

AD/A-003 398

PROCEEDINGS OF AFCRL SCIENTIFIC
BALLOON SYMPOSIUM (8TH) HELD AT HYANNIS,
MASSACHUSETTS ON 30 SEPTEMBER TO
3 OCTOBER 1974

Andrew S. Carten, Jr.

Air Force Cambridge Research Laboratories
Hanscom Air Force Base, Massachusetts

21 August 1974

DISTRIBUTED BY:

NTIS

National Technical Information Service
U. S. DEPARTMENT OF COMMERCE

Preface

The AFCRL Scientific Balloon Symposia have over the years become established as the principal forum for the exchange of ideas and technical information within the wide community of balloon systems users and developers. This Eighth Symposium has been planned to maintain the high standards of its predecessors and at the same time introduce some major innovations. For example, these Proceedings are for the first time being published as preprints instead of after-the-fact documentation. The reader's indulgence is requested for any unevenness in format and any discrepancies that may have occurred. Such unwanted results frequently accompany this mode of publication. Timeliness has been given the greatest priority. This has placed the burden of editing primarily on the individual authors so that photoready copy could be obtained for quick reproduction. It is hoped that the prompt availability of these Proceedings compensates for their flaws of production.

I sincerely thank my colleagues in the Aerospace Instrumentation Laboratory for their help and encouragement in this endeavor, and the individual authors who did such a magnificent job of meeting the stringent time schedules for photoready copy. To the Chairmen who assisted so nobly in the planning of the sessions, and to the typists at AFCRL and elsewhere who worked so hard to turn out the final copy, a special debt of gratitude is owed and acknowledged.

ASC

Hanscom AFB, 21 August 1974

3

Preceding page blank

Contents

1. <u>POWERED BALLOONS</u>	
UNMANNED POWER BALLOONS A. Korn	11
HIGH-ALTITUDE SUPERPRESSURED POWER AEROSTAT (HASPA) <u>(Abstract)</u> F. J. Petrone and P. R. Wessel	31
REGENERATIVE FUEL CELL POWER SYSTEM FOR AEROSTATS P. R. Wessel and F. J. Petrone	33
THE INFLUENCE OF FINENESS RATIO ON POWERED ELLIPSOIDAL BALLOON WEIGHT AND OTHER CHARACTERISTICS N. J. Mayer	51
2. <u>TETHERED BALLOONS</u>	
TECHNOLOGY UPDATE ON TETHERED AEROSTAT MATERIALS DEVELOPMENTS L. B. Keen	65
STRATOSPHERIC TETHERED BALLOONS <u>(Abstract)</u> R. Regipa	87
THE MINNESOTA 1973 ATMOSPHERIC BOUNDARY LAYER EXPERIMENT D. A. Haugen, J. C. Kaimal, C. J. Readings and A. J. Marks	89
A NEW MOORING SYSTEM FOR TETHERED AEROSTAT E. L. Haak and K. Turner	99
THE TCOM SYSTEM - TECHNOLOGY AND APPLICATIONS I. R. Sussman and D. L. Spritzer	125
AERODYNAMIC PERFORMANCE OF THE FAMILY II TETHERED BALLOON SYSTEM R. G. Ollila and M. A. Duffy	143

Contents

AN EXPERIMENTAL INVESTIGATION OF THE DYNAMIC STABILITY OF THE FAMILY II BALLOON J. D. DeLaurier	161
EXPERIMENTAL INVESTIGATION OF BALLOON STRUCTURAL RESPONSE E. J. Mills and J. J. Groom	177
BALLONET GAS MOTION IN LARGE BALLOONS C. F. Holt	189
A NEW KIND OF POWERED OR TETHERED BALLOON (Abstract) A. Balleyguier	203
DESIGN, DEVELOPMENT, AND TESTING OF NEW AEROSTAT MATERIAL E. E. Alexandroff	205
LOCAL MOTIONS OF A PAYLOAD SUPPORTED BY A NOLARO TRI-TETHERED BALLOON R. C. LeClaire, 1/Lt, USAF and H. L. Schumacher, Jr., 2/Lt, USAF	233
A FABRIC STRAIN MONITOR FOR BALLOON FLIGHT TEST E. L. Crosby, Jr.	257
MOBILITY OF LARGE TETHERED AEROSTATS H. D. Masch	277
TESTING THE PERFORMANCE OF A LARGE AEROSTAT T. H. Yon, Jr.	299
TETHERED BALLOON POWER PLANT GASEOUS FUEL SUPPLY VIA TUBULAR TETHER C. H. Duggins	313

3. FREE-BALLOON TECHNOLOGY

FREE BALLOON CAPABILITIES: A CRITICAL PERSPECTIVE (Abstract) J. F. Dwyer	327
GORE PANEL STRESS ANALYSIS OF HIGH ALTITUDE BALLOONS Dr. H. Alexander and P. Agrawal	329
THERMAL ANALYSIS OF LONG DURATION FLIGHT PACKAGES (Abstract) L. A. Carlson and Penny M. Brandeberry	347
BALLOON DESIGN (Abstract) J. L. Rand	349
BALLOON SYSTEMS STRENGTH AND FAILURE ANALYSIS (Abstract) L. D. Webb	351
DEVELOPMENT OF DACRON-REINFORCED POLYETHYLENE FILM FOR HEAVY-LOAD FREE-FLIGHT BALLOON APPLICATIONS (Abstract) J. B. Munson	353
TWELVE YEARS AFTER THE FIRST LAUNCH: CNES OPERATIONAL ACTIVITY WITH STRATOSPHERIC BALLOONS (Abstract) M. Rougeron	355

Contents

AN ADVANCED BALLOON LOCATING SYSTEM H. Laping and A. R. Griffin	357
UPDATING FREE BALLOON TECHNOLOGY (<u>Abstract</u>) J. R. Nelson	371
COMPOSITE MATERIALS CONCEPT AND BALLOONS APPLICATION M. Ferronniere	373
COMPUTER TECHNIQUES FOR BALLOON OPERATIONS B. D. Gildenberg	385
ATMOSPHERIC TEMPERATURES MEASURED NEAR 48 KILOMETERS BY BALLOON-BORNE THERMISTORS H. N. Ballard, M. Izquierdo, C. McDonald and J. Whitacre	401
SCIENTIFIC BALLOONING AND RADIATIONS MONITORING ORGANIZATION (SBARMO): ORIGIN, PURPOSE AND POSSIBLE FUTURE H. Trefall	417

4. BALLOON-BORNE EXPERIMENTS

BACKGROUND ON BALLOON-BORNE EXPERIMENTS A. H. Howell	425
VENUS BALLOON SYSTEMS P. C. Carroll and C. L. Deats	433
A CONTROL AND TELEMETRY SYSTEM FOR A BALLOON BORNE AIR SAMPLING PACKAGE R. H. Cordella, Jr., Capt. USAF	451
A DESCRIPTION OF THE LACATE BALLOON EXPERIMENT AND SOME PRELIMINARY RESULTS J. M. Russell, III, J. C. Gille, R. E. Davis and P. L. Bailey	477
DESIGN AND OPERATING CHARACTERISTICS OF A BALLOON-BORNE VACUUM SYSTEM R. O. Woods	495
BALLOON GONDOLA MEASUREMENTS P. B. Herrington	511
AMES BALLOON-BORNE TELESCOPE FOR INFRARED ASTRONOMY C. D. Swift	517
FLIGHT PERFORMANCES OF THE GENEVA STELLAR PLATFORM D. A. Huguenin	527

Contents

5. SPECIAL APPLICATIONS

SPECIAL APPLICATIONS; AN OVERVIEW J. A. Winker	539
MANNED HOT-AIR BALLOONS AS WARM FOG RESEARCH VEHICLES R. G. Reinking	553
A MANNED, NONRIGID THERMAL AIRSHIP R. A. Pohl	567
PRESSURE HOT AIRSHIP DESIGN AND PERFORMANCE <u>(Abstract)</u> J. F. Hebel	577
ROCKET-LAUNCH BALLOON-BORNE SYSTEMS (RLBS) R. C. Geiss	579
SPHERE DESIGN FOR A STATIC DETONABLE GAS EXPERIMENT - GEST M. G. Marcucci, Capt., USAF	589
APPENDIX A: Publicati of Proceedings of Past AFCRL Balloon Symposia and Workshops	613

Session 1
Powered Balloons

Arthur O. Korn, Chairman
Air Force Cambridge Research Laboratories

Contents

1. Introduction
2. Background
3. History
4. High Altitude Flights
5. Low Altitude Flights
6. Studies
7. Summary

Unmanned Powered Balloons

Arthur O. Korn
Air Force Cambridge Research Laboratories
Bedford, Massachusetts

Abstract

In the late 1960's several governmental agencies sponsored efforts with private industry to develop unmanned, powered balloon systems for scientific experimentation and military operations. Some of the programs resulted in hardware and limited flight tests; others generated system designs and concepts that, to date, have not progressed beyond the paper study stage. Silent Joe I, Silent Joe II, and Microblimp flew at low altitudes. The first powered balloons to fly in the 60,000 to 85,000-ft region of minimum wind fields were High Platform I, High Platform II and POBAL. Several paper design studies also have been completed for unmanned, remotely controlled, high altitude powered balloon systems with higher speed capabilities and much longer flight durations. HASKV (High Altitude Station Keeping Vehicle) was an overview of high altitude, station keeping vehicles as applicable to powered balloon concepts. High Platform III is a 600,000-ft³, Class C hull design for flight at 85,000 ft, solar powered for a 4-month duration. The POBAL-S program resulted in design of a superpressured, stern-propelled airship to fly at 70,000 ft. It is powered by a H₂-O₂ fuel cell/electric motor combination rather than by solar cells so that more electric power will be continuously available to the user's payload. Useful payload capacity on the POBAL-S system is 200 lb. Speed capability is 16 knots continuously for a 7-day duration. The HASPA (High Altitude Superpressure Powered Airship) program is the largest active effort in this field. Its goal is to carry a 200 lb useful payload at 70,000 feet for longer than one month, with a continuous speed capability of 15 knots, and maximum, shorter duration capability of 25 knots. Four test flights are planned, the fourth to be an all-up, long duration, solar-cell powered flight. The program will take place during the next three years.

This paper briefly describes the various balloon system designs, materials and propulsion units and highlights the capabilities of the systems, and points out critical problem areas that require further study in order to achieve operational, high altitude powered balloon flight.

1. INTRODUCTION

This morning's opening session deals with powered balloons. Most of you are more familiar with the conventional, free floating balloon that drifts wherever the prevailing winds happen to carry it. For many balloon-borne experiments the drift is inconsequential -- it even can be an asset. There are other very important applications, however, for which the balloon is an ideal atmospheric vehicle provided that drift can be minimized. Various governmental agencies have been studying methods for minimizing drift by adding a propulsion source to the balloon. Several of these systems have been fully developed and have been flown.

Today I shall present some history, and a brief overview of recent powered balloon efforts. Then, individual papers will be presented by specialists who are currently working in this field. My discussion will include powered balloon systems and completed system design studies for both high and low altitudes, but the recent programs will be limited to unmanned systems in the USA. Several of these programs were conducted on a classified basis; however, the design and test performance data have been declassified. This paper reports on these declassified data.

2. BACKGROUND

For many years balloon flight managers have been attempting to minimize horizontal displacement by preselecting the float altitude where the winds are known to be near minimum, monitoring the trajectory, and correcting the drift by ballasting or valving to nearby altitudes where the wind will drive the balloon in the proper direction.

Many unpowered flights have been very successful in this type of station keeping. This success is based upon the seasonal atmospheric phenomenon illustrated in Figure 1. The westerly winds above easterly winds in the lower stratosphere result in a transition level where the winds are essentially zero. Just above and below this level are bands of altitude where the winds are less than 10 knots.

It was reasoned that if some small amount of propulsion could be added to a free balloon, the station-keeping capability in the minimum wind fields could be greatly enhanced. With some margin in available thrust, such a powered balloon is not limited to station-keeping, of course, but can travel in any direction.

3. HISTORY

The early balloons would only go up and down or float in the direction of the prevailing winds. In order to make the balloon more useful it was soon concluded that it should be "dirigible" or directable. Throughout the nineteenth century ingenious men such as Meusnier, Giffard, Tissandier, Renard and Krebs worked on this problem. They built manned airships shaped as spindles, torpedos, cigars, stringbeans and even whales. Their biggest problem was the lack of a lightweight, efficient power plant. The steam engine, while dependable, was very heavy. In 1852, Giffard built a small engine using steam, but it weighed 100 pounds per horsepower. (Today's automobile engines weigh as little as 2 pounds per horsepower, and airplane engines, less than 1 pound per horsepower). Those early inventors experimented with feather-bladed oars and screw propellers turned by hand using a crew of eight men! Engines were built that used coal gas or hydrogen lifting gas from the airship. In 1884, Renard built an electric motor powered from a storage battery.

Real progress in powered balloons had to wait for the discovery of petroleum in Pennsylvania and the invention of the internal combustion engine. In the 1890's the gasoline engine was being developed and it proved to be the long sought key to the (low altitude) propulsion problem. In 1901, Santos Dumont's work on small airships in France won him the 100,000 franc prize for flying across Paris to circle the Eiffel Tower and return to his starting point. In the early 1900's Count Zeppelin started to develop big ships in Germany. The airship Clement Bayard II flew the English Channel in 1910 and made a 242-mile trip to London in 6 hours. Great progress continued throughout World War I and thereafter. The blimp proved

its usefulness during World Wars I and II. All of these airships flew at very low altitudes.

I will not dwell on the era of the blimps and zeppelins, since they are well recalled, but will now skip in history to the late 1960's when several U.S. government agencies sponsored efforts with private industry to develop unmanned powered balloon systems for scientific experimentation and military operations. Some of the programs resulted in hardware and limited flight tests; others generated system designs and concepts that, to date, have not progressed beyond the paperwork stage. This paper gives an overview of these various programs.

4. HIGH ALTITUDE FLIGHTS

High Platform I was one of the earliest attempts at powering a balloon at high altitude. It was developed and flown on a classified program by Goodyear Aerospace and Winzen Research Inc. In Figure 2 the system is shown being launched. The program objectives were (1) to demonstrate that it is feasible to maintain a free balloon on-station at high altitude using an electrically-driven propeller; (2) to examine the accuracy and output of a simple, single-axis-oriented silicon solar array for application as the eventual primary power source for the electrically powered balloon. The program was limited in scope in that off-the-shelf hardware was required for all systems. This requirement necessitated using a natural shaped balloon which has an undesirably high coefficient of drag. Because of the high drag force the flight test was planned during a period when the speed of the upper atmosphere winds was at a minimum. The flight design goals were: (1) float altitude--70,000 feet; (2) maximum airspeed--10 knots; maximum deviation from station +50 miles. Flight duration was dependent on battery life. The flight was conducted at Minneapolis, Minnesota in Sept., 1968. The balloon had a volume of 106,000 cu ft and was 63 ft in diameter. A 2.75 H.P. motor drove a 14 ft diameter propeller with power from 112lbs of silver zinc batteries. The goal was to control balloon orientation and heading at an airspeed of 10 knots by remote control of a

styrofoam rudder that rode in the propeller slipstream. The wooden propeller was designed to provide 25 lbs thrust at 1,000 R.P.M.. Total system weight was 555 lbs of which 106 lbs was balloon. The system in flight is shown in Fig 3. It was launched in the early morning and ascended at nearly 1,000 ft/min. On its first power cycle the motor was run for 31 minutes. Directional response to rudder commands was good and no evidence of instability was noted. However, time delay between command and rudder actuation, the rate of rudder movement, and the time required to calculate and verify the actual heading resulted in a rather erratic flight path. During the second power cycle the rudder control was erratic. Although the gondola changed azimuth orientation in response to rudder commands, it was found to be almost impossible to hold a given heading. Rudder response then disappeared and recovery procedures were initiated. The direct current motor, when recovered, was severely charred and showed evidence of brush arcing. The motor was completely destroyed from overheating. During the first 30 minute power cycle the system did demonstrate the capability to fly into the wind at an airspeed in excess of 10 knots, and to change the direction of the flight path. The sun sensor was successful in consistently tracking the sun accurately enough to estimate the maximum output of the solar array. The results show that an electrically driven propeller is a feasible method of station keeping a high altitude balloon.

The High Platform II program (HP II) began in early 1969. This was a classified effort conducted by Raven Industries. The statement of work called for the development of a unique airship having a capability of operating for very extended durations at an altitude of 70,000 feet. The flight system is shown in Fig 4. The duration requirements defined a completely sealed, superpressure balloon which should have a duration capability of greater than 6 months. Desired speed capability was 20 knots. Solar cells were to be used to power the motor-propeller assembly.

A 3/1 fineness ratio, class C hull configuration was used on HP II because of its greatly reduced coefficient of drag as compared with the HPI envelope. The envelope was constructed of a bi-laminate of 1.0 mil and .35 mil Mylar S and was

81 feet in length. Control surfaces on the hull included one vertical stationary fin, one rudder, two horizontal stabilizers and two elevators. Rudder and elevators were servo motor controlled. The lightened, molded foam propeller, 10 feet in diameter was designed to operate at 360 RPM with an efficiency of 78%. Propulsion motor characteristics were: .25 brake horsepower at a speed of 8,200 RPM with an input of 24VDC, predicted efficiency; 72%. The motor drove a belt speed reducer to drop the high speed of the motor to the desired 360 RPM of the propeller. The power supply was a 300 watt cadmium sulfide solar array of 13 panels connected in parallel. CdS cells were chosen over silicon because of their greater flexibility and greater potential for weight reduction.

The basic purpose of the gondola was to support mechanical components of the propulsion system. An anemometer was suspended beneath the gondola. In January and March 1970 two test flights were accomplished to check out system components. Several changes to the all-up flight system were made as a result of these test flights. In May, 1970, the airship was test flown. The airship gross weight was 136 lb. The tow balloon launch technique was used for better control of the very fragile system. The tow balloon was detached from the airship at 50,000 ft. When the motor was turned on, the airship immediately swung into the selected heading. After 76 minutes operation the motor was turned off. Reflected light falling on the solar cell array prevented further acquisition of accurate heading data. Immediately after the motor was turned on the system rose in altitude. This is indicative of a positive angle of attack and forward speed which provided the airship with some aerodynamic lift. The experimenters concluded that the airspeed was 10 knots rather than the desired 17 knots, and that the primary factors reducing speed below the design value were too low a design value for drag coefficient (actual value of $C_d = 0.11$ rather than design value, $C_d = 0.045$, based upon wind tunnel data) and mismatch between the solar cell array and propulsion system. They further concluded that a high altitude airship having a superpressure envelope to obtain extremely long duration flight, and thin film solar cells for power can be designed, constructed, successfully launched and remotely controlled.

POBAL (Powered Balloon) was an unclassified program started in 1969 by AFCRL with Goodyear Aerospace Corp. under contract to study feasibility of station keeping by remote control of a powered balloon at high altitudes. Both streamlined (blimp) and natural shaped (or round) balloon configurations were considered, with reciprocating engines, turbines and electric motors as candidates for propulsion, and fuel cells, solar cells and batteries, for electric power sources. As a result of this study it was decided to design an economical system for flight demonstration. The system that was built and flown by AFCRL was larger, heavier and more powerful than High Platform I (Figure 5). For reasons of economy, the parachute system, rigging hardware, balloon and control system were off-the-shelf items currently used for conventional ballooning. A 711,000 ft³, double wall polyethylene balloon was used on POBAL to carry a load of nearly 4,000 pounds to 60,000 ft. altitude. An 8HP DC electric motor drove (through a gear reducer) a 35 foot diameter FH-1100 helicopter rotor at 200 RPM. Based on $C_d = .19$ the system was designed to have a speed capability of 15 knots. Planned duration of flight was to be 8 hrs, the life available from the residual silver zinc F-105 fighter starter batteries. (Nearly 2,000 lbs of the payload were comprised of these batteries). The direction of motor thrust was controlled by a rudder located in the slip stream of the propeller. After the mission the balloon was expended and the gondola recovered by parachute.

The first flight was flown in September 1972. All systems functioned for the first 43 minutes of power. The propulsion motor was then allowed to cool for 11 minutes and then another powered cycle was initiated. Various headings were commanded into the autopilot system during these powered cycles. The system was also flown via manual control of right and left rudder.

After a total of four power "on" cycles (3 hrs of flight time) control of the azimuth heading was no longer possible. It was then confirmed that the rudder had broken free of the payload. Subsequent examination of the failed rudder support tube indicated improper heat treatment after a welding process. The system did however, attain air speeds in excess of 11 knots and demonstrated that the

concept is feasible. It is felt that the design speed of 15 knots was not attained because of one or a combination of both of the following: (1) too low a design drag coefficient for the round balloon or (2) the propeller was not producing the calculated thrust.

5. LOW ALTITUDE FLIGHTS

Silent Joe I is shown in Figure 6. The balloon was a 5,500 ft³ Class C hull with a 3 to 1 fineness ratio developed on a classified program by the Sheldahl Co. Design speed for this system was 12-15 knots. The first version used two 3HP McCulloch chain saw engines for propulsion. Steering was accomplished by varying the speed of either outboard-mounted engine. Some problems were encountered in the synchronization of the motor throttles and the gasoline engines were replaced with electric motors. This second version of Silent Joe I shown in Figure 7 used 2-2½HP electric motors powered by nickel cadmium batteries. This combination gave a planned flight duration of two hours. Silent Joe I was successfully flown on several occasions in Southeast Asia. It had well controlled performance with flight speeds being 10-12 knots.

Silent Joe II followed Joe I. Its configuration is shown in Figure 8. This program was conducted by Goodyear Aerospace Corporation and used the 150,000 ft³ Goodyear Mayflower I blimp as the system hull. The hull was modified to add a propulsion unit in the stern of the airship. The propeller was driven by a hydraulic motor, pressure for which was generated from a unit located in the forward end of the hull. The propulsion unit had a servo-controlled pitch and yaw gimbal system for vectoring the propeller thrust in order to achieve flight-path control. Nine flights of Silent Joe II were conducted in 1968 and 1969.

Micro Blimp was a classified, low altitude airship program accomplished by Raven Industries. The hull was a class C shape with a 3:1 fineness ratio. The system is shown first prior to launch in Figure 9. Hull volume was 2,750 ft³ and length was 37 feet. Propulsive power was provided by a stern mounted, 4 HP Wankel engine

driving an 8 foot diameter molded polyurethane three bladed propeller. Directional control was obtained by gimbaling the engine-propeller assembly. Heading and pitch stability were maintained by an autopilot in the system. Micro Blimp had a maximum cruise altitude of 5,000 feet MSL and a cruise speed of 30 knots. Its maximum radio controlled range is 5 miles with a control accuracy of 1500 feet. Endurance was 10 hours with a full load of fuel. Payload capacity was 20-50 pounds depending upon the amount of fuel carried. Many successful flights were accomplished with the Micro Blimp. The major problem with the system was propeller breakage. This however was solved with propeller stiffeners. Micro Blimp in flight is shown in Figure 10.

6. STUDIES

Several programs generated system designs and concepts that, to date, have not progressed beyond the paperwork stage.

The High Platform III paper study performed by Raven Industries required the design of a solar-powered aerostat and the definition of a development program for a prototype system. The airship designed under the program has a volume of 600,000 cubic feet. The envelope length is 309 feet and the diameter is 62 feet. The airship is designed to be a constant altitude system and as such is superpressured. Nylon film is used for the hull. Fins are pressurized by a small air-compressor. Propulsion and control of the airship is accomplished by use of a rear mounted, gimballed propeller powered by an electric motor. The motor's power supply is a solar array. The system is designed to be capable of maintaining air speed of 15 knots continuously, 24 hours a day for 4 months. Flight altitude is 85,000 feet. Payload capacity is 10 pounds.

Several assumptions were made throughout the design study. These include:

- (a) A high strength nylon film will be sufficiently developed for superpressure balloons.
- (b) The coefficient of drag of the airship is .048.

(c) Pulse charging techniques can be developed to increase the life of the battery.

(d) Cadmium sulfide thin film solar cells of characteristics equal to or better than the cells used on High Platform II will be available.

Until these items are developed the airship cannot be built to meet the specifications. If the assumptions cannot be met, changes in system size or capabilities will result. The proposed High Platform III airship is shown in Fig 11. The High Platform III Design Study was complete in August, 1971.

The HASKV (High Altitude Station Keeping Vehicle) program had as its objective to review and study all high altitude station-keeping powered balloon concepts. All past efforts were reviewed, a comprehensive analysis of various system concepts was undertaken and a preliminary design for a system was completed. Primary emphasis was placed on superpressure airships capable of flying for durations up to several months at altitudes ranging from 60,000 feet to 85,000 feet with speeds up to 30 knots. The major effort on HASKV was devoted to parametric analysis and trade-off studies of the many system components and concepts. Much valuable information was thus generated and reported upon in the HASKV Final Report. Using this information a system was designed that is similar to that proposed in the High Platform III Study. The major differences concern the construction of the balloon envelope and the use of the power cycle. The final HASKV design was for a vehicle capable of supporting a 200 lb payload at an altitude of 70,000 feet for a four month duration. It is to be solar powered, to operate at 30 knot air-speeds during the day and 10 knots during the night. This program was completed in 1973.

The AFCRL POBAL-S design effort with Raven Industries resulted in an airship very similar to the HASKV vehicle. Jack Beemer of Raven Industries, Inc. will report on this system later in this session. I will report only briefly on the salient characteristics of the POBAL-S Program. The major difference between HASKV and POBAL-S lies in the system used to power the electric propulsion motor.

You will recall that the HASKV airship is solar cell powered; POBAL-S obtains electrical energy from a H_2-O_2 fuel cell. The fuel cell was selected for this airship rather than solar cells so that more electric power could be made available on a continuous basis to the operational payload. On this system 500 watts are available to operate the user's payload. Duration for the system is 7 days rather than 4 months for the solar powered version. The two systems are obviously designed for different operational missions. POBAL-S is shown in Figure 12. To summarize the capabilities of AFCRL's POBAL-S; it flies at a 70,000 foot altitude; has a payload capacity of 200 lb; continuous power of 500 watts available on a continuous basis for operation of the payload; speed capability of 16 knots continuously for a 7 day duration. The final report and drawings for the fabrication of a POBAL-S airship are due to be completed in the fall of 1974.

The U. S. Navy (NRL, NOL) HASPA (High Altitude Superpressure Powered Airship) program is the largest active effort in high altitude powered ballooning. Messrs. Frank Petrone and Paul Wessel of the Naval Ordnance Laboratories will report in detail on the effort during this session. It is listed as a "Study" only because the contract award for its development was still being negotiated at this writing. The program's goal is to carry a useful payload of 200 pounds at 70,000 feet for durations exceeding one month. HASPA is to have a continuous speed capability of 15 knots, with a maximum shorter duration capability of 25 knots. Four flight tests are planned; the first, an unpowered flight to evaluate the launch technique and the integrity of the superpressured hull; the second, a battery-powered flight to evaluate the propulsion system; the third, a fuel-cell evaluation flight; and the fourth, an all-up, long-duration, solar-cell powered flight. The program will take place over the next three years. The HASPA vehicle is shown in Figure 13.

7. SUMMARY

In the past six years much useful work has been accomplished in developing unmanned powered balloons without a great expenditure of funds. Several governmental

agencies have been involved with all of the major balloon companies in the various systems studies and developments. The total result has not been outstanding but, considering the very low funding and manning budget available and the magnitude of the problem, very good progress has been made toward achieving operational, long duration, high altitude powered balloons with usefully large payloads. The experimental systems that have been flown have clearly defined the remaining practical and theoretical problems to be solved. For example, future high altitude, powered balloon programs should spend more effort to obtain accurate drag coefficient measurements at the low Reynolds numbers encountered in the minimum wind fields. Another important area of uncertainty is the propeller design. More basic work is required to accurately predict propeller performance in the 60,000 to 85,000 ft altitude levels. Propellers have not normally been used at those altitudes; conventional procedures for "scaling" from ground level data are not valid, and no guidance is available from the literature. We also must make use of the modern analytical tools for accurately determining the dynamic stresses in the structure and their distribution over the airship surface. If the pressurized hull volume to support a usefully heavy payload is to be kept within manageable limits without sacrificing structural reliability, then the allowable weight to strength and elastic properties of the materials are critical design parameters. It is hoped that future high altitude powered balloon programs will benefit from the experience reported herein.

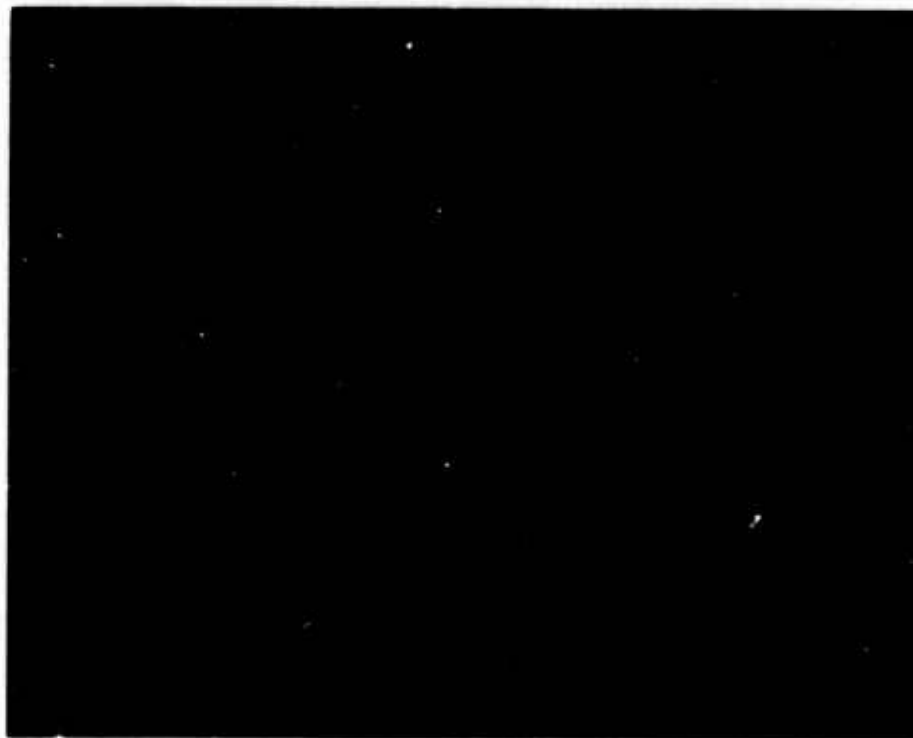


Figure 1. Minimum Wind Field Phenomenon



Figure 2. High Platform I at Launch

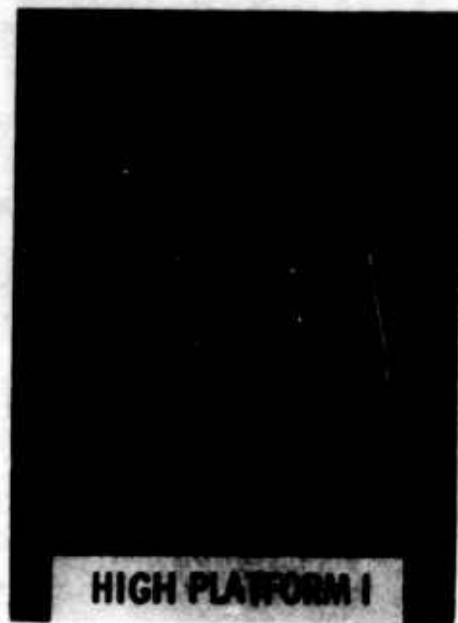


Figure 3. High Platform I in Flight

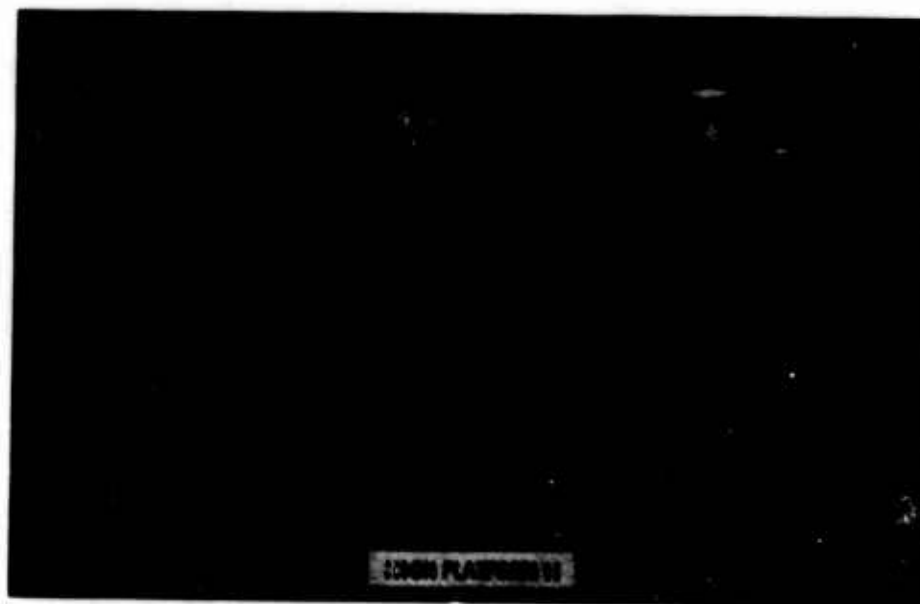


Figure 4. High Platform II During Test



Figure 5. Pobal Undergoing Hanger Tests

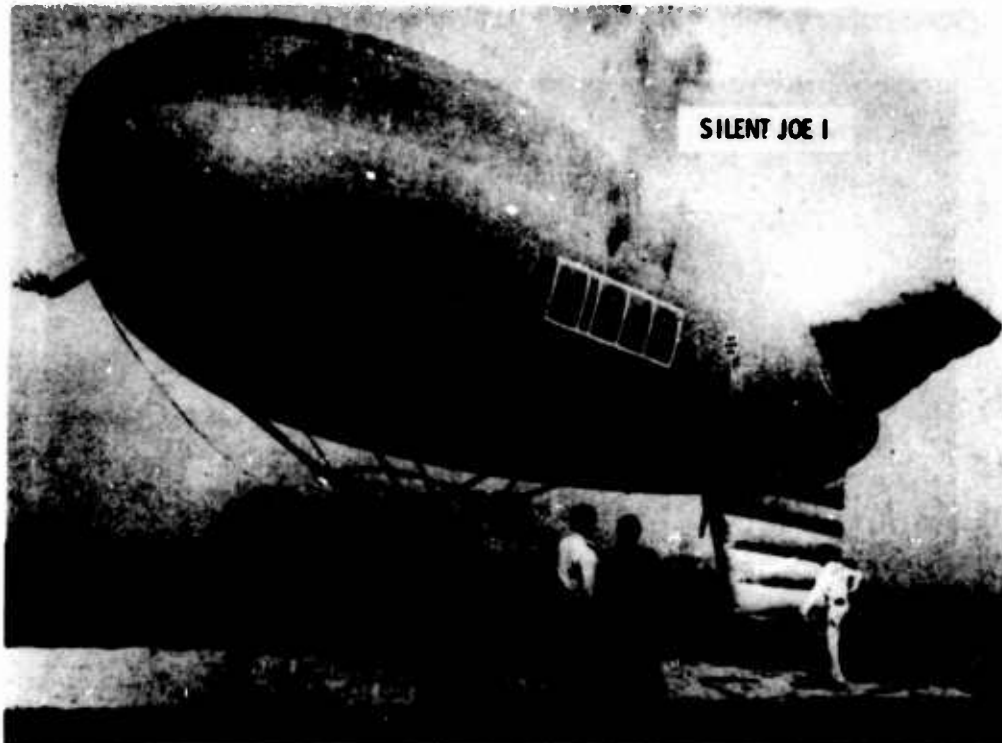
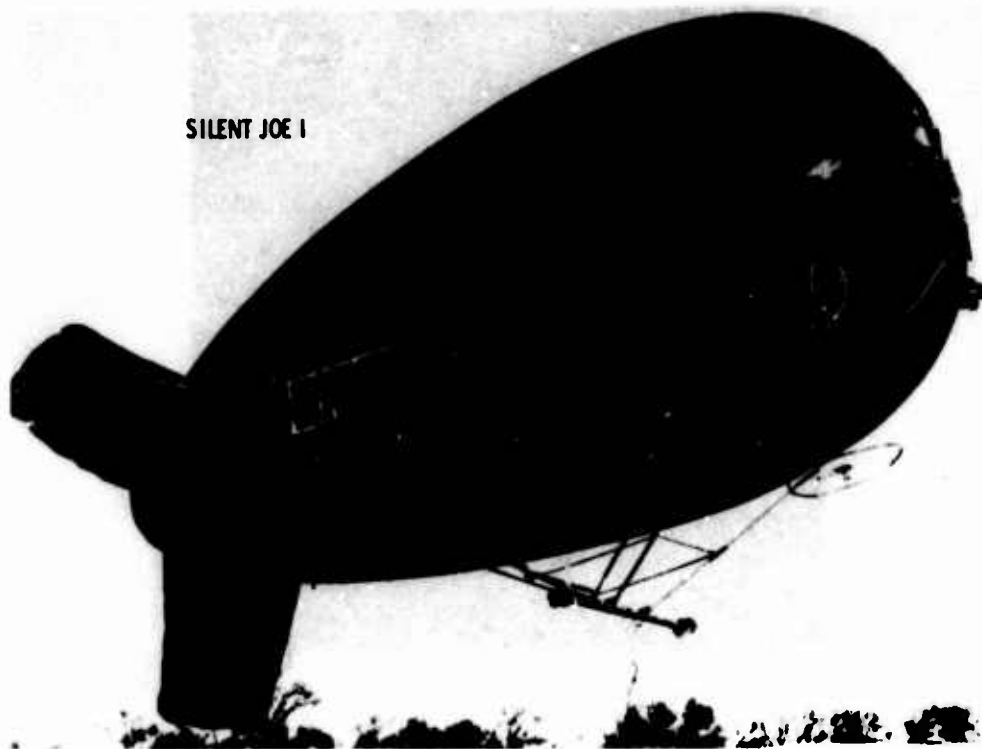
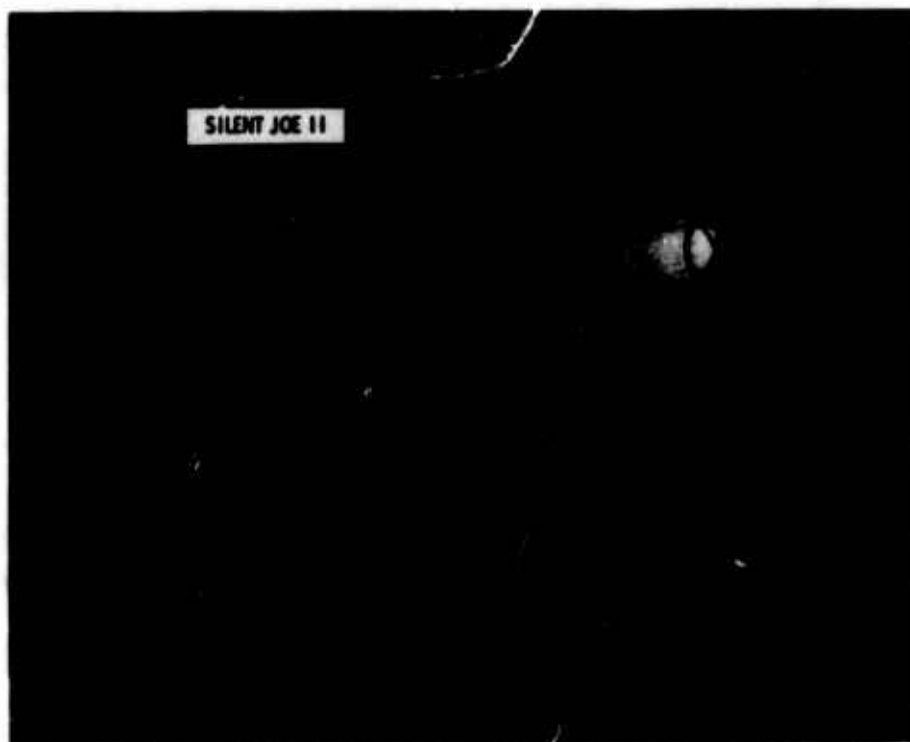


Figure 6. Silent Joe I, Initial Configuration



SILENT JOE I

Figure 7. Silent Joe I, Final Configuration



SILENT JOE II

Figure 8. Silent Joe II in Flight



Figure 9. Micro Blimp at Launch

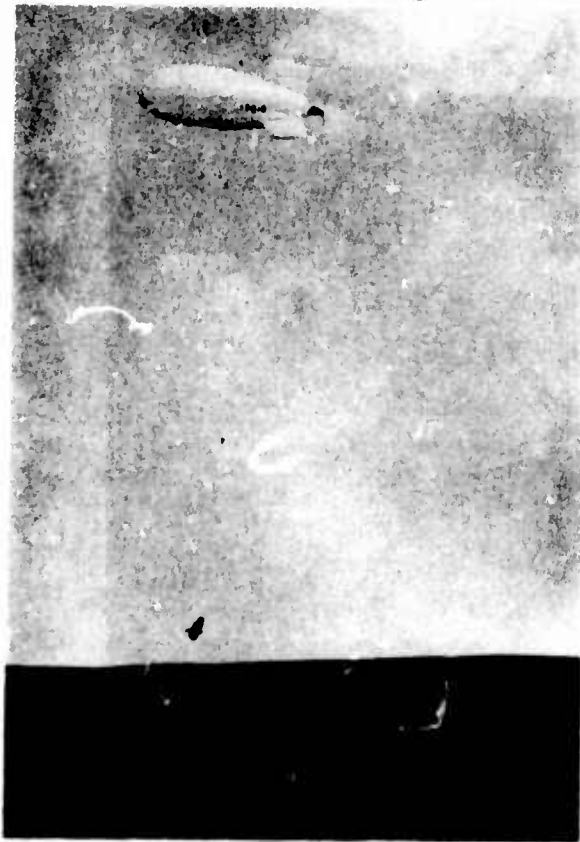


**Figure 10. Micro Blimp
in Flight**

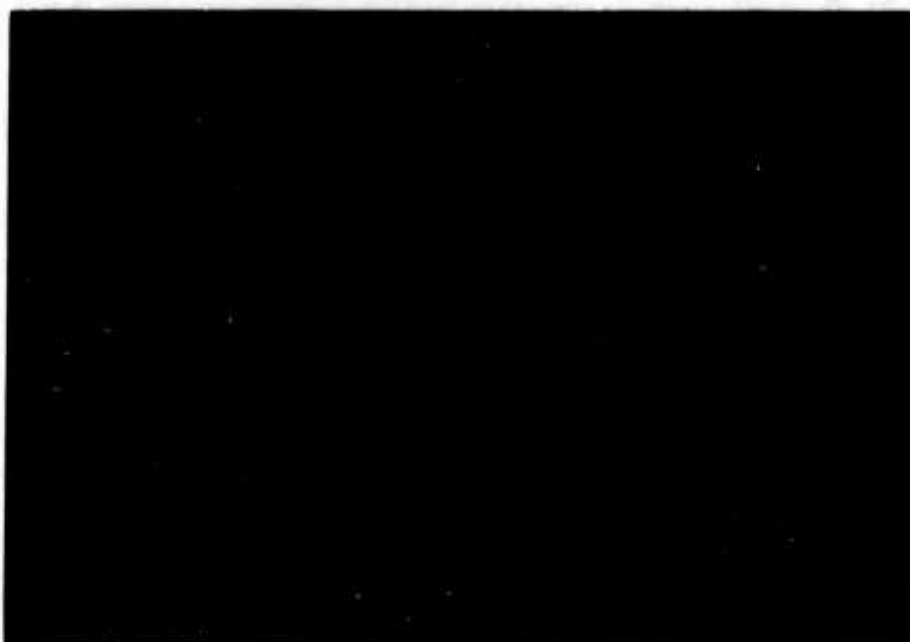
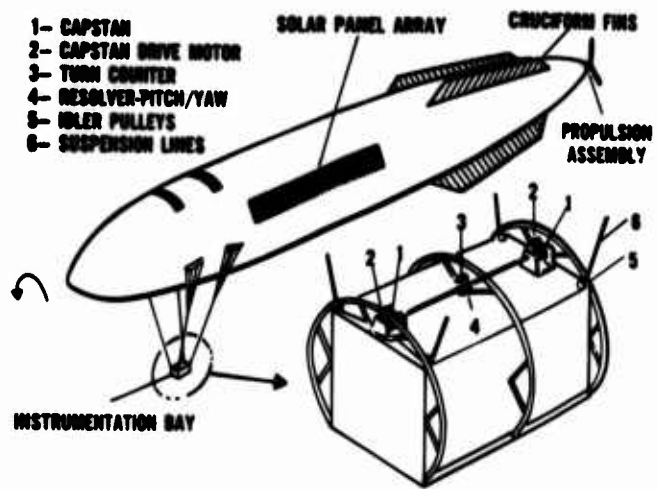


Figure 11. High Platform III Arrangements



Figure 12. Pabal-S Arrangement



HASPA CONFIGURATION

Figure 13. HASPA Arrangement

References

- Allen, H., (1943) The Story of the Airship (Non-Rigid), The Lakeside Press, Akron, Ohio.
- Goodyear Aerospace Corp., (1968) Report BB-2304, High Altitude Powered Balloon Test Program.
- Raven Industries, Inc., (1970), Report R-0870025, High Platform II.
- Raven Industries, Inc., (1971), Report 0871005, High Platform III, Design Study.
- Raven Industries, Inc., (1973), Report 0373003, Study of High Altitude Station Keeping Vehicles.
- Korn, A., Leclaire, R., 1st Lt, USAF, Rice, C., (1973), Report AFCRL-TR-73-0424, LDF Powered Balloon Program.
- Raven Industries, Inc., (1971), Report 1271010, Micro Blimp Final Report.

High-Altitude Superpressured Power Aerostat (HASPA)

F. J. Petrone and P. R. Wesel
Naval Ordnance Laboratory
Silver Spring, Maryland

Abstract

A demonstration program is now underway in which the feasibility of a High Altitude Super-pressured Powered Aerostat (HASPA) will be determined. Basically the HASPA is an unmanned platform that would operate continuously at high-altitude for long periods of time and maintain an assigned station through powered maneuverability taking advantage of the low wind fields between the stratospheric and tropospheric winds. HASPA would serve as an extended duration airborne platform from which sensors or communication relay links can be operated. The present 32 month time frame of this program will include four demonstration flights (one unpowered and three powered) with expected flight durations of from a few days to over one month. This presentation will emphasize present flight objectives, vehicle design status, and potential problem areas with the proposed resolutions.

Contents

1. Introduction
2. Power System Requirements
3. Regenerative Fuel Cell System
4. System Weights, Costs, and Alternatives
5. Summary

Regenerative Fuel Cell Power System for Aerostats*

P. R. Wessel and F. J. Petrone
Naval Ordnance Laboratory
Silver Spring, Maryland

Abstract

A regenerative hydrogen-oxygen fuel cell is an attractive alternative as a power supply for high altitude super-pressured balloons and powered aerostats. The state of the art is sufficiently advanced that systems operating continuously in the 10 kW power range can be expected to weigh less than 1000 pounds. Such systems will provide power that is virtually unlimited in duration and will operate as completely closed cycle units. The use of the regenerative system is particularly advantageous for applications requiring the availability of high power levels on a continuous basis for extended periods of time. Other advantages of the system and its cost-effectiveness compared to other alternatives are discussed. Improvements to be expected in the future are also reviewed.

*Work supported by the Naval Electronics Systems Command

1. INTRODUCTION

Interest in high altitude powered balloons or aerostats has been steadily increasing in recent years. This interest has led to a greater awareness of the unique problems and requirements which such systems pose for engineers, particularly in the areas of materials technology and high energy density power systems. The latter area is the one we have addressed in this description of a regenerative fuel cell system. Before describing the power system concept we would like to take a brief look at the overall power requirements.

2. POWER SYSTEM REQUIREMENTS

Power consumption can be conveniently divided into three general categories, propulsion, payload operation, and control and telemetry. For a powered aerostat the greatest consumption will result from propulsion requirements. To estimate the power needed we will assume baseline system parameters as follows:

Volume - 1,000,000 cu.ft

Shape - Class "C" airship (approximately)

Operating Altitude - 70,000 ft

Maximum Speed - 30 knots

Propulsion - large diameter propeller

2.1 Propulsion

An appropriate expression for the drag, D , (or thrust, T) of an aerodynamically shaped balloon is,

$$T = D = \frac{1}{2} \rho C_D v^2 V^{2/3} \quad (1)$$

where ρ is the atmospheric density (slugs/ft³)

C_D is the drag coefficient

v is the flight velocity, (ft/sec)

V is the volume of the vehicle (ft³).

Substituting the nominal system parameters Eq. (1) leads to an estimated thrust requirement of

$$T = 0.1 v^2 \text{ lbs}$$

where v is expressed in knots, and a value of 0.05 is assigned to the drag coefficient.

To produce this thrust level the power input to the propeller, P_i , reduced by the propeller efficiency ($E_p \approx 0.75$) must equal the product of thrust and forward velocity. Thus

$$P_i E_p = Tv,$$

or

$$P_i = \frac{0.167 v^3}{E_p} \frac{\text{lb.ft}}{\text{sec}}, \quad (2)$$

where an additional factor of 1.67 is introduced by the conversion of knots to ft/sec. Additional efficiency factors must be introduced for the mechanical drive system ($E_d \approx 0.9$) and for the electric motor conversion of electrical power to mechanical power ($E_c \approx 0.8$) for operation from an electrical power system. Introducing an additional factor of 0.74 for the conversion of lb-ft/sec to watts leads to the final expression for propulsive power:

$$P_i = \frac{0.22 v^3}{E_p E_d E_c} \text{ watts.} \quad (3)$$

For the particular case under discussion this leads to a power requirement of 11kW. The factor v^3 has been retained to emphasize its driving influence on the power requirement. Fractional improvements of perhaps 5 to 10% in all of the efficiency factors will only provide a 5 to 10% increase in speed capability.

It is evident that speed will be strictly limited by power system capacity. Unfortunately the precise capability required

depends on the nature of the high altitude winds. Wind velocities over continuous time periods of long duration are only approximately known for altitudes near 70,000 ft. Consequently we have chosen 30 knots as an approximation of what may be required for a practical system. To operate at this speed would require a continuous power consumption of the order of 10 kW.

2.2 Payload

A variety of scientific and military payloads may be considered for a powered aerostat. The purpose of this paper is not to make an exposition of these, but to consider the added requirement they would place on the power system. Within the limits of the few hundreds of pounds of payload that the baseline system might carry, it is unlikely that payload power requirements will exceed the kilowatt level on a continuous basis. This would represent a small increase in the total power system capability required.

2.3 Control and Telemetry

Very efficient and sophisticated control and telemetry units have been developed and used for both high altitude balloon operations and for remotely piloted vehicles. The power consumption of such systems is typically a fraction of a kilowatt. This would also represent a small addition to the propulsion power requirements.

It is evident that the power requirements of a powered aerostat will be largely determined by its propulsion needs. These needs will be determined by unpredictable wind conditions and must therefore be considered as a continuous requirement for a long term system. By comparison to the 10 kW required for propulsion, the 1 kW required for payload and control functions is of lesser concern.

3. REGENERATIVE FUEL CELL SYSTEM

3.1 System Outline

The regenerative fuel cell system is composed of four basic components, as shown in Figure 1, and associated controls and plumbing. The system operates around a hydrogen/oxygen fuel cell

which derives electrical energy from the conversion of those gaseous reactants into water. The water produced by the fuel cell reaction is pumped into an electrolysis chamber where the passage of an electrical current reconverts it to the gaseous state. Product gases are then held in high pressure storage until needed by the fuel cell. Electrical energy for operation of the electrolysis cell is obtained from a solar array distributed on the upper surface of the aerostat.

Each of these major components has been developed and is available in some form today, though not optimized for the aerostat power application. We have attempted to determine the capabilities of existing hardware and project the results of anticipated modifications and improvements to estimate the performance of future systems.

3.2 Fuel Cell

The basic element of the power system is a hydrogen/oxygen fuel cell of the type used in space programs. Information on several units is available. One particular unit in which we are interested is illustrated in Figure 2 and has the general characteristics listed in Table 1.

(General Electric, 1971).

Table 1. Fuel Cell Characteristics

Average Power Output per Module	5 kW
Maximum Power Output per Module	10 kW
Specific Reactant Consumption	0.8-0.9 lb/kWh
Specific Weight @ ave. output	25-30 lb/kW
Anticipated Cell Life	> 10,000 hrs.

This unit was developed for the space shuttle program. It therefore must meet very stringent safety and reliability requirements, and be capable of operating in the zero gravity space

environment. A relaxation of these requirements, appropriate for the unmanned aerostat in a less demanding environment, would result in appreciable weight savings. This would be primarily achieved by operating at a higher power density, which may result in slight increases in specific fuel consumption and a reduction in system life and reliability.

Systems designed expressly for aerostat use should achieve a 10 kW output with a specific weight of about 15 lb/kW and a specific fuel consumption of 0.8 lb/kWh in the not too distant future. Significant advances beyond this point will be difficult since operating efficiency will be approaching realistic limits and weight reductions would result in more fragile and more costly components. The size and power characteristics described above are for systems in the size range of several kW. Smaller units have been constructed with comparable efficiencies but with significantly higher specific weights. It will be difficult to obtain sub-kilowatt power levels in packages of less than 30 pounds.

3.3 Solar Array

The point of departure we have chosen for considering solar array technology is the FRUSA or Flexible Rolled-Up Solar Array (Felkel, 1972). This array development indicated that it was possible to place solar cells on a flexible plastic sheet with imbedded interconnections and achieve excellent reliability with very lightweight panels. A weight breakdown for individual cell parts is shown in Figure 3. For conditions in orbit the FRUSA array was capable of providing a power level of 52 W/lb. At that time advanced array systems utilizing lightweight cells were expected to produce 70 W/lb. Utilizing the FRUSA design without the protective glass cover slide, which may be unnecessary for terrestrial applications, would result in a power density of nearly 80 W/lb.

The FRUSA approach could possibly be stretched somewhat further but it is unlikely to exceed 100 W/lb through changes made to lighten existing components. Recent announcements of advances in solar array performance, through increased light conversion efficiency, indicate that the present 10 to 11% efficiency may be raised to 14 to 16% levels. Indeed there are some suggestions that the influx of new efforts and support in energy research may raise the efficiency to 20% over the next few years. In any event it is

not unreasonable to expect that the specific weights of 12-15 lb/kW available with existing technology will be reduced to 7-8 lb/kW in the future.

The life time of the solar array will be more than adequate. Mission durations extending to several years are already a reality for space systems powered by solar arrays.

While the specific weight of the solar array may be low it must be remembered that it will be the ultimate source of all power. Since power can be generated only during the daylight hours the size of the array will have to be approximately doubled to account for the power needed during night hours. The exact factor will depend on geographic location and time of year. Since all parts of the array cannot be oriented directly toward the sun at all times another factor of two must be included to account for the average sun angle. A minimal roll control system on the aerostat would provide this level of capability in sun alignment. Finally, the fuel cell/electrolysis cycle, water/H₂-O₂/water, is no more than 60% efficient. Thus, an additional expansion of the solar array must be made to account for this power loss. To generate power adequate for a 10 kW continuous level of consumption will require a total generating capacity of 53.4 kW. This level can be reduced somewhat by improving the fuel cell efficiency.

At a nominal generating capacity of 10 W/ft² (15 W/ft² in future systems) such an array would cover an area greater than 5000 square ft. The required array area will be reduced by improvements in both fuel cell and array efficiencies.

3.4 Electrolysis Unit

An electrolysis unit has been developed for space applications. This unit has an efficiency of better than 90% at all levels of operation. The space system is much heavier than that required for terrestrial applications as a result of the difficulty in maintaining contact between the water and the electrode surfaces in a zero-g environment. Present indications are that an electrolysis unit would have a specific weight of about 3 lb/kW. Output will have to be adjusted according to the length of day and night conditions.

The electrolysis process is inherently stable and self regulating. It is unaffected by pressure, produces very pure

reactants, and does not require sophisticated electrical power regulation equipment. The simplicity of the system would seem to indicate a capability for extended duration operations but we do not have good data on this point as yet.

3.5 Reactant Storage

To supply the fuel cell with reactant to produce 10 kW for 12 hours at a specific fuel consumption of 0.8 lb/kWh will require nearly 100 pounds of reactant, or roughly 11 pounds of H₂ and 88 pounds of O₂. At atmospheric pressure this would represent 2000 cubic ft of H₂ and 1000 cubic ft of O₂. Storage volume can be greatly reduced by increasing the storage pressure. This will not, in general, significantly increase the container weight.

A somewhat higher pressure is required to meet the nominal gas pressure of 50 psi for the fuel cell. Some recent developments in the fabrication of filament wound pressure vessels (Chiao, 1973) have greatly reduced the weight required for such storage. Converting the values for test bottles to more appropriate dimensions indicates a storage specific weight requirement of about 0.025 lb/ft³- atmosphere, after allowing an adequate safety factor. This would imply a storage weight requirement of 50 pounds for H₂ and 25 pounds for O₂, or a specific weight of 7.5 lbs/kW. Making full use of the available strength of these new materials would reduce the specific weight for reactant storage to about 5 lbs/kW. The availability of higher strength materials in the future is impossible to predict. Pressure vessel tests over hundreds of cycles, to a pressure equivalent to 75% of ultimate stress loading, indicate that storage chambers will have long life capability.

The electrolysis unit can generate gas, under pressure, directly into the storage chamber. Since the product water from the fuel cell is at a relatively low pressure, a boost pump will be required to introduce it into the electrolysis unit. The capacity required for this unit is only one gallon per hour, so this should be a relatively minor problem.

4. SYSTEM WEIGHTS, COSTS, AND ALTERNATIVES

4.1 Summary of Component Weights

We have estimated current and future specific weights for each of the major components of the regenerative fuel cell system. In addition to these items an allowance must be made for power conditioning, for interconnecting cables and plumbing, and for excess heat rejection. A propulsion system designed to accommodate the output characteristics of the fuel cell and solar array will minimize the power conditioning requirements. On this basis we would estimate power conditioning to require about 5 lbs/kW. The relatively high current levels between the solar array and electrolysis units will require heavy conductors. If the equipment can be kept approximately centrally located to major array sections the cabling requirements will be approximately 3 lb/kW. Plumbing requirements will be minimal since the electrolysis unit can be physically located adjacent to the fuel cell.

Heat rejection may require a liquid heat exchanger or may be accomplished by forced air cooling. A heat exchanger would be more efficient but is somewhat heavier and more complex. The principal cooling requirement will occur at night, when ambient temperatures are lowest, as the fuel cell generates approximately 2500 Btu/kWh of waste heat that must be dissipated. Some of this heat will be used to maintain the operating temperature of the fuel cell and surrounding equipment. The remainder will require a cooling system estimated at 4 lb/kW.

The present and future weight requirements estimated for all system components are summarized in Table 2. All of the component's specific weights will be relatively insensitive to system size with the exception of the fuel cell and electrolysis unit. These items would require about twice the single kW weight for a subkilowatt, low power unit.

Table 2. Summary of Component Weights for a 10 kW Regenerative Fuel Cell System

Component	Estimated Weight (lb/kW)		Future 10 kW System Weight (lbs)
	Current	Future	
Fuel Cell	35	15	150
Solar Array	13	8	430*
Electrolysis Unit	3	3	30
Reactant Storage	7.5	5	50
Reactants	10	10	100
Power Conditioning	5	5	50
Cabling	3	3	30
Heat Rejection	4	4	40
TOTAL SYSTEM WEIGHT			880

*Solar Array Weight Contains Required Factor of 5.34

Each of the components that make up the regenerative fuel cell system should have extremely long life capabilities. Thus it appears possible to contemplate a power system for high altitude use that will provide 10 kW of power, continuously, with less than 1000 pounds of total weight. It is not unreasonable to contemplate operating periods of a year or longer, and indeed, such periods are desirable to reduce the handling inherent in launch and recovery operations and to amortize the substantial investment that such a system will represent. It is obvious that a key element in achieving this low power system weight is the development of lightweight solar arrays for terrestrial use.

4.2 Estimated System Costs

In attempting to determine current costs and project future ones on an estimated basis, we have obtained a variety of opinions. The values given in Table 3 represent a distillation of those opinions into what we believe are reasonable estimates for each system component. As is apparent from the table the cost of the solar array is the dominant factor in the overall cost, even for the lowest of the range of costs estimated. This results in part from the additional factor of 5.34 that must be applied to the solar array size to provide an equivalent 10 kW constant power level.

If the powered aerostat becomes a 10,000 hour capability system, then the one to three million dollar cost of the power system is amortized at the rate of 100 to 300 dollars per hour. A significant portion of this cost, which by itself compares favorably to aircraft costs, may be recovered if the system components can withstand the long exposure to the high altitude environment and the disruptions inherent to recovery.

Table 3. Estimated Costs for a 10 kW Regenerative Fuel Cell System
(Costs in Thousands of Dollars)

Component	Estimated Cost Per kW	10 kW System Cost
Fuel Cell	20	200
Solar Array	10 - 15	534 - 2670
Electrolysis Unit	1	10
Reactant Storage	1	10
Reactants	-	-
Power Conditioning	5	50
Cabling	1	10
Heat Rejection	5	50
TOTAL		864 - 3,000

4.3 Effects of Variation in Day/Night Duration

The discussion, to this point, has assumed equivalent day and night periods. Under the worst case conditions, of the winter solstice in northern latitudes, the daylight period would be reduced to 9 hours. This would increase the multiplication factor for the solar array from 5.34 to 7.55 since more energy must be generated in a shorter period of time.

The required capacity of the fuel cell and heat rejection will be unchanged. However the quantity of reactant, reactant storage and electrolysis capacity would have to be increased. The first two will be increased by 25%. Electrolysis capacity must be increased by 67%. We will assume that changes in cabling and power conditioning will be minimal. Under the conditions of 9 hours daylight and 15 hours darkness the total future system weight would

rise from 880 to 1112 pounds. A similar increase in cost will also occur since much of the change concerns an increase in size for the solar array. For optimum conditions where daylight periods are longest the situation is obviously reversed. The point to be made is that such changes in operating conditions are matters of considerable concern to a system designer, particularly where the system may be aloft for a full year.

4.4 Effect of Energy Storage and Day/Night Speed Variation on System Design

The solar array is the dominant single item in both system weight and cost and particular attention should be given to optimum utilization of the power generated by it. We have conducted a brief study to minimize power system weight as a function of two variables, the power generation density (ρ_g in watts/lb) of the solar array and the energy storage density (ρ_s in w-hrs/lb) of the regenerative fuel cell or secondary battery system. Some of the basic results of this study are shown in Figures 4 and 5.

In Figure 4 we have estimated the weight/kW (W) for a constant output system just as we have done in this analysis. In this figure it can be seen that the slope of the weight curve is still relatively steep for ρ_s equal to 100 Wh/lb. This is about the maximum storage efficiency now foreseen for batteries if all packaging, power conditioning, and conversion inefficiencies are included in that rating. By contrast the regenerative fuel cell system provides an equivalent storage density of 200 Wh/lb even when all other components and its own inefficiencies are charged against it.

The storage of energy has a certain weight penalty associated with it. This implies some advantage to using all of the energy immediately for propulsion as it is generated. The penalty for this increases according to the cube of the velocity, hence there must be an optimum division for utilizing some energy immediately and storing the remainder. This will require that the vehicle travel more slowly at night than during the day.

The calculation is relatively simple and the results are shown in Figure 5 for the same two parameters ρ_g and ρ_s . The upper curves show the optimum day/night speed ratio (R_{DN}) necessary to obtain motion equivalent to the constant speed (constant power) system,

while the lower curves shows the system weight (W_0) required for the equivalent optimum power output. Comparing these two figures reveals that substantial power system weight reduction can be obtained if one is willing to go much slower at night than during the day. This is particularly true for a less efficient storage system than the regenerative fuel cell. The analysis also shows that the size of the solar array is not greatly affected by variations in the power profile.

5. SUMMARY

The regenerative fuel cell system offers a significant improvement over secondary batteries for long duration, high-altitude power requirements. Considering the likely course of current developments, it should soon be possible to construct such a system that would provide a continuous power output of 10 kW with a total system weight of less than 1000 pounds. The expected lifetime of such a system will be many thousands of hours. This combination of low weight and long duration makes the regenerative fuel cell a desirable choice for powered aerostat use.

Even the relatively high cost of the regenerative fuel cell appears to be acceptable when long mission durations are required. In fact, to meet such requirements, it, or a secondary battery system, may be the only alternatives. An equivalent Wankel engine, using consumable fuel to generate 10 shaft horsepower, would not last long even if it could be made to run at high altitudes. With a specific fuel consumption of 0.3 lb/shp-hr the fuel would be exhausted in less than 10 days.

Low power units, in the 1 kW range, would be less efficient on a weight basis than larger ones. Performance levels and lifetimes may still compare favorably with secondary battery systems.

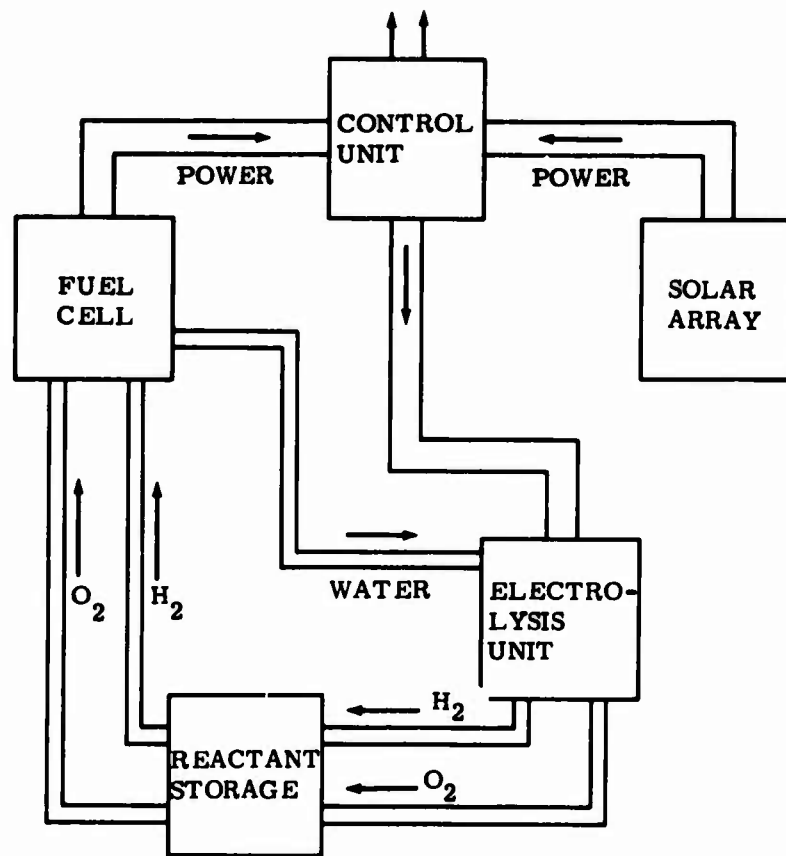


Figure 1. Regenerative Fuel Cell System Block Diagram

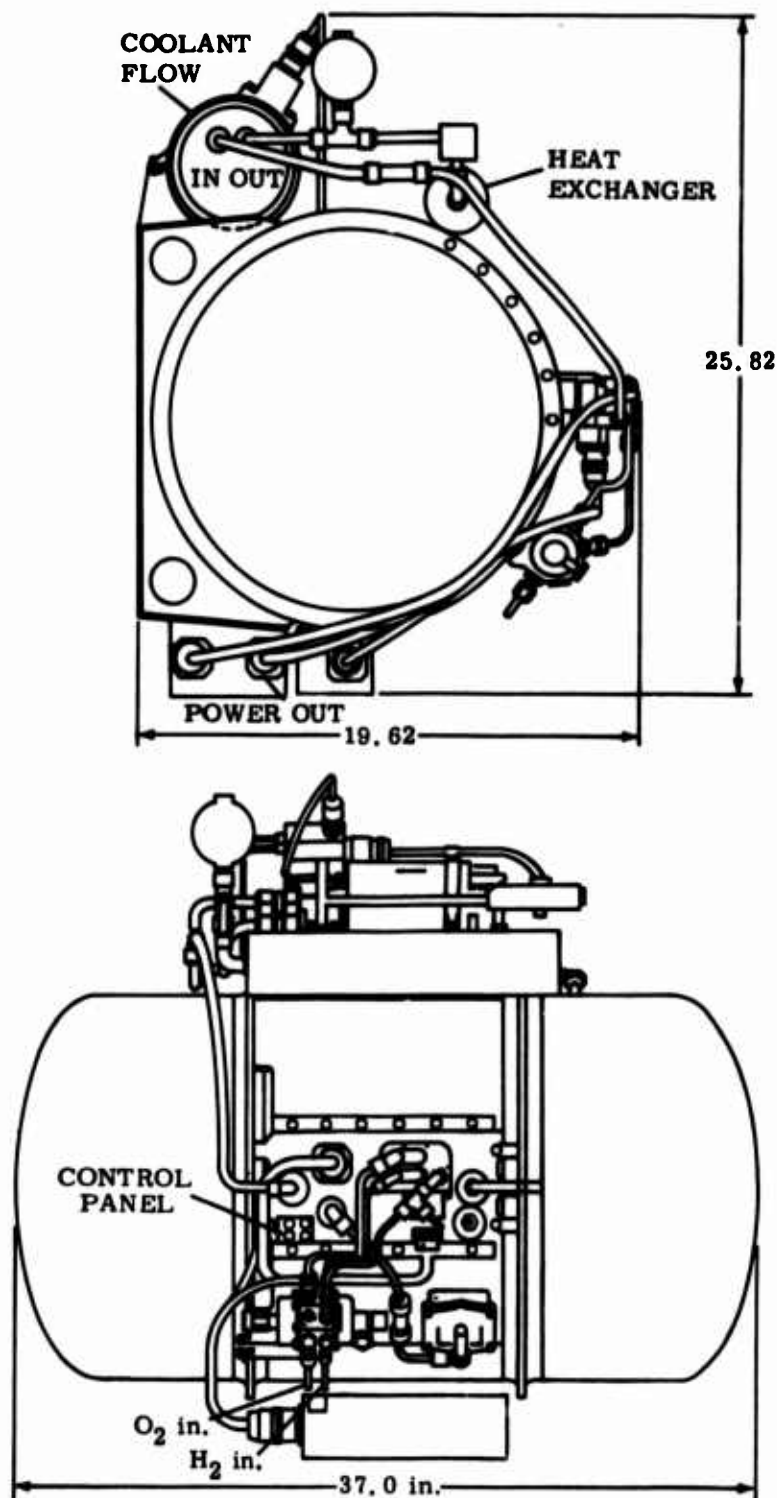
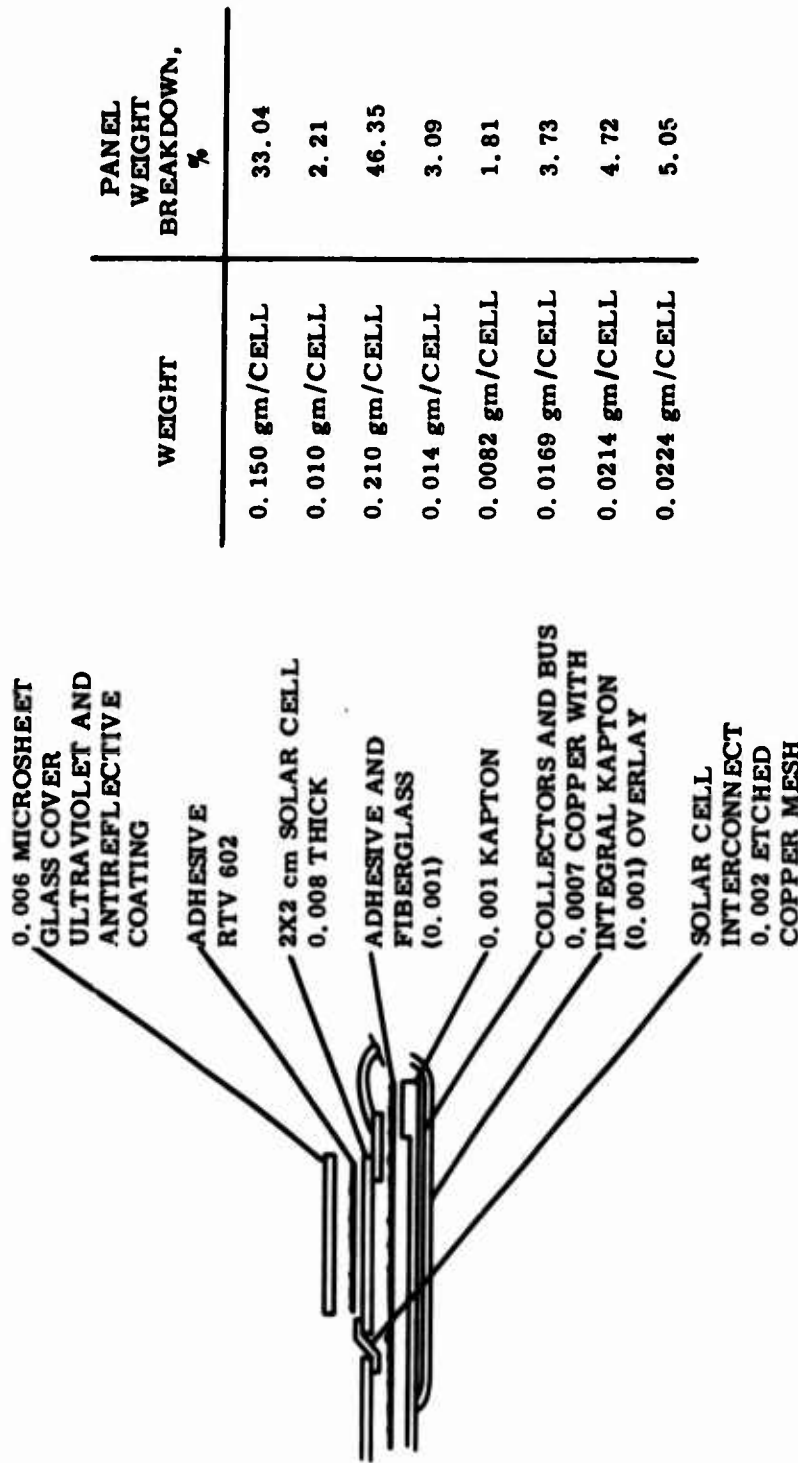


Figure 2. General Electric Fuel Cell Module



WEIGHT	PANEL WEIGHT BREAKDOWN, %
0.150 gm/CELL	33.04
0.010 gm/CELL	2.21
0.210 gm/CELL	46.35
0.014 gm/CELL	3.09
0.0082 gm/CELL	1.81
0.0169 gm/CELL	3.73
0.0214 gm/CELL	4.72
0.0224 gm/CELL	5.05

Figure 3. Solar Array Panel Configuration and Weight Breakdown

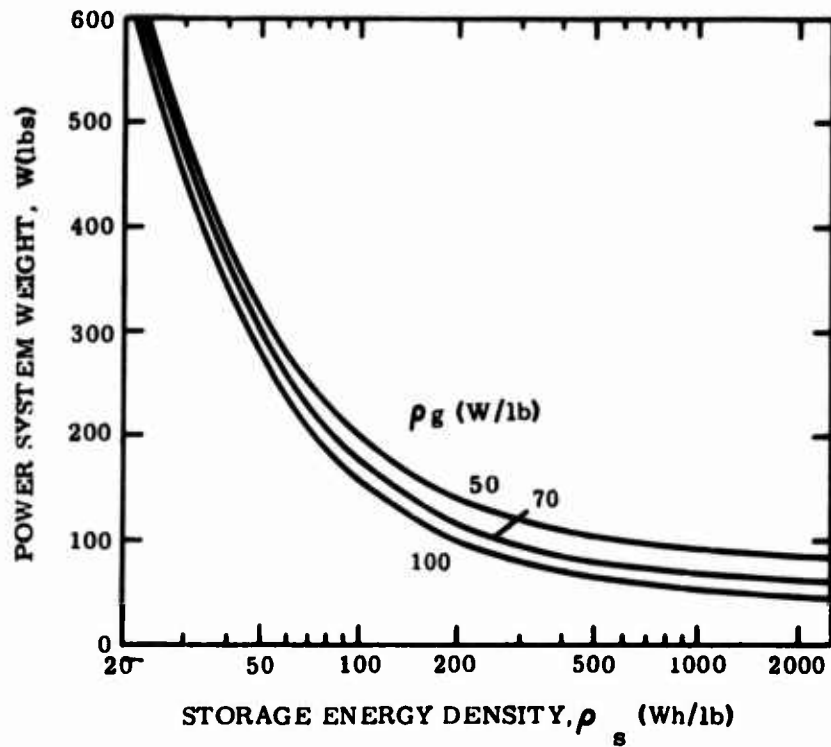


Figure 4. Power System Weight for a Constant Power Level of 1 kW

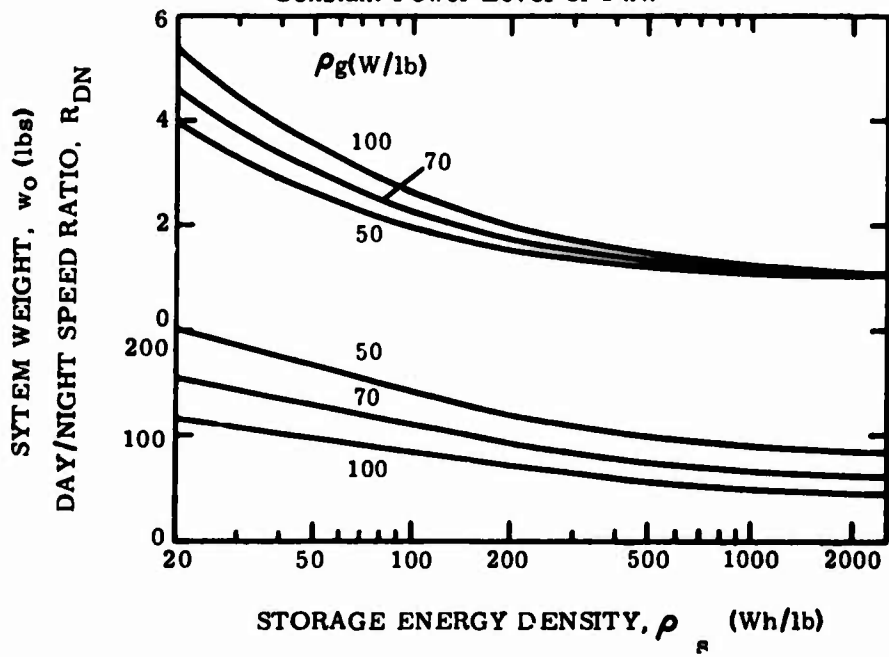


Figure 5. Power System Weight for an Optimized Effective Power Level of 1 kW and Day/Night Speed Ratio

References

- Chiao, T. T. et al (1973) Filament Wound Kevlar 49/Epoxy Pressure Vessels, UCRL 51466, Contract NASA C-13980-C, University of California, Livermore
- Felkel, E. D., Wolff, G. et al. (1972) Flexible Rolled-Up Solar Array, AFAPL-TR-72-61, Contract F 33615-68-C-1676, Project B/682J, Hughes Aircraft Co.
- General Electric (1971) Fuel Cell Technology Program, GE SPR-044, Final Report, Contract NAS 9-11033, General Electric

Contents

1. Introduction
2. Design Parameters
3. Discussion
4. Conclusions

The Influence of Fineness Ratio on Powered Ellipsoidal Balloon Weight and Other Characteristics

Norman J. Meyer
NASA Headquarters
Washington, D.C.

Abstract

The choice of fineness ratio influences the weight, drag, and stability of powered balloons. These are examined, using airship design theory, to determine the relationships. It is concluded that the major effect of increasing fineness ratios is an increase in overall weight of the vehicle.

1. INTRODUCTION

In recent years, several programs have been suggested or initiated for use of high altitude station keeping balloons in scientific or military missions. Such missions dictate utilization of some means of propulsion to maintain or achieve station over a designated geographic location. Power requirements must be minimized for efficiency and therefore balloon shapes of streamlined form are dictated. Although power and speed requirements may be low, these balloon systems become, for purposes of engineering and design,

dirigibles. Therefore, much of the aerodynamic and structural principles developed for dirigibles, and particularly for non-rigid airships, can be applied.

Investigators have found it convenient to use ellipsoids (ellipses rotated about their major axes) to represent airship envelope or hull forms. Most forms are, in reality, combinations of ellipsoids or mathematical derivations of same. When this is done, the geometric characteristics such as volume and surface area are easily calculable. Also, the form expression may be entered into various other analyses such as drag, stability, and dynamics equations.

The final index of efficiency for any airship is the total or gross weight required to perform a given mission. Various parameters must be considered in design which influence this weight.

The selection of a suitable proportion of length to maximum diameter (fineness ratio) is one of the important steps which must be taken. Fortunately, this was a subject which occupied a substantial portion of research activity during the 1920's and 30's in connection with determination of minimum aerodynamic drag for airplane fuselages and airships, and many references exist from this period which remain valid today.

Drag, however, is not the only parameter which must be considered in the choice of fineness ratio for airships. While this paper does not purport to be an exhaustive treatment of the subject, it does examine several of the more important parameters to determine their relationship and influence on the choice of fineness ratio and the net effect on weight.

2 DESIGN PARAMETERS

The weight of an airship or powered balloon includes the total propulsion system including fuel (or batteries) necessary to balance the drag forces produced at any selected velocity. This drag is produced by the hull or envelope and by various appendages. The hull drag is a function of its shape. The appendages must also be shaped to produce minimum drag, but a major factor here is the overall size of such components as determined by the dimensions required to provide the function (such as stability).

In this section, two of the major components (hull and fins) are examined to determine their characteristics as influenced by

fineness ratio.

2.1 Hull Drag

The total drag (D) of a streamlined body of revolution in an airstream can be regarded as consisting of a form or pressure drag (D_p) and a frictional drag (D_f). Early aerodynamic studies by Zahn, Munk, VonKarman, Jones, and others (1916-1929), established that the primary source of drag is frictional for bodies whose fineness ratio is greater than 1.0. The relationship between d , D_p and D_f can be expressed by the equation: $\frac{D}{D_f} = A$ where A is the longitudinal inertia coefficient and is equivalent to $1 + k_1$.

Values of k_1 have been derived for equivalent ellipsoids and can be found in various references. For fineness ratios above 3.0, k_1 is < 0.1 . The results of tests, including many conducted by Abbott (1931) led to the conclusion that minimum drag can be obtained in the ranges of fineness ratios (n) from 4 to 8. Other sources such as Upson and Klikoff (1931) would allow a value of as low as 3.0. Indeed, one airship was actually built using a ratio of 2.8, the choice being based on wind tunnel tests which indicated lowest drag at this value. Upson (1926).

An expression for total drag, developed by Upson and Klikoff (1931) is:

$$D = \frac{A^{2.775} n^{1.158} (n+2)^{0.925} VOL^{0.617} v^{1.85}}{22000 (n+1)^{1.85}} \quad (1)$$

Where VOL is the total volume of the hull or envelope and v is the velocity in the direction of the major axis.

A simplified version of this expression is:

$$D = C_D VOL^{0.617} v^{1.85} \quad (2)$$

Values of C_D are dependent on A and n and are plotted against n in figure 1. The dotted curve is an average of NACA wind tunnel test values (Abbott, 1931). It can be noted that these show a shift to the higher values of n .

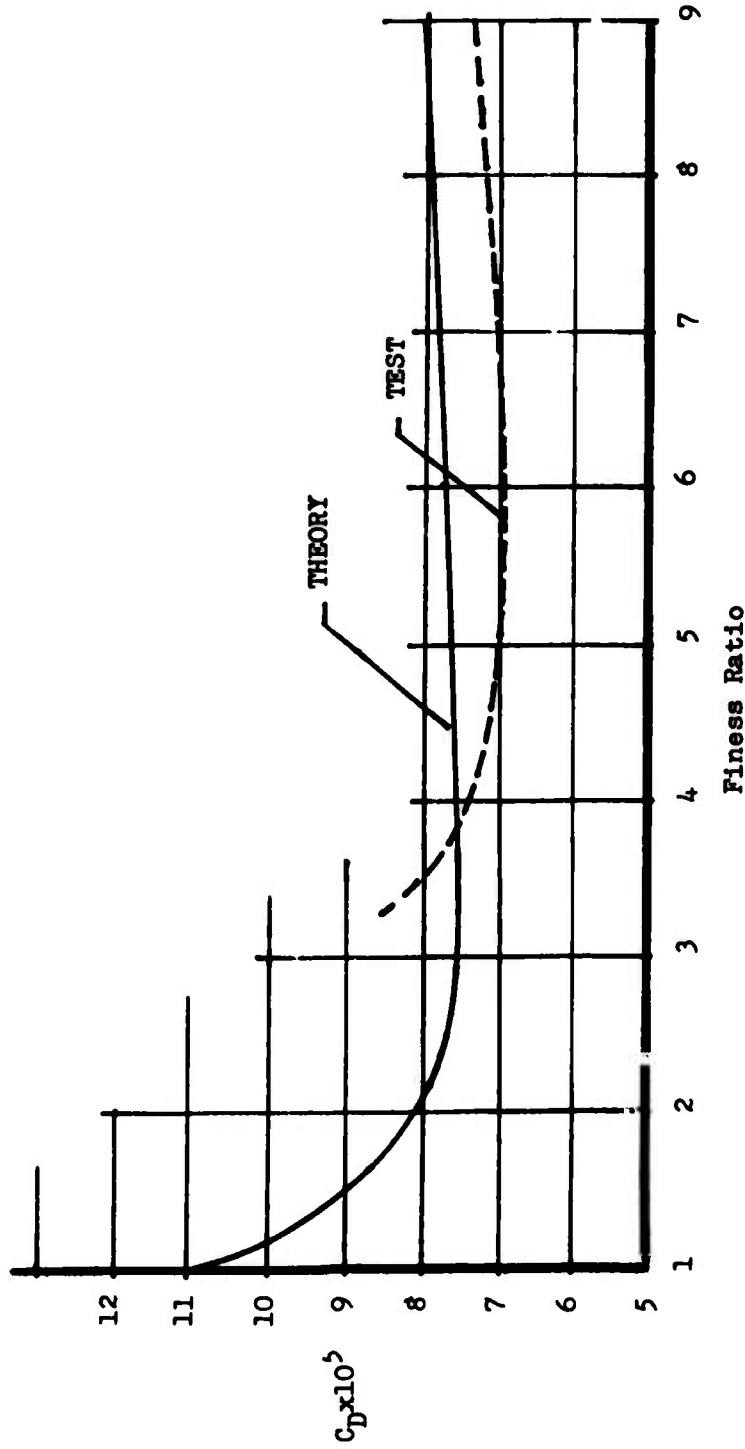


Figure 1 Plot of Total Drag Coefficient vs. Fineness Ratio

All wind tunnel tests performed with models of airship hulls suffer from the common deficiency of low Reynold's number. Reynolds numbers for scale models tested by Abbott in the NACA variable density tunnel (1931) reached maximum values of 4×10^7 . Even small Goodyear type blimps operate at Reynold's numbers of twice this value at maximum speeds. Investigators have concluded that for large airships the flow in the boundary layer is entirely turbulent, whereas wind tunnel tests were conducted in the ranges where the flow is partially laminar and partially turbulent. Before this was fully appreciated, there were a number of erroneous conclusions drawn by experimentors and designers regarding merits of particular hull shapes.

Subsequent tests of body forms of various fullness (cylindric coefficients) (Abbott, 1937) revealed that form drag was sensitive to the curvature aft of the maximum section. Upson (1931) concluded that this factor was difficult to control for values of n under 4.0.

The body of knowledge on drag of various shapes of ellipsoidal form is now reasonably extensive. Much of this data can be applied (with proper corrections) to contemporary designs. The effects of features which would alter aerodynamic characteristics in a major manner (boundary layer, control, stern propellers, new empennage forms, etc.) would require additional testing.

2.2 Stability and Control

The stability of a dirigible is dependent upon the pitching and yawing characteristics of the hull and its appendages and the effectiveness of the fins or stabilizing system. Pitch stability is not usually a problem - particularly for low speed flight since the static moment due to metacentric height usually adds a substantial increment to that produced by the tail.

Stability in yaw is a different problem. It can either be diminished or amplified by various appendages such as control cars, payload packages, and other external items. Ellipsoidal hull shapes are not inherently stable. Wind tunnel tests and theory both show that the instability tends to increase slightly with finess ratio. Hulls, which have been elongated by insertion of parallel middle body, particularly show poor force distribution and produce higher pitching or yawing moments at small angles of deviation. (Upson and Klikoff, 1931).

All ellipsoidal bodies, therefore, must have stabilizing fins of some kind added to the stern. Criteria for evaluating stability have been developed by various investigators and organizations. Upson and Klikoff developed a criteria which utilizes a simple wind tunnel test to determine rotary derivatives. Burgess (1938) has modified this to develop a stability criterion as follows:

$$\frac{(B-A) - \frac{1}{2} (d C_m / d\alpha)}{(A/B) (B-A)} \geq 1.0 \quad (\text{Criterion (1)}) \quad (3)$$

where: $B = 1 + k_2$

$A = 1 + k_1$

k_1 and k_2 are additional inertia coefficients

for ellipsoids

$d C_m / d\alpha$ = rotary derivative as determined in wind tunnel

Another criteria, using a more detailed approach to obtain the rotary derivatives, has been applied to design of non-rigid airships by Liebert and Eager (1951).

$$S.C \#2 = -1 \left\{ m' + \left[\frac{n'm'' - m'n''}{2A} \right] \right\} \geq 0 \quad (\text{Criterion (2)})(4)$$

where m' = total static yawing moment derivative

n' = total static side force derivative

m'' = total rotary yawing moment derivative

n'' = total rotary side force derivative

Both criteria require wind tunnel tests or other experimental apparatus to determine $\frac{dm}{d\alpha}$ values. Both criteria also indicate a degree of stability by virtue of the range of values it is possible to achieve. Values near or at 1.0 for S.C. #1 indicate marginal stability and values near 1.1 indicate positive stability. Likewise, for S.C. #2, values near or at 0.1 are not as satisfactory as values approaching 0.4.

Table 1 shows a comparison of a variety of airships for directional stability using both criteria.

TABLE 1. COMPARISON OF STABILITY FOR VARIOUS AIRSHIPS

<u>Airship</u>	<u>Total Vert. Fin Area(S)</u>	<u>VOL^{2/3}</u>	<u>$\frac{S}{VOL^{2/3}}$</u>	<u>n</u>	<u>Crit.(1)</u>	<u>Crit.(2)</u>
ZRS-4&5	7200	37,974	.19	5.9	1.09	.38
ZPG-1	1516	9,150	.17	4.4	1.03	.34
ZSG-2	815	5,924	.14	4.3	1.00	.11
ZMC-2	342	3,419	.10	2.8	1.01	.09

It can be seen that although larger values are indicated for airships of larger fineness ratios, the ratio of total fin area (vertical fins and rudders) to $VOL^{2/3}$ also increased. A better comparison can be shown between the ZRS - 4&5 and the ZPG-2. If an equivalent ratio of fin area to $VOL^{2/3}$ had been used for the ZRS-4&5 airships, their stability criteria value would have been approximately equal to the ZPG-2.

As a matter of interest, the ZMC-2 was marginally stable at low angles of yaw and unstable at higher angles.

2.3 Maneuverability

The same factors which favor stability auger against maneuverability. If a highly maneuverable vehicle is required, the designer could select a combination of characteristics which would produce the desired results. These would be:

- Large control surfaces
- Small stabilizing fins
- Low aspect ratio

The last item is suggested on the basis that the transverse inertial coefficients for lower ranges of fineness ratio are less. Once acceptable stability and controllability is indicated, the efficiency of any design must be determined by the total fin and control surface area compared to some normalizing base such as $volume^{2/3}$ as used above. The weight of the empennage is subject to the designer's talents to some extent.

It can be concluded that fineness ratio has little influence on stability and that stability can be achieved with equal efficiency on hulls of low values of n as well as the higher values particularly

for the range between 4 and 6.

2.4 Envelope Weight

The weight of an envelope is a function of its strength and its surface area. Burgess (1937) calculated the surface area (S_e) for ellipsoidal envelopes vs. finess ratio by normalizing against a sphere of equal volume, based on the expression:
 $S = C_n \sqrt{\text{VOL}} (L)$ where C_n is a coefficient depending on finess ratio and L is the overall length. Values of S_e/S_s are plotted against n in Figure 2. As is expected, the surface area increases with finess ratio but the change is not great unless large differences in finess ratio are compared.

The envelope must function as a beam with sufficient strength to resist bending moments resulting from various static and aerodynamic loads. The strength is derived from internal pressure, which in turn causes stress in the envelope fabric. The level of stress determines the weight of material that must be used for construction.

A relationship between bending moments and the internal pressure was determined by Burgess (1933) as a limiting value for the bending moment coefficient (C_m) in the expression:

$M = C_m q \text{VOL}^{2/3} L$ (where q is aerodynamic pressure) as:

$$C_m = C_1/n^{5/3} \quad (5)$$

Values of C_1 can be calculated to give constant values of C_m . A value of .018 gives the various values of C_1 shown in Table 2. The value of C_1 is equivalent to the increase of pressure required for equal bending strength. Since p has a linear relationship with stress and tension, C_1 also becomes an index of the increase in envelope fabric strength required under the same flight conditions.

The last column shows this proportion normalized for a value of $n = 4$. This illustrates the penalty of higher finess ratio values on required strength. A change between $n = 4$ to $n = 6$ almost doubles the strength required to carry the moments. If this is taken in proportion to stress caused by normal pressure loads, a 50% increase in envelope weight is indicated.

TABLE 2. PRESSURE INCREASE REQUIRED FOR EQUIVALENT BENDING STRENGTH

<u>n</u>	<u>C₁</u>	<u>C₁/₄C_{1n}</u>
2	.057	0.31
3	.112	0.62
4	.181	1.00
5	.263	1.45
6	.357	1.97
7	.461	2.55
8	.576	3.17

3. DISCUSSION

The three parameters reviewed herein represent important ones which influence the selection of finess ratios for conventional dirigibles.

The designer may choose to interpret wind tunnel data as inconclusive in the range of $n = 4 - 6$, and perhaps choose a higher value of n for minimum drag. Likewise, particular combinations of empennage design and envelope shape may indicate higher values of n are favored for satisfactory stability. However, both these choices must be made knowing that an increase in envelope weight will result, and must be offset by the gains produced by, perhaps, lower weight propulsion or lower weight empennage. This is fairly well demonstrated by most of the naval non-rigid airships which generally used ratios of about 4.25 - 4.5.

Particular designs for special missions would have to be checked carefully considering the large sensitivity of weight to finess ratio. Other considerations might require either higher or lower values of n than the general case indicates. One such consideration would involve the sensitivity of a particular vehicle to pressure changes and consequently wrinkling during flight. Naturally, superpressure should not be greater than absolutely required to meet the flight condition. If a superpressure design is chosen (no ballonets), a very careful analysis of the conditions of density and temperature should be made to determine the lowest practical maximum pressure required. With this determined, the balloon may experience, in flight, conditions where the envelope is operating at near zero tension. This condition combined with atmospheric disturbances could cause bending or wrinkling and hence

a drag increase. Shapes of low finess ratios are less sensitive to moment and load changes.

If a propeller is located on the major axis of the envelope, such propeller should be designed to operate most efficiently in accelerating the frictional wake. This concept would favor envelope shapes with higher values of D_f which are characteristic of hulls with higher values of n . Unfortunately, the weight concentration at the stern produces high static (and dynamic, if vectored thrust is used) bending moments which are better handled by hulls of low values of n . Such designs would indeed demand a careful trade-off analysis.

A final note on Reynold's number effects is in order. Values of Reynold's number are dependent on density. At high altitudes, e.a. 70,000 ft., the Reynold's number would be approximately $.06 RN_{sl}$, and could be within actual wind tunnel test number ranges. If this is the case, wind tunnel data might be applied more directly to compute drag.

4. CONCLUSIONS

In conclusion, the following points can be made:

1. Drag of ellipsoidal envelope shapes is approximately constant over a range of finess ratios between 4 - 6.
2. Stability can be achieved with equivalent fin areas for envelopes of low finess ratios provided streamline flow can be maintained and fins are fully effective under all flight conditions.
3. Good maneuverability can be achieved at low values of finess ratio provided the surfaces are fully effective under all flight conditions.
4. Envelope weight is greatly reduced by favoring low finess ratios.

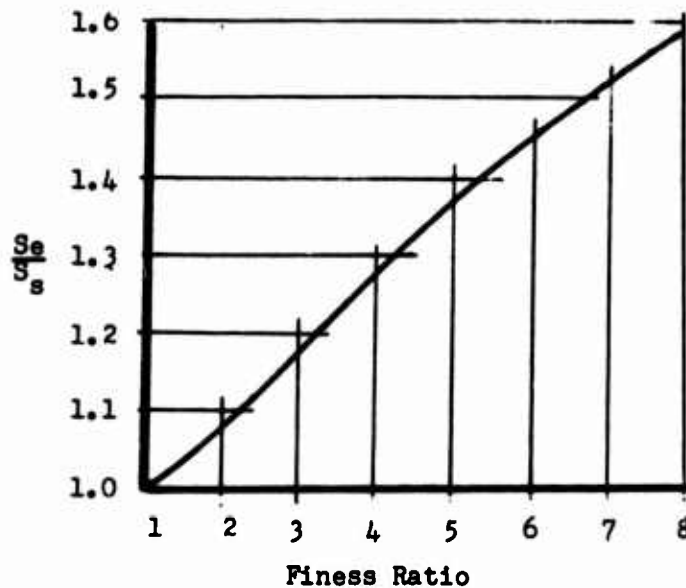


Figure 2 Surface Area Increase with Finesse Ratio

References

- Abbott, I.H. (1931) Airship Model Tests in the Variable Density Tunnel, NACA TR 394 (1937) Fuselage Drag Tests in the Variable Density Wind Tunnel; Streamline Bodies of Revolution, Finesse Ratio of 5, NACA TN 614
- Burgess, C.P. (1937) The Surface Area of Ellipsoids, Design Memorandum No. 276 (1933), Comparative Bending Strength and Weight of Structural and Pressure Airships, Design Memorandum No. 142 (1938) A Criterion for the Dynamic Stability of Airships, Design Memorandum No. 300
- Jones, R. (1925) The Distribution of Normal Pressures in a Prolate Spheroid, R&M No. 1061 British A.R.C.
- Liebert, H.R., Eager, R. (1951) Aerodynamic Analysis of the Dynamic Stability and Lateral Maneuverability Characteristics of the ZPN Airship
- Munk, M.M. (1929) Fundamentals of Fluid Dynamics for Aircraft Designers, Ronald Press (1924) Note on the Pressure Distribution over the Hull of Elongated Airships with Circular Cross Section, NACA TN 192
- Upson, R.H., Klikoff, W.A. (1931) Application of Practical Hydrodynamics to Airship Design, NACA TR 405 (1926) Metalclad Rigid Airship Development SAE Journal, Feb.
- VonKarman, T.H. (1924) Calculation of Pressure Distribution in Airship Hulls, NACA TM 574

Session 2
Tethered Balloons

Richard S. Cesaro, Chairman
TCOM Corporation

Technology Update On Tethered Aerostat Materials Developments

**Larry B. Keen
Sheldahl, Inc.
Northfield, Minnesota**

Abstract

Tethered aerostat systems of today are complex flexible structures that must operate under extreme environmental conditions and in winds of at least 70 knots. Aerostat life times of ten years are expected while twenty years are desired under continuous around-the-clock operation in worldwide weather conditions. Lighter weight vehicles are needed to increase payload capacity. These requirements are placing new demands on the materials engineer to develop materials and materials technology to meet the needs of today. This paper deals primarily with aerostat hull materials. Recent history, the state of the art, and advanced material concepts are covered. In addition, Sheldahl's qualification test program is discussed, including several previously unreported innovations in aerostat material testing.

1. INTRODUCTION

Sheldahl, since early 1967, has been actively involved in the development of large aerodynamically shaped tethered aerostat systems. The result of this concentrated development activity is represented by the Sheldahl CBV-250A Tethered Aerostat vehicle illustrated in Figure 1. This vehicle, used in the TCOM Corporation's telecommunications system, has successfully undergone qualification and operational testing for the past 18 months and has demonstrated the capability to support 4000 pounds of electronics at 10,000 feet to allow continuous, around-the-clock commercial broadcasting.

The realization of an operational all-weather, tethered aerostat vehicle was the result of advances made in various technical disciplines. Perhaps the most important work, and the focus of this paper, was the development of improved materials and materials test methods and equipment which led to significant enhancement of the performance capability of the aerostat. Materials, as used herein, refers to the *flexible* materials used in the construction of the envelope, empennage, and ballonnet.

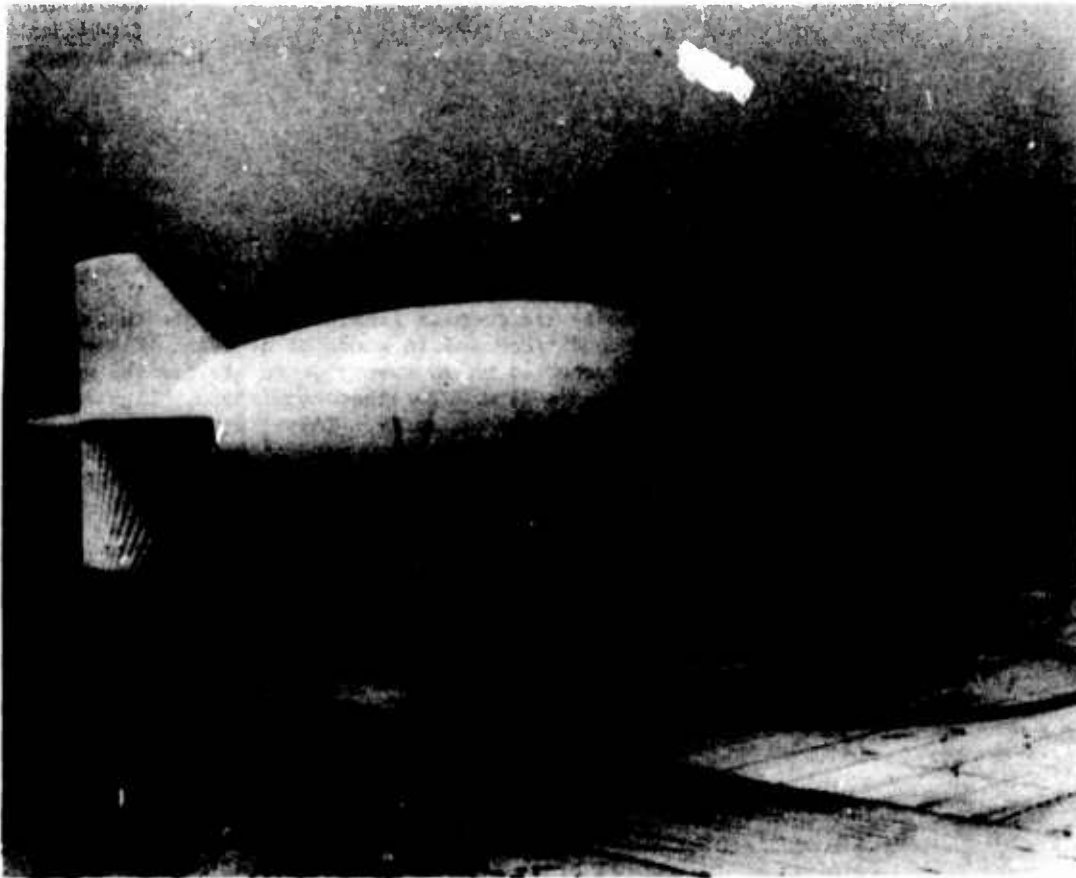


Figure 1. Sheldahl's CBV-250A Aerostat

The best way to illustrate the significance and the benefits of the materials development work is as follows. The CBV-250A vehicle hull is constructed from a material weighing 7.8 ounces per square yard, with a rated tensile strength of 225 pounds per inch. The best material available in 1967 weighed 12.9 ounces per square yard, and had a tensile strength of 195 pounds per inch. Thus, we see a 40-percent reduction in material weight and at the same time, a 30 pound per inch increase in strength. In terms of payload, the CBV-250A aerostat can carry an additional 1000 pounds as a result of these improvements. Already, the new materials have demonstrated a maintenance-free operation of 18 months, and laboratory test results give confidence for 20-year life expectancies.

Although major improvements in aerostat materials technology have been made over the past seven years, there are exciting new materials at Sheldahl currently undergoing development. For example, Sheldahl, under contract to NASA, Langley Research Center, has been investigating the new DuPont KEVLAR cloth. Potential hull materials using KEVLAR cloth show significant improvements in strength-to-weight ratios.

It is the purpose of this paper to summarize the results of Sheldahl's materials development work over this seven-year period. Although material test data and material descriptions will be presented as they relate to the CBV-250A vehicle, the emphasis of the report is the definition of material performance requirements, including the new methodology and test equipment used to measure material properties for materials selection and qualification.

2. MATERIALS REQUIREMENTS

Each material in Sheldahl's CBV-250A aerostat, from the hull and ballonnet materials to the seal tapes and T-tapes, is tailored to its specific task. The requirements for each material differ, of course, but the design approach is the same for all materials: (1) define material requirements; and (2) perform qualification tests on the candidate material. For the sake of brevity, only the hull material requirements and testing will be spotlighted in detail.

The hull envelope for a nonrigid aerostat must possess high strength-to-weight and low permeability. Depending on anticipated hazards, it may be essential that the envelope resists the attacks of weather or that repeated handling not degrade other required properties. Minor damage should not lead to catastrophic failure. The cost of the hull envelope, although secondary to most other requirements, must remain within reason. Lastly, a material is viable only if seaming and repair techniques are available to weld panels into a continuum that possesses all essential envelope characteristics. These requirements are illustrated in Figure 2. No monolithic material satisfies all requirements. A composite of materials, either a coated fabric or a laminate is needed.

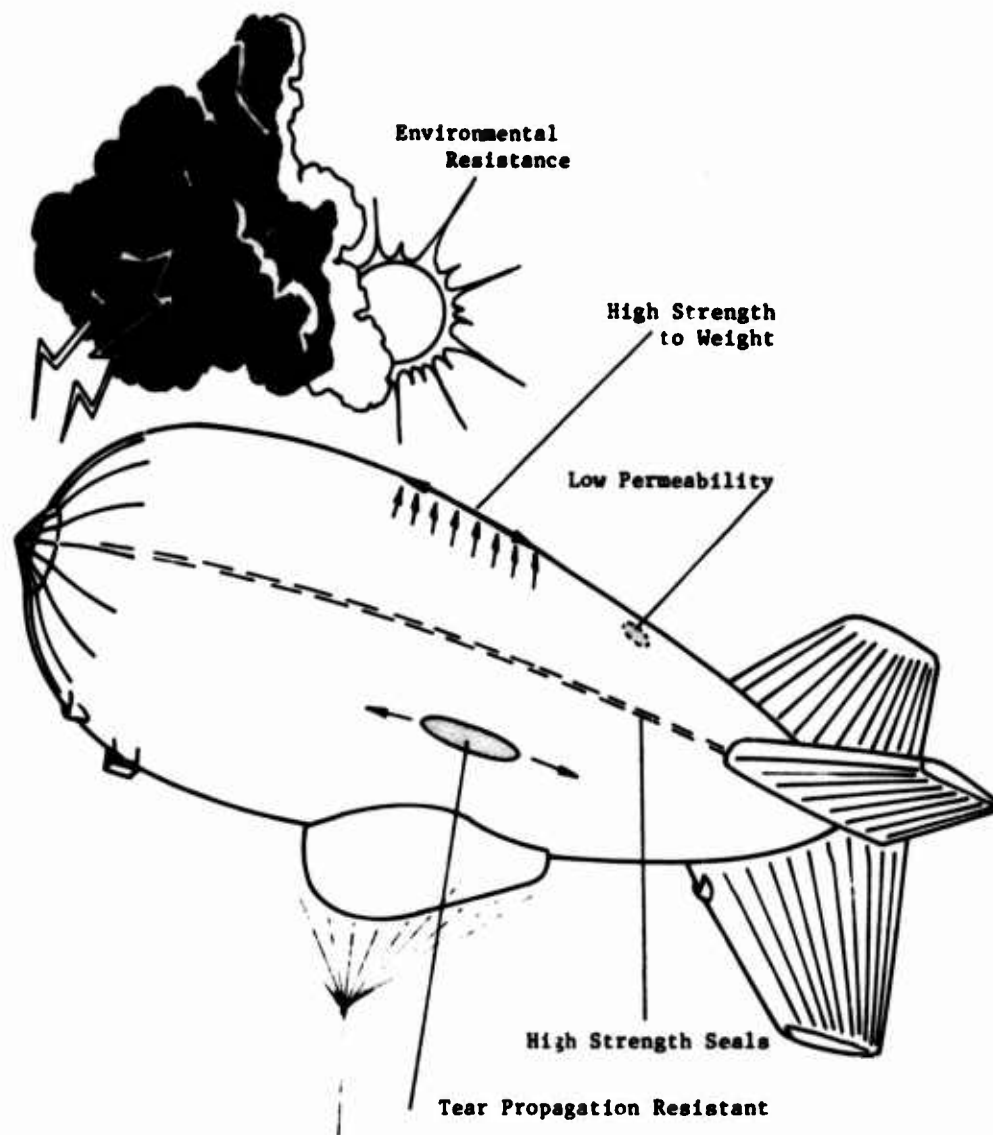


Figure 2. Hull Envelope Requirements

2.1 Strength Requirements

2.1.1 TENSILE

A thorough review of climatic conditions at potential deployment sites around the world, plus computerized structural analysis of the hull, have led to the basic CBV-250A strength requirement--a safety factor of two (2) in a 70-knot wind at 120°F. The computer analysis, defined technically as a large deflection, finite element

approach, provides a detailed picture of stresses over the entire hull as shown in Figure 3. Concentrated loads, such as those at suspension patches, are accounted for along with the overall stresses resulting from pressurization. The two most important results of this analysis are the hull biaxial stress and shear stiffness requirements. At flight placard extremes--70-knot winds, a high angle of attack, etc.--the maximum hull skin stress is found to be 70 pounds per inch in the hoop direction. Applying the safety factor of two (2) results in a static load requirement of 140 pounds per inch at 120°F. A material is considered acceptable if these conditions can be maintained for two (2) weeks without a failure.

2.1.2 SHEAR

Shear stress in the hull envelope is found to be highest near load concentrations. The portions of the hull adjacent to nose beams are typical high shear stress areas. Shear stiffness must be adequate to prevent large envelope distortions and buckling in these areas. For the CBV-250A, a minimum shear modulus (modulus = stress/strain) of 200 pounds per inch is required.

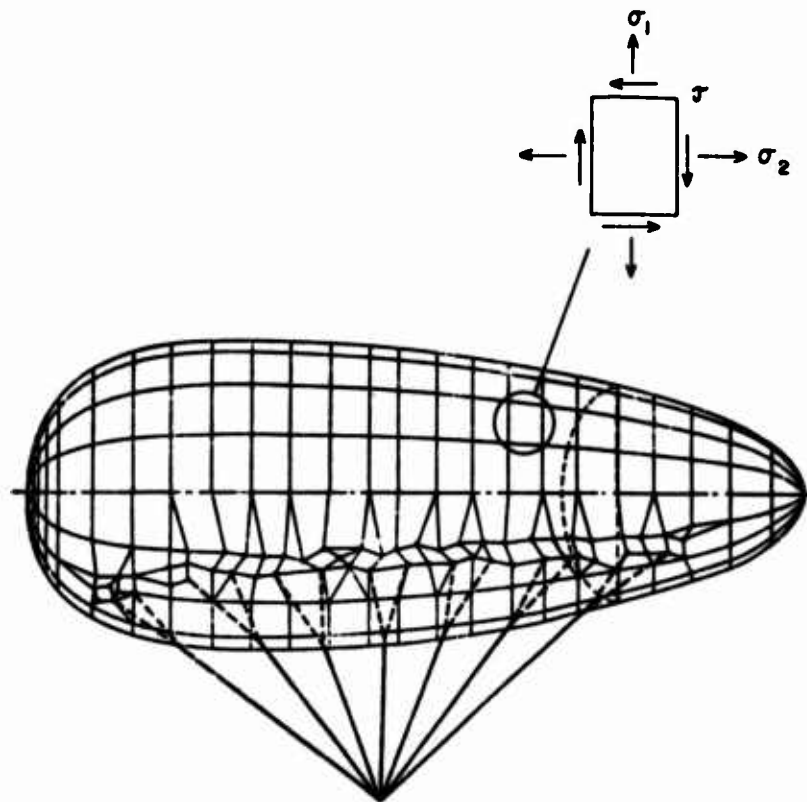


Figure 3. Finite element Analytical Model of the CBV-250A Hull

2.1.3 TEAR

Handling procedures for large aerostats are adequate to eliminate tearing as a hazard to an uninflated vehicle. This is especially true in view of the high tongue tear requirement of 60 pounds for a CBV-250A aerostat. However, the real tear hazard for aerostats is spontaneous tear propagation, initiated by minor damage to an inflated vehicle. A realistic requirement is that minor damage, defined as having a maximum dimension of one (1) inch or less, should not lead to catastrophic failure.

2.1.4 PLY ADHESION

Another strength requirement is inter-ply or coating adhesion. This quantity is generally measured in terms of the force required to peel one layer from another. A minimum required peel value is typically 8 pounds per inch. However, where two structural materials are bonded together, such as in a bias-ply fabric, higher values may be required. Where thin films are employed, plies may become physically inseparable at lower values.

2.1.5 FLEX LIFE

Aerostats are handled repeatedly, folded and unfolded, during manufacture and deployment. The envelope material must be capable of surviving hundreds of crease cycles.

2.2 Permeability Requirements

Permeability characteristics of the aerostat envelope are no less important than the strength requirements. The ratio of surface area to volume is high in a 250,000 cubic foot aerostat--about 11 cubic feet per square foot. Add to this the need for long duration flights plus low cost operation and the result is that low helium permeability has become a major design requirement for the CBV-250A. The present requirement is 0.5 liter per square meter per 24 hours, maximum, for virgin hull material.

2.3 Environmental Resistance

"Environment" is here defined as all forces acting to degrade the envelope fabric, including the necessary handling involved in the aerostat manufacturing and deployment operations. The aerostat environment can often be simulated or even accelerated. These simulations will be referred to as "conditioning".

The conditioning procedures employed by Sheldahl include high and low temperature exposure, handling simulations, water immersion, weather aging, and biaxial stress cycling. For design purposes, a material should be judged primarily on its post-conditioning performance. Sheldahl's environmental goal is a 20-year lifetime.

24 Seams

The strength, permeability, and environmental resistance requirements discussed above apply as much to seams as to the envelope material itself. Seams have the very difficult job of providing panel-to-panel continuity for all required envelope characteristics without introducing deficiencies such as excessive stiffness. Also, aerostat economics are highly dependent on efficient seaming techniques.

3. MATERIAL QUALIFICATION TEST PROGRAM

Standard aerostat material tests, sanctioned by an organization like the American Society for Testing and Materials (ASTM), do not exist. Some standard textile and plastic film tests are applicable to aerostat materials, but in many cases realistic and meaningful tests must be invented.

Sheldahl has a continuing program to develop test procedures aimed at qualifying aerostat materials. It is essential that qualification testing go well beyond the product assurance tests that are used to control the quality of virgin materials. The everyday handling and exposure of a material must be simulated, followed by thorough post-simulation testing of properties such as strength and permeability.

3.1 Conditioning Procedures

Several simulation or conditioning procedures have been developed for the CBV-250A, including:

1. Temperature extremes (+120°F, -40°F)
2. Water immersion (72 hours at 72°F)
3. Weather aging
4. Twist-Flex, a handling simulation
5. Biaxial stress cycling

The first three conditioning procedures are not accelerated, because of the difficulty of relating accelerated exposure to "normal" conditions. High and low temperature samples are simply allowed to come to temperature (five minutes minimum) prior to testing. Water immersion samples are submerged in distilled water for three days. Weather aging is accomplished using 18-foot diameter, low stress diaphragms, Figure 4, exposed to southern Minnesota weather.

Twist-Flex describes the operation of the handling simulation apparatus in Figure 5. Two 12-inch diameter by 48-inch long cylinders of hull envelope material with a common axis of symmetry are alternately inflated and deflated. The inflating cylinder twists the deflating cylinder 180° and crushes it from 48 inches down to 6 inches. The skin stress in the crushed cylinder is low during the crushing operation

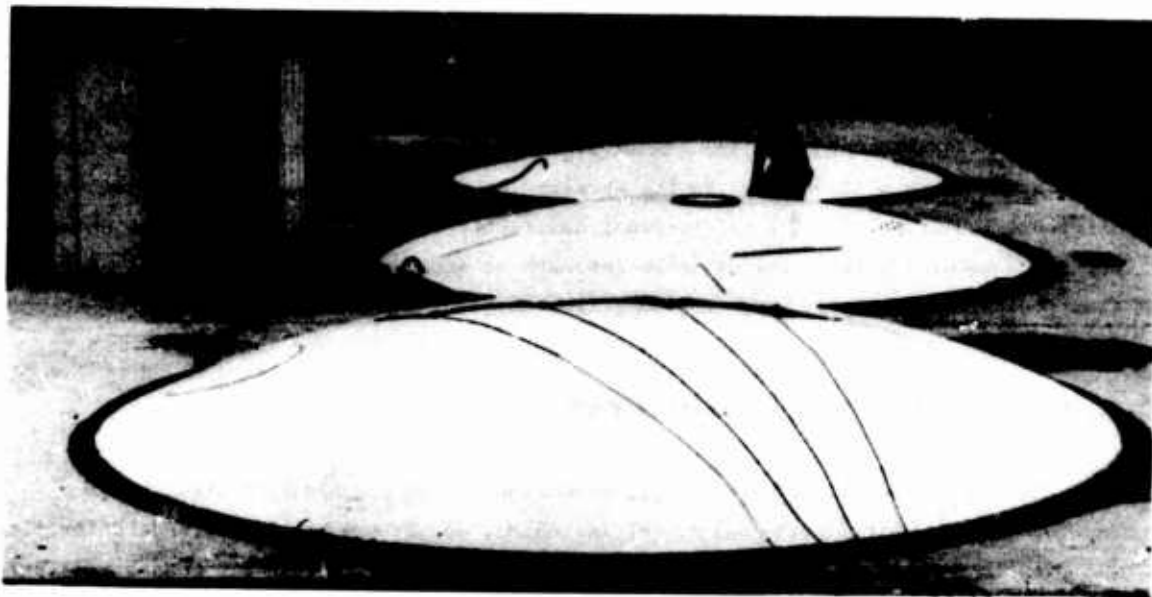


Figure 4. Weather Exposure Diaphragms
(18-foot diameter)

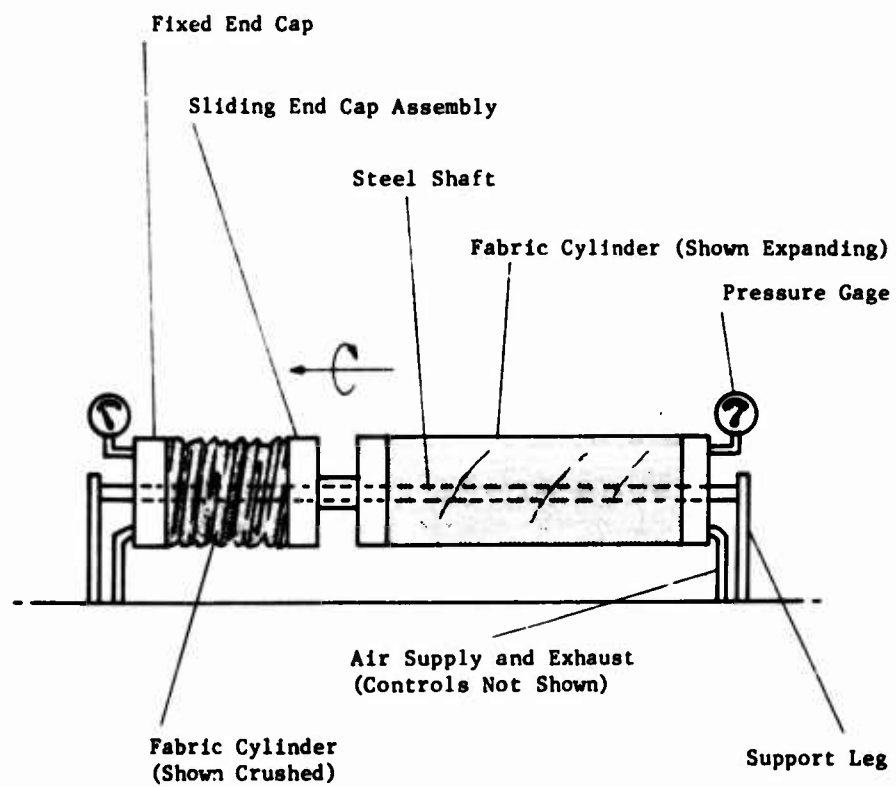


Figure 5. Twist-Flex Apparatus

and zero at the end of the cycle. Skin stress in the inflating cylinders builds to 70 pounds per inch at the end of the cycle. The process is then reversed--the previously inflated cylinder is exhausted, and the crushed cylinder begins to inflate. Normal handling of a CBV-250A aerostat, including manufacturing and deployment, is approximated by 100 Twist-Flex cycles.

Biaxial stress cycling is accomplished by "pulsing" an inflated diaphragm, Figure 6, between a low skin stress value and a maximum biaxial stress of 70 pounds per inch. The cycle rate is one per second and 100,000 cycles are adequate to detect any tendency toward material degradation from stress cycling.

3.2 Property Tests

After conditioning the aerostat hull material, one or more of the following property tests is performed.

1. Weight (FTMS-191-5041)
2. Strip tensile (FTMS-191-5102)
3. Tongue tear (FTMS-191-5134)
4. Ply adhesion (ASTM-D-1876)

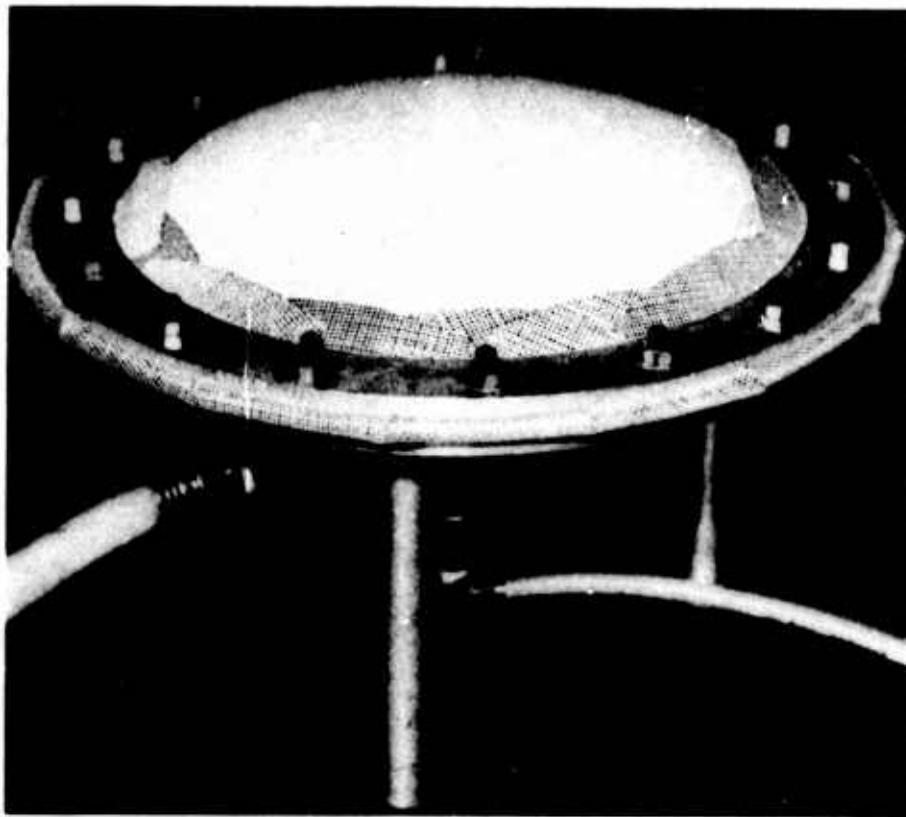


Figure 6. Biaxial Stress Apparatus
(12-inch diameter diaphragm)

5. Helium permeability (FTMS-191-5460)
6. Static tensile
7. Tear propagation
8. Shear stiffness
9. Bally-Flexometer

Property tests (1) through (5) are standard ASTM or FTM procedures. Tests (6) through (9) are discussed below.

The static tensile test samples, Figure 7, are one-inch wide and are looped around D-rings at each end in a manner that prevents slippage. The D-rings, spaced at least six (6) inches apart, provide a means of hanging the sample and applying a load. For the CBV-250A envelope, two weeks at a stress of 140 pounds per inch and a temperature of 120°F is required.

Tear propagation is defined as the spontaneous extension of a tear away from a point of damage. The minimum stress at which a tear will propagate is called the critical stress. The following method has been used to establish the critical stress

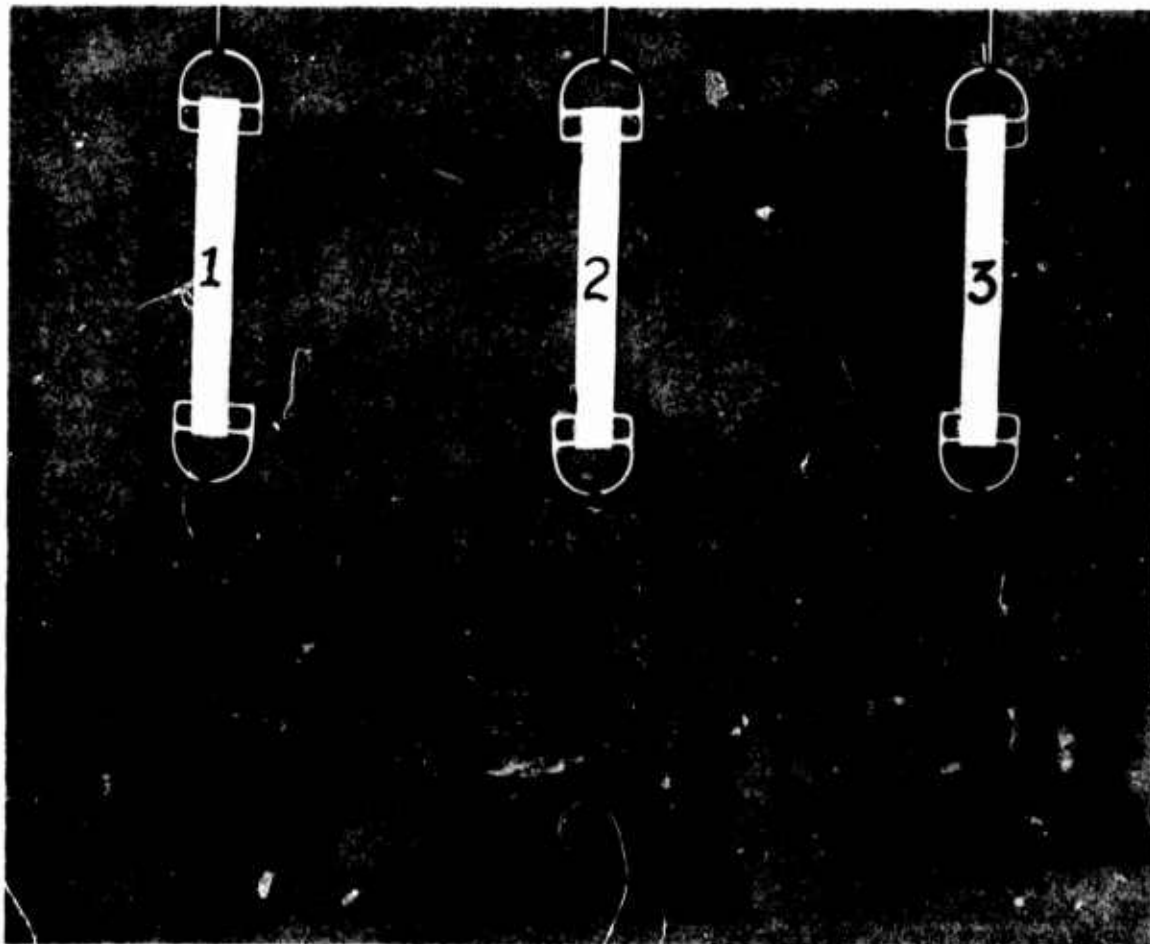


Figure 7. Static Tensile Samples

for aerostat materials. A 12-inch diameter diaphragm is slit as shown in Figure 8. The slit is covered with elastic, pressure-sensitive tape applied to the high pressure side of the diaphragm. The pressure differential across the diaphragm is then increased at a rate of 5psi per minute until the fabric ruptures. By varying the slit length, a plot of critical stress versus damage length, Figure 9, is obtained.

Shear stiffness is evaluated by twisting a pressurized cylinder and measuring the torsional deflection as shown in Figure 10. This machine is also used to obtain the biaxial stiffness coefficients used in the aerostat stress analysis.

The Bally-Flexometer, shown in Figure 11, is a walking crease test that was originally designed to measure the durability of shoe leather. There are 12 sample stations, and the crease point of each sample is worked back and forth until the sample cracks or pin holes form.

The CBV-250A hull qualification test program is summarized in Table 1. Matrix format was chosen for this table to give visibility to all important conditioning/ material property combinations.

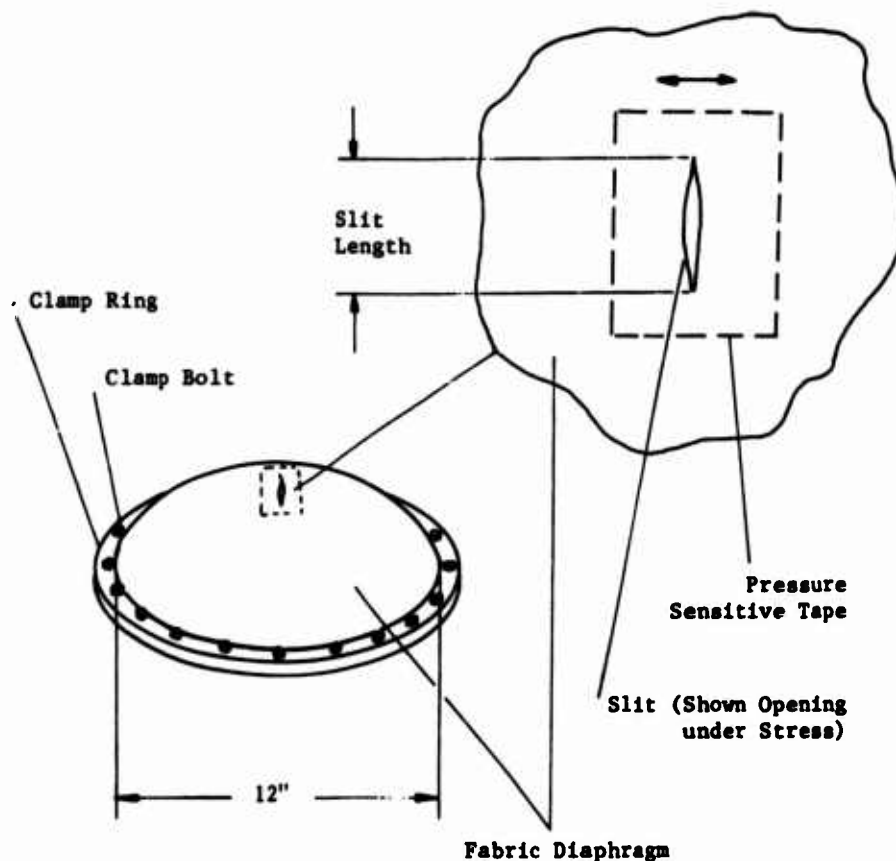


Figure 8. Tear Propagation Test

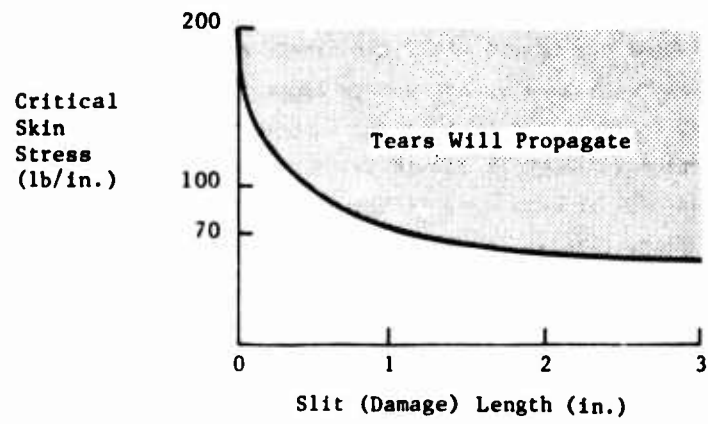


Figure 9. CBV-250A Tear Propagation Characteristics

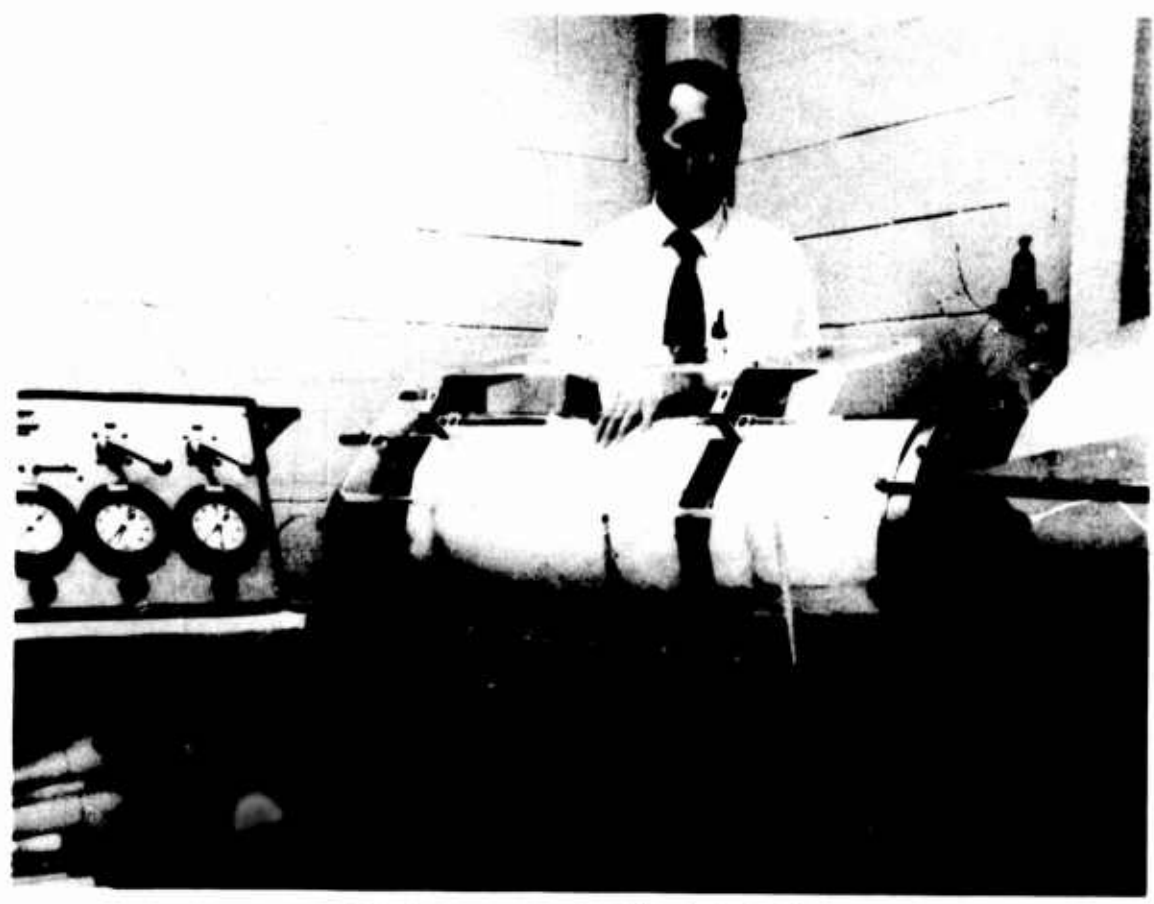


Figure 10. Cylinder Test Apparatus (14-inch diameter)



Figure 11. Bally-Flexometer

Table 1. Summary of the CBV-250A Hull Qualification Test

Conditioning Procedures	Property Tests									
	Weight (oz/yd ²) FMS-191-5041	Strip Tensile (lb/in.) FMS-191-3102	Tongue Tear (lb) FMS-191-5134	Ply Adhesion (lb/in.) ASTM-D-1876	Ballum Permeability (liters/m ² /24 hr) FMS-191-5460	Static Tensile (lb/in.)	Critical Tear Propagation Stress (lb/in.)— slit length, 1 inch	Shear Modulus (lb/in.)	Bally-Flexometer (cycles)	
New Material at Room Ambient	8.0 max.	225 min.	60 min.	8 min.	0.5 max.	140 min.	70 min.	200 min.	1000 min.	
Hot (120°F)		225	60			140				
Cold (-40°F)		225	45							
Water Immersion	8.0	225	60	8						
Weather Aging*		225	60	8	1.0					
Twist-Flex		225	60	8	0.5					
Biaxial Stress Cycling		225	50	8	0.5					

*Data available to date is for one (1) calendar year of exposure.

- NOTE: 1. An empty box indicates that no requirement has been identified for the conditioning/property test combination associated with that box.
2. All values are for the warp direction (where applicable); fill values are similar.

4. MATERIAL DESIGN, CBV-250A

The only material in use today that satisfied all of the requirements stated in Table 1 is the CBV-250A hull laminate. This material, described in detail in Figure 12, is a "bench mark" by which future materials may be judged.

DACRON was chosen as the structural cloth for its excellent dimensional stability, high tenacity, and hydrolytic stability. The 13 by 13 count, 1000-denier cloth has low twist, low crimp, and a balanced weave. This results in minimum elongation, low crimp interchange, and high tear resistance.

Both MYLAR film and elastomer coatings were considered for use as a helium gas barrier, but MYLAR was chosen for the following reasons. MYLAR film satisfies the helium permeability requirement at 1/5 the weight of an elastomer such as neoprene or polyurethane. This is a savings of several ounces per square yard which translates into an increase in payload capability of over 500 pounds for the CBV-250A. Also, films are generally more uniform. Sheldahl has experienced very few quality control problems with MYLAR. One roll is virtually identical to the next. The record for coated fabrics is not as consistent.

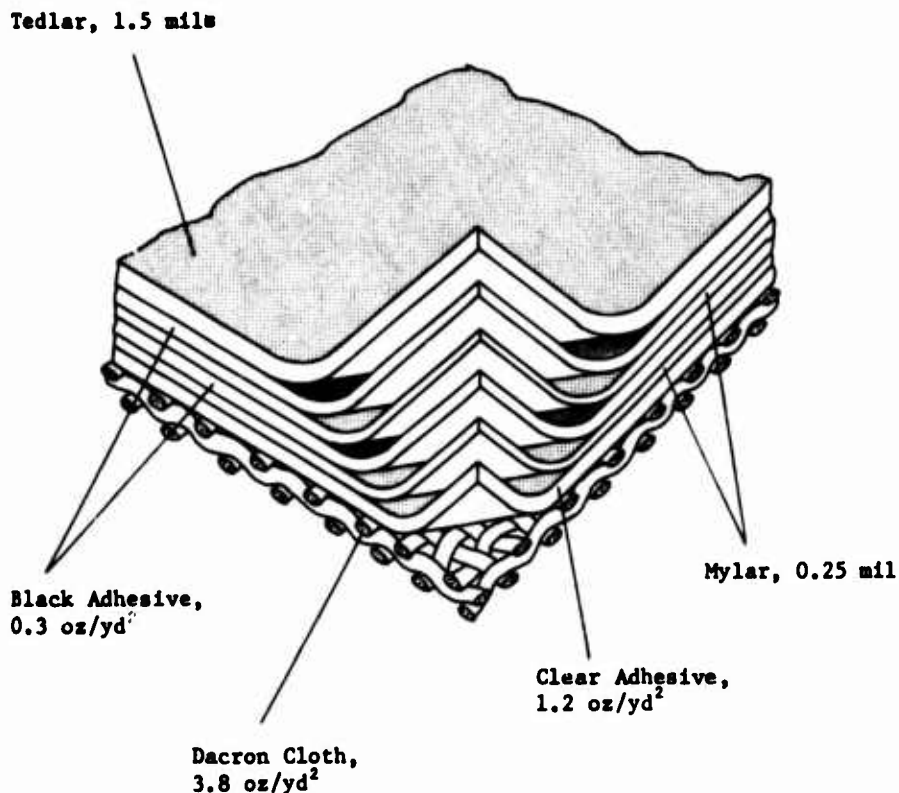


Figure 12. CBV-250A Hull Envelope Laminate

Increased porosity caused by stress cycling is a common deficiency of coated fabrics. By comparison, the CBV-250A laminate shows no increase in permeability after 100,000 cycles to a biaxial stress of 70 pounds per inch. In addition, MYLAR's high tensile modulus, 550,000 psi, provides adequate shear stiffness. This eliminates the need for a bias cloth, thus providing an additional weight saving of 1 to 3 ounces per square yard.

The TEDLAR exterior weathering surface represents another advance in aerostat technology. Experience with coated fabric radomes shows that elastomer weather coatings require periodic, usually annual, maintenance. TEDLAR, on the other hand, has been in service as a maintenance-free protective coating for building roof and siding panels for over twelve years, according to DuPont technical data. By conservative extrapolation, twenty-plus years of protection from weather and UV can be expected with no maintenance.

Table 2 summarizes Sheldahl's aerostat material progress from 1967 to 1974. The hull material strength-to-weight ratio has increased 95 percent over the past seven years. This translates into a 1000-pound weight reduction (payload increase) for a 250,000 cubic foot aerostat, due to improvements in the hull material alone.

The CBV-250A hull seam construction, Figure 13, is efficient in that loads are carried directly from the structural cloth in the hull laminate to the structural yarns in the splice tape. This seam construction satisfies all hull envelope strength, permeability, and environmental resistance requirements. Seams are fabricated economically at a rate of several feet per minute using a continuous "wheel" sealer.

Table 2. Aerostat Hull Material Progress, 1967 - 1974

Material Property	1967	1974	Δ
	CBV-200A Hull ARPA Balloon No. 201 Bias Ply, Coated Fabric	CBV-250A Hull Six (6) TCOM Balloons Laminate Construction	
Weight (oz/yd ²)	12.9 nom.	7.8 nom.	40 percent
Strength - Warp and Fill (lb/in.)	195 min.	225 min.	30 lb/in.
Permeability (l/m ² /24 hr)	1.0 max.	0.5 max.	50 percent

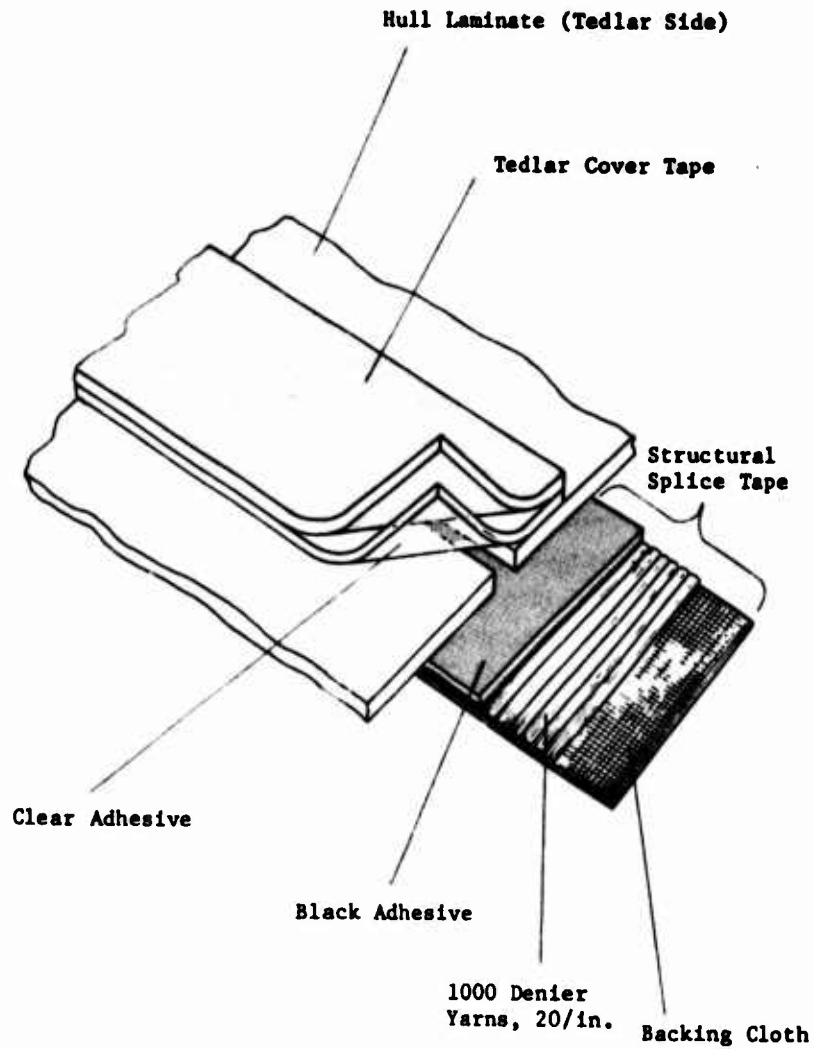


Figure 13. Hull Seam Construction, CBV-250A

5. ADVANCED MATERIALS

Looking toward the future needs of tethered aerostats, the engineer is continually looking at ways to carry heavier payloads on vehicles of existing design. This can only be accomplished by reducing the weight of the vehicle. In addition, the engineer is looking at ways to improve the safety factors with respect to high wind performance requiring additional material strength, and larger vehicles capable of higher altitude operation and, again, heavier payloads. In order to satisfy these future needs, a research program was undertaken jointly by the National Aeronautics

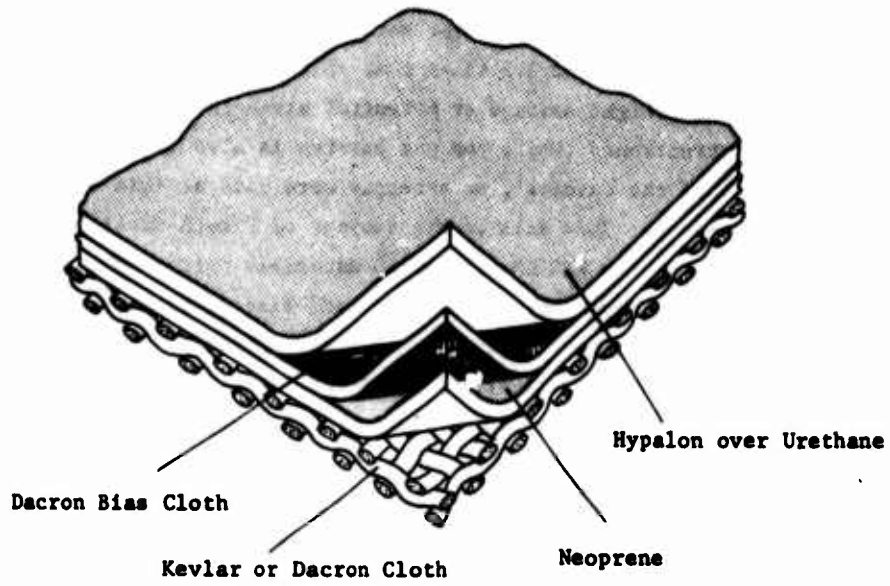
and Space Administration, Langley Research Center, and Sheldahl, the results of which have been reported in NASA CR-132411. The objective of this program was to investigate whether a new DuPont fiber PRD-49 (KEVLAR), could be incorporated into a coated fabric two-ply construction and a single-ply film laminate construction similar to that used today on CBV-250-type aerostats. The KEVLAR yarn offers a strength-to-weight ratio of 2 to 3.5 times that of DACRON and ten times that of steel, offering a significant weight savings or potential strength improvement over the present DACRON constructions. While the gas barrier is also a significant portion of the total weight of the material, no attempts were made at this time to vary this portion of the composite. This will be the subject of future development work.

In addition to the two KEVLAR-reinforced materials patterned after the materials used today, a unique construction using thread laid bias KEVLAR yarn of sufficient denier and count to tailor the bias strength was also tried. The technique used is similar to that developed by Sheldahl for Air Force high altitude, free-flight balloons which have been used very successfully for the very heavy and expensive payloads requiring high reliability. This construction, called SHELWEAVE, offers the potential of high production rates as the threads can be laid down at the same time as laminating the woven fabric to the environmental and gas seal membranes. This offers considerable advantages over the two-ply fabrics where the bias fabric must be hand cut and laid on a bias prior to combining with the main structural fabric. Also, by thread laying, the yarn count can be varied easily. This is not the case with woven materials used in a coating process where the fabric must be a sufficient count and weight to hold the elastomer during the coating process. The coating manufacturer generally does not want to work with a fabric weighing less than 2.2 ounces per square yard, and 2.2 ounce bias fabric is often more strength than is required for producing the desired bias strength. In thread laying, it is possible to put down a bias construction weighing as little as 0.1 ounce per square yard.

In this test program, three constructions were designed and built using KEVLAR as the strength member. Two were compared with a similar DACRON construction produced at the same time. Figure 14 describes these constructions. Table 3 shows an analysis of the component weights.

In the case of the KEVLAR reinforced two-ply coated fabric, we elected to use DACRON fabric as the bias ply because a lightweight KEVLAR fabric falling within the desired weight range was not available at the time. We were informed by the elastomer coater that he would have to have a minimum count weave construction to carry the elastomer coating through his equipment. He was skeptical of anything less than 2.2 ounce per square yard; however, he did agree to try a 1.4-ounce DACRON construction. There was also considerable skepticism with respect to the flatness of a very lightweight KEVLAR fabric which would result in fold-overs or creases when the bias construction was mated with the base structural fabric. It was recognized at the

TWO-PLY COATED FABRIC



SINGLE-PLY LAMINATE

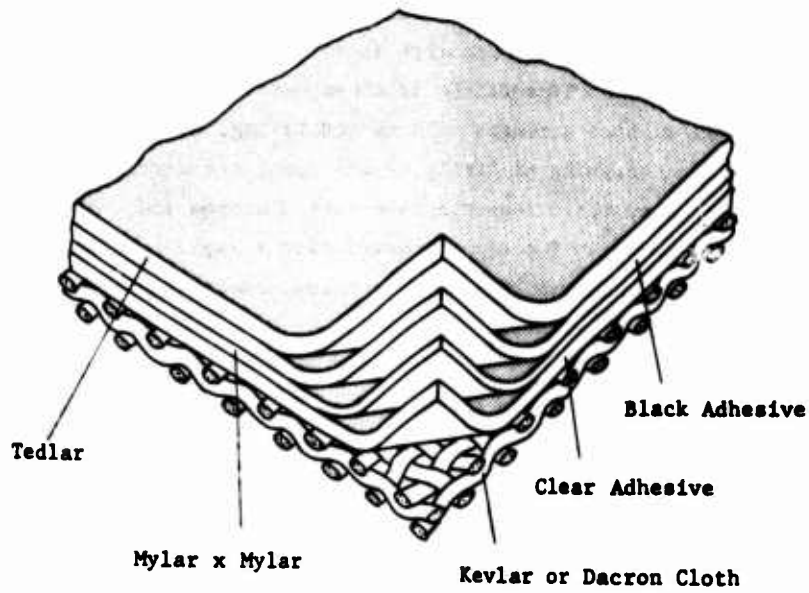


Figure 14. Advanced Materials

SHELWEAVE

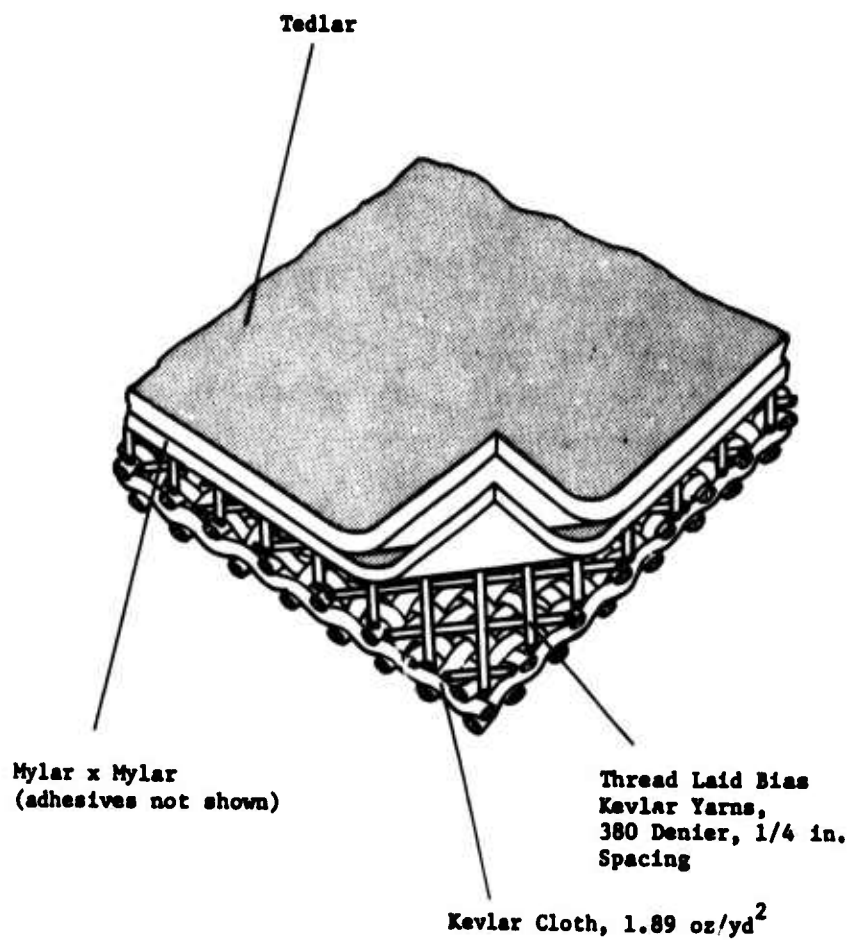


Figure 14. Advanced Materials (Continued)

Table 3. Analysis of Constituent Weights

Controls				Experimental Materials		
Constituent		kg/m ²	(oz/yd ²)	Constituent	kg/m ²	(oz/yd ²)
Laminated Materials	Tedlar	0.064	(1.89)	Tedlar	0.064	(1.89)
	Adhesive	0.007	(0.20)	Adhesive	0.007	(0.20)
	Mylar	0.008	(0.25)	Mylar	0.008	(0.25)
	Adhesive	0.005	(0.15)	Adhesive	0.005	(0.15)
	Mylar	0.008	(0.25)	Mylar	0.008	(0.25)
	Adhesive	0.040	(1.17)	Adhesive	0.040	(1.17)
	Dacron	0.129	(3.80)	Kevlar	0.064	(1.89)
	Adhesive	0.010	(0.29)	Adhesive	0.010	(0.29)
TOTAL		0.271	(8.00)	Total	0.213	(6.09)
Coated Materials	Hypalon	0.068	(2.0)	Hypalon	0.068	(2.0)
	Urethane	0.085	(2.5)	Urethane	0.085	(2.5)
	Dacron	0.065	(1.9)	Dacron	0.048	(1.4)
	Neoprene	0.119	(3.5)	Neoprene	0.119	(3.5)
	Dacron	0.119	(3.5)	Kevlar	0.092	(2.7)
	TOTAL		0.456	(13.4)	TOTAL	0.412
Shelweave (Quadaxial)				Tedlar	0.064	(1.89)
				Adhesive	0.007	(0.20)
				Mylar	0.008	(0.25)
				Adhesive	0.005	(0.15)
				Mylar	0.008	(0.25)
				Kevlar (bias)	0.007	(0.40)
				Adhesive	0.040	(1.17)
				Kevlar	0.064	(1.89)
			Adhesive	0.010	(0.29)	
TOTAL				TOTAL	0.213	(6.49)

time that the modulus of the DACRON and KEVLAR were sufficiently different to cause problems in any weave construction where the fibers were used in parallel. The KEVLAR yarn would be carrying the load first, having an ultimate elongation of approximately 4 percent compared to 20 percent for the DACRON yarn. This way the DACRON yarn would not be loaded until after failure of the KEVLAR. However, in this particular bias two-ply construction, the DACRON and KEVLAR are not used in parallel but rather at 45° from one another. The KEVLAR serves as the main structural member and the DACRON serves to stabilize the material with respect to bias loading.

Cylinder torsion tests verified that these two materials could be used successfully in this manner; however, should the coater be able to solve the problem of coating the very light open weave KEVLAR constructions, it would be desirable to try KEVLAR throughout in order to save additional weight. This problem prompted our looking at thread laying KEVLAR yarn to the main structural fabric as used in the third construction tested. Table 4 summarizes the test results and compares these to the DACRON controls.

5.1 Summary and Conclusions

All three of these new KEVLAR constructions are producible on existing weaving, laminating, and coating equipment. While some problems were experienced in the flatness of a KEVLAR woven fabric, this was attributed to the newness of this product and equipment adjustment.

Comparing the KEVLAR to the DACRON controls, tensile strength-to-weight increased by about 35 percent for the single-ply laminates and by 135 percent for the two-ply coated fabrics. Tensile stiffness was increased about threefold for one-ply and tenfold for two-ply materials. Shear stiffness of the one-ply material was doubled.

The one-ply KEVLAR laminates exhibited some strength loss after sharp creasing. By pre-wash coating of the KEVLAR yarn prior to laminating, this problem seems to disappear.

Bias KEVLAR yarns can be laid on the structural fabric at just about any angle and spacing to produce the desired bias strength with little penalty in weight over plain fabric film laminate.

It appears the KEVLAR yarn reinforced material is an effective improvement in strength and weight-saving for aerostat composite materials and warrants further qualification testing and prototype balloon fabrication. In designing a vehicle using this material, one must take into consideration its lack of "forgiveness" resulting from its relatively low ultimate elongation. Considerable care must be given to manufacturing tolerances and stress risers at seams, seam crossovers and subassemblies.

Table 4. Summary of Characteristics of Control and Experimental Materials

Characteristic	Control (Dacron)		Experimental (Kevlar)		Shelveave (Quasidaxial)
	1-Ply Laminates*	2-Ply Coated	1-Ply Laminates	2-Ply Coated	
Weight - kg/m ² (oz/yd ²) FTMS - 191 - 5041	0.271 (8.0)	0.456 (13.4)	0.206 (6.09)	0.412 (12.1)	0.219 (6.49)
Tensile Strength at 22°C (72°F), N/m (lb/in.) FTMS - 191 - 5102	46 (262)	32 (184)	47 (269)	69 (394)	58 (334)
Trapezoidal Tear Strength, N (lb) FTMS - 191 - 5136	167 (38)	53 (12)	58 (13)	93 (21)	108 (25)
	209 (47)	Ply delamination	35 (8)	100 (23)	113 (26)
Abrasion Resistance (Cycles to Failure) Relative Data	40,000	21,000	69,000	21,000	69,000
Flex Life - Bally- Flexometer (Cycles to Failure)	1,000	24,000	3,000	24,000	3,000
Blocking (mg) Sheldahl Spec. Q000041	<10	<10	<10	<10	<10
Permeability 1/m ² / 24 hr FTMS - 191 - 5460	0.4	0.7	0.3	0.5	0.3

*CBV-250A Hull Laminates

Stratospheric Tethered Balloons

R. Regipa
CNES
Toulouse, France

Abstract

In October-November 1973, at the 'Centre Spatial' in French Guiana, CNES (Centre National D'Études Spatiales) and the French 'Météorologie Nationale' jointly conducted a series of experiments with stratospheric tethered balloons.

After a first flight failure, due mainly to the winch lapse, it was possible to get a successful flight at 17,000 m for 12 hr with a balloon volume of 10,000 m³ and a 350-kg payload. The ambient temperature was under -80°C.

About 60 sensors allowed the following measurements at the flight level:

Temperatures (and their variation) of the atmosphere and of different points into the gondola.

Vibrations and inclinations.

Wind speeds.

Proper balloon motions.

For the next program, the French 'Météorologie Nationale' is developing a new winch and the CNES is studying a new way to reach the flight level and avoid stresses in crossing the jetstream.

A device of gondolas moving along the cable will allow permanent soundings while stationary or during gondola ascent or descent.

The Minnesota 1973 Atmospheric Boundary Layer Experiment

Duane A. Heugen, J. Chandran Kaimal
Air Force Cambridge Research Laboratories
Bedford, Massachusetts

and

Christopher J. Readings, Alan J. Marks
Meteorological Research Unit
RAD, Cardington
Bedford, England

Abstract

A field program to obtain detailed data on turbulent transport of heat and momentum in the first 4000 feet of the atmosphere was conducted in Minnesota during August and September 1973. Five probes, designed to measure wind and temperature fluctuations, were furnished and operated by the British team. These probes were spaced along the tethering cable of a large kite balloon between heights of 200 and 4000 feet. Detailed transport properties close to the ground were measured by the AFCRL team on a 100-foot tower. Over seventy hours of data were obtained during meteorological conditions appropriate to studying the increase of turbulent mixing and boundary layer depth during day time hours and the decrease during night time hours. Some of the significant features of boundary layer flow that can be studied using tethered balloons as a sensor platform will be discussed in this paper. The most important result to have emerged from the analyses to date is that measuring turbulent transports directly by the so-called eddy correlation technique is indeed possible with sensors mounted on the tethering cable to a degree of accuracy not expected from considerations of averaging time and the diurnal variations in the boundary layer.

1. BACKGROUND

The purpose of this paper is to describe a field program for studying the turbulent structure of the atmospheric boundary layer. The predominant feature of this program was the use of a captive balloon to carry turbulence probes to depths of the atmosphere just recently attracting the interest of meteorologists. It is believed that the day time atmospheric boundary layer extends to several thousand feet in the temperate latitudes, but to date little is known of the significant features of the flow within this layer. The fundamental properties we set out to measure in this program were the turbulent fluctuations and average values of the wind and temperature from the surface up to heights of 4000 feet. This was a joint program utilizing experimental techniques that had been independently developed by the various research groups involved. A team from the Meteorological Research Unit, (MRU), RAF Cardington, Bedford, England, installed and operated probes which were mounted on the tethering cable of the captive balloon. A team from the Meteorology Laboratory, AFCRL, Bedford, Massachusetts, installed and operated probes mounted on fixed booms on a 32m tower. The balloon was a 45000 cu. ft. kite balloon, manufactured by Lea Bridge Industries, England, trimmed to fly at heights of roughly 5000 to 7000 feet MSL. The balloon flights were accomplished by a team from Aerospace Instrumentation Laboratory, AFCRL, Det. 1, Balloon R & D Test Branch, Holloman AFB, N. Mexico. Rawinsonde observations of the mean wind and temperature from the surface to heights of about 10,000 feet were taken during each experimental period by a team from the 6th Mobile Weather Squadron, AWS, Tinker AFB, Oklahoma.

Planning and preparation for these experiments dates back to 1969 when members of the British and AFCRL meteorology groups compared sensor performance with probes mounted side by side on a tower. In 1971, a balloon-tower comparison program was conducted to determine the effects of balloon movement on the cable-mounted turbulence probes. The results of that experiment were particularly gratifying and were reported at the Seventh AFCRL Scientific Balloon Symposium

(Haugen, et al, 1973; See also Haugen et al, 1974). It was concluded that balloon movements generally occur at frequencies sufficiently removed from those which are important for studying the turbulent structure of the atmosphere to justify plans for the Minnesota boundary layer experiment.

The experiments took place during August and September of 1973 at the APCRL experimental site near Donaldson, Minnesota. This site is in the Red River valley where the terrain closely approximates a uniformly flat plane for tens of miles. Data were gathered only under northerly wind directions for which an unobstructed fetch of about 7 miles exists.

The data to be presented here have been selected to illustrate the potential of the captive balloon technique for exploring the boundary layer. Balloon movement effects were one concern we had prior to embarking upon this overall joint program. Another concern was whether statistically-stable estimates of turbulent quantities could be obtained at large heights in the boundary layer using fixed probes rather than aircraft-mounted probes. (See, e.g., Wyngaard, 1973) These fundamental concerns are significant not only to these Minnesota experiments, but to a number of other programs which also use captive balloon techniques for probing the boundary layer, e.g., Thompson, 1972; Yokoyama, 1969.

2 EXPERIMENTAL DETAILS

The MRU probe is shown in Fig. 1 as it is being mounted on the tethering cable. It consists of an arm with a fin at one end and an array of sensors at the other. The arm is attached to the tethering cable at the probe's balance point such that it freely rotates and keeps the sensors facing into the wind. These consist of an 8-cup anemometer for measuring total wind speed, a magnetic field sensor for measuring the arm position relative to the earth's magnetic field and thus the wind direction, a double-"V" hot wire oriented on its side for measuring the instantaneous differences between the arm position and the wind direction, a double-"V" hot wire oriented in a vertical plane to measure the inclination of the wind to the horizontal, and a platinum-wire resistance thermometer. Three oil

dash pots are used to damp out any cable-induced motions. Five probes were used in these experiments, in two spacing patterns on the cable depending on the anticipated height of the boundary layer top. One pattern had the probes at 200, 500, 1000, 1500, and 2000 feet with the balloon at 4000 feet; the other had them at 200 (or 500), 1000, 2000, 3000, and 4000 feet with the balloon at 6000 feet above terrain. Radio-telemetry was used to relay the signals from the four uppermost probes to the ground but a signal cable was used for the lowest probe. Rechargeable battery packs mounted just below each probe had a usable life time at least twelve hours, thus permitting the observation of boundary layer transitions from the deep, turbulent layer of a sunny day to the shallow, smooth layer of a clear night.

The tower-mounted probes consisted of two three-axis sonic anemometers and two platinum-resistance thermometers, mounted at 4m and 32m for measuring turbulent fluctuations in the wind and temperature fields; two-axis sonic anemometers mounted at 1, 2, 4, 8, 16, and 32m to measure the mean horizontal wind; quartz crystal thermometers mounted in aspirated radiation shields at 0.5, 1, 2, 4, 8, 16, 24 and 32m to measure the mean air temperature. Total solar radiation and net radiation were measured at 32m; two surface drag plates were installed north of the tower to measure the earth's frictional drag on the overlaying air. A photograph of the tower installation is given in Fig. 2.

All data from the tower and balloon probes were recorded digitally on magnetic tape by AFCRL's computer-controlled data-acquisition system (Kaimal, et al, 1966). Seven periods were studied during the experiment. Five of these lasted ten to twelve hours and covered the transition from the afternoon convective situation to the night time inversion; one lasted ten hours and covered the transition from night time inversion to mid-morning; one covered a full twenty-four hour period starting at 8:00 A.M. local time.

Prior to each of these observation periods, each MRU probe was placed on a platform next to an AFCRL three-axis sonic anemometer and a temperature sensor to obtain detailed comparison data. In this way, we effectively established the

relative calibration of the instruments in the same turbulent flow unaffected by balloon movement.

3. DATA ANALYSES

The first goal of our data analysis effort is to determine whether it is possible to observe accurately enough the turbulent processes believed to be important in the development of the boundary layer using the captive balloon technique. This question is basic to the so-called eddy-correlation techniques for determining the rate of vertical transfer of heat and momentum through the boundary layer by turbulent motions. For purposes of illustration, let us consider the vertical transport of heat. Define T' as the instantaneous departure of the temperature from its mean value at any height, z . Let w' be the simultaneous value of the vertical wind fluctuation at the same point. It can then be shown the net vertical transport of heat across a plane at height z due to turbulent motion is directly proportional to the covariance, $\overline{w'T'}$, where the bar indicates an appropriate time average of the indicated cross-product. The question now becomes the proper definition of "an appropriate average" for this covariance.

Close to the ground, long-period, large-amplitude fluctuations in the vertical component, w , are inhibited by the ground itself. Hence, in many instances, it is a relatively straight forward process to define an appropriate averaging time for the tower data in order to obtain statistically stable estimates of the transport quantities. As one moves higher in the boundary layer, however, there is no immediately obvious low-frequency damping of vertical motions so that one would expect longer averaging periods to be necessary to obtain stable estimates. It has been shown that five to thirty minutes are usually adequate close to the ground, the shorter periods being applicable to night time situations and the longer periods to daytime ones. Extrapolation of these results to the heights used in Minnesota indicate that several hours might well be necessary. (Wyngaard, 1973) If it develops that such long averaging periods are required, a further complication will enter in that it will then be necessary to filter diurnal trends

(periods of 12 to 24 hours) from the data before computing the covariances. Thus, if a suitable combination of averaging and filtering cannot be established, it would tend to devalue the captive-balloon approach to boundary layer experiments (time-averages) relative to an instrumented aircraft approach (space-averages).

Computations of $\overline{w'T}$ have been performed for the tower and balloon probe data for averaging periods varying from 15 minutes to 150 minutes. In addition, the data have been subjected to numerical high-pass filters which retain fluctuations of 15-minute periods or smaller.

4. RESULTS

In Fig. 3 we show vertical profiles of $\overline{w'T}$ for a typical daytime convective situation. Each data point is the average of five successive fifteen-minute averages, i.e., roughly equivalent to the high-pass filter just mentioned. Also plotted are theoretical profiles predicted for "typical" convective situations with a numerical model of boundary layer turbulent flow (Wyngaard and Coté, 1974). The agreement is excellent and clearly indicates that direct measurements of turbulence with probes mounted on captive balloon cables is indeed an extremely valuable research tool. Analyses currently underway at AFCRL and MRU are now being directed to such topics as investigation of universal similarity parameters to characterize the flow, spectral distribution of the turbulent energy, and application of various filtering techniques for removing known trends from the data.

5. ACKNOWLEDGMENTS

We would particularly like to express our appreciation to Capt D. E. Jackson, SSgt T. J. LaChance, and SSgt J. A. Caronna of the Holloman balloon crew for their expert and enthusiastic contributions to these experiments. In addition, it is a pleasure to acknowledge the contributions made by every member of our research team at AFCRL and MRU to all aspects of the program, contributions without which this program would not have been possible.



Figure 1. MRU Turbulence Probe

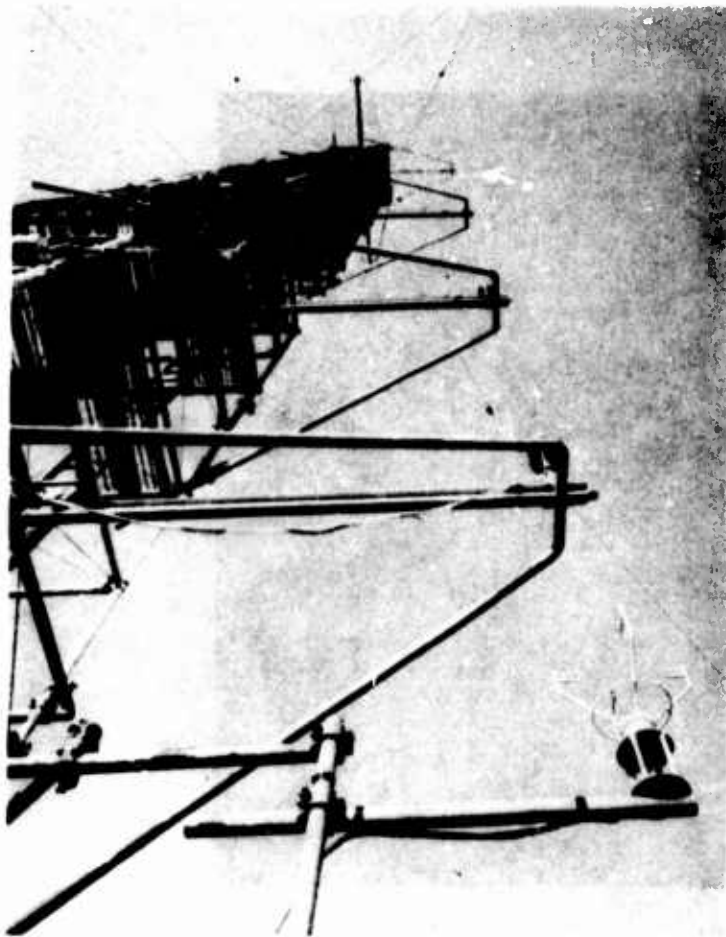


Figure 2. AFCRL Tower Instrumentation

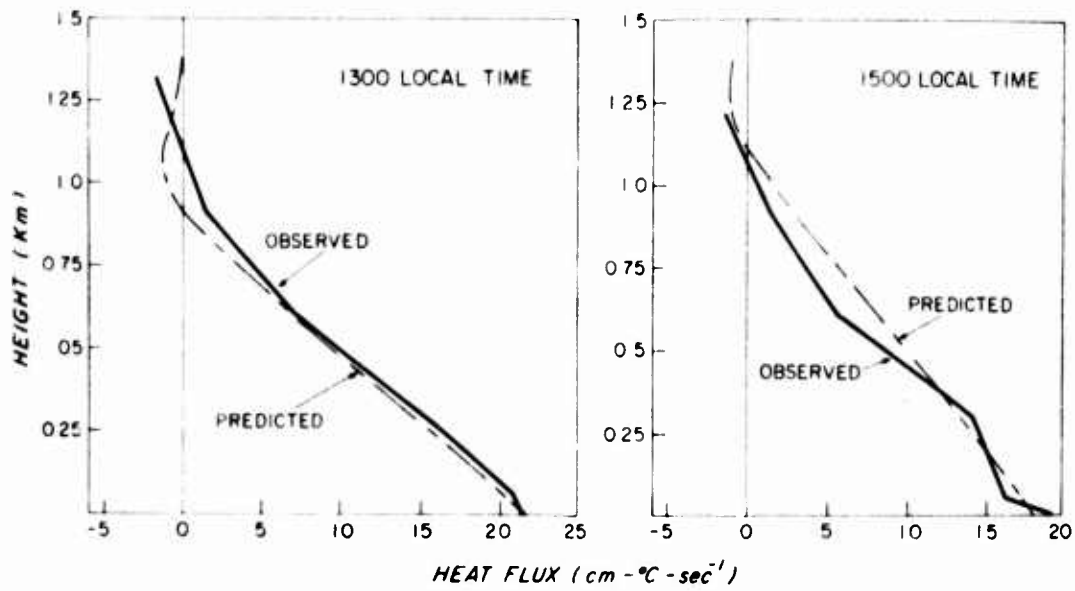


Figure 3. Heat Flux Profiles

References

- Haugen, D. A., Pellegrini, J., Readings, C. J., and H. E. Butler (1973), Comparison of balloon-borne and tower-mounted turbulent wind and temperature sensors, Proc. Seventh AFCRL Scientific Balloon Symposium, AFCRL-TR-73-0071, 93-101.
- Haugen, D. A., Kaimal, J. C., Readings, C. J., and R. Rayment (1974), A comparison of balloon-borne and tower-mounted instrumentation for probing the atmospheric boundary layer, J. Appl. Meteor., to be published.
- Kaimal, J. C., Haugen, D. A., and J. T. Newman (1966), A computer-controlled mobile micrometeorological observation system, J. Appl. Meteor., 5, 411-420.
- Thompson, N. (1972), Turbulence measurements over the sea by a tethered-balloon technique, Quar. J. Roy. Meteor. Soc., 98, 745-762.
- Wyngaard, J. C. (1973), On surface layer turbulence, Workshop in Micrometeorology, D. A. Haugen, Ed., Boston, Amer. Meteor. Soc., 101-149.
- Wyngaard, J. C., and O. R. Coté (1974), The evolution of a convective planetary boundary layer - a higher-order-closure model study, Bound. Lay. Meteor., to be published.
- Yokoyama, O. (1969), Measurement of wind fluctuations by a vane mounted on a captive balloon cable, J. Met. Soc. Japan, 47, 159-165.

Contents

1. Introduction
2. The TCOM Mooring System -
A General Overview
3. Capabilities
4. Site Requirements
5. Power, Controls and Winch Systems
6. Future Systems
7. Operations

A New Mooring System For Tethered Aerostat

**Eugene L. Haak
Sheldahl, Inc.
Northfield, Minnesota**

**Kebbie Turner
OECO
Dallas, Texas**

Abstract

A unique mooring system and maintenance station has been in service with 250,000 cubic feet aerostats for about 1-1/2 years. This paper presents the design requirements and performance capability of this new system as evidenced by the year and one-half of successful operation in actual field conditions. A description of the winches, hydraulic system, nose latch, flying sheave and structural components along with the theory of operation are presented. Typical launch and recovery operations and "on-station" performance are described. Some of the experiences encountered and the operational tests performed during the year of operation are described and the related changes and improvements are noted. A discussion of manpower and site requirements is also given.

1. INTRODUCTION

1.1 Background

Mooring systems for tethered balloons, blimps and rigid airships have a history that is nearly as old as streamlined aerostats themselves (Figures 1, 2 and 3), and most of our modern mooring systems use the same concepts that were prevalent 50 years ago. Although through the years a great number of innovations and new ideas have been tried, and sometimes endured, until recently all mooring systems had one thing in common -- the need for a large ground crew for launch and recovery operations. In the case of the large rigid airships, a crew in excess of 400 people was sometimes required (Figure 4). For military operations this crew was usually readily available at a nominal cost. In recent years, particularly in commercial ventures, the cost of maintaining a crew has become prohibitive, and the trend has been to design systems which require minimum manning. Goodyear, for many years, has been operating their blimps with a surprisingly small number of well-trained men. The tethered balloon operations at Cape Kennedy, and later at Cujoe Key (Figure 5), have also been carried out with relatively few personnel. With the emergence of the telecommunications concept using tethered aerostats, however, the need to minimize crew size became critical. Since this concept requires that the aerostat remain aloft for weeks or months at a time, the maintenance of a large, full-time ground crew is cost prohibitive. This fact, then, dictated the requirement for mooring system which could be operated by a small crew.

Another relatively unique requirement imposed upon the mooring system by the nature of the telecommunication concept is a need for all-weather capability on a global scale. The system, both mooring system and aerostat, had to be designed to withstand the environment, primarily wind and temperature, anywhere in the inhabited world without hangar facilities or any other assistance.

These two requirements, weather and crew size, prompted the design of a mooring system which incorporates several new features while attempting to retain the knowledge and experience of the past.

2. THE TCOM MOORING SYSTEM -- A GENERAL OVERVIEW

2.1 General Description

This mooring system is a permanent installation with primary functions to a) serve as the ground anchor for a CBV-250A or a CBV-350A aerostat when it is on station, and b) serve as a service and maintenance station for the aerostat



Figure 1. ZR-1 (Shenandoah) Mooring Mast,
Lakehurst, N.J. (Ref. 1)

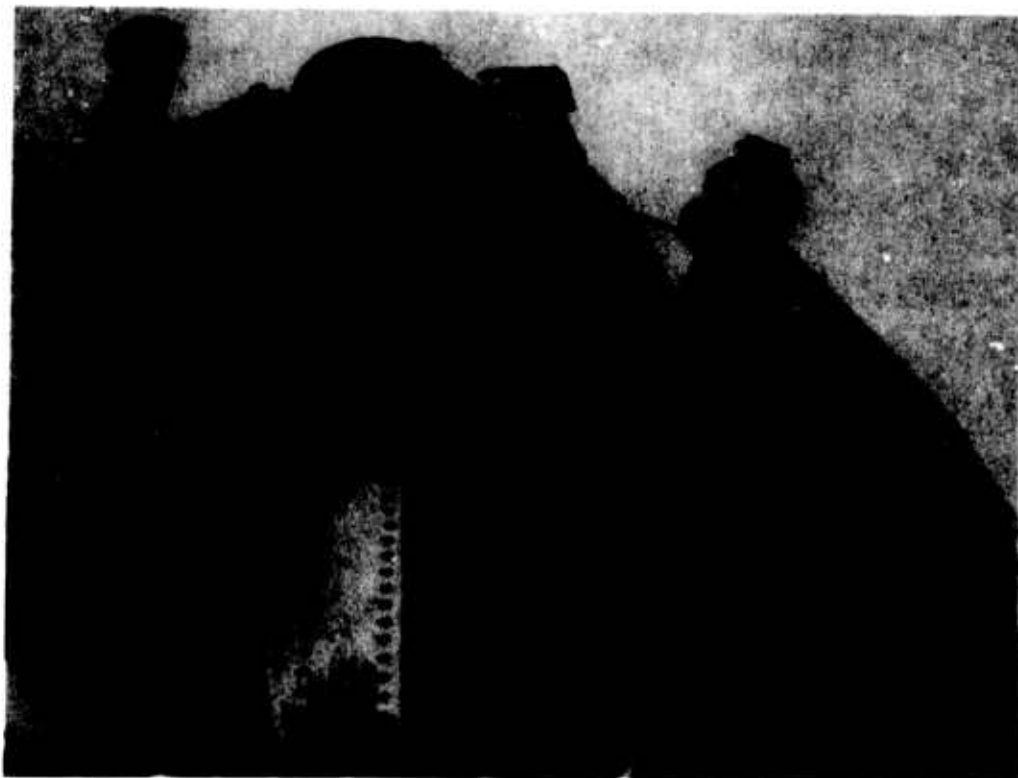


Figure 2. ZR-1 Nose Cone and Latch (Ref. 1)



Figure 3. ZR-1 Mooring at Sea, 1924 (Ref. 1)



Figure 4. Typical Ground Crew for Large Airships (Ref. 1)

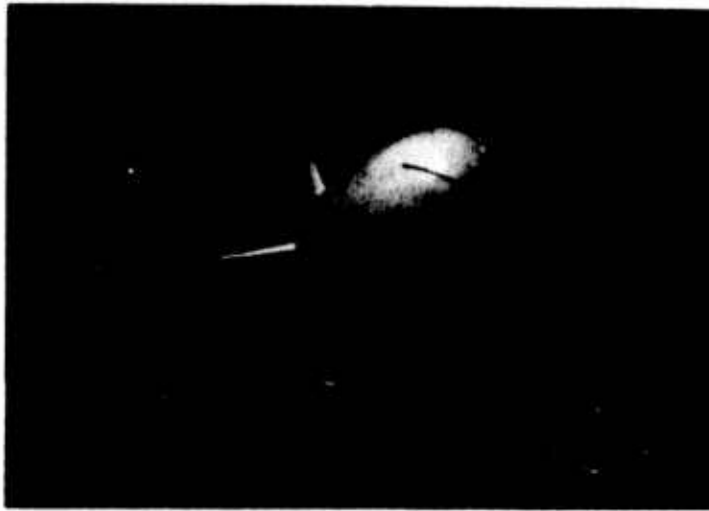


Figure 5. Cujoe Key Operations, 1972

between missions. The mooring system, Figure 6, consists of a central machinery enclosure and mast mounted on a large central bearing, a horizontal compression member or boom, and a circular mono-rail which supports the boom end, flying sheave and close-haul winches on rollers. A mechanical lock with a remote electrical release is provided at the top of the mast. Work surfaces are provided on the top deck of the machinery enclosure, on the boom and at the location of the aerostat payload when it is moored. A diesel powered main winch and an auxiliary power unit located within the machinery enclosure furnish the power required to launch and retrieve the aerostat and to moor the balloon in the close-hauled mode. The main winch is used to control and store the tether cable during flight operations. Three smaller winches, one at the base of the mast and two on the circular rail, provide the restraints and control during early stages of launch and during final recovery. A completely enclosed operator's cab is located on the forward side of the machinery enclosure, providing visibility to all operational areas.

The principle feature of this design is its ability to be rotationally driven, either by the forces generated by the aerostat or externally, to align, in azimuth with the aerostat or its tether cable. This allows a single operator to maintain the balloon in flight and a minimum-sized crew to launch and recover the balloon. During servicing and maintenance when moored, the crew moves with the system thereby providing improved accessibility and greater safety and again reducing the crew size.

The following paragraphs describe typical procedures as evidenced by operational experience with mooring systems of this type.

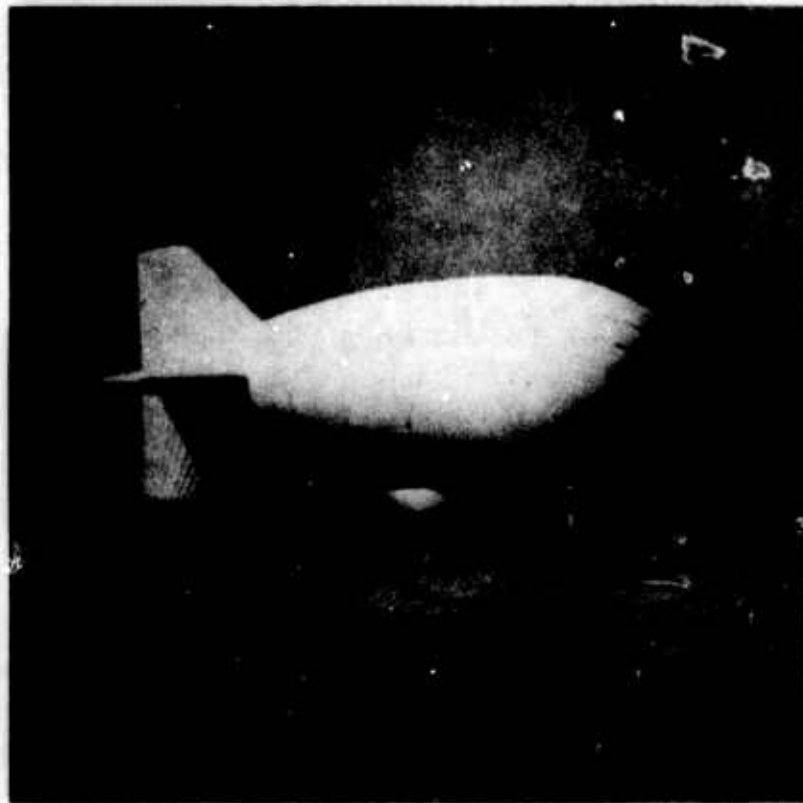


Figure 6. The TCOM Mooring System, 1973

2.2 Moored Mode

When moored the aerostat is mechanically locked to the mooring mast at the nose and secured by its suspension lines to the service platform under the aerostat payload. In this configuration any changes in wind direction will cause a rotation of the complete system and maintain the balloon headed into the wind. It also allows the field crew to "ride" the mooring system and work without concern for shifting winds and gusts. In relatively calm weather (winds less than 15 knots), the brakes can be engaged so that heavy loads, such as the aerostat payload, can be transferred from truck to work platform. In all other moored operations, the system is free to rotate with the wind.

2.3 Flight Mode

When the aerostat is at altitude, the tether cable is routed from the main winch through the boom to the flying sheave and thence up to the balloon (Figure 7). The tether cable tension is generally strong enough to rotate the mooring

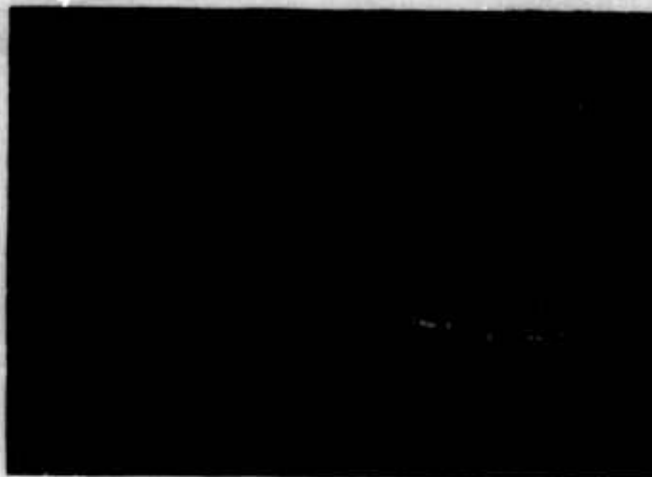


Figure 7. Mooring System with Aerostat Aloft

system into direct alignment with the horizontal projection of the tether cable. If not, final adjustments are made by driving the system to this condition with the hydraulic rotating motor located on the central bearing. Once aligned, the brakes on the close-haul winch trolleys are engaged. The system remains in this condition until changes in the direction of winds aloft dictate re-orientation. Aerostat altitude variations with wind speed are controlled by inhauling or out-hauling of the main winch.

3. CAPABILITIES

3.1 Performance

3.1.1 WIND

Figure 8 shows wind velocity versus altitude for several selected geographical locations and the velocities for which the aerostat is designed. The mooring system with the aerostat attached is designed for this same wind velocity at sea level (90 knots). With the balloon aloft or detached, the system will withstand wind loads in excess of 120 knots.

3.1.2 ALIGNMENT WITH WIND

With the aerostat moored, it has been estimated from visual observation that a 3 to 5 knot wind 10 degrees off the balloon heading will cause the mooring

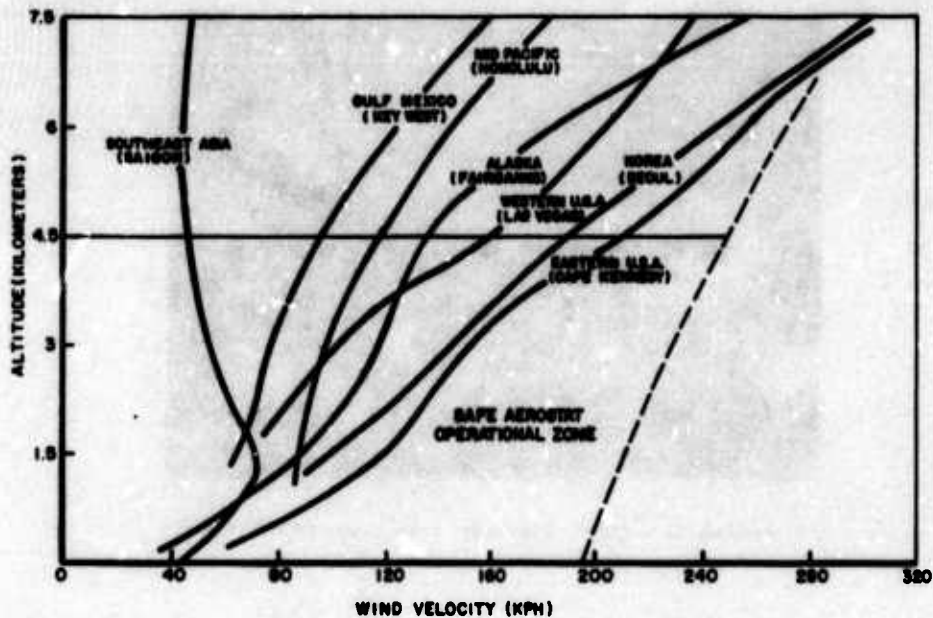


Figure 8. Safe Aerostat Wind Velocities Versus Representative Maximum Wind Profiles

system to realign itself into the new wind directions. When the balloon is aloft, tether cable side loads of this same magnitude would cause mooring system rotation if it were not braked during flight (see paragraph 2.3).

3.1.3 MANPOWER

The system was originally designed for operation by a six-man crew. Field operations, however, have demonstrated that normal launch and recovery operations can be performed by four men.

3.1.4 OTHER PERFORMANCE CAPABILITIES

Table 1 summarizes the performance and design features of the mooring system.

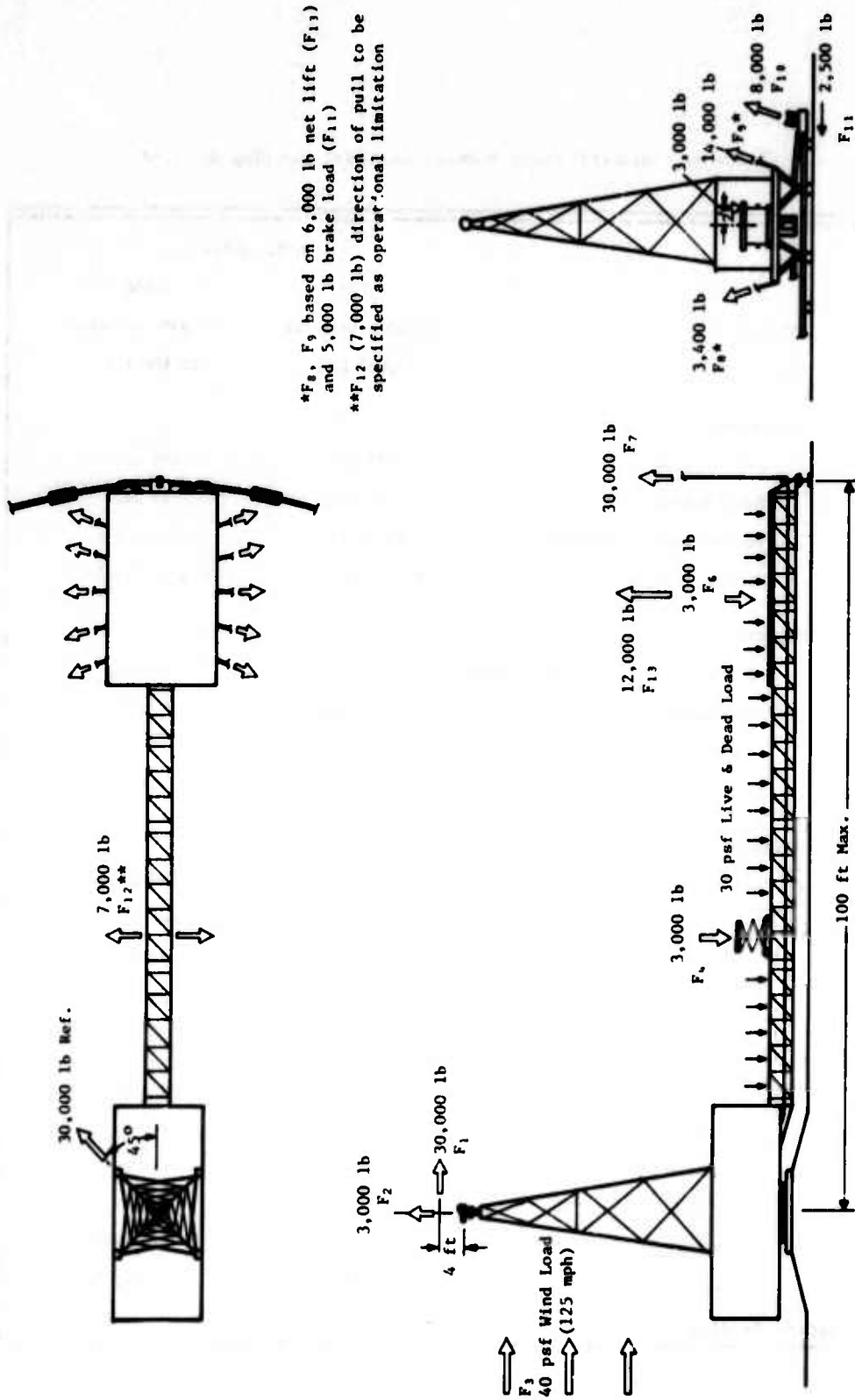
3.2 Structure and Loads

The winds described above, a dynamic analysis of the moored aerostat (reference 2 and 3) and the live and dead loads expected on the system, resulted in the loadings shown in Figure 9 in the combinations described in Table 2. The primary forces are the 30,000 pound nose latch load and the 30,000 pound (20,000 pounds on earlier systems) tether cable load.

Table 1. Specification Summary Aerostat Mooring System*

APPLICATION	MODEL NUMBER	
	18500	18600
	CBV-250A Aerostat	CBV-350A Aerostat
WEIGHT	95,600 lbs.	99,600 lbs.
DIMENSIONS		
Rail Diameter	173 ft.	203 ft.
Tower Height	47 ft.	47 ft.
Payload Service Platform	16' x 22'	16' x 22'
Machinery Enclosure	12' W x 9' H x 31' L	12' W x 9' H x 31' L
STRUCTURAL CAPABILITY		
Wind Speed (With Aerostat Moored)	90 knots	90 knots
Wind Speed (Without Aerostat)	120 knots	120 knots
Operating Temperature	-30°F to +120°F	
Design Criteria	AISC Standards, 7th Edition	
OPERATOR CAB		
Dimensions	6' W x 5' L x 6.5' H	6' W x 5' L x 6.5' H
Note: Full Console With All Engine Instruments, Tether Cable Indicators, and Hydraulic Controls.		
HYDRAULICS (Supplied by OECO)		
Main Winch		
Tether Cable Capacity	20,000'	20,000'
Maximum Pull	30,000 lbs.	30,000 lbs.
Maximum Line Speed	200 fpm	200 fpm
Close Haul Winches (3)		
Maximum Pull	12,000 lbs.	12,000 lbs.
Maximum Line Speed	140 fpm	140 fpm

*Patent Pending



* F_8, F_9 based on 6,000 lb net lift (F_{13}) and 5,000 lb brake load (F_{11})

** F_{12} (7,000 lb) direction of pull to be specified as operational limitation

Figure 9. Mooring System Loads

Table 2. Mooring System Load Definitions and Combinations

<u>EXTERNAL LOAD DEFINITIONS</u>	
\vec{F}_1	Dynamic reactions at balloon nose probe/latch interface resulting from wind loads on balloon structure
\vec{F}_2	Vertical load at nose probe resulting from tendency of balloon to pitch up under all wind conditions
\vec{F}_3	Loads imposed under survival type wind conditions (without balloon)
\vec{F}_4	Combination of loads including dead weight of cart, personnel weight, and weight of electronic hardware. This combined load can be off-center.
\vec{F}_5	Combined dead load and live load on boom and platform
\vec{F}_6	Concentrated weight of payload acting anywhere on work platform
\vec{F}_7	Tether load imposed by balloon flying in 70 knot winds (including appropriate load factor)
\vec{F}_8, \vec{F}_9	Loads transferred from the balloon suspension lines to the platform - resulting from both buoyancy loads and balloon side forces. These loads are affected by the braking friction loads (\vec{F}_{11})
\vec{F}_{10}	Balloon aft close-haul line loads
\vec{F}_{11}	Braking load
\vec{F}_{12}	Emergency forward close-haul line load
\vec{F}_{13}	Maximum net lift
<u>LOADING COMBINATIONS</u>	
.	Balloon moored in 90 knot winds: $\vec{F}_1 + \vec{F}_2 + \vec{F}_5 + \vec{F}_8, \vec{F}_9$
.	Balloon flying in 70 knot winds ($q = 3.2'' H_2O$): $\vec{F}_5 + \vec{F}_7$
.	Balloon close-hauling in 40 knot winds: $\vec{F}_5 + \vec{F}_{10} + \vec{F}_{12}$
.	Balloon/electronic maintenance in 40 knot winds: $\vec{F}_4 + \vec{F}_5 + \vec{F}_6 + \vec{F}_8, \vec{F}_9 + \vec{F}_{11}$
.	Mooring system survival in hurricane winds: $\vec{F}_3 + \vec{F}_5$

The structural analysis is based upon these load combinations, using a minimum factor of safety of 1.5. In addition, a dynamic magnification factor of 2.0 is used on all design loads where shock loading occurs. AISC specifications are used whenever applicable.

4. SITE REQUIREMENTS

A reasonable level area approximately 500 feet in diameter is needed to provide adequate ground clearance for the moored aerostat. A 12 foot x 12 foot x 2-1/2 foot high concrete pedestal is located at the center of this area. This pedestal contains forty-eight 1-1/4 inch diameter studs in a circular pattern to which the central bearing mounts.

Concrete footings are also provided for the monorail. These footings can either be a full circle of concrete or smaller footings at each rail anchor point. One inch diameter studs are imbedded in these footings for anchoring the monorail.

The remaining area need not be paved. However, gravel or some other stabilizer is necessary to carry erection and maintenance equipment.

A second level surface is necessary in the immediate area where the aerostat can be laid out and inflated. This area should be about 100 x 300 feet, with the long axis aligned with the prevailing wind direction, and located such that the transfer of the aerostat to the mooring system can be accomplished over a minimum distance.

4.1 Component Description

4.1.1 STRUCTURAL COMPONENTS

4.1.1.1 Nose Latch (Figure 10)

This is the mechanism which attaches the nose structure of the balloon to the mooring system. It restrains longitudinal and lateral motion of the aerostat nose, but allows ± 15 degrees of angular mis-alignment in the horizontal and vertical planes during the docking maneuver. The nose line from the aerostat is threaded through the center of the latch, around a pair of 10 inch diameter sheaves, through the center of the mooring mast and finally onto the nose line winch located at the top center of the machinery enclosure. Unlatching is accomplished by activating two electrical solenoids in the latch using a single switch in the operator cab. Latching requires no electrical current and is accomplished simply by pulling the aerostat nose structure probe into the latch with the nose line winch. Two indicator lights in the operator cab show the state of the solenoids in the latch.

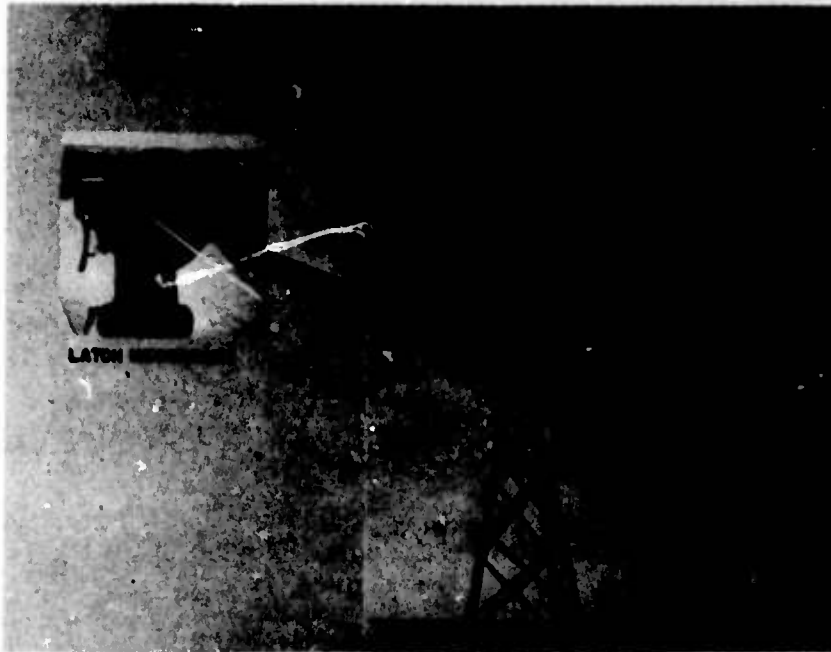


Figure 10. Nose Latch

4.1.1.2 Mooring Mast (Figure 11)

A 34-foot tapered mast bolts to the top center of the machinery enclosure. It is square in cross section and fabricated from steel tubing and angle structural members. A steel plate at the top supports the latch mechanism. A ladder with a safety climb device is provided on one face of the tower.

4.1.1.3 Machinery Enclosure (Figure 12)

A 9-foot high x 12-foot wide x 31-foot long structure provides a base for the main tether winch and the auxiliary power unit (APU), support for the mooring mast and attachment for the nose line winch and operator's cab. The center base area of this structure mates to the central bearing using forty-eight 1-1/4 inch diameter bolts. It is fabricated from structural steel, pre-drilled for field assembly. The inside machinery deck is steel tread plate and the upper deck is steel and aluminum plate. The siding is corrugated, translucent fiberglass or galvanized iron. Access doors are provided at each end of the structure. Stairway, ladders and railings are provided for access to all areas.



**Figure 11. Mooring System
under Construction**

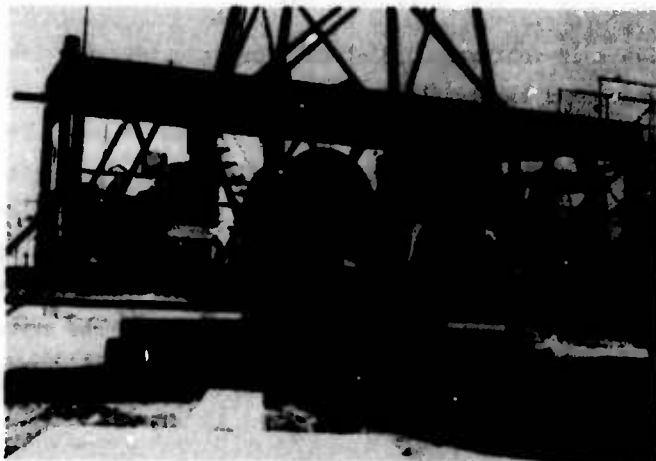


Figure 12. Machinery Enclosure Prior to Siding

4.1.1.4 Central Bearing (Figure 12)

An 8-foot nominal diameter ball bearing supports the mooring system on the central axis. The lower race of this bearing attaches to a ring of concrete anchored studs. The upper race is bolted to the main superstructure of the system. This bearing has integral gear teeth on its inner circumference through which the torque to rotate the system is transmitted.

4.1.1.5 Boom Assembly (Figure 11)

The current boom* consists of four welded structural members, each 45 inches square. Three of the sections are 22-1/2 feet long. The fourth section is 11-1/4 feet long and is used with the CBV-350A aerostat. These are bolted together, end to end. The inboard end is bolted to mounting brackets on the machinery enclosure, and the outboard end is attached to a tubular bearing structure (boom end assembly) which rests in the mating tubular frame of the fairlead trolley assembly. The main aerostat tether cable is routed through the center area of the boom. When slack the tether cable is supported by a sheet metal tray within the boom. The top surface of the boom is covered with steel tread plate for its full length to provide a walkway. Two auxiliary tie points are located at midspan and have a load capacity of 7,000 pounds each. The top chords of the boom are completely flat end to end and are designed to accommodate a scissor-type, traveling platform used to service the underside of the aerostat.

4.1.1.6 Payload Service Platform (Figure 11)

A 16-foot wide x 22-foot long platform is located at the outboard end of the boom to provide a work area for installing and servicing the airborne payload. It is supported by the boom and by two rollers which rest on the circular rail. The platform is fabricated from structural steel and covered with steel tread plate. When the aerostat is moored, its auxiliary suspension lines are attached to the side edges of this platform and the excess suspension lines are stowed in boxes provided with the platform. The platform surface is flush with the top of the boom and provisions are made on this surface to allow the traveling service platform to traverse the full length of the payload service platform. A stairway is mounted to the outer end of the platform for access from ground level.

*Note: Earlier booms were triangular in cross section and somewhat shorter. Also, at that time the tether cable was located above the boom.

4.1.1.7 Fairlead Trolley Assembly

This trolley or truck, located on the circular rail at the outboard centerline of the boom, supports the boom end and provides the mounting for the flying sheave. Four steel rollers support this assembly on the rail in normal operation. In extreme flight conditions (i.e., when tether cable tension is high), the assembly is restrained from lifting away from the rail by four additional trolley wheels which contact the underside of the rail flange. The boom end is attached to the fairlead trolley through a longitudinal slip joint which allows for rail eccentricities and thermal expansion differences up to \pm one inch. The flying sheave has a nominal pitch diameter of 22 inches and is mounted such that the horizontal component of tether cable tension is transferred to the boom as a compressive load while the vertical component transfers directly to the circular rail. The sheave assembly is free to rotate in the plane perpendicular to the boom, but is counterbalanced to remain erect under no load. When not in use, the sheave assembly can be rotated and locked in a horizontal position. Any tether cable groove diameter for the sheave pulley can be used up to about 1-1/4 inches, depending upon the tether cable selected. The cable diameter must also be specified for the main winch.

4.1.1.8 Circular Rail (Figure 11)

Ten inch standard I-beam sections nominally 20 feet in length are rolled to form the circular rail. Each rail section has three mounting plates for stud attachment to the concrete base. The rail sections are connected end to end using steel link plates and bolts. The rail assembly is fabricated from corrosion resistant steel and requires no surface finishing once installed.

4.1.1.9 Close-Haul Trolleys (Figure 7)

Two additional steel wheeled trolleys ride on the rail nominally 15 feet on either side of the flying sheave trolley. The close-haul winches which operate the center handling lines of the balloon are mounted on these trolleys. The trolleys are connected to the flying sheave trolley by pin-ended steel tension members. Like the fairlead trolley, they are restrained from upward movement by four flanged trolley wheels which bear against the underside of the circular rail flange. These trolleys have hand-wheel operated brakes which, when set against the top of the circular rail, restrain rotational movement of the entire system. Two hydraulically operated winches furnish the main mooring restraint to the balloon. These winches are located on the close-haul winch trolleys.

4.1.1.10 Electrical System

Standard equipment furnished with this unit includes a slip-ring assembly and all the electrical components to provide service to the machinery enclosure. The slip-ring assembly, located at the center of the central bearing, has 48 conductors (40 each, 5 amp and 8 each, 25 amp). The feeder service to the slip-ring assembly can be obtained from a local source or from on-site generators. The electrical service to the machinery enclosure consists of a four circuit, 25 amp breaker box with main breakers, internal vapor-tight, overhead lights, exterior lights at each doorway, internal and external duplex receptacles, and the circuitry to operate the nose latch. Thin wall EMT conduit is used throughout. Two 24-inch exhaust fans provide ventilation to the machinery enclosure. An intercom system links the operator cab, the ground crew and the central van. Flood lights on the structure and on mobile carts provide illumination for night operations.

4.1.1.11 Lightning Protection

The entire mooring system is internally grounded. A large slip-ring, concentric with and outside of the central bearing, carries the common ground to earth. When the balloon is moored its lightning protection system is electrically coupled to the mooring system. When aloft lightning and/or atmospheric potential is carried off from the steel tether cable to ground through brushes on the circular rail.

5. POWER, CONTROLS AND WINCH SYSTEMS

5.1 Main Tether Winch (Figure 13)

The main tether winch utilized on the TCOM system is the OECO Model 30W traction type. This dual-capstan, line-pulling system is 18 feet long, 9 feet 2 inches wide, and 7 feet 8 inches high. It weighs approximately 19,000 pounds. It has a maximum line pull capability of 30,000 pounds and a maximum line speed in excess of 200 feet per minute. The triangular design of the capstan frame allows the line tension sheave to be located just below the top capstan. The tether line passes from the upper traction sheave, around the tension measuring sheave, to the flying sheave. The load cell on the tension sheave is a hydraulic diaphragm compression unit. This unit supplies pressure to the visual tension indicator gauge in the control cab, and also supplies the signal for the high and low tension alarms. The load cell supplies pressure to an electrical transducer for remote transmission of the tension readings.

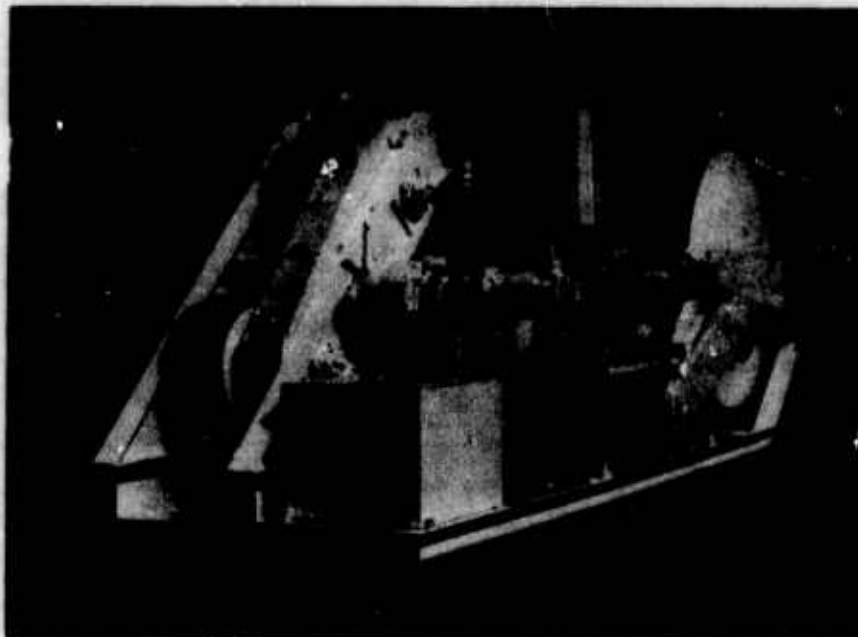


Figure 13. Main Tether Winch

The power to rotate the traction capstans is a hydraulic motor driving into a planetary gear box to a chain drive to the upper capstan. Both capstans are linked together by a quad chain drive.

The storage drum on the 30W winch has a capacity of 16,500 feet of one inch tether cable. The storage drum is driven by a high torque hydraulic motor through a roller chain drive.

The power for the main tether winch is a six-cylinder, two-cycle diesel engine which supplies 154 net continuous horse power at 1,800 rpm. This prime mover drives four hydraulic pumps: one pump on the flywheel end; one on an auxiliary drive on the front of the engine; and two pumps on the cam shaft towers.

The hydraulic fluid for the traction drive is supplied by a variable volume bi-directional axial piston pump mounted on the flywheel end of the engine. The auxiliary pump on the front of the engine supplies fluid to the nose line winch and to the rotary drive for the machine enclosure and tower structure. This pump is a variable volume pressure compensated design.

The variable volume pressure compensated pump on the cam tower supplies the fluid for the drum drive motor and brake controls. Both the main winch and the close-haul winches are equipped with brakes that are automatically applied when the controls are placed in the neutral position or in the event of loss of hydraulic pressure.

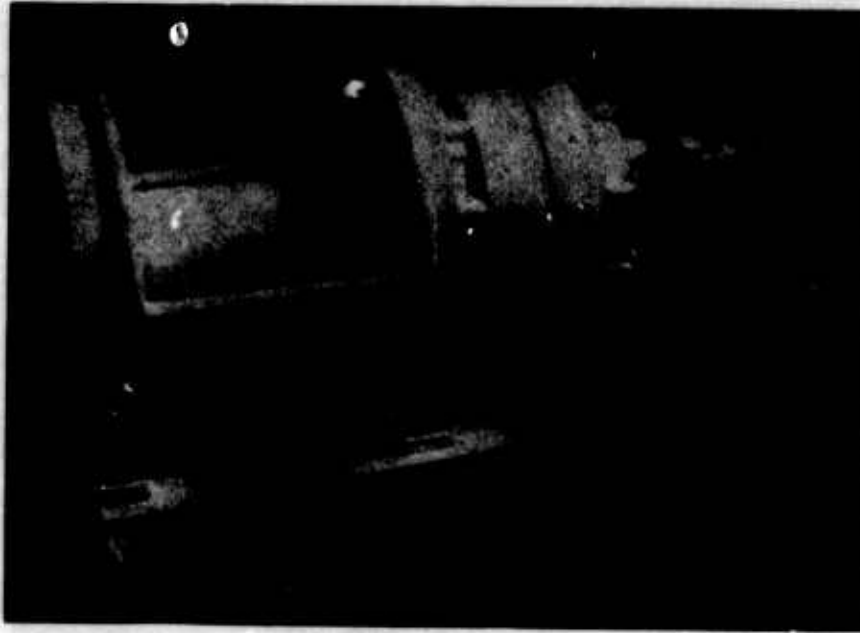


Figure 14. Close-Haul Winch

5.2 Close-Haul Winches (Figure 14)

There are four close-haul winches on the TCOM system and one nose line winch. These are all conventional windlass type winches identical in structure and performance. The drum is powered by a fixed vane hydraulic motor through a gear box with an automatic brake. The drum has a capacity of 300 feet of 3/4 inch rope and will provide 140 feet per minute line speed at 8,000 pounds pull. The drum core has a recessed knob for attaching the line to the winch. The knob is designed so that the eye splice on the end of the handling line can be easily attached and will also fall free when all the line is spooled off.

5.3 Rotating Drive

A gear train attached to the structure, powered by a high torque hydraulic motor, provides the rotary motion for the structure. Installed in this hydraulic circuit are adjustable valves. These valves are used to provide dynamic braking of the mooring system.

5.4 Auxiliary Power Unit (Figure 15)

The mooring system has a 140 horsepower auxiliary power unit for powering the close-haul winches. This unit is self-contained having its own fuel tank,

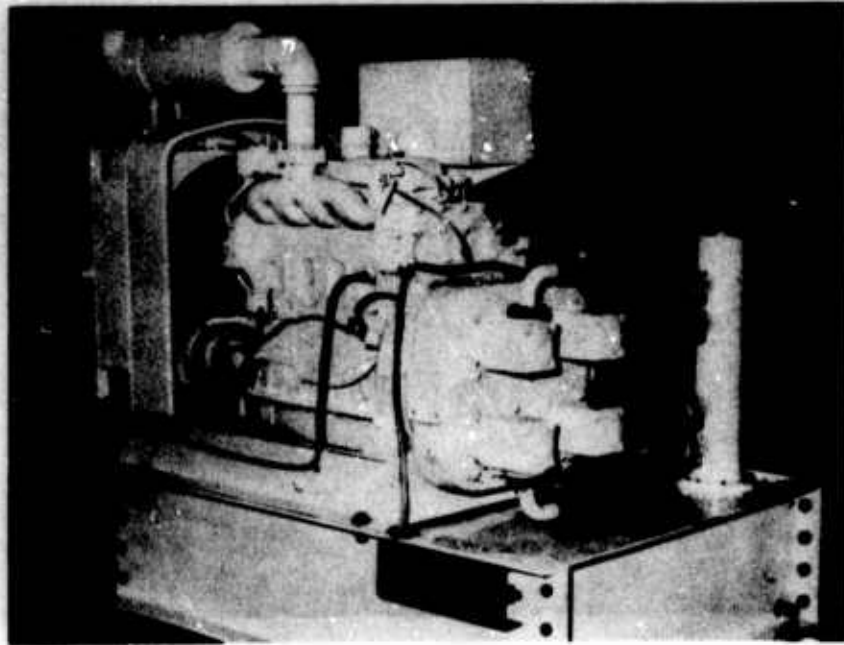


Figure 15. Auxiliary Power Unit

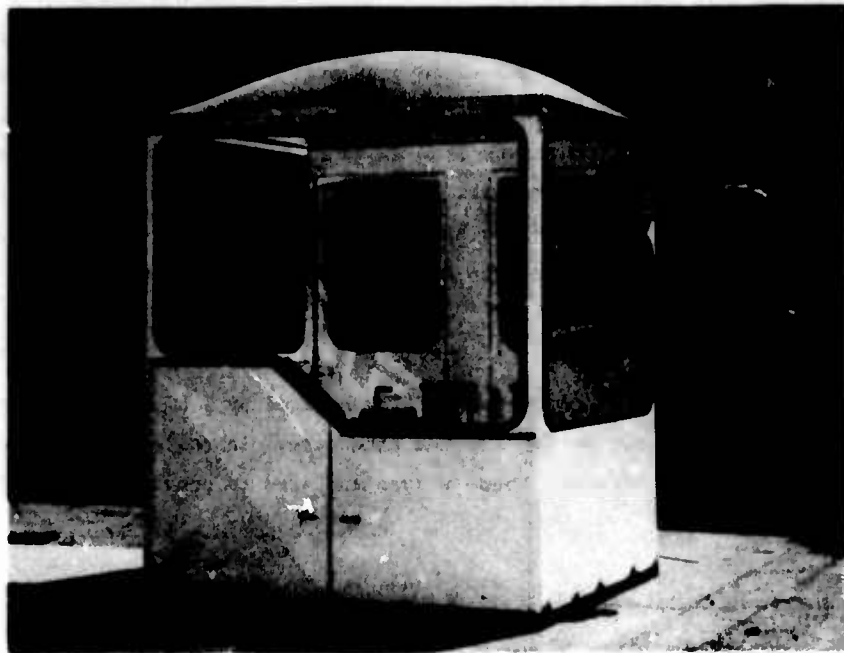


Figure 16. Control Cab

hydraulic reservoir and filter system. The four-cylinder, two-cycle diesel engine drives four 35 gallons per minute fixed vane pumps through a quad drive gear box. The hydraulic fluid is piped to the throttling control valves in the control cab where it is directed to the four close-haul winches.

5.5 Controls and Control Cab (Figures 16, 17 and 18)

A control cab is mounted to the front left side of the machinery enclosure. This cab is fabricated from steel and transparent lucite providing the operator with a clear visibility of the area. The transparent dome top of the control cab provides unlimited visibility upward.

When the operator is facing outward toward the flying sheave end of the boom, all the controls for the winches are in easy reach in front of him. The main tether winch control is on the right side; the close-haul, nose line winch and the rotating control are on the left side of the panel. The instrument panel is on the right side of the cab and is tilted for better visibility. This panel contains all the engine instruments and controls. These are in two groups; one for the main winch and one for the auxiliary winches and functions. The line tension gauge, line footage counter and the line speed and direction indicator are also located on the left side of the instrument panel in view of the operator. The panel also has indicator lights to alert the operator of various functions. Colored lights are used to indicate the nose latch condition, hydraulic filter condition and power-on or off conditions.

6. FUTURE SYSTEMS

Experience with the present aerostat mooring system and the stability of the balloon has prompted the elimination of the two inboard close-haul winches. This will eliminate the auxiliary drive on the front of the main tether winch engine. The nose line winch and the rotator can be powered by the separate pumps from the APU.

The forward close-haul lines will, however, remain on the balloon and can be used in an emergency to stabilize the aerostat.

The line tension sheave has been lowered in the substructure of the machinery enclosure to allow the tether line to pass through the boom structure.

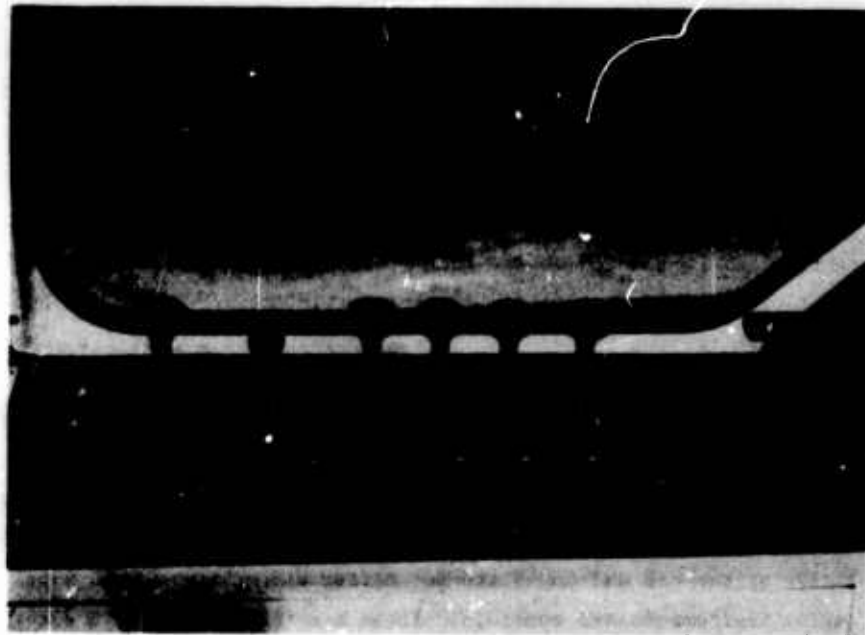


Figure 17. Control Panel

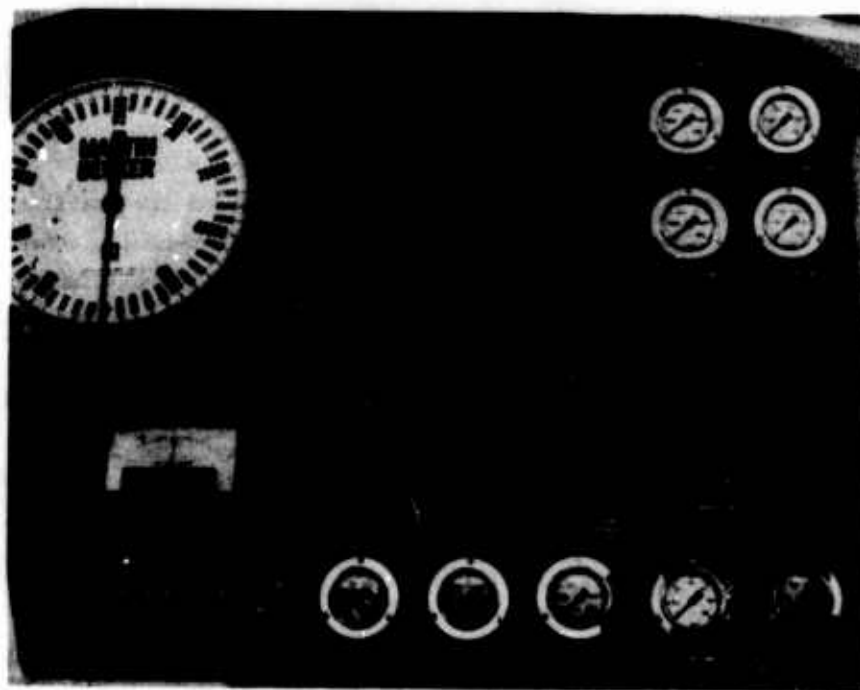


Figure 18. Instrument Panel

7. OPERATIONS

7.1 Launch

At the commencement of flight activities, the mooring system is braked with the aerostat into the wind. The close-haul winches on the rail inhaul the balloon slightly to loosen and release the aerostat suspension lines where they attach to the work platform. The nose is then unlatched and the nose winch and close-haul winches allow the balloon to rise. When the confluence of the balloon suspension system is clear, the outhauling is stopped long enough to attach the tether cable. Outhauling then continues, now on the three small winches and on the main tether winch, until the close-haul lines are completely unspooled. When the end of the nose line, to which is taped a smaller tag line, is approximately 50 feet above the latch, the nose winch is braked while outhauling on the main tether winch continues. The tape breaks and the free end of the tag line falls to the ground while the other end remains threaded through the latch and secured on or near the nose winch. This eliminates the need to re-thread the nose line through the latch during the recovery operation.

The aerostat is now restrained by the tether cable alone and is allowed to ascend to altitude at a nominal rate of 200 feet per minute. The mooring system brakes may be released and reset to allow for changing wind direction and tether cable azimuth during ascent.

7.2 Recovery

The retrieval operation is essentially the reverse of the launch sequence, with primary efforts directed at getting the nose line attached to its winch as quickly as possible.

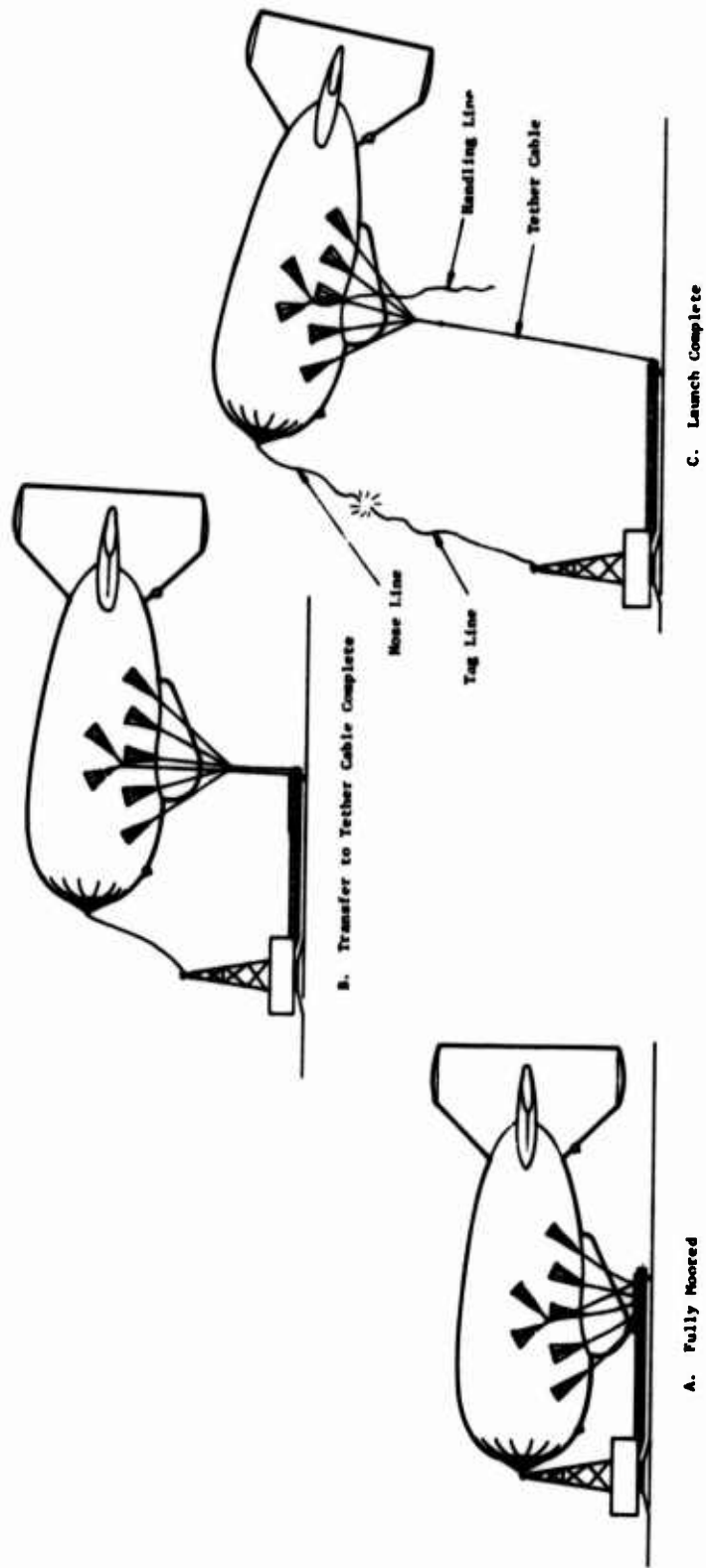


Figure 19. Launch Sequence

References

1. Hook, Thom (1973) Shenandoah Saga, Air Show Publishers, Annapolis, Maryland.
2. DeLaurier, J. D. (1972) A Dynamic Analysis for a Moored Aerodynamic Shaped Balloon Subjected to Atmospheric Turbulence, Sheldahl Engineering Report 150.
3. Lagerquist, D. R. (1974) CBV-250 Mooring Loads Parameter Variation Study, Sheldahl SAM-56-062.

Contents

- 1. Introduction**
- 2. Basic System Principles**
- 3. System Technology**
- 4. Applications**
- 5. Conclusions**

The TCOM System - Technology and Applications

**I. R. Susman and D. L. Spritzer
TCOM Corporation
Rockland, Maryland**

Abstract

This paper provides a summary description of a system which employs tethered aerostats as high altitude platforms for wide-area telecommunications and broadcast functions, and discusses some of the basic applications.

1. INTRODUCTION

TCOM systems capitalize on the height advantage of tethered aerostats to provide economical and dependable telecommunications and broadcast services over a large ground area. By suspending light-weight electronics payloads from stabilized platforms beneath the aerodynamically shaped aerostats, point-to-point and omni-directional communications can simultaneously be accommodated. The aerostats operate at altitudes between 10,000 and 15,000 feet above sea level. From these heights, line-of-sight extends to distances of 125 to 150 miles and the ground area covered ranges from 50,000 to over 70,000 square miles.

2 BASIC SYSTEM PRINCIPLES

The concept of using lighter-than-air vehicles as high altitude platforms for communication equipments has received much attention over a considerable span of time. Clearly, the extensive line-of-sight achievable and the free space electromagnetic environment indicated that low powered equipments carried aloft could be used to economically provide services over a rather wide area. However, problems relating to maximum achievable stability, load carrying limitations and availability of suitable power sources prevented practical realization of such a system until certain key technological advances were made. The most significant of these advances were development of high-strength but low-weight balloon hull materials, introduction of computer aids in optimizing aerodynamic design, and the miniaturization of electronic devices.

The TCOM system is capable of relaying voice communications, broadcasting TV, AM and FM radio directly to users, and providing many other specialized services. The design of the system permits these services to be provided simultaneously without experiencing interference. There are two major elements which make up the overall system: an airborne communications payload suspended beneath a tethered aerostat (referred to as the "airborne package") and a ground control station. When required for voice channel communications, any number of remote terminals are added to the system.

A single payload, suspended beneath an aerostat, at 10,000 feet, provides coverage over distances of 250 miles and serves a ground area greater than 50,000 square miles. Operating at 15,000 feet, the payload range increases to 300 miles and the ground area covered is in excess of 70,000 square miles. This is considered the local coverage area.

Long-line equipment permits transmission and reception of communications data between two or more aerostats to greatly extend this coverage area. For example, when a second TCOM system is added to the first one (Figure 1), long-line information transfer is available from anywhere within the ground area covered by the first airborne package to anywhere within the ground area covered by the second. Since the distances between aerostats operating at 10,000 feet are on the order of 250 miles, communications between two points as much as 500 miles apart can be accommodated and the combined ground area covered is at least 100,000 square miles.

The equipment that controls the airborne electronic system, monitors the status of the airborne equipment, monitors vital aerostat operating parameters, and performs signal processing functions is located at the ground control station. Typically, this equipment is housed in a mobile van, located near the aerostat launching complex, which acts as the hub of system operation.

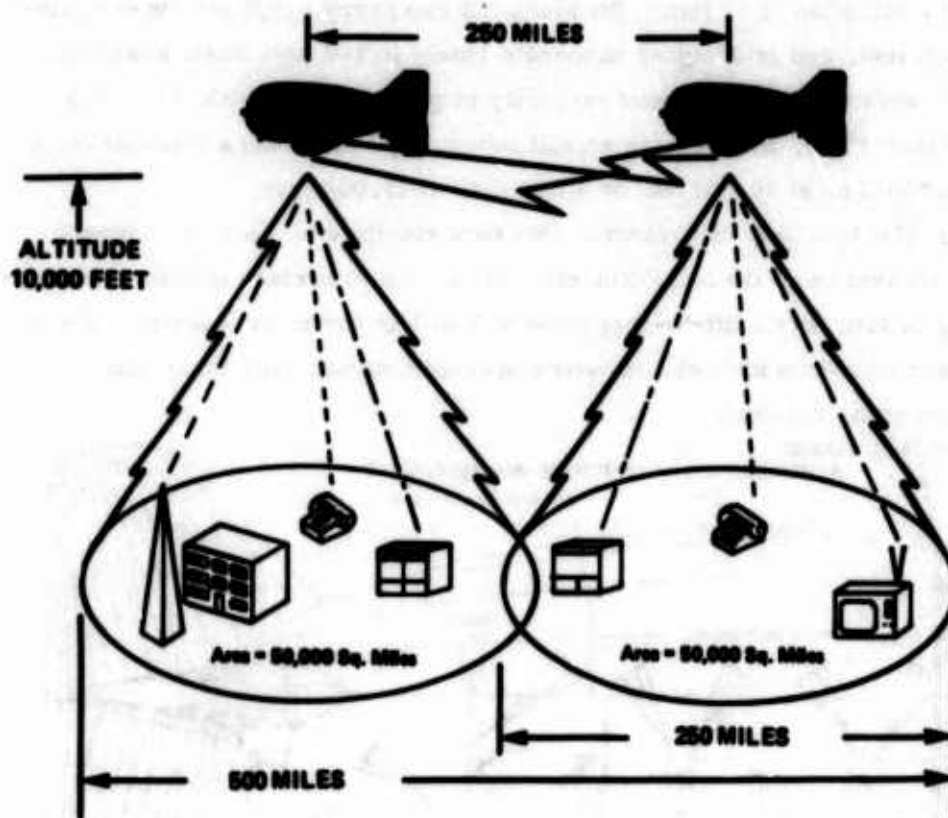


Figure 1. TCOM System Concept

3. SYSTEM TECHNOLOGY

3.1 Aerostats

TCOM aerostats are unmanned, lighter-than-air, tethered vehicles that not only derive buoyancy from helium but also have aerodynamic lift that positively offsets drag in a wind environment. The general arrangement of these aerostats is typically represented by the Mark VII configuration shown in Figure 2. This vehicle has a minimum volume of 250,000 cubic feet, a length of 175 feet, a diameter of 56.8 feet and a tail span of 82 feet. The Mark VII can carry 4,000 pounds of equipment to 10,000 feet, and is designed to operate safely in 100 knot winds at altitude. A "stretched" version of this aerostat currently in production, the 380,000 cubic foot volume Mark VII-S, will have an overall length of 215 feet and a load-carrying capacity of 8,000 lbs at 10,000 feet or 4,000 lbs. at 15,000 feet.

Each aerostat is a body of revolution with four stabilizers spaced 90 degrees apart on the aft section of the hull. The ratio of volume to surface is high, the aerodynamic drag is low, and a lift-to-drag ratio of 3 to 1 is normally obtained. Electrically-powered blowers and release valves operate automatically to maintain pressurization of the ballonnet.

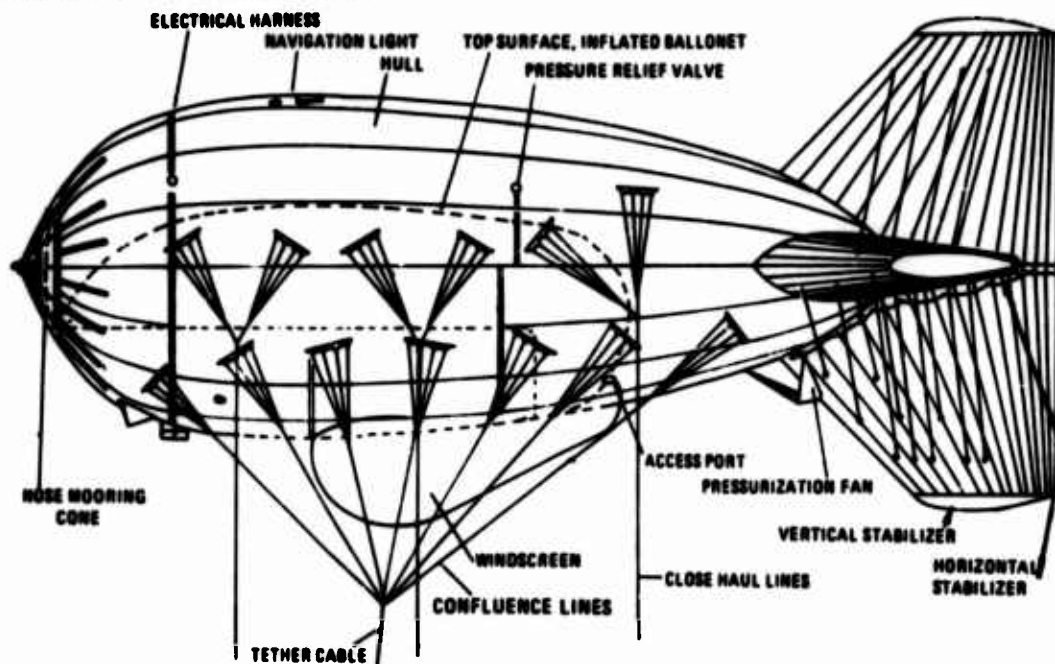


Figure 2. Mark VII Aerostat Configuration

To optimize the load-carrying capability of TCOM aerostats, advantage is taken of the latest developments in material engineering such as the light-weight but high-strength laminate used for the aerostat hull. The laminate weighs only 8.25 ounces per square yard and consists of adhesive bonded layers of tedlar, mylar films, and dacron fabric arranged as shown in Figure 3.

The tedlar film has excellent weather and abrasion resistance which protects the other components in the laminate. The two mylar layers form an efficient gas barrier. The dacron fabric provides the strength to withstand the loads induced by normal inflation, attachment of payload and inflight loading, with a $\geq 100\%$ safety factor. The dacron also has good dimensional stability and imparts a high degree of tear resistance to the laminated material.

The aerostat maintains its position in the immediate vicinity of the launch site by means of a single steel tether with a .4-inch diameter, a weight of 260 lbs/1000 feet and a breaking strength of $>20,000$ lbs. Under development is a conductive steel tether which will carry high voltage from a ground source up to the aerostat. This tether will be an electromechanical coaxial cable consisting of a copper inner conductor insulated with TPX and armored with high strength steel wires providing the strength member and the outer conductor. The conductive tether will have a diameter of $\approx .45$ inches, a weight approximating 330 lbs/1000 feet and will provide a breaking strength of 28,000 lbs. Utilization of this conductive tether will extend continuous at-altitude operating time up to six months.

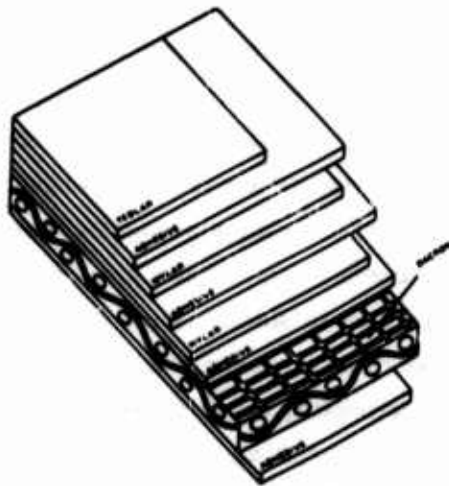


Figure 3. Mark VII Hull Material

3.2 Airborne Payload

The airborne electronic equipment which requires stabilization and the directional antennas are integrated into a compact, accessible, modularly-constructed airborne package. Off-the-shelf, light-weight, reliable electronics with low power consumption utilizing integrated circuits, thin film, thick film, stripline and microstrip techniques form the package. This unit, referred to as the stabilized electronics structure (SES), is suspended from the aerostat by means of a gimbal assembly which decouples the electronics platform and reduces the effects of aerostat movement. The airborne electronic units not requiring stabilization are typically mounted on aluminum structures laced to the aerostat skin. During flight, an aerodynamically-shaped windscreen provides environmental protection.

The TV broadcast antennas are usually vertical masts providing omni-directional coverage. Separate radiating elements are used for visual and aural broadcast.

Because the beamwidth of the TV broadcast antenna varies inversely with frequency, Band I VHF antennas do not require stabilization. Consequently, a broadcast antenna for Band I can be fixed rigidly in the vertical fin of the aerostat. A Band III VHF antenna, however, normally requires a degree vertical stabilization and is suspended within the aerostat gas envelope.

A typical payload mounting arrangement is shown in Figure 4.

For each system, the payload configuration depends on the particular application. A typical payload might include commercial and educational TV, AM and FM radio broadcast equipment; off-the-air receivers; translating equipment; high and low density wide-band communications equipment for fixed and mobile multichannel voice and data transmission. The payload may also include equipment to perform other diverse functions such as wide area paging, emergency radio broadcasting, wide area data collection; remote area meteorological observation and optical scanning and monitoring. A stabilized structure now providing television broadcasting and point-to-point communications is shown during final checkout in Figure 5.

The payload is stabilized by an airborne mechanical system that provides almost an order of magnitude decoupling between aerostat and payload movement. Since the aerostat movements are gradual, small changes, the decoupled platform is extremely stable, with package motions seldom exceeding .5 degrees. The airborne mechanical system consists of a two-axis gimbal assembly acting as a two-axis pivot from which the entire airborne payload is suspended, in pendulum

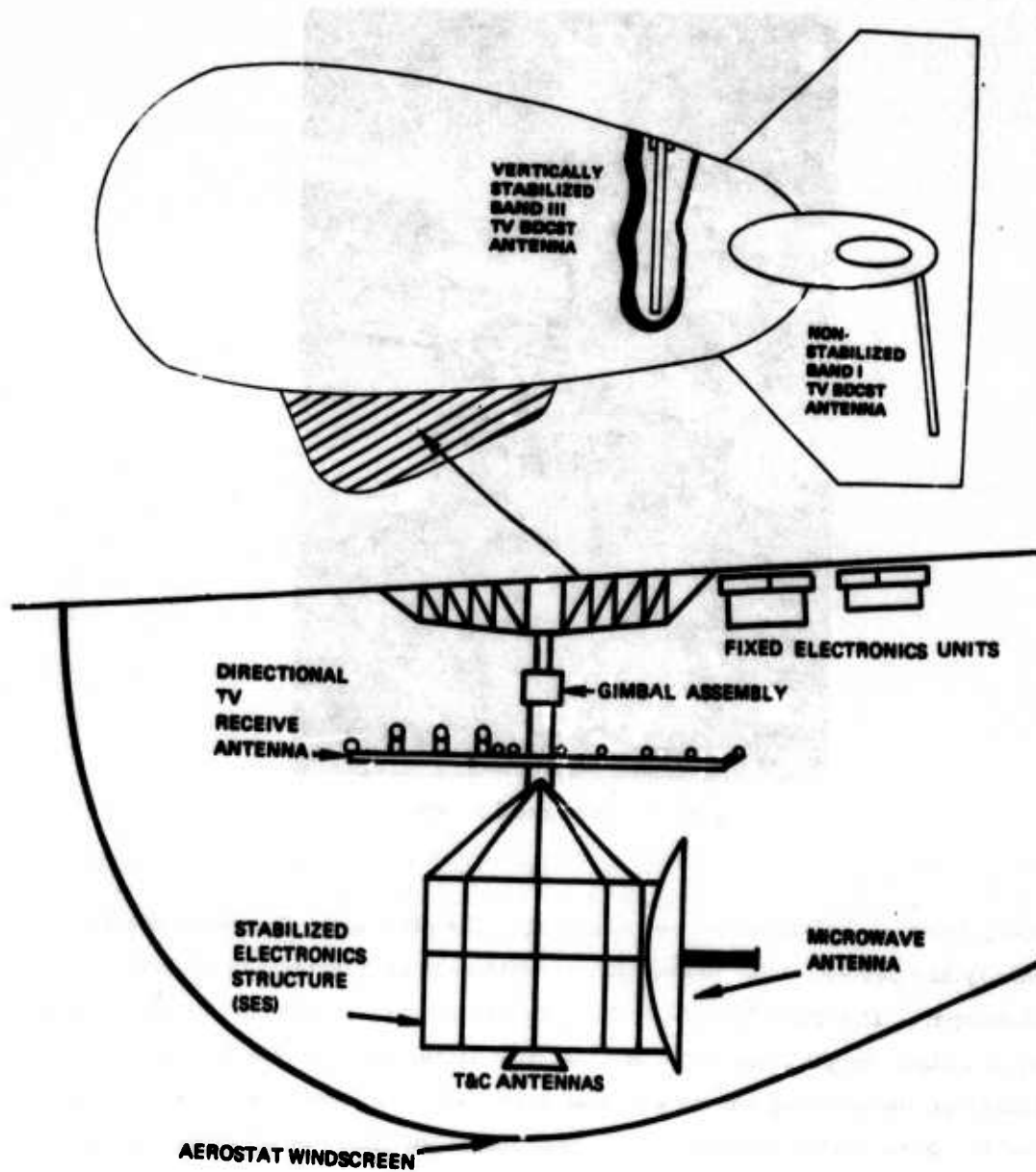


Figure 4. Typical Payload Mounting Arrangement



Figure 5. Stabilized Structure

fashion, from the bottom of the aerostat hull. The pitch and roll axes of the gimbal assembly are perpendicular to each other, with each axis damped by a rotary viscous damper. The upper linkage on the gimbal assembly is mounted to the aerostat through a light-weight truss structure that distributes the airborne package weight and inertial loads throughout the aerostat skin. The azimuth drive shaft, attached below the lower gimbal linkage, is the mechanical portion of an azimuth heading servo loop. The drive system receives an electrical signal from the servo electronics and converts it into mechanical rotation of the payload package to maintain proper heading referenced through a magnetometer to magnetic north, as the aerostat yaws. The slip ring assembly incorporated into the airborne package allows unrestricted azimuth motion between the payload and the aerostat. The ring is located at the upper end of the azimuth drive where it is attached to the lower linkage of the gimbal. An azimuth positioning of $\pm 0.5^\circ$ pointing accuracy, controllable in 0.1° increments is achieved.

3.3 Airborne Power Generation

The primary airborne power unit consists of a Sachs-Wankel rotary combustion engine of approximately 18 hp (at 4500 RPM) directly coupled to a three-phase brushless generator with a voltage regulator. Several such engine-generators are carried aloft on each aerostat. Compared to conventional engines, the rotary engine is lighter, consumes less fuel, has superior remote start-up characteristics and contains fewer moving parts. Each 400 Hertz, 120/208 volts AC alternator provides a 5-kilowatt power output at operational altitudes. A power distribution unit, a "thin-skin" 200-gallon spherical aluminum fuel tank, and a fuel supply system including pumps, hose manifold, pressure controls and fuel filters complete the airborne power system.

3.4 Telemetry and Command System

The telemetry and command system controls and monitors all the communications equipment on board the aerostat. Vital aerostat data including such functions as altitude, pitch, roll, heading and temperatures are also monitored. The system consists of a ground control section, typically housed in the mobile van at the ground control station, and an aerostat control section carried aloft by the aerostat.

Two different frequencies are used: one for commands (uplink); the other for telemetry (downlink). The aerostat control section contains two identical downlink (aerostat to ground) transmitters and two identical uplink (ground to aerostat) receivers. The ground control section similarly contains redundant uplink transmitters and downlink receivers. This redundancy, coupled with an automatic switchover capability, affords a high level of system reliability.

The 28 volts dc power for the telemetry and command system's transmitters and receivers aboard the aerostat is normally provided by the main airborne power supply system. A trickle charge is also supplied to maintain a backup battery pack. In the event of loss of prime power, automatic switchover to the backup battery pack ensures continued operation.

3.5 Mooring System

During periods of maintenance and servicing operations, the aerostat is docked to a ground service installation, commonly called the mooring system. The nose structural members, attached to the forward section of the aerostat, provide the

mechanical attachment for the flexible aerostat to the rigid mooring tower. The aerostat nose structure is capable of safely carrying the wind loads impressed upon the aerostat. The entire nose structure is fabricated from high strength aluminum alloys.

The mooring system, shown in Figure 6, is a carefully integrated design which incorporates all the mooring equipment such as the mooring tower, main tether winch, nose line winch, close haul winches, monorail, flying sheave, and work platform. Each mooring system provides complete facilities for aerostat launch, flight and retrieval. A rotational drive system orients the moored aerostat nose forward for least resistance into the wind.

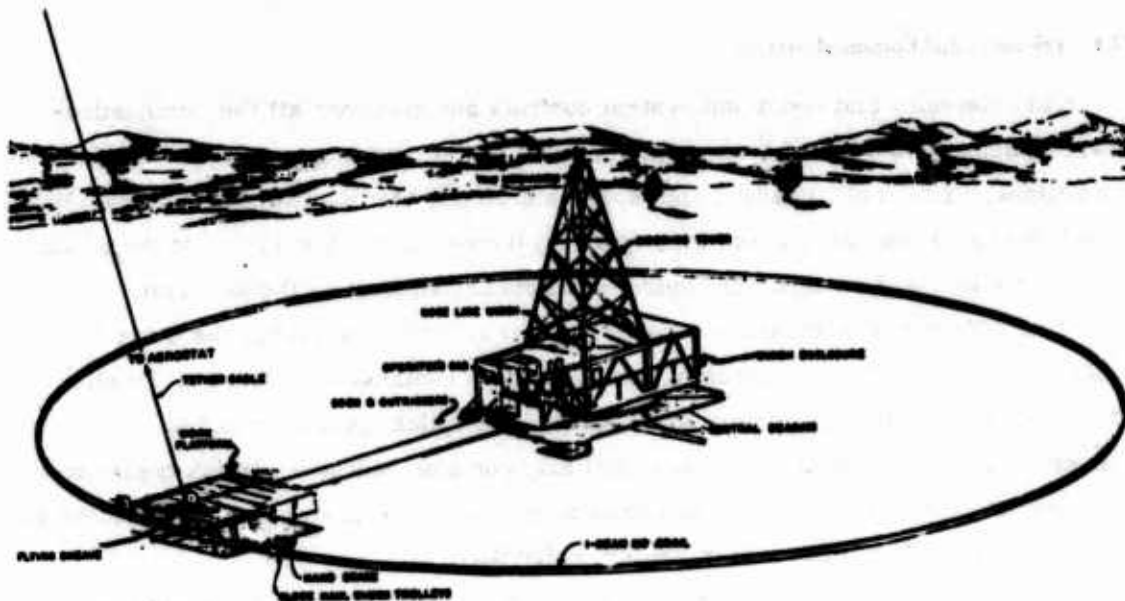


Figure 6. Aerostat Mooring System

4. APPLICATIONS

Several important applications for the system have been previously noted in this paper. In this section, a generalized model system will be used to demonstrate how a number of these applications are implemented. While a detailed discussion of propagation theory and analysis of performance are outside the scope of this paper, pertinent data are included for each application.

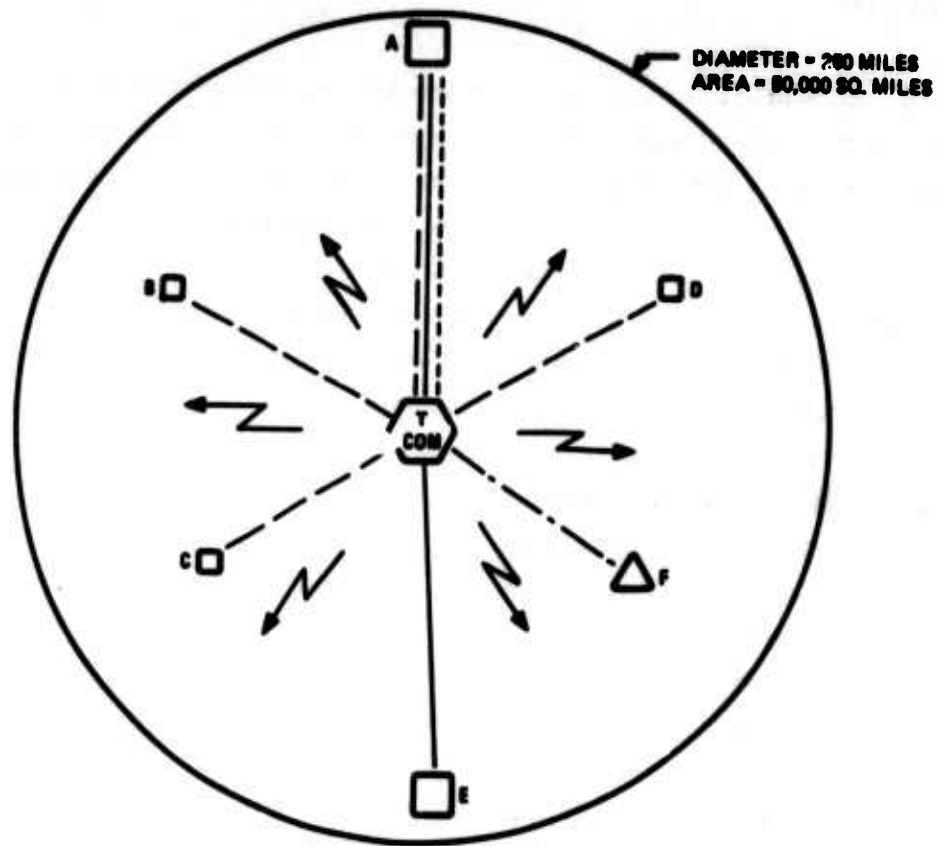
The generalized model system is represented by Figure 7, which diagrams the approximate coverage area of an aerostat system operating at 10,000 feet above sea level. The services provided by this system are:

- 1 color television broadcast program
- 1 FM radio broadcast program
- 1 high density radio relay system
- 1 low density radio relay system
- 1 VHF transponder

The system is based on the following set of assumptions.

- (a) City A is a major city within the aerostat coverage circle with a broadcast studio for originating television and radio programming.
- (b) Cities B, C and D are minor cities within the aerostat coverage circle. There is a requirement for 20 telephone and 10 telegraph channels from Cities B and C to City A. City D requires 10 telephone and telegraph channels to City A.
- (c) City E is a major city within the aerostat coverage circle. There is a requirement for 900 voice channels and 100 telegraph channels between City A and City E.
- (d) Point F is a control post. There is a requirement to contact vehicles traveling anywhere within the coverage circle from Point F.

Referring to Figure 7, the broadcast signals (TV video + audio, FM audio) are transmitted from City A to the aerostat over a one way studio/transmitter type radio relay link. TV audio and FM radio are carried on the radio relay baseband above the video on frequency modulated subcarriers. In the aerostat electronics systems, Figure 8, an airborne receiver demodulates the radio relay signal and passes the TV video + audio to the TV broadcast transmitter, the FM audio to the broadcast transmitter.



APPROXIMATE DISTANCES (MILES)

CITY A TO CITY B: 105
 TO CITY C: 175
 TO CITY D: 105
 TO CITY E: 235

LEGEND

- HIGH DENSITY RADIO RELAY
- VIDEO RADIO RELAY
- · - · - · LOW DENSITY RADIO RELAY
- VHF
- BROADCAST

Figure 7. Generalized System

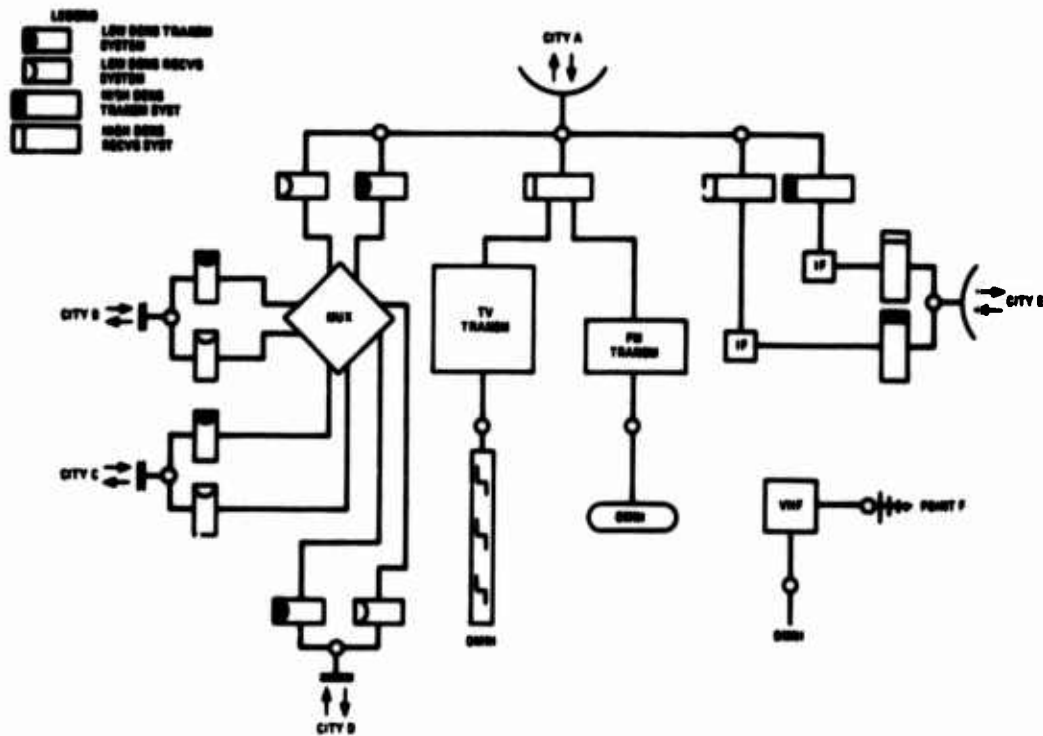


Figure 8. Airborne Electronics System

The voice and telegraph channels connecting Cities A and E are multiplexed at the city terminals and form a baseband which modulates a microwave carrier. Transmission to the aerostat is over a high-density type radio relay link, with the aerostat acting as a heterodyne repeater. Signal amplification occurs at an intermediate frequency. Demodulation to baseband at the aerostat is not necessary.

In the low density radio system all radio signals are demodulated to baseband at the aerostat. A multiplexer (basic group translators) rearranges the circuit groups originating in Cities B, C and D and forms them into one baseband for

transmission to City A. (The low density radio link between City A and the aerostat also carries supervisory and telemetry information for retransmission to the aerostat ground station.)

Control point F amplitude or frequency modulates a VHF carrier and transmits this signal over a directional antenna to the aerostat. A VHF transponder translates the VHF signal to a new frequency and retransmits it with an omnidirectional antenna over the entire coverage circle. Vehicle to control point communications are achieved in the reverse manner.

A typical frequency allocation scheme for the model system would be:

- Television broadcast Band I or III
- FM broadcast Band II
- Video radio relay 1.7 - 2.3 GHz
- High density radio relay 1.7 - 2.3 GHz
- Low density radio relay 380 - 470 MHz or 790 - 960 MHz
- VHF land mobile 140 - 170 MHz

Other possibilities include Band IV for television, 4 and 6 GHz for video and high density radio relay, 2 GHz for low density radio relay, and UHF for land mobile control. Medium wave AM broadcast is also feasible. The telemetry and command system would operate in the 1.7 - 2.3 GHz band.

4.1 Broadcast Coverage

The TCOM system has an inherent advantage over conventional broadcast systems in its ability to cover a vastly greater area with a single transmission system. Lower costs, frequency conservation and performance improvement are the ultimate results. Since broadcasting in the United States is regulated by the Federal Communications Commission (FCC), FCC regulations are used here as a basis for comparing the TCOM system performance with that of conventional broadcast systems. FCC describes coverage in terms of field strength leading to Grade A or B picture quality. Considering lower VHF band, the median field strengths required for channels 2 - 6 are $2,500 \mu\text{v/m}$ (68 dB_U) for Grade A, and $225 \mu\text{v/m}$ (47 dB_U) for Grade B service. The factors affecting the actual received field strength are so numerous and difficult to predict that a statistical approach is used. This approach predicts field strength present in the best 50% of receiving locations for 50% of the time. Using the results of actual observations and considering a typical receiving

To make the long radio relay paths more reliable, TCOM usually provides these in a frequency diversity configuration. The system availabilities indicated in Table 1 are based on CCIR report 338-1 (Volume II, Part 1, Pages 114-127) and prove the high performance quality of the TCOM system for high density telecommunications and wideband intelligence (TV) applications.

5. CONCLUSIONS

This revolutionary telecommunications and broadcast system is now operational and offers great economical and technical advantages over many conventional systems as well as augmenting existing systems. While the electronics configuration is engineered for each program's applications, the basic platform, aerostat and mooring system are completely developed. Consequently, the system is available with short delivery schedules. A complete system for modern, wide-band communications, broadcast and other applications can be operational in approximately one year. A TCOM aerostat system has been operating in The Bahamas for the past year at altitudes up to 13,500 feet above sea level, providing communication and TV broadcast coverage over an area of some 60,000 square miles with excellent performance substantiating predictions. Figure 9 shows this aerostat system in flight.



Figure 9

system with assumed noise figure and antenna gain, the FCC (in Volume III of The Rules and Regulations of the Federal Communications Commission 1972, Part 73, pages 289 and 291) provides charts to be used for estimation of field strength. Conventional transmission is normally restricted, by practical considerations, to an effective tower height of 1000 feet. A TCOM relay is nominally at an altitude of 10,000 feet.

The standard TCOM Band I TV Transmitter coupled with an omni-directional antenna radiates with a minimum ERP of 2.5 KW, while the Band III TV transmitter yields at least 5.0 KW ERP. From an altitude of 10,000 feet the following field strengths in dB above $1 \mu\text{V}/\text{m}$ are obtained:

<u>Distance (Miles)</u>	<u>Band I</u>	<u>Band III</u>
30	77	80
62	68	72
125	47	54

Even at the extreme, the field strengths at 125 miles from the transmitter site are sufficient to provide acceptable TV picture quality with standard receivers and normal antennas. With high gain receiving antennas and low noise preamplifiers the picture quality at 125 miles is excellent and the acceptable coverage range extends on to approximately 155 miles. Similar considerations apply to AM and FM radio. This performance is possible because the TCOM transmitter is operating essentially as a free space transmitter and does not experience the normal ground losses associated with terrestrial systems.

It is important to note that these coverages are conservatively based on line of sight from an aerostat operating altitude of 10,000 feet. Since operating altitude is normally between 10,000 and 15,000 feet and radio waves normally follow a 4/3 earth curvature, superior coverage may be expected.

4.2 Telecommunications Performance

The TCOM platform acts as a very tall tower for relaying signals carrying multichannel voice, data or program messages. Table 1 indicates performance analysis for a hypothetical microwave path of approximately 90 miles, at 2, 6 and 8 GHz.

The size of the airborne antenna is limited by the space availability, while the size of the ground antenna is constrained by the maximum beamwidth that can be

tolerated by the required performance level. With the pointing error and the indicated permissible blow-down figures, a blow-down and pointing loss, proportional to the calculated antenna beamwidth, is included in the table. Free space losses are calculated and atmospheric absorption estimated for moderate rain conditions per Bell Telephone Laboratories: Transmission Systems for Communications (4th edition, 1970, pages 442-444). Antenna gains are calculated for 55% efficiency. The receiver noise figures represent typical off-the-shelf equipments. The bandwidth is adequate for high density multichannel voice or equivalent TV transmission. Receiver threshold is the calculated value for the parameters included in the table. Adequate available fade margins are obtained for this illustration. In CCIR Recommendation 441-2 (Volume V, Part 2, Annex III, pages 188-189), the TV S/N ratio is calculated for CCIR white noise weighting of the M-system as used in the U. S. A. The worst channel noise figures, based on the receiver input power, can be realized by solid-state off-the-shelf equipment available on today's market with the received signal strength indicated in the table. These figures meet or exceed all relevant CCIR requirements in CCIR Recommendation 395-1 (Volume IV, Part I, page 43).

Table 1. Typical Microwave Performance (\approx 90 Mile Link)

Frequency (GHz)		2	6	8
Antenna Diameter (feet)		15	15	15
Antenna Beamwidth ($^{\circ}$)	} Ground	2.34	0.78	0.58
Antenna Gain (dB)		36.88	46.42	48.92
Tx Power (dBm) (20 W)	} Terminal	43.00	43.00	43.00
Tx Losses (dB)		1.00	2.00	2.50
EIRP (dBm)		78.88	87.42	89.42
Free Space Loss (dB)		141.92	151.48	154.00
Permissible Blowdown (miles)		3.7	1.3	.9
Blowdown & Pointing Loss (dB)		1.50	3.50	4.50
Atmospheric Absorption (dB)		0.15	7.00	10.50
Antenna Diameter (feet)		6	6	6
Antenna Beamwidth ($^{\circ}$)	} Airborne	5.84	1.95	1.46
Antenna Gain (dB)		28.92	38.47	40.97
Rx Losses (dB)	} Terminal	2.00	2.5	3.50
Rx Input Power (dBm)		-37.77	-38.59	-42.11
Rx Noise Figure (dB)		8.00	9.00	10.00
Rx Bandwidth (MHz)		30	30	30
Rx Threshold (dBm)		-81.23	-80.23	-79.23
Available Fade Margin (dB)		43.46	41.64	37.12
TV S/N Ratio Weighted (dB)		78.16	76.34	71.82
Worst Channel Noise (pWpO)		85	90	150
Availability w/Freq. Diversity (%)		99.999	99.999	99.99

References

Bell Telephone Laboratories: *Transmission Systems for Communications*, 4th Ed., 1970, pages 442-444.

CCIR Report 338-1, Volume II, Part 1, pages 114-127.

CCIR Recommendation 395-1, Volume IV, Part 1, page 43.

CCIR Recommendation 441-2, Volume V, Part 2, Annex III, pages 188-189.

FCC: Volume III of the Rules and Regulations of the Federal Communications Commission 1972, Part 73, pages 289 and 291.

Contents

1. Introduction
2. Nomenclature
3. Derivation of the Aerodynamic Coefficients
4. Test Procedures
5. Experimental Results and Analysis
6. Balloon System Performance
7. Concluding Remarks

Aerodynamic Performance of the Family II Tethered Balloon System

R. G. O'Hila and M. A. Duffy
Battelle Columbus Laboratories
Columbus, Ohio

Abstract

A design verification test program of the ARPA Family II tethered balloon system was conducted at the Cape Canaveral Air Force Station during late 1973 and early 1974. Objectives of this program were to describe the aerostatic, aerodynamic, structural, and performance characteristics of the IID-7A design. This paper addresses the aerodynamic performance of the balloon system.

Experimental methods for determining the aerodynamic coefficients of lift, drag, and pitching moment of an aerodynamically-shaped tethered balloon are described. Experimental data obtained from flight tests are presented and compared with theoretical and wind tunnel results. Expected system performance, based on these newly derived aerodynamic coefficients, is presented for various tether lengths in winds up to 65 knots.

1. INTRODUCTION

The objective of the Design Verification Program (DV) was to measure the performance capabilities of the Family IID-7A balloon system for potential users. A specific objective was to determine the aerodynamic lift, drag, and pitching moment coefficients of the full-scale balloon system. These data are needed to define the balloon system payload/altitude capability, blowdown distance, dynamic stability coefficients, and the influence of aerodynamic loads on structural response.

The series of flight tests were planned and conducted as a joint effort between the Range Measurements Laboratory (RML) of the Air Force Eastern Test Range and its support contractors and Battelle-Columbus personnel at the Cape Canaveral Air Force Station, Florida. A total of 30 flights, including 29 fixed-tether flights and one helicopter tow flight, were conducted to collect aerodynamic and performance data on the balloon system during the period of November, 1973, to March, 1974.

Presently, there is a very limited amount of full-scale experimental data which can be applied to the aerodynamic design or operation of aerodynamically-shaped tethered balloon systems. This paper presents the results obtained during the DV program and a description of a novel method for determining the aerodynamic lift coefficient of tethered balloons.

2. NOMENCLATURE

A	constant in lift coefficient equation
B	buoyant lift, lb
C_D	aerodynamic drag coefficient
C_L	aerodynamic lift coefficient
$C_{L\alpha}$	aerodynamic lift curve slope, 1/deg
C_M	aerodynamic moment coefficient
D	drag, lb
K	constant in drag coefficient equation
L	aerodynamic lift, lb
M	moment, lb-ft
T	tether tension at tether point, lb
V	wind speed, knots

V	balloon hull volume, ft ³
$v^{2/3}$	characteristic area of balloon, ft ²
W	weight, lb
X	balloon station in X-direction measured from the nose of fabric structure, ft
Z	balloon station in Z-direction measured from centerline of balloon (down positive), ft
\bar{c}	hull length, 138 ft
q	free stream dynamic pressure, lb/ft ²
α	angle of attack, deg
ϵ	tether angle at tether point, deg

Subscripts:

a	after
B	center of buoyancy
b	before
CG	center of gravity
CP	center of pressure
TP	tether point

3. DERIVATION OF THE AERODYNAMIC COEFFICIENTS

A specific purpose of the DV program was to measure the steady aerodynamic forces and moments acting on the balloon at various angles of attack and relative wind speeds.

The free body diagram of the balloon system at equilibrium is shown in Figure 1. This diagram indicates the forces and the aerodynamic moment acting on the balloon; it also establishes the coordinate system used in locating these forces.

3.1 Aerodynamic Drag

The aerodynamic drag is obtained by summing the forces on the balloon which act in the free stream wind direction. Assuming horizontal winds,

$$D = T \sin \epsilon . \quad (1)$$

Aerodynamic drag coefficients are obtained by nondimensionalizing the above expression with respect to the dynamic pressure, and the characteristic area of the balloon. Thus, at any equilibrium position, the aerodynamic drag coefficient is defined by

$$C_D = \frac{T \sin \epsilon}{q V^{2/3}} . \quad (2)$$

Different equilibrium positions, characterized by different angles of attack, will yield different values for C_D . Theoretically, these values will define the balloon drag curve, comprised of the profile drag and the induced drag, which has the familiar form

$$C_D = C_{D_0} + K\alpha^2 \quad (3)$$

3.2 Aerodynamic Lift

The aerodynamic lift is obtained by summing the vertical forces on the balloon such that

$$L = T \cos \epsilon + W - B . \quad (4)$$

Calculating the aerodynamic lift is straightforward if the weight and buoyancy are known accurately. Unfortunately, the specific values of W and B could not be determined with sufficient accuracy on a day-to-day basis. The uncertainty in the value of B arises because of the inability to calculate precisely the mass of helium in the balloon at a given time after the initial fill. Losses occur due to leakage and programmed helium dumps. The uncertainty in the value of W arises because of the inability to calculate accurately the weight of water that is collected within the balloon from precipitation and condensation. Therefore, it was necessary to devise a means of calculating the aerodynamic lift coefficient that would eliminate the need for knowing the absolute values of the buoyant force and the balloon weight.

By releasing a known weight from the balloon while at steady-state equilibrium, two different trim angles can be obtained at identical external conditions. Resolving vertical forces at the tether point before and after the release will yield the difference due to the change in weight, any change in buoyancy due to altitude change, and the change in aerodynamic lift. Since the change in aerodynamic lift is a function of the change in angle of attack, and is independent of

how this change in α occurs, the slope of the lift curve can be determined directly from the before and after steady-state conditions.

Data taken during the water drop tests provided the means of eliminating weight and buoyancy effects. The lift equation can be written as

$$L_b - L_a = (T_b \cos \epsilon_b - T_a \cos \epsilon_a) + (W_b - W_a) - (B_b - B_a) . \quad (5)$$

The aerodynamic lift coefficient is linearly dependent on the angle of attack and is expressed as

$$C_L = A + C_{L\alpha} \alpha . \quad (6)$$

Since the aerodynamic lift is related to C_L by

$$L = C_L q V^{2/3} , \quad (7)$$

substitution of Eq. (6) and Eq. (7) into Eq. (5) yields

$$C_{L\alpha} = \frac{(T_b \cos \epsilon_b - T_a \cos \epsilon_a) + (W_b - W_a) - (B_b - B_a) - A(q_b - q_a)V^{2/3}}{(\alpha_b q_b - \alpha_a q_a)V^{2/3}} \quad (8)$$

This equation is justified because the slope of the lift curve remains essentially constant as a function of angle of attack until the onset of flow separation or stall occurs.

Although the absolute value of total balloon weight may not be known with sufficient accuracy, the term $(W_b - W_a)$ which is equal to the weight of water released is easily determined prior to launch. Similarly, even though the buoyant lift before and after the water drop may not be known precisely, their difference should be included in the lift slope calculations, especially at empty ballonnet conditions. Increases in balloon altitude of 100 feet are not uncommon during these water drop tests. This could mean as much as a 40 to 50 lb decrease in buoyancy at empty ballonnet conditions, which is significant when compared to the 200 to 400 lb of water that is released. The uncertainty in calculating the absolute value of buoyant lift becomes insignificant when forming this difference term. For example, if it is assumed that the error in calculating buoyancy directly were ± 5 percent and entirely attributed to uncertainties in helium purity and volume, then the error would be approximately 500 lb. However, the error in calculating the difference would be only 2 lb.

3.3 Aerodynamic Pitching Moment

The aerodynamic moment (M_{aero}) required to maintain the balloon at equilibrium, when the aerodynamic lift and drag forces are applied at a particular location, can be determined by summing moments about any known reference point. If moments are summed about the tether point, the required pitching moment is

$$\begin{aligned} M_{aero} = & B[(X_B - X_{TP}) \cos \alpha + Z_{TP} \sin \alpha] \\ & - W[(X_{CG} - X_{TP}) \cos \alpha + (Z_{TP} - Z_{CG}) \sin \alpha] \\ & + L[(0.624\bar{c} - X_{TP}) \cos \alpha + Z_{TP} \sin \alpha] \\ & - D[Z_{TP} \cos \alpha - (0.624\bar{c} - X_{TP}) \sin \alpha] , \end{aligned} \quad (9)$$

assuming that the lift and drag act on the centerline of the hull at $X = 0.624\bar{c}$ and $Z_{CB} = 0$.

The aerodynamic pitching moment coefficient is expressed as

$$C_M = \frac{M_{aero}}{qV^{2/3} \bar{c}} \quad (10)$$

Although the aerodynamic pitching moment coefficient is a function of the external configuration only, determining its value requires a precise knowledge of all forces (and their points of application) acting on the balloon. Because of the uncertainty in locating the tether point, the center of buoyancy, the center of gravity, the weight and buoyancy, it is impossible to calculate a pitching moment coefficient, as a function of angle of attack, which is consistent between flights. Therefore, the location of the center of pressure (X_{CP}) versus angle of attack was assumed to be the same as determined during the wind tunnel tests. Then, C_M can be determined relative to any point of application of the aerodynamic lift and drag forces from the following relationship

$$C_{M@x_{ref}} = - (C_L \cos \alpha + C_D \sin \alpha) \left(\frac{X_{CP}}{\bar{c}} - \frac{X_{ref}}{\bar{c}} \right) \quad (11)$$

4. TEST PROCEDURES

4.1 Test Vehicle and Instrumentation

The Family IID-7A balloon is a 200,000-cu-ft (approximately), all-weather balloon that is designed to operate in winds up to 65 knots at altitudes from sea

level to 10,000 ft. In flight, the balloon is tethered with a 0.775-inch-diameter NOLARO cable, weighing 0.202 lb/ft, with a minimum breaking strength of 26,000 lb. A more comprehensive description of the system is reported by the EML (1974).

The balloon system was instrumented to obtain data for determining steady-state aerodynamic coefficients. Table 1 is a description of the primary sensors related to the aerodynamic data requirements. Systematic errors and the full-scale range of each sensor are also noted in the table. Figure 2 shows the arrangement of various sensors on the vehicle and the location of the instrumentation and telemetry package.

Table 1. Primary Sensors for Aerodynamic Data

Physical Parameter	Sensor	Model Number	Full-Scale Reading	Systematic Error
Wind Speed	Belfor: anemometer	5600	0 to 60 knots	± 0.5 knot
Tether Tension	MLM load cell	UCG-1	0 to 10,000 lb	± 25 lb
Tether Angle and Angle of Attack (Pitch Angle)	Humphrey gyroscope	VO-24-0601-1	-10 to +30 deg	± 0.5 deg
Ambient and Ball Temperature	Farnel thermostat	K-1979	40 to 140 F	± 2.0 F
Ambient Pressure	Statham pressure transducer	PA-505-15	0 to 15 psia	± 0.15 psia
Ball Pressure	Statham pressure transducer	FM-203-TC	0 to 5 ING	± 0.05 ING

In order to ensure an accurate determination of wind velocity, two anemometers were attached to the balloon. The prime unit, which was also designed to measure wind direction off the horizontal, was originally located on the tether approximately 100 feet below the confluence point (Figure 2). A second anemometer was suspended from the horizontal empennage on a 100-ft line. Both anemometers were outside the flow region influenced by the balloon and when both were functioning properly, their readings agreed within one knot. Eventually the tether unit had to be abandoned because of repeated damage caused by tether vibration. Thereafter, redundancy was provided by two trailing anemometers. Unfortunately, this eliminated the only means of measuring wind direction, so that the wind relative to the balloon had to be assumed horizontal.

Bags filled with water were used as ballast to change the trim angle of the balloon. These bags, which could hold up to 400 lb of water, were attached to guy wires on the lower vertical empennage. The water was released by severing a cord

which held the bags in an upright position. The water ballast located in this position was sufficient to cause changes in balloon trim angle of 1.5 to 7 deg, depending upon the amount of water released, the wind speed at altitude, and the basic trim configuration of the balloon.

All of the physical parameters measured in flight were transmitted to a ground recording station via telemetry. The aerodynamic data were simultaneously recorded on analog strip chart recorders and on a digital magnetic tape recorder.

The magnetic data tape was processed on a Xerox Sigma-7 computer prior to the next flight. Figures 3-6 are some representative output sheets. Figure 3 is a listing of some of the input measured data. Figure 4 is a listing of a typical static aerodynamic data sample. Figure 5 shows the calculation of the aerodynamic lift slope based on data collected before and after the release of water ballast. In addition to the printed output, it is possible to obtain plots of any output parameter versus any other output parameter. Figure 6 is a typical time history of the balloon pitch angle and tether pitch angle for a water release test.

4.2 Fixed Tether

During the DV program, two types of balloon flights were conducted to obtain aerodynamic data. Early in the DV program, each water drop experiment was conducted while the balloon had an empty ballonet. This required that the balloon ascend to an altitude of at least 7,500 ft, steady-state data being collected at certain intermediate altitudes during both ascent and descent. At the maximum altitude, steady-state data before and after the water drop were recorded. These two steady-state conditions were used to calculate the slope of the aerodynamic lift curve (they also provided aerodynamic drag data at two different trim conditions).

As the DV program progressed, it became clear that both water drop and static equilibrium tests could be conducted at low altitudes, if the winds were steady at these altitudes. Thus, as many as four water drop tests were conducted in one day at altitudes of 2,000 to 4,000 ft.

4.3 Helicopter Tow Test

In order to demonstrate the balloon performance and to collect structural and aerodynamic data up to its design wind speed, a procedure to tow the balloon behind a helicopter was devised. A sketch of the tow configuration is shown in Figure 7. This configuration was selected because the balloon would have the same load as it would in a standard fixed-tether flight and no changes in instrumentation or data reduction routines were required. The cable lengths and the ballast weight were chosen so that the balloon would be towed above the helicopter downwash during the data collection periods.

5. EXPERIMENTAL RESULTS AND ANALYSIS

A total of 30 flights, including 29 fixed-tether and one helicopter tow, were conducted during this phase of the program. Winds from near zero to 38 knots were encountered at balloon altitudes from 2,000 to 12,000 ft. During the helicopter tow test, the balloon experienced a relative wind speed of 45 knots. Reynolds numbers, based on hull length, ranged from 6×10^6 to 65×10^6 .

5.1 Aerodynamic Drag Coefficient

Figure 8 presents the aerodynamic drag coefficient data as a function of angle of attack. Seventy data points, from 22 of the fixed-tether flights and the helicopter tow test, are included. Since steady-state conditions were experienced before and after a water drop and since data was generally recorded at intermediate altitudes, one flight could yield several data points at different angles of attack. However, some flights resulted in no usable data, either because of unsteady conditions, or because of improper functioning of critical instrumentation.

The solid line on Figure 8 is a least squares fit of the data to an expression of the form

$$C_D = C_{D_0} + K \alpha^2 ,$$

which becomes

$$C_D = 0.11 + 0.0007 \alpha^2 .$$

The one-sigma deviation about C_{D_0} is ± 0.026 or ± 24 percent. This one-sigma spread is also indicated on the figure.

5.2 Aerodynamic Lift Coefficient

Valid data for determining the slope of the aerodynamic lift coefficient (C_{L_α}) were obtained from 16 of the 22 flights during which the water ballast was released. Figure 9 presents the results of C_{L_α} calculations and the corresponding change in angle of attack for each flight. A weighted average of all data points and the one-sigma deviation are also shown

$$C_{L_\alpha} = 0.05 \pm 0.014 .$$

Each data point was weighted according to the reciprocal of the total error (random plus systematic, in percent/100) expected for that flight. Thus, a data point with an associated error of ± 25 percent would have a weight of 4.0 (1/0.25), whereas one with an error of ± 50 percent would only have a weight of 2.0. The average error was calculated to be ± 28 percent.

Integrating the aerodynamic lift slope by the balloon angle of attack yields the following equation for the aerodynamic lift coefficient

$$C_L = 0.050 \alpha .$$

5.3 Aerodynamic Pitching Moment Coefficient

The aerodynamic pitching moment coefficient (C_M) could not be determined directly from in-flight measurements. Therefore, C_M was determined by assuming that the X-location of the center of pressure (X_{CP}) for IID-7A balloon is the same as that of the wind tunnel model as reported by Haak (1971). The wind tunnel variation of X_{CP} , as a fraction of hull length, with angle of attack, is shown in Figure 10. Figure 10 also presents C_M as a function of α for C_L and C_D as derived from flight data and $\frac{X_{ref}}{c} = 0.624$.

5.4 Discussion of Results

The flight derived and wind tunnel measured lift and drag coefficients are shown in Figure 11. These results are similar to those reported by Ollila (1973). Comparison of the flight aerodynamic lift data to the wind tunnel data shows that the nominal value of the flight test lift data is approximately 50 percent higher than the wind tunnel data. This increase is probably caused by the reduced interference effects between the hull and tail of the full-scale balloon as compared to those of the wind tunnel model.

Comparison of the flight drag data to the wind tunnel data shows that the profile drag of the total balloon system is about twice that of the wind tunnel model. This increase in drag is attributed to the parasite drag caused by addition of ram-air scoops, confluence and load lines, tail guy wires, the power supply and its frame, and the nose cone/batten assembly. The wind tunnel model was much cleaner aerodynamically, consisting of only the hull, tail, and payload windscreen.

The maximum lift-to-drag ratio (L/D) based on flight data is approximately 2.85 at an angle of approximately 12.5 degrees. The maximum L/D based on wind tunnel data is 3.8 at 10 degrees. The reduction in L/D and its shift are attributed to the large increase in the drag of the actual balloon system as compared to the wind tunnel model.

6. BALLOON SYSTEM PERFORMANCE

Balloon system performance is calculated using a computerized equilibrium analysis of the balloon cable system. This program has been validated by comparing data obtained in-flight to calculated values by Ollila, Duffy, and Brown (1974). The comparison showed that predicted altitudes were within ± 5 percent of the measured value and tether tensions were within ± 10 percent.

6.1 Operational Performance

The performance of the Family II operational balloon system was calculated for winds of 0 to 65 knots. The performance curves shown in Figure 12 are based on the aerodynamic characteristics derived from flight data and the following physical characteristics: total weight of 6,291 lb (including a 750-lb payload and a 284-lb fuel supply); center of gravity at $X_{CG} = 65.8$ ft and $Z_{CG} = 11.9$ ft; hull volume of 204,000 cu ft; center of buoyancy at $X_{CB} = 57.7$ ft and $Z_{CB} = -0.5$ ft; helium purity of 98 percent; tether point location at $X_{TP} = 51.8$ ft and $Z_{TP} = 52.8$ ft; and a tether weight of 0.202 lb/ft with a maximum length of 15,000 ft.

This configuration has a zero-wind trim angle of 7.6 deg. Although a low trim angle reduces the maximum achievable dynamic altitude and results in greater blow-down distances, it does yield lower tether tensions for a given tether length and wind speed. For comparative purposes, a curve, representing the hypothetical performance of the same balloon always flying at its maximum aerodynamic lift-to-drag ratio, is shown on each plot. At high wind speeds, a significant increase in altitude and decrease in blowdown is achieved at the expense of almost doubling the tether tension. Of course, a tethered balloon cannot be designed to fly at a constant angle of attack, independent of wind speed, without active control devices. However, it can be designed to operate at maximum L/D for a particular wind speed.

6.2 Effect of the Uncertainty of Lift and Drag on Performance

Two additional sets of performance curves, which illustrate the influence of the uncertainties in the C_L and C_D expressions, are indicated on Figure 12. One set of curves pertains to lift and drag coefficient expressions, respectively, of

$$C_L = (0.05 + \sigma_L) \alpha$$

$$C_D = 0.11 + 0.0007 \alpha^2 - \sigma_D$$

and the other to

$$C_L = (0.05 - \sigma_L) \alpha$$

$$C_D = 0.11 + 0.0007 \alpha^2 + \sigma_D .$$

σ_L (=0.014) is the one standard deviation error associated with the calculation of C_L ; σ_D (=0.03) is the one standard deviation error associated with the calculation of C_D . The errors attributable to lift and drag were combined to yield the maximum and minimum expected lift/drag ratios. Thus, the initial set of the above equations combines the greatest expected aerodynamic lift with the smallest expected aerodynamic drag, producing the maximum expected L/D (4.3). The latter set produces the minimum expected L/D (1.8). In terms of altitude and blowdown, there is little difference among the nominal, upper, and lower extremes. Appreciable differences in tether tension occur at the higher wind speeds only. The behavior of balloon angle of attack, although not critical, is quite different for the minimum L/D case.

7. CONCLUDING REMARKS

The aerodynamic coefficients obtained from flight data are substantially different than those obtained from wind tunnel tests utilizing a small rigid scale model. The full-scale balloon is aerodynamically dirty, compared to the wind tunnel model, which accounts for the increase in drag. The increase in aerodynamic lift cannot be accounted for so easily and must be attributed to reduced interference effects and possibly scale effects.

Calculations based on the flight-derived aerodynamic data show that the operational balloon system can lift a useful, 750-lb payload to an altitude of 10,000 ft for all wind conditions up to the design wind speed. Uncertainties in the estimation of the aerodynamic lift and drag do not alter this conclusion, except to increase the design strength requirement of the tether cable.

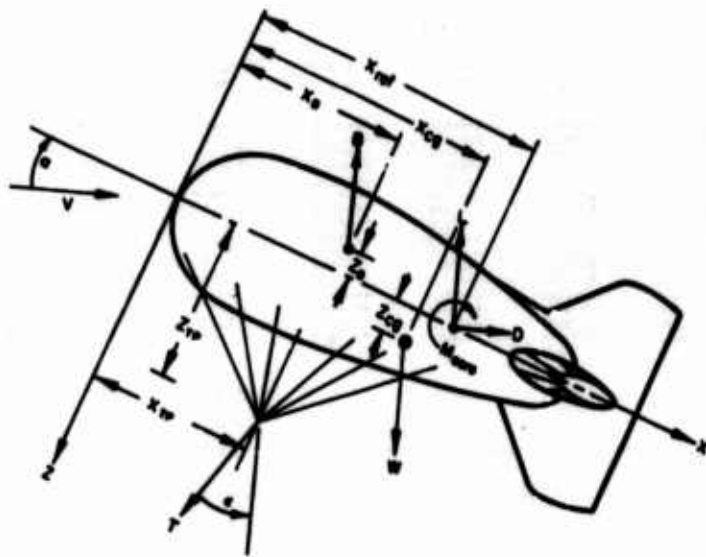


Figure 1. Free Body Diagram of Balloon System

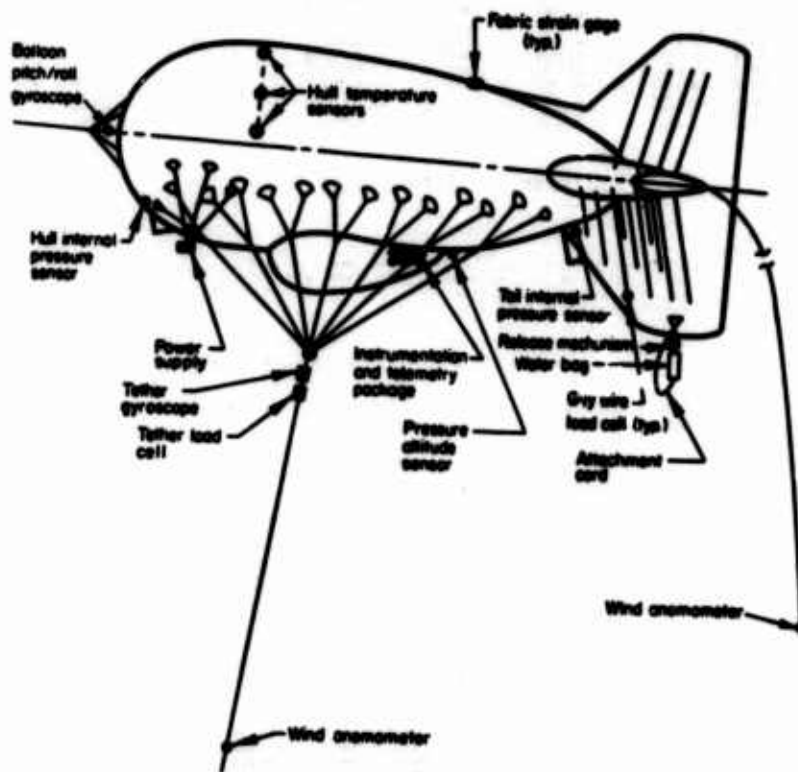


Figure 2. Location of Balloon Instrumentation

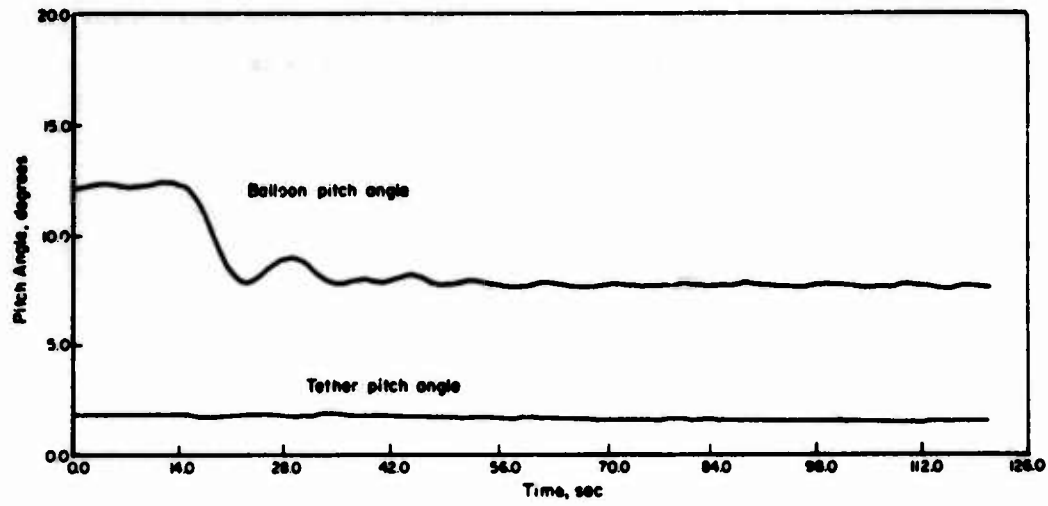


Figure 6. Time History of Pitch Angle During A Water Drop Test

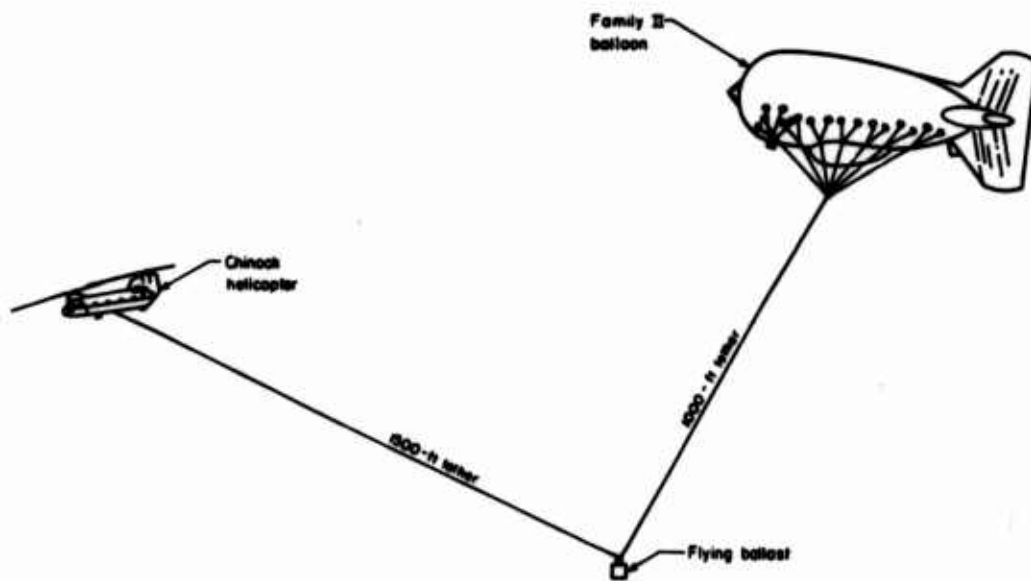


Figure 7. Helicopter Tow Test Configuration

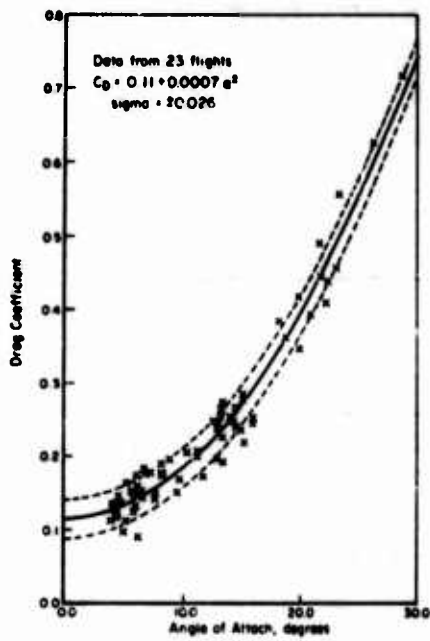


Figure 8. Drag Coefficient Versus Angle of Attack

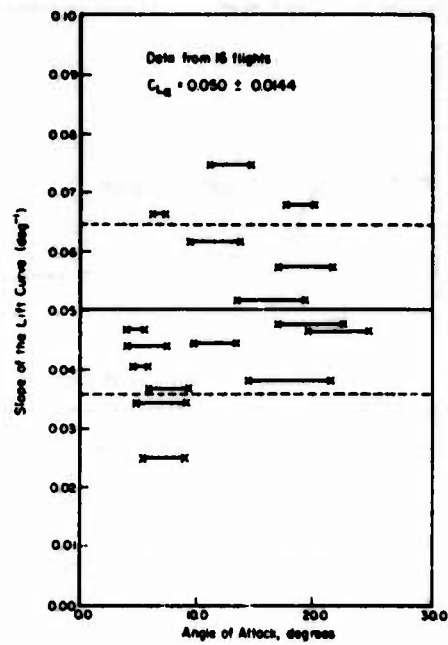


Figure 9. Aerodynamic Lift Coefficient Slope Data

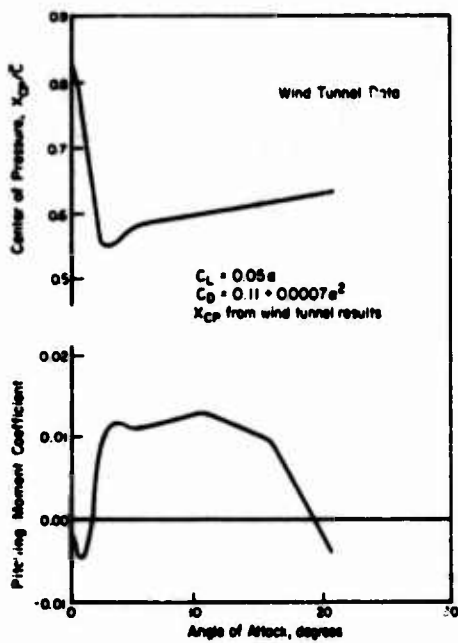


Figure 10. Center of Pressure and Aerodynamic Pitching Moment Coefficient Versus Angle of Attack

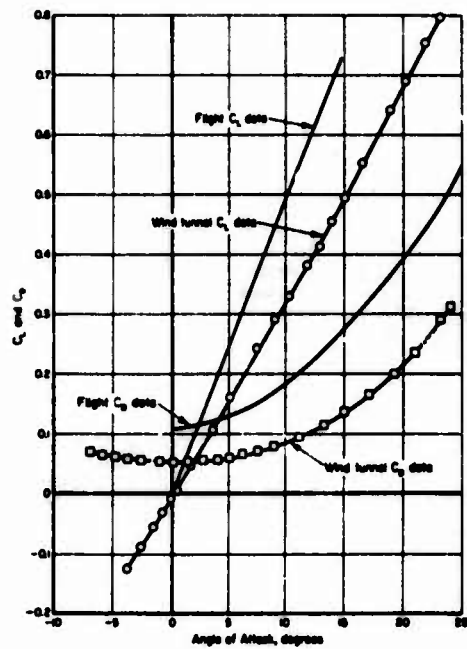
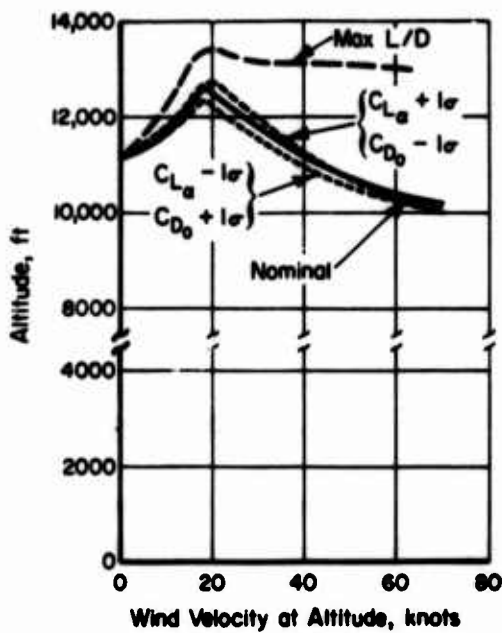
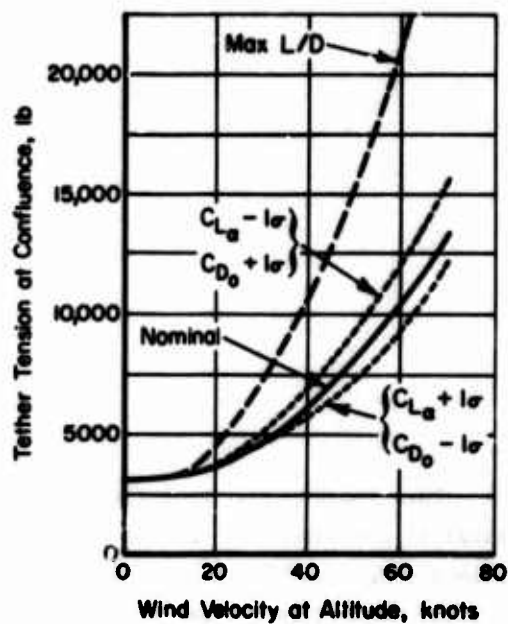


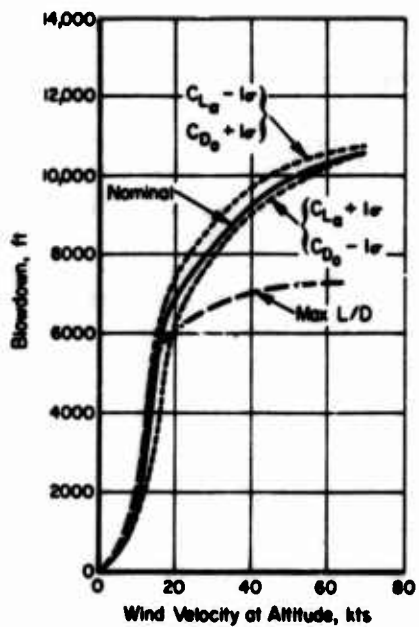
Figure 11. Family II Balloon System Lift and Drag Coefficients



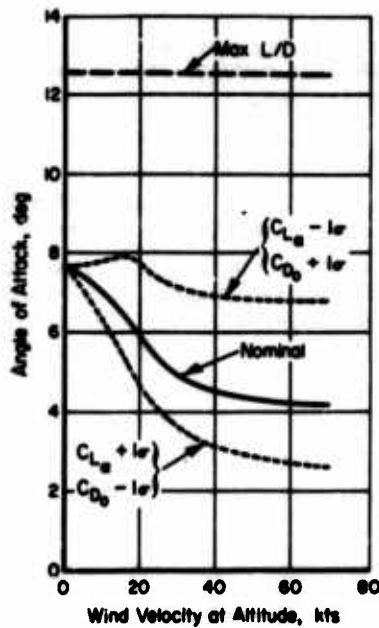
(a)



(b)



(c)



(d)

Figure 12. Family II Balloon Operational Performance

Acknowledgments

This research was supported by the Defense Advanced Research Projects Agency (ARPA) of the Department of Defense and was monitored by the U. S. Army Missile Command under Contract Number DAAH01-73-C-0924. Col. G. H. Greenleaf (USAF) of the Tactical Technology Office of ARPA monitored the effort. Review of this material does not imply DoD endorsement of factual accuracy or opinion.

References

- Design verification test program, Final Report, TELTA TR-74-058, Contract No. F08606-74-C-0025, ARPA Order No. 2176, The Range Measurements Laboratory, Patrick AFB, Florida (to be issued).
- Haak, E. L., Wind tunnel test results--family II-D aerodynamically-shaped balloon, SER0093, March, 1971, G. T. Schjeldahl Company, Northfield, Minnesota.
- Ollila, R. G., Flight tests of a large low-altitude tethered balloon. Paper presented at the AERALL Symposium, November, 1973, Paris, France.
- Ollila, R. G., Duffy, M. A., and Brown, J. H., Jr., Analysis of family II design verification program data--aerodynamic coefficients and system performance, Topical Report, July, 1974, Battelle-Columbus Laboratories, Columbus, Ohio

An Experimental Investigation of the Dynamic Stability of the Family II Balloon

J. D. DeLaurier
Battelle Columbus Laboratories
Columbus, Ohio

Abstract

A series of tests were performed on a Family II balloon in order to characterize its dynamic stability. These tests consisted of perturbing the balloon a known distance, and then recording its subsequent motion upon release. In particular, longitudinal perturbations were accomplished by drawing back the balloon's confluence point with an auxiliary cable. This cable was released at the confluence point, and the balloon's displacement and pitch time histories were recorded. Similarly, the balloon's lateral stability was investigated by displacing the confluence point normal to the wind's direction. The data recorded were the balloon's lateral displacement, yaw, and roll.

These perturbations were accomplished for tether cable lengths of 1000, 1500, 2000, and 2500 feet for a variety of wind speeds varying from 11.8 to 31.3 ft/sec. During the test program, there were several days when the winds were extremely steady. These allowed perturbation responses with minimal influence from atmospheric turbulence. This gave smooth plots of the data which clearly show the influence of the system's various dynamic modes, and the effect of cable length and wind speed on the system's dynamic stability.

1. INTRODUCTION

The objective of this work was to characterize the dynamic stability of a 200,000 ft³ tethered balloon by measuring its dynamic responses to given perturbations from its equilibrium flight configurations. These tests were performed under ARPA contract during February, 1974, at Cape Kennedy Air Force Station, Florida, and this paper presents the results and the methodology.

Although the dynamic response results are the primary consideration of this report, the methodology of the tests is of particular interest since much of it had to be specifically developed for this program. This is because quantitative measurements of a tethered balloon system's dynamic stability involve considerable practical difficulty. Part of the problem is that normal atmospheric turbulence causes a random dynamic response of the system which is a "background noise" to any measurements of the balloon's response to given experimental inputs. Random response information is, itself, of considerable operational value, and has been measured by various investigators beginning with Baird in 1915. However, it is extremely difficult to obtain quantitative measures of the system's stability parameters (such as time to half amplitude) from such data.

For their investigation of a tethered balloon's frequency and stability boundaries, Radd, et al (1973), avoided atmospheric turbulence by towing their system at various speeds through more or less quiescent air. This was a very suitable technique for their small balloon (25.1-foot length), but poses considerable difficulties for application to large balloons such as the Family II (167-foot length). Other problems arise if one wants to investigate the balloon's response to given initial conditions. This would entail devising some means to perturb the balloon while towing it. Whereas such a problem is not insolvable, it appears far simpler to perturb a system which is tethered to the ground. This approach was used by Vorachek and Doyle (1973) in their investigation of the dynamic response of a BJ balloon (107-foot length). The perturbations were generated by a light auxiliary tether which was attached to the confluence point and pulled and released from the ground. The difficulty, then, is that one has to wait for winds of suitable velocity and smoothness.

The tethered perturbation technique was used for this dynamic response study. Because three weeks of testing were allowed, there were sufficient days with suitable atmospheric conditions to permit a good range of tests. Within certain limitations, these were sufficient to characterize the 204 balloon's dynamic stability, as elucidated in the balance of this report.

2. THE SYSTEM'S PROPERTIES

As mentioned above, the cable-body system tested is a balloon tethered to the ground. The balloon, shown in Figure 1, is the fourth in the Family II series constructed under ARPA contract, and is designated SN 204. Its geometrical properties and coordinate definitions are shown in Figure 2, and its confluence point location is

$$l_{tp} = 57.6 \text{ ft} , \quad h_{tp} = 52.8 \text{ ft} \quad . \quad (1)$$

Also, its nominal volumetric properties are

$$\begin{aligned} \text{Hull volume} &= 204000 \text{ ft}^3 \\ \text{Empennage volume} &= 36900 \text{ ft}^3 \\ \text{Windscreen volume} &= 7530 \text{ ft}^3 \\ \text{total volume} &= 248400 \text{ ft}^3 \\ l_{cv} &= 70.08 \text{ ft} , \quad h_{cv} = 79 \text{ ft} \quad . \end{aligned} \quad (2)$$

The balloon's weight and center-of-gravity location differed slightly from test to test, but very close nominal values were

$$\begin{aligned} \text{Total weight} &= 7000 \text{ lb} \\ l_{cg} &= 66.1 \text{ ft} , \quad h_{cg} = 12.0 \text{ ft} \quad . \end{aligned} \quad (3)$$

Also, from the measured weights of the balloon's components, the balloon's moments of inertia relative to its center of gravity (see Figure 2) were calculated to be (note that the contribution of enclosed air and gas is not included):

$$\begin{aligned} I_a &\equiv \text{Moment of Inertia about the } \bar{a} \text{ axis} = 94650 \text{ slug-ft}^2 , \\ I_c &\equiv \text{Moment of Inertia about the } \bar{c} \text{ axis} = 544300 \text{ slug-ft}^2 , \\ I_b &\equiv \text{Moment of Inertia about the axis normal to } \bar{a} \text{ and } \bar{c} = \\ &\quad 583200 \text{ slug-ft}^2 , \\ I_{ac} &\equiv \text{Product of Inertia with respect to the } \bar{a} \text{ and } \bar{c} \text{ axes} = \\ &\quad 37900 \text{ slug-ft}^2 . \end{aligned} \quad (4)$$

The balloon's static longitudinal aerodynamic properties were obtained from water-drop tests described by Ollila and Duffy (1974). Upon using

$$\begin{aligned} S &\equiv \text{Reference Area} = 3465 \text{ ft}^2 , \\ b &\equiv \text{Reference Length} = 138 \text{ ft} , \end{aligned} \quad (5)$$

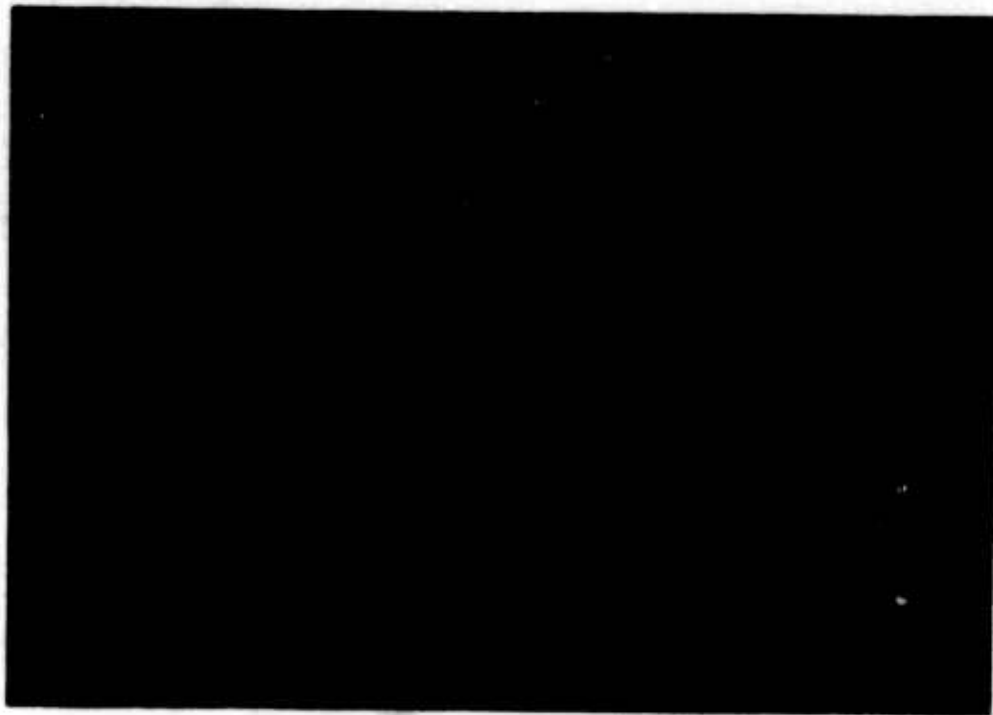


Figure 1. SN 204 Balloon

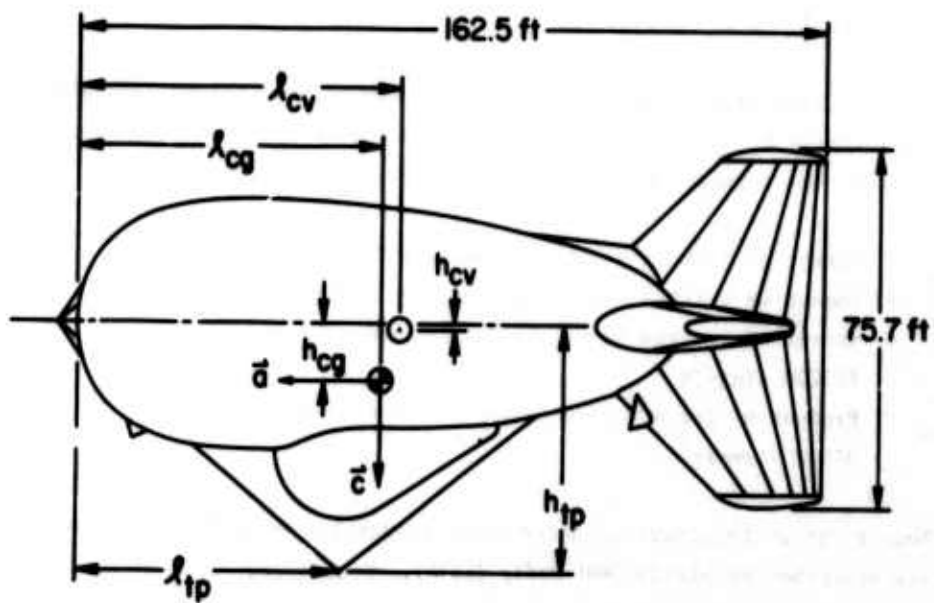


Figure 2. Balloon Dimensions and Coordinates

the aerodynamic properties are given by

$$C_L = 2.90 \alpha \quad , \quad (6)$$

$$C_D = .11 + 2.36 \alpha^2 \quad , \quad (7)$$

and the balloon's pitching moment coefficients about its nose were obtained from the above equations and the longitudinal center-of-pressure locations found from wind-tunnel tests by Haak (1971). Upon fitting these values with an equation, one obtains

$$(C_m)_{\text{nose}} = -.0027 - 1.65\alpha - .698\alpha^2 \quad , \quad (8)$$

where α is the balloon's angle of attack in radians. The lateral static aerodynamic properties also were calculated from Haak (1971), which gave

$$C_Y = 1.91 Y \quad , \quad (9)$$

where Y is the balloon's yaw angle in radians. Also, the lateral center of pressure was approximately constant at 80 feet from the nose.

Finally, the cable was a smooth-jacketed NOLARO line (manufactured by the Columbian Rope Company) with the following properties:

$$\begin{aligned} R &= \text{Radius} = .0323 \text{ ft} \quad , \\ \tilde{p} &= \text{Mass/Length} = .00621 \text{ slugs/ft} \quad , \end{aligned} \quad (10)$$

and from Hoerner (1965)

$$\begin{aligned} C_{d_o} &= \text{Tangential Drag Coefficient} = .035 \quad , \\ K &= \text{Normal Drag Coefficient} = 1.19 \quad . \end{aligned} \quad (11)$$

3. TEST PROCEDURE

A drawing which illustrates the perturbation technique is shown in Figure 3. The auxiliary tether was attached directly below the confluence point swivel. Upon launching the balloon, the auxiliary tether was left slack until the desired length of main tether (L) was let out. At that point, both the main winch truck and the auxiliary winch truck maneuvered within the flight area to give the desired perturbation direction and baseline (L_p). For longitudinal perturbations, the balloon was drawn in the direction of the wind, and lateral perturbations were obtained

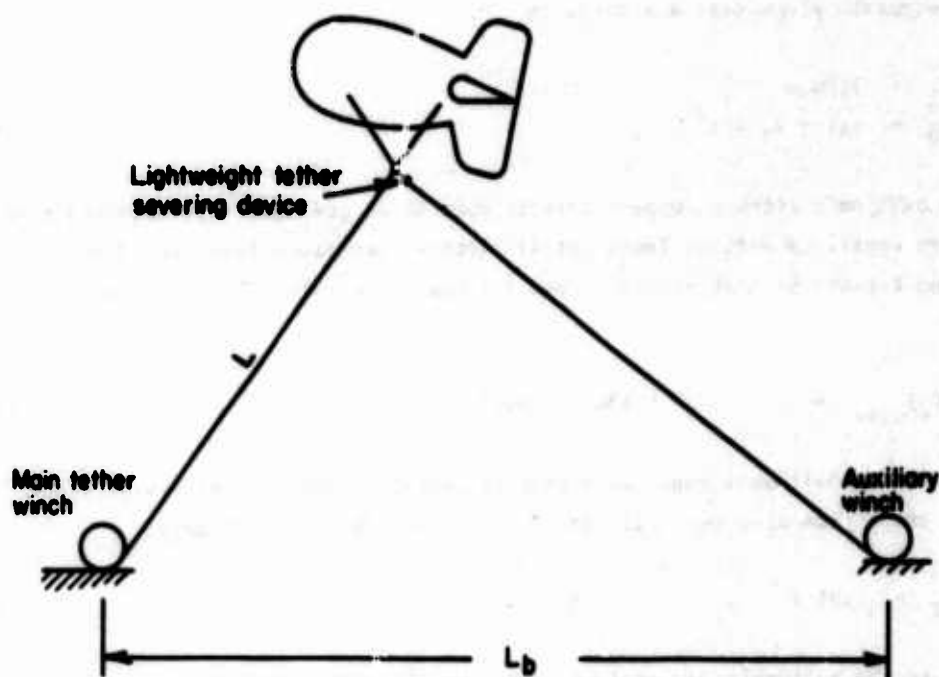


Figure 3. Schematic of Balloon Perturbation Technique

by drawing the balloon normal to the wind. Baselines ranging between 1500 and 2000 feet were used, and the change in the balloon's altitude while the auxiliary winch was reeling-in was utilized in a simple calculation to give an approximate value to the horizontal perturbation. An accurate value was later obtained from the recorded data.

When ready, the auxiliary tether was released at the confluence point by a remotely controlled burn device. The subsequent motions were then recorded in a variety of ways: the horizontal displacements, X and Y , and the yaw angle, Ψ , were obtained from film data recorded by a vertically oriented movie camera shown in Figure 4. The roll angle, ϕ , and the pitch angle, θ , were obtained from balloon-mounted gyro sensors. These signals were sent via a balloon-mounted telemetry package to ground-based strip chart and magnetic-tape recorders. This same telemetry package handled the signals for equilibrium tether tension, wind speed, and angle of attack. Further details on the instrumentation (its type and location) are described by Ollila (1974).

Data reduction of the movie film entailed the reading of individual frames. Trigonometric corrections were applied to account for altitude variations and

camera distance from the main winch. The results were then presented in tabular and graphical forms as functions of time. The magnetic tape data were directly read into a computer, which then produced the results in tabular and graphical forms. The sampling time for all of the data collection was small enough to allow the results to be plotted as continuous curves. However, for most cases, values plotted at 5-second intervals were sufficient to characterize the experimental dynamic responses, which are given in Figures 5 through 12.

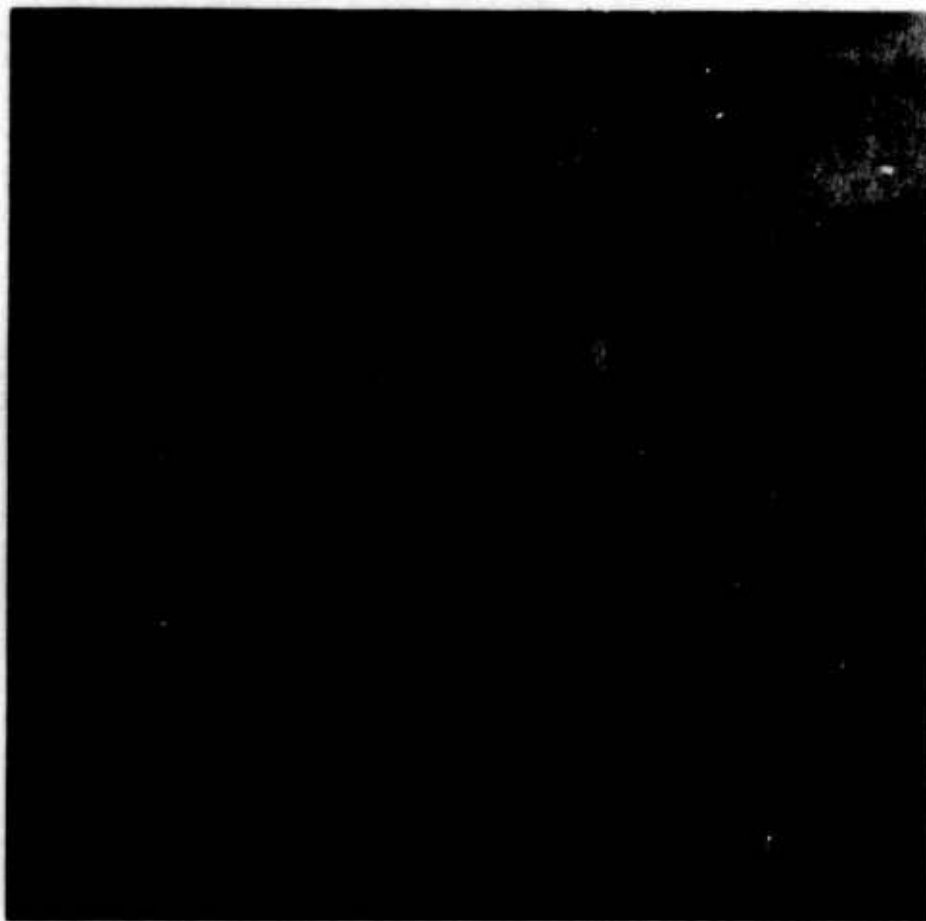


Figure 4. IFLOT Movie Camera

4. DISCUSSION OF THE EXPERIMENTAL RESULTS

The dynamic response tests covered a wind-speed range of $11.8 < U < 31.3$ ft/sec, and a cable-length range of $1000 < L < 2500$ ft. This did not cover the

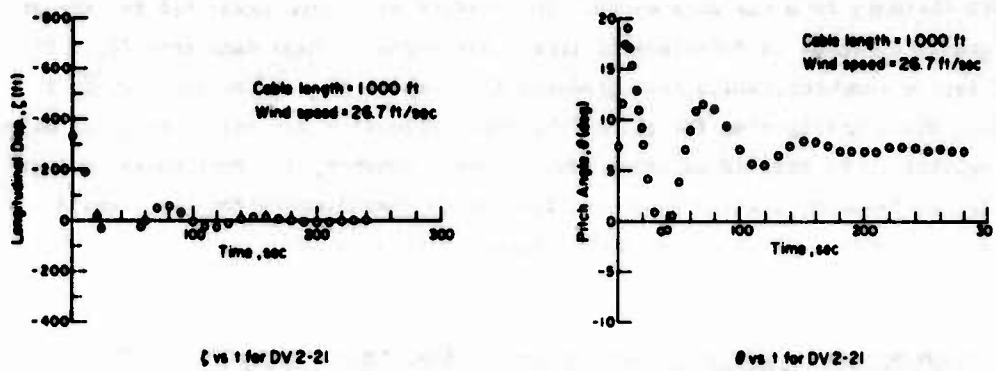


Figure 5. The Dynamic Responses of Test DV2-21

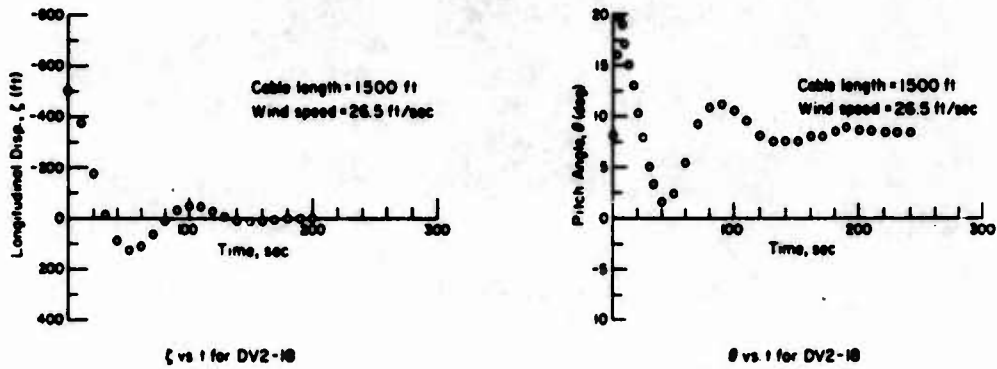


Figure 6. The Dynamic Responses of Test DV2-18

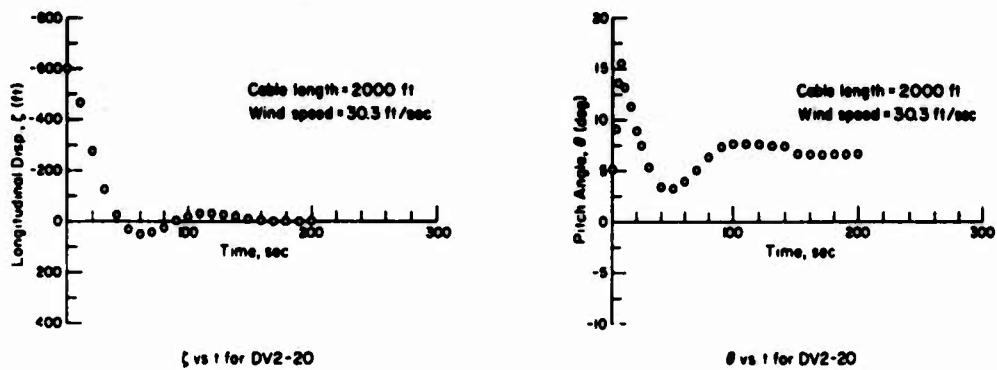
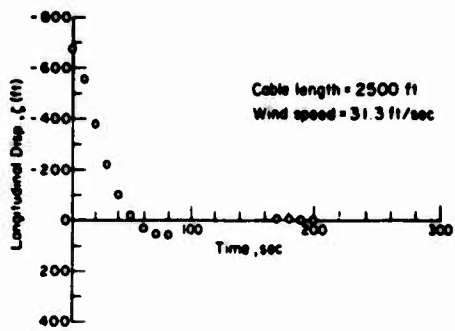
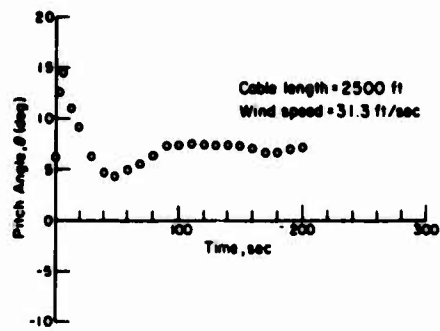


Figure 7. The Dynamic Responses of Test DV2-20

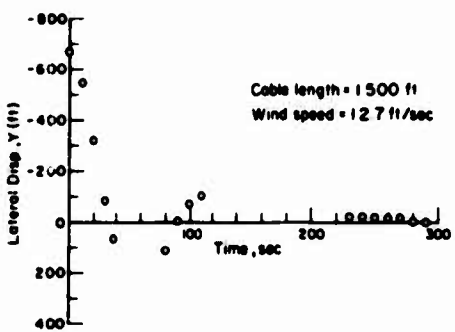


ζ vs t for DV2-19

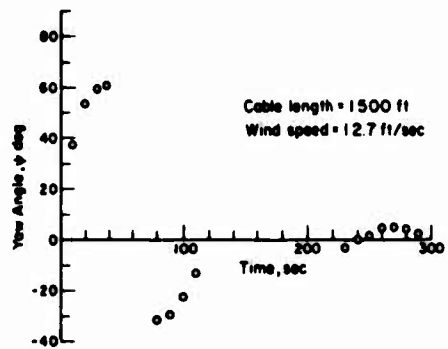


θ vs t for DV2-19

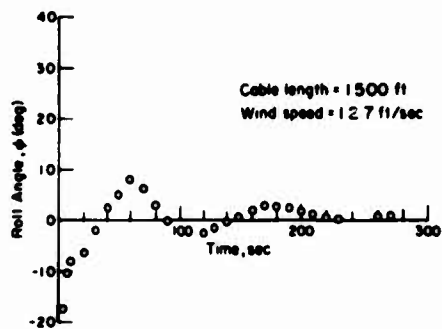
Figure 8. The Dynamic Responses of Test DV2-19



Y vs t for DV2-8

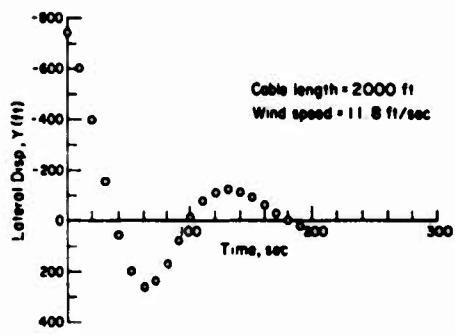


ψ vs t for DV2-8

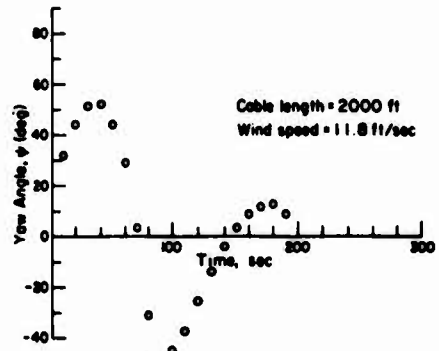


φ vs t for DV2-8

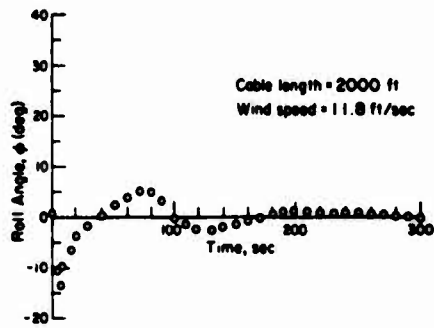
Figure 9. The Dynamic Responses of Test DV2-8



Y vs t for DV2-9



ψ vs t for DV2-9



φ vs t for DV2-9

Figure 10. The Dynamic Responses of Test DV2-9

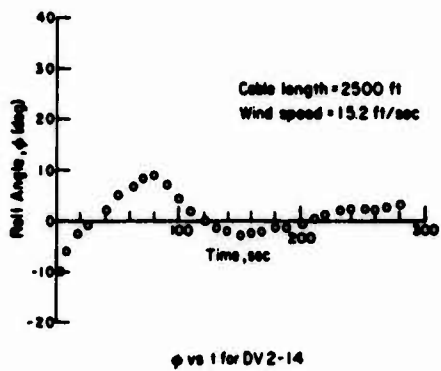
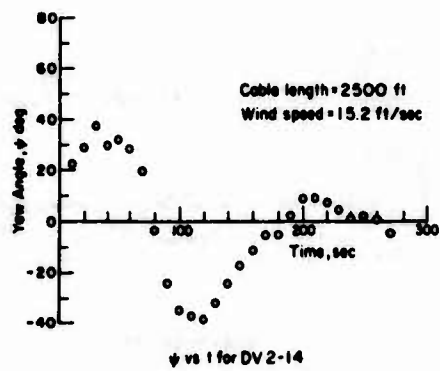
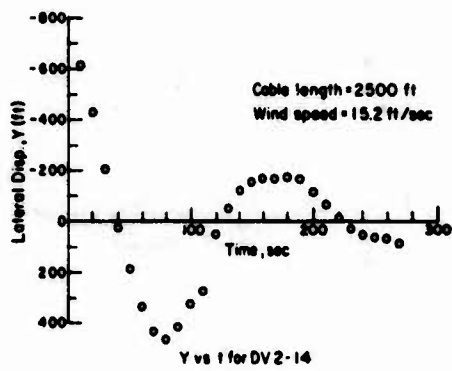
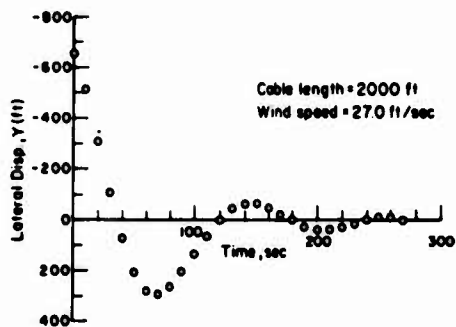
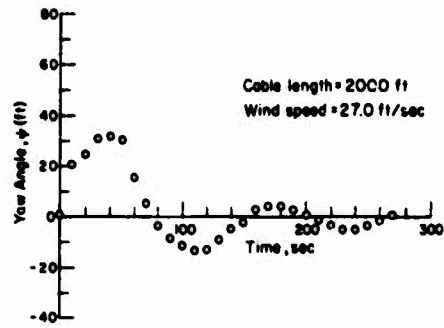


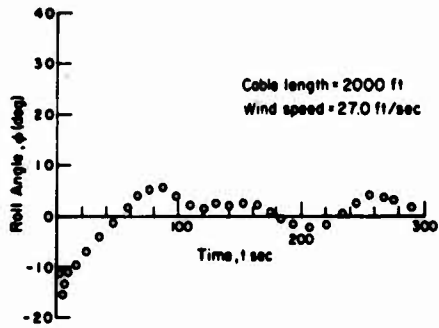
Figure 11. The Dynamic Responses of Test DV2-14



ψ vs t for DV2-13



ψ vs t for DV2-13



ϕ vs t for DV2-13

Figure 12. The Dynamic Responses of Test DV2-13

system's entire operational flight envelope ($0 < U < 117$ ft/sec $0 < L < 10,000$ ft) because of limitations on the perturbation technique and the wind speeds encountered. However, operational experience with the Family II balloon has shown that the system is qualitatively stable throughout its flight envelope, and that it has the most observable motion (least qualitative stability) in the flight regime of lower altitudes and wind speeds. Thus, it is felt that the scope of the present tests was adequate to characterize the dynamic stability of the 204 balloon.

The dynamic response results are shown in Figures 5 through 12, from which one may see that in each case the system has complete dynamic stability. For instance, there was no dynamic response where the number of cycles to half amplitude was greater than 1. Also, the shapes of the response plots are very similar to those for damped simple harmonic motion. The displacement response plots, ζ and Y versus t , have the greatest similarity, whereas the pitch and roll plots, θ and ϕ versus t , have a quick initial jump before settling into the simple damped motion. What this shows is that all of the possible dynamic modes of this system are heavily damped, except for a long period motion which is characterized by relatively large longitudinal or lateral displacements. This is the "upside-down pendulum" mode described by DeLaurier (1972), and since it has the least damping, the dynamic stability may be adequately described in terms of this mode.

The response plots for the longitudinal perturbations are given in Figures 5 through 8. The mean wind speed at the balloon varied somewhat from test to test, but the values remained close enough that variations of period and damping of the system with cable length may be assessed. First of all, one sees that the period of the oscillation increases with increasing cable length. This behavior is consistent with the mode's characterization as an "upside-down pendulum"; and, in fact, one may approximately obtain the value of the period, T , from the simple pendulum equation,*

$$T = 2\pi \left(\frac{\text{Total Balloon Mass} \times L}{\text{Net Static Lift}} \right)^{1/2} \quad (12)$$

Next, the plots show that the damping of the mode also increases with increasing cable length. This is consistent with the previously mentioned qualitative observation that the system appears least stable at lower altitudes and wind speeds. Unfortunately, no useable longitudinal data were obtained for a given cable length at different wind speeds. But atmospheric conditions were more cooperative for the lateral tests, and Figures 9 through 12 show the system's lateral responses for four combinations of wind speed and cable length.

Figures 9, 10, and 11 show responses with similar mean wind speeds at the

*Note that the Total Balloon Mass should include its enclosed gas and air.

balloon but different cable lengths, and one sees that the period increases with increasing cable length. This is the lateral version of the "upside-down pendulum" mode, and in fact, the magnitude of the periods are very similar to those of the longitudinal responses with the same cable lengths. However, the damping of the lateral mode is not as large as it is for the corresponding longitudinal mode. Again, this is consistent with operational experience where lateral balloon motion is more often seen than longitudinal motion. Qualitative observation is further confirmed by Figures 10 and 12, which show that the damping also increases with increasing wind speed.

Further, note that the lateral displacement, Y , is more strongly coupled with yaw angle, Ψ , than roll angle, θ . Also, after the initial perturbation has settled down into the single mode motion (about 1/2 of a period), the θ response is generally in phase with Y , and may be approximately described by

$$\theta \approx -\arcsin(Y/L) \quad (13)$$

This suggests that an appropriate physical model for analyzing the lateral "upside-down pendulum" motion of a balloon would be to assume that a short tether always stays in a plane defined by the balloon's $\bar{a} - \bar{c}$ axes (Figure 2).

Finally, note that the longitudinal plots do not suggest an analogous relationship between the longitudinal displacement, ζ , and the pitch angle, θ .

5. CONCLUSIONS

The auxiliary tether method for balloon perturbation proved to be a very suitable technique for studying the dynamic stability of the 204 system. The only constraint was the maximum available baseline distance between the main and auxiliary winches, which restricted the main cable length to 2500 feet or less for adequate perturbations. If larger baselines were available, there appears to be no major reason why this technique could not be applied to studying balloons at higher altitudes. For such applications, it would be helpful if the fall of the auxiliary tether could be slowed (perhaps by parachute) and the auxiliary winch speeded-up so that it could reel-in most of the tether before it reaches the ground. Winching-in the auxiliary tether along the ground was no problem for the present tests, but it was seen how this could be time restrictive and inconvenient for longer cable lengths.

The instrumentation for recording the dynamic responses was found to be very suitable, and gave accurate and usable data. The movie data required more time and labor for reduction than the information recorded on magnetic tape, which could

be directly reduced and plotted through a computer program. If the movie camera could be located directly next to the main winch, this would simplify the data reduction, and help insure that the balloon would stay within the camera's field of view during the perturbation. Also, note that the yaw information recorded by the camera could have been obtained by a directional gyro slaved to magnetic north.

Finally, it was shown that the 204 system had strong dynamic stability for the configurations of wind speed and cable lengths tested. Further, it was shown that the longitudinal stability increased with increasing cable length, and the lateral stability likewise increased with cable length, as well as with increasing wind speed. These quantitative measurements confirmed the qualitative observations that the system has good operational stability throughout its flight envelope.

Acknowledgments

This research was supported by the Defense Advanced Research Projects Agency (ARPA) of the Department of Defense and was monitored by the U. S. Army Missile Command, Redstone Arsenal, Alabama, under Contract Number DAAH01-73-C-0924 (Advanced Balloon Technology). Col. G. H. Greenleaf (USAF), of the Tactical Technology Office of ARPA, monitored the effort.

The tests were performed with the cooperation of the RCA/TELTA organization at Cape Kennedy Air Force Base, Florida; and it was through a close working relationship with their operations personnel, in particular: Louis Anelli, Carl Emery, William Pilcher, and their project manager, Robert Murkshe, that the test methodology was developed.

The data were reduced at Patrick Air Force Base, Florida, where the magnetic

tape information was processed by Michael Duffy of BCL with the cooperation of the Range Measurements Laboratory. Also, the camera data were processed by the RCA optical data reduction group, of which Ralph Gugol was particularly helpful.

References

- Bairstow, L., Relf, E. F., and Jones, R., (1915) The Stability of Kite Balloons: Mathematical Investigation, Advisory Committee for Aeronautics.
- DeLaurier, J. D. (1972) A Stability Analysis for Tethered Aerodynamically Shaped Balloons, Journal of Aircraft, 9 (No. 9) : 646-651.
- Haak, E. L. (1971) Wind Tunnel Test Results, Family II-D Aerodynamically Shaped Balloon, G. T. Schjeldahl Co. Report SER 0093.
- Hoerner, S. F. (1965) Fluid Dynamic Drag, Hoerner, Midland Park, N.J.
- Ollila, R. G., Duffy, M. A. (1974) Aerodynamic Performance of ARPA Family II Tethered Balloon System, Proceedings, Eighth AFCRL Scientific Balloon Symposium, Publication Pending.
- Redd, L. T., Bennett, R. M., and Bland, S. M. (1973) Analytical and Experimental Investigation of the Stability of a Balloon Tethered in Wind, Proceedings, Seventh AFCRL Scientific Balloon Symposium, AFCRL-TR-73-0071.
- Vorachek, Jerome J., and Doyle, George R., Jr. (1973) Comparison of Analytically and Experimentally Determined Dynamic Behavior of Tethered Balloons, AFCRL-TR-73-0284.

Experimental Investigation of Balloon Structural Response

E. J. Mills and J. J. Groom
Battelle Columbus Laboratories
Columbus, Ohio

Abstract

Balloon fabric strains were measured during the design verification test program on the ARPA Family II tethered balloon system. The strains were converted to membrane stresses or fabric loads using a constitutive relationship developed by Battelle's Columbus Laboratories. The numerical coefficients of this relationship were obtained from an experimental evaluation of the balloon hull material. Using the resulting balloon fabric stresses, the effects of static internal pressure loads and flight dynamic pressure loads were evaluated.

1. INTRODUCTION

Structural response to operating wind loads was examined in the Defense Advanced Research Projects Agency (ARPA), Family IID-7A tethered balloons. This balloon system includes a 200,000 cubic foot all-weather balloon that is designed to operate in winds up to 65 knots at altitudes up to 10,000 feet. In flight, the balloon is tethered with a 0.775-inch-diameter NOLARO cable weighing 0.202 lb/ft., with a minimum breaking strength of 26,000 pounds. In this paper, structural

response refers to the balloon fabric stress resulting from internal pressure and aerodynamic pressure loads during flight. Stress is a derived physical condition which is calculated either from the measured strain in the actual structure and its material properties or from mathematical relationships describing the structure's geometry and loading. For the ARPA balloon SN204, no theoretical analysis of the structure was available at the time of the testing program other than that for simple geometries, so the measured strain approach was selected to determine the structural response.

2. STRAIN MEASUREMENT

Strain was measured on the hull fabric using a linear variable displacement transducer designed and built by RCA/DELTA personnel under the direction of Range Measurement Laboratories, Patrick Air Force Base. These devices were designated as fabric monitors and included a linear variable displacement transducer (LVDT), mounting block, core displacement rod, and tail block. Both the transducer mounting block and the tail block were bonded to the balloon fabric surface. The spacing between the fixed tail block and the transducer was 2.5 inches. This spacing can be considered as an equivalent gage length, and, when divided by the travel distance of the core displacement rod, ± 0.125 inch, the resulting maximum strain capability of the fabric monitor is $\pm 50,000$ microstrain (one microstrain = 1×10^6 in/in.).

The signals from these fabric monitors were amplified and transmitted to a receiver in the telemetry van on the ground where they were recorded. Selected signals were recorded on Brush strip-chart recorders and all transmitted signals were recorded on FM tape in addition to the BCL Incre-Data digital tape recorder. The digital tape was then used in a data reduction computer program to obtain a printout of computed fabric stresses.

During the fixed-tether flight tests, only the steady-state conditions were used for the fabric monitor data acquisition periods. In steady winds, a one- or two-minute data run was made and the data recorded on the digital tape recorder. During the helicopter tow test phase of the program, several bursts of data were recorded when the helicopter speed was relatively steady, both during the high-speed and turn-around portions of the flight.

The fabric monitors were placed either in pairs aligned with the machine and transverse directions of the major fabric ply or in a three-element rosette with the third element at 45 degrees to these machine or transverse elements. A total of 21 fabric monitors were attached to the balloon hull. Figure 1 shows the general arrangement of these fabric monitors.

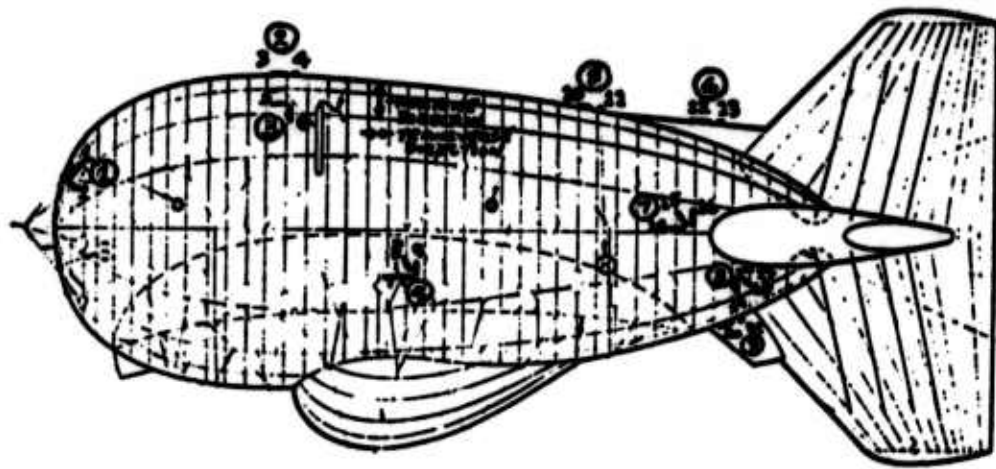


Figure 1. Family II 200,000 cu-ft Tethered Balloon

3. STRESS DETERMINATION

The hull fabric strain data recorded during the flight tests were converted to stresses using a constitutive relationship developed by BCL during this ARPA program. In order to utilize the relationship, the necessary material coefficients were required. These material coefficients are similar to the elastic or Young's modulus, shear modulus, and Poisson's ratio, which are used to convert measured strains to stresses in isotropic materials such as most common metals. For example, in a plane stress case, such as in-plane (membrane) loading of a thin plate, the strains are related to the stresses by the following relationships:

$$\epsilon_x = \frac{\sigma_x - \nu\sigma_y}{E} \quad (1)$$

$$\epsilon_y = \frac{\sigma_y - \nu\sigma_x}{E} \quad (2)$$

$$\gamma_{xy} = \frac{\tau_{xy}}{G} \quad (3)$$

where ϵ_x and ϵ_y are the tensile/compressive strains associated with the stresses σ_x and σ_y ; γ_{xy} is the in-plane shear strain associated with τ_{xy} , the shear stress normal to the x-y axes; E is the elastic or Young's modulus for the isotropic plate material; G is the shear modulus; and ν is Poisson's ratio. Note that the shear strains and stresses are related as a function of the shear modulus. The tensile/compressive strains and stresses are functions of ν and E , and these terms are also coupled to G for isotropic elastic materials. Thus, the shear stresses and strains are coupled to the tensile/compressive stresses and strains through the relationship,

$$G = \frac{E}{2(1+\nu)} \quad (4)$$

For a fabric material, however, and particularly a two-layer composite fabric, the relationship between the measured strain and the calculated stress is much more complex. The composite material used for the SN204 balloon has material properties which vary with the orientation in the material plane and which are nonlinear. The fabric tests also showed that the material tended to creep (strain continued to increase with no increase in load), and its Poisson's ratio was unusually large when compared with that determined for most common structural materials. These

observations of unusual material behavior are partially explained by the nature of a woven material itself, in that the fibers in the machine or warp direction are straight and the transverse or weave direction fibers are bent to go over and under the machine direction fibers. Other factors governing the behavior are the properties of the fiber and the coating or inter-ply material.

The material coefficients were obtained from a series of laboratory tests using a 12-inch-diameter by 42-inch-long cylinder of balloon fabric. The specimens were supplied by ILC Industries, the manufacturers of the balloon using this particular fabric. Strain gages were attached to the fabric specimens and data recorded during sequential loading combinations of internal pressure, axial and torque loads. The resulting strains were plotted as a function of the applied membrane loads. The slopes of these strain versus load curves were used to determine the material coefficients in a matrix equation relating the membrane loads to the resulting membrane strains. The resulting constitutive relationship for the SN204 hull fabric is

$$\begin{aligned}
 \begin{bmatrix} \epsilon_t \\ \epsilon_m \\ \gamma_{tm} \end{bmatrix} \times 10^6 &= \begin{bmatrix} 1524. & -(669.+62.) & 0 \\ -(669.-62.) & 1053. & 0 \\ 0 & 0 & 5490. \end{bmatrix} \begin{bmatrix} N_t \\ N_m \\ T_{tm} \end{bmatrix} \\
 &+ \begin{bmatrix} 0 & 10.6 & 0 \\ 10.6 & 0 & 0 \\ 0 & 0 & 0 \end{bmatrix} \begin{bmatrix} N_t^2 \\ N_m^2 \\ T_{tm}^2 \end{bmatrix} \\
 &+ \begin{bmatrix} 0 & -0.11 & 0 \\ -0.11 & 0 & 0 \\ 0 & 0 & 0 \end{bmatrix} \begin{bmatrix} N_t^3 \\ N_m^3 \\ T_{tm}^3 \end{bmatrix} \\
 &+ \begin{bmatrix} 0 & 0.0006 & 0 \\ 0.0006 & 0 & 0 \\ 0 & 0 & 0 \end{bmatrix} \begin{bmatrix} N_t^4 \\ N_m^4 \\ T_{tm}^4 \end{bmatrix}
 \end{aligned} \tag{5}$$

where the following notation is used:

- ϵ_t = transverse direction strain
- ϵ_m = machine direction strain
- γ_{tm} = shear strain in the t-m plane normal to the t and m axes
- N_t = transverse direction membrane stress
- N_m = machine direction membrane stress
- τ_{tm} = shear stress in the t-m plane and subscripts
 - t = transverse direction of fabric
 - m = machine direction of fabric.

In contrast to the isotropic material discussed earlier, there is no convenient equation, such as Eq. 4, relating the coefficients for the fabric material. This may be explained partly by the inherent nature of woven materials in that the fibers tend to behave as mechanisms and not as a homogeneous material.

In the balloon, the strongest direction of the fabric (machine direction) was carefully aligned to the hoop direction which is the direction of highest stress. The fabric monitors were also carefully aligned to these expected major load axes. Eq. 5 applies only to such an orientation.

The measured fabric strains can thus be converted to stresses by inverting this equation. A computer program for converting the strains to stresses was written by BCL and incorporated into the overall data reduction program used with the RML computer facility.

4. INTERNAL PRESSURE STRESS

An internal pressure test on balloon SN204 was performed in the Vehicle Assembly Building at Kennedy Space Flight Center. The purpose of conducting the test indoors was to eliminate any dynamic pressure effect on the balloon structure. Twenty-one fabric monitors were placed on the balloon as shown in Figure 1. The machine and transverse fabric directions are also indicated on the figure. The circled numbers refer to the gage set number. Some gage sets included two elements (biaxial) and others included three elements (rosette). During the internal pressure tests, the hull pressure was increased through a sequence from 1.5 to 3.75 IWG while the empennage pressure was held constant. The empennage pressure was also increased from 1.5 to 6.0 IWG while the hull pressure was held constant. During each test, the pressures were held at the designated levels for a period of two minutes before the fabric monitor strains were recorded.

5. DYNAMIC PRESSURE STRESS

During the tethered flights and the helicopter tow test, data were recorded from the fabric monitors and reduced to stress values using the computer. Figures 2 and 3 show selected fabric stresses for Gage Sets 3 and 8, respectively. Gage Set Number 3 is at the balloon mid-body near the top surface, and Gage Set Number 8 is on the port side aft-body near the horizontal stabilizer as seen in Figure 1. The background gridwork used on Figures 2 and 3 represents the tensile stress region of the constitutive relationship. The gridwork is arranged to aid the conversion from strains to stresses. The static hull internal pressure curves are those shown as solid lines and marked in hull pressure units of inches of water (IWG). The dashed lines on the figures represent the difference between the internal pressure stress and the total measured stress as calculated from the fabric monitor recorded strains. The numbers at the dashed line segments are the dynamic pressure values, q . At some of the gage sets, the total stress values follow a fairly obvious pattern related to wind speed.

One purpose of the structural data reduction is to predict structural response to higher winds than those already experienced by the balloon. This prediction can be made by determining the structural stress due to the dynamic pressure load, q , at the extrapolated wind speed conditions and then adding that stress component to the expected differential pressure stress component. The differential pressure stress component can be found at the specific gage set location from the experimental results.

As an example, the total membrane tensile stress state at Gage Set Number 3 will be calculated for a balloon wind speed of 65 knots ($q = 2.7$ IWG). The differential pressure, Δp , for a given flight configuration is determined by the following equation:

$$\Delta p = p_0 + C_p q$$

where p_0 is the internal pressure of the hull and C_p is the pressure coefficient for that gage set location on the balloon. The internal pressure at 65 knots was defined by

$$p_0 = 1.5 + q = 1.5 + 2.7 = 4.2 \text{ IWG}$$

Using a C_p value of 0.4, the total differential pressure Δp becomes

$$\Delta p = p_0 + 0.4q = 4.2 + 0.4(2.7) = 5.3 \text{ IWG}$$

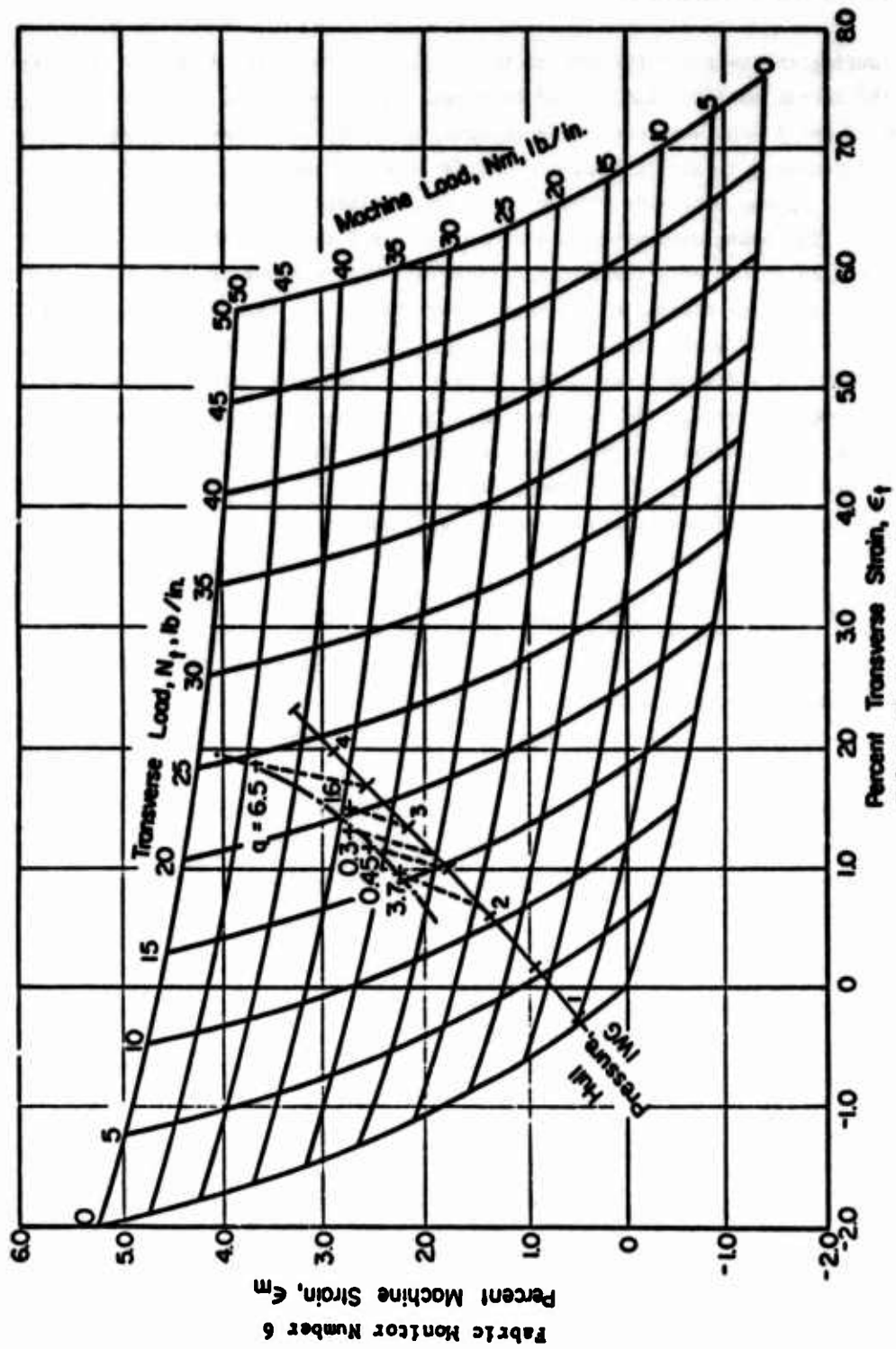


Figure 2. Fabric Stresses at Cage Set Number 3
Fabric Monitor Number 5

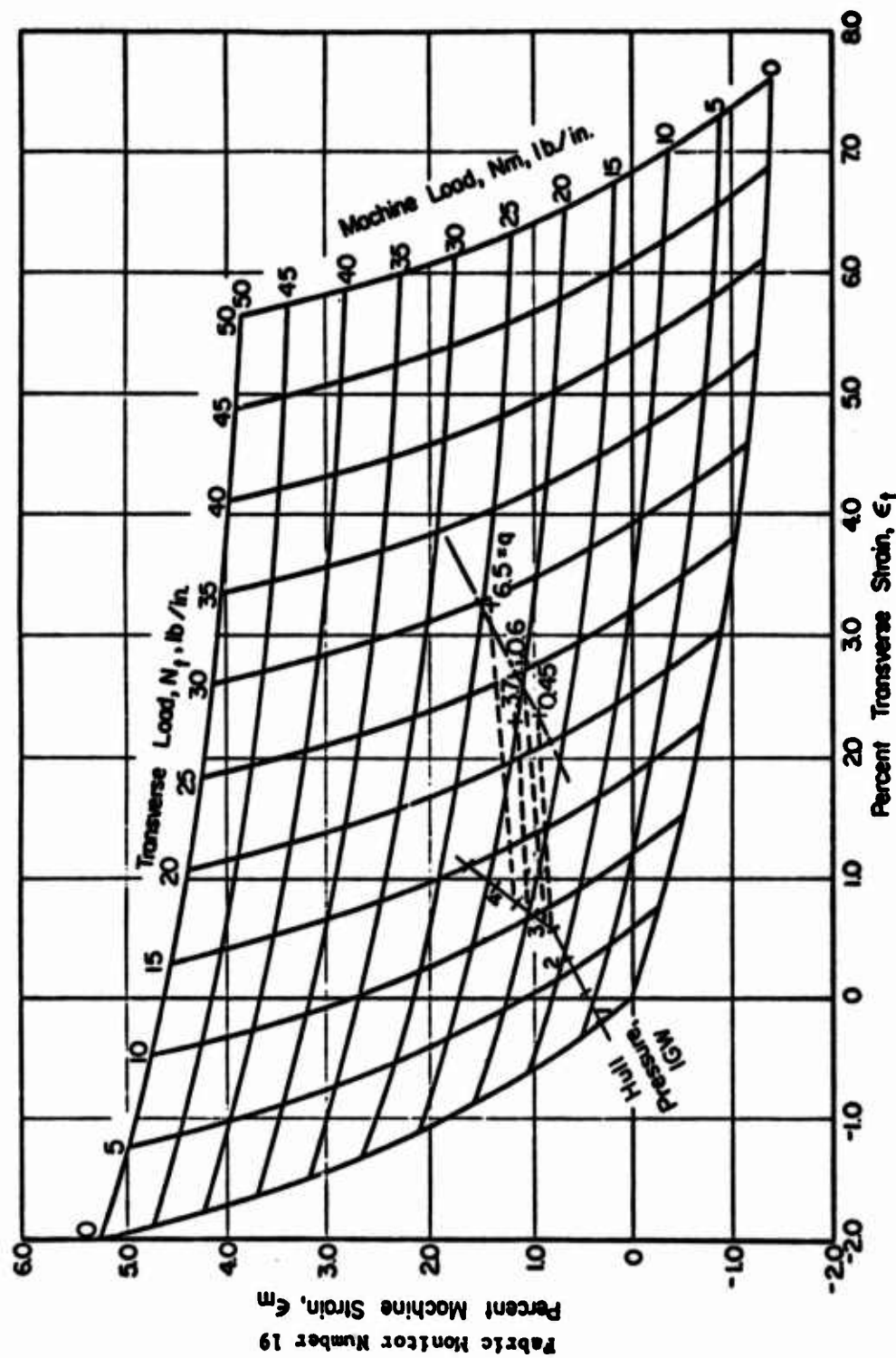


Figure 3. Fabric Stresses at Gage Set Number 8
Fabric Monitor Number 17

Applying this to Figure 2 gives the following differential pressure stresses.

$$N_m = 47 \text{ lb/in (machine direction)}$$

$$N_t = 32 \text{ lb/in (transverse direction)}$$

Next, the dynamic pressure stress must be added to those differential pressure stresses to obtain the total expected stress level. The dynamic pressure structural stress component can be derived from the data in Figure 2 for Gage Set Number 3. The dynamic pressure structural stress as a function of $q\alpha$ (for angle of attack $\alpha = 5$ degrees) for this gage set was plotted separately as shown on Figure 4. At 65-knot wind speed, the value of $q\alpha = 1.22 \text{ lb/ft}^2$ and the resulting extrapolated machine and transverse direction stresses are

$$N_m = 15 \text{ lb/in}$$

$$N_t = 2 \text{ lb/in}$$

Therefore, the extrapolated total fabric stresses at 65 knots are

$$N_m = 47 + 15 = 62 \text{ lb/in}$$

$$N_t = 32 + 2 = 34 \text{ lb/in}$$

This technique can be used to determine the expected stress magnitudes at selected wind speeds provided that an adequate material investigation has been performed to allow a determination of a sufficiently reliable constitutive equation for converting strains to stresses. In addition, the differential pressure stresses on the structure need to be understood along with the dynamic pressure stress behavior.

Acknowledgments

This research was supported by the Defense Advanced Research Projects Agency (ARPA) of the Department of Defense and was monitored by the U.S. Army Missile Command under Contract Number DAAH01-73-C-0924. Col. G. H. Greenleaf (USAF) of the Tactical Technology Office of ARPA monitored the effort. Review of this material does not imply DoD endorsement of factual accuracy or opinion.

q	q _a	Actual		Pressure		Difference	
		N _M	N _T	N _M	N _T	N _M	N _T
0.64	0.12	27.6	17.0	25.0	16.0	2.6	1.0
3.70	0.28	28.4	16.2	19.0	11.0	9.4	5.2
1.33	0.12	27.6	16.3	24.0	15.0	3.6	1.3
0.39	0.02	22.1	13.8	19.0	11.0	3.1	2.8
1.58	0.14	34.4	20.9	29.0	18.5	5.4	2.4
6.50	0.62	44.2	23.7	32.5	21.5	11.7	2.2

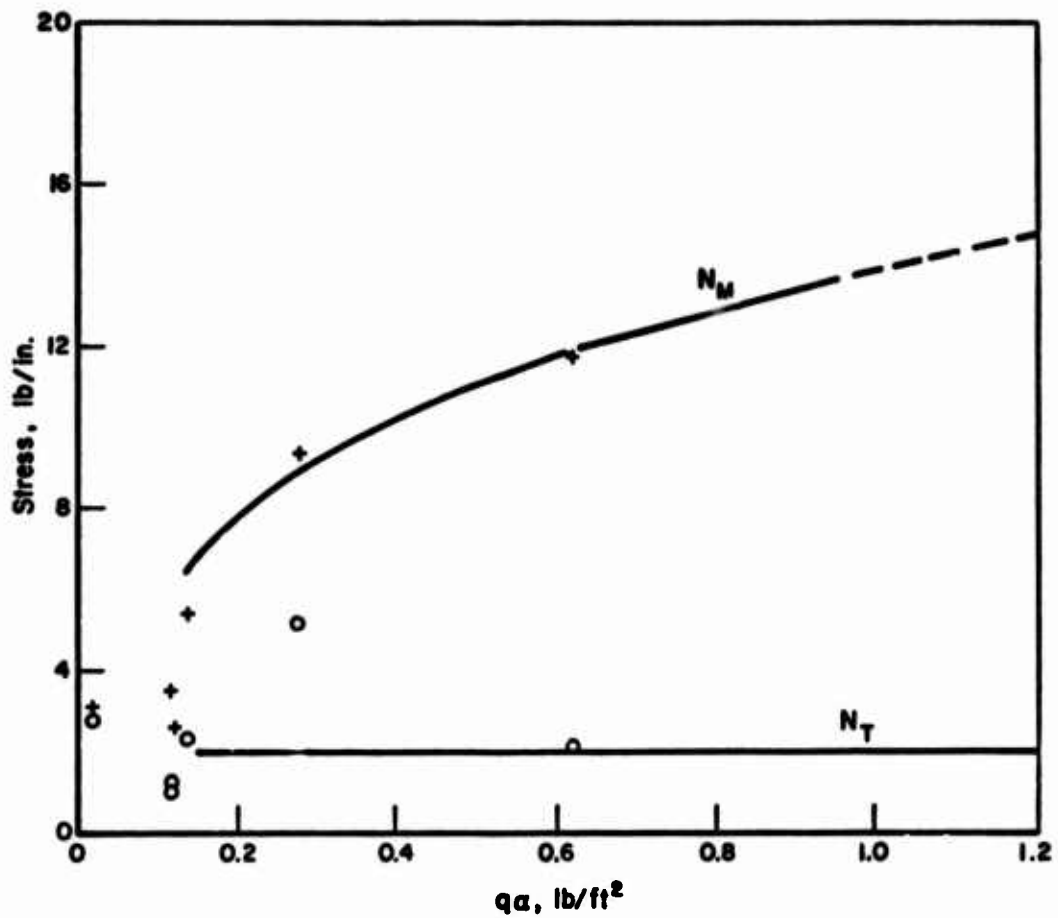


Figure 4. Dynamic Stress at Gage Set Number 3

Ballonet Gas Motion in Large Balloons

Charles F. Holt
Battelle Columbus Laboratories
Columbus, Ohio

Abstract

A study of ballonet gas motion in the ARPA Family II tether balloon was made using a 1/30th scale model. The shift of the center of gravity of the model as a function of pitch attitude was related to the movement of the center of buoyancy (CB). From these data, predictions of CB movement of the Family II balloon, for changes in pitch attitude up to ± 20 degrees, were made.

1. INTRODUCTION

Constant volume balloons operating at high altitudes require large initial ballonet volumes. Since the weight of air is over six times that of helium, the motion of the air (termed sloshing) at partial ballonet inflation levels may have a significant effect on the handling qualities of the balloon. The air shifting within the flexible constraint of the ballonet curtain causes a change in the shape of the helium compartment, thus causing a change in the location of the center of buoyancy. Because the actual shape of a partially full ballonet is not describable analytically, scale-model tests appear to be the best method for

obtaining information on center-of-buoyancy shift and the nature of the ballonnet gas motion.

In what follows, model-scaling criteria along with the results of an experiment with a 1/30 scale model of the ARPA Family II balloon, are presented.

2 SCALING CONSIDERATIONS IN MODELING BALLONET SLOSH

2.1 Fluid Forces

In scaling the sloshing phenomenon, no consideration was given to external aerodynamic forces. Frictional scaling effects are neglected because they are considered to be insignificant so long as the model is not made unreasonably small and the fluids used are not of obviously large viscosity.

Consideration of the physics of the sloshing phenomena leads one to conclude that the major forces acting on the fluid are inertial and gravitational. Dynamic similarity requires that the ratio of these forces, termed the Froude number, be the same at every point in model and prototype.

The gravitational forces arise due to fluid displacement when the slack ballonnet changes shape (due to a change in pitch attitude, for example) as shown in Figure 1. An equivalent volume of helium counterbalances the displaced air and is indicated by the dotted line. The net gravitational force driving the motion is then:

$$(\rho_A - \rho_H) g l^3 \quad (1)$$

where ρ_A and ρ_H are the densities of air and helium, respectively, and l is a characteristic linear dimension of the raised fluid.

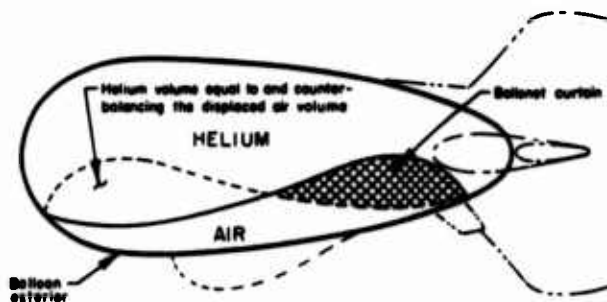


Figure 1. Unbalanced Mass or Fluid Driving the Ballonet Motion

The inertial resistance to the motion includes the entire mass of air plus that of the helium. This resistance is in the form of an inertial force developed during the motion of the air and helium which is:

$$\rho_A U_A^2 l^2 + \rho_H U_H^2 l^2 \quad (2)$$

Here U_A and U_H are representative of the velocities in the air and helium, respectively. For the case when the ballonet is half-full, it seems reasonable to neglect the inertial forces in the helium for those in air due to the large density differences and the fact that the characteristic velocity in helium will be lower than that in air. Using the dimensions of the Family II balloon, the magnitudes of the inertial forces in helium were estimated to be lower than those in air by at least an order of magnitude. Therefore, the Froude number may be written as

$$F \sim U_A^2 l^2 / (1-\alpha) g l^3 \quad (3)$$

where the density ratio, $\alpha = \rho_H / \rho_A$.

For modeling purposes, scale factors may be determined by requiring that the Froude number be equivalent in both model and prototype ($F_m = F_p$). The characteristic velocity may be represented by the length, l , divided by a characteristic time of the motion, say one period of oscillation, t , then equating Froude numbers yields,

$$t_p^2 / t_m^2 = l_p (1-\alpha_m) / l_m (1-\alpha_p) \quad (4)$$

It is not surprising that the time scale depends upon the length scale and the density ratio. Both model and prototype are to be operated in the same gravitational force field so that size will determine the forces and resultant motion. The above relation allows the choice of two parameters, fixing the third among the three variables of length, time, and density.

2.2 Choosing a Scale

In Table 1 two length-scale ratios are illustrated along with the choice of gases or liquids as the test fluids. The density ratio is fixed for illustrative purposes as 0.14 which is the ratio for helium/air as used in the full scale. It is assumed for illustration that this ratio can be maintained with a pair of liquids so that the time scale [from Equation 4) is simply the square root of the length ratio. For case (a) the ballonet fluid is air and for (b) it is water. Any

Table 1. Scale Parameters For Two Models

Design Parameters	$l_p = 5l_m$	$l_p = 24l_m$
Model density ratio	$\rho_H/\rho_A = 0.14$	$\rho_H/\rho_A = 0.14$
Time scale	$t_p = \sqrt{5} t_m$	$t_p = \sqrt{24} t_m$
(a) Ballonet fluid	Air	Air
Fluid above	Helium	Helium
Ballonet weight	18.4 lbf	0.166 lbf
Displaced weight*	3.1 lbf	0.0288 lbf
(b) Ballonet fluid	Water	Water
Fluid above	$\rho = 0.14 \rho_{\text{water}}$	$\rho = 0.14 \rho_{\text{water}}$
Ballonet weight	15,000 lbf	135 lbf
Displaced weight*	2,580 lbf	23.3 lbf

*Weight is for 20 percent ballonet displacement offset by an equivalent volume of fluid above ballonet.

density ratio other than $\beta_m = 0.14$ may result in a somewhat different shape (however slight) from the prototype shape under the same relative conditions.

Table 1 also contains the ballonet volume when 50 percent full and the total ballonet weight for each fluid. The figures indicated as "displaced weight" have been calculated by taking the weight of 20 percent of the ballonet fluid diminished by the weight of an equal volume of the fluid above the ballonet. This gives an indication of the experimental measurement requirements. From an inspection of the ballonet weights, it may be concluded that it is impractical to use water in the larger two models and gas in the smaller models. In the former case, the weights are prohibitively large and in the latter case they are too small for reasonable measurement.

2.3 The 1/30th Scale Model

A model of the order of 1/24 full scale with liquids used for the test fluids was considered to be the most suitable choice giving measurable force differentials with a reasonable size model. The length scale finally chosen was 1/30 for economy and manageability.

It was not possible to reproduce the prototype density ratio of $\beta_p = 0.14$ with available liquids. The actual choice was to have acetylene tetrabromide (ATB) as the ballonet fluid with water above the ballonet. Thus, the density ratio was set at $\beta_m = 0.337$. Dupont Surlyn[®] was chosen as the ballonet fabric because of its formability over a mold to the exact shape required and because of its resistance to attack from ATB.

The basic scale factors are shown in Table 2.

Table 2. Descriptive Characteristics of the 1/30 Scale Model

Time Scale	Density Ratio	Model Fluids
$t_p = 4.8t_m$	$\beta_m = \frac{\rho_H}{\rho_A/m} = 0.337$	Water acetylene tetrabromide

3. MODEL TESTS

3.1 Apparatus

The model was fabricated in two half-shells by vacuum forming from sheets of clear plastic material. The ballonet curtain was designed to lie flat against the hull when completely deflated by stretch-forming the Surlyn[®] over the mold used for the hull. The transparent shell was supported in a cradle formed of plywood and 2-inch angle iron [see Figure 2], then suspended from the ceiling by steel cables fitted with load cells. Figure 3 illustrates the support structure.

Direct measurement of the motion of the ballonet was obtained as a movement in the center of gravity of the scale model through the shifting support cable loads. For the CG measurements, the model was placed at several pitch attitudes by rotating and locking the upper frame in each position. With a nonhomogeneous body where the mass distribution changes with orientation, the CG can only be located at some point between supports. The response of the ballonet to sinusoidal pitching motion and to step changes in pitch attitude was recorded on 16 MM film.

3.2 Center of Buoyance

In a balloon with a ballonet partially inflated, the attitude of the balloon will determine, within limits, the location of the center of buoyancy. The centroid of the balloon is not coincident with the centroid of the helium volume. This situation is illustrated in Figure 4(a) and (b). In Figure 4(a) the buoyant force on the entire shell, without regard to the interior distribution of gases, is considered. In Figure 4(b) the same situation is depicted, but the buoyant force on the two-gas volume (helium/air) is shown separately. Since the gases are homogeneous within their respective volumes, the buoyant forces and the gravitational forces act through the centroid of volume for each gas as shown. Because the gas in the ballonet is air, the buoyant force balances the gravitational force. Both 4(a) and 4(b) are two descriptions of the same situation, and moments taken about the hull centroid (Point O) may be equated. The result is a relation

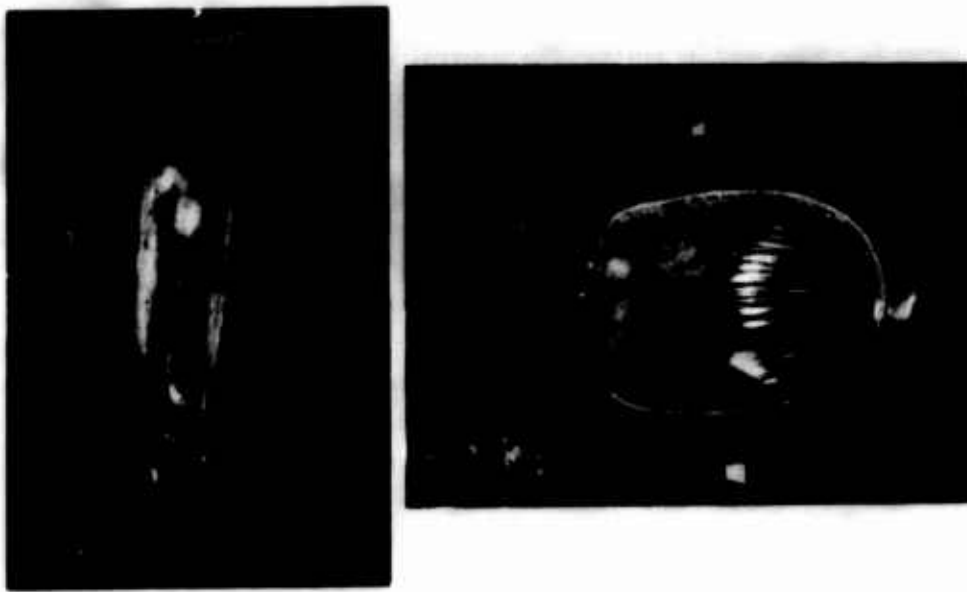


Figure 2. 1/30 Scale Model (Lower Half Shell)
With Fully Inflated Ballonet

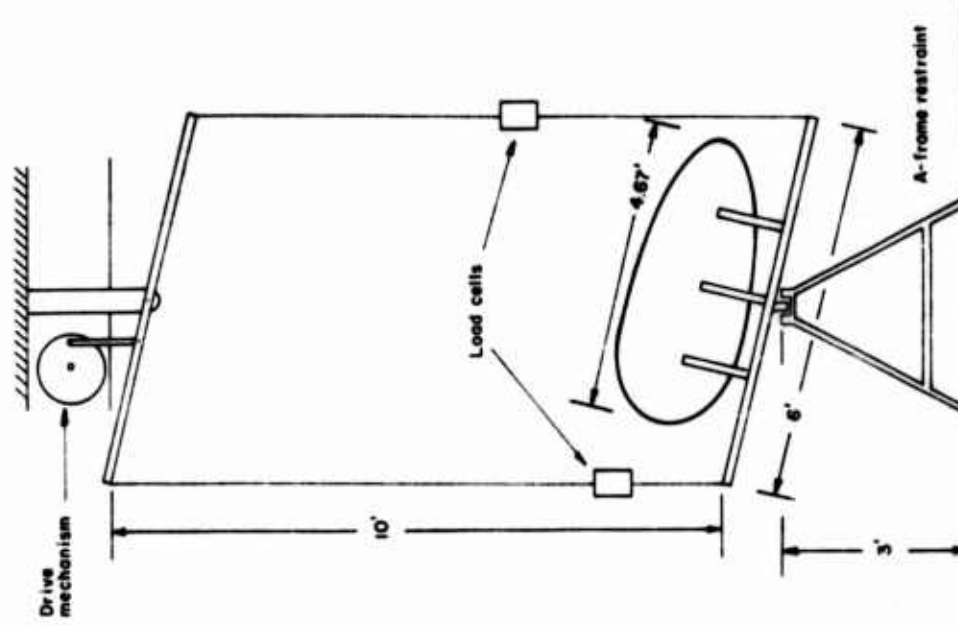


Figure 3. Support Assembly

between the center of gravity of the fluid system and the center of buoyancy of the helium which can be written as

$$X'_{CG}/X'_{CB} = (1-\theta)/(V_A/V_H + \theta) \quad (5)$$

where X'_{CG} and X'_{CB} are the perpendicular distances between point O and the forces F_g and F_{B_H} , respectively and V_A , V_H represent gas volumes.

As θ approaches zero the ratio X'_{CG}/X'_{CB} approaches the value V_H/V_A . The opposite extreme is that of a homogeneous body, $\theta = 1$. In this case both the center of buoyancy and the center of gravity are located at the volume centroid of the body and the ratio X'_{CG}/X'_{CB} has no meaning since both distances are zero. Thus, by measuring X'_{CB} from tests, the value X'_{CG} may be found in Equation (5). The position of the CG and CB measured along the axis of the balloon from the volume centroid is $X'_{CG}/\cos \alpha + Z_{CG} \tan \alpha$ and $X'_{CB}/\cos \alpha - Z_{CB} \tan \alpha$, respectively. For the present work the Z components are neglected since they are unobtainable from the experimental setup.

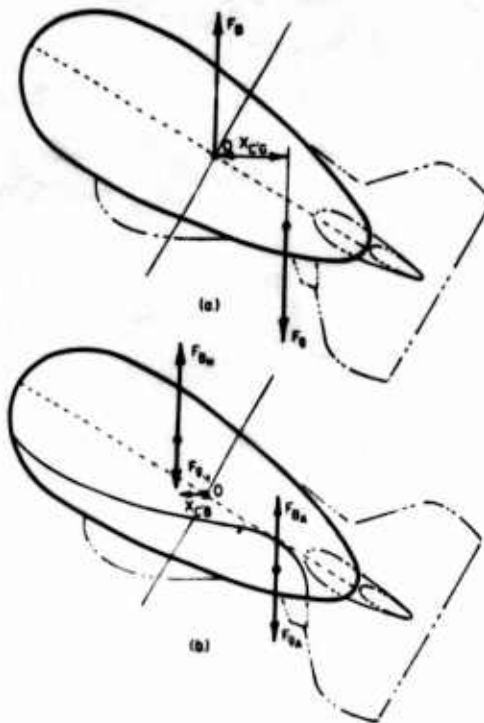


Figure 4. Buoyant and Gravitational Forces

4. EXPERIMENTAL RESULTS

4.1 Movement of the CG

Two photographs of the model at pitch attitudes of ± 20 , degrees are shown in Figure 5. The displacement of the ballonet fluid is clearly indicated in the lower half of the hull. Subtracting out the influence of the model assembly leaves only the CG of the fluid system. This point, X_{CG} (measured from the nose) shifts due to the changing shape of the ballonet with pitch angle, α . The value of X_{CG} (computed as a percentage of the length of the model measured from the nose) is illustrated in Figure 6.

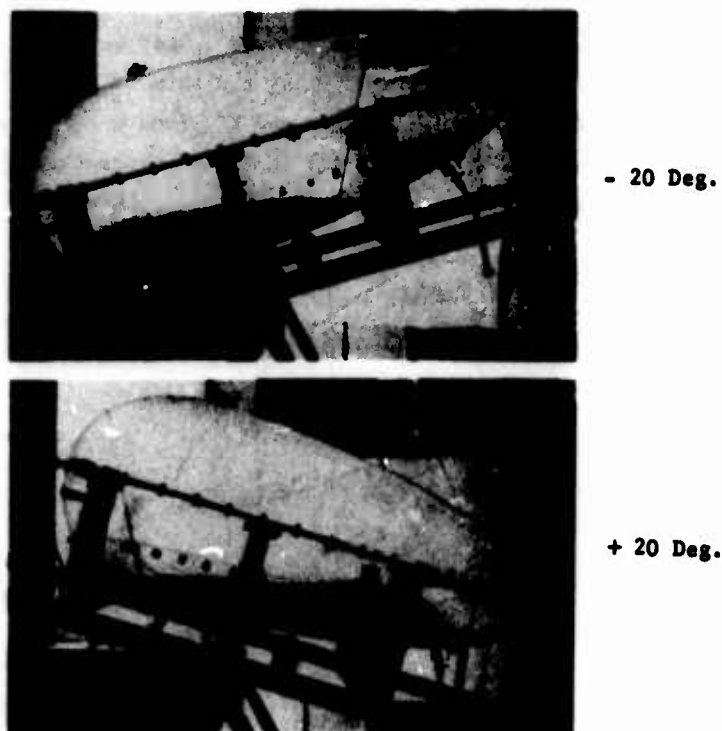


Figure 5. Model At Various Pitch Attitudes

The vertical line through the 42 percent position is the center of volume for the hull and represents the CG and CB for the special case where the density ratio is unity. For $\sigma = 0.337$, the movement of X_{CG} of the fluid system in the model is almost linear between the angles ± 20 degrees. The slight deviation from the linear may be seen at either end of the α range, due to the ballonet restricting fluid movement. The data indicate that the maximum travel of the CG is about 20 percent of the total length of the hull. This is a variation of ± 10 percent

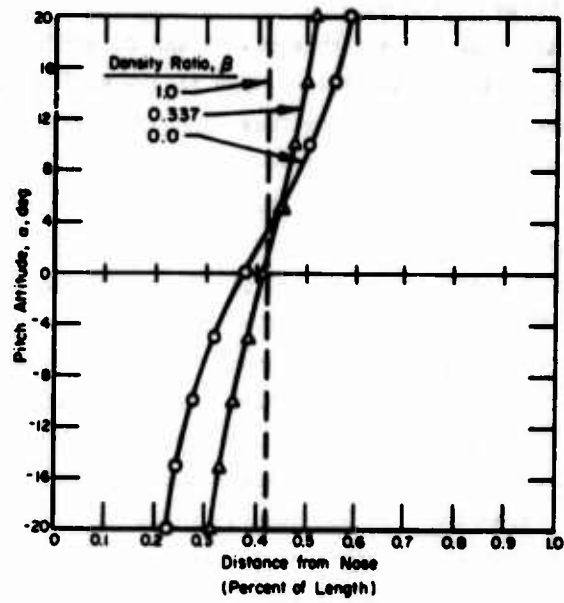


Figure 6. C.G. Dependence on Pitch Angle, α

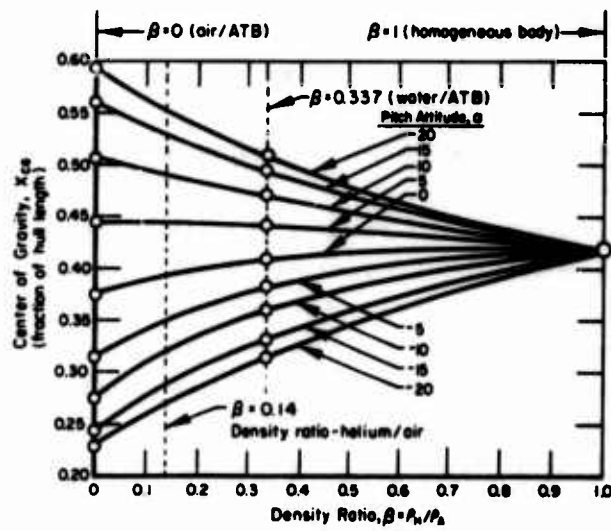


Figure 7. C.G. Dependence on Density Ratio, β

about the volume centroid of the hull.

The shape of the ballonet, and thus the CB and CG shift, can be expected to depend on the density ratio of the fluids. The larger θ , the smaller the CG variation and, conversely, for smaller values of θ , larger CG variations will result, up to a maximum defined by the ballonet constraints.

The density ratio was decreased to approximately zero by removing the water from the model and leaving the ATB in the ballonet. With the air/ATB system the movement of the CG with pitch angle is more pronounced as can be seen in Figure 6. For this system, the CG moves slightly further forward than it moves aft of the volume centroid (19 percent forward as opposed to 17 percent aft).

For a density ratio of 0.14 (helium/air) the CG migration should fall somewhere in between the experimentally determined curves for $\theta = 0.337$ and $\theta = 0.0$. To obtain this location, the curves of Figure 6 are replotted in Figure 7 with the pitch angle as a parameter. As the density ratio is decreased, the maximum travel of the CG for the limiting pitch angles (± 20 degrees) increases and reaches a limit at $\theta = 0.0$. The family of curves drawn through the points is approximate. The estimated travel of the CG for $\theta = 0.14$, as determined from Figure 7 is presented in Figure 8.

4.2 Predicted CB Movement

The CB, for the fluid above the ballonet can be determined with the aid of Equation (5) using $\theta = 0.14$.

Thus, the movement of the center of buoyancy as a function of pitch angle is obtained as shown in Figure 8.

For a helium/air system with a half-full ballonet, the CB is shown to move 4.5 percent forward and about 5.5 percent aft of the volume centroid at the extreme pitch angles. This represents a total movement of 10 percent between ± 20 degrees pitch. However, the balloon can be realistically expected to fly between 0.0 and + 20.0 degrees pitch under normal conditions. This restricts the possible CB movement between -1.0 and + 4.5 percent, or a total of 5.5 percent. Translated into full-scale dimensions, this implies a movement of 6.9 feet. If a buoyant lift of 6,000 pounds moving over this distance is assumed, then the moment due to a shifting CB can be over 41,000 ft-lb. For comparison, the moment generated by the lift on the balloon in a 15-knot wind at an angle of attack of 15.0 degrees is about 20,000 ft-lb when measured about the volume centroid of the hull. Although the balloon would not normally be expected to experience angle of attack changes as violent as 20 degrees, it seems clear that the moment due to CB shift can easily be of the order of the aerodynamic moment.

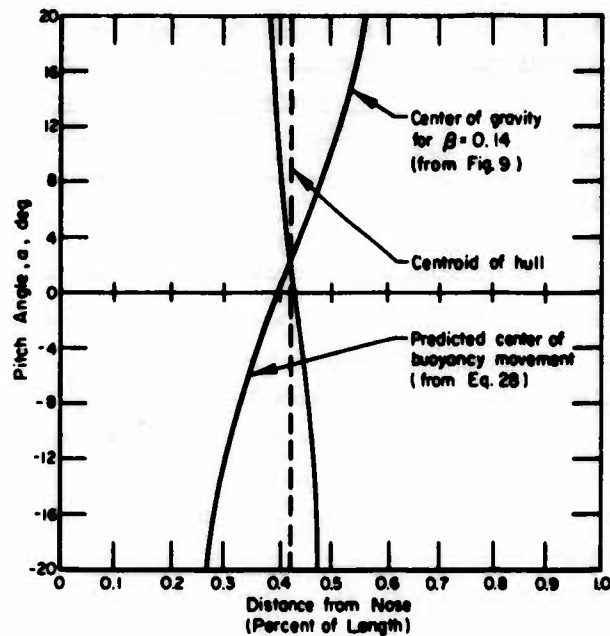


Figure 8. Predicted Center of Buoyancy Location As A Function of Pitch Angle

4.3 Motion-Picture Data

The upper frame of the model assembly was connected to a drive mechanism which was designed to impart a sine wave-like oscillation to the frame. In order to avoid possible damage to the ballonet due to heavy inertia loads imparted by the ATB, the amplitude was restricted to ± 10 degrees. The maximum rotational output from the gear reduction drive to the frame was rpm. This speed corresponds to a full-scale time period for the oscillation of $T = 48$ seconds. The results of the pitch tests were recorded at 32 frames per second.

Observation of the motion during the experiment suggests that the ballonet slosh is in phase with the forced oscillation of the shell. Thus, the ballonet responds rapidly to changes in the balloon pitch angle so that the motion appears to be quasi-steady.

To obtain some indication of the ballonet slosh period, a series of tests was run to note the response of the ballonet to a given step change in pitch angle. The model was placed in either a nose-down or nose-up position and then manually brought to the horizontal (within 1 second) and held there by causing the frame to come to rest against a stop. Motion pictures provided the means by which the period of slosh was measured (via counting frames between peaks). In all cases, the ballonet motion damped out within three cycles. These results are presented in Table 3.

Table 3. Slosh Periods For A Half-Full Ballonet

Pitch Angle Change degrees	Time Required to Change seconds	Estimated Period, seconds			
		First Cycle		Second Cycle	
		Model	Full Scale	Model	Full Scale
-20 0	1.19	2.00	9.6	2.80	13.4
+20 0	0.78	2.35	11.3	3.00	14.4

The pitching motion of the ballonet appears to have a period of about 10 to 14 seconds. Of course, much longer periods may be present but the amplitudes of the motion are insignificant. It seems reasonable to conclude that full-scale balloon pitching motions with periods greater than 20 seconds will be accompanied by in-phase ballonet sloshing motion. This period is much shorter than the theoretical period for all reasonably long tether lengths throughout the speed range of the Family II as shown in Reference 1.

The slosh period of 10 to 14 seconds compares favorably with the values calculated by an approximate analytical technique which considers the ballonet to behave as a modified fluid pendulum. This simple approach gives a period of about 10 seconds.

5. CONCLUSIONS

The CB movement for a balloon of the ARPA Family II type with a half-full ballonet appears to be about 7 feet when the balloon goes from +20 to 0 degrees pitch. Such changes in the location of the buoyant force can result in significant moments possibly affecting the static trim and stability of the balloon.

From the dynamic tests the period of motion of ballonet slosh appears to be about 10 to 14 seconds. Approximate analytical computations yield similar results. This indicates that for any balloon pitching period significantly longer than 10 seconds the ballonet motion may be considered quasi-steady. Thus, the static CB versus pitch attitude may be used in the equations of motion and in any stability analysis.

Acknowledgments

This study was performed as a part of the Battelle Balloon Technology Support Task (Task No. 3), sponsored by the Defense Advanced Research Projects Agency (ARPA) of the Department of Defense, and monitored by the U.S. Army Missile Command, Redstone Arsenal, Alabama, under Contract No. DAAH01-72-C-0982. Dr. Francis W. Niedenfuhr and Colonel George H. Greenleaf, of the Tactical Technology Office of ARPA were technical monitors for the program.

References

Brown, J. H., et al., (1973), "Balloon System X - Systems Analysis", Tactical Technology Center, Battelle-Columbus Laboratories.

Appendix A

Fabric Scaling Considerations

The need to choose a ballonet fabric for the model raises the question of suitability in the context of the experimental objectives. Briefly, these objectives are that: (1) the ballonet surface assumes a geometrically similar shape under similar loading, and (2) that the fabric not unduly influence the response of the sloshing liquid by either being too heavy or too stiff. The first requirement is really no problem so long as the fabric is not obviously resistant to bending or is not made irregular. The second requirement is more difficult to evaluate.

In an attempt to evaluate the importance of bending stiffness, a comparison was made between the bending strain energy, U , of a sheet (of unit width and length, l) and the translational kinetic energy, KE , due to an assumed harmonic motion of the sheet. The calculation was only approximate, since the nature of the edge clamping of the fabric was not included. For the materials, lengths, and periods of motion considered in this work the ratio U/KE was found to be much less than unity, thus suggesting that fabric stiffness was not a critical factor in model scaling.

Fabric scaling criteria suggested by Sedov* was designed to insure that the stresses imposed on the model fabric are geometrically similar to those produced in the full scale. The system of parameters for obtaining geometric similarity of fabrics prepared from materials with the same stress-strain relations are; the difference in densities of the fluids across the fabric, the elastic modulus of the fabric, a characteristic length, and the weight of the fabric. These may be grouped into scaling conditions linking the fabric properties and the model fluid system. The material finally chosen for the ballonet was judged to be relatively lighter and more flexible than the prototype fabric.

*Sedov, L. L. (1959), Similarity and Dimensional Methods in Mechanics, Academic Press, New York, pp 48-52.

A New Kind of Powered or Tethered Balloon

Alain Balleyguier
Cheville, France

Abstract

This paper contains four sections, divided as follows:

- Part 1: Presentation of research principles and models selected. Calculations and wind tunnel results.
- Part 2: Tethered unpowered balloons: scheduled production models, all-weather, in a wide range of sizes.
- Part 3. Powered balloons: (a) probatory model (2600 lb of useful load, moored high above the ground; (b) a 40-ton load-under-sling model—mainly for oil companies in areas lacking transport facilities; (c) a 400-ton load-under-sling model, whose scheduled main use is for transportation of nuclear pressure vessels between factories and power unit locations (volume is $28 \times 10^6 \text{ ft}^3$; length, 750 ft [twin-hulled]; cruising speed, 70 to 75 mph). This semirigid balloon will be constructed of high-performance new fabrics made with PRD 49 fibers. It will have a performance/weight ratio 2 to 3 times better than Dacron. The mooring cables will also be made with this material, with a resistance/weight ratio about 8 times better than equivalent steel cables.
- Part 4. New types of configurations.

Contents

1. Introduction
2. Ripstop Development
3. Triaxially Woven Fabric
4. Conclusions

Design, Development, And Testing Of New Aerostat Material

Eugene E. Alexandroff
ILC Dover
350 Peer Street
Dover, Delaware

Abstract

A series of new candidate materials for use in aerostats have been designed, developed, tested and compared with present state-of-the-art materials. The tests were conducted under contract to the Air Force Cambridge Research Laboratories. This effort was very extensive and produced two promising advancements in aerostat fabric.

One new material is a ripstop fabric made from Dacron* and Kevlar 29* yarns. This fabric affords an excellent strength-to-weight relationship and exhibits much improved tear strength over commercially available ripstop fabrics.

The other new material is a triaxially woven fabric incorporating a three yarn system. Unlike conventional fabrics having warp yarns and fill yarns intersecting at 90°, triaxially woven fabric has two warp yarn systems and one fill yarn system intersecting at 60° and forming a triangle. This construction provides bias strength to the fabric, increasing dimensional stability and tear strength. New testing procedures required for this fabric and coating techniques are also discussed.

*DuPont Tradename

1. INTRODUCTION

Under contract to the Air Force Cambridge Research Laboratories (F19628-73-C-0155), the ILC Materials Department has recently developed new superior materials specifically for aerostat applications. This effort was very extensive and has produced two major advancements in the state-of-the-art of balloon fabric. The effort was not limited to improved envelope material but also included an extensive effort in the development of new empennage materials.

The disadvantage of present lightweight empennage fabric is poor tear strength. One way to improve the tear strength is the utilization of ripstop weaves. Use of conventional yarns in conjunction with ripstop weaves affords a two and one-half fold increase in uncoated fabric tear strength; however, when coated, the improved tear property is lost. To obtain the advantage of the ripstop weave requires the judicious use of dissimilar moduli materials, such as, Kevlar 29 and high tenacity Dacron yarns.

There are basically two types of fabric geometries that are now being used to meet the requirements of structural envelope material. These types are: double substrate coated two sides, and single substrate coated two sides. The double substrate ply construction provides exceptional dimensional stability with increased tear resistance but high weight penalties. Single substrate fabrics are generally lower in weight but in order for a single substrate fabric to have good dimensional stability, it must be combined with films having a high modulus which usually results in a stiff material having poor flex life. One way to solve the high weight and dimensional stability problems with double and single substrates is the use of triaxial weaves.

Although the two experimental fabric constructions were designed to meet the requirements for a 100,000 ft³ balloon, they are still low enough in weight to use in a 45,000 ft³ balloon. As a result, a 45,000 ft³ balloon, made from these experimental fabrics is now under construction for AFCRL.

2. RIPSTOP DEVELOPMENT

The distinctive characteristics of lightweight, plain-weave orthogonal fabrics include high tensile strength, tight weave, low

racking characteristic, and relatively low tear strength. However, tear strength is dependent upon the fabric weave, crimp distribution, yarn strength, and yarn elongation. It is important to note that the yarns fail individually in tension, and this is the reason that the fabric's tear strength is so much lower than its tensile strength where all the yarns fail at the same time.

It will be apparent that fabric weave can have a great influence on tear strength. All other construction factors being equal, a ripstop weave will have more than two and one-half times the tear strength of a 1 x 1 plain weave, the reason being that the two ripstop yarns act as one in the del and they break at the same time. The higher original tear strength of a ripstop weave may not be retained when such fabrics are coated. A 2.0 oz/yd² plain weave Dacron fabric has an uncoated tear strength of four pounds and a coated fabric tear strength of two pounds. A 2.0 oz/yd² Dacron ripstop fabric has an uncoated tear strength of ten pounds and a coated fabric tear strength of five pounds.

In order to further improve the tear strength of the ripstop weave after coating, it is necessary to integrate a second, stronger yarn system into the construction. In this case, Dacron and Kevlar 29 yarns are used where the Kevlar 29 yarns function as the ripstop and the Dacron yarns provide the body of the fabric.

2.1 Ripstop Fabric Design Criteria

Due to the high cost of the Kevlar 29 yarn, ILC Dover ran a study to minimize the Kevlar 29 usage in the structural ripstop fabric. The following equation was used to determine what percentage of the construction should be Kevlar 29 and what percentage should be Dacron, Type 52.

$$\sigma(\text{lbs/in}) = cE_X D_X X + cE_Y D_Y Y \quad (1)$$

where: σ = ultimate fabric stress (lbs/in)
 c = ultimate elongation (in/in)
 E = Tenacity (GPD)
 D = denier
 X, Y = numbers of yarns per inch

$$140 = \frac{(.033)(75)(70)X}{454} + \frac{(.033)(630)(200)Y}{454}$$

$$100 = X + Y \quad (2)$$

solving simultaneously:

$$Y = 11.6$$

$$X = 88.4$$

2.2 Problems Encountered

The development of the Dacron/Kevlar ripstop fabric was initiated using commercially available yarns. Because of this decision, the resulting fabric was unacceptable for coating due to the excessive shrinkage in the Dacron yarns and the absence of shrinkage in the Kevlar 29 yarns.

The dissimilar moduli of the Kevlar 29 and Dacron Type 52 yarns prevented the satisfactory culmination of this design effort. Although one physical fabric was woven, two definite breaking strengths resulted. The first breaking strength indicated the breakage of the Kevlar 29 yarns. The second breakage indicated the breaking strength of the Dacron yarns. Analysis of this phenomenon indicated that this type of failure defeated the purpose of the fabric design. When the Kevlar 29 yarns failed, although the Dacron yarns maintained adequate tensile to sustain static loads, the increased tear strength provided by the Kevlar 29 yarns is lost. Therefore, this construction was functionally unacceptable.

Thorough analysis of the problems encountered in mixing dissimilar moduli materials resulted in a design modification to perfect the Dacron/Kevlar ripstop construction. The approach was to change the orientation and crystallinity of the Dacron yarn, thus increasing the modulus, while twisting and plying the Kevlar 29 yarn to reduce the modulus.

The next design iteration consisted of lowering the twist per inch in the Dacron yarn, increasing the twist per inch in the Kevlar 29 yarn, 2-plying the Kevlar 29 yarn and changing from two strands of Kevlar 29 for the ripstop to one strand. These changes effected an increased ultimate elongation of the Kevlar yarn and resulted in a fabric having a minimum breaking strength in either yarn system of 80 pounds per inch; however, the Kevlar 29 yarn still broke first. In addition, the single strand of Kevlar 29 yarn only had 10 pounds of tear strength and the two-ply Kevlar 29 yarn presented excessive bulk at the cross-over. This bulk presented considerable coating difficulty. Consequently, another design iteration was initiated. Considerations for this design iteration were:

- cold-stretched, pre-shrunk 140 denier Dacron yarn
in lieu of 55 denier preshrunk Dacron yarn
- lower twist per inch in the Dacron yarn
- higher twist per inch in the Kevlar 29 yarn

The rationale for this design iteration was to provide for a flatter fabric, thus enhancing the coating capability, while bringing the yarn moduli closer together to effect complementary load sharing between the two yarn systems.

During the course of this materials program, it was decided to pursue the development of triaxial materials for the balloon hull and utilize the advanced Dacron/Kevlar ripstop construction for the empennage. Because of this decision, the scope of the ripstop design criteria was changed to reflect the lower strength requirements of the empennage application. Continued development efforts with the Dacron/Kevlar ripstop construction were sized to these lower requirements.

2.3 Results

Preproduction samples of the ripstop configuration were obtained for physical properties testing; both coated and uncoated samples were evaluated. A cross section of the finished coated fabric is shown in Figure 1. The tensile and tear test results are listed in Table 1 for both coated and uncoated fabrics.

Table 1. Dacron/Kevlar Ripstop Material

<u>Characteristic</u>	<u>Design Goal</u>	<u>Value</u>	
	<u>Uncoated</u>	<u>Uncoated</u>	<u>Coated</u>
Weight, oz/yd ²	2.0	2.0	6.0
Tensile, lbs/in			
Machine	70	96	96
Transverse	70	101	101
Tear, Tongue, lbs			
Machine	15	27.0	24.2
Transverse	15	30.4	26.8

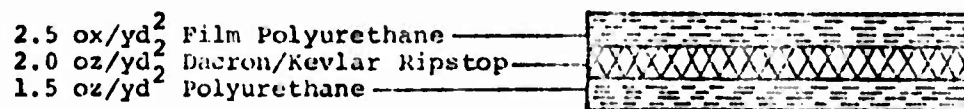


Figure 1. Cross Section of Single Ply Coated Dacron/Kevlar Ripstop

3. TRIAXIALLY WOVEN FABRIC

Triaxial fabric is a three yarn system with the yarns oriented 60 degrees apart as shown in Figure 2. The name given to this new weaving system is "DOWEAVE".

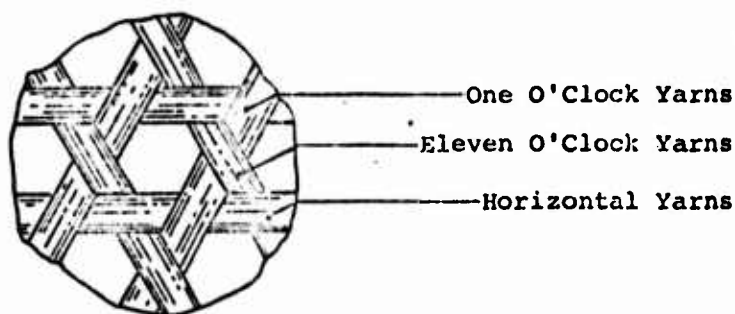


Figure 2. Basic-Weave

As a result of this construction, the fabric yarn geometry forms triangular intersections which serve to prevent bias distortion, insure dimensional stability, and increase tear strength over comparable biaxial fabric. Conventional balloon technology requires the bias lamination of two biaxial fabrics or the use of high modulus films to obtain dimensional stability. Triaxial fabric, by its construction, eliminates the need for either of these operations.

In the performance of the present investigations, ILC with a view toward the simplification of fabric design, elected to study and develop the basic-weave pattern for acrostat envelope material.

The basic-weave, the simplest possible triaxial configuration, has no counterpart in conventional fabric construction. The yarn courses are not interwoven at all, that is, they do not pass alternately over and under each other. The horizontal yarns are over all

the "eleven o'clock yarns" and under all the "one o'clock yarns"; the "elevens" are also over all the "ones", as shown in Figure 2. Thus, the impossibility of finding a two-way counterpart to this weave is evident; if the warp simply lay on top of the fill throughout the fabric no weave would exist to hold them together.

In contrast to the complete instability of a lay-up of two yarns, the basic-weave is stable both in the small and in the large. In the small, the locking characteristics of the yarn cross-over resists sideways slippage of any of the yarn courses. In the large, the tri-axial symmetry is such that there is no bias direction at all, and for the first time, a fabric can approach isotropy, that is, it provides essentially uniform resistance to distrotion in all directions.

Radically new fabric testing and evaluation methods have been developed by ILC Dover for both coated and uncoated triaxial fabrics. These efforts have resulted in several new test fixtures which were developed to overcome the shortcomings encountered with conventional biaxial fixtures.

3.1 Bias Stability

To illustrate the bias stability of triaxially woven fabric, ILC Dover designed and fabricated a shear testing device. The purpose of this test fixture was to measure the amount of load required to deform a fabric in the bias direction through a given length (1/2 inch). The three major fabric geometries were tested using the test fixture shown in Figure 3. The test results are shown in Table 2.

Table 2. Fabric Dimensional Stability

<u>Fabric Geometry</u>	<u>Weight (Oz/Yd²)</u>	<u>Breaking Strength (Lb/In)</u>	<u>Shear Resistance (Lbs)</u>
Two-Ply Biased Fabric Construction (1.1 oz/yd ² Biased at 45° to the 3.25 oz/yd ² Fabric)	10.85	160 x 160 x 120	99
Biaxially Reinforced Film Construction (4 oz/yd ² Laminated to 2 Layers .25 Mil Mylar and 1.0 Mil Tedlar)	8.5	200 x 200 x 90	89

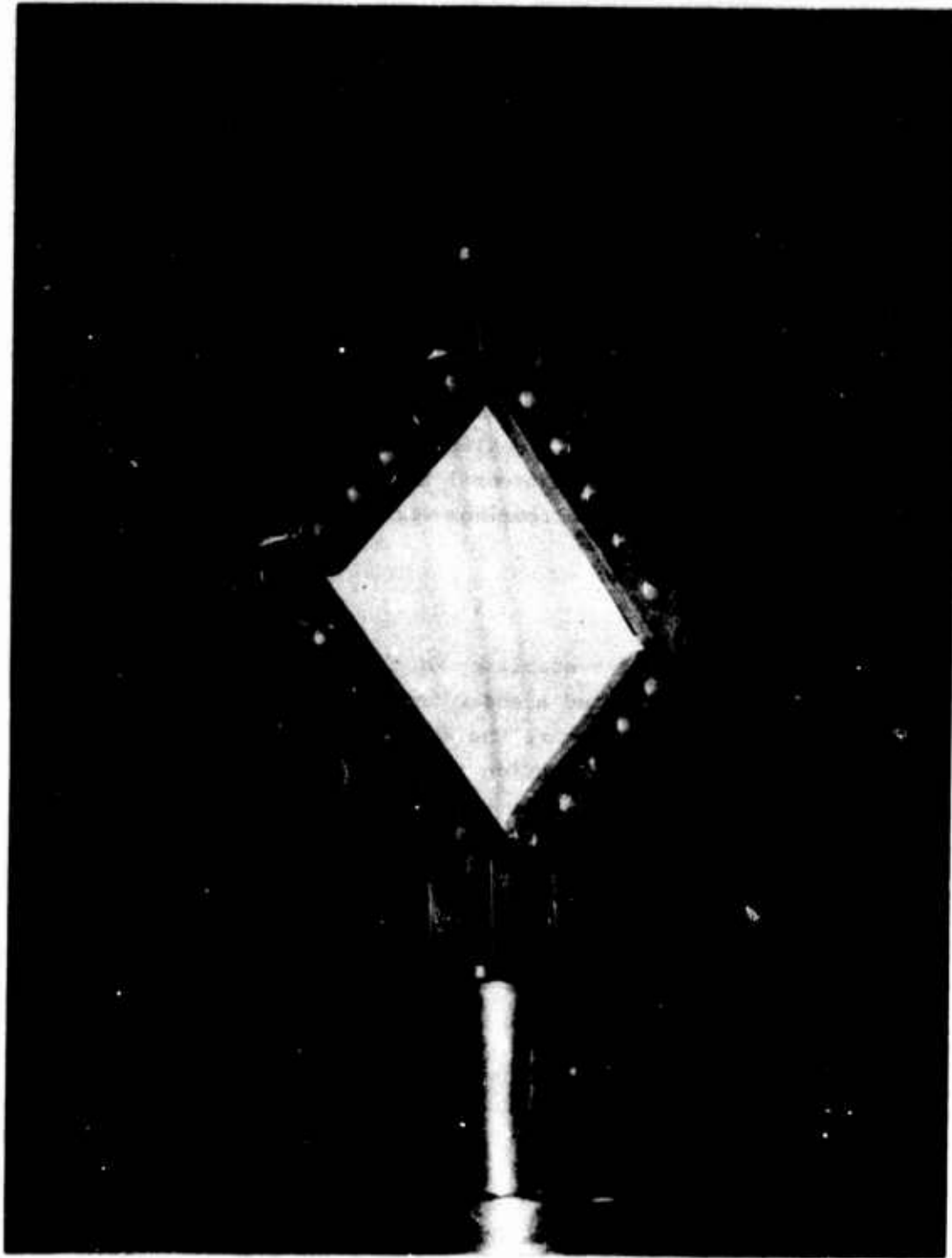


Figure 3. Dimensional Stability Fixture

Table 2. Fabric Dimensional Stability (Cont'd)

<u>Fabric Geometry</u>	<u>Weight (Oz/Yd²)</u>	<u>Breaking Strength (Lb/In)</u>	<u>Shear Resistance (Lbs)</u>
Triaxially Reinforced Film Construction (1.5 oz/yd ² Urethane Laminated)	5.0	150 x 150 x 150	252

3.2 Tensile Testing

The geometric characteristics of triaxial fabrics have necessitated the development of new tensile testing techniques and apparatus. The basic biaxial testing methods and equipment which were previously the standards of the textile industry have been found to be incapable of accurately measuring the strength of the triaxial system. ILC Dover has pioneered the testing of triaxial fabrics and has developed several pieces of tensile testing equipment during the course of these efforts.

3.2.1 One x Six Inch Ravel Strip Tensile

Test Method 5104 from Federal Test Method Standard No. 191 utilizes a 1 x 6 inch ravel strip sample to determine fabric tensile and elongation. Samples are typically cut parallel to the machine or transverse direction and test either the "warp" or "fill" yarns respectively.

Triaxial fabric, when subjected to this test procedure in the machine direction, yields very poor results since individual warp yarns are not held in both jaws, but tend to "run-off" the side of the 1 x 6 sample. See Figure 4.

It was attempted to run this test with successively smaller initial jaw separations in an effort to minimize the warp yarn run-off. The test was finally conducted with the jaws initially butted together; however, the mode of failure in each test was a single yarn system break. It was believed that jaw travel before break was too short to allow the second yarn system to shift and share the total load.

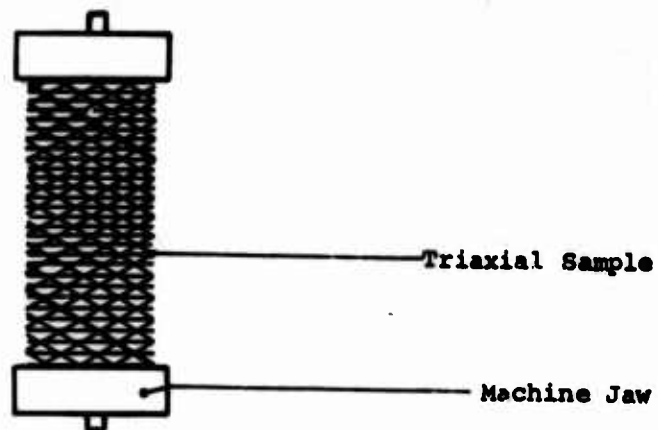


Figure 4. Triaxial Fabric Strip Tensile. Note the "run-off" of the warp yarn systems

3.2.2 Six Inch Wide Tensile Test

Since initial efforts to minimize or eliminate warp yarn run-off were unsuccessful, it was then decided to design a test fixture that would minimize the effect of the run-off. Using a one inch jaw separation, the length of test sample affected by run-off is .578 inches on a side. Thus, it was expected that a total of 1.16 inches of sample would be affected. See Figure 5.

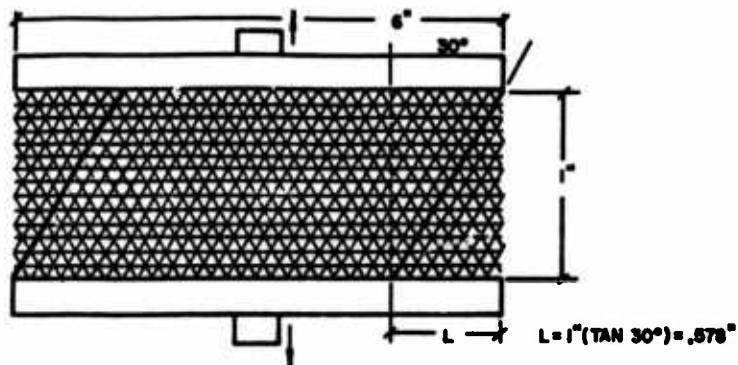


Figure 5. Six Inch Wide Edge Effects

ILC fabricated a six inch wide jaw fixture (Figure 6) for the

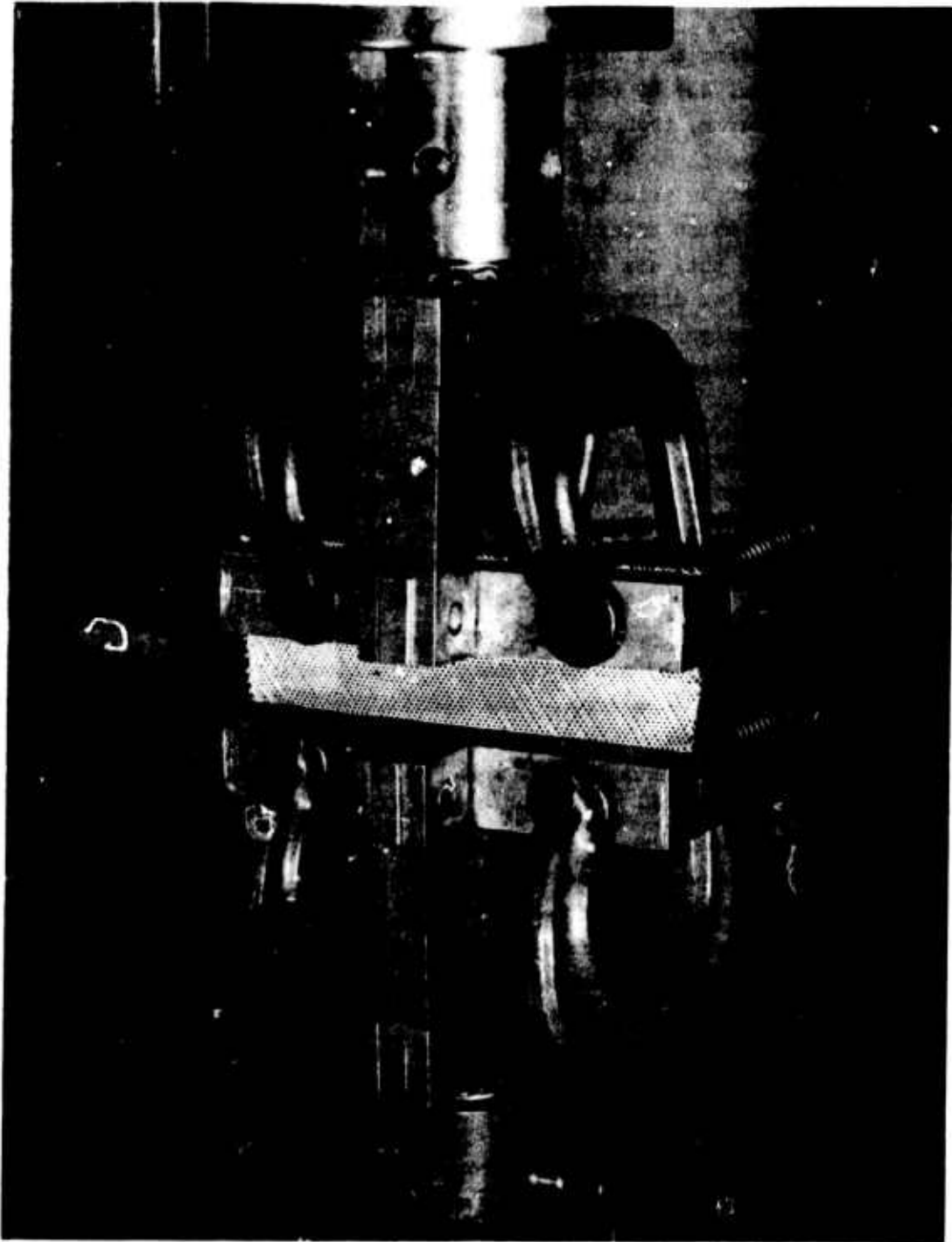


Figure 6. Six Inch Wide Tensile Test Fixture

Instron machine. Using this apparatus, larger samples could be tested and a loss factor, due to edge effects, could be applied to the triaxial tests; however, the magnitude of this factor was still questionable.

Up to this point in triaxial testing technology, there existed no accurate test on which triaxial and biaxial fabrics could be compared. ILC has used this six inch test fixture for preliminary relative evaluations of different triaxial fabrics but is not suitable for use as a design test apparatus to simulate actual loads encountered in an inflatable product application.

3.2.3 Cylindrical Tensile Test

As the testing of triaxial fabrics progressed it became apparent that the edge effects of the test sample were very important. Previous testing procedures had attempted first to minimize the amount of run-off in triaxial fabric testing and then to minimize its effect on the total test article. The cylindrical tensile test was intended to remove or lock out the edge effects from the test sample.

A two inch diameter by six inch long cylindrical test sample was prepared from the fabric specimen. The longitudinal seam of the cylinder was made with a one-half inch overlap sealed with a heat set polyester adhesive. The entire sample was then placed into a set of circular jaws fabricated for the test. These jaws loaded the fabric cylinder and continuously held the sample around its perimeter to lock the yarn ends in place. See Figure 7.

The test results obtained from this test were found to be of limited value in determining a fabric tensile because the sample exhibited a localized failure mode. It was impossible to position the fabric sample evenly enough to ensure total failure around the cylinder circumference, consequently the ultimate fabric tensile in lb/in was not apparent from the test results.

3.2.4 Mullen Burst Method

At this point in the testing program, it was recognized that the pressurized behavior of triaxial fabric presented an interesting phenomenon in that the crossing yarn systems add stability and strength to the principal direction yarns. ILC thus began to consider methods of utilizing pressure forces to achieve uniform fabric stress loading. The first test procedure designed to accomplish this effect utilizes the standard Mullen Burst Tester.

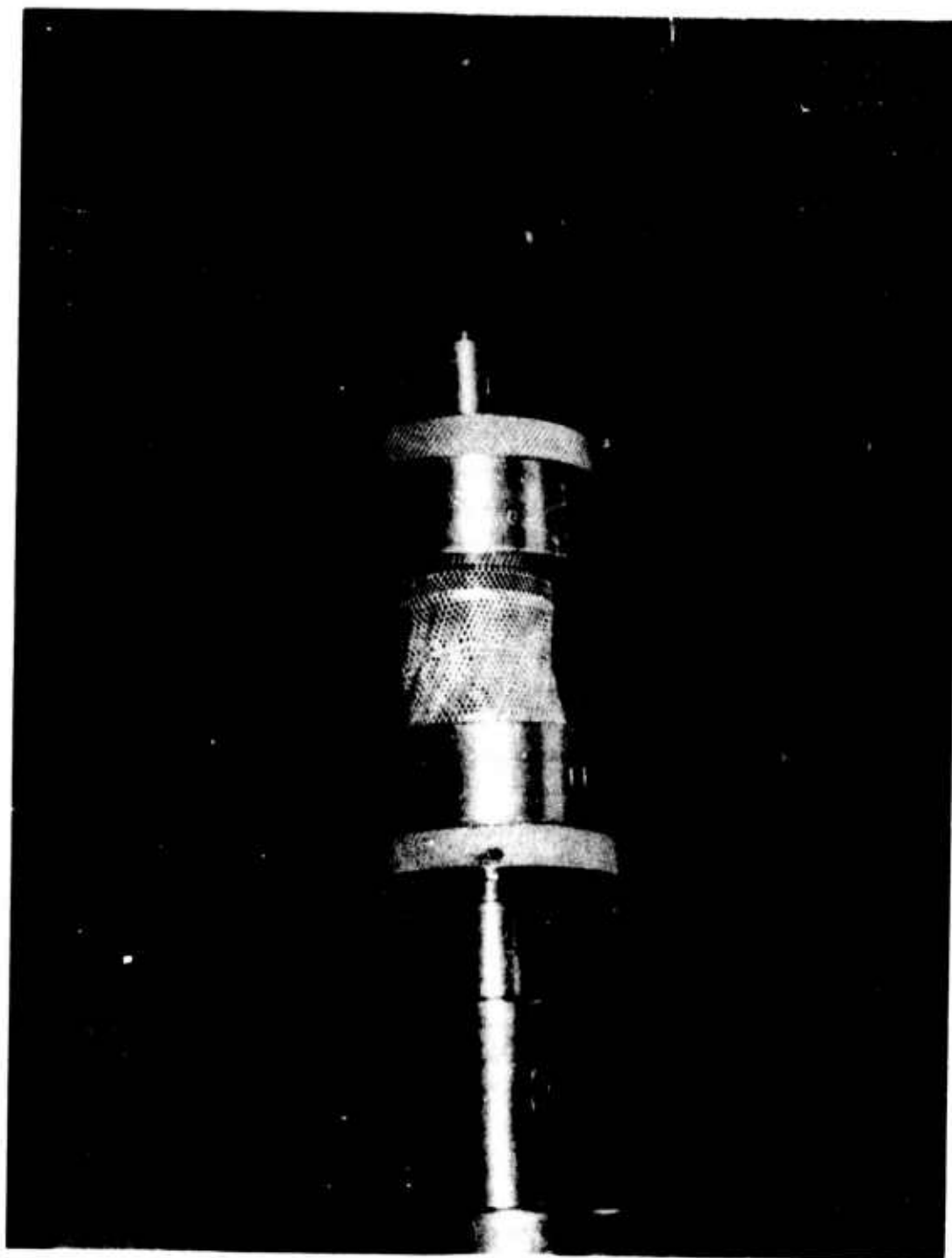


Figure 7. Cylindrical Tensile Test Fixture

The approach taken was to apply increasing pressure to a fabric sample until failure occurred. Then, knowing the internal pressure and the shape of the distorted sample at break, the fabric stress in lb/in could be calculated. It was projected that the sample deformation would follow a spherical shape. It was therefore only necessary to be able to determine the radius of curvature of the surface at the time of break.

Utilizing the volumetric flow rate specifications of the standard Mullen Burst machine, we were able to establish the spherical section volume and hence its radius of curvature with respect to the real time base of the test duration. The equation describing the radius of curvature as a function of elapsed time from start to break was generated and plotted to serve as an aid in evaluating the test data.

It was apparent that in order for any test procedure to be totally credible its accuracy had to be verified by the use of conventional biaxial fabrics of known strengths. Efforts to so correlate the Mullen Burst test procedure in this manner consistently yielded tensile results on the order of 80% of the true value established by standard strip tensile methods. Several attempts were made to improve the test timing apparatus including the use of an audio actuated timer that would automatically indicate the elapsed time between the start of the machine and the sample failure.

After considerable efforts to refine the procedure and equipment for this test it was decided to develop a second approach which would subject the fabric samples to a real life load configuration and eliminate the timing problems encountered previously.

3.2.5 Bag Burst Test

In an effort to more accurately simulate the fabric loading characteristics encountered in actual balloon applications, a cylindrical bag burst test (Figure 8) was developed. It was desired to provide a testing procedure which served to load the test sample with a uniform hoop stress and be able to determine the value of that stress from the internal pressure and the radius of the cylinder. It was also felt to be advantageous to subject the triaxial test samples to stress loading values which were σ and 2σ respectively in the two principal directions. The cylindrical bag burst test accomplished all of these intents.



Figure 8. Bag Burst Tensile Apparatus

It was desired to record the bag growth as a function of internal pressure during the test. Having this data available, the fabric modulus could be determined as well as the ultimate tensile strength.

The test bag was designed to be six inches in diameter and hold a six inch long sample of material in its center section. The ends of the bag were hemispherical end caps made from heavy Kevlar fabric.

The bag growth was measured by recording the movement of a circumferential cord wound around the bag center. The cord, as it moved, rotated the shaft of a calibrated potentiometer which recorded the change in circumference. The bag pressure was recorded by a pressure transducer. Both signals were recorded on a multiple pen Sandborn strip chart recorder. Initial tests were conducted using air pressure, however, the failure mode was extremely explosive and it was impossible to observe the failure either visually or with high speed photography. A change was made in the system to include a reservoir tank and water was used as the pressurizing fluid. This enable close-up visual observation of the fabric failure.

Utilizing this equipment and test procedure, samples of biaxial fabrics of known tensile strength were tested and found to exhibit tensile strengths which agreed with the values obtained by standard coupon test methods. The correlation of results between the bag test and standard unidirectional tensile tests was verified with numerous biaxial tests; it is therefore apparent that the bag test procedure is a valid and accurate method of determining ultimate fabric tensile strength.

3.3 Tear Resistance

The tearing behavior is extremely important in many fabric applications, particularly those for aerostats. The significance of this property can be illustrated by analyzing personal tearing experiences. As is known, the tearing resistance "on the bias" is greater than in the warp or fill direction. To tear a triaxial fabric, one is always tearing "on the bias", and the overall improved tear properties result.

Because the basic weave is the simplest possible triaxial configuration, the analysis of its tearing behavior forms an ideal starting point, on both theoretical and experimental grounds, in the investigation of the tearing characteristics of triaxially woven fabric.

Theoretically, the basic-weave should possess the lowest tear strength of any triaxial configuration. As the interlacings become more complex, as in the first, second and third variants, the tear strength should similarly increase. This has been empirically shown to be true by virtue of comparison of the basic-weave with the sixteenth variant.

For the purposes of evaluating the tear strength of triaxial fabric three different tear methods were investigated: tongue tear, trapezoid tear and slit tear.

In the tongue tear test a specimen 6 x 8 inches is cut so that the yarns to be ruptured during the tear lie in the shorter dimension. A cut three inches in length is made along the longer centerline of the fabric. This cut thus produces two 3 x 3 inch tongues which are placed in the upper and lower jaws of the testing machine. As the jaws move apart the specimen assumes a configuration typified as shown in Figures 9 and 10.

As the yarn courses are subjected to increasing tension the angle between the eleven o'clock and one o'clock warp yarns increases allowing the yarn courses to bunch up against each other. As the tear progresses the tongues become progressively longer. The del becomes very large, and the yarns bunch up to reinforce each other, so that tearing is extremely difficult. The tearing action is manifested on the tensile tester recorder as a diagram of progressively increasing and then sharply decreasing loads. Results of the tongue tear tests are shown in Table 3.

For the trapezoid tear test the specimen is 8 1/2 x 5 3/8 inches with a one inch slit placed midway along the longer direction. The sample is inserted on the bias between the jaws of the testing machine so that the yarns are caused to fail progressively. This test is entirely of a tension type, and has little meaning in terms of the practical tearing characteristics of the fabric. In fact, unless the sample size is extremely large, the warp yarns are never placed in tension. Therefore, comparative test results are only obtainable in the machine direction. The phenomenon of trapezoidal tear is illustrated in Figures 11 and 12. Results of the trapezoid tear tests are shown in Table 3.

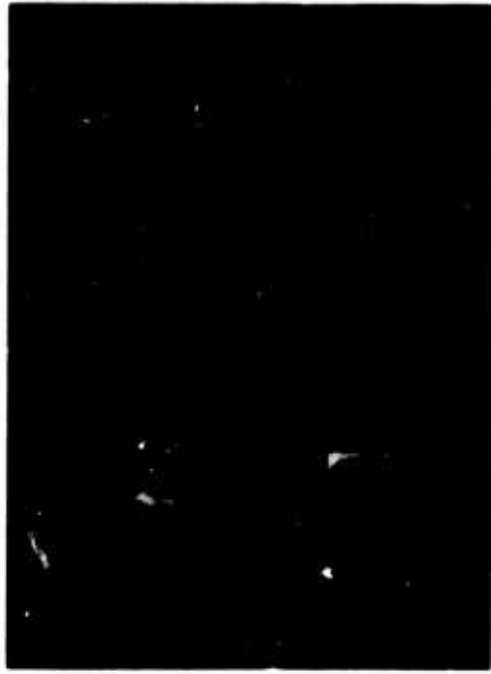


Figure 9. Tongue Tear Test Machine Direction

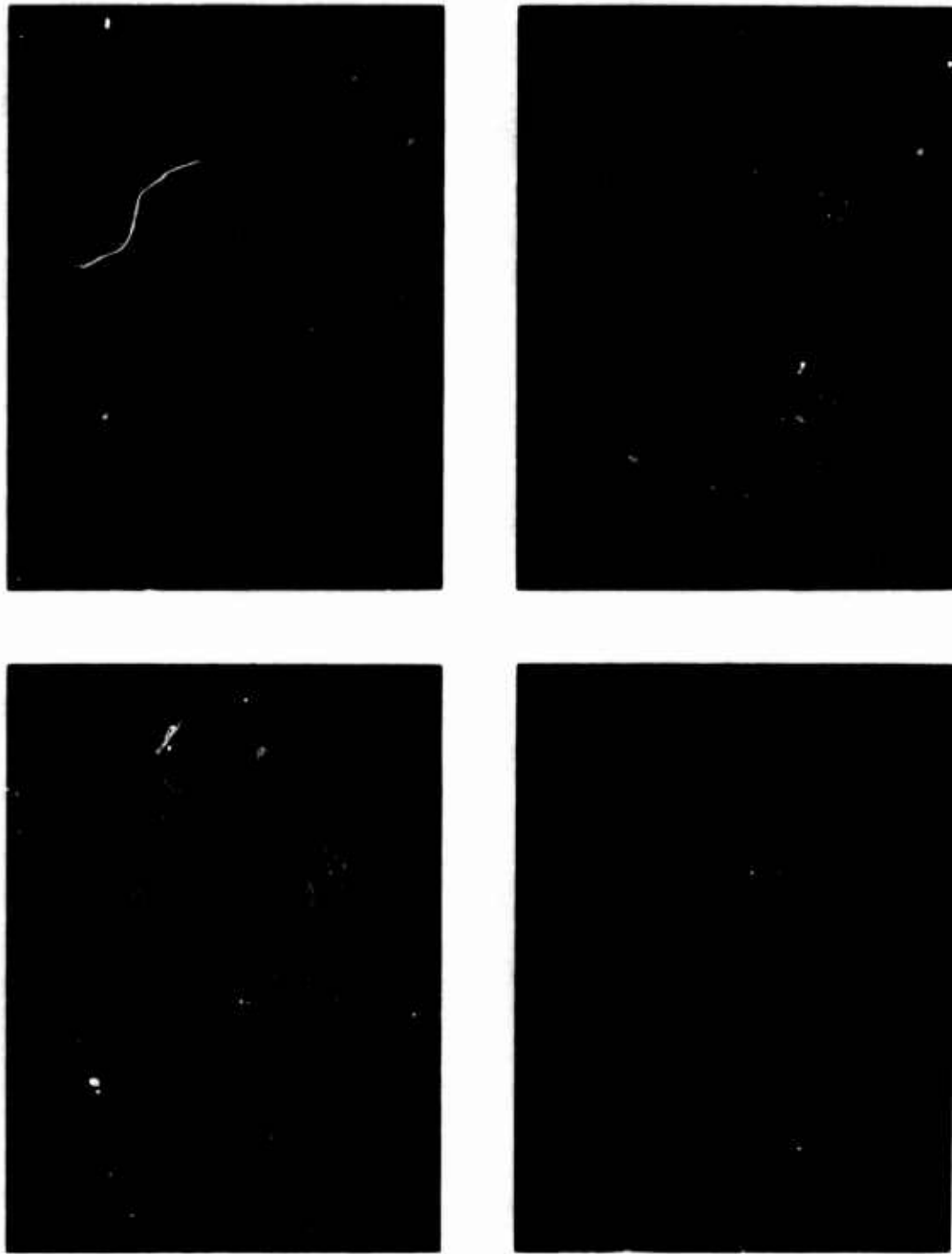


Figure 10. Tongue Tear Test Transverse Direction



Figure 11. Trapezoid Tear Test Machine Direction



Figure 12. Trapezoid Tear Test Transverse Direction

For the slit tear test a specimen 6 x 7 inches is cut such that the sample has 1 1/4 inch wide slit across the center of the sample at right angles to the longest dimension. This test is designed to determine the force necessary to propagate a tear in damaged fabric. Unlike conventional orthogonal woven fabric, the triaxially woven fabric shows no sign of tear propagation. Figure 13 illustrates the effects of the slit tear test on a triaxial fabric where the slit is normal to the transverse direction. The transverse yarns are brought into tension until rupture occurs with no evidence of tear propagation. Figure 14 illustrates the effect of the slit tear test on a triaxial fabric where the slit is normal to the machine direction. Although only a few warp ends are placed in tension, no tear propagation results. Results of the slit tear tests are shown in Table 3.

Table 3. Triaxial Fabric Tear Tests, 16 x 16 x 20 Basic Weave

Test	Fabric Weight (oz/yd ²)	Tear Strength, Lbs.	
		Machine	Transverse
Tongue Tear	1.5	90*	50*
Trapezoid Tear	1.5	104	65**
Slit Tear	1.5	265***	860***

* The tear did not propagate at the tongue slit, but took the path of least resistance.

** The warp yarns were not under tension, therefore the resultant tear strength is not comparative to a similar orthogonal construction.

*** Failure was in tensile. The sample showed no signs of tear propagation.

As a result of the in-depth study of the tearing behavior of triaxial fabric, the following conclusions are drawn:

- a. The nature of the triaxial configuration precludes tear propagation.
- b. Tongue tear results are a magnitude better than conventional orthogonal fabrics.
- c. Trapezoidal tear tests have little meaning in terms of practical tearing characteristics.

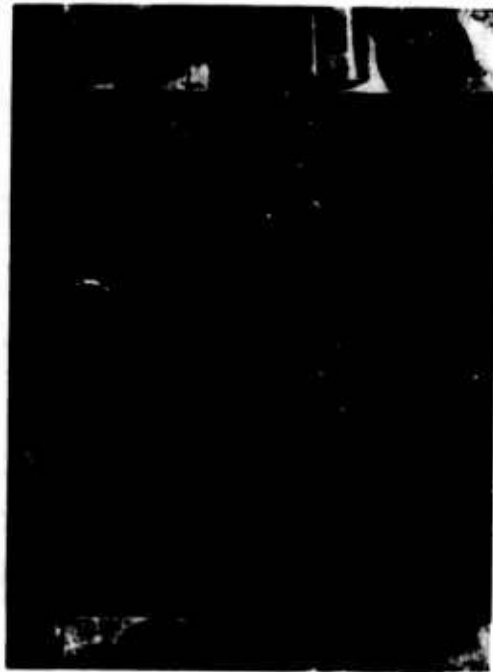
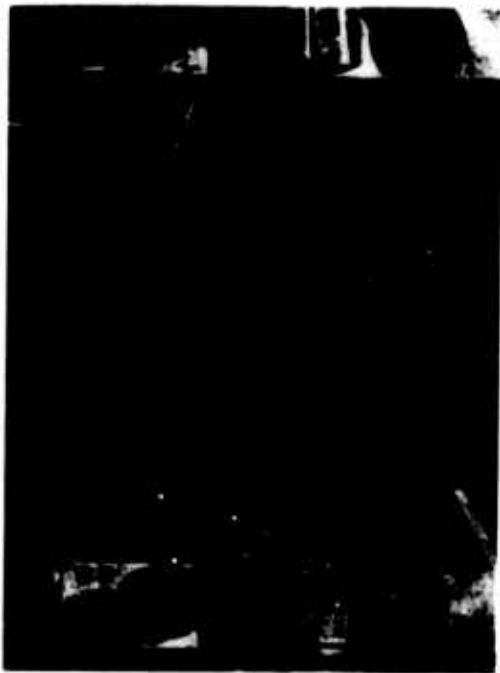
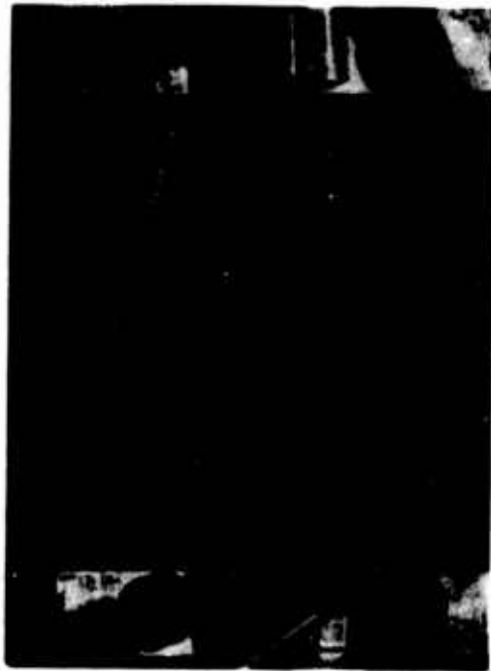
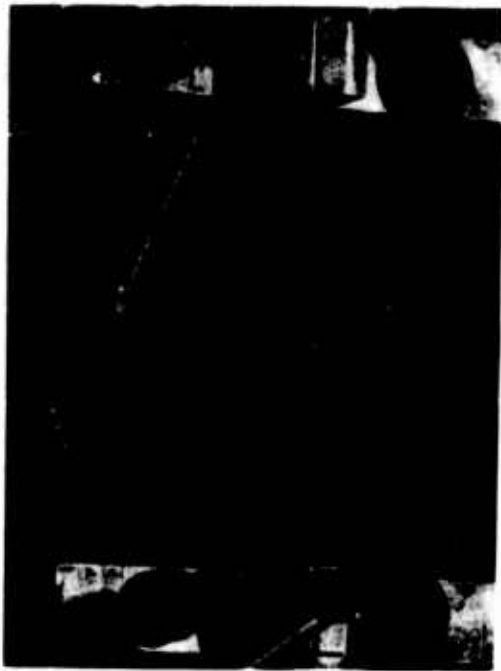


Figure 13. Slit Tear Test Transverse Direction

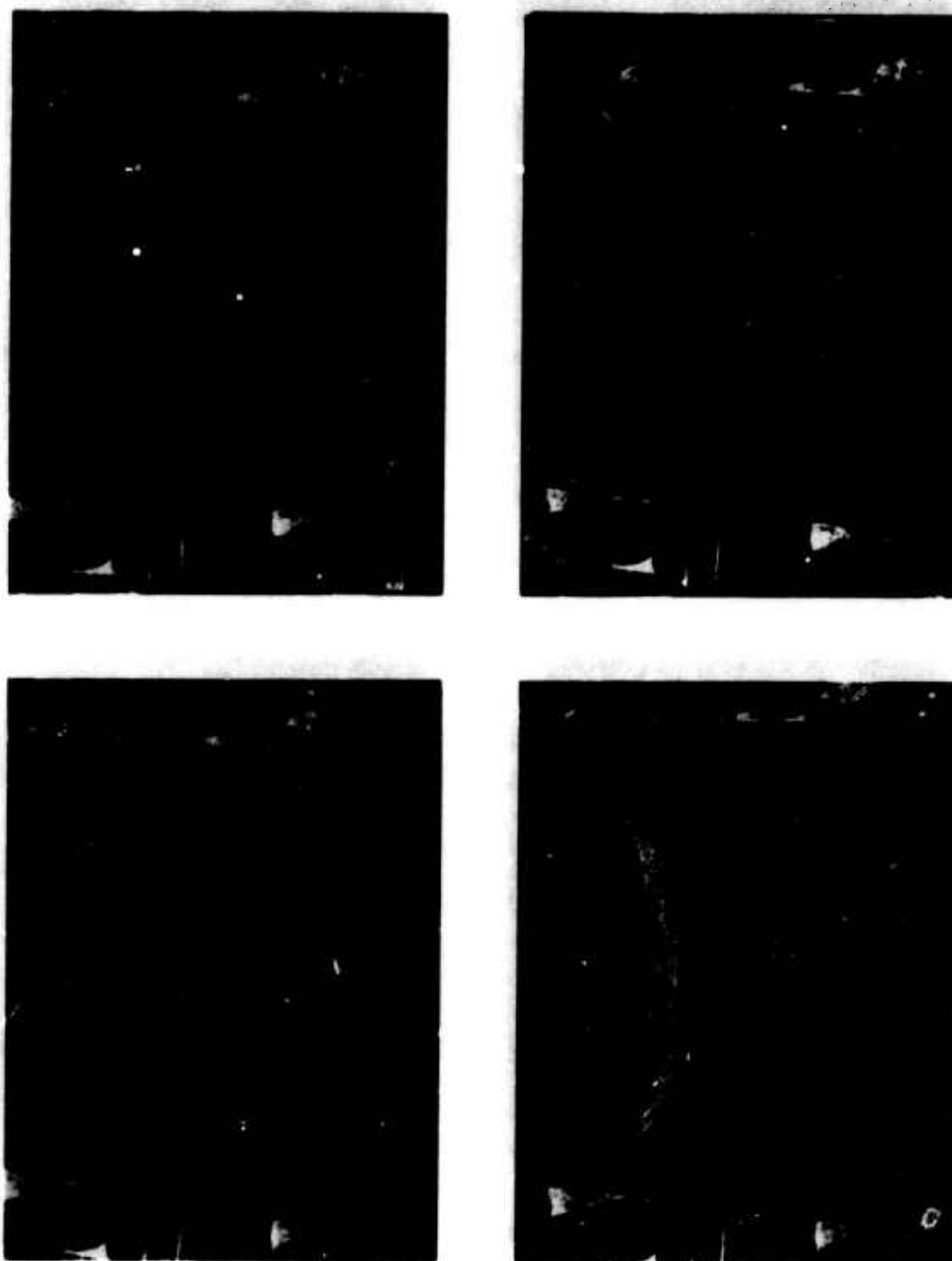


Figure 14. Slit Tear Test Machine Direction

3.4 Triaxial Fabric Design

Due to the revolutionary nature of the triaxial configuration and the limited capabilities of those machines available, only two variants of triaxial weave were considered; the basic-weave, and the sixteenth variant. The nature of triaxial machinery and the mechanisms associated with them, unlike conventional textile machinery, dictate certain design parameters, such as yarn count and yarn diameter. Investigation was initiated with the triaxial fabric manufacturer, Doweave, Inc., to develop a lightweight triaxially woven fabric of the basic-weave configuration. Included in this development effort were the following fabrics: 1.89 oz/yd² triaxial fabric made from all Dacron, and a 1.5 oz/yd² triaxial fabric made from all Kevlar 29.

It was learned from the preliminary run of experimental triaxial hull laminate constructed of all Kevlar 29 yarns, that the anticipated lower elongation (vs. all Dacron) was attained; however, the higher strength-weight ratio was not reflected in the cylinder bursting strength. The use of polyacrylic acid sizing on the Kevlar 29 yarns reflects not only a 50 percent reduction in yarn breaking strength, but also a severe reduction in yarn elongation. This elongation reduction prevents the fabric from stretching or shifting to share the load more efficiently.

As a result, another design iteration was considered. Considerations for this design iteration were: the elimination of all sizing on yarns and the twisting of the Kevlar 29 yarns with 9 turns per inch of Z twist. The rationale for this design iteration was to provide for lower yarn modulus thus resulting in higher fabric elongation. Figure 15 shows the cross section of the finished triaxial envelope laminate and the associated physical properties are given in Table 4.

Table 4. Finished Triaxial Envelope Laminate

	<u>Design Goal</u>	<u>Actual</u>
Weight, oz/yd ²	5.0	5.2
Breaking Strength, lb/in		
Machine	120	150
Transverse	120	150
Bias	120	150

Table 4. Finished Triaxial Envelope Laminate (Cont'd)

	<u>Design Goal</u>	<u>Actual</u>
Tear Strength, lbs.		
Tongue Method		
Machine	20	35
Transverse	20	35
Leakage		
L/M ² /Day	1.0 max.	.6
Shear Resistance, lbs.	150 min.	252

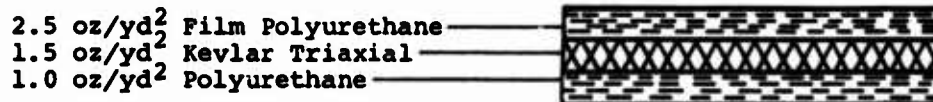


Figure 15. Cross Section of the Triaxial Envelope Laminate

3.5 Economic Benefits

The inherent strength of triaxially woven fabric will allow lighter weight fabric substrates to be used in coated and multi-ply fabrics. In some applications the lighter substrates will result in raw material savings in excess of 30 per cent. Since raw material costs represent approximately 60 per cent of fabric costs, this savings is significant.

An inherent characteristic of the weaving process is the potential to produce 50 per cent more fabric than conventional weaving for each pass of the shuttle across the loom. The number of shuttle passes is a main factor limiting production speeds, and since, in a triaxial machine, only one third of the yarns must be carried across the loom by the shuttle, rather than half, two triaxial machines will do the work of three conventional looms.

Triaxial woven fabrics will be competing with conventional woven, knitted, and non-woven products produced by the large textile organizations. Improved fabric performance, potential manufacturing cost reductions, and raw materials savings are significant reasons why triaxial woven fabric should fare well in the aerostat marketplace.

ILC Dover is working closely with the triaxial fabric

manufacturer, Doweave, Inc., to develop optimum substrate fabrics for aerostat programs. ILC Dover's efforts in coating development for these materials have been consolidated with the E. I. DuPont de Nemours Co., Inc. DuPont is presently engaged in an extensive effort to develop coatings and techniques to fully exploit the capabilities of triaxial fabric. Foremost in this effort is their integrated activity with ILC Dover and Doweave to optimize the coating system for aerostat materials.

4. CONCLUSIONS

As a result of this materials development program, new frontiers have been created in the field of aerostat softgoods. The new concepts explored by ILC during this effort are expected to establish new guidelines in materials development for advanced aerostats being considered today.

With the vast amount of interest currently being shown in large aerostats and hybrid LTA vehicles, it is expected that such programs will soon progress beyond the drawing board to working scale models and then on to full size systems. Aerostat materials development will also progress with these programs as the need for stronger materials for these larger ships is realized. The new triaxial and ripstop materials are expected to lead the way for future "super" fabrics in these applications.

The knowledge of triaxial Kevlar fabrics obtained during this program, has already been applied to one such hybrid called the Aerocrane, designed by All American Engineering Company. ILC Dover has conducted a preliminary materials study encompassing strength requirements, weight analysis and coating options for this application.

Fabrics which have been proposed for larger models of the Aerocrane will require tensile strengths on the order of 3000 lb/in. With the triaxial Kevlar construction, it should be quite possible to build such a fabric, but it is anticipated that a major effort will be required to improve current fabric joining or seaming technology.

The two materials advancements explored during this effort represent the beginning of two new classes of aerostat materials. It is hoped that subsequent programs will be able to build upon this base work by providing a suitable growth environment for the new triaxial and ripstop technologies.

Contents

1. Introduction
2. Test Arrangement
3. Test Program
4. Results
5. Discussion
6. Conclusions and Suggestions

Local Motions of a Payload Supported by a Nolaro Tri-Tethered Balloon

R. C. Lactaire, 1/Lt, USAF and
H. L. Schumacher, Jr., 2/Lt, USAF
Air Force Cambridge Research Laboratories
Bedford, Massachusetts

Abstract

This report studies the local motions of a payload supported by a NOLARO tri-tethered natural shape balloon. A $793M^3$ ($28,000 \text{ ft}^3$) natural shape balloon on a 13.2mm (0.52 in) diameter NOLARO tri-tethered cable array was flown with the payload at an altitude of 140M (460 ft) AGL. Test constraints included separating the payload from all metal by 15M (50 ft) and from the balloon by 45M (150 ft). The payload had to remain within a 3 meter radius sphere for all 25 test runs. These tests were conducted at Holloman AFB and White Sands Missile Range, New Mexico. Target position, tangential speed and acceleration were determined by using the White Sands Missile Range cinetheodolite system. Actual results are compared with theoretical data.

1. INTRODUCTION

Several papers have been written on the use of steel cable in forming a tri-tethered balloon system. These systems are stable, easy to erect and well defined. The distinct advantages of the steel cable supported system are well known and include readily available tether cable, off the shelf winches adapted to the operation, high safety factors, etc. The prime disadvantage is the low strength/weight ratio, elasticity and resulting instability of the balloon system, and radar reflectivity.

As a result of the steel cable limitations, the use of NOLARO rope was identified as possibly providing a superior tri-tether arrangement to exceed those previously established and tested. The one immediate advantage of higher strength/weight ratio for supporting cable created a higher payload capability with established balloon systems. The design, development, and application of this system is described in this paper, with the culmination of direct Army program support in March 1974.

1.1 Requirement

On 22 January 1974 Detachment 1, AFCRL was approached by personnel from the Missile Electronics Warfare, Technical Area (MEWTA) Group at the White Sands Missile Range (WSMR) to provide a tethered balloon platform in support of a Chaff Dispersion mechanism. From 25 March to 1 April 1974 a flight series was flown at the Radar Target Scattering Facility (RATSCAT) WSMR, New Mexico to support this program. Test constraints included separating the payload from all metal by 15 meters and from the balloon by 45 meters. The payload had to remain within the same 3 meter radius sphere for 25 separate test runs over several days. Metal cables could not be used as it would have interfered with the radar acquired data. The experimenter imposed a two meter/second wind limitation in order to evaluate the chaff dispersion separate from wind effects.

1.2 Requirement Evaluation

From the constraints outlined, a detailed evaluation of the requirements immediately led to the conclusion that systems previously flown were not acceptable. Target position, target speed and acceleration, the effect of cable catenary, and the variation of balloon motion versus target motion led to the system integrated for initial testing and program support. Final determination of a test program included a 79M^3 ($28,000\text{ ft}^3$) natural shape balloon on a 13.2mm (0.52 in) diameter NOLARO tri-tethered cable with the payload at an altitude of 140M (460 ft) AGL. (See Figure 1). The test program demonstrated the advantages of this type of support. This report describes the results of two preliminary flights to show feasibility of supporting this program, the actual flight series, and a flight after the fact using an identical configuration to further evaluate the system. The flights were conducted at Holloman AFB and the White Sands Missile Range, New Mexico.

2. TEST ARRANGEMENT

2.1 The Balloon and Cable

The natural-shape balloon, made of urethane-coated nylon, weighed 1290N (290 lbs). When fully inflated and pressurized, the nominal 79M^3 ($28,000\text{ ft}^3$) balloon had a total volume of 87M^3 ($31,000\text{ ft}^3$). (This balloon is illustrated in Figure 2)

The cable used was 13.2mm (0.52 in) diameter rope manufactured by the Columbian Rope Company. It consists of prestretched polyester yarns contained in an extruded polyethylene jacket. The cable has 60 yarns and a nominal jacket thickness of 1mm (40 mils). It has a rated break strength of 50,600N (11,500 lbs) and weighs 396N (90 lbs) per 305M (1,000 ft).

This cable has been used on tethered balloons successfully for years. Its biggest advantage for this test was that it is non-radar reflective. It is less susceptible than steel cables to damage due to lightning, less likely to transmit

dangerous electric potential, has limited stretch, and a very high strength to weight ratio. However, it is susceptible to failure due to dirt damaging the jacket and abrading the fibers. It cannot be wound upon a drum while under tension without the use of a traction drive to prevent crushing of the cable and jacket.

2.2 Erection of the Balloon System

Due to the use of NOLARO cable, the technique of erecting the system was different from that normally used by AFCRL.* We had no on-hand mobile winches with traction drive capable of handling the large diameter rope. We therefore put fittings on the end of three pre-cut lengths and tied them to the bumpers of vehicles.

As the vehicle system has less positive control of the balloon than a winch, a fourth line was tied to the tri-plate.** This line was a braided dacron line (12.5mm) not requiring a traction driven winch. This line was used solely to raise and lower the balloon. Due to its high stretch characteristics it was kept slack on all data runs, and was not used as the sole support line during any portion of the test program. After reaching the proper altitude with this line, the NOLARO legs took up the tension and positioned the balloon.

The other change from the normal configuration was the use of a 30M extension line between the balloon and tri-plate. (See Figure 3) As a result two lines were flown here. One NOLARO line was the flying line, and the other, a woven coreless braid, was used for balloon handling. Through use of a ground shieve, the braided line raised and lowered the balloon 30M in order to attach the tri-plate and tri-tether legs to the flying line.

* Leclaire, R. C. and Rice, C. B. (1973), The Local Motions of a Payload Supported by a Tri-tethered Natural Shape Balloon, AFCRL-TR-73-0748.

** The tri-plate is at the confluence point of the three tether lines and is shown in Figure 3.

The payload was suspended 15M below the tri-plate. A pulley was attached to the base of the tri-plate and the package support line was run from the top of the package around the pulley and down to the ground. By this technique we were able to raise and lower the package as required without repositioning vehicles or moving the balloon.

2.3 Instrumentation and Data Collection

Since the experimenter required no instrumentation support from AFCRL, a standard tethered balloon safety package (developed by Mr. Arthur Giannetti, AFCRL) was used. This package will open and close the balloon valve by command or by a preset aneroid.

The experimenter gathered data through the use of cameras, radar and visual observations. The data used in this report was gathered by cinetheodolites, theodolites, visual observations, and pibals. Correlation of the data indicated that the theodolites show the position of the balloon very accurately, although they do not show small scale variations over time. Thus they can show position within a small radius very accurately and if the balloon was out of position by a significant amount, it would be immediately obvious from the data.

2.4 Flight Geometry

The March preliminary test configuration and the RATSCAT configuration were basically the same. On the first day of the preliminary tests, the cinetheodolite data show an altitude of 127M for the target. We took the data at this altitude to show the effects of elevation angle on stability. On the second day of testing the system was located (within 3 meters) at 153M and two data runs were made. The vehicles were at a 187M radius and the triangle they formed was approximately equilateral. From experience, the authors feel that as long as the triangle is approximately equilateral there will be no significant change in system stability. The theodolite computer program used at that time gave altitude and not position relative to a ground point. Therefore, we were not able to accurately locate the target relative to ground zero.

Cinetheodolite data is highly accurate, although data reduction takes 2 to 3 weeks. Therefore, we required an alternative system to provide real time target position. Prior to the RATSCAT tests the computer program was modified to give ground position as well as altitude.

In the July tests, we used surveyed locations at Scat Site to position the vehicles and let the target seek its own position. Three different triangles were used at radii of 87.5M, 127.5M and 181M. (See Figure 4) These were equilateral triangles with ground zero as the centroid. The altitude of the tri-plate was then compared to that calculated by assuming no catenary in the cable. An uplooking ground camera was placed at ground zero to evaluate balloon motion versus target box motion. Finally the suspension line length between the tri-plate and target was varied from 5 to 56 feet to determine pendulum effects.

2.5 Operational Constraints

Due to time and money limitations, the system actually flown was not optimized. The least satisfactory portion of the system was the use of pre-cut lengths of NOLARO. The NOLARO is subject to damage to a much greater extent than steel as described above. Positioning was somewhat more difficult because vehicles had to be moved rather than inhauling or outhauling a winch. This was partially ameliorated by marking the positions of the vehicles the first time and returning to these spots on subsequent days. In the light wind/high lift system used, this worked very well, although we believe that if the system had been more marginal on lift or if the winds had been higher this would not have sufficed. The other major problem inherent in NOLARO is its vulnerability to damage during ground handling. Due to lack of winches, there were times when the NOLARO was laid out on the ground and care had to be taken to prevent tearing the jacket by either human error or natural events. Although no damage was incurred, we were unable to prevent some dragging on the ground, and in different terrain this could have been a real problem.

The severe wind limitation imposed by the experimenter was another operational constraint. At the start of the test a 2 meter/second wind limit was used. As the tests progressed it became apparent from the radar data that this was more stringent than required, and was relaxed to 3 meters/seconds. This constraint resulted in a limited period each day when tests could be run due to the local climatology. Cameras were used to record experimenter data so we were also limited to daylight operations. As a result we could only test from about one hour after dawn until approximately 1030 hours local time.

3. TEST PROGRAM

3.1 March Tests

On 13 and 14 March 1974 preliminary tests were performed at Scat Site, Holloman AFB, New Mexico to determine if the proposed technique of suspending the payload was feasible. Four cinetheodolite runs were taken for after the fact analysis. The prime purposes of these tests were to insure that the system would be acceptably stable, positioning the balloon at the proper position was possible, and the method of using NOLAN cable would not result in flying line failure due to an unforeseen problem.

It was determined that the system was safe to operate, and the system could meet the operational requirements imposed by the experimenter.

3.2 RATSCAT Tests

From 25 March to 1 April 1974 tests were run at RATSCAT to actually support MENTA. The system was flown over a ground radar with the payload at 140 meters. Sixteen test runs were originally scheduled. As a result of excellent data, and 4 misfires, a total of 25 actual test runs were made. Two theodolites were used to assure that the balloon was in the same position for every test. The "quick-look" radar data verified the target was satisfactorily positioned and not moving excessively.

Table 1. Summary - Tri-tether, Target Nominally 15.2M (50 ft) Below Confluence Point, 793M³ (28, 000-Pt³) Natural-Shaped Balloon, 13.2mm Diameter NOLARO Cable

Flt	Date	Pibal Wind Speed (M/Sec)	Wind Direct. (Deg)	Mander						Flt Date	Max Tangential			Elv Angle	Altitude (M) AGL
				M			Ft				Grd Speed (M/Sec)	Accel (M/Sec ²)	Altitude (M) AGL		
				X	Y	Z	X	Y	Z						
1	3/26	2.1	-04 kts	.915	1.24	.915	3	4	3	1	3/26	0.305	0.0	37.8°	140
2	3/13	5.7	-11 kts	.305	.305	.305	1	1	1	2	3/13	0.305	0.0	31.25°	127
3	3/13	4.6	-09 kts	.305	.61	.305	1	2	1	3	3/13	0.305	0.0	31.25°	127
4	3/14	6.2	-12 kts	2.44	2.44	1.24	8	8	4	4	3/14	0.305	0.0	41.8°	152
5	3/14	5.2	-10 kts	2.44	.61	.61	8	2	2	5	3/14	0.305	0.0	41.8°	152
6	3/14	5.2	-10 kts	2.14	1.52	.61	7	5	2	6	3/14	0.305	0.0	41.8°	152

Table 2. Summary - Tritether, 793M³ (28,000 ft³) Natural-Shaped Balloon, 13.2mm Diameter NOLARO Cable

Data Run	Times (MDT)	Pibal Wind Speed (M/Sec)	Wind Direct. (Deg.)	Triplate Height (M)		Anchor Pt. Rad (M)	Target Position (M)	Mender						
				Calc	Actual			X	Y	Z	X	Y	Z	
1	7:22:45	Start: 1.5 (3 kts)	Start: 180	138	142.5	181	1.8 (6 ft)	0	0	0	0	0	0	0
	7:37:15	Finish: 1.5 (3 kts)	Finish: 250											
2	7:45:00	Start: 2.6 (5 kts)	Start: 210	138	142.5	181	7.9 (26 ft)	.64	.52	.27	2.1	1.7	0.9	
	7:55:00	Finish: 1.1 (2 kts)	Finish: 060											
3	7:58:00	Start: 0.5 (1 kts)	Start: 115	138	142.5	181	15.2 (50 ft)	.64	.52	1.06	2.1	1.7	3.5	
	8:08:00	Finish: 1.1 (2 kts)	Finish: 130											
4	8:59:00	Start: 3.1 (6 kts)	Start: 185	190	192	127.5	13.7 (45 ft)	1.16	.52	1.25	3.8	1.7	4.1	
	9:09:00	Finish: 1.5 (3 kts)	Finish: 175											
5	9:17:00	Start: 3.1 (6 kts)	Start: 190	190	192	127.5	3.0 (10 ft)	.52	.52	.88	1.7	1.7	2.9	
	9:27:00	Finish: 2.1 (4 kts)	Finish: 190											
6	9:46:00	Start: 2.1 (4 kts)	Start: 225	211.9	212	87.5	17.4 (57 ft)	2.34	2.13	1.76	7.7	7.0	5.8	
	9:56:00	Finish: 1.5 (3 kts)	Finish: 225											
7	10:02:00	Start: 2.6 (5 kts)	Start: 235	211.9	212	87.5	3.0 (10 ft)	1.19	1.58	1.37	3.9	5.2	4.5	
	10:12:00	Finish: 2.1 (4 kts)	Finish: 255											

3.3 July Tests

On 17 July 1974 an additional flight was flown at Scat Site to further study system stability, evaluate how much effect the cable catenary had on altitude, and look at the balloon motion relative to target motion. Seven data runs were made while measuring cable tension at each of the three vehicles and plotting target positions. The target was suspended at various distances below the tri-plate to determine if this had a significant effect.

4. RESULTS

Table 1 summarizes the results of all flights flown with a fixed elevation angle and fixed distance from the tri-plate to the target. The same data is represented on Table 2, for Flight 7, using changing elevation angles and target position below the tri-plate. On all flights data was taken on the target motion.

The least amount of wander was encountered on Flight 7, run 1. On this run the payload did not move at all. The maximum wander was encountered on Flight 4, and this was only 2.5 meters. The wind speeds present during these runs ranged from 0 to 6.2 meters/second. As can be seen from Table 1, this system, utilizing an elevation angle of approximately 40° , is very stable in the 0 to 6.2 meters/second wind regime. It should be noted that payload ground speed and acceleration was minimal.

On Flight 7, runs were conducted varying elevation angle and payload distance from the tri-plate. As can be seen from Table 2, as the elevation angle increases, payload stability decreases. It is felt by the authors that increased balloon motion accounts for this trend. For as the elevation angle increases, the tri-tether system more closely approximates a single tether system.

Figures 5 through 8 show time-displacement curves for the data collected on Flights 1 through 6. Table 1 reflects the maximum values of wander collected.

5. DISCUSSION

5.1 Cable Catenary and Cable Stretch

The test series in which cable catenary was investigated is summarized in Table 2. Tri-plate height was calculated by assuming rigid links with neither catenary nor stretch. Looking at Table 2, it is apparent that the actual height is consistently higher than predicted. The actual height was obtained from double theodolite readings. If a catenary were present with no stretch, the actual height would be lower than the calculated height. From this it is apparent that cable stretch offsets any effect of cable catenary.

This amount of stretch exceeds predictions based upon manufacturer's data on stretch at these low loads. It is the opinion of the authors that this discrepancy is due in part to heating of the cable by the sun. As the cable has carbon black in the jacket, it will be significantly warmer than ambient. Further tests will have to be conducted to determine the relationship of solar heating, cable age, and cable loading.

5.2 Payload Positioning

The accurate placement of the test payload over a specified ground point was easier in practice than anticipated. The first time we located the system over a particular point, an iterative procedure was used. The crew chief directed the positioning of vehicles until the system was reasonably close. At that time the theodolites would determine the target position relative to the proper location. The crew chief would reposition the vehicles to adjust the payload position. Several iterations were required to properly position the payload. Once ground points were located and marked, the positioning was merely a process of having the vehicles move to those locations. Fixed cable lengths eased the process substantially.

The use of double theodolite positioning data aided the fine tuning of position immeasurably. The procedure used to position this system is applicable to all systems where the requisite control is present.

One problem was the requirement to survey the site prior to placing the theodolites. We are presently in the process of rewriting the program so that one can go to any location and by knowing which direction north is, and picking two convenient locations for theodolites, set up a viable theodolite system. The only measuring required would be the distance between the theodolites, and the angle from true north to ground zero from each theodolite.

5.3 Balloon Motion Versus Tri-plate Motion

An extension line was flown between the balloon and the tri-plate on all tests. This had two major benefits and one minor drawback. The most important benefit was to separate the balloon radar signature from that of the chaff and dispenser. This allowed the experimenter to analyze the data without making a correction, by use of a "range gate". The other advantage is to greatly enhance the positional stability of the experimental payload. It was visually obvious using a bore sight, in winds of approximately 5 knots at the balloon, that the target had no apparent motion while the balloon above it was sweeping a disk approximately 1.5 balloon diameters in radius. Thus the balloon would move approximately 35 meters in both x and y while the target stayed within 3 meters.

In the follow up tests at Scat Site this effect was filmed by an uplooking camera at ground zero. A clip of film will be shown in conjunction with this presentation at this symposium. The minor drawback associated with the extension cable is in the increased difficulty of ground handling and maintenance. However, any time test stability is required, the benefits far outweigh the disadvantages.

5.4 Pendulum Effects of a Hanging Package

Table 2 shows that as the distance between tri-plate and payload increases, payload motion increases. During Data Run 1 winds of approximately 1.5 meters/second were encountered. With the payload 1.8 meters below the tri-plate, no motion was detected. Run 3, utilizing the same elevation angle, shows payload motion in a weaker wind field. In this case the payload was 15.2 meters below the tri-plate. When other elevation angles were used, the same situation occurred.

The greater the pendulum, the more payload motion. This is due to the fact that a longer pendulum will show more displacement for the same energy.

6. CONCLUSIONS AND SUGGESTIONS

6.1 Conclusions

The following conclusions were made from the test program described in this report:

- (1) The NOLARO tri-tether system with a natural shape balloon resulted in excellent stability for a payload in low winds.
- (2) Very precise positioning requirements can be met with little problem in low winds if a double theodolite system is used.
- (3) The tri-tether system with a lower elevation angle tends to be more stable regardless of cable type.* This tends to indicate system geometry is more important to stability than the type of cable used.
- (4) The double theodolite system is valuable for assuring proper system location.
- (5) Cable catenary has no appreciable effect on a low altitude, high lift system such as was flown.
- (6) The use of NOLARO cable was satisfactory, even though it went through handling it was not designed for.
- (7) The use of a pulley to reel a package up and down while leaving the balloon on station significantly speeds up an operation.
- (8) The use of a long extension line between the balloon and the tri-tether apex significantly enhances system stability.

* Leclair and Rice, Ibid.

6.2 Further Work and Improvements

Several areas of improvement have presented themselves to the authors. One of these is to improve the theodolite data analysis computer program as mentioned earlier in this paper.

Data acquisition on the total system could be improved by the more complete use of theodolites and cinetheodolites. This could be done by using them to record simultaneous data on balloon, tri-plate, and payload motions. Data of this sort would allow the various components to be looked at as a total system. Relationships between motions of the components might be determined with this data.

The extraordinary stretch found to be present in the cable needs further study. Solar radiations impact on this characteristic needs to be determined. Does the cable in fact stretch more under the influence of heat? Recommended additional study in this area is felt by the authors to be necessary.

The use of winches in place of trucks would aid in the proper care of the NOLARO cable. As explained before, time consideration required the use of cable too big for use on winches on hand. Future work would be greatly facilitated by the use of NOLARO cable on winches with a compatible traction drive system.

The optimum extension length between balloon and tri-plate should be determined. This would enhance the stability of the system without unnecessarily hampering ground handling.

Relationships between elevation angle, system weight and stability should be investigated.

A study utilizing an identical cable array but using an aerodynamically shaped balloon appears called for. The system using the aerodynamically shaped balloon should be extremely stable, especially in higher wind regimes.

NOLARO TRI-TETHER SYSTEM

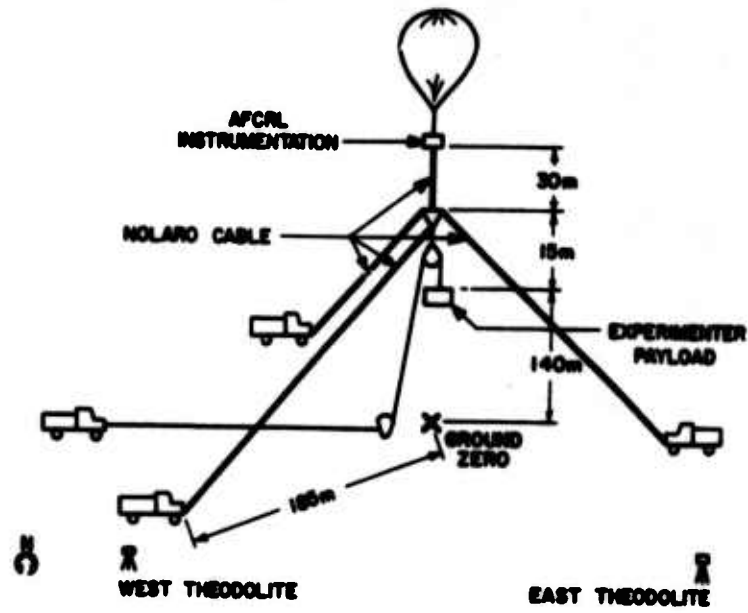


Figure 1. Erected System in Operation

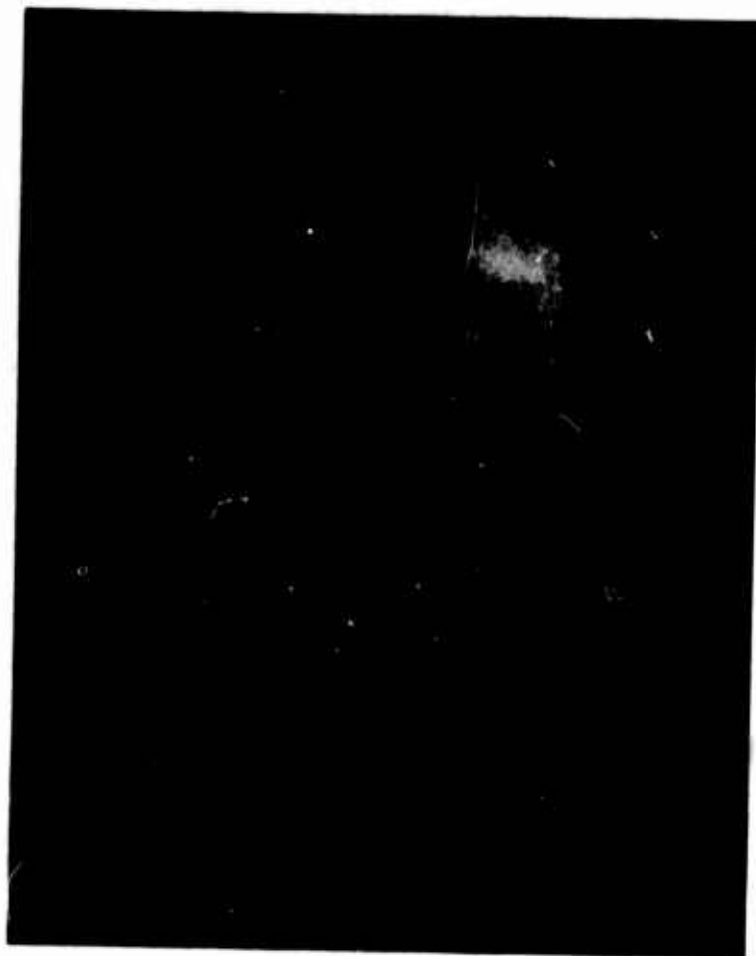


Figure 2. The Balloon at the Ground

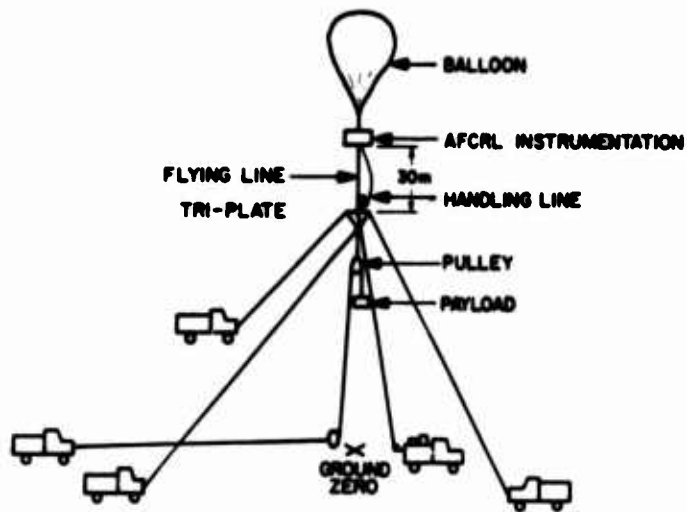


Figure 3. Operational Setup to Erect

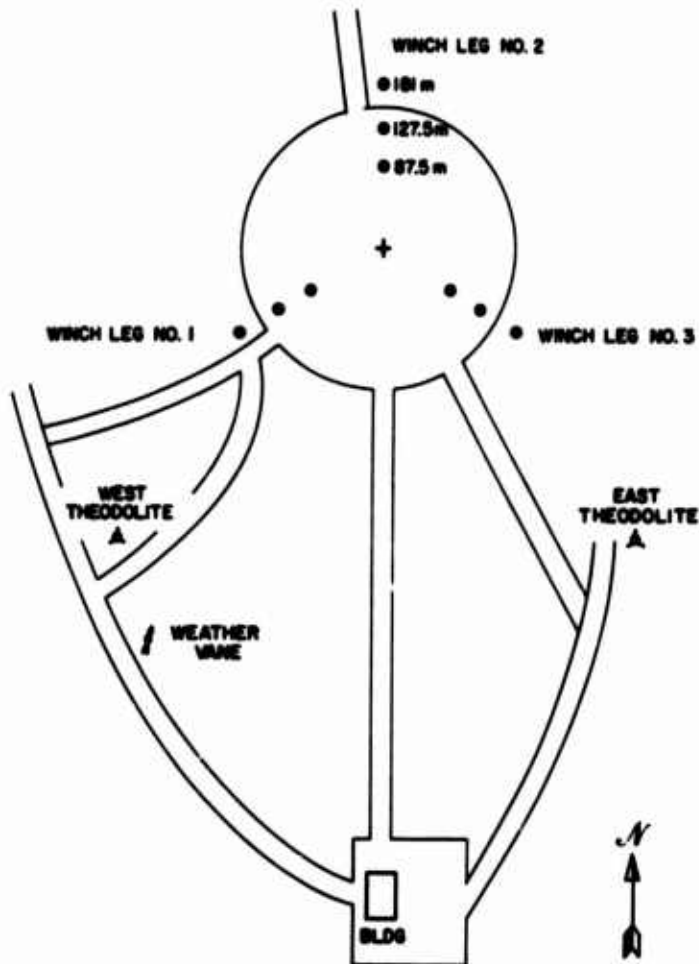


Figure 4 View of Scat Site Ground

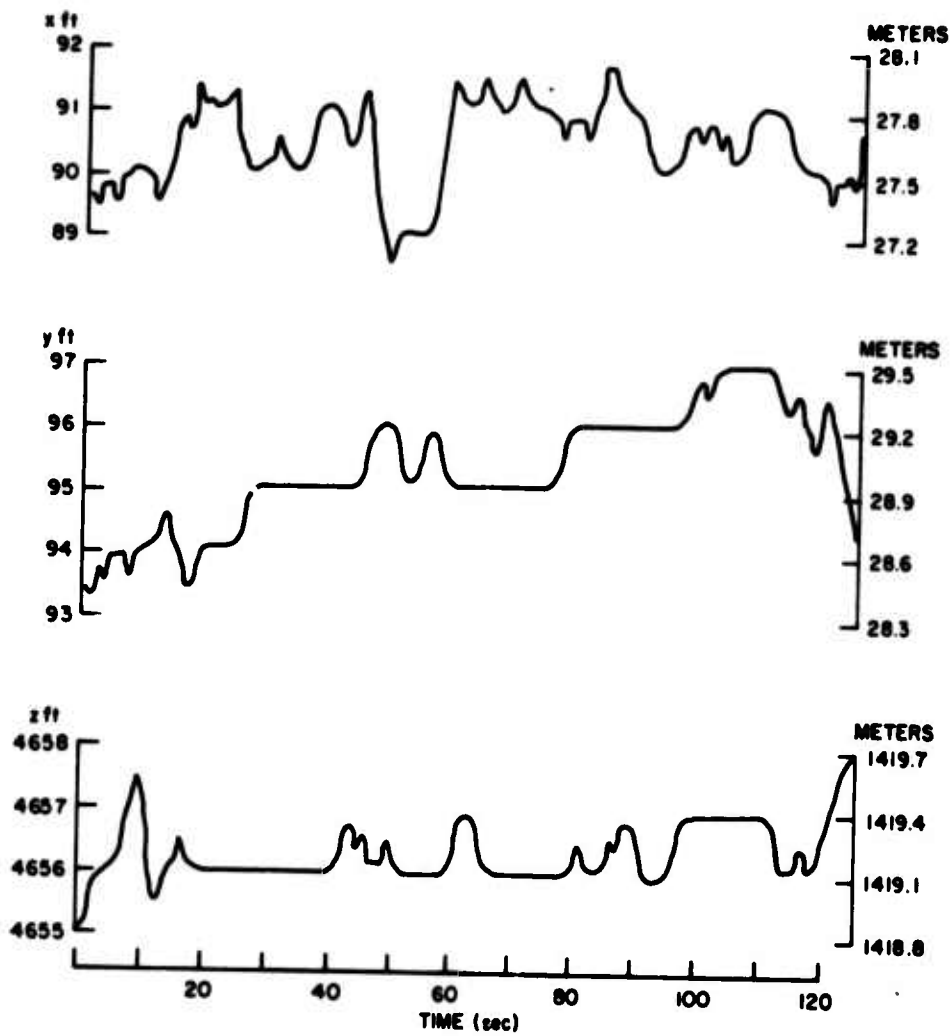


Figure 5. Data Run, Flight 1

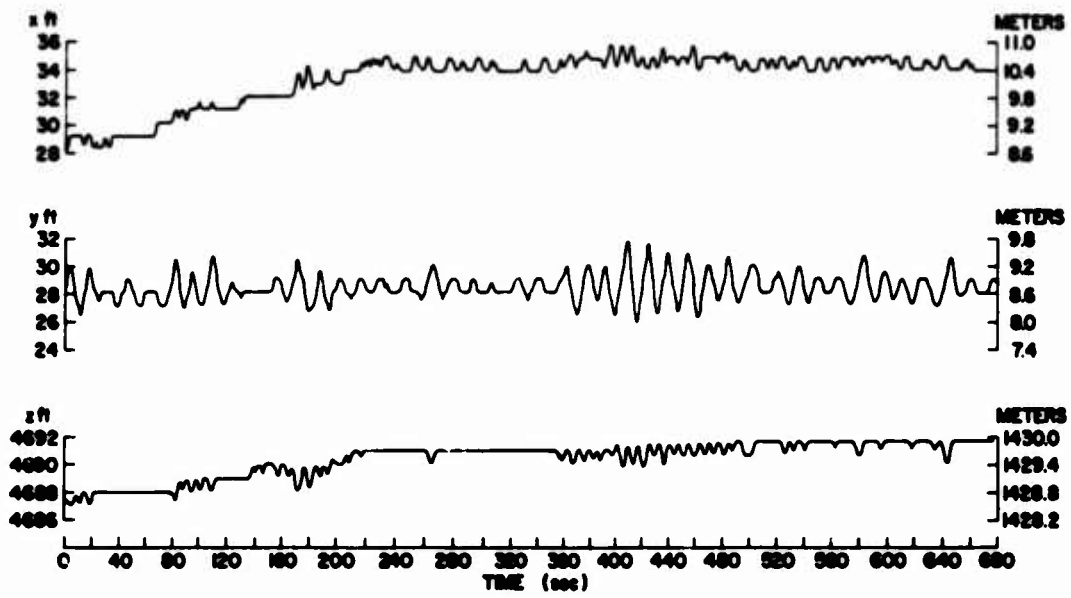


Figure 6. Data Run, Flight 4

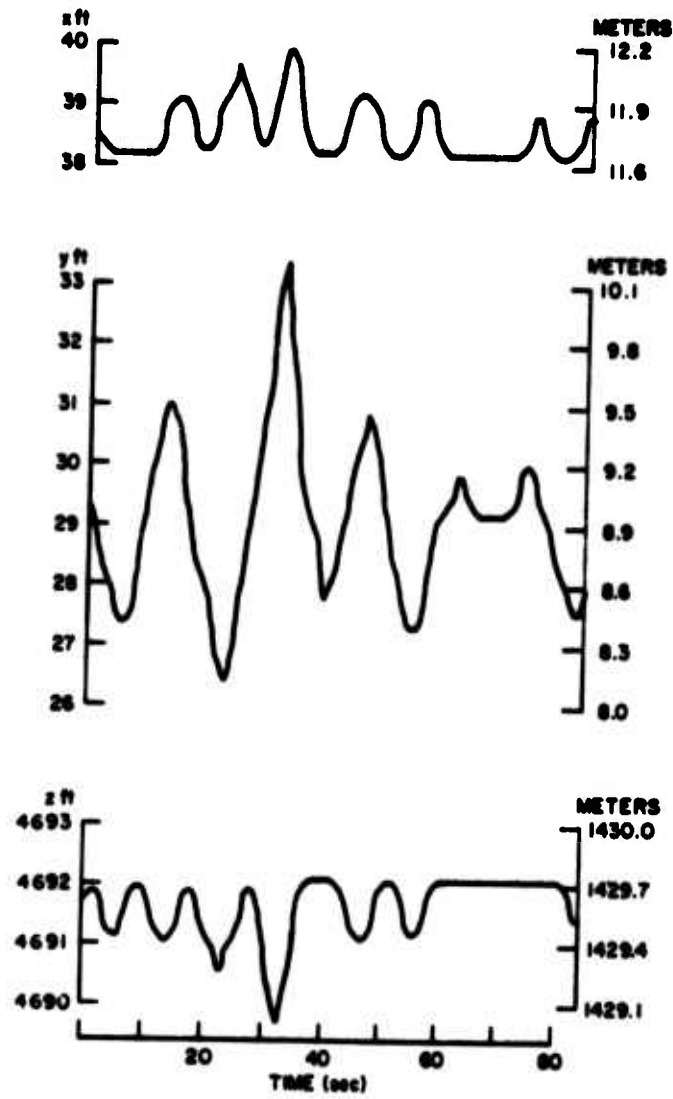


Figure 7. Data Run, Flight 5

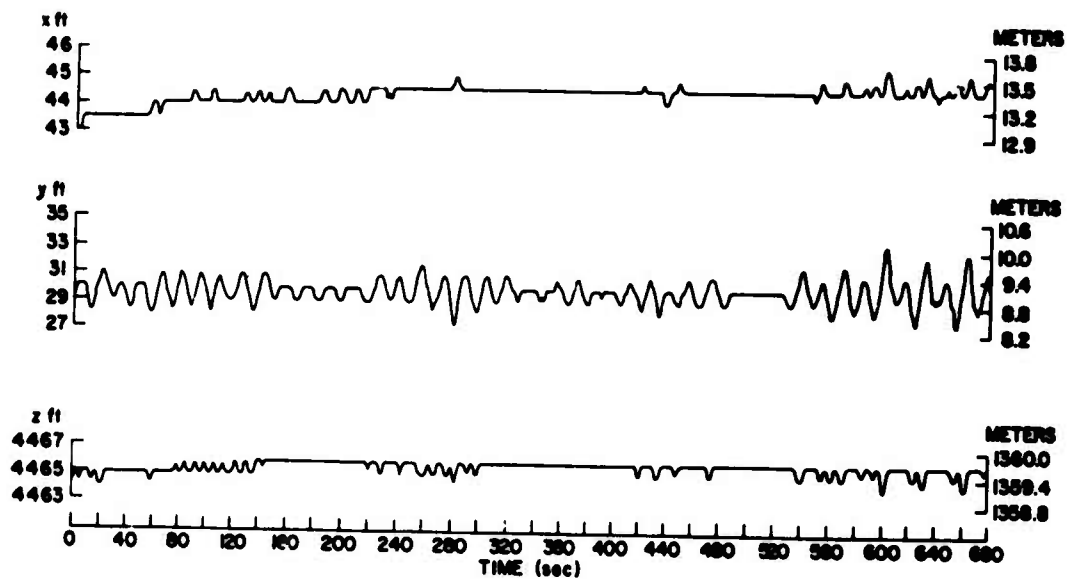


Figure 8. Data Run, Flight 6

Acknowledgments

The authors would like to thank 1st Lt J. R. Greenlee for helping during the performance of these tests and by proofreading the paper for technical accuracy. We would also like to thank Mr. James K. Hall for his help in computerized data reduction and depiction.

References

- Bennett, R. M., Bland, S. R., and Redd, L. T. (1973) Computer Programs for Calculating and Plotting the Stability Characteristics of a Balloon Tethered in a Wind, NASA TN X-2740.
- DeLaurier, J. D. (1970) A First Order Theory for Predicting the Stability of Cable Towed and Tethered Bodies Where the Cable Has a General Curvature and Tension Variation, Von Karman Inst. TN-68.
- DeLaurier, J. D. (1972) A Stability Analysis of Cable-Body Systems Totally Immersed in a Fluid Stream, NASA CR-2021.
- DeLaurier, J. D. (1972) A stability analysis for tethered aerodynamically shaped balloons, J. Aircraft 9(No. 9):646-651.
- Doyle, G. R. Jr., and Vorachek, J. J. (1971) Investigation of Stability Characteristics of Tethered Balloon Systems, AD731570.

References

- Doyle, G. R. Jr., Vorachek, J. J., and Block, D. B. (1973) Stability and Dynamic Behavior of Two Tethered Balloon Systems, AFCRL-TR-0396.
- Hoerner, S. F. (1958) Fluid-Dynamic Drag, published by the author.
- Leclaire, R. C., and Rice, C. B. (1973) The Local Motions of a Payload Supported by a Tritethered Natural Shape Balloon, AFCRL-TR-73-0748
- Peters, P. A., Lysons, H. H., and Shindo, S. (1973) Aerodynamic Coefficients of Four Balloon Shapes at High Attack Angles, Proceedings, Seventh AFCRL Scientific Balloon Symposium, AFCRL-TR-73-0071.
- Pohl, R. A., and Odney, K. D. (1973) Tethered and Cable Powered Heavy Lift Balloon Systems Design, Operations and Applications, Proceedings, Seventh AFCRL Scientific Balloon Symposium, AFCRL-TR-73-0071.
- Potter, R. C. (1965) The Stability of Captive Balloons for Instrument Flying, including Analysis of Multi-Cable Configurations, N67 11729.
- Redd, L. T. (1970) A Towing Technique for Determining the Aerodynamic Forces on Tethered Balloons, Proceedings Sixth AFCRL Scientific Balloon Symposium, AD717149.
- Redd, L. T., Bennett, R. M., and Bland, S. R. (1972) Analytical and Experimental Investigation of the Stability of a Balloon Tethered in a Wind, Proceedings Seventh AFCRL Scientific Balloon Symposium, AFCRL-TR-73-0071
- Redd, L. T., Bennett, R. M., and Bland, S. R. (1973) Experimental and Analytical Determination of Stability Parameters for a Balloon Tethered in a Wind, NASA TN F-7222.
- Redd, L. T., Bland, S. R., and Bennett, R. M. (1973) Stability Analysis and Trend Study of a Balloon Tethered in a Wind, With Experimental Comparisons, NASA TN-7272.
- Vorachek, J. J., Burbick, J. W., and Doyle, G. R. Jr. (1972) Investigation of Dynamic Behavior of Tethered Balloon Systems, AD740723.
- Vorachek, J. J., and Doyle, G. R. Jr. (1973) Comparison of Analytically and Experimentally Determined Dynamic Behavior of Tethered Balloons, AFCRL-TR-0284.
- Waters, M. H. L. (1959) Some Observations on the Wander of a Kite Balloon, Royal Aircraft Establishment TN Mech Eng 305.

Contents

1. Purpose and Scope
2. Objectives and Requirements
3. Prior Experience
4. Design of the Telta Fabric Elongation Monitor
5. Performance and Results
6. Conclusions

A Fabric Strain Monitor for Balloon Flight Test

Edward L. Crosby, Jr.
Chief, Analysis & Advanced Development
RCS TELTA Project
Cape Canaveral Air Force Station, Florida

Abstract

The performance characteristics required of an elongation transducer for in-flight monitoring of balloon fabric are somewhat unusual. The design, use, and results obtained with a fabric monitor used extensively on the IID7, 200,000 cubic foot aeroform balloon are presented and discussed.

1. PURPOSE AND SCOPE

This paper describes the design of a new fabric strain measuring instrument which has been used successfully for in-flight monitoring of induced strains in balloon fabric. Rather than as an academic "tour-de-force", in addressing conferees of the technical balloon community, we will emphasize the practical aspects of the development, hoping to provide the most useful information.

2 OBJECTIVES AND REQUIREMENTS

2.1 Background

In dealing with structural fabrics, the designer of inflated structures applies the classical principles of structural dynamics as applied to thin plates or membranes. His task is made more difficult and his methodology is modified because the materials of preference differ from metals in several important ways. They are anisotropic, usually strongly so; that is, their strength is much greater along certain directions than others. They are non-Newtonian in that their stress-strain ratios are not constant; in fact for most modern balloon fabrics the stress-strain slope is not only not linear, but has an arbitrarily curved shape. They exhibit "stress-creep" and stress memory. And, finally, their physical properties are more or less strongly temperature dependent.

The designer, obviously, must understand the capabilities and limitations of his materials; and the method of applying structural fabrics, very briefly, is as follows. The selected material is measured in the laboratory by instruments which provide stress data from applied strain in each of several selected directions while maintaining selected stress levels in each of one or more of the other significant axes. For "bias-ply" balloon fabric these directions are longitudinal, transverse and shear as related to the bolt of fabric. With these "materials properties", a measured strain, which is the elongation of the material, can be equated to the stress which produced it. This process of converting measured strain to applied stress may be performed by inspection of suitably plotted data, or it may be accomplished by reduction of the laboratory-generated data to an empirical mathematical definition for entry in a computer. The strain values measured on the structure are then entered and the

stresses print out. More will be said about this process by other speakers.

2.2 Utility of the Data

An accurate knowledge of the stresses to which the fabric is subjected provides the following essential information to the balloon designer:

- (1) The circumferential and longitudinal hoop tension due to inflation.
- (2) The loads imposed by load patches, fin attachment structures and other structural discontinuities.
- (3) The adequacy of the distribution (or the risk of the concentration) of these loads.
- (4) The stress imposed by hull body-bending or tail-lift under aerodynamic influence.
- (5) Incipient buckling due to aerodynamic forces which is revealed as a decrease in the static strain of inflation.
- (6) The creep of the material as shown by increasing strain (elongation) with time, accompanied by pressure drop.
- (7) The partition of stress between panels and seams, and between circumferential and longitudinal seams.

2.3 Requirements of the Monitoring Instrument

2.3.1 GENERAL REQUIREMENTS

Measurement of fabric elongation on a flying balloon imposes the obvious problems of remote measurement in an uncontrolled if not hostile environment. The instrument must be impervious to all effects of weather and sunlight and operate in a temperature range of

-50 to +150° F. Its longevity should be equal to the test period because of the inconvenience of reinstalling and recalibrating a replacement.

2.3.2 DETAILED REQUIREMENTS

The characteristics desired in any remote sensor apply in the present case and will be merely mentioned here. They include sensitivity, resolution, accuracy, good retrace (no hysteresis) electrical stability, durability and minimum effect on the measured phenomenon. This last requirement means minimum "force to operate" in this case.

2.3.3 SPECIAL REQUIREMENTS

The foregoing desiderata are primarily applicable to the transducer itself. There are other characteristics which must be maximized in the design of the monitor. Because of the physical nature of an inflated flexible envelope, two problems arise which are difficult to deal with and which are centrally important.

First, since the fabric is uniform in its elongation along a given direction, the attachment of a gauging structure creates an inelastic area which is, in effect, prohibited from elongating. Secondly, the somewhat indeterminate contour of the surface of a balloon, and the elongation of the fabric in several directions requires care in restricting the response of the elongation monitor to the single direction intended for measurement. A third characteristic which is rather universal but very significant in balloon instrumentation is output voltage level. Signals from balloon instrumentation transducers are of necessity carried on long leads and are subject to induced electrical noise of surprisingly high amplitude. An output level in the order of 100 millivolts is satisfactory. Of marginal usefulness

are 10 mV signals while those in the region of 1 mV and below are virtually useless unless complex and cumbersome signal conditioning amplifiers are used at the transducer site. Note that the voltage levels mentioned above are those of the range of the variable analog, regardless of the d-c pedestal. Thus a 5 volt half-bridge with ± 2.0 mV delta is entirely unsatisfactory.

3. PRIOR EXPERIENCE

The art of fabric strain measurement is not extensive. Beside "scratch gauges" and similar devices of the aerospace technology which indicate maximum excursions, there were no useful instruments available. Bonded strain gauges have greatly insufficient physical range. An arrangement of multiplying levers (actually dividing levers) is conceptually possible for use with bonded strain gauge elements but their complexity and fragility as well as other objectives are unattractive. A fluid-metal capillary resistance gauge developed by Battelle Columbus Laboratories appears to have excellent applicability in the controlled environment of the laboratory. However, stability, problems of secondary instrumentation, its low-level output, and its strong temperature dependence prevent its use on flying balloons.

3.1 The Mark I Fabric Strain Monitor

Developed by TELTA in 1971, this gauge used a linear (push-pull) potentiometer as the transducer. It was used more or less successfully for two years. Because of the relatively large physical excursion and the limited resolution of the potentiometer, the gauge required a span of 10 inches of fabric to provide acceptable results. This gauge-length is inconvenient. The associated hardware had an undesirably large "footprint", and the impossibility of adequately

sealing the potentiometer necessitated its periodic replacement, and recalibration of the gauge. At one time, the gauge was criticized because of the temperature coefficient of the 10 inch actuating rod. It was pointed out however that the brass rod had a temperature coefficient of expansion which is minute when compared with that of the polyester fiber under measurement which, in turn, is very small when compared with its elongation which is being measured.

4. DESIGN OF THE TELTA FABRIC ELONGATION MONITOR

The Mark I fabric strain monitor was built in considerable numbers and used for about two years. The service life of this instrument was in the order of six months. For this and the other reasons given in paragraph 3.1, above, it was decided to design a new instrument. The decision to do so was precipitated, in part, by the "discovery" of a nearly ideal transducer.

4.1 Selection of the Transducer

Space does not permit a discussion of the selection process but it should be stated that the search was aggressive and many transducers were investigated, some of them in considerable detail. The one selected is the linear variable differential transformer (LVDT) as manufactured by Schaevitz Engineering; the particular model is designated 125 HCD. As stated above, it was very well suited to this application. It is hermetically sealed, has a high output level, infinite resolution, satisfactory physical excursion and a compact and very convenient shape.

4.2 Electrical Characteristics of the Transducer

The detailed characteristics of the 125 HCD LVDT are given in

the manufacturer's literature, Reference 1, and will be synopsised here since the interested prospective user will and should use the prime information. A simplified schematic of the transducer is given in Figure 1. As shown the unit requires a ± 15 V d-c supply. It incorporates intrinsic regulation so that its performance is unaffected by ± 2 volt variation in the external supply. It draws only 20 mA on each leg so that line drop is no problem. The principle of the transducer is variation in reluctance of the iron circuit of a transformer. The variation is provided by the depth of insertion of a ferromagnetic cylindrical slug, hermetically external to the sealed unit. The a-c for the transformer is provided by the oscillator and the transformer secondary signal is demodulated and amplified. The output signal is a single-ended d-c analog voltage and is impressed upon a potentiometer at the input to the telemeter equipment. This potentiometer is used to set the signal level; as will be discussed later. The maximum linear input range, i.e., the maximum slug excursion for linear output is ± 0.125 inch.

4.3 Mechanical Characteristics of the Transducer

The LVDT is a stainless steel cylinder, 0.75 in diameter and 3.625 inches long, terminating in a shrouded male receptacle at one end and having a cylindrical hole in the other. This cavity receives the slug and is lined with an anti-friction polymer. The separate slug is of non-corrosible alloy and is concentrically bored and tapped.

4.4 Detail Design of the Gauge

The entire assembly is shown in Figure 2, as it is attached to the balloon. The LVDT is held to the saddle block by a stainless-steel screw-type hose clamp. A neoprene buffer pad under the clamp prevents crushing. The slug is driven by a wire assembled between

two screws. The screw on the slug-end is non-magnetic stainless-steel. The wire is nickel alloy wire chosen for its temper. It is 0.02 inch diameter and non-corroding. The screw on the tail-block end is brass and screws into the tail block.

Figure 3 shows the components. The drive-wire assembly is fabricated by boring #48 drill holes in the screws, loop-heading the wire, and joining with epoxy cement. The screw in the slug is retained on final assembly by a thread staking compound. On the tail block, which is a slice of a 5052 aluminum alloy angle, is riveted an aluminum/nylon elastic-stop anchor-nut. The installation crew added a jam nut on this screw but it is not needed. The saddle block is a weldment made of 6061 aluminum alloy parts. The base corners are rounded so that the blocks may be removed by peeling them off the balloon without damaging it. The saddle and tail blocks are finished with white epoxy varnish over zinc chromate primer, except for their base surfaces which are sanded bright.

4.5 Discussion of the Geometry

The small size of the transducer permits a reduction in the footprint of the gauge. Although any rigidly stiffened fabric is undesirable, some is unavoidable. The base area of the saddle block, in this case, was considered small enough that for the elongation to be expected, the mounting cement would provide some compliance at the edges. Compliance over the bonded area however is not desired since it has the effect of increasing the gauge length. None of the gauges used during the Design Verification Test Program peeled, even at the edges. Figure 4 is a sketch of the gauge geometry.

The drive wire permits various combinations of axial and angular misalignment, but drives the core along the gauge axis. The

height of the gauge axis above the fabric surface suggests the possibility of tipping, particularly of the tail-block. This can only occur, however, if there is an appreciable restraining force, such as friction, applied to the slug. Of course there is some but it is very small. To check it, the operating force of the drive wire was checked, with the tail-block screw axis misaligned 5 degrees from that of the slug. The friction required to move the slug was less than 0.1 ounce (0.006 lb). Since the force responsible for the elongation being measured is in the range of 10 to 150 lbs., we can dismiss the matter. Furthermore as the strain increases, and hence the stress, not only does the slug resistance become less important, but the firmness of the base greatly increases. And, finally, slug friction would produce directional hysteresis unless it were negligible, and none has been recorded or observed.

4.6 Calibration; Basic Coefficients

A full account of calibration philosophy and procedures is given by E. T. Johnson in Reference 2. The summary below provides the presently relevant data. With the telemetry-channel input potentiometer set so that maximum slug excursion is 0.125" from null and the gauge-length of 2.5" established by the separation of the juxtaposed edges of the saddle block and the tail block as mounted, the following data, based on 204 hull fabric characteristics, are examples of fabric strain monitor performance:

	<u>output</u>	<u>extension from null</u>	<u>strain</u>
Maximum Scale	2.5 V	0.125"	50,000 μS
Practical Null	0.005 V	2.5×10^{-4} "	100 μS
High Hull Pressure (50 lb/in hoop stress)	0.19 V	9.5×10^{-2} "	3,800 μS

4.7 Transducer Accuracy and Linearity

The transducers (25 units) were measured for linearity by the Physical Standards Laboratory of Cape Canaveral Air Force Station of the Air Force Eastern Test Range. The procedure was to record the departure from the expected output for each 0.025" increment of core movement from null to 0.125" from null in each direction. The measuring machine was a Pratt-Whitney with a certified accuracy of $\pm 10 \times 10^{-6}$ inch. The measured maximum departure of the units was the specification limit of 0.25% of full scale or 1% of the indicated value, whichever was least. Each slug was related to the LVDT with which it was tested by serial numbering the same.

4.8 Pre-Installation Checkout of System

In order to operate the system before installation, a piece of hull fabric was fastened to a test frame so equipped as to put variable tension on the fabric. The maximum tension which can be applied is approximately 800 lbs. For a yard of fabric this is about 22 lbs per inch, a moderate strain. A fabric strain monitor was cemented to the fabric and mechanically nulled. Using a 4-place digital voltmeter the gauge output was read for several tension increments. Tension was measured with a Dillon tension scale with an accuracy of $\pm 2\%$ of full scale of 2000 lbs. This test setup, though crude, provided assurance that the gauge was functional. Of more importance, we soon learned, it provided practice in setting the null on the gauge. The sensitivity and response-width became apparent when the voltmeter reading varied with shouting at the fabric.

5. PERFORMANCE AND RESULTS

5.1 Installation on the Balloon the Balloon

Twenty-one gauges were installed on the Balloon SN 204 for the Design Verification Tests. Figure 5 is a sketch illustrating their location. The gauges were oriented longitudinal, circumferential or shear. The LVDT's were positioned cavity-down or cavity-aft so as not to fill with water and be damped. (No pun is intended; the dash-pot effect would be obviously undesirable.) Gauge sites were chosen on the basis of structural significance as will be discussed in detail by other speakers. Figure 6 is a photograph of a cluster of gauges, set No. 4. A template was prepared which was used as a stencil by the installer. The gauge outlines were stenciled on the hull using a ball-point pen. The saddle block was cemented in place and the tail block was then cemented into position using a 2.5 inch spacer. The drive-wire was then screwed into the tail block half way. Next, the LVDT was mated to its connector and, introducing the slug into the transformer cavity, it was clamped. Before final tightening, the LVDT was slid along the saddle block to that position at which the core was at mid-position in the cavity, approximately. The clamp was tightened.

5.2 Calibration

To calibrate the gauge, the technician substituted a test-box cable for the balloon cable. This box supplies power and reads output. The adjustment is made by carefully turning the tail block screw until null is read. The very high sensitivity together with the rather "rubbery" nature of the gauge's foundation makes this a rather exacerbatng exercise. After some thought, and with substantial pressure from the crew, we agreed to accept ± 5 mV as null

limits. To check the rest of the system, the technician supplies a "par" voltage to the gauge cable before replacing it on the gauge. This is a signal simulation and should drive the telemeter strip-chart pen from zero to full scale as it is keyed "on" and "off". The full scale strip chart readout (i.e. the scale factor) may be selected in the T/M Ground Station for any channel. With these two operations, the calibration is complete. The procedure is performed with the hull pressure at 1 IWG pressure. This is a compromise between excessive tension in the area of the maximum diameter (maximum hoop-stress) and insufficient tension of the fabric to remove creases in those areas of small inflation stress. In data reduction, the bias is known and can be handled as desired. The elongation at 1 IWG is small, in any case, and the bias is a small part of any significantly large stress.

5.3 Inflation Test

The static pressure and hull growth test of Balloon SN 204 was conducted in the Vehicle Assembly Building, Kennedy Space Center, NASA. This was an unusually complex operation and the large number of measurements made produced very interesting information on the effects of pressure on hull geometry. A detailed account of the test is reported in Reference 3. The fabric strain monitors were installed on the balloon as shown in Figure 5. Their calibration had been checked just prior to the test and valid data were recorded for all. The nulls at 1 IWG pressure were offset from "pen zero" on the charts so as to provide for buckling.

Although none was expected in this static test, it was desired to operate the instrumentation as was contemplated during the then forthcoming flights tests. The reduction of the fabric strain

monitor data is reported in Reference 4 along with a discussion of the results. The stress levels computed from the strain data were moderate and they varied from site to site in very good accordance with expectations. Figure 7 is a reproduced excerpt from one of the recorders -- the one on which hull and tail pressures appear. This portion of the test includes "test sequence one" and, quite dramatically shows the response of the gauges to rapid fluctuations in hull pressure. This unscheduled event, immediately preceding the test, was caused by failure to disconnect the hull pressure servo; and the ballonet valve cycled to prevent the attainment of 3 IWG hull pressure, which was the intent at that step of the test.

5.4 Flight Test

In the Design Verification Test Program, the fabric strain monitors were used on all of the 50 flights. One gauge failed on the last tow test flight. The failure was caused by a catastrophic electronic circuit failure within an LVDT. The unit was promptly replaced by the manufacturer. The telemetered data were reduced by the Range Measurements Laboratory computer and an analysis of the results has been prepared by Battelle Columbus Laboratories in Reference 4. The DV Program Final Report which will be shortly released contains this information also, in Appendix "H". This report is Reference 5.

These fabric monitors have been used on two other tests in addition to the regular flight test series. A pair was attached to the hull fabric as close as possible to a nose beam at the point of its intersection by a spoke. The purpose of instrumenting the fabric at this point was to ascertain what load was transmitted into this region of the envelope by high transverse loads on the nose post.

Interestingly, no load of significance above static could be detected. Evidently the cross load on the nose structure is very generally distributed.

The second special test consisted of instrumenting a gore seam and a panel seam immediately adjacent to a pair of gauges already in use on a panel. The purpose was to determine the magnitude of inflation stress on seams as compared with that of the panels. The balloon was moored. The seams chosen were adjacent to gauge set 3 so as to be removed from patch loading and be near maximum hoop tension. The information was obtained; the seams carry substantially higher loads than the panels as would be expected because they are 3 times the thickness (in this balloon) than the panels. An unexpected result also eventuated. It was found that the tension on the panel seams was roughly equal to that of the gore seams, notwithstanding that circumferential hoop stress is twice that of longitudinal. The explanation is obvious when the geometry is considered. In this region of the balloon, as in most areas, the panel seams divide the load because on an area basis there are more than twice as many as there are of the gore seams.

6. CONCLUSIONS

The fabric strain monitor design project which was addressed was completed. Twenty-five have been fabricated. They have been exposed to the environment continuously for several months and read during many tests and flights. The gauge is reliable, highly sensitive, and accurate.

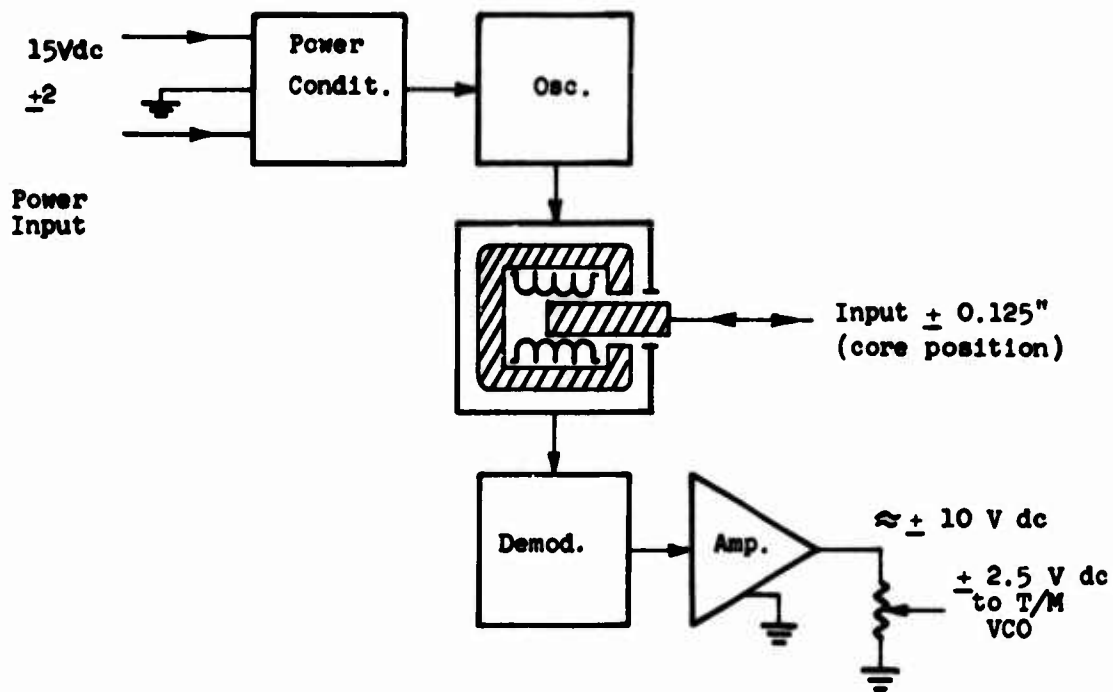


Figure 1. Functional Block Diagram, LVDT



Figure 2. Fabric Strain Monitor Assembly

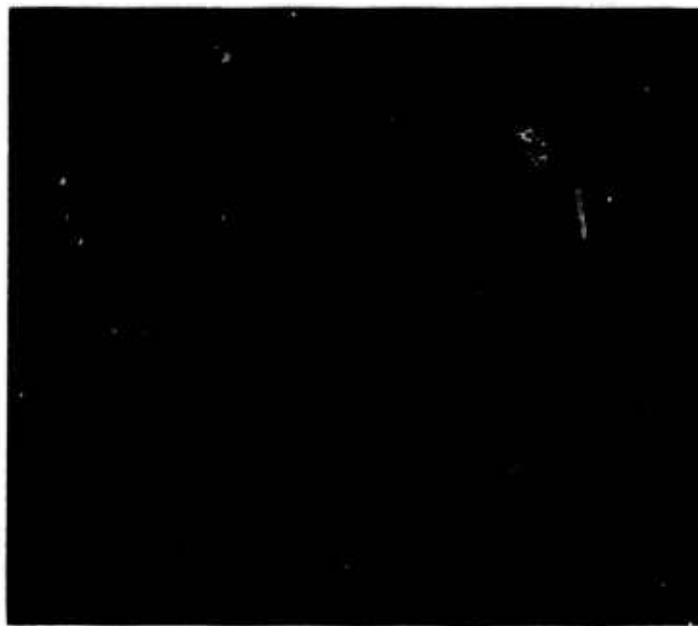


Figure 3. Fabric Strain Monitor Components

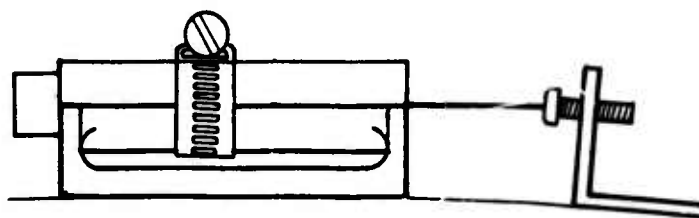


Figure 4. Diagram, Horizontal Side View, Fabric Strain Monitor

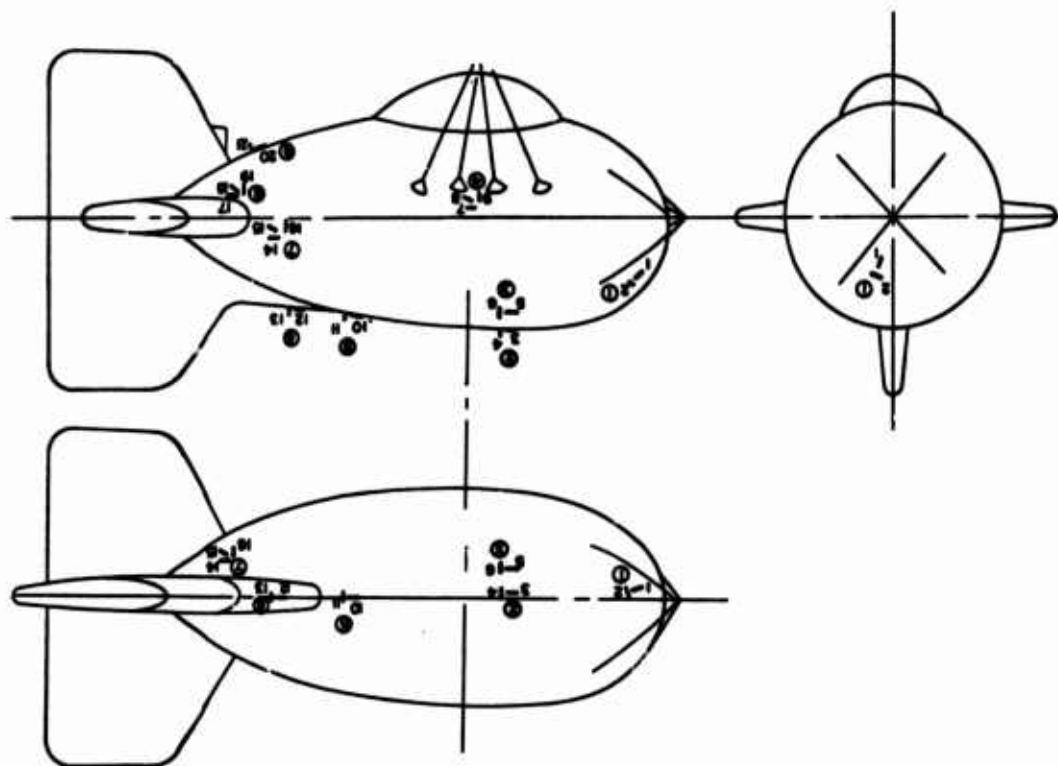


Figure 5. Diagram IID7 Balloon, Showing Fabric Monitor Locations



Figure 6. Cluster of Three Fabric Strain Monitors Mounted on Hull of Balloon S/N 204

Acknowledgments

The support of the Tactical Technology Office of the Defense Advanced Research Projects Agency, the Sponsor, is gratefully acknowledged as is the Range Measurements Laboratory, Air Force Eastern Test Range, and Walter H. Manning, Jr., its Director. Lt. Col. L. J. Del Do, Chief, and Lt. Col. J. H. Watts, Assistant Chief of the Sensor Platforms Branch of the RML have managed the Balloon Program and provided the opportunity for our participation. Gratitude is extended to Robert P. Murkshe, RCA TELTA Project Manager for his encouragement and priority aid. Ted Yon, DV Project Engineer and Ed Johnson, TELTA Electronics Engineer are due my special thanks for their many decisive contributions to the success of this development.

References

Catalog on Linear Variable Differential Transformers, Schaevitz Engineering, Rte 130 at Union Avenue., Pennsauken, N. J. 08110

Design Verification Program Instrumentation System Calibration. E. T. Johnson TELTA Report TR 74-059, RML, June 1974.

Design Verification Program Balloon Physical Measurements and Pressure Growth Test Results, Balloon SN 204, H. D. Masch; TELTA Report TR 73-036, RML, December 1973.

Data Analysis of the Family II Balloon Design Verification Program - Structures, E. J. Mills and J. J. Groom, Battelle Columbus Laboratories, August 1974.

Design Verification Test Program TELTA Report TR 74-058, Range Measurements Laboratory, to be published.

Contents

1. Introduction
2. Background
3. Methods
4. Experience
5. Special Problems
6. Future Concepts

Mobility Of Large Tethered Aerostats

H. D. Masch
Chief, Operations Planning
RCA TELTA Project

Abstract

One of the more significant limitations of a large tethered aerostat system operating at a permanent or a temporary site has been the inherent lack of quick reaction mobility. Quick reaction mobility is that system capability to relocate both ground support and aerostat systems to new operating locations with minimum effort and time consistent with aerostat safety. This paper presents a synopsis of TELTA Project methods and experiences in moving large tethered aerostats from one operating location to another. The relocation tests used such prime movers as bulldozers, flight winch vehicles, and helicopters. The synopsis is followed by a discussion of the impact on future aerostat systems concepts resulting from TELTA Project demonstrated mobility of large tethered aerostats. Typical of this future impact on mobility is the pending mobility test with a large aerostat using a sea-going vessel to move an in-flight aerostat several hundred miles by sea from one site to another.

1. INTRODUCTION

Before reviewing current large aerostat mobility methods and experiences it is best that the scope of the terms Large Aerostat, and Mobility be defined to establish a common plane for reference.

(1) Although basic experience in aerostat mobility was acquired by the TELTA Project (Figure 1-1) through the movement of small size aerostats (nominally 3,000 to 5,000 cubic feet) (Redd, 1970) and medium sized aerostat (nominally 80,000 cubic feet) (EGYPTIAN GOOSE PROJECT), the mobility of large aerostats in this paper refers to those of 200,000 cubic feet in size (Figure 1-2). Thus, the range of a large aerostat covered by this paper may be assumed to be those from 100,000 to 300,000 cubic feet in size.

(2) Mobility is a more complex term in that the distance to be moved, the reason necessitating the move, and the time allowed in which to accomplish the move are all inter-related. Distance to be moved may be in the order of 100 yards (i.e. moving an aerostat from a mooring location to a flight location); or the move may be a few to hundreds of miles (i.e.: relocation from one operational location to another). The reasons necessitating the movement are in themselves complex; they may be due to economical constraints (i.e.: to avoid costly deflation and reinflations); or to better fulfill a tactical or scientific mission; or the move may be necessitated by the approach of excessively severe weather (i.e.: hurricane). The distance to be moved is a direct function of mission objectives and requirements. These will be expanded upon in appropriate parts of this paper.

2. BACKGROUND

Interest in aerostat mobility is not of contemporary origin. It has been, however, and continues to be one of predominately military interest from time to time thru the previous several centuries until today. There exist recorded examples of attempted aerostat mobility, with varying degrees of success, over land and water

during the American Civil War (Haydon, 1941). There are recorded examples of aerostat mobility by the Germans (by land and sea) and the A.E.F. in France (Widmer, 1918; Myers, 1969). Without exception, aerostat mobility in the above applications was for aerial observation missions. In more recent times, aerostat mobility was exercised most fully by sea during the Normandy Invasion in World War II by the Allies (Myers, 1969). In this latter instance, the aerostats were barrage balloons transported by ships to hamper enemy aircraft attacks upon the D-Day Invasion Armada.

Even the movement of a small tethered aerostat (6,500 cubic foot) was successfully accomplished by Goodyear Aerospace Corporation in 1966, utilizing a Bell Model 47G helicopter (GER-15317, 1971).

From this background, it is clear that work in tethered aerostat mobility has been accomplished by our predecessors in tethered aerostat operations. The point of departure herein covered is, however, that the feasibility and techniques related to the mobility of the large tethered aerostats has now been successfully accomplished and demonstrated.

3. METHODS

Basically, all methods concerning tethered aerostat mobility are directly influenced by two simple matters. First, consideration of the ground tether point (anchor) relative to a tethered aerostat aloft. And second, consideration of the nature and types of obstructions along the route of travel. Weather and winds are an influence, but these are common considerations to all facets of tethered, aerostat operations. In effect, if the weather and winds are compatible to tethered flight operations, then they are also compatible to an aerostat relocation operation.

(1) To create tethered aerostat mobility, one need only to provide mobility to the "ground" tether point. In essence, move the anchor point by some means while an aerostat is aloft, and the standing tether and aerostat will follow the moving anchor point. The "ground" tether point may be a flying sheave, or a shackle assemble, as appropriate.

TELTA Project mobility tests utilizing the tether winch truck (Figure 1-3) were directly feasible because the flying sheave was already truck mounted and therefore already mobile.

TELTA Project mobility tests with a bulldozer (Figure 1-4) utilized a modified shackle assembly in lieu of a flying sheave.

The helicopter mobility tests utilized a flying ballast (Figure 1-5) to simulate an anchor point with a modified shackle assembly in lieu of a flying sheave.

In all of the tests, the anchor point was made mobile, or movable relative to the ground.

Of the three methods cited, movement with bulldozer and movement with Helicopter/flying ballast each required an especially fabricated, fixed length tether assembly. Movement with the winch truck was done directly with the on-board flight tether contained on the winch tether drum.

(2) Obstructions along the route of travel may be by-passed, or passed over; dependent upon the mobility technique used and the surrounding terrain. Perhaps the most troublesome of obstructions to overcome are power lines and bridge overpasses along the relative route of travel. However, such obstructions are more challenging than prohibitive. By-passing such obstructions should always be the first consideration when feasible. Movement by helicopter and flying ballast directly overcomes all normally encountered obstructions save mountains and seas.

4. EXPERIENCE

Before reviewing TELTA Project aerostat mobility experiences in greater detail, let me cite the gross benefit the project gained through the effective application of aerostat mobility. This gain was in time, costs, and material expenditures avoided during 1972 then 1974. During this period eleven major large tethered aerostat mobility exercises were accomplished while fulfilling primary mission assignments.

The following salient facts are essentially representative of project expenditure avoidance directly distributed to aerostat mobility.

- Eleven aerostat deflation and eleven inflation operations were avoided. This most effectively reduced inherent handling wear to the aerostats through packing and unpacking.
- The consumption of 1,760,000 cubic feet of helium was avoided. This volume nominally represents 39 GHe tube-bank trailers, or \$89,760 in helium costs.
- 112 manweeks of flight crew effort were avoided.
- 33 work days were saved for direct application to primary aerostat mission commitments.

In substance, effective use of tethered aerostat mobility saves mission time, money, and material. In addition, such mobility allows that added necessary element of quick reaction to mission requirements.

(1) During the first years of TELTA Project operations fundamental experience was gained in aerostat mobility through three assigned programs. These programs were POCKET VETO, Phase I; PROJECT BALDY; and a follow-on Tow Test Project. All were on a small scale with respect to aerostat mobility, but valuable experience was gained on a modest scale.

(a) In POCKET VETO, Phase I, a BJ+3 barrage balloon type aerostat of 84,000 cubic feet was utilized (Figure 1-6). The primary Balloon Facility at Complex 1/2, Cape Canaveral, Fl., was set up such that the aerostat mooring location was 300 yards from the aerostat launch location. To maintain aerostat safety and control, it was necessary to move the BJ+3 Balloon from its mooring location to its launch location each morning; and back, each evening. Anchor point mobility was provided by using an aircraft tug. The balloon was tethered on a short cable to the tug and moved as needed. This was a direct application of the first rule

for mobility: render the ground tether point mobile.

(b) Project BALDY utilized a 5,300 cubic foot balloon (Figure 1-7). To avoid daily inflation and deflation, the balloon was left inflated but moored in Hangar C, Cape Canaveral. The hangar is one-half mile from the launch location. Mobility with the BALDY balloon was accomplished via two methods, each dependent upon surface wind conditions. On relatively calm days, a small tether winch was mounted on the rear of a 1½ ton truck, with the balloon secured with minimum tether length. Again, the "ground" tether was thus rendered mobile. However, there were obstacles along the route of travel: power lines. But due to the modest size of this aerostat, we were able to pass under these obstructions. On more windy days, the small winch was secured on a flat bed trailer; and the balloon was closehauled and snubbed to the trailer. As before, the size still allowed for passage under the power line obstacles.

(c) The follow-on Tow Test mission was with the Langley Research Center balloon system (Redd, 1970) (Figure 1-7). This was a small balloon of 25 feet in length, tethered to the top of a panel truck. The entire system was parked, when not in use, in Hangar C. Tow Test missions were conducted at the Skid Strip on Cape Canaveral, Fl., about 1½ miles by road from Hangar C. Although, power line obstacles were along the route, mobility was unimpeded because the entire system could pass under these obstacles.

(2) In early 1972, delivery was taken on the first large tethered aerostat, a 200,000 cubic foot Family II balloon (Figure 1-2). To avoid work interference by weather, this first aerostat, SW 201, was given complete checkout, inflation and assembly in the NASA Vertical Assembly Building (VAB) at the Kennedy Space Center. Upon completion of this activity the full value of mobility capability was recognized. The VAB is nominally 15 miles distance from the primary Balloon Pad Facility on Cape Canaveral Air Force Station.

The immediate consideration was to evaluate the feasibility of moving the inflated aerostat from the VAB to the flight facility. Two methods were evaluated

initially: helicopter tow and tow over land. A survey revealed that neither a helicopter nor a pickup zone was readily available. Thus, the decision was limited to an attempt at tow over land.

Two tasks needed resolution before true mobility and VAB-to-Pad transfer could be achieved. First, develop a mobile anchor point; and second, determine a suitable route of travel. In this case, the route of travel was evaluated first because the route would affect the mobility method chosen.

(a) An examination of the route of travel revealed that a run, with no obstacles, existed from the VAB to the beach road, a distance of three miles. The route down the beach road had some 14 power line obstacles before reaching the balloon pad. However, it was noted that the balloon pad could be made accessible from the beach if a patch were bulldozed through the palmettoes. It was obvious that there were no overhead obstacles along the beach, but none-the-less, the full route along the beach was also examined to assure that no low lying blockades existed. The route evaluation revealed that a clear run existed from the VAB to the Pad, at low tide. We were, in essence, thus planning to by-pass the existing overhead obstacles. The next task then was to determine the means of acquiring the necessary mobility.

(b) The task of providing aerostat mobility between the VAB and the beach was readily resolved by planning to use the winch truck (Figure 1-2). Based upon past experience of moving aerostats with an aircraft tug and a short, fixed length tether, it was decided to borrow a vehicle heavy enough to control the balloon in flight, yet capable of driving along the beach at low tide. Either of two tracked vehicles were considered: an M-24 Tank or a bulldozer. The bulldozer was immediately available and was thus chosen for this portion of the mobility task. With the route and the means chosen, the next task was to develop a special tether compatible to the winch and the bulldozer.

(c) Again, previous experience assisted in the development of this

special tether. One of the first balloon missions of the TELTA Project was to test and evaluate tandem balloon operations with BJ+3 balloons. The upper tether assembly, connecting the upper balloon to the lower balloon was an ideal design. In the original design this special tether was 3,000 ft long. This length was shortened to 1,000 ft for this mobility exercise because at this height, the balloon could be easily monitored visually and would be flying at an effective height above any normal ground air turbulence.

In the tandem application, the aerostat was ascended under winch control until an in-line eye splice was readily accessible. At this time, a short section of tether was connected to this in-line splice and to the top attachment point on the lower tandem balloon. Once connected, the upper balloon was ascended until it was supported by the lower balloon. At this time, the remainder of this special tether was removed from the winch drum and its lower end secured to the lower balloon's tether point assembly.

In the mobility exercise, the bulldozer was used to simulate the lower balloon and to serve as the mobile anchor point. A sling and shackle assembly was used to secure the in-line tether eye to the bulldozer blade. The remaining length of special tether was removed from the winch, coiled, and suspended from the standing tether at the shackle attachment location (Figure 1-4).

After egress from the VAB, with the balloon supported by the winch truck, the balloon was ascended to 500 ft. At the beach, the balloon was attached to the bulldozer then proceeded along the beach to the flight pad complex where the balloon was again transferred back to the winch truck and then moored. The total mobility event, from egress at the VAB to Mooring at Complex 1/2 took about 8 hours to accomplish.

(3) The next significant mobility exercise occurred in late 1972 with the same aerostat. In essence, the requirement for this particular balloon design was to be capable of sustaining 65 knots in flight. However, because such wind speeds had not been encountered during routine flight test missions, the mission requirements were revised to include an inflight tow with a helicopter (Figure 1-8).

The primary mission was to achieve 65 knot relative wind speed on the balloon. The secondary mission was to determine mobility feasibility using a helicopter.

In preparation for this mission, the balloon was relocated by routine means (deflation and reinflation) to an open field site adjacent to Port Canaveral. This particular location was selected because it affords immediate access to over water flight, east of Cape Canaveral Air Force Station.

Three tasks were involved in this mobility exercise: Acquisition of a helicopter to conduct the test; determination of the size mobile anchor required (flying ballast) (Figure 1-4) for this mission; and the special tether assembly needed.

(a) The helicopter acquired for this test was a CH-47 Chinook (Figure 1-8) provided by the U.S. Army.

(b) The mobile anchor, or flying ballast, was fabricated to weigh 9,000 lbs. The objective of such high weight was to prevent excessive distance from developing between the helicopter and balloon while in flight at 65 knots. A secondary problem surfaced before the test was conducted. This problem concerned the effect of emergency jettison by the helicopter while over water. Analysis revealed that should jettison occur, the free fall force from the total flying ballast weight would cause the balloon to continue to dive and strike the water surface with sufficient impact to probably destroy the balloon.

As a result, the final configuration of the flying ballast (Figure 1-5) contained two sections. In essence, the lower section of 5,000 lbs could be separated on command in the event of emergency jettison. Thus the free fall force of the remaining flying ballast weight would bring the balloon down to a soft impact without striking the water surface.

(c) The special tether assembly developed was made in two parts. The portion for tethering the balloon to the flying ballast was the same configuration as was used with the bulldozer. It provided a fixed distance of 1,000 feet between balloon and ballast. A tri-plate/swivel assembly on the ballast head (Figure 1-5) allowed for the connection of the other portion of the special tether assembly,

a single 1,500 foot length of tether.

The basic design purpose here was to ensure that the helicopter maintained a 500 ft vertical separation between it and the balloon when the tethers were under tension and the helicopter was in flight near the balloon.

(d) The helicopter tow test was conducted in two parts on two consecutive days. On the first day, the balloon/ballast was picked up and flown in an approximate 12 mile round trip at a maximum speed of 40 knots. The balloon/ballast was then landed at the take-off site and moored.

This test was not only an unqualified success, but was also a record maker in that this was the largest known tethered aerostat towed by helicopter to date.

On the second day, the balloon/ballast was picked up and flown in an approximate 30 mile round trip at a maximum speed of 68 knots. With the primary mission thus achieved, the helicopter then returned the balloon/ballast to the primary Balloon Pad Facility, and landed the system just outside the designated landing zone at the facility.

Herein the secondary objective of testing aerostat mobility with a helicopter was totally achieved.

The balloon was then moved from its landing point at the facility using the truck mobility technique, and then moored for a subsequent major balloon inspection.

(4) In late 1973, the second large tethered aerostat mobility exercise was conducted when Balloon SN 204 was moved from the VAB to the flight pad. This transfer was accomplished in the same manner as was the first exercise with Balloon SN 201.

The only material change was in the tether to bulldozer assembly. It had been noted that during the bulldozer run along the beach a potential problem was occurring. Each time the bulldozer passed over tidal washouts, the blade would drop, transmitting a severe pull down jerk to the balloon aloft. To provide a degree of damping and cushioning, an old but pull tested truck tire was installed in the sling and shackle, rigging above the bulldozer blade (Figure 1-4). The insertion

of this tire successfully damped out all observable down shocks to the balloon. This method was crude, but effective.

With confidence gained through experience, this transfer was accomplished in a little over three and one-half hours.

Most significant in this mobility exercise was that the winds at 1,000 ft. altitude and below were significantly higher than desirable. During peak periods, the winds were 20 knots gusting to 30 knots, after having been a steady 30 knots earlier in the move.

(5) Not long after a series of flight tests had been flown with SN 204, at the primary Balloon site, it became evident that a helium leak had developed. The leak was determined to be in such a location that deflation and repair would be required. In addition, it was also evident from air leakage in the new tail design that intensive tail repairs were needed. Thus, the VAB-to-Pad transfer was accomplished in reverse order.

The mobility exercise was another milestone event. This was the first time a large tethered aerostat had been relocated a significant distance and moved into a large non-airship structure for maintenance and repair. A rare luxury to those who work with large tethered aerostats.

(6) After the repairs were completed to Balloon SN 204, a VAB-to-Pad transfer was again conducted as a routine operation. The same methods as used with the initial SN 204 transfer were followed; that is, movement by the winch truck to the beach, and movement along the beach to the pad by the bulldozer.

(7) In the spring of 1974, additional helicopter tow tests were conducted. The primary mission was to verify new balloon tail performance at wind speeds of 65 knots. The secondary mission was to test mobility. This time, the Cape Canaveral Air Force Station Skid Strip was selected as the test site. In addition a Sikorsky S-61A (CH-3B) Jolly Green Giant was used in lieu of the helicopter originally used (Figure 1-9).

A preliminary inspection of the route of travel revealed that a clear path

was available around the end of power lines at LightHouse Point, east of the balloon facility. This meant that the entire one and one-half mile could be traversed by using a winch truck for mobility. Because part of the route was unstabilized fire lane and open sand dune, the Army M-55 winch truck was selected to conduct the transfer (Figure 1-10).

Inasmuch as the route was unobstructed and the distance relatively short, it was decided to leave the mooring tower in place at the Balloon Facility. On each of the two flight test days, transfer operations were initiated upon confirmation that the helicopter was doing preflight checks at Patrick Air Force Station, some twenty miles South of the Skid Strip.

Each morning, the balloon was unlatched from the mooring tower, transferred to the M-55 winch truck, and driven to the Skid Strip within one hour's time. At the Skid Strip, the balloon was transferred to the Flying Ballast and made ready for helicopter arrival. At the end of each day, the balloon was driven back to the mooring site and secured for the night. Both helicopter tow tests, although with a new crew inexperienced in balloon pickup and towing, were routinely accomplished. All mission objectives were achieved.

(8) Preliminary work was accomplished in late 1972 in the Ship-to-Shore Tests conducted in Oregon (TR-024 & TR-030). Although the mission at that time was not one of mobility, the methodology learned will be directly applicable to a currently planned mobility test. In substance, the plan is to transfer an inflated, large tethered aerostat from Cape Canaveral, Florida, to the southern balloon test facility at Cudjoe Key, Florida, by sea. This will be a mobility test over a distance of about 400 miles. The ship presently identified for this mission is the U.S. Army LT/Col Paige, berthed at Norfolk, Va. All the plans and logistics have not been completed, but this mobility test is tentatively scheduled for late fall or early winter of 1974.

5. SPECIAL PROBLEMS

No unresolvable or prohibitive problems have yet surfaced in any of the TELTA large aerostat mobility tests. Only future challenges are anticipated.

Through the test missions already conducted, significant aerostat mobility was achieved. Although not used in any mobility exercise, a mobile mooring system was developed for the CEFAR YONDER Project. In that project, a mast erector truck (Figure 1.11) and a Mooring Gondola (Figure 1.12) were developed. These units are presently in the equipment inventory.

6. FUTURE CONCEPTS

TELTA demonstrated balloon mobility has clearly revealed that operations with a large tethered aerostat need not be considered as a fixed location operation. Future tethered aerostat system designs may freely incorporate any and all methods of achieving total mobility. The only true limit to tethered aerostat mobility is the designers scope of innovation and skill. The swiftness of exercising mobility for relocation will be directly proportional to the built-in mobility capability or available mobility support. Let me close on an example of one suggested means of achieving rapid mobility. It was suggested that a small, properly ballasted gondola containing small aircraft engines be developed. With such a gondola, the aerostat could become self-propelled. It could be flown via ground radio control or an on-board pilot from one location to another. An ultimate in mobility! Is this feasible for a tethered aerostat? I say most definitely, yes. It's merely a simple, but temporary metamorphosis from a tethered aerostat to a blimp to achieve the mobility mission.

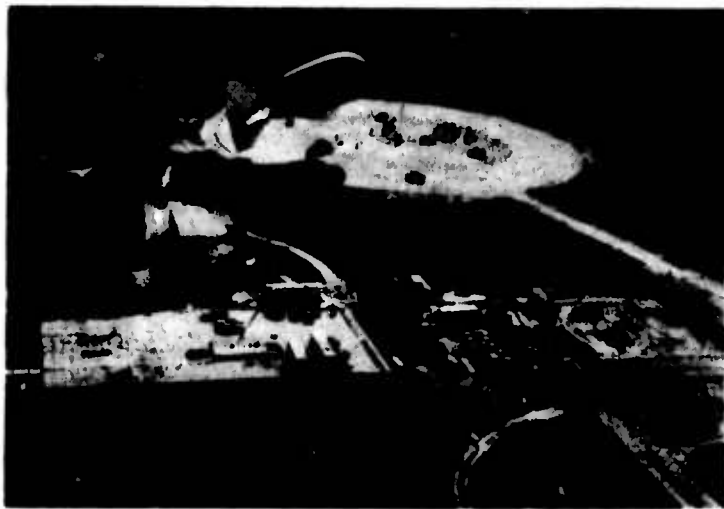


**Figure 1. Telta Balloon
Test Facility, Cape
Canaveral**

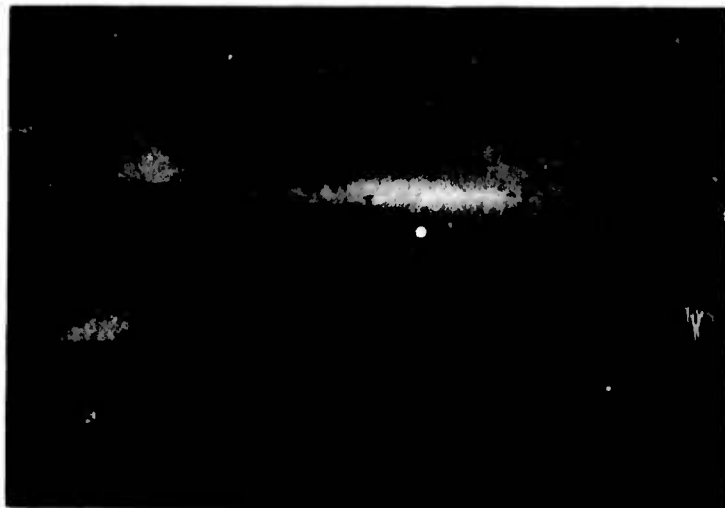


**Figure 2. Large Tethered
Aerostat, Balloon SN 201,
200,000 Cubic Feet**



Figure 3. 45K LB Winch Vehicle

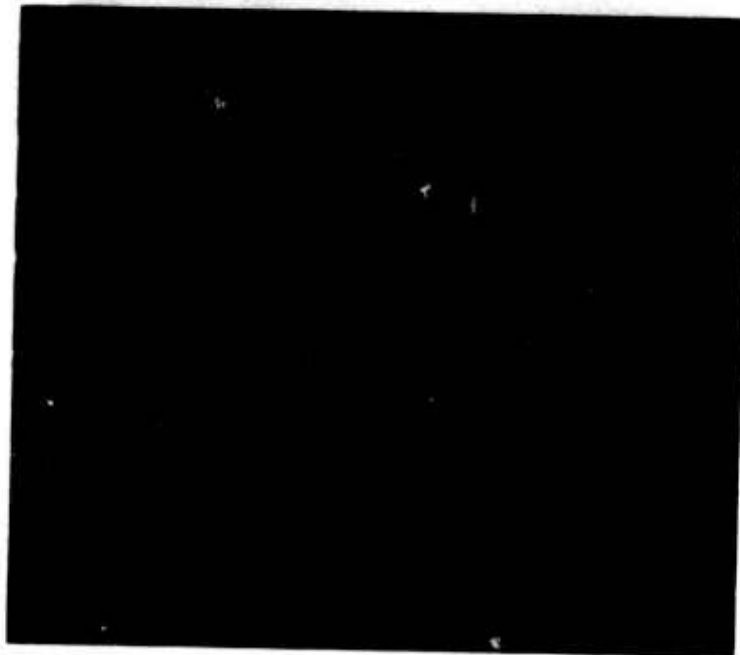


Figure 4. Bulldozer for Beach Mobility

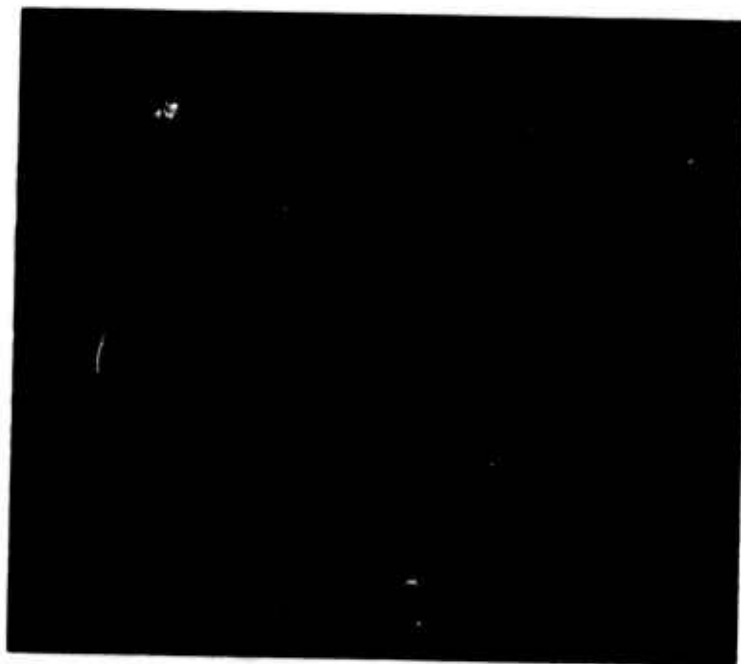


Figure 5. Flying Ballast for Helicopter Tow



Figure 6. BJ+3 Balloon



Figure 7. Baldy and LRC Balloons

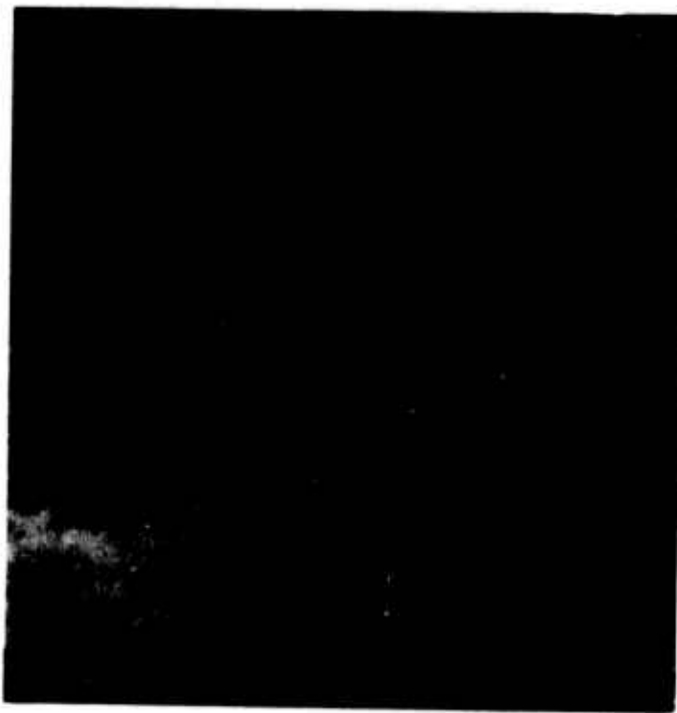


Figure 8. CH-47 Helicopter and Balloon SN 201



Figure 9. CH-3B Helicopter and Balloon SN 204



Figure 10. M55 Winch Truck



Figure 11. Mast Erector Truck



Figure 12. Mooring Gondola

Acknowledgments

This research was supported by the Defense Advance Research Projects Agency (ARPA) of the Department of Defense and was monitored by the Range Measurements Laboratory of the Air Force Eastern Test Range, W. H. Manning, Jr., Director. Program management for the various aerostat activities was provided by Lt. Col. Louis J. Del Do, USAF, Chief, RML Sensor Platforms Branch and Lt. Col. John H. Watts, RML Project Officer.

Special acknowledgment is made to the U.S. Army Aviation Detachment (HIFA), ECOM, Ft. Monmouth, N.J., for the CH-47C helicopter support with Capt. Geo. Barry, pilot, utilized in the SN-201 aerostat tow test. Also to Lt. Col. J. A. Crupper, CO, Det 15, 39th Aerospace Rescue & Recovery Wing, Patrick AFB, Fl., for the CH-3B helicopter support rendered in the SN-204 tow test. Grateful acknowledgment is also given to the Kennedy Space Center, NASA, for use of the Vertical Assembly Building concurrent with the heavy demands of their Apollo program commitments.

References

- GER-15317. (July 1971) Study of LTA Ground Handling and Operational Problems as Applicable to the TELTA Project, Goodyear Aerospace Corporation.
- Haydon, F. Stansburg. (1941) Aeronautics in the Union and Confederate Armies, Johns Hopkins Press.
- Myers, Philip F. (1968) Tethered Balloon Handbook, AFCL-69-0017, Goodyear Aerospace Corp.
- Range Measurements Laboratory, AFETR, TELTA Technical Reports:
TELTA Report #72-024, Ship to Shore Oregon Demonstration Tests, 9 Nov. 1972
TELTA Report #73-030, Ship to Shore Oregon Test Series II, Final Report, 11 June 1973.
- Redd, L. T. A Towing Technique for Determining the Aerodynamic Forces on Tethered Balloons, Proceedings, Sixth AFCL Scientific Balloon Symposium
- TELTA Project, Flight Test Reports, 201-Series and 204-Series

References

- Widmer, Emil J. (1918) Military Observation Balloons, Van Nostrand (New York).
- Young, Edward F., Captain USAF (1968) Tethered Balloons: Present and Future,
AIAA Paper No. 68-941

Contents

1. Introduction
2. Parameters of Interest
3. Accuracy Requirements
4. Types of Instruments
5. Placement of Instruments
6. Windspeed
7. Angle of Attack and Yaw Angle
8. Tether Tension
9. Tether Angle and Pitch Angle
10. Concluding Remarks

Testing The Performance Of A Large Aerostat

Terrell Higdon Yen, Jr.
RCA TELTA Project
Cape Canaveral, Florida

Abstract

This paper provides a summary of the development of some of the sensors necessary to the determination of the aerodynamic and dynamic stability performance of a large aerostat.

1. INTRODUCTION

The aerodynamic flight testing of a full size IID-7 200,000 cubic foot tethered balloon necessitated the development of instrumentation capable of measuring the pertinent forces, angles and velocities; within the scope of this paper we will cover some of the data requirements with the desired accuracies, the development of the instrumentation, the problems encountered while attempting to gather data

with this instrumentation and some of the alternate approaches substituted for the initial concepts applied in attempting to acquire the desired data to the desired accuracies.

2. PARAMETERS OF INTEREST

During the design verification test program on the IID-7 balloon there were 54 parameters of balloon performance data measured. Of these, the following are of interest within the context of this paper:

- Balloon windspeed
- Balloon pitch angle
- Balloon angle of attack
- Balloon yaw
- Tether tension
- Tether angle.

Figure 1 graphically presents the relationship of these parameters.

The tether angle is measured from local vertical and the balloon pitch is the angle between the balloon X axis and local horizontal. Throughout this program we attempted to reduce only data in which the wind velocity vector was horizontal - that is, where the pitch angle and angle of attack were coincident.

3. ACCURACY REQUIREMENTS

Early in the planning for the test program, goals were established for desired accuracies in the measurement of these parameters.

Windspeed	<u>+0.5</u> knots
Pitch Angle	<u>+0.25</u> degrees
Angle of attack	<u>+0.25</u> degrees
Yaw	<u>+0.25</u> degrees
Tether tension	<u>+0.1</u> percent
Tether Angle	<u>+0.5</u> degrees

The windspeed is the most critical in terms of accuracy because of its squared value in the dynamic pressure definition, $q = \frac{1}{2} \rho v^2$.

4. TYPES OF INSTRUMENTS

The acquisition of the foregoing six data values initially involved four types of instruments, as listed below, although test experience brought about a number of changes.

<u>Parameter</u>	<u>Instrument</u>	<u>Manufacturer</u>	<u>Model Number</u>	<u>Range</u>
Windspeed	Anemometer	Belfort	5688	0 to 60 knots
Pitch Angle	Gyro	Humphrey	VG-24-0801-1	-20 to +40 degrees
Angle of Attack	Potentiometer	TELTA		-20 to +40 degrees
Tether Angle	Gyro	Humphrey	VG24-0801-1	-10 to +50 degrees
Tether Tension	Load Cell	BLH	USG1	0 to 10,000 pounds

5. PLACEMENT OF INSTRUMENTS

Of prime importance in the placement of instruments designed to measure the speed and angle of the wind mass relative to the balloon is the elimination of the balloon hull effect on the airstream in which the instrument is operating. It is contemporary practice to assume that a distance of two body diameters between the instrument and the hull will sufficiently remove the instrument from body effects. The windspeed instrument was therefore mounted 100 feet down the tether. The windspeed instrument was also to be used as an indication of the balloon angle of attack. It was fitted with a tailplane which gave excellent alignment with the airstream. The actual instrument was thoroughly tested in the low speed wind tunnel with excellent results. Essential in the rationale supporting the use of the location 100 feet down the tether and in addition to the reasonable assurance of its removal from the balloon hull body effects, is the assumption of a homogenous air mass, at least for the vertical airspace occupied by both the balloon and the instrument.

5.1 Past Experience With Body Effects

An experimental note of interest, as regards body effect, occurred during the tow tests of the NASA Langley Research Center 25 foot balloon. This balloon was fitted with a "windbird" instrument (shown in Figure 2) which was intended to measure windspeed, balloon yaw and balloon pitch. The positioning of the instrument mount placed the "windbird" location very near the X-axis station of maximum diameter and approximately one hull radius away from the balloon hull. As can be seen in Figure 2 this location places the hull X-axis, the tangent to the hull surface at this station, and the windbird axis at zero deviation all mutually parallel.

When tow testing with the "windbird" in this location the yaw measurement obtained was quite satisfactory. The windspeed indication, although appearing to be very linear and rational in its recorded value, never quite agreed with a second anemometer which was mounted on a boom above and ahead of the tow truck. Both were soon abandoned in favor of a distance and time method of calculating velocity which was extremely accurate. The discrepancies in the balloon windspeed readings were attributed to the body effects of the balloon hull on the airstream in the area of the windbird.

Of particular relevance to this discussion is the pitch measurement. Keeping in mind that on the Langley balloon a full balloon hull radius separated the pitch instrument from the hull, one may be tempted to discount hull effects on the pitch readings; however, hull effects on the windbird were very clearly evident. The balloon was towed at a matrix of pitch angles from 0 to 20 degrees and windspeeds from 5 to 100 feet per second, but the pitch angle indication throughout remained at 0 degrees, just as if the instrument was mechanically "frozen". On more than one occasion the "bird" was physically deflected by hand, just to make sure it was still functioning. This is undoubtedly one of the more dramatic illustrations in balloon testing of body effects on the airstream and on instruments immersed in it.

6. WINDSPEED

6.1 Instrument Mounted on Tether

The initial effort to construct an instrument to measure both windspeed and the angle between the wind and the tether resulted in the instrument shown in Figure 3. As can be seen from the figure the instrument was quite ruggedly built. Figure 4 is a picture of the fourth redesign of this sensor in an attempt to make it both lighter and more resistant to vibrational loads imposed on it.

6.1.1 TETHER STRUMMING

Thru the years we have been quite aware of the effect of wind on the tether and the strumming which occurs when spontaneous oscillation results under certain combinations of tether tension, tether length and windspeed. When this instrument was clamped to the tether, the forces imposed on the instrument shook it to destruction. This instrument went thru numerous redesigns but to no avail as on the next flight the first occurrence of tether strumming would destroy it.

6.2 The "It's" Windbird on Tether

After the failure of the tether instrument we reverted to an earlier windspeed measurement instrument which had been successfully used on many "Interim Test Sequence"* flights. This windbird, shown in Figure 5, successfully withstood the ravages of tether strumming because it was loosely mounted to the tether rather than hard mounted as the first instrument; however, it measured only windspeed and was not capable of any angle measurement.

6.3 Trailing Anemometer

Because of the accuracy requirements necessary for windspeed, a second anemometer was added early in the program. This anemometer was suspended by about 100 feet of its own coax signal line, the top end of which was attached to the tip of the port horizontal fin. The Belfort anemometer on the end of the cable hung

* The "ITS" program was a brief period of aerodynamic testing performed at Cudjoe Key, Florida, prior to the design verification test, performed to gather, principally, lift and drag data with some dynamic testing in the longitudinal plane.

nearly vertical as the cable trailed aft in the windstream. Toward the end of the program the "ITS" windbird was removed from the tether and trailed off the horizontal stabilizer at the end of a hundred feet of coax signal line as shown in Figure 6.

6.3.1 COMPARISON ACCURACIES

For the short periods of time that the first tether mounted anemometer was operational, its indication compared quite consistently within one knot or less with that from the trailing anemometer. When the "ITS" anemometer was installed and its measurements were compared to the trailing anemometer, they agreed within one knot or less. The same results were obtained with both anemometers trailed from the horizontal stabilizers.

6.3.2 EXPERIMENTAL NOTES

One rather interesting observation of basic atmospheric characteristics occurred while testing with the "ITS" bird and the trailing anemometer. When a wind gust would pass the tether anemometer, as indicated by a Spike in the wind-speed recording, the velocity reading was compared with the distance between the tether anemometer and the trailing anemometer and rather accurately corresponded to the time delay before the spike appeared on the trailing anemometer wind-speed recording.

7. ANGLE OF ATTACK AND YAW ANGLE

As noted earlier, the plan was to derive the angle of attack of the airstream by measuring its angle to the tether and then adding this to the tether angle gyro indication from the confluence point.

A second and alternate method was also utilized in an attempt to measure the angle of attack, by installing a wind direction instrument on the side of the hull as shown in Figure 7. The location was chosen to reduce to a minimum the effect of the flow around the side of the balloon hull which results from the pressure gradient due to hull lift. This instrument was far too sensitive to yield useful

angle of attack data. When the airflow in the area of this windbird was either up or down the windbird would give very large angle indications. It was suspected that a minor change in the direction of the general overall airflow was amplified by the body effect on the direction of local flow, this close to the hull. This data channel was converted to a more useful assignment, and for the remainder of the program the pitch angle, as read from the pitch gyro, was used in lieu of angle of attack.

The same approach used for the angle of attack instrument on the side of the balloon hull, was applied to the design of a yaw instrument to measure the yaw angle of the balloon relative to the airflow. This instrument was mounted on a pylon on the top centerline of the hull as may be seen in Figure 7. The resultant yaw signals were acceptable during periods of steady winds but during variable light to moderate winds the indications of yaw angle generated by the instrument were amplified much as were those of angle of attack. Although testing was completed before the yaw measurement problem was completely resolved, a north reference indication would have sufficiently defined balloon yaw in all but gusty, shifting winds.

8. TETHER TENSION

The tether tension was measured by a BLH electronic load cell of 10,000 pounds capacity. As sturdy as this instrument was it was still affected by the strumming of the tether cable. It never was damaged by these vibrations however, and performed its function quite well through the test period.

9. TETHER ANGLE AND PITCH ANGLE

Humphrey gyroscopes were used to measure both the tether angle and the pitch angle. The pitch and roll gyroscope may be seen attached to the centerpost strut of the nose beam structure in Figure 7. The pitch gyro was positioned and cali-

brated to the balloon X-axis while the balloon was held in a fixed position. The pitch angle and roll angle were recorded throughout the program with good reliability.

The tether angle gyroscope was mounted on a two foot link between the confluence point fan plates and the tether tension load cell. Throughout the program there were periods when the tether angle could not be read because of the vibrations caused by the tether strumming. An earlier configuration placed the tether gyro and link below the load cell. In that position the gyro units had a very short life before they had to be rebuilt; however, when the load cell was moved below the gyro unit, the lifespan of the gyro was greatly increased and the percentage of time that useful angle data was acquired was increased manyfold. The load cell itself, which weighs about 30 pounds, obviously acted as a damper on the cable end to reduce the amplitude of the cable strumming at the gyro instrument.

10. CONCLUDING REMARKS

In measuring the relative motion of the balloon in the air mass, the initial concern was the effect of the hull on the quality of data intended to define the general airflow characteristics. This concern was well founded because the body effects caused many problems in acquiring these measurements; however, as the methods of acquiring these data were modified, the test program moved forward with excellent results. In planning a tethered balloon test program it is always an extreme temptation to use the tether cable as a mounting place for instrumentation. This is true because it is necessary to get the instruments away from the balloon and the tether "is there". The tether cable "strumming" is not an occasionally occurring phenomenon, but is nearly always present somewhere on the tether to some degree and will frequently involve the entire length of the tether. When undertaking a test program on a tethered balloon, it would be advisable to not require instrumentation to be attached to the tether cable if at all possible.

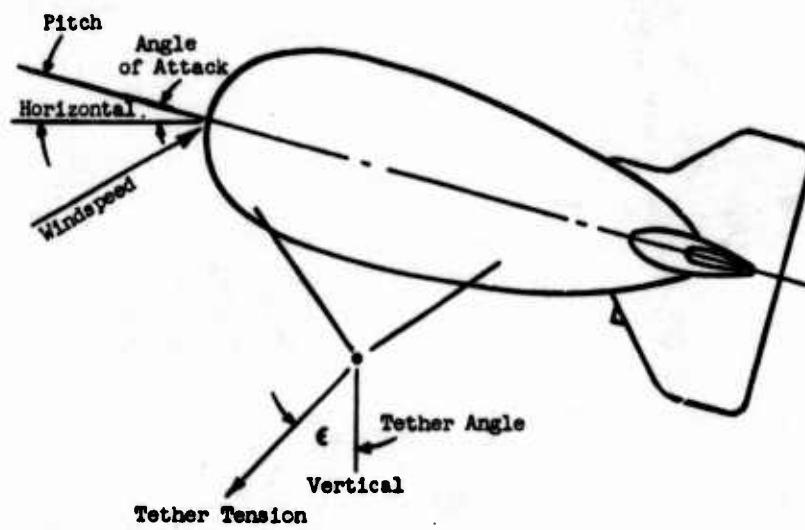


Figure 1. Measured Parameters

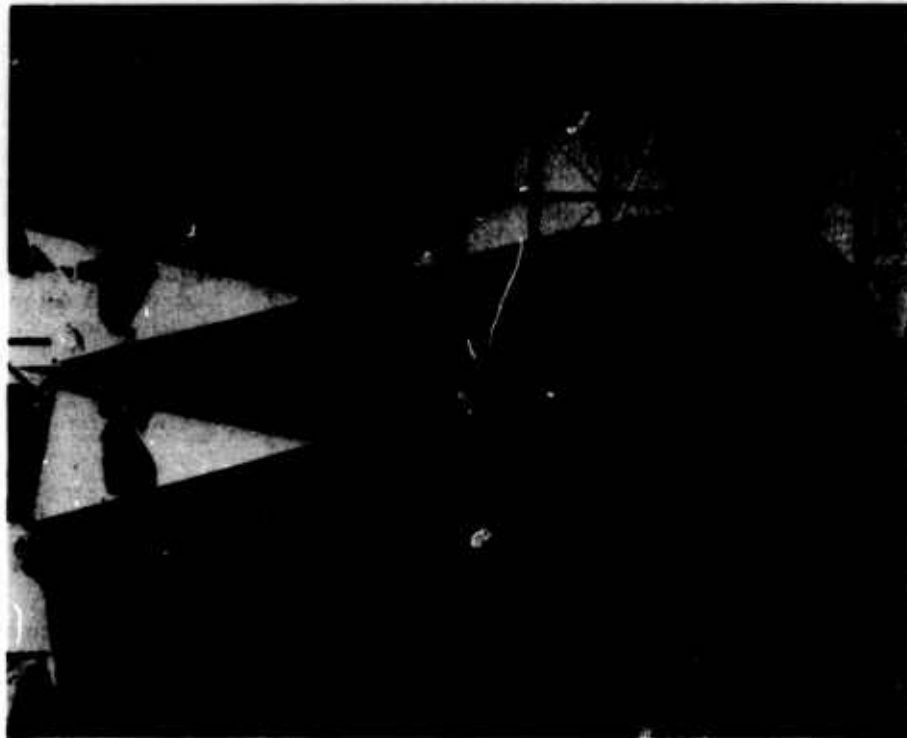
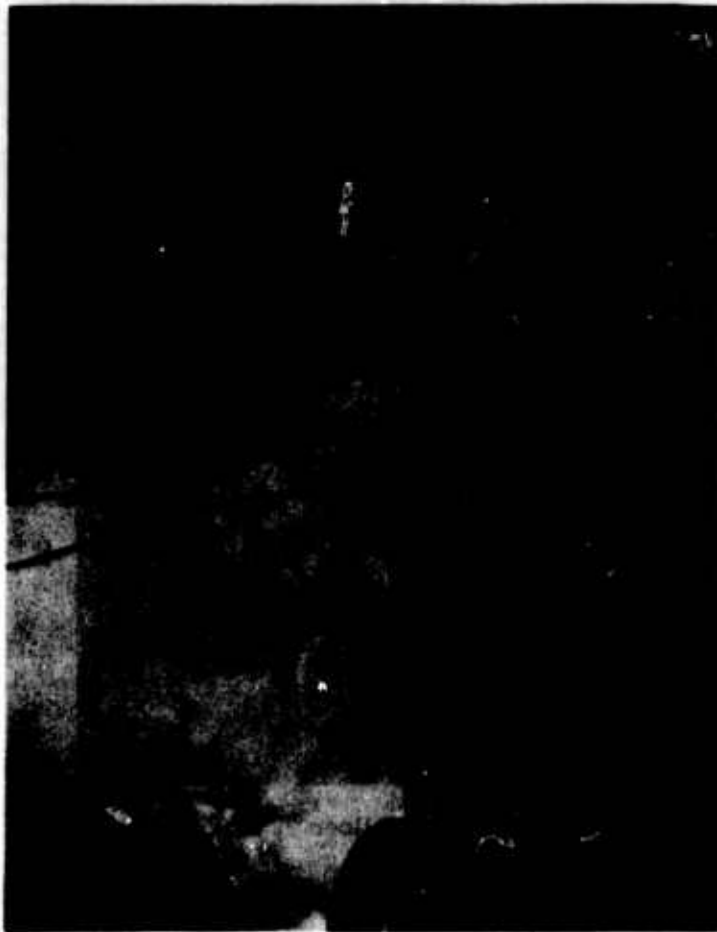


Figure 2. LRC 25 Foot Balloon



Figure 3. Tether Instrument



**Figure 4. Tether
Instrument After
Modification**



Figure 5. "Its" Windbird on Tether



Figure 6. "Its" Windbird on End of Coax Cable



**Figure 7. IID-7 Balloon Showing Angle-of-Attack,
Yaw and Pitch/Roll Sensors**

Acknowledgments

The author wishes to acknowledge the efforts of Mr. Fred Minning, Mr. Charles Duggins and Mr. James Sechrist, RCA-TELTA Engineering Staff for their contribution in the design and fabrication of the described aero instrumentation devices. Also, the Battelle Columbus Laboratories for the use of their low-speed wind tunnel and assistance in the calibration of the aero instrumentation.

Contents

1. Introduction
2. Power Sources
3. Tubular Tether
4. Flight Test of Propane Fueled Generator
5. Tests of Tubular Tether Samples
6. Conclusions

Tethered Balloon Power Plant Gaseous Fuel Supply Via Tubular Tether

C. H. Duggins
RCA TELTA Project
Cape Canaveral Air Force Station, Florida

Abstract

A study of various systems for providing electric power to a tethered balloon led to experiments with the concept of a tubular tether feeding gaseous fuel to an on-board engine-generator set. The experiments are described and their results discussed.

I. INTRODUCTION

The on station time and/or operating altitude of tethered balloons using on board gasoline fueled engine-generator sets for electrical power is severely limited by the fuel load-lifting capability tradeoff. The Power and Tether Systems (PATS) Program was initiated to study methods of providing higher power/weight ratios for balloonborne power sources and/or alternative methods of supplying power to the balloon system. The emphasis of this program was on reliability, operability, maintainability and on-station time in excess of 72 hours.

2 POWER SOURCES

The problem of power sources for tethered balloons was investigated and analyzed extensively by R. C. Hamilton, Institute for Defense Analysis, and his work is reported in "Performance, Analysis and Selection of Balloon Electrical Power Systems" dated December 1968. The systems investigated included:

- A. Windmills
- B. Nuclear Power Systems
- C. Thermoelectric and Thermionic Energy Converters
- D. Solar Cells
- E. Thermodynamic Energy Converters
- F. Fuel Cells
- G. Microwave Power Transmission
- H. Electric Power Transmission Through A conductive Tether

Another report dealing with balloon power sources is "An Evaluation of Potential Balloon Electrical Power Supply Techniques" (Report No. A-3966-B) by R. F. Badertscher et. al., Battelle Columbus Laboratories, dated May 1972. A considerable amount of this study was devoted to methods of fuel supply and resupply for on-board electric power generating system. Among the methods investigated were:

- A. Tether Crawler
- B. Direct Pumping of liquid fuel from the ground
- C. Direct Pumping of Gaseous Fuel from the Ground
- D. Refueling by Auxiliary Balloon
- E. On-board Unpressurized Gas Bag

These two reports were reviewed and the advances in the state of the art of the various suggested systems was investigated. This led to the conclusion that two systems showed promise of most nearly meeting the criteria and time schedule set forth in the PATS Program.

The systems are:

- A. Electric power transmission through a conductive tether
- B. Internal combustion engine-generator set supplied with gaseous fuel through a tubular tether

The use of a conductive, wire rope tether or even a nonconductive strength member containing conductors presents a potential lightning hazard. This potential hazard, the extent of which is unknown, precluded further investigation of a conductive tether system. The Atmospheric Sciences Program, a companion program to PATS, was currently in progress and was expected to provide the answers to the questions concerning personnel hazard and tether survivability. Thus it was decided to concentrate on development of the tubular tether concept.

3. TUBULAR TETHER

An Onan generator set modified to operate on methane gas would have a fuel consumption of 126 ft³/hr at an output of 6.5 KW or about 2 ft³/min. From "Fluid Power" by Daugherty & Ingersoll.

$$P_1^2 - P_2^2 = \frac{W^2 RT}{g A^2} \left(\frac{f L}{D} + 2 \ln \frac{P_1}{P_2} \right) \quad (1)$$

A = .0376 in² (.225 I.D. Tube)
D = .0187 ft
L = 10,000 ft
f = .02
R = 96.4
T = 528°R
W = 1.4 x 10⁻³ lb/sec (2 ft³/min)
P₂ = 65 psi

$$P_1^2 - (65)^2 = \frac{(.0014)^2 \times 96.4 \times 528}{32.2 (.0376)^2} \left(\frac{.02 \times 10^4}{.0187} + 2 \ln \frac{P_1}{65} \right) \quad (2)$$

P₁ = 159 psi

The pressure (159 psi) required to supply 2 ft³/min of methane through 10,000 feet of 0.225 I.D. tube is well within the capability of commercially available Nylon tubing which has an operating pressure rating of 625 psi and a short-time burst

rating of 2,500 psi. A safety factor of 4 to 1, applied from the short-time burst rating is considered good engineering practice for most applications.

Long-time burst strength of Nylon tubing somewhat lower than short-time values. However, if Nylon tubing is pressurized at 50% of its short-time burst strength, it should last more than 10 years. Nylon tubing has excellent resistance to flex and vibration fatigue. So long as fiber stress stresses do not exceed 4,000 psi, Nylon tubing is virtually immune to fatigue. One company reported that $\frac{1}{4}$ " and $\frac{5}{16}$ " O.D. nylon tubing, internally pressurized at between 700 and 1,000 psi flexed over $1\frac{1}{2}$ million times without failure. The tubing had a bend radius of $4\frac{3}{4}$ " and one end was reciprocated 3" at $2\frac{1}{2}$ Hertz. Useful temperature range of some types of Nylon tubing is from -65°F . to $+225^{\circ}\text{F}$. Cold brittleness tests demonstrate that the tubing will function at temperatures as low as -65°F .

A point of concern in the use of a tubular tether is the possibility that the gas flow will be shut off by flattening of the internal tube as the tether passes over the fairlead and traction sheaves or as it is compressed by the overlaying coils of the tether on the reel.

Two tests were conducted in an attempt to evaluate this problem. A short length of tubular tether was fabricated by removing some of the strands from the center of a piece of .625" diameter Molaro tether and inserting a piece of nylon tubing. The tubing was .250" O.D. x .062" wall thickness, type 6/6 Nylon. The tubular tether was passed through a pulley with a 20" diameter sheave and a 4,000 lb. load applied as in Figure 1 to produce a tether tension of 2,000 lbs. Using one standard lung power as a pressure standard the air flow rate through the tube was determined before and after the load was applied. The load was maintained for 24 hours. There was no detectable change of air flow rate which indicated that the tube was not flattened.

In this test the tube was centered within the tether and the strands ran parallel to it and therefore only the strands above the tube exerted pressure on it. A most severe case would exist if the tube was off center of the tether and the

tether was twisted. In this case all of the tether strands would cross the tube at some bias angle and exert the full tether load on the tube. This situation was simulated by helically winding a bundle of tether strands around the tube and applying a tether tension of 2,000 lbs. (See Figure 2). The air flow rate at the standard pressure was reduced by 40% within one half hour. After four hours of constant load the flow rate was down by 50% and at the 24 hour mark it was still 50%. When the load was released the springback of the tube allowed the original 100% flow rate to be regained although visual inspection showed that the tube was still slightly flattened.

A 3 KW Continental engine-generator set was converted to use either propane or methane gas. 5,000 feet of Nylon tubing (.375 O.D. x .075 wall) was procured to use with the converted generator set to determine fuel consumption, flow rate, pressure drop and other operating parameters. Several tubing and rope manufacturers were contacted about the possibility of producing long, continuous lengths of tubing and fabricating it into a tether. A manufacturer of Nylon tubing stated that fabrication of long (10,000 ft) lengths of tubing is within the state of the art. They have manufactured some 3,000 ft lengths.

A 700 ft length of experimental tubular tether was procured from the Columbian Rope Company. It was manufactured to the following specifications:

Diameter	0.625 in.
Jacket	0.055 in. thick Polyethylene
Fiber	Polyester
Fiber Lay	No lay (Parallel Strands)
Tube	3/8" O.D. x 0.075" Wall Thickness, Type 6/6 Nylon
Breaking Strength	8,000 lbs

The manufacturer was initially concerned with tube centering within the tether. With no lay construction there is no positive centering action and with an extruded jacket the rope making machine cannot be stopped in mid-run to adjust the infeed of the tube and strands. As it turned out inspection of the finished tether showed

that the centering of the tube was almost as good at the end as at the beginning and it does not appear that there would be any great difficulty in fabricating a tether 10,000 ft or 12,000 ft. long.

4. FLIGHT TEST OF PROPANE FUELED GENERATOR

A BJ+3 84,000 ft³ balloon was used to flight test the 3 KW engine-generator set which had been modified to use gaseous propane or methane fuel. Approximately 4,500 ft. of Nylon tubing (.375" O.D. x .075" Wall thickness) was wound on the drum of one of the BJ+3 tether winches. The winch drum was modified and a rotary union was installed to permit an uninterrupted flow of propane gas from the tank as the tubing was reeled out or back in. (See Figure 3). The second BJ+3 winch was used to provide the tether for the balloon. As the tubing and tether were paid out from their respective winches they were secured together with Nylon plastic Ty-wraps at intervals of approximately 50 ft. A standard confluence point swivel was modified in-house to have the added capability of a rotary union (See Figure 4). The engine-generator set was installed on the balloon at the normal location for the balloon's power source and provided all the power required for normal balloon operation. An altitude of 3,700 ft was attained and the generator and all other components of the system operated satisfactorily. Propane gas was used and the vapor pressure of the propane in the tank was 150 psi which was quite sufficient to push the gas through the 4,500 ft of tubing.

Propane was used for these tests of the tubular tether concept because of its ready availability although methane (natural gas) is the fuel intended for an operational system. Propane has a boiling point of -44° at atmospheric pressure and at +30°F the vapor pressure is only about 60 psi which would be insufficient to push the gas through a 10,000 ft tube at the required flow rate. Methane has a boiling point -259°F and the vapor pressure is over 2,000 psi at any temperature encountered in balloon operations. In order to provide methane to an operational system it was proposed that the gas be compressed and stored under pressure (2,200

psi) in the type of tank trailer used for helium. These trailers have a capacity of 40,000 ft³. At a generator consumption rate of 2 ft³/min one trailer would provide fuel for 13.8 days.

The tubular tether could also be used for helium make-up supply to the balloon. It is proposed to use three solenoid valves mounted to the power unit frame which would be actuated by ground command to provide three functions; fuel supply, purge or helium supply. The fuel valve would be normally open and the other two normally closed types. The methane gas would be fed to an airborne storage tank with a volume of 1.21 ft³, pressure rating of 400 psi and weight of approximately 20 lbs. At 350 psi this tank would hold approximately 30 ft³ of gas which would supply the generator for about 15 minutes. A tubular tether 10,000 feet long with an inside diameter of .225" would have a volume of about 2.76 ft³. A head pressure of 500 psi would produce a helium flow of about 4.4 ft³/min which would double flush the tube in 1.25 min.

Allowing two (2) minutes for each purge and a one (1) minute reserve in the fuel tank, ten (10) minutes would be available for a helium make-up of about 44 ft³ in each 15 minute cycle. The generator engine would be equipped with a ground command restart capability in case of human error in using this system.

5. TESTS OF TUBULAR TETHER SAMPLES

It was believed that the use of a nonconducting Nylon tube within a tether would not change its characteristics relative to lightning as would the inclusion of conductors in a conductive tether. There was some reservations however that if lightning struck the tether, as has occurred once during a TELTA Project flight, the tube might be punctured and release gas which would burn the tether through causing break-away of the balloon. In order to test this possibility, samples of tubular tether containing gas under pressure were subjected to simulated lightning strikes in the Lightning Transients Laboratory in Miami, Fl. Though the tether jacket and fibers were damaged there was no puncture of the tube. In order to make

the test more severe wires were inserted into the tether fibers from both ends of the sample so that the simulated lightning arc would occur inside the tether adjacent to the tube. The fibers and jacket were exploded away from the tube but the tube was not punctured.

Samples of the experimental tubular tether purchased from Columbian Rope Co. were tested on an in-house designed tension fatigue testing machine which cycles the tether over a 10 in. diameter sheave at tension values from 10% to 70% of its breaking strength. These tests showed that the tube did not cause any loss of strength or fatigue life of the tether. A flow of air at constant pressure was maintained during these tests and measured with a flow meter. No change of flow rate was observed thus indicating no appreciable flattening of the tube.

6. CONCLUSIONS

The development of the tubular tether was not pursued further due to lack of a firm requirement for long on-station operation of tethered balloons. It is believed that if such a requirement should exist, at some time in the future, the tubular tether would be a prime candidate to fulfill the need.

Acknowledgments

This research was supported by the Defense Advance Research Projects Agency (ARPA) of the Department of Defense and was monitored by the Range Measurements Laboratory of the Air Force Eastern Test Range under contract Number F08606-74-C-0025. Lt. Col. Louis J. Del Do, USAF, Chief RML Sensor Platforms Branch monitored the effort. Mr. E. E. Sheppard, the RML Project Officer, provided invaluable technical and operational support for the test program implementation.

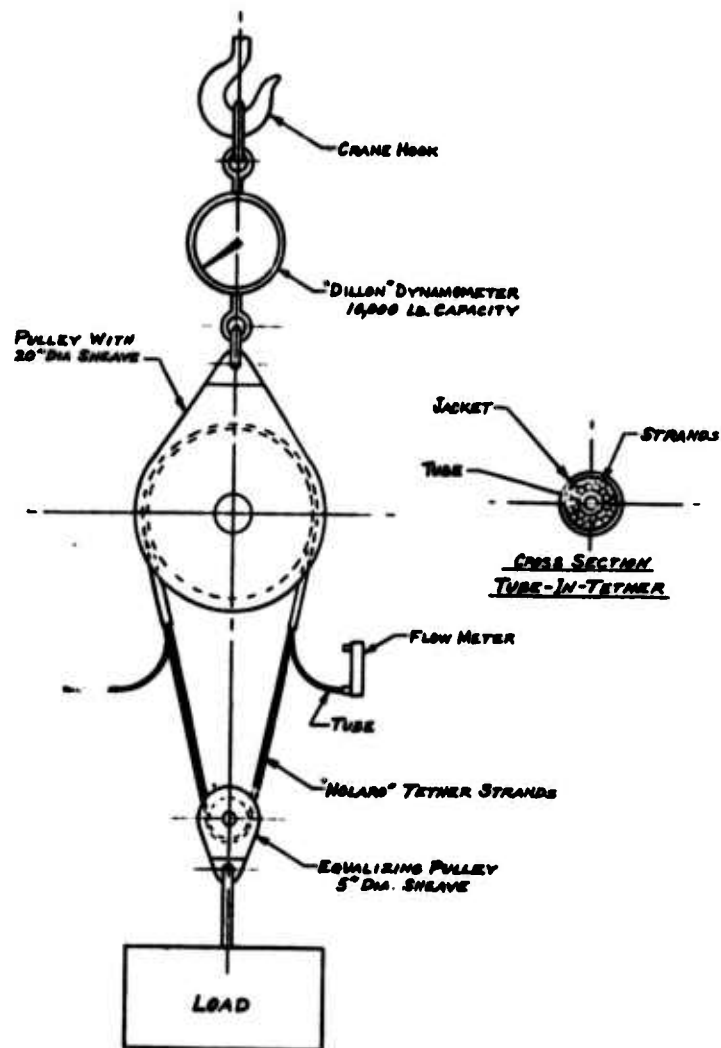


Figure 1. Tube Crush Test

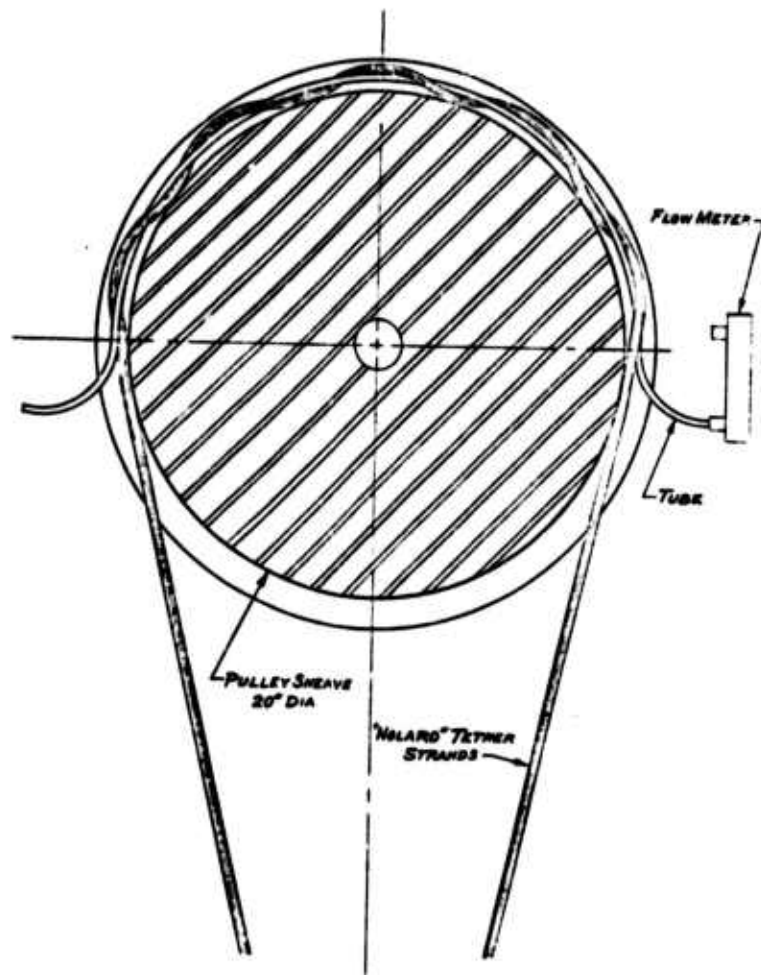


Figure 2. Crossed Strand Tube Crush Test

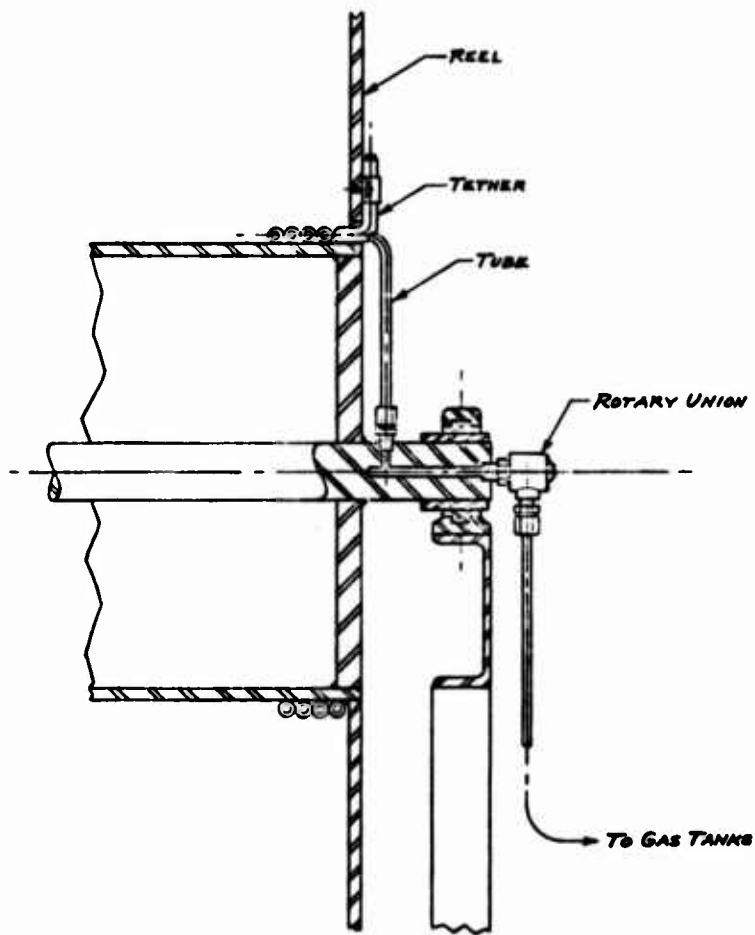


Figure 3. BJ Winch Modification

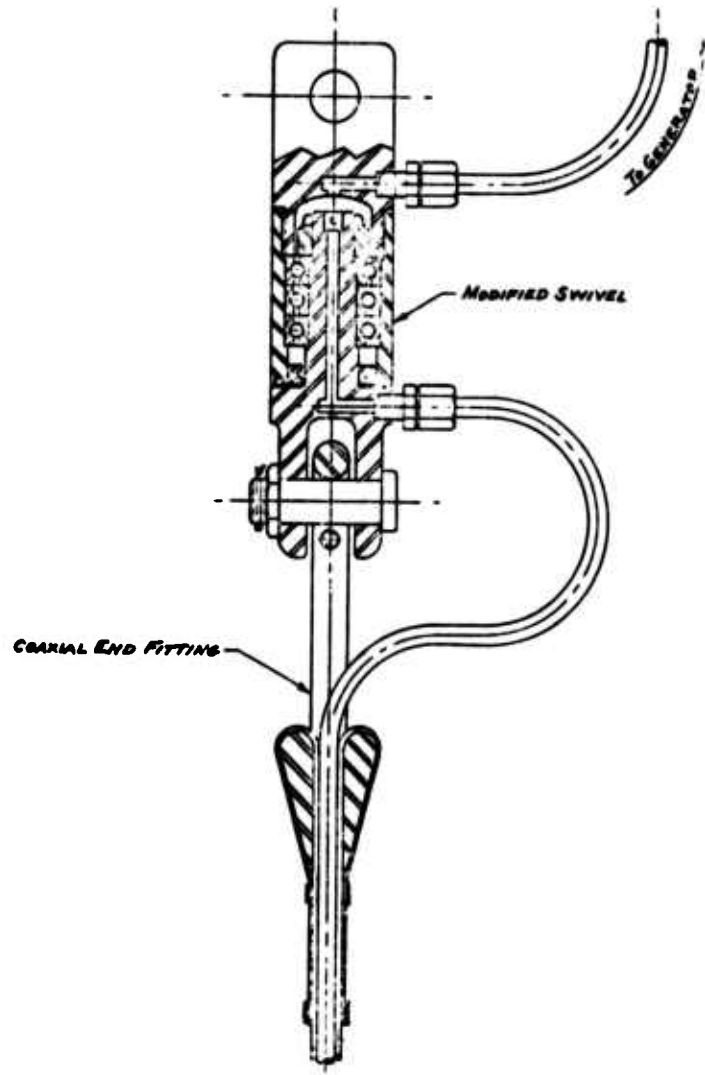


Figure 4. Swivel Rotary Union Modifications

Session 3
Free-Balloon Technology

James F. Dwyer, Chairman
Air Force Cambridge Research Laboratories

Free Balloon Capabilities: A Critical Perspective

James F. Dwyer
Air Force Cambridge Research Laboratories
Bedford, Massachusetts

Abstract

Free balloon systems, classified as zero-pressure, superpressure and air-ballast systems, are reviewed with respect to both achievable flight profiles (in terms of possible flight stages) and the payload subsystems necessitated thereby. Air-ballast systems, with noted exceptions, are treated as having merely theoretical capabilities, sufficiently documented elsewhere. The capabilities and potential of the superpressure balloon are briefly considered and recommended as warranting a thorough independent analysis (some capability trend data are appended). For zero-pressure balloons, a capability in-the-large is numerically defined and this macroparameter is proposed as suitable for assessing and planning capability growth. Implications are stated with respect to the historical trend of this parameter and, based thereon, suggestions are offered concerning future research and development of zero-pressure balloons. Historical data are appended and references are given.

Contents

1. Introduction
2. Shape Analysis
3. Gore Panel Stress Analysis
4. Application to Four Balloons
5. Conclusions

Gore Panel Stress Analysis of High Altitude Balloons

Dr. H. Alexander and P. Agrawal
Stevens Institute of Technology
Hoboken, New Jersey

Abstract

A method for determining the stress state of a balloon gore panel was presented at the 7th AFCRL Scientific Balloon Symposium. In this method it is assumed that the load tapes take the design shape and the gores bow out between the tapes. Using experimentally determined constitutive relations for the film and the load tapes both the circumferential and meridional stresses in the gore panel have been determined at all altitudes from launch to ceiling.

This analysis has been improved to include the subpressure region noted in a partially inflated balloon and the weight of the fittings and the tapes. In the partially inflated state, the uninflated material is assumed to be partially suspended from the top end fitting with the remainder added to the payload at the bottom. Gore panel stresses have been determined for a number of tailored taped balloons varying in volume from five to forty-seven million cubic feet. The effect of number and strength of load tapes and changes in payload are assessed.

1. INTRODUCTION

As a result of the requirements placed on the balloon designer by the user to carry heavier payloads to even higher altitudes, the demands placed on the balloon structure have increased to the point where the usual assumptions of zero circumferential stress and no

material deformation in the design of natural shape balloons are no longer valid approximations of the actual stress and deformation states. The need for a realistic analysis of the stresses actually developed in a balloon was recognized a number of years ago by the authors. Such an analysis must account for the effect of material deformation and should be an adjunct to any balloon design program. It could be an important aid in modifying balloon design procedures to better utilize material strength and prevent regions of high stress concentration.

A stress analysis procedure that assumes that the load tapes take the design shape and the gores bow out between the tapes was presented at the Seventh AFCRL Scientific Balloon Symposium (Alexander, Agrawal, 1972). Using experimentally determined constitutive relations for the film and the load tapes both the circumferential and meridional stresses in the gore panel were determined at all altitudes from launch to ceiling for a sample 5×10^6 cubic foot balloon. However, the shape analysis used in this work ignored the subpressure region at the base of the balloon and did not properly account for the weight of the fittings and the uninflated material. A subpressure region exists in all balloons at altitudes below the ceiling altitude. This paper deals with the necessary modifications to the shape analysis and demonstrates the combined shape-stress analysis procedure by examining the stress fields developed in three popular balloon systems in a number of different design configurations carrying various payloads.

2. SHAPE ANALYSIS

In the determination of gore panel stresses, it is assumed that the load tapes, which are fairly rigid in comparison to the film, follow the design shape at ceiling and a computed bubble shape at all other altitudes. The film is then assumed to deform into a circular cross-section shape between adjacent tapes. The computed bubble shape is determined using classical membrane theory assuming zero circumferential stress (Smalley, 1963, 1964). The procedure starts with a computer program that calculates the shape and the ratio of payload at the bottom of the balloon to the total payload at a given subpressure value. The computation is repeated until the opening angle at the base of the balloon, θ , has been found which allows the

satisfaction of the equation

$$F/P + L/P = 1 \quad (1)$$

to $\pm 0.1\%$ accuracy; where F is the payload at the top plus the excess top material, P is the payload and all excess material and L is the payload at the bottom plus the excess bottom material. It is assumed that all the excess material weight from the bottom to the maximum radius is acting as a payload from the bottom of the balloon and all of the excess material from the maximum radius to the top is acting as a payload from the top of the balloon. This procedure was repeated for a range of subpressure ratios, α , from -1 to -5, a range of L/P ratios from 1.00 to .55 and various values of the shape parameter, Σ . ($\alpha = a/\lambda$, where a is the pressure head at the bottom of the balloon and $\lambda = (P/b)^{1/3}$ with b being the difference in weight densities of air and the inflation gas. $\Sigma = (2\pi)^{1/3} (w/b\lambda)$, where w is the unit weight of balloon material.) The results of the calculations were curve fitted by functions of the form,

$$\theta = C_0 + C_1\Sigma + C_2\Sigma^2 + C_3\Sigma^3 \quad (2)$$

for all combinations of values of α and L/P.

A second program is utilized to determine the shape of the balloon at a desired altitude. First a subpressure value is chosen that is well below that expected at the computation altitude. The subpressure ratio is chosen so that in the shape computation, the gore length does not exceed the designed gore length of the balloon. If this should inadvertently occur, a higher subpressure ratio is chosen and the calculation is repeated. The computed gore length being less than the designed gore length does not cause any difficulty since the volume of gas in the lower portion of the partially inflated balloon is negligible.

The opening angle is calculated from Eq. 2 for various values of L/P. A value of total payload is then assumed. For a given value of L/P, the shape of the balloon is then computed. The computed balloon volume is then compared with the volume of the lifting gas in the design balloon at that altitude. If the volumes are not within $\pm 0.5\%$, the value of the payload is changed and the shape calculations are repeated until the volumes are matched. This procedure is repeated for a range of values of L/P.

To determine the correct value of L/P, the following procedure has been adopted. First, the balloon material acting as a payload, W_p , is computed as

$$W_p = W - (W_1 + W_2) \quad (3)$$

where W is the nominal weight of balloon material, W_1 is the weight of inflated balloon material up to the maximum radius and W_2 is the weight of inflated balloon material from the maximum radius to the top. The total payload, P , is then given by

$$P = P_h + W_p \quad (4)$$

where P_h is the actual hanging payload.

The total gore length up to the maximum radius, l_t , is determined to be

$$l_t = (l - l_0) + l_1 \quad (5)$$

where l is the fully inflated balloon gore length, l_0 is the gore length determined in the shape calculation and l_1 is the determined gore length up to the maximum radius. The weight of this lower section of the balloon is calculated from the design configuration as W_0 . Then L , the payload at the bottom plus the excess bottom material, is found to be

$$L = P_h + W_0 - W_1 \quad (6)$$

The ratio of L/P is then calculated and the shape determination at the value of L/P closest to that obtained in Eq. 6 is then stored by the computer program for use in the gore stress analysis. The determined shapes of a 5.025×10^6 cubic foot capped 1.0 mil balloon with a 488 lb. payload are shown at launch, 40,000 ft., 60,000 ft. and 90,000 ft. in Figure 1 and at ceiling (119,000 ft.) in Figure 2. A comparison with photographs taken at launch and during flight appears to indicate that the computed shapes are fairly realistic determinants of the load tape configurations.

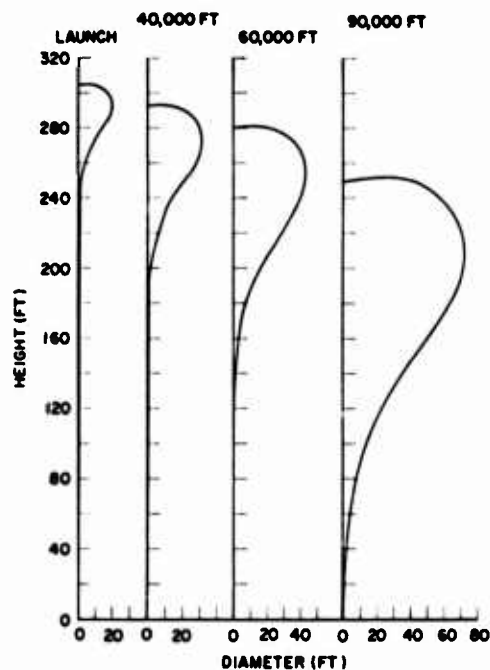


Figure 1. Shape (Load Tape Configuration) of a 5.025×10^6 cu. ft. Balloon at Launch, 40,000 ft., 60,000 ft. and 90,000 ft. Altitude

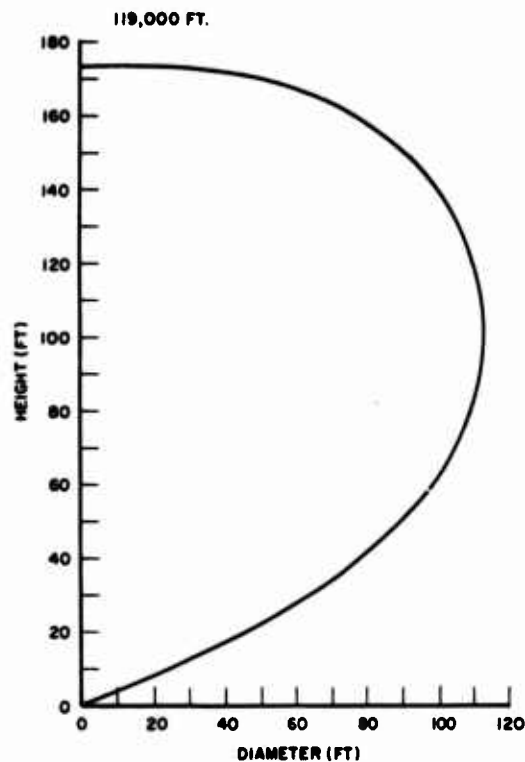


Figure 2. Shape (Load Tape Configuration) of a 5.025×10^6 cu. ft. Balloon at Ceiling (119,000 ft. Altitude)

3. CORE PANEL STRESS ANALYSIS

The stress analysis procedure was presented in detail at the Seventh AFCRL Scientific Balloon Symposium (Alexander, Agrawal, 1972). It is assumed that the film deforms into a circular cross-section perpendicular to the principal curvature of the load tape configuration determined in 2. above (see Figure 3). All excess material sustains no pressure load and all loaded gores are assumed to be similarly loaded. Using previously determined film and load tape constitutive theories the analytical procedures of the earlier paper (Alexander, Agrawal, 1972) have been utilized to obtain the circumferential and meridional stresses developed in the gores of four tailored taped balloons; a 5.025×10^6 cubic foot 1.0 mil capped balloon, a 5.025×10^6 cubic foot 1.5 mil uncapped balloon, a 20.8×10^6 cubic foot 0.8 mil capped balloon and a 47.8×10^6 cubic foot .35 mil

capped balloon. For each balloon the effect of number and strength of load tapes and changes in payload have been assessed.

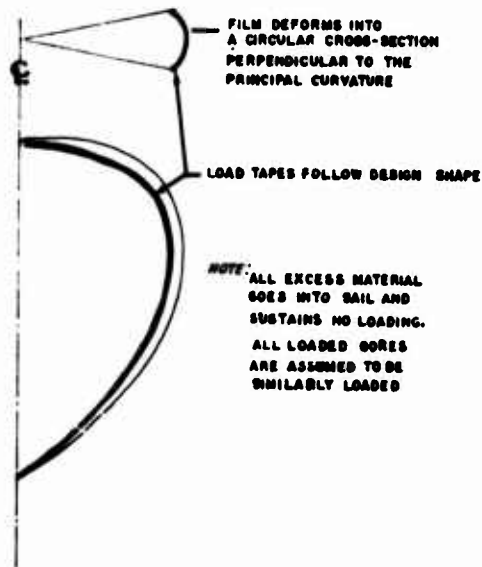


Figure 3. Scheme of Analysis for a Taped, Natural Shape Balloon

4. APPLICATION TO FOUR BALLOONS

4.1 5.025 x 10⁶ Cubic Foot Capped Balloon

This balloon, a quite successful design that was flown many times constructed of DFD-5500 film is described in the following table:

Gore Pattern: Tapered Tangent Base, Fully Tailored Apex
Maximum Volume: 5.025 x 10⁶ cu. ft.
Diameter: 238.9 ft.
Tape Type: Polyester, 500 lb.
Number of Gores: 120
Gore Material: 1.0 mil Polyethylene
Gore Length: 324 ft.
Cap Length: 110 ft.
Cap Material: 1.0 mil Polyethylene

Design Minimum Payload: 488 lbs. floats at 119,000 ft.

Maximum Payload: 4500 lbs. floats at 92,100 ft.

Gore panel stress analysis results for a 488 lb. payload at launch, 60,000 ft. and ceiling (119,000 ft.) are shown in Figures 4, 5 and 6 for the design configuration, 120 gores with 500 lb. load tapes, and a test configuration, 240 gores with 250 lb. load tapes. All results are shown for the top portion of the balloon only; from the top to the maximum radius. At launch, both the circumferential and the meridional stresses are found to be of similar magnitude in the range from 100 to 200 psi for the 120 gore balloon with the maximum stresses developing near the maximum radius. Increasing the number of gores lowers the stresses appreciably. The ratio of maximum circumferential stress with 240 gores to maximum circumferential stress with 120 gores is 0.66; approximately a 35% stress advantage by increasing the number of gores. A stress advantage continues to exist through most of the ascent. However, it diminishes with altitude, until at ceiling, increasing the number of gores causes a slight stress disadvantage near the maximum radius.

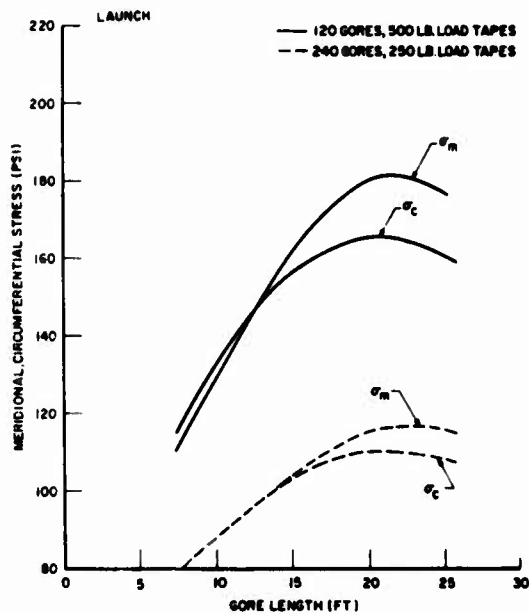


Figure 4. Gore Panel Stress Analysis of a 5.025×10^6 cu. ft. Balloon with a 488 lb. Payload at Launch

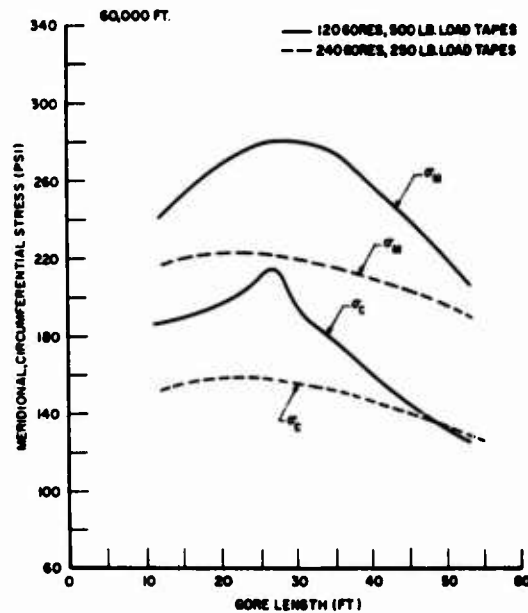


Figure 5. Gore Panel Stress Analysis of a 5.025×10^6 cu. ft. Balloon with a 488 lb. Payload at 60,000 ft. Altitude

It should also be noted that the shape of the stress curves changes with ascent from having a maximum near the maximum radius at launch to having a maximum at the apex at ceiling. This is due to the balloon's approaching the flat top design configuration as it inflates. The stresses tend to increase with increasing altitude. However, they are always far below a yield or failure value at the associated temperature of the flight. The 1.0 mil cap on this balloon has certainly been effective in keeping the film stresses quite low. This balloon design has had an excellent flight record except in situations where a high launch temperature and a cold tropopause were encountered (Dwyer, 1966). This combination has been shown to cause brittle balloon film failures (Kerr, 1968).

4.2 5.025×10^6 Cubic Foot Uncapped Balloon

This balloon is essentially the same as the balloon described in section 4.1 above except for the absence of the cap and the consequent construction with a 1.5 mil film instead of the 1.0 mil film of balloon 4.1. This balloon has successfully carried a 3000 lb. payload to 101,500 feet. The stress analysis during such a flight is shown in Figures 7, 8 and 9 for the design configuration, a balloon with 240 gores with 250 lb. load tapes and a

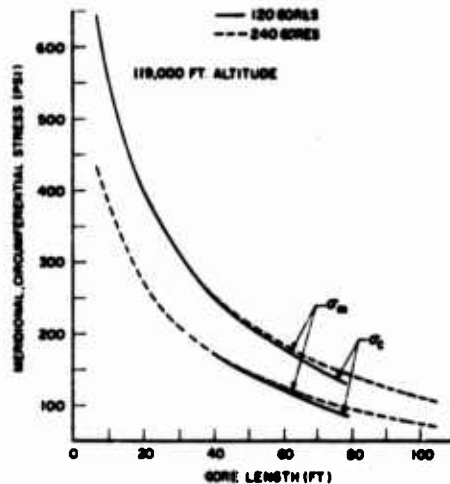


Figure 6. Gore Panel Stress Analysis of a 5.025×10^6 cu. ft. Balloon with a 488 lb. Payload at Ceiling (119,000 ft. Altitude)

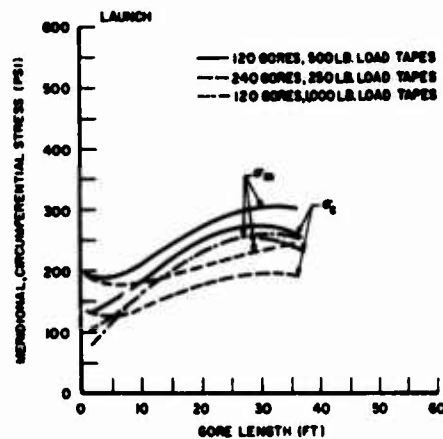


Figure 7. Gore Panel Stress Analysis of a 5.025×10^6 cu. ft. Balloon with a 3000 lb. Payload at Launch

balloon with 120 gores and 1000 lb. load tapes. The stresses are higher than those predicted for the capped balloon. However, the trends appear to all be similar to those of balloon 4.1 with a 35% stress advantage gained at launch by the doubling of the number of gores. At launch, there does not appear to be much advantage to using the 1000 lb. load tapes. However, at ceiling, the stresses near the top are appreciably lowered through the use of high strength tapes.

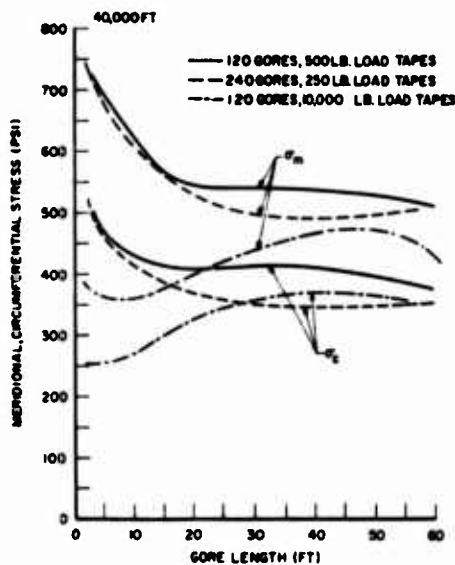


Figure 8. Gore Panel Stress Analysis of a 5.025×10^6 cu. ft. Balloon with a 3000 lb Payload at 40,000 ft. Altitude

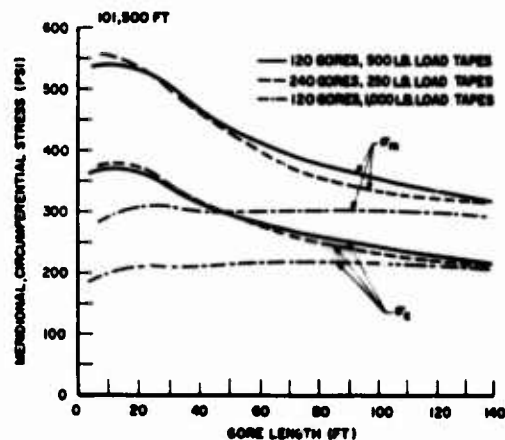


Figure 9. Gore Panel Stress Analysis of a 5.025×10^6 cu. ft. Balloon with a 3000 lb. Payload at Ceiling (101,500 ft. Altitude)

In any event, the stresses are always within allowable limits of strength accounting for the excellent success record of this configuration.

4.3 20.8 x 10⁶ Cubic Foot Capped Balloon

This is a heavy load balloon with 2 caps described in the following table:

Design: Natural Shaped, Taped
 Maximum Volume: 20.8×10^6 cu. ft.
 Diameter: 375.08 ft.

Tape Type: Polyester, 400 lb.
 Number of Gores: 140
 Gore Material: 0.8 mil Polyethylene
 Gore Length: 529.7 ft.
 Cap Lengths: 172 ft., 168 ft.
 Cap Material: 0.9 mil Polyethylene
 Design Minimum Payload: 2700 lb. Floats at 126,000 ft.
 Maximum Payload: 5250 lb. Floats at 117,000 ft.

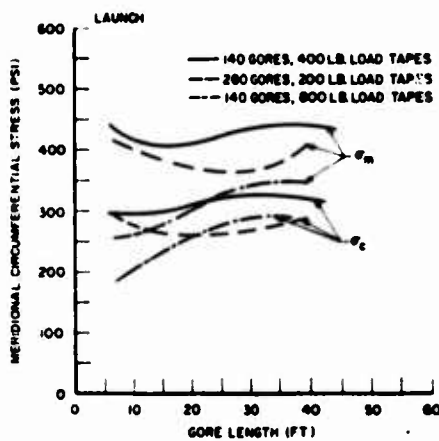


Figure 10. Gore Panel Stress Analysis of a 20.8×10^6 cu. ft. Balloon with a 2700 lb. Payload at Launch

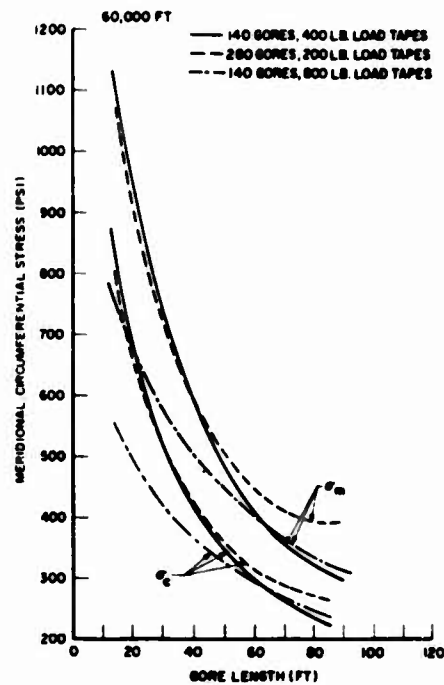


Figure 11. Gore Panel Stress Analysis of a 20.8×10^6 cu. ft. Balloon with a 2700 lb. Payload at 60,000 ft. Altitude

Gore panel stress analysis results for launch, 60,000 ft. and ceiling with both the minimum and maximum payloads are shown in Figures 10-15. At launch, with both payloads there appears to be an advantage to increasing the number of gores and an even greater advantage in doubling the load tape strength. However, with increasing altitude, the stress advantage diminishes and is eventually eliminated. The stresses in this balloon are much higher than in the 5×10^6

cu. ft. balloon. At the maximum payload, the stresses are approaching yield or failure at almost all altitudes. This design is probably only nominally safe.

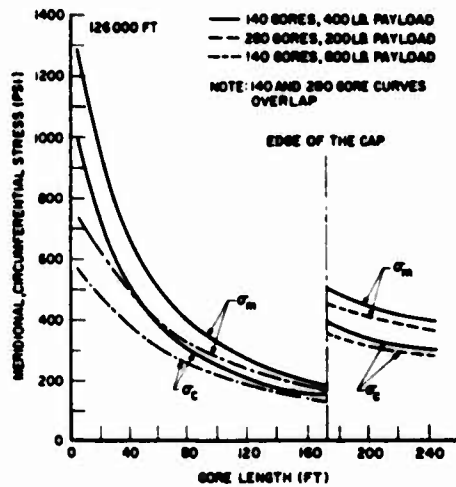


Figure 12. Gore Panel Stress Analysis of a 20.8×10^6 cu. ft. Balloon with a 2700 lb. Payload at Ceiling (126,000 ft. Altitude)

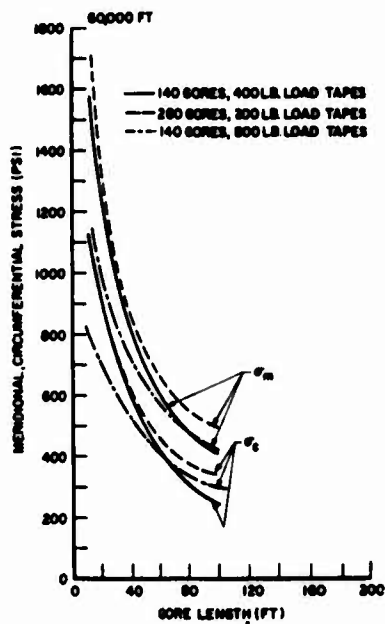


Figure 14. Gore Panel Stress Analysis of a 20.8×10^6 cu. ft. Balloon with a 5250 lb. Payload at 60,000 ft. Altitude

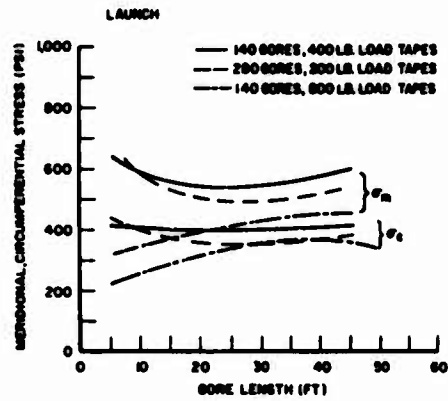


Figure 13. Gore Panel Stress Analysis of a 20.8×10^6 cu. ft. Balloon with a 5250 lb. Payload at Launch

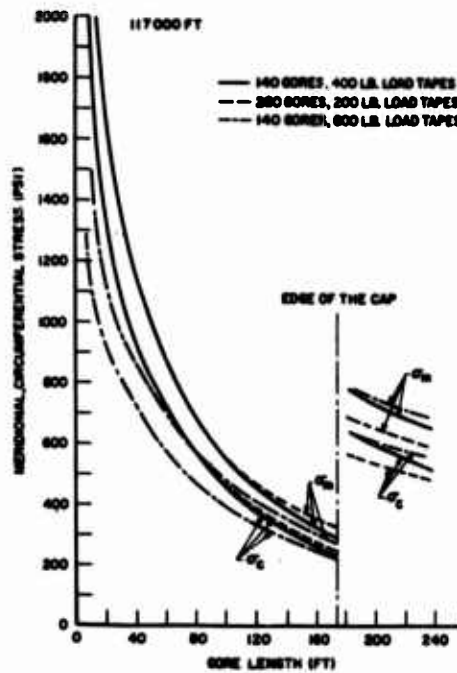


Figure 15. Gore Panel Stress Analysis of a 20.8×10^6 cu. ft. Balloon with a 5250 lb. Payload at Ceiling (117,000 ft. Altitude)

4.4 47.8 x 10⁶ Cubic Foot Capped Balloon

This is a very large, extremely high altitude balloon produced of a very thin (.35 mil) film. Its specifications are given in the table below:

Design: Natural Shaped, Taped
 Maximum Volume: 47.8 x 10⁶ cu. ft.
 Diameter: 521.43 ft.
 Tape Type: Fortisan, 60 lb.
 Number of Gores: 197
 Gore Material: 0.35 mil Polyethylene
 Gore Length: 682.71 ft.
 Cap Length: 128 ft., 121 ft.
 Cap Material: 0.35 mil Polyethylene, 0.5 mil Polyethylene
 Design Minimum Payload: 100 lb. Floats at 172,000 ft.
 Maximum Payload: 500 lb. Floats at 166,500 ft.

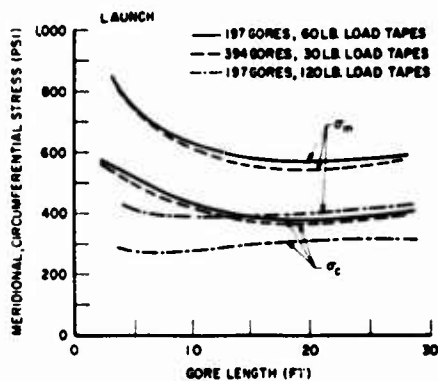


Figure 16. Gore Panel Stress Analysis of a 47.8 x 10⁶ cu. ft. Balloon with a 100 lb. Payload at Launch

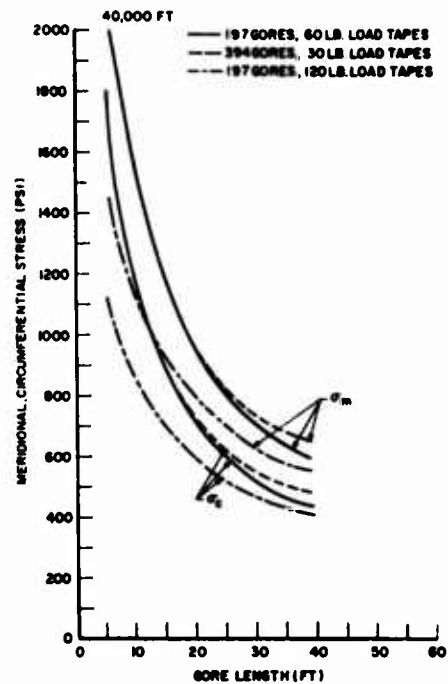


Figure 17. Gore Panel Stress Analysis of a 47.8 x 10⁶ cu. ft. Balloon with a 100 lb. Payload at 40,000 ft. Altitude

Gore panel stress analysis results for launch, 40,000 ft., 90,000 ft. and ceiling at both minimum and maximum payloads are presented in Figures 16-23. In the launch configuration, this balloon was found to have a very flat upper region yielding the stress curves shown in Figures 16 and 20. Consequently, there appeared to be little advantage to increasing the number of gores. However, approximately a 40% stress advantage was realized by doubling the load tape strength. Here is a situation where it appears that stronger load tapes should be used to secure a safe launch. With both payloads, the launch stresses are dangerously close to yield stresses. In fact, launching in high temperature conditions would probably result in a launch failure if not for the high orientation and an absence of a low yield stress in this thin polyethylene film.

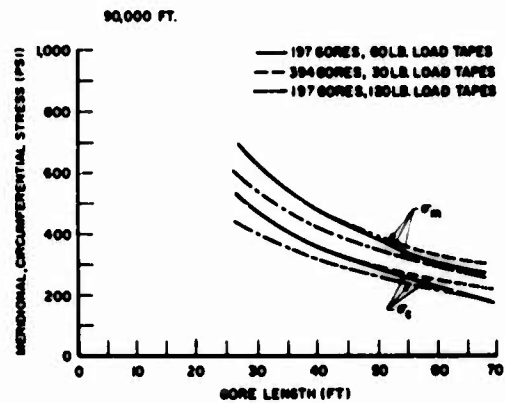


Figure 18. Gore Panel Stress Analysis of a 47.8×10^6 cu. ft. Balloon with a 100 lb. Payload at 90,000 ft. Altitude

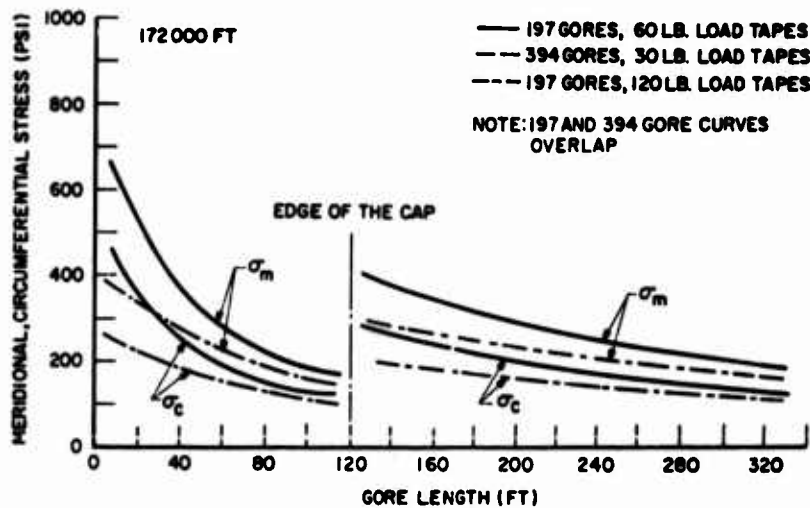


Figure 19. Gore Panel Stress Analysis of a 47.8×10^6 cu. ft. Balloon with a 100 lb. Payload at Ceiling (172,000 ft. Altitude)

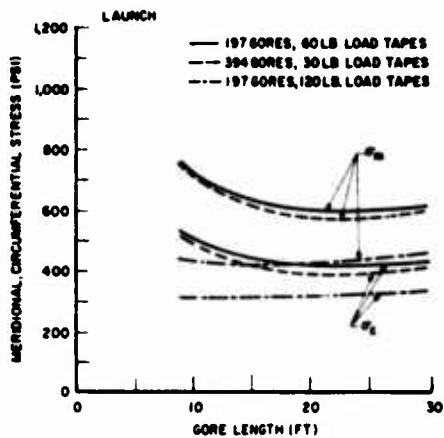


Figure 20. Gore Panel Stress Analysis of a 47.8×10^6 cu. ft. Balloon with a 500 lb. Payload at Launch

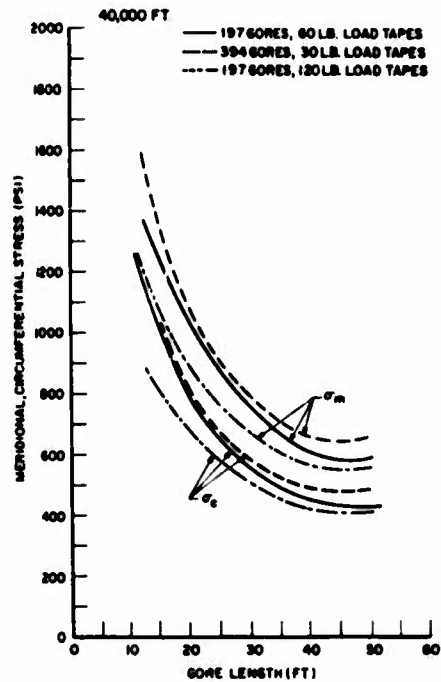


Figure 21. Gore Panel Stress Analysis of a 47.8×10^6 cu. ft. Balloon with a 500 lb. Payload at 40,000 ft. Altitude

The advantage in increasing load tape strength continues with ascent for both payloads. However, the advantage is diminished as ceiling is approached. This balloon has probably been successful to date only because of the use of a highly equibiaxially oriented film that has better ultimate strength behavior than heavier gauge films. The balloon should probably be produced with stronger load tapes than the designed 60 lb. tapes.

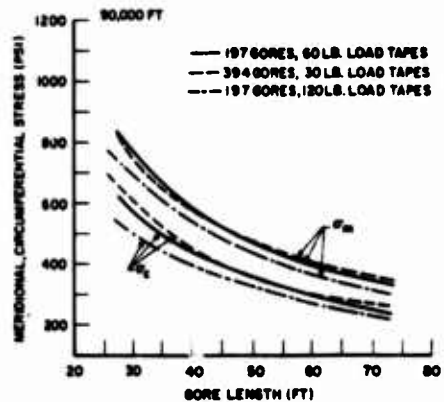


Figure 22. Gore Panel Stress Analysis of a 47.8×10^6 cu. ft. Balloon with a 500 lb. Payload at Ceiling (166,500 ft. Altitude)

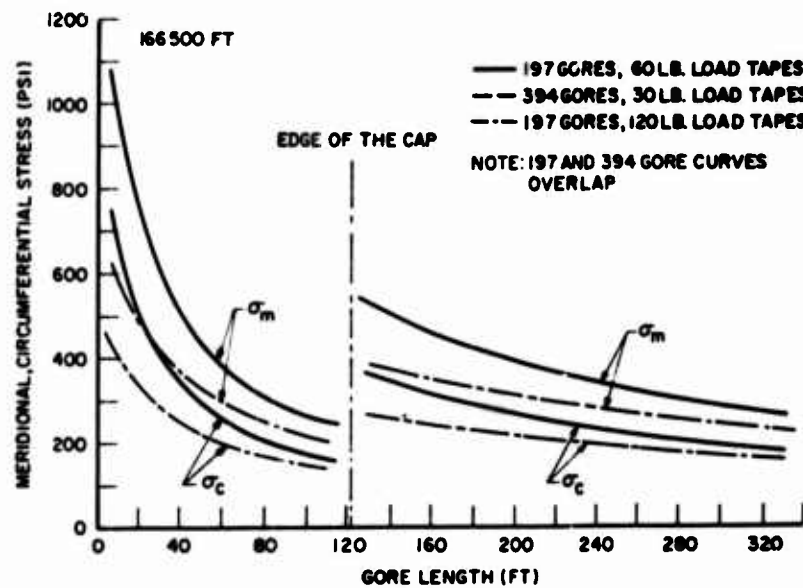


Figure 23. Gore Panel Stress Analysis of a 47.8×10^6 cu. ft. Balloon with a 500 lb. Payload at Ceiling (166,500 ft. Altitude)

5. CONCLUSIONS

The procedure presented in this paper and the earlier work of two years ago (Alexander, Agrawal, 1972) provides a simple calculation of the stress field in a high altitude balloon throughout its entire flight history. Using four popular balloon designs the effect of payload and number and strength of load tapes has been demonstrated. With the availability of the proper material properties data, the procedure can be incorporated into the balloon design procedure. The designer will then have a rational basis on which to decide such design parameters as number of gores, film thickness, cap size and thickness, and load tape strength.

Acknowledgments

The authors acknowledge the enthusiastic support of Mr. J.F. Dwyer of the Air Force Cambridge Research Laboratories throughout the performance of this research. This project was supported by the Air Force Cambridge Research Laboratories through Contract No. F19628-72-0100.

References

- Alexander, H. and Agrawal, P. (1972) The Effect of Material Deformation on the Shape and Stress State of a High Altitude Balloon, Proc., Seventh AFCRL Scientific Balloon Symposium, pp. 397-414.
- Dwyer, J.F. (1966) Some Polyethylene Balloon Statistics, Proc., AFCRL Scientific Balloon Workshop, 1965, pp. 49-58.
- Kerr, A.D. (1968) Balloon Strength in the Troposphere as Affected by Creep at Launch, Proc., Fifth AFCRL Scientific Balloon Symposium, pp. 7-17.
- Smalley, J. (1963) Determination of the Shape of a Free Balloon. Theoretical Development, General Mills Report No. 2421 (AFCRL-63-951).
- Smalley, J. (1963) Determination of the Shape of a Free Balloon. Balloons with Zero Super Pressure and Zero Circumferential Stress, General Mills Report No. 2500.

References

Smalley, J. (1964) Determination of the Shape of a Free Balloon. Balloons with Super Pressure, Sub Pressure and Circumferential Stress; and Capped Balloons, General Mills Report No. 2560 (AFCRL-65-72).

Thermal Analysis of Long Duration Flight Packages

Leland A. Carlson* and Penny M. Brandeberry**
Texas A&M University, College Station, Texas

Abstract

With the development of super pressure balloon technology long duration balloon flights, measured in days and weeks, will become common. Because of restrictions on package size, weight, and internal power dissipation, the package thermal protection system will have to be passive. This paper presents a model suitable for predicting the transient thermal behavior of such packages. To verify the model, comparisons with actual flight measurements are presented for several twelve and twenty-four hour flights. In addition, the configuration and environmental factors that affect the package thermal behavior are discussed. Emphasis is placed upon those factors that are particularly important in long duration flights. Finally, predictions for a typical around the world package are presented. It is shown that several days are required before a steady state thermal behavior is established and that wide temperature variations are encountered.

* Assistant Professor, Aerospace Engineering Department

** Graduate Research Assistant, Aerospace Engineering Department

Manuscript will be available from author at Symposium.

Balloon Design

James L. Rand*
Texas A&M University
College Station, Texas

Abstract

The design of high altitude scientific balloons has evolved over the years strongly influenced by material quality and manufacturing techniques. However, demands by scientists for heavier payloads and higher altitudes have resulted in dramatic failures since the design of these balloons must be without the advantage of prior experience. Therefore, a need exists to review existing design procedures as well as the history of balloon failures in order to determine if and how these designs might be improved.

All design procedures require some knowledge of the balloon shape at float. Therefore, the classic works of Upson and the detailed description of the "natural" shape by Smalley are reviewed. Designers then incorporate the effects of material strength, flight temperature, and experience to iteratively obtain the necessary envelope and cap thicknesses. These designs are reviewed along with the success and failure histories of these designs. Both experimental and theoretical stress analyses are reviewed and graphically demonstrate the existence of circumferential stresses in "natural" shape designs. The role of material characterization is described as well as the state of stress in the critical cap portion of the envelope.

* Associate Professor, Aerospace Engineering Department

It is hoped that a detailed stress analysis coupled with adequate material characterization will permit the reliable design of balloons in environments not yet attained.

Manuscript will be available from author at Symposium.

Balloon Systems Strength and Failure Analysis

L. Dale Webb
Texas A&M University
College Station, Texas

Abstract

A 'race track' biaxial testing system developed in our Extreme Environment Laboratory is capable of subjecting balloon components to flight environments while measuring their mechanical response. The sample used in the TAMU system requires no special trimming or preparation, thus alleviating the major problem of edge effects in uniaxial testing. It is capable of measuring the following quantities over a wide range of strain rate and temperature: (1) multiaxial mechanical properties for films; (2) heat seal strengths, including mode of failure; (3) creep behavior of films, adhesive tapes, and heat seals; (4) cold brittle behavior, including the influence of prestressing and creep enhancement of the cold brittle points.

Application of fracture mechanics to the failure behavior of balloon systems shows that a measure of the energy required to cause system failure provides a useful tool in establishing the influence of temperature, strain rate, and previous stress history on the tendency of a system to fracture in a cold brittle fashion.

Development of Dacron-Reinforced Polyethylene Film; Heavy-Load Free-Flight Balloon Applications

James B. Munson
Sheldahl Company
Northfield, Minnesota

Abstract

A composite, sheet material, consisting of multi-axial arrays of parallel Dacron yarns, bonded with adhesive to one side of polyethylene film is shown by test to equal or exceed the biaxial tensile and shear strength of similar Mylar film-Dacron yarn composites previously used in free-flight balloons. Theory shows a potential gain of one-third in structural efficiency from the change from Mylar to polyethylene. A new thermal seaming method yields joint efficiencies of 80 percent between panels of the polyethylene composite. A taped, butt-type joint is produced by passing the area through a pair of rollers in which an axial temperature gradient is maintained from a maximum at the tape center to a minimum at the edge of the lap. This graduates the bond level across the seam and minimizes the usual stress discontinuity present at edges of bonded lap joints. Since the seaming process rate is more than twice the rate for Mylar film composites, and polyethylene film costs are less than half that of Mylar, significant balloon cost savings are projected.

Twelve Years after the First Launch: CNES Operational Activity with Stratospheric Balloons

M. Rougeron
CNES
Toulouse, France

Abstract

Besides spectacular developments such as in stratospheric tethered balloons, CNES maintains its effort in the well-known stratospheric free balloons activity.

At the Seventh AFCRL Symposium, CNES announced initiation of a natural-shape balloon production unit. This unit, located in Zodiac-Espace Cy., is now in operation; it allows launching by CNES of about 50 balloons ($350,000$ to $100,000\text{ m}^3$), in addition to the same number of tetraon balloons ($85,000\text{ m}^3$), restricted to payloads of less than 150 kg.

CNES is also improving such airborne equipments as telemetry transmitters, telecommand receivers, decoders, and various other mechanical devices; and such ground equipments as telemetry stations, real-time data processors; and launching devices.

The original launching techniques with auxiliary balloons have for many years allowed successful launchings from any point on the earth and from small and unprepared areas.

Contents

1. VHF Omnirange
2. Balloon-borne VOR instrument
3. Balloon position plotting
4. An advanced balloon locating instrument
5. Flight test results
6. World-wide tracking capability

An Advanced Balloon Locating System

H. Laping and A. R. Griffin
Air Force Cambridge Research Laboratories
Bedford, Massachusetts

Abstract

A third generation balloon locating instrument using VHF Omnidirectional Range (VOR) navigation has been designed, developed and flight tested by AFCL's Aerospace Instrumentation Laboratory. The report that follows will lead into a discussion of this new instrument after first presenting VOR theory and its use in locating a balloon position.

1. VHF OMNIRANGE

The VHF Omnidirectional Range system is a network of ground transmitters operated by the FAA for aircraft navigation across the United States. It is widely used by all types of commercial and military aircraft.

At present there are approximately 1200 VOR stations across the United States operating on 100 channels in the 108-118 MHz frequency band. Each station is assigned a carrier frequency within this range. Stations that transmit on the same frequency are separated by a sufficient distance and radiation controlled to minimize interference with one another. The radiation pattern from the station's transmitter is an omnidirectional, horizontally-polarized, vertical cone which can be received within line-of-sight.

The omnirange transmission principle is based on the creation of a phase

difference between two 30 Hz modulating signals on a VHF carrier. One of these signals is called the 30 Hz reference signal. Its phase remains constant around the ground station. The other signal is called the 30 Hz variable signal. Its phase varies with azimuth around the ground station. In order that these two signals are distinguishable from each other when looking at the transmission of the station, the 30 Hz reference signal frequency modulates a 9960 Hz subcarrier which, in turn, amplitude modulates the RF carrier of the station. The 30 Hz reference and variable signals are aligned at the station so that at magnetic north they are exactly in phase and then each electrical degree of phase shift between them corresponds to a degree of azimuth around the station with respect to magnetic north.

In addition to these signals, a VOR station also broadcasts voice and Morse Code transmissions on its RF carrier. These transmissions are used for identifying the particular station, for weather broadcasts and for communication with enroute aircraft.

2. BALLOON-BORNE VOR INSTRUMENT

AFCLR's balloon locating system utilizes these signals from VOR stations to establish the geographic position of its free-floating balloons.

A simplified block diagram of a balloon-borne VOR instrument is shown in Figure 1. Before a balloon flight the instrument is pre-programmed for several VOR stations. The selection of these stations depends upon the forecast trajectory of the balloon. Upon command from the ground control station or a start signal from its own timer, the balloon-borne instrument receives the complex radiated signal from the first programmed station. A signal processor then resolves this signal into a bearing that represents the angle between magnetic north and the line-of-position of the balloon with respect to the station. An encoder then converts this information into Morse Code which is transmitted to the ground tracking station. This operation is repeated for all of the programmed stations before the unit stops and awaits the next start signal.

3. BALLOON POSITIONING PLOTTING

3.1 Present Method

At the tracking station the Morse Code is received and recorded in a bearing log. A code dictionary is then used to convert the Morse Code into bearing angles

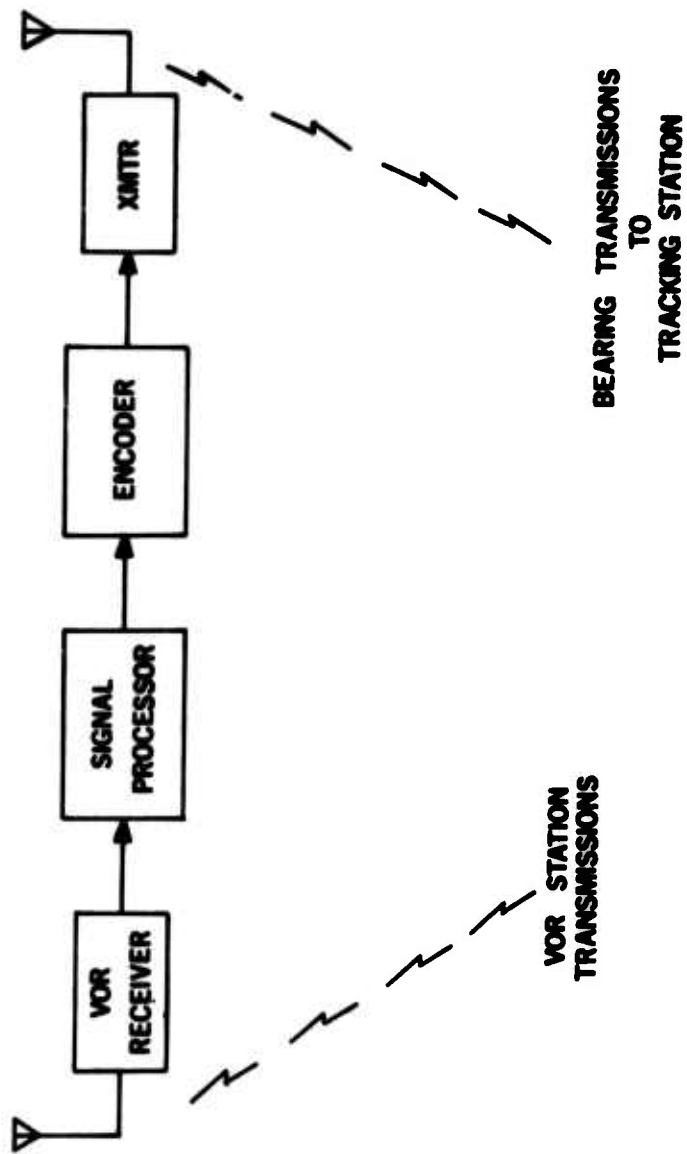


Figure 1. Simplified block diagram of a balloon-borne VOR instrument

and this is entered into the log. A typical bearing log section is shown in Figure 2. The code dictionary is shown in Figure 3.

VOR BEARING LOG				
Date <u>18 Mar 74</u> Flight No. <u>C74-05</u>				
LOCAL TIME	CH	READOUT		STATION
		CODE	BEARING	
0938	1	UDWD	099.5	Chico
	2	SDWS	035.0	Williams
	3	SUKS	013.0	Marysville
	4	KDSD	352.5	Sacramento
	5	SGWD	052.5	Ukiah
	6	DRFD	274.5	Lake Tahoe
	7	UWGD	094.5	Fortuna
	8	WOWD	251.5	Reno
0945	1	UDGD	102.5	Chico
	2	SDDD	036.5	Williams
	3	SUWD	011.5	Marysville
	4	KDSS	352.0	Sacramento
	5	SGWD	051.5	Ukiah
	6	DRUS	273.0	Lake Tahoe
	7	UDSD	096.5	Fortuna
	8	WOUS	249.0	Reno

Figure 2. A section of a typical bearing log

Personnel at the ground station take the bearings and plot them on standard aeronautical charts. Then, by means of triangulation, the balloon position is fixed. An example of a plot is shown in Figure 4.

3.2 Automated Method of Plotting

The process of plotting fixes on aeronautical charts and triangulating a position is a slow and tedious one. It requires one person for the entire duration of a balloon flight. In its operational form, the new system will utilize an automatic plotter operating in conjunction with a minicomputer to automatically

	S	U	R	W	D	K	G	O
SS	0	1	2	3	4	5	6	7
SU	8	9	10	11	12	13	14	15
SR	16	17	18	19	20	21	22	23
SW	24	25	26	27	28	29	30	31
SD	32	33	34	35	36	37	38	39
SK	40	41	42	43	44	45	46	47
SG	48	49	50	51	52	53	54	55
SO	56	57	58	59	60	61	62	63
US	64	65	66	67	68	69	70	71
UU	72	73	74	75	76	77	78	79
UR	80	81	82	83	84	85	86	87
UW	88	89	90	91	92	93	94	95
UD	96	97	98	99	100	101	102	103
UK	104	105	106	107	108	109	110	111
UG	112	113	114	115	116	117	118	119
UO	120	121	122	123	124	125	126	127
RS	128	129	130	131	132	133	134	135
RU	136	137	138	139	140	141	142	143
RR	144	145	146	147	148	149	150	151
RW	152	153	154	155	156	157	158	159
RD	160	161	162	163	164	165	166	167
RK	168	169	170	171	172	173	174	175
RG	176	177	178	179	180	181	182	183
RO	184	185	186	187	188	189	190	191
WS	192	193	194	195	196	197	198	199
WU	200	201	202	203	204	205	206	207
WR	208	209	210	211	212	213	214	215
WW	216	217	218	219	220	221	222	223
WD	224	225	226	227	228	229	230	231
WK	232	233	234	235	236	237	238	239
WG	240	241	242	243	244	245	246	247
WO	248	249	250	251	252	253	254	255
DS	256	257	258	259	260	261	262	263
DU	264	265	266	267	268	269	270	271
DR	272	273	274	275	276	277	278	279
DW	280	281	282	283	284	285	286	287
DD	288	289	290	291	292	293	294	295
DK	296	297	298	299	300	301	302	303
DG	304	305	306	307	308	309	310	311
DO	312	313	314	315	316	317	318	319
KS	320	321	322	323	324	325	326	327
KU	328	329	330	331	332	333	334	335
KR	336	337	338	339	340	341	342	343
KW	344	345	346	347	348	349	350	351
KD	352	353	354	355	356	357	358	359
KK	360							

Figure 3. Code Dictionary

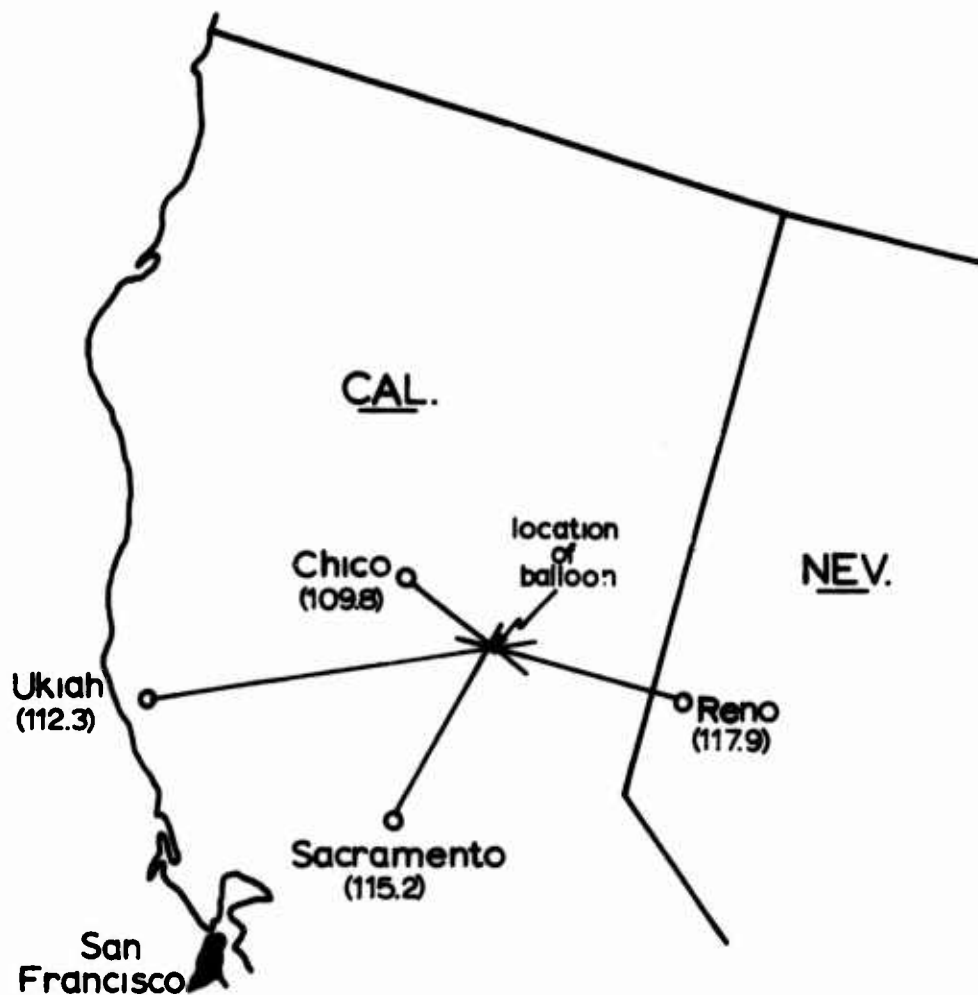


Figure 4. A sample balloon position plot

fix the position of the balloon. This capability is currently being developed. When put into operation, it will allow the code copier to feed the Morse Code bearing information directly into the computer. The computer will convert the Morse Code into bearing angles and compute the corresponding latitude-longitude position of the balloon. This position will be fed directly to the plotter and automatically marked on a map. Any type of map will be usable with this plotter as long as the scale is accounted for in the computer program.

4 AN ADVANCED BALLOON LOCATING INSTRUMENT

4.1 History of Development

AFCRL started to experiment with a balloon tracking system in the mid-sixties. This locating system used mostly analog circuitry to derive a bearing angle from the VOR station to a free-floating balloon. The phase difference between the two 30 Hz signals was measured with a servomotor and resolver, and digitized with a 9-bit Gray Code shaft encoder. The 9 bits of information were transformed into Morse Code and transmitted to the ground tracking station. Large size, weight and power consumption made this instrument impractical for a standard VOR navigational flight package.

The second generation model is an all digital processor except for an electromechanical channel selector. This unit is still in our inventory, but it is slowly being phased out as the third generation system becomes available. The power consumption of this unit is still fairly high, since all digital logic circuits are of the DTL (Diode Transistor Logic) family. The instrument has a limited operating temperature range which makes it impractical for long duration flights unless a power consuming electrical heater is installed. This instrument has a bearing resolution of 0.7 degrees and an accuracy of ± 2.5 degrees. Since the FAA VOR ground stations maintain a tolerance of ± 1.0 degrees, the overall system accuracy becomes ± 3.5 degrees. This means a possible error of about ± 6 miles at a distance of 100 miles from a VOR station.

A third generation system has been designed and fabricated by AFCRL. This instrument (BLS-3) takes advantage of the latest technological advances, especially in the integrated circuits field. COS/MOS circuits are used wherever possible. This technology provides high noise immunity, micropower dissipation and MSI (Medium Scale Integration) in a single package. As a result this instrument has a low power drain. The accuracy of this unit is ± 0.5 degrees over a temperature range of -40°C to $+55^{\circ}\text{C}$. Figure 5 shows the BLS-3 instrument next to the models from the two previous generations. The BLS-3 instrument itself is shown in Figure 6.

4.2 The BLS-3 Instrument

A block diagram of the BLS-3 instrument is shown in Figure 7. The VOR navigation receiver is Model RNA-26C manufactured by Bendix Corporation. It was slightly modified for our specific needs. Only the RF and IF sections are used.



Figure 5. Three generations of VOR locating instruments

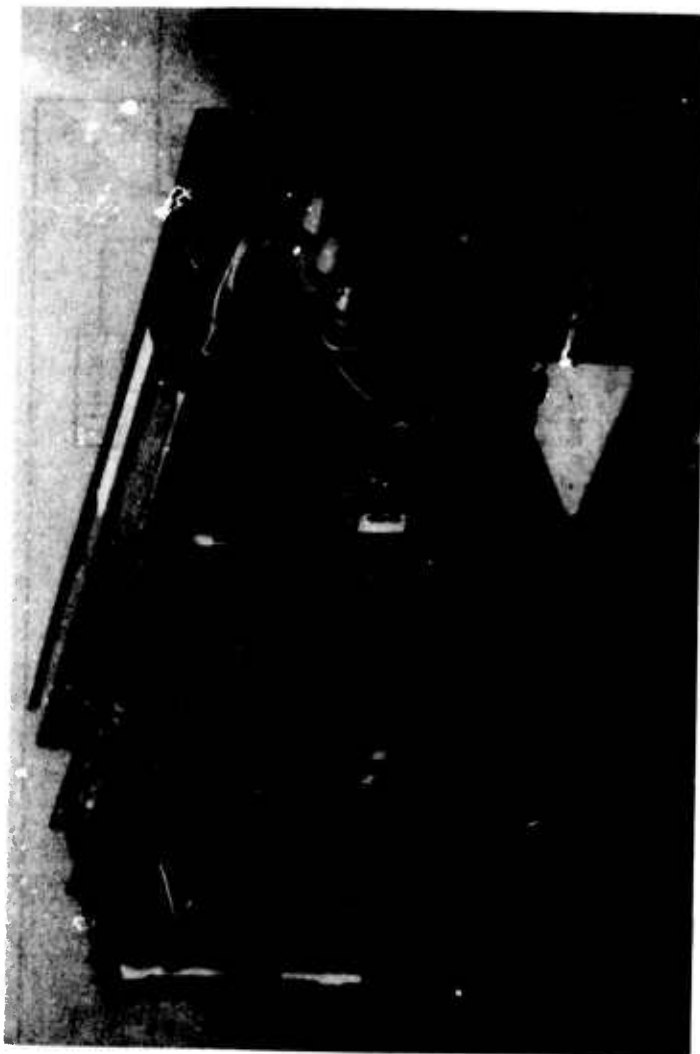


Figure 6. The BLS-3 prototype model

BLS-3 INSTRUMENT

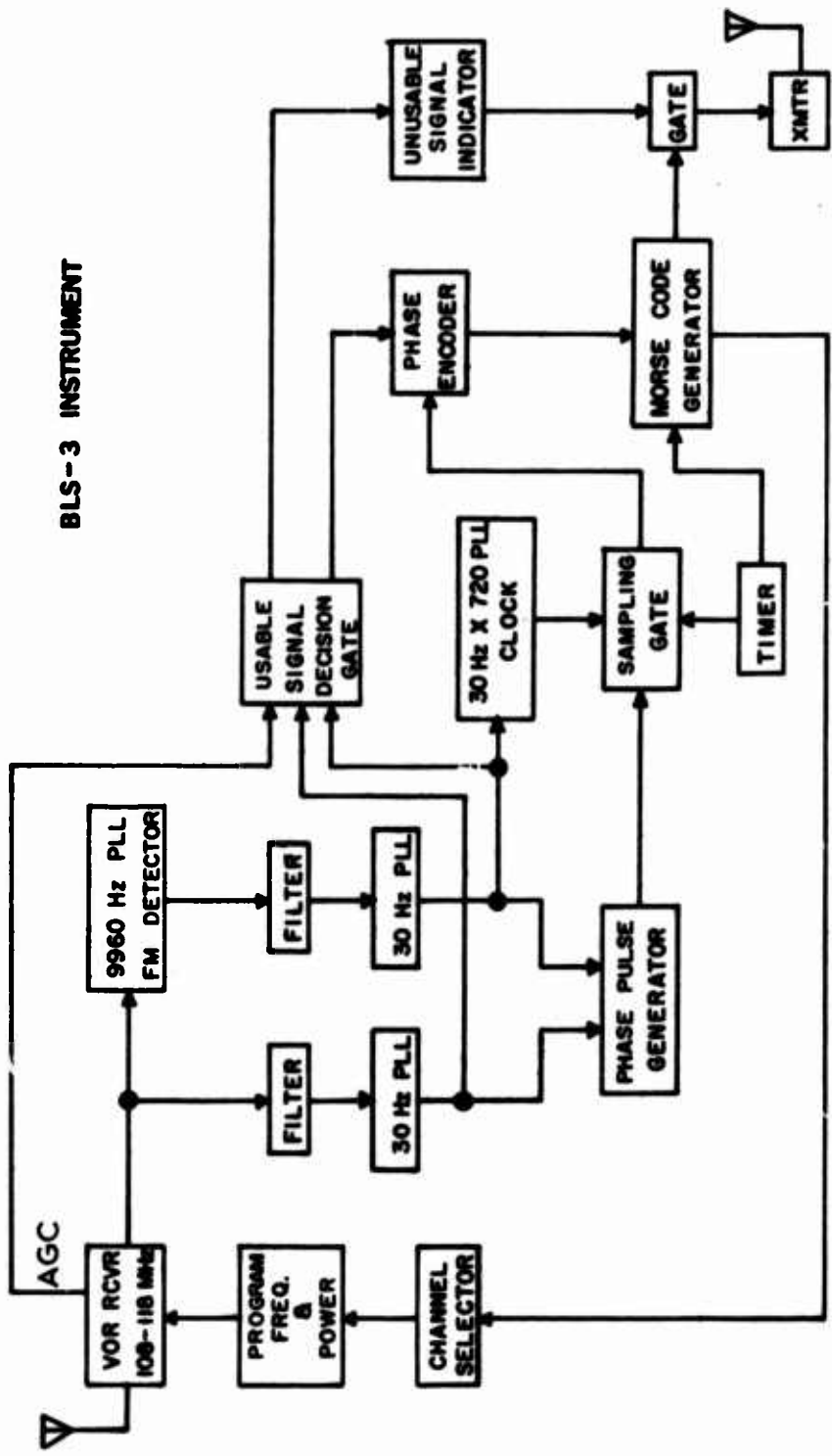


Figure 7. Block diagram of the BLS-3 instrument

The system is activated by command or by its own internal timer. This timer is programmed before every balloon flight to establish the desired frequency of readout cycles. Eight VOR frequencies are digitally selected before flight by a PROM (Programmable Read Only Memory). Upon system activation the complex bearing signal from the receiver is fed into a PLL (Phase-Locked Loop) FM detector which extracts the 30 Hz reference signal. This signal is filtered and phase-locked to a 30 Hz PLL. The 30 Hz variable signal, which amplitude modulates the RF carrier, is also filtered and phase-locked to another 30 Hz PLL.

It should be noted that both 30 Hz signals are derived from the 60 Hz power line frequency at the ground station, therefore, phase jitter and small variations of frequency can exist. The problem of phase jitter on the 30 Hz variable signal is even more pronounced because a station's identifier and voice modulation creates a number of intermodulation products and distortion of the signal. By using phase-locked loops as signal conditioners, in the BLS-3, these problems are nearly eliminated. In fact, laboratory bench tests comparing the BLS-3 with the second generation instrument showed an accuracy improvement of 5 to 1. Both units were operated from the same test generator with an identical signal. The BLS-3 varied only $\pm 0.5^\circ$ while the second generation unit varied $\pm 2.5^\circ$. These figures are based on 300 continuous measurement and readout cycles for each unit.

The output of each 30 Hz PLL is gated into a flip-flop circuit which generates pulses that represent the phase difference between the two 30 Hz signals. The output of the 30 Hz reference PLL is multiplied by 720 to generate the clock frequency for the phase encoder, therefore, this clock frequency is also phase-locked to the local power line frequency. Any variation of the power line frequency between 55 and 65 Hz does not introduce any error in the phase measurement. Since the clock frequency is derived from the 30 Hz reference signal, synchronized gating is established and thus eliminates the ± 1 bit ambiguity of the usual digital system. The width of one phase pulse determines how many clock pulses the phase encoder counts. Because the clock frequency is 30×720 Hz, we get a bearing resolution of 0.5 degrees.

The Morse Code generator transforms the number of counts stored in the phase encoder into dots and dashes. The dots correspond to binary zeroes and the dashes to binary ones. The Morse Code is grouped into 3 bits per letter and 4 letters per word. One word represents the bearing angle from one station. The decimal equivalent of the first three letters of each word represents whole degrees, while the last letter indicates the addition of either 0 degrees or 0.5 degrees to the reading.

After the first channel readout, the instrument automatically sequences through the remaining channels, measuring and reading out each one until it has

gone through all eight channels.

Up to now it has been assumed that a Morse Code bearing was generated for every channel, however, this condition will only exist if the instrument receives a usable signal from every station. A signal is usable if the magnitude of the RF carrier is above a preset level and both 30 Hz modulating signals are present. The RF level of the receiver is usually set to 10 microvolts to give a good signal to noise ratio. If one of these conditions is not met, a decision gate overrides the Morse Code and a two-second steady keydown is transmitted to the ground station indicating that a non-usable signal exists.

In order to compute or plot a balloon position, at least two of the eight channels must have a usable signal. With eight VOR frequencies, provided they are carefully chosen, it is possible to locate a balloon anywhere in the continental United States.

5. FLIGHT TEST RESULTS

To date the BLS-3 instrument has been flight tested on two occasions. The first flight was launched from Chico, California and flown for a duration of six hours. During the flight, radial bearings from the programmed VOR stations were plotted on an aeronautical chart. The crossings from these radials were observed to generate either a point, or small triangles no greater than 0.5 miles on a side. The final fix from the BLS-3, just before impact, placed the payload in the actual area where it was found by the recovery crew.

The second test flight was launched from Holloman AFB, N.M. and flown for a duration of twenty-three hours. White Sands Missile Range provided a radar track on this flight which gave an excellent source of comparison for the BLS-3 instrument. At random intervals a fix was taken from both radar and the BLS-3. Table 1 lists a group of fixes that are representative of all the comparisons taken during the flight. As can be seen, the results are very good. Before termination, the radar lost its track on the balloon. The BLS-3 kept tracking until just after termination when the payload was descending on its parachute. Even though it lost track at that time, the impact area was predicted through the use of parachute drift data.

6. WORLD-WIDE TRACKING CAPABILITY

The VOR balloon locating system will be complemented by an Omega tracking system in areas where no VOR coverage exists. This will result in a world-wide

balloon tracking capability. An Omega balloon tracking system has been developed for AFCRL by Beukers Laboratories, Inc. and is ready for flight test as soon as the Omega network becomes fully operational.

Table 1. Comparison of radar and BLS-3 fixes

Radar fixes		BLS-3 fixes	
Distance (mi)	Angle ^o	Distance (mi)	Angle ^o
9	143	9.5	144.5
33.5	93	34	92.5
85	85.5	84	84
63	84	63	83
53	93	52	94.5
41	97	40.5	97
28.5	120	28	120.5
19	173	18.5	173
41	277	40	277
49.5	289	49.5	288
66	281	66.5	279.5
97	282	98	281.5

Note: All distances and angles measured from Holloman VOR station

Updating Free Balloon Technology

Jean R. Nelson
Winzen Research Inc.
So. St. Paul, Minnesota

Abstract

Balloon sizes continue to increase with fabrication of two balloons in excess of 50 million cubic feet. Dynamic launch of heavier payloads in the range of 5000 to over 6000 pounds has progressed in the operations field. A review of size and performance data since the last AFCRL symposium is presented. While the size of balloons and payloads have increased, a new method of launching for heavier payloads and larger balloons has proceeded further toward successful development. This reefing sleeve vertical inflation procedure was reported in the earlier phases of development at the Seventh AFCRL Symposium and has now been used at NCAR and AFCRL. Updated results will be reported. Some computer studies have been directed toward learning more about vertical ascent control. The above development work and studies have been conducted under sponsorship of ONR.

Contents

1. Introduction
2. Choise of assembly type
3. Joining requirements
4. Technological devices developped
5. Example of application
5. Range of products developped
7. Conclusion

Composite Materials Concept And Balloons Application

**M. Ferronniers
Zodiac-Espace
61, Quai Carnot
Saint-Cloud (F)**

Abstract

This paper will endeavour to analyse the different possibilities for joining composite materials. It will describe the technology contrived and show an application in ballon construction.

1. INTRODUCTION

Users of either free or captive stratospheric balloons require balloons capable of carrying increasingly heavier loads and of increasingly longer flight duration. The requirements impose changes in construction of materials and techniques for the balloons. The critical function in balloon construction is that of joining of two materials of the same composition or of differing composition. The study in hand will endeavour to analyse the possible types of sealing, to justify the type favoured and to describe the range of its possibilities.

The account will be illustrated with a description of the technology contrived and perfected to meet required specifications and with a concise description of production line for the balloons.

Finally, instances will be given of the type of assembly produced and the range of products issuing from these methods.

2 CHOICE OF ASSEMBLY TYPE

2.1 Types of Sealing

2.1.1. THE THREE TYPES

Three types of assembly can be used to join two films or flexible materials :

- the "peeling" assembly
- assembly by "overlapping"
- "butt seam" assembly

2.1.2. THE "PEELING" TYPE

The "peeling" assembly is subject to delamination and can only be used for joining thin homogenous films. It cannot be used at all for any composite materials, notably those with a textile reinforcement layer which is then subject to delaminating stress giving a much lesser strength equivalent to the join than that of the material itself.

2.1.3. "OVERLAPPING" AND "BUTT SEAM" ASSEMBLIES

"Overlapping" and "butt seam" assemblies are both subject to shear along the join in the direction of the material. The strength of the assembly itself is determined by the adhering capacity of the adhesive itself or that between the different layers of the material. It can be increased in absolute terms by enlarging the surface of the assembly. These methods of assembly make it possible to obtain a joint-strength which is always superior to that of the actual material, within the limits of its field of use. These methods are indispensable in assembling coated materials or complexes (laminates).

2.2 Type Chosen for Balloon Application

2.2.1. DEFINITION

The type of assembly favoured for every balloon application is the "butt seam" assembly, characterised by the putting together of the edges of the pieces to be assembled. The assembly in fact consists of two lap tapes placed above and below the pieces to be joined. These tapes can be made of the same material as the pieces to be assembled or from different, but compatible materials.

2.2.2. SPECIFIC ADVANTAGES OF "BUT SEAM"

The specific advantages of "butt seam" as opposed to "overlapping" are as follows :

- very good impermeability and complete elimination of leakage from joins.
- very good geometrical definition of the assembly, in respecting both the geometry of the objects to be manufactured and the length of the joins.
- Lessening the width of the joins by half-as compared with a similar join by "overlapping" - due to the use of the two tapes multiplying the contact surface by two.
- Possible specification of assembly tape to be used, in instances of dissymmetrical complexes. On one side the assembly can provide mechanical functions and on the other ensure impermeability.
- Finally, easy mechanisation of lead in and positioning devices for assembling pieces.

2.3 Gluing or Welding

2.3.1. THE ALTERNATION

From the same geometrical outline, assemblies can be made either by gluing or welding. The choice depends on the constituents to be assembled.

2.3.2. GLUING

2.3.2.1. The proceed

In the case of gluing (as with polyester films) the adhesives used are of a resinous thermosetting type. The assembly bands are precoated with adhesive material with or without interlinings and the tape is heat pressed at the moment of assembly. This heating initiates a setting of the resin; a setting which stops at room temperature.

2.3.2.2. Advantages and disadvantages of gluing

Gluing makes excellent quality assemblies possible, but at a high cost, due to the following :

- quite slow working speed, in the region of one to two yards per minute, because of the resin setting time,
- high cost of assembly adhesives and preparation of tapes

2.3.2 THE WELDING AND THE THE MANUFACTURE OF BALLOONS

For these reasons we have chosen to concentrate mainly on assembly by thermofusion of a coating, without introducing an extraneous substance. In the case of balloons, this coating is a polyethylene film whose properties have long been used in the field of stratospheric balloons. The assembly tape has a substrate whose melting point is higher than that of the polyethylene. The coating is brought into fusion by passing the tape over a heated roller; in this way the assembly tape conveys its coating in a state of fusion to be applied to the materials to be assembled and provides the heat necessary for the welding.

The application is made by pressure and, at the same time, cooling allows regulation of the extent of weld penetration across the width of the tape, thus avoiding any cutting in at the edge of the join. This effect is obtained by selective heat absorption along the length of the assembly.

In applying this technique, it is easy to obtain the kind of weldings which are independent of tape heating time once the thermal equilibrium is reached, and which stay independent of the running speed of the assembly tape and any intermittency in the running of the machine.

The high production speed (in the region of 20 yds per minute) and the low cost of assembly material make it possible to execute joins of excellent quality at a much lower cost than that for gluing. Furthermore, the reliability of the joins depends only on the thermal parameters of the operation. It can be guaranteed by correct setting up and control of the technologies used.

3. JOINING REQUIREMENTS IN THE DEVELOPMENT OF LAMINATES

3.1 Laminated Materials

3.1.1. REQUIRED SPECIFICATIONS

The principal features required for a laminated material are the following :

- mechanical strength and tear resistance
- qualities of impermeability
- resistance to ultra-violet effects, to abrasion and effects of environment
- ease of joining

3.1.2. COMPOSITION OF LAMINATES

Laminates are composed of several layers of material with specific characteristics to meet best either one or more of the requirements established by the specifications. For instance, the "mechanical strength" requirement can be met either by a textile fabric, a scrim, or a film. The textile fabric can use one or more different types of fibre of varying moduli. The weaving technique also can have an effect : on mechanical strength and tear spreading resistance.

3.2 Joining

3.2.1. REQUIRED SPECIFICATIONS

The joining requirements must be considered in the same light as the other requirements for the laminate. There is in fact a regrouping of the same requirements as for the complex, and as with the latter, these can be put into three categories:

- mechanical joining requirements
- joining impermeability film requirements
- protective film requirements.

3.2.2. CHOICE OF THE METHOD

The exact method of joining must be based on the make-up of the individual laminate and be in complete harmony with the evaluations laid down for the laminate. Where there is a very high performance laminate, the assembly, like the laminate, will have to break down the three above groupings, and the requirements can then read:

- mechanical assembly by stitching fabrics of laminates to be assembled
- a thermo-sealing impermeable tape which is continuous with the barrier film of the laminate
- a protective tape of the same kind as the protective layer on the laminate, to cover and protect the joint.

For lighter complexes, several or all of these requirements are combined so as to simplify the assembly.

4 TECHNOLOGICAL DEVICES DEVELOPED FOR JOINING PURPOSES

4.1 Purposes

These devices have been developed to meet the following needs :

- symmetrical " but seam " assembling with two covering tapes
- assembly by thermofusion or thermoadhesion
- range of assembly temperatures from 50 to 350°C

These devices make possible, among others, the following assemblies :

- welding of triplex (polyethylene, polyester, polyethylene) reinforcing tapes on polythene film
- joining of scrim reinforced polyethylene films - (poly-plus type)
- joining of reinforced triplexes (polyethelene, polyester, Dacron scrim, polyethylene)
- joining of triplex type polyurethane, Dacron scrim, polyurethane - or-Teldar, Dacron scrim, Teldar.

4.2 The Machines are as Follows:

4.2.1. "POSITIONER" OR GUIDING DEVICE :

The positioners guide and bring into contact two films or laminates whose thickness varies from some hundred microns to 10 microns, without creasing or crumpling and without causing longitudinal strain in the film. What is most difficult, here, is the bringing and keeping in position of polyethylene films - which are extremely ductile at these very slight thicknesses - without wrinkling, at a running speed of up to 30m per minute.

The positioner consists of a group of guide wheels fitted with flexible conical rubber skirts, set slightly convergently in relation to the running of the film. The films to be assembled are thus brought into position on both sides of a guide blade and are placed in contact with each other at the point at which sealing tapes are applied.

Because of the obliquity of their plane of rotation, the guide wheels with flexible skirts, by exerting slight pressure on the film, force its edge into constant contact with the edge of the guide blade. Should the edge of the film move away from the positioning reference, the conical skirt of the guide wheel will, with a jamming effect due to its distortion, exert greater than usual pressure on the film, thus resisting further movement away and tending to bring it back to its normal position.

This positioner is easy to adjust and provides excellent film positioning at running speeds of up to 50 yards a minute with 10 micron films.

4.2.2 HEATING HEAD :

The heating head consists of a heated roller around which runs the assembly tape. Thus roller must possess the following special characteristics :

- a teflon rim to stop any sticking from the substance in fusion
- considerable heating power located as near as possible to the exterior of the rim
- maximum thermal insulation between the rim and the hub
- a temperature regulation device - as precise as possible

This precision has been obtained by using a standard proportional regulation connected to an electronic measurement circuit placed in the turning part of the roller in such a way as to eliminate any problem of contact resistance that could come from the revolving joint. This regulation unit makes it possible to guarantee fluctuations of temperature smaller than one degree on the outside of the rim, placed in normal conditions.

4.2.3. COOLER:

This device consists of a wheel with high thermal inertia whose profile is calculated so as to provide the required cooling characteristic.

This wheel can, if necessary, be cooled by circulation of fluid.

5. EXAMPLE OF APPLICATION. PRODUCTION LINE NATURAL SHAPED BALLOONS

5.1 The Balloons

All these devices are used on the machines which make up the assembly line for natural shape balloons.

These balloons are made of a thin film of polyethylene - thickness of film , 25 to 10 μ . They are formed of gores cut from this film, on the edge of which are welded tapes of polyester-polyethylene complex. These tapes join the vertex of the balloon to its hook, from which is suspended the load.

The shape of the balloon is calculated so that the principal stresses are all longitudinal and transmitted by these reinforcing edging tapes.

5.2 The Machines and the Manufacture Method

5.2.1. EDGING AND CUTTING MACHINE :

The same machine ensures cutting-out of the half gores from the reel of polyethylene film and the placing of polyester reinforcing tapes on each of these edges. The machine consists of two edging and cutting heads, one fixed and the other movable, moving transversely across the film movement. Each head consists of a knife and an assembly head which welds the edging tape. The cut out edged half gore is then rewound onto a mandrel by pulling the edging tapes. These tapes are indispensable and ensure a correct definition of the cut-out shape of the half gores as well as a definition of their length. For instance, there is a tolerance of 20 cm on gore lengths of 150 m, which represents a relative error approaching 1/1000.

This machine works at 20 m per minute. It has a certain number of accessory devices : for leading in and straightening creases in the film; rewinding of off cuts; marking off the lengths of the gores etc .. The moving head is driven by a computer which directs its movement by following indications on a computer read out " listing ". The flexibility and adaptability of this machine is therefore large, for it only takes a change of programming tape to make it possible to manufacture another type of balloon.

5.2.2. JOINING OF HALF-GORES :

Two successive half-gores are unrolled conjointly and assembled along their straight edge. The films are positioned by two positioning devices similar to those described before. The made up gore is stocked in a basket ready for the next assembly position.

5.2.3. JOINING OF GORES

Assembly of the panels is carried out on a fixed machine with a fitting for placing supplementary tapes on edging tapes. Guiding devices and assembly heads are standard. The pairs of assembled gores are stocked in handling baskets and run through on the same machine. Above groups of four gores the volume of film to be handled is such that it is preferable to work on the final assembly bench.

5.2.4. MOVABLE JOINING MACHINE

A movable assembly head with standard devices, positioners and assembly rollers, is placed on the carriage to be driven along the assembly bench. The groups of 4 gores are placed on the bench by an automatic device and the edges to be joined are " pinched together " by a set of fold-away holding arms which keep them in place until the arrival of the positioners on the movable assembly head. The balloon is thus put together by welding the groups of 4 pre-assembled gores. The final operations are the fitting of the vertex and accessories - operations which are carried out by specific welding devices.

5.3 Control

The reliability of the assemblies carried out by these machines is assured by an extremely rigorous control and recording by machine adjustment parameters.

Requirements for the assembly parameters as well as their tolerances, or limits, for guaranteeing a correct assembly, are determined carefully on a laboratory machine specially developed for this purpose, for every type of material and every product. These requirements are set on each machine on the assembly line and their values readjusted several times a day by measuring the temperature in the assembly area with infra-red temperature sensing. Samples of assembly tapes are tested statistically. A control slip makes it possible to note at each assembly position the difficulties or anomalies observed. The personnel on the machines is in fact a control personnel, very aware of the importance of quality and the absolute priority of reliability in every respect.

5.4 Present Production and Future Plant

Thus constructed, this production line can present the following figures : Every week a balloon of 350,000 m³ is produced, with a man-power capacity of 12 persons. This balloon has an assembly length of 26,500 m and uses 38,000 m² of film. An extension of the assembly bench in the near future will make it possible to double the rate of production of balloons and to make balloons reaching cubages of over 1 million m³.

6. RANGE OF OTHER PRODUCTS DEVELOPED USING THIS JOINING TECHNOLOGY

6.1 Natural Shape Captive Stratospheric Balloon

The material used is laminated material combining polyethylene - polyester - dacron scrim-polyethylene. The sealings are carried out by two tapes using the same material.

The whole assembly line is used with no modification, the first machine only effecting the cutting out of the half gores.

6.2 Superpressure Balloons and Balloons With Ballonets

These balloons are made either from a bi-laminated polyester film or from a triplex polyethylene - polyester - polyethylene. The choice between these two materials depends on the expected performance of the balloon and the means of transport and launching. The joinings are carried out by two triplex tapes or by two adhesive tapes. The same machines are used for assemblies, the cutting out done by hand from former for balloons of less than 5 M diameter.

A variant of high pressure balloon with interior ballonet has been developed. It is possible to direct the balloon at altitude by controlling the fullness of the interior ballonet.

6.3 Captive Tropospheric Balloons

These balloons are made from a complex polyethylene - polyester - dacron scrim - polyethylene and the assemblies are made with tapes of the same composition. The range developed reaches from 30 to 100 m³ and the tail fins are sheets stretched on an umbrella type frame. A unit of techniques " parabolic patch extendable gores etc... " have been designed for application to the types of materials used.

6.4 Captive Balloons With Dilatable Envelope

These balloons are made from a stretch polyurethane film. The assembly is a double seam " peeling " weld effected by two heated rollers. These balloons of limited volume (3 to 12 M³) have taught tail fins. They are used principally in meteorological and publicity contexts.

7. CONCLUSION

The assembly devices developed make it possible to treat assemblies of both simple and complex films as a uniform technology.

The techniques are not restricted to one type of material and can easily be adapted to meet the needs for assembly of the highest performance materials. They guarantee, through positioning edge to edge, that the geometrical design of the object to be manufactured will be perfectly respected - a fact which is very important when dealing with materials of limited stretch.

Finally, the reliability of the assemblies is fully guaranteed by the continual recording of the thermal parameters. In short, these assembly techniques are the indispensable complement of new materials developed within the sphere of high performance balloons.

Contents

1. Introduction
2. Advantages
3. Sample Programs
4. Results
5. The Future

Computer Techniques for Balloon Operations

B. D. Gildenberg
Air Force Cambridge Research Laboratories
Bedford, Massachusetts

Abstract

Advantages and some sample programs are examined, as AFCRL evaluates computer techniques for its balloon operations in the field.

1. INTRODUCTION

During the past four years, AFCRL has made increasing use of a modest mini-computer to facilitate balloon operations in the field. The model is a Wang Laboratories 700C with printer-plotter, 120 storage locations and 960 programable steps, with data/program sharing core. Time sharing over hard line to a full scale computer was considered briefly, but is not practical at remote sites, particularly over the long duration of a typical mission.

Although computers have been utilized frequently for specific balloon engineering applications, this marks the first general integration with actual flight operations. For a wide variety of reasons, the mating was a case of pre-destination. Most of the pre-launch calculations take place in the very early morning hours when manual mathematical manipulations are especially prone to error. With computers, the intricate computations have actually been performed at a more rational hour when the program was conceived. Now, during the operation phase, one need only mechanically index raw data.

2. ADVANTAGES

2.1 Response Time

This is a rather obvious factor, especially when taking into account the long, awkward hours of typical operations. Consider one of the larger helium inflations requiring a nominal 8 helium trailers. Manual computations dictate one division, eight additions, 21 subtractions, 21 multiplications, 8 excursions into the tables and another into a graph. With a cross-check system, which was necessary to minimize potential errors, the whole process required some 20 minutes. A computer program has reduced that interval to 30 seconds. Thus, personnel can devote extra time to other problems which require more thought, than this purely mechanical exercise.

For special operational problems, computer speed is almost mandatory, and periodic encounters with such problems, expedited adaption of this facility. One such case occurred during support of NASA Project Viking, the Martian Soft Lander. AFCRL provided a balloon test bed for that recovery system. The mission required forecast intercept times and latitudes for three different target longitudes crossing WSMR, every ten minutes. Only use of a computer program made the exercise feasible.

Another instance was provoked during the recent upsurge of tethered balloon activity. Both altitude and position are often accurately desired, just prior to

some event such as a missile drop from the balloon. Tethered altitudes are usually too low for radar, optics do not provide real time data, and radar altimeters telemeter only one dimension. AFRL, therefore, generates its own preliminary measurements via a double theodolite system. Reduction originally required some six minutes, using a desk calculator and trigonometric tables. Now, the program delivers answers in a scant 30 seconds, with cross-checked solutions, in a form neatly typed for final file. Since various events from the tethered balloon have to proceed on a precise countdown, the vehicle would often move out of position during the marginally long manual computations, then this whole process had to be recycled. A significant number of extra events are achieved today, with the computer in the system.

Probably the most important operational factor effected by this new dimension in response time is balloon control. Here, command valving and ballasting are employed to describe a complex, pre-determined vertical profile. For effective balloon control, altitude, and ascent rate, various ballasting and altitude parameters must be monitored rather closely, and continuously updated. This equates to detailed, very busy bookkeeping, eventually real time functions, and inexorably, computers.

2.2 Accuracy

In the double theodolite example, an individual performing manual computations was under considerable pressure for rapid answers. With precarious interpolations in the trigonometric tables, while dueling with the law of sines, errors were inevitable during this kind of stress. One would be much less apt to err, if the only activity demanded was indexing of four raw angles. Indeed, by substituting programmed equations for the graphs and tables, we eliminate necessity for any interpolations, thus increasing accuracy, and even more, consistency. We also eliminate a periodic requirement for expanding the ranges of various graphs and tables.

A more subtle advance in accuracy is that in programming various problems one has been led to examine original equations more carefully. Some have been consequentially improved or expanded, but in all cases, a better understanding of the basis of the process is obtained.

With a computer, indexing errors are possible, of course, but one can minimize this potential by having the printer display raw data together with solutions.

2.3 Simplicity

The layman may not correlate simplicity with computers, but I am referring here to practical operational use. Once a program has been loaded, any untrained individual can proceed by simply supplying raw data as requested by the program, in a printed conversation. Thus the normal operator, especially with a mini-computer, can break for a more urgent task and have almost anyone associated with the mission, process the data.

2.4 Presentation

Manual operations result in a wide variety of handwriting, some of which must be decoded and transcribed by irate secretaries, or draftsmen. The computer printer-plotter provides a finished table or graph, almost immediately ready for file, and with sufficient capacity, extra copies. AFCRL has eliminated significant drafting and typing workloads at its operational station in this way.

2.5 Versatility

Not only may the computer be utilized for a wide variety of tasks during flight operations, but also for equally numerous pre and post test activities. It becomes especially valuable for instrument calibration, data analysis, and as a training or problem prototyping vehicle for advanced computers.

2.6 Summation

These itemized advantages add up to an order of magnitude increase in bookkeeping during a mission, with parallel jump in accuracy, despite a decrease in actual time dedicated to mechanical computations.

3. SAMPLE PROGRAMS

3.1 Trajectory Forecast

One activates this program (Figure 1) by loading the proposed ascent rate. This, of course, can be optionally varied to describe a complex profile. Eventually, we hope to incorporate a parachute descent time program for descent trajectories.

One proceeds by indexing wind direction and speed for successive layers. Printed items are left relatively unlabeled, so that a variety of units can be used. For instance, either 5,000 foot or 10,000 foot intervals can be assigned to the numbered levels. Headings could be true or compass, speed in knots or miles per hour.

An advanced form of this program may see the tabular summary accompanied by an x-y plot, for both climb-out and parachute drift trajectories.

3.2 Radiosonde Data Processing

Figure 2 shows raw data from a run preceding the launch is digested to provide a variety of information. Inputs from the run are pressure, temperature, and relative humidity for significant layers only. This is substantially less data than handled in the standard final form, and permits us to obtain the run one hour earlier than normal.

The program computes geopotential altitudes for standard as well as significant levels via the hydrostatic equation. Corresponding temperatures, pressures and humidities are listed so that one can pick out tropopause and cloud boundaries. Ambient temperature lapse rate is computed and listed in the fifth column. The latter is one of the most important variables in determining ascent

rate. By scanning this column, qualitative changes in rate can be predicted in advance, an important feature in planning ballasting and valving exercises. Eventually, we hope to print out the forecast ascent rate in an adjacent column.

One additional item is indexed into this program, namely gross inflation. It, together with the density ratio from column 6 is incorporated in an appropriate equation to present, in the last column, apex gas valving seconds for 1% of the gross inflation. This is more accurate than using the Standard Atmosphere density ratio, but since the ascent rate is not yet known accurately in advance, there is no corresponding correction for ram pressure on the apex valve. Moreover, the time would change with prior valving exercises, as the gas head decreases. But this column is still of practical use in determining estimated valve times and therefore the altitude at which valving should commence. The density ratio will eventually be fed into another routine to provide parachute descent times.

3.3 Single Trailer Helium Inflation

The legend (Figure 3) is on the bottom so that the first solution can be read immediately. The latter is the first number printed, a cut off pressure in psi, for the designated free lift and number of tubes open. Following, we provide solutions for increments of 1% free lift and 1 tube. This is very useful in that it provides ready answers if a last minute change in any of these variables is required. It also optimizes the number of tubes selected.

Inputs are gross load, free lift, pressure, temperature, and number of tubes. No tables or graphs are required. Figure 4 presents the basic equations which were developed to duplicate the General Mills inflation tables and graph. These, with modifying substitutes, are discussed in a recent report, AFCRL-TR-74-0200. The computer program approximates the tables to within 0.1 pounds of lift per tube for a range from 1200 to 2700 psi initial pressure. Lift per tube is printed out so discrepancies can be checked for fringe pressures.

3.4 Local Area Weather Map

The specific advantage of this process is that the program (Figure 5) computes sea level pressure from altimeter readings. Thus we can include pertinent local Class C stations in the analysis, which are not found on the national facsimile charts. It permits the kind of microanalysis especially pertinent to the launch of large, plastic balloons. With suitable, peripheral equipment, this map could be produced directly from the weather teletype machine, thus providing some material even before personnel arrive on shift.

3.5 Height-Time Curve

Once airborne, we switch to this rather basic program (Figure 6). The entire graphical framework and legend are printed out by activating only one key. This accelerates transfer as we proceed to higher altitudes in 50K intervals.

The first number next to each position plot is overall ascent rate from launch followed by the rate between successive points. To prevent overcrowding, print out is optional, with the rates also displayed on the registers. We do not have a real time clock as yet, so inputs are altitude in kilofeet, and time in minutes from an elapsed timer next to the computer. Nevertheless, the program is a significant improvement over manually plotted curves, where only the slope indicates ascent rate.

If the altitude telemetry originates from a simple aneroid device, the incremental rates can be rather noisy, but they will indicate a trend, which is substantiated by the first number. Incremental rates do become more consistent, as the balloon decelerates.

There is a supplementary version of this program with expanded scales for flight profile exercises in a limited altitude slice.

Future plans call for this program forecasting minutes to float, or time of arrival at float, with each plot. This is not a simple problem since ascent rate above the point must be forecast.

3.6 Ballast-Valve Bookkeeping

On a previous program (3.2), we computed initial apex valving rates, presuming a static head. It is primarily used for making preliminary estimates. This program (Figure 7) is the dynamic version. It adjusts gross load and gross inflation as control is exercised, which in turn vary the ballast and valving times. To illustrate, at 1430Z, there was a ballasting event. Input is percent (of gross load) ballast desired. The computer then displays corresponding minutes and seconds. Next step is to index minutes and seconds actually commanded, which could vary from the original intent. Now our computer prints out updated values. Free lift is shown in percent and pounds, ballast residue in percent, pounds, and minutes required to dump the total residue. The new gross load and unchanged gross inflation follow. The register notes the updated time for 1% ballast.

For a valving exercise, one indexes the percent desired, plus altitude. The print out readjusts the gross inflation and free lift. This program incorporates density ratios from the earlier program (3.2) for valving rates.

Mathematics of such bookkeeping is obviously straightforward, but during the rapid ballasting and valving events required for a complex flight profile, this program becomes an invaluable tool.

3.7 Target Trajectories

At WSMR, particularly, AFCRL has periodic requirements to overfly a designated ground target area or hover within minimum range of a laser site. For these problems, sophisticated missile radar tracking may be employed, but real time digital display of various flight parameters is not available in the Balloon Control Center. Accordingly, a program (Figure 8) was devised which would accomplish both, although not precisely in real time. It incorporates elevation and azimuth angles from the target point, plus balloon altitude, to plot a position with respect to the target. Next to each plot is the incremental x, y vector. Simultaneously, the registers display horizontal distance and slant

range from the target center. By climbing very slowly during approach to the target, one can select an optimum altitude for intercept or hover, by watching changes in the various displays and print out.

3.8 Double Theodolite Solution

Figure 9 shows how we determine x, y, and z positions with respect to a fixed ground point. The first section is a question and answer session for establishing complete geometrical layout of any given site. Then, inputting elevation and azimuth angles from both theodolites, it prints the altitude for two different solutions, plus component displacement from ground zero. Differential in altitude for the two solutions provides a calibration of the accuracy of each set of observations.

3.9 Supplementary Programs

We now list supplementary routines (Figure 10) which are used indirectly or not on every operation.

The "aiming angle" program displays look angles for any latitude and longitude and give the latitude and longitude of the balloon. It was derived from a satellite application.

The University of Minnesota equations are being used experimentally, thus far, to establish a free lift choice based upon the past performance of similar systems.

The altitude sensor calibrations furnish a finished, errorless copy in about 30 minutes. Formerly, a hand copy required some three hours.

4. RESULTS

The facility has substantially proved its worth, in a wide variety of operational activities, and further advances are forthcoming as the programmers accumulate more skill. With precision bookkeeping during balloon control exercises, post test analysis attains more quantitative value. Response time to

changes in balloon performance has improved appreciably. Mission paper workload was decreased and improved in appearance. More detailed computations are performed during a mission, with significantly increased accuracy and speed. Today, these characteristics become a necessity, as vehicle performance expands in response to computer amplified complexity of experimental payloads.

5. THE FUTURE

The major weakness of current, modestly priced mini-computers, is that only one large program can be handled at a time on the basic units. Expensive peripheral equipment is required to manipulate a nominal five operational balloon programs, more or less simultaneously. Advances in the next three to five years promise that same capability without peripherals, and probably even more portability. Indeed, some of the programs reviewed in the previous section may then be packed into pocket computers.

Designs for near future balloon on-board instrumentation should make provision for real time computer processing of altitude and trajectory. The Locate navigation system is an important step in that direction.

Some type of reasonably priced optical display that allows the various computer outputs to be seen from any part of the room would be another goal.

Further downstream, consider real time decision making/control for vertical flight control.

CLIMB OUT TRAJECTORY

(JUNE 10, 1974)

LAYER	SUBVECTOR		SUMVECTOR	
1	330/	.50	329/	.50
2	/	.80	348/	1.25
3	150/	.50	359/	.80
4	180/	.80	315/	.00
5	40/	.50	39/	.50
6	30/	1.00	33/	1.49
7	70/	1.50	51/	2.84
8	60/	1.50	54/	4.33
9	90/	.50	58/	4.74
10	240/	.50	57/	4.24
11	290/	1.50	38/	3.55
12	290/	1.50	13/	3.37
13	280/	1.50	348/	3.61
14	270/	3.00	313/	5.12
15	270/	3.00	297/	7.58
16	270/	3.00	290/	10.32
17	280/	3.50	287/	13.78
18	280/	3.50	286/	17.26
19	280/	3.50	285/	20.74
20	270/	4.00	282/	24.63

Figure 1. Trajectory Forecast

HYDROSTATIC EQUATION WITH VALVE TIMES

JUNE 10, 74, 75000 GROSS INFLATION

• 4387.7	863.000000	24.600000	19.000000	-4.23		
• 4824.2	850.000000	25.900000	21.000000	2.97		
• 4926.3	847.000000	27.100000	20.000000	11.74		
4993.4	845.124115	26.985721	20.000000		.798231	41.308436
• 8034.9	760.000000	21.800000	20.000000	-1.70		
9984.4	709.391065	16.401713	23.373928		.695128	46.354538
• 10346.1	700.000000	15.400000	24.000000	-2.76		
14973.0	592.183104	3.411404	32.046036		.607968	51.829727
• 16096.6	566.000000	.500000	34.000000	-2.59		
• 19306.7	500.000000	-8.600000	42.000000	-2.83		
19959.2	487.972165	-10.115194	42.937233		.527088	58.377219
• 23483.6	423.000000	-18.300000	48.000000	-2.32		
• 24845.9	400.000000	-21.100000	30.000000	-2.05		
24943.1	398.519306	-21.228471	29.716926		.449741	66.631102

Figure 2. Radiosonde Data Processing

INFLATION PROGRAM PRINTOUT

521.6	38	8.0
473.1	37	8.0
567.7	39	8.0
611.8	40	8.0
538.2	38	7.0
504.9	38	9.0
488.4	38	10.0
CUTOFF	TUBES	1.1
LB LIFT / TUBE	-	92.60

Figure 3. Single Trailer Helium Inflation

EQUATIONS FOR HELIUM INFLATION
COMPUTATIONS

$$\text{LIFT (LB/TUBE)} = \frac{12.545 P^{0.92683}}{1.9333} \left(\frac{P}{2400} \right)^{0.001} \left(\frac{P}{100} - 24 \right)$$

$$\text{FINAL PRESSURE (psi)} = \frac{L(T)}{10.95}$$

$$\text{LIFT (LB/TUBE FOR 220 psi)} = \frac{2401.5}{T(^{\circ}\text{K})}$$

$$\text{CUTOFF PRESSURE} = 10,000 + 0.5 (1P) - \sqrt{10,000 + 0.5 (1P)^2 - 20,000 (FP)}$$

Figure 4. Basic Equations for Helium Inflation Computations

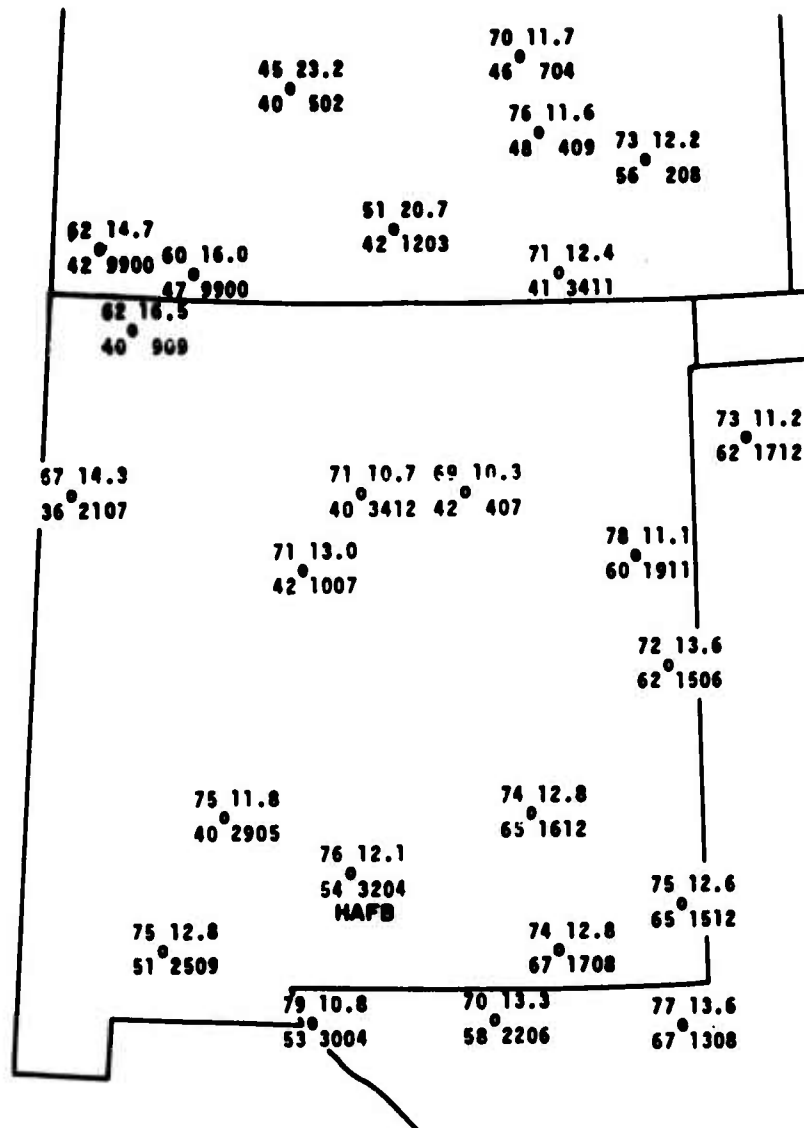


Figure 5. Local Area Weather Map

FLIGHT H74-19/H-39
 22 APRIL 1974
 LAUNCHED 1404Z

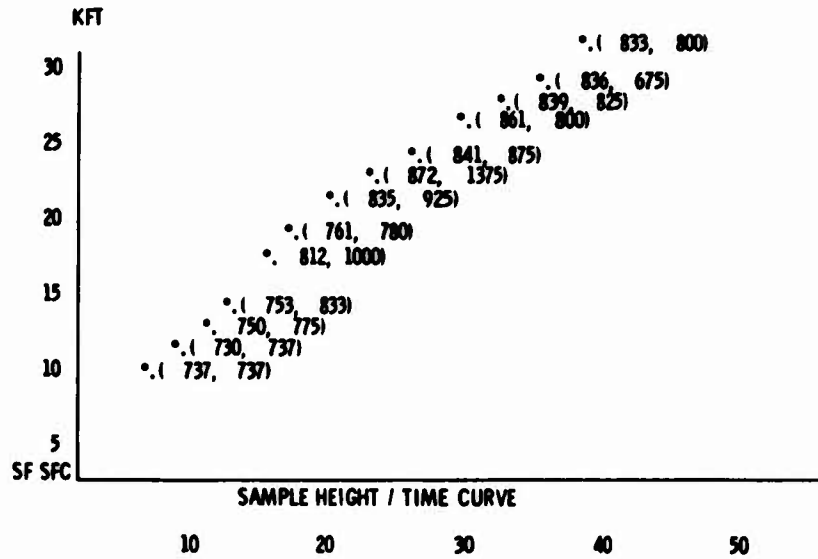


Figure 6. Height-Time Curve

BALLAST-VALVE PROGRAM

1438Z FL	11.0%	588.1 #	BALLAST RESIDUE	12.0%	618.8 #	12.2 MIN. GL	4818.8 #	GL.	5408.8 #
1438Z FL	10.4%	618.5 #	BALLAST RESIDUE	12.0%	618.8 #	12.2 MIN. GL	4818.8 #	GL.	5428.3 #
1448Z FL	12.0%	682.8 #	BALLAST RESIDUE	10.8%	523.5 #	10.4 MIN. GL	4823.5 #	GL.	5428.3 #
1448Z FL	10.4%	688.3 #	BALLAST RESIDUE	10.8%	523.5 #	10.4 MIN. GL	4823.5 #	GL.	5328.8 #

Figure 7. Ballast Valve Bookkeeping

TARGET TRAJECTORY PLOT

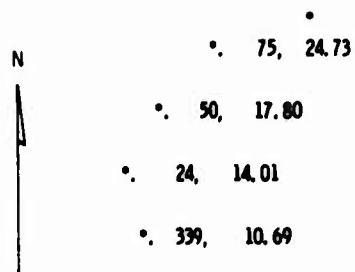


Figure 8. Target Trajectory

DOUBLE THEODOLITE PROGRAM
FOR TETHER OPERATIONS

AZM. FOR THEOD. #1 LOOKING AT GND. ZERO - 45.00
 AZM. FOR THEOD. #1 LOOKING AT THEOD. #2 - 90.00
 BASELINE LENGTH - 3000.00
 AZM. FOR THEOD. #2 LOOKING AT GND. ZERO - 315.00
 ELEV. OF THEOD. #1 LENS ABOVE GND. ZERO - 3.00
 ELEV. OF THEOD. #2 LENS ABOVE GND. ZERO - 2.00
 ANGLE C-A-B - 90.00
 ANGLE A-B-C - 45.00
 ANGLE B-C-A - 45.00
 LENGTH A-B - 2121.32
 LENGTH B-C - 3000.00
 LENGTH C-A - 2121.32

	<u>READINGS</u>		<u>RESULTS</u>		
	<u>AZMUTH</u>	<u>ELEV.</u>	<u>NORTH DISP.</u>	<u>EAST DISP.</u>	<u>ALTITUDE</u>
EAST THEOD.	311.10	17.50			691.9
WEST THEOD.	43.20	19.60	-61.4	-149.0	705.7

Figure 9. Double Theodolite Solution

SUPPLEMENTARY PROGRAMS IN USE

1. TRAJECTORY PLOT FROM GMD
2. HORIZONTAL DISTANCE OUT COMPUTATION
3. PARACHUTE IMPACT SPEED
4. FLOAT ALTITUDE CRUISE VECTOR
5. AIMING ANGLES
6. DENSIOMETER CALIBRATION
7. BARACODER CALIBRATION
8. U. OF M. EQUATION OF MOTION
9. RADAR DATA CONVERSIONS
10. BALLOON SUN ANGLE
11. BALLAST TELEMETRY
12. VECTORIAL WIND SHEAR

Figure 10. Supplementary Programs

Contents

1. Introduction
2. Experimental Results
3. Experimentally Determined Solar Radiation Correction
4. Calculated Solar Radiation Corrections
5. Atmospheric Temperatures at 48 KM, 0600-0845
6. Summary

Atmospheric Temperatures Measured Near 48 Kilometers By Balloon-Borne Thermistors

Harold N. Ballard
Atmospheric Sciences Laboratory
U.S. Army Electronics Command
White Sands Missile Range, New Mexico

Miguel Izquierdo, Carlos McDonald, and John Whitacre
University of Texas at El Paso
El Paso, Texas

Abstract

Modified rocketsonde film-mounted spherical bead thermistors are presently serving as temperature sensors on balloon-borne atmospheric composition experiments conducted in the 40-50 km altitude interval. The thermodynamic parameters of temperature and pressure (density derived) serve as basic background data for these composition experiments. Because of the stability of the balloon-supported instrument platform, solar radiation absorbed by the thermistor and thermistor mounts causes the measured temperatures to be considerably warmer than the true atmospheric temperatures. Through the known geometric orientation of two film-mounted thermistors relative to the known direction of incident solar radiation and determination of instrument platform rotation rate from magnetometer data, the solar radiation correction to the measured temperatures was experimentally determined and compared to that theoretically predicted from the heat transfer equation for the film-mounted thermistors. The resulting atmospheric temperature at 48.5 km vs time data are presented. Also presented, for comparison with the balloon-borne measurements, are temperature profiles from 0-65 km as determined from radiosonde and rocketsonde temperature sensors launched in support of the balloon flights.

1. INTRODUCTION

Particularly extensive studies, both theoretical and experimental, were conducted in the period 1961 to 1969 to determine the proper corrections to temperatures measured by rocket-borne sensors in the 30-65 km height interval. Much time and effort have been expended in examining the heat transfer equation for the temperature sensors. Various authors have contributed to an understanding of the physical principles underlying the design of a proper rocket-borne temperature sensor. [Wright Instruments Inc. (1961); Ney et al. (1961); Wagner (1961, 1964); Ballard (1961, 1967, 1968); Pearson (1964); Hind (1966); Drews (1966); Thompson and Kelly (1967); Thompson (1968); Ballard and Rubio (1968); Hyson (1968) and Ballard and Rofe (1969).] Each of these papers is either a theoretical or a theoretical-experimental study related to a spherical bead thermistor temperature sounding device for the 30-65 km atmospheric region. These studies presently continue as different mounting configurations are utilized to adapt the thermistor temperature sensor to various rocket systems.

The progression of balloon technology to the point that it became possible to launch a constant altitude balloon to 50 km led previously to two integrated experiment balloon flights to 50 km which were related to the study of atmospheric tides by the Atmospheric Sciences Laboratory (ASL), White Sands Missile Range (WSMR). The first was launched to 48 km on 11 September 1968 (Ballard et al. 1970; Beyers and Miers, 1970). The second was launched to 50 km on 22 September 1969 (Ballard et al., 1972). Modified rocketsonde film-mounted spherical bead thermistors served as the atmospheric temperature sensors on both these flights. Five hours of stratospheric temperature data were obtained near 48 km during the 1968 flight while 16 hours of temperature data were obtained between the altitudes of 32 and 50 km during the 1969 flight.

These experiments led to the fabrication of the payload shown in Figure 1 consisting of solar uv photometer, quadrupole mass spectrometer, positive ion sensor, Lyman - lamp, atmospheric sampler, ozone sensors, pressure gauges, cosmic ray detector, water vapor sensors and film-mounted spherical bead thermistor temperature sensors, launched to 48.7 km on 18 September 1972. In Figure 1, of the seven cylindrical rods extending below the top of the truck in the photograph background, counting from left to right, rods 3 and 6 served as mounts for the temperature sensors.

Figure 2 is a photograph of the two film-mounted bead thermistors which shows the orientation of the film mounts relative to one another as they were mounted on the balloon-borne instrument platform. When solar radiation was incident in a direction which was perpendicular to the plane of one film, then the direction of the incident solar ray was parallel to the second film. The argument was made that if the payload platform rotated during the balloon flight, there would come a time when the above condition of perpendicular and parallel incident rays, relative to the two film surfaces, would exist and the maximum difference in temperatures recorded at this time by the two identical sensors would be an experimental determination of the maximum solar radiation correction to the temperatures recorded by the film-mounted thermistors. The experimental results and the theoretical considerations related to this aspect of the balloon-borne measurements of atmospheric temperature are discussed in a following section of this paper.

From the time of launching at 0304 MST until 0421 (23 km), the principal payload was suspended at distance of 20 m beneath the balloon. At 0421 this payload was reeled downward a distance of 370 m from its original position.

Figure 3 is a photograph of the instrument and telemetry package on the apex valve at the top of the balloon. A spherical bead thermistor to determine balloon-skin temperature was attached to the balloon surface 2 m from the outer circumference of the apex valve. This sensor and instrument transmitted balloon-skin temperature continuously throughout the balloon flight. Since the balloon diameter, when the balloon was fully inflated near 48.5 km, was approximately 150 m, the upper and lower temperature sensors were separated by approximately 540 m.

2. EXPERIMENTAL RESULTS

In Figure 4 are summarized altitude vs time data as determined by the FPS-16 radar track of the target at the base of the balloon and the temperature vs time data as measured by the two film-mounted spherical thermistors (B_1 and B_2) on the principal payload beneath the balloon. Also shown in Figure 4 is the balloon-skin temperature as a function of time as measured by the thermistor sensor near the top of the balloon.

Figure 5 presents a summary of the atmospheric temperature vs altitude data obtained by (1) the two film-mounted thermistors B_1 and B_2 , (2) the rod thermistor of the radiosonde (RAOB) launched at 0215 MST, and (3) the bead thermistor sensor of the Loki rocket launched at 0645 MST.

2.1 Comments on Experimental Results

The comments which follow (a - j), are made concerning some aspects of the atmospheric and balloon-skin temperature data presented in Figures 4 and 5. All times are stated as MST:

a. From the time of balloon launching at 0304 until approximately 0335 (12 km), the temperatures recorded by sensors B_1 and B_2 and the balloon-skin temperature sensor all recorded approximately the same temperature, which was considerably colder than the temperature recorded by the RAOB sensor at the same altitude. At 0345 (15.3 km), sensors B_1 and B_2 , which were located 20 m beneath the balloon, registered -68°C . The temperature thus does not accurately represent the lowest tropopause temperature of -74°C recorded by sensors B_1 and B_2 shortly after 0855 when the payload was floating downward on its parachute. This difference was caused by the proximity (20 m) of sensors B_1 and B_2 to the balloon at a temperature of -64°C . In Figure 5, the tropopause temperature at 15.3 km measured by the RAOB temperature sensor as -73°C .

b. From 0345 to 0421 (23 km), the rates of increase of temperatures registered by sensors B_1 and B_2 , and the balloon-skin sensors were approximately equal. At 0421 the payload was reeled downward 370 m. From this time forward the balloon-skin temperature remained much colder than the temperature registered by sensors B_1 and B_2 located 390 m beneath the balloon.

c. After the time of sunrise (0528, 40 km), the differential absorption of solar radiation by the film-mounts of the thermistors can be seen, this differential absorption being caused by the relative orientation of the planes of the film mounts (Figure 2) with respect the direction of incident solar radiation as the payload rotated about its vertical support line.

d. The balloon reached its float altitude near 48.5 km at 0555. The differences between the temperatures recorded by sensor B₁ and B₂ between 0555 and 0757 are caused by the differential absorption of solar radiation by the thermistor film mounts as discussed above. At 0757 (solar elevation angle 27°) sensors B₁ and B₂ became shaded from direct solar radiation. The recorded data points in Figure 4 are plotted without correction for solar radiation effects. The solar radiation correction to the film-mounted thermistor is discussed in following sections.

e. Very shortly after the time of sunrise at the balloon altitude (0528, 40 km), the balloon-skin temperature began to slowly increase from -55°C with an abrupt increase to -50°C occurring at 0540. Shortly after 0600, the balloon skin temperature again increased sharply followed by a sharp drop in temperature in turn followed by a relatively steady rise in temperature to -30°C just prior to the time of flight termination. It is perhaps not just coincidental that the 2990 Å radiation from the sun appeared in the balloon-borne photometer at 0540 and the 2400, 2500 and 2550 Å solar radiation appeared in the photometer between 0600 and 0610, correlating quite well with the times of abrupt increase in the balloon skin temperature.

f. As a point of interest relative to the comparison of temperature data from the balloon, RAOB, and rocketsonde sensors presented in Figure 5, note that when the balloon payload was floating downward on its parachute after flight termination, the temperature recorded by film-mounted sensor B₂ was -20°C at 40 km (Figure 3), while the rocketsonde also recorded a temperature of -20°C at this altitude. As noted above, the atmospheric temperature measured by sensors B₁ and B₂ at 15.3 km (Figure 4), when descending on a parachute, registered -74°C while the RAOB sensor measured -73°C at this altitude (Figure 5).

Based upon the data presented in Figures 4 and 5, and the above comments a - f, it appears that the large balloon has a marked effect upon the temperatures recorded by sensors mounted on the payload following on its wake. As it ascended to 5 km, the balloon was considerably colder than the air temperature at that altitude, this effect being produced by the adiabatic expansion of the helium as the balloon was inflated and its continued expansion and cooling (2°C/km), as the balloon further ascended. This effect was recorded by sensors B₁ and B₂ following in the balloon wake. It gradually diminished as the balloon ascended to the cold (-74°C) tropopause since, because of the relatively long thermal time constant of the balloon and helium, the balloon temperature became warmer than that of the surrounding air; thus at the tropopause the situation has reversed with the balloon being at a temperature of -64°C, the atmosphere at -74°C and the sensors following in the wake measuring -68°C. After passing through the tropopause the balloon and air were at the same temperature near 20 km with the temperature sensors following in the balloon wake registering the correct air temperature. At altitudes above 20 km with the balloon remaining at -55°C and the air temperature increasing, the sensors following in the balloon wake again registered values colder than the true air temperature. After visible sunrise (0528, 40 km), the balloon temperature began to increase slowly with marked increases in balloon temperature occurring at 0540 and 0606-0610, corresponding to times of appearance of 2990 Å and 2400-2550 Å radiation, respectively, at the balloon altitude. The balloon reached float altitude at 0555. After this time the temperature recorded by the sensors 390 m beneath the balloon were not influenced by the presence of the balloon. Therefore, a determination of the solar radiation correction to the temperature measured by the film-mounted thermistors permits a corresponding determination of the correct air temperatures.

3. EXPERIMENTALLY DETERMINED SOLAR RADIATION CORRECTION

Figure 6 (a and b) is an expanded-in-time section of the temperature vs time data presented in Figure 3 as determined by the film-mounted thermistors on the payload 390 m beneath the balloon when the balloon was at its float altitude near 48.5 km. Figure 6a is the telemetered temperature record as determined by sensors B₁ and B₂ in the time interval 0559 to 0607. That portion of the record marked reference is the signal that is received corresponding to the introduction of a fixed resistance (the reference resistance) into the temperature sensing circuit so as to detect any drift in the electronic circuitry; thus the resistance (corresponding to temperature) of thermistors B₁, B₂, and the reference were alternately sampled.

Figure 6b is the time-shared record of Figure 6a with the dashed lines indicating the temperatures that were being sensed by thermistors B₁ and B₂ in the time intervals when their data were not recorded. A study of Figure 6b shows that the maximum difference between the temperatures recorded by sensors B₁ and B₂ occurred at approximately 0604. The magnitude of this difference is 12°C. A study of Figure 2 concerning the relative orientation of the thermistor film-mounts indicates that the plane of film B₁, was perpendicular to the direction of incident solar radiation at 0604 while the plane of film B₂ was parallel to this direction, thus implying that the solar elevation angle at 48 km (the altitude of the thermistor sensors) was zero degrees at 0604.

A further study of Figure 6b shows that the rotation period of the sensors on the principal payload was 3 min 48 sec at times near 0604. The rotation period of the principal payload relative to the earth's magnetic field, as determined by the magnetometer on the principal payload, was also 3 min 48 sec. The planes of the thermistor film-mounts were established to be vertical from the payload pendulum data, thus substantiating the time of 0604 as the time of zero solar elevation angle at 48 km.

Figure 7 is a plot of solar elevation angle at WSMR as a function of time on 18 September 1952. A study of this figure shows that zero solar elevation angle at 48 km occurred at 0553 with the solar elevation angle at 0604 being +2.5°; thus the maximum temperature difference registered by sensors B₁ and B₂, as caused by solar radiation, should have occurred at 0553 rather than at 0604. This would be true if all wavelengths of solar radiation were transmitted equally and at the same time through the atmosphere. As was stated above, ultra violet radiation at 2990Å did not initially appear at the balloon altitude (45 km) until 0540 and reached its maximum intensity at approximately 0610. Ultra violet radiations at 2400, 2500 and 2550Å did not initially appear at the balloon altitude (48.5 km) until 0610 and reached their maximum intensities at approximately 0810 (48.5 km). The maximum radiation intensity at 2900Å to the maximum total radiation intensity at 2400, 2500, and 2550Å was in the ratio of approximately 25 from 0700 to the time of flight termination at 0845.

A study of Figure 4 shows that some wavelengths of solar radiation were incident upon thermistor sensors B₁ and B₂ at approximately 0528 when they were near 40 km altitude, this incidence being indicated by the orientation of the film-mounts relative to the direction of incidence. A marked effect, as caused by this relative orientation, can be observed beginning at 0540 when radiation at 2990Å was incident upon the thermistors, becoming of maximum intensity at 0610. Recall from Figure 6 (a and b), the maximum difference in temperatures registered by B₁ and B₂ occurred at 0604 (thermistors at ≈ 48 km) before wavelengths 2400, 2500 and 2550 were incident on the thermistors. Thus it would appear that solar radiations at wavelengths greater than 2990Å were responsible for increasing the film-mounted thermistor temperatures.

A study of Figure 7 shows at 0610, the time at which solar radiation at 2990A reached its maximum value, the solar elevation angle was approximately four degrees. It would appear from the above considerations that the maximum solar radiation correction to the film-mounted thermistors at 48 km is $12^\circ/\cos 4^\circ = 12^\circ/0.998 = 12^\circ\text{C}$.

To determine whether or not this experimentally-determined solar radiation correction to the film-mounted thermistors is in agreement with a theoretically determined value, the solar radiation correction is calculated below utilizing the heat transfer equation for a film-mounted thermistor.

4. CALCULATED SOLAR RADIATION CORRECTIONS

Based upon realistic simplifying assumptions, it can be shown (Ballard and Rofe, 1969) that the heat transfer equation for the bead thermistor can be solved to give explicitly the difference in temperature, ΔT_{te} , between the thermistor and the atmosphere environment. This temperature difference is

$$\Delta T_{te} = \frac{-m c_t dT/dt + h_t A_t r v^2 / 2 c_p + (2KB/l) \Delta T_{se} + 1/4 J_{cs} A_t + T_e A_t n}{[4T_e h_t A_t T_e^3 + 2KB/l + h_t T_t]} \quad (1)$$

In Eq. (1), the first term in the numerator gives the correction due to the time lag of the thermistor; the second term is the aerodynamic heating correction; the third term is the correction caused by heat conduction through the thermistor leads from the thermistor support when there is a temperature difference ΔT_{se} between the thermistor support and the environment; the fourth term is the correction caused by the absorption of shortwave solar radiation by the thermistor; and the fifth term gives the error introduced by the simplifying assumption.

The denominator of Eq. (1) is the dissipation factor, S_t , for the thermistor to include the heat transfer processes of radiation, conduction, and convection.

All terms in the numerator of Eq. (1) can be shown to be negligibly small for a film-mounted thermistor (Figure 1) floating on a balloon near 48 km, with the exception of $(2KB/l)\Delta T_{se}$ and $1/4 J_{cs} A_t$.

In Figure 2, the thermistor thin-film mounts are fabricated from aluminum-coated mylar. The aluminum coating is on both sides of the mylar film.

Using a reflection coefficient for aluminum of 0.90 and an absorption coefficient for mylar of 0.05, and using time rate of absorption of solar radiation by a film of the dimensions of that shown in Figure 2, one obtains a value of

$$\frac{dR_f}{dt} = J(0.10) A_f = 60,200 \text{ } \mu\text{watts} \quad (2)$$

where J is the solar constant and A_f is the film area. Here the plane of the film is perpendicular to the direction of incident solar radiation. The heat dissipation factor S_f for the film is given by

$$S_f = 4\sigma\epsilon_e T_e^3 + h_f A_f \quad (3)$$

Evaluation of this expression for an altitude of 48 km and a vertical velocity for the temperature sensor of 1 meter/second (as determined from the radar track of the balloon between 0600 and 0610) gives

$$S_f = 2890 \text{ } \mu\text{watts}/^\circ\text{C} + 890 \text{ } \mu\text{watts}/^\circ\text{C} = 3780 \text{ } \mu\text{watts}/^\circ\text{C} \quad (4)$$

thus,

$$\Delta T_{se} = \frac{dR_f/dt}{S_f} = \frac{60,200 \text{ } \mu\text{watts}_s}{3780 \text{ } \mu\text{watts}/^\circ\text{C}} = 16.0^\circ\text{C} \quad (5)$$

The difference in temperature recorded by the two film-mounted thermistors when the incident rays of solar radiation were perpendicular to one film and parallel to the other is given by

$$\Delta T_{B_1, B_2} = \frac{(2KB/l)\Delta T_{se}}{S_t} \quad (6)$$

For the mounting configuration shown in Figure 2, $2KB/l$ equals $10.4 \text{ } \mu\text{watts}/^\circ\text{C}$, while S_t has a value at 48 km given by

$$S_t = 4\sigma\epsilon_e A_t T_e^3 + 2KB/l + h_t A_t = 1.5 + 10.4 + 2.8 = 14.7 \text{ } \mu\text{watts}/^\circ\text{C} \quad (7)$$

Substitution of the values of the quantities in Eq. (6) from Eqs. (5) and (7) gives

$$\Delta T_{B_1, B_2} = \frac{(2KB/l)\Delta T_{se}}{S_t} = \frac{(10.4)(16.0)}{14.7} = 11.3^\circ\text{C} \quad (8)$$

Thus the theoretically determined correction is in excellent agreement with the solar radiation correction determined experimentally; i.e., 11.3°C and 12°C , respectively.

5. ATMOSPHERIC TEMPERATURES AT 48 KM, 0600-0845

A study of Figure 6b shows that the shape of the continuous temperature records for sensors B_1 and B_2 gives the orientation of the two sensor mounts relative to the direction of incident solar radiation. For example, minimum points on the temperature trace delineated by B_2 occur when the plane of thermistor mount B_2 is parallel to the incident rays. Minimum points on trace B_1 are at times when the plane of thermistor mount B_1 is parallel to the incident rays. At these times the solar radiation correction caused by heating of the film is zero, and thus the recorded temperatures represent the actual air temperature (all other corrections being negligible).

The temperature records obtained near 0700 were expanded about 0700, and it was determined that the plane of thermistor mount B₂ was parallel to the direction of incident solar radiation at 0700. Sensor B₂ registered a temperature of -4°C at this time.

A close examination of the photographs of the film-mounted thermistors (Figure 2) shows that both sensors B₁ and B₂ became totally shaded from directly incident solar radiation when the solar elevation angle exceeded +27°. From Figure 7, a solar elevation angle of +27° occurred at 0757. Thus the temperatures recorded by both sensors B₁ and B₂ were independent of incident solar radiation after 0757.

The temperatures recorded by sensors B₁ and B₂ at 0800 were -3.0 and -3.5°C, respectively. At 0815 B₁ and B₂ both recorded -1.5°C. At 0830 both B₁ and B₂ recorded +1.0°C. At 0844 both sensors registered -0.5°C, while near 0845, just prior to flight termination, sensor B₁ registered 0°C.

While the balloon was floating near 48.5 km with the temperature sensors near 48 km, the air temperature was -7.0°C at 0600, -4.0°C at 0700, -3.0°C at 0800, -1.5°C at 0815, +1°C at 0830, and approximately 0°C at 0845. The total atmospheric temperature change from 0600 to 0845 would thus be approximately 7°C.

6. SUMMARY

From the data presented in this paper, it would appear that temperatures recorded by balloon-borne, film-mounted thermistors of the configuration described herein are greatly influenced by the presence of the large balloon, as the balloon floats upward with the sensors following in the balloon wake (Figures 4 and 5). When the balloon reaches its float altitude near 48.5 km during daylight hours, the distance of 390 meters between the balloon and sensors is sufficient to allow the thermistors to measure the correct air temperature, if the recorded temperatures are corrected for the absorbed solar radiation effect.

By mounting two film-mounted thermistors in the configuration described, it is possible to experimentally determine the magnitude of this absorbed solar radiation correction and thus determine the correct air temperatures. A comparison of the magnitude of the experimentally and theoretically determined corrections gives 12°C versus 11.3°C, respectively, at an altitude of 48 km for the maximum solar radiation effect. This value gradually diminishes with changing solar elevation angle, becoming zero when the thermistors and mounts are totally shielded from directly incident solar radiation.

A comparison of the air temperatures at 48 km as determined by the film-mounted thermistor carried aloft by the Loki rocket launched at 0645, 18 Sep 1972, and the air temperature at 48 km at 0700 as determined by the film-mounted balloon-borne thermistors, gives comparison values of -5°C and -4°C, respectively.

Rocketsonde temperature sensors similar to this Loki-borne sensor were utilized by Beyers *et al.* (1966) in their experimental studies of the diurnal temperature fluctuations associated with the diurnal atmospheric tide in the stratosphere. Contrary to values predicted by theoretical studies, they found a diurnal variation in temperature at 48 km having an amplitude of 5°C (minimum-maximum, 10°C), with the minimum and maximum values occurring at 0400 and 1600 LST, respectively.

It would appear that the temperatures determined by the balloon-borne sensors utilized in this experiment verify that the magnitude (minimum to maximum) of the observed diurnal temperature change at 48 km is at least 10°C, in that in the time interval extending from 0600 to 0845, when the balloon was floating near 48 km, the air temperatures were -7, -4, -3, and 0°C at 0600, 0700, 0800, and 0845, respectively. All stated temperatures are believed to be correct to within +1°C.

If the diurnal temperature variation is assumed to be sinusoidal with an amplitude of 5°C and a period of 24 hours, then the temperature change between 0600 and 0900 would be approximately +3°C.



Figure 1. Principal Payload Prior to Launching

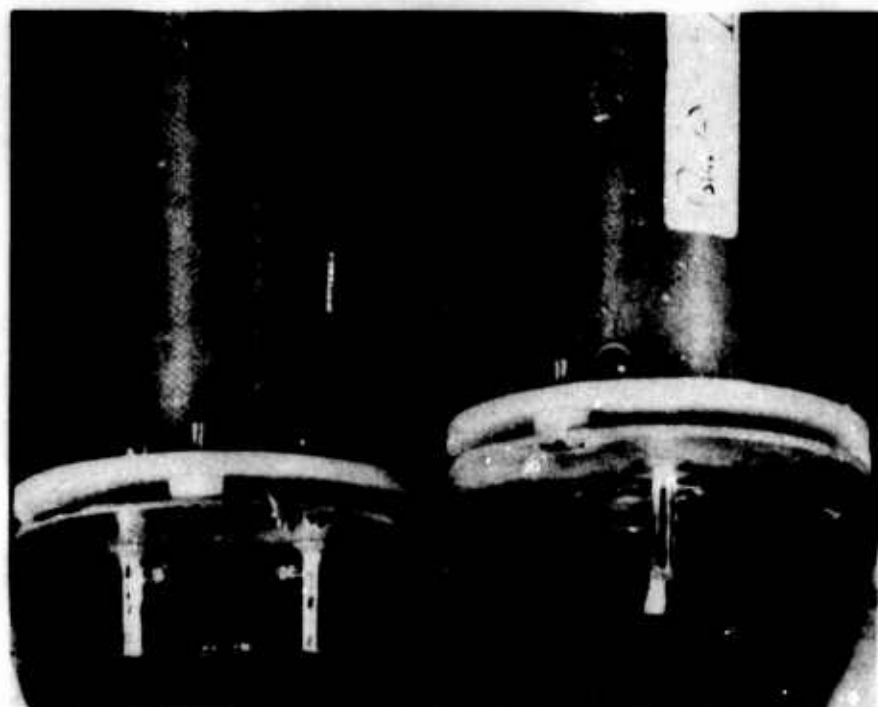


Figure 2. Film-Mounted Spherical Bead Thermistor Temperature Sensors



Figure 3. Payload on Balloon Apex Valve

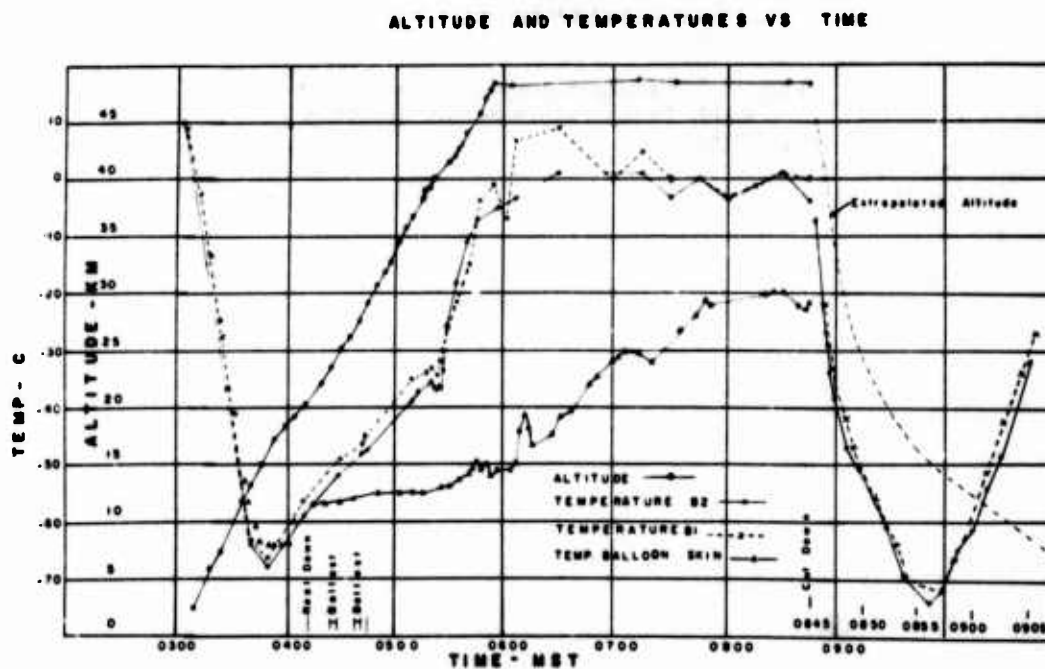


Figure 4. Balloon Altitude, Air and Balloon-skin Temperature vs Time

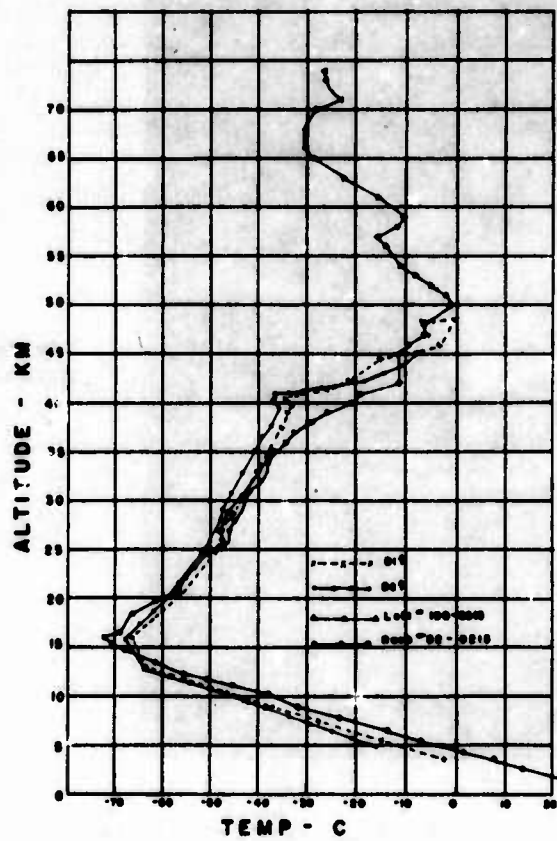


Figure 5. Balloon-borne, Rocket-borne, and Raob Temperature Sensor Records vs Altitude

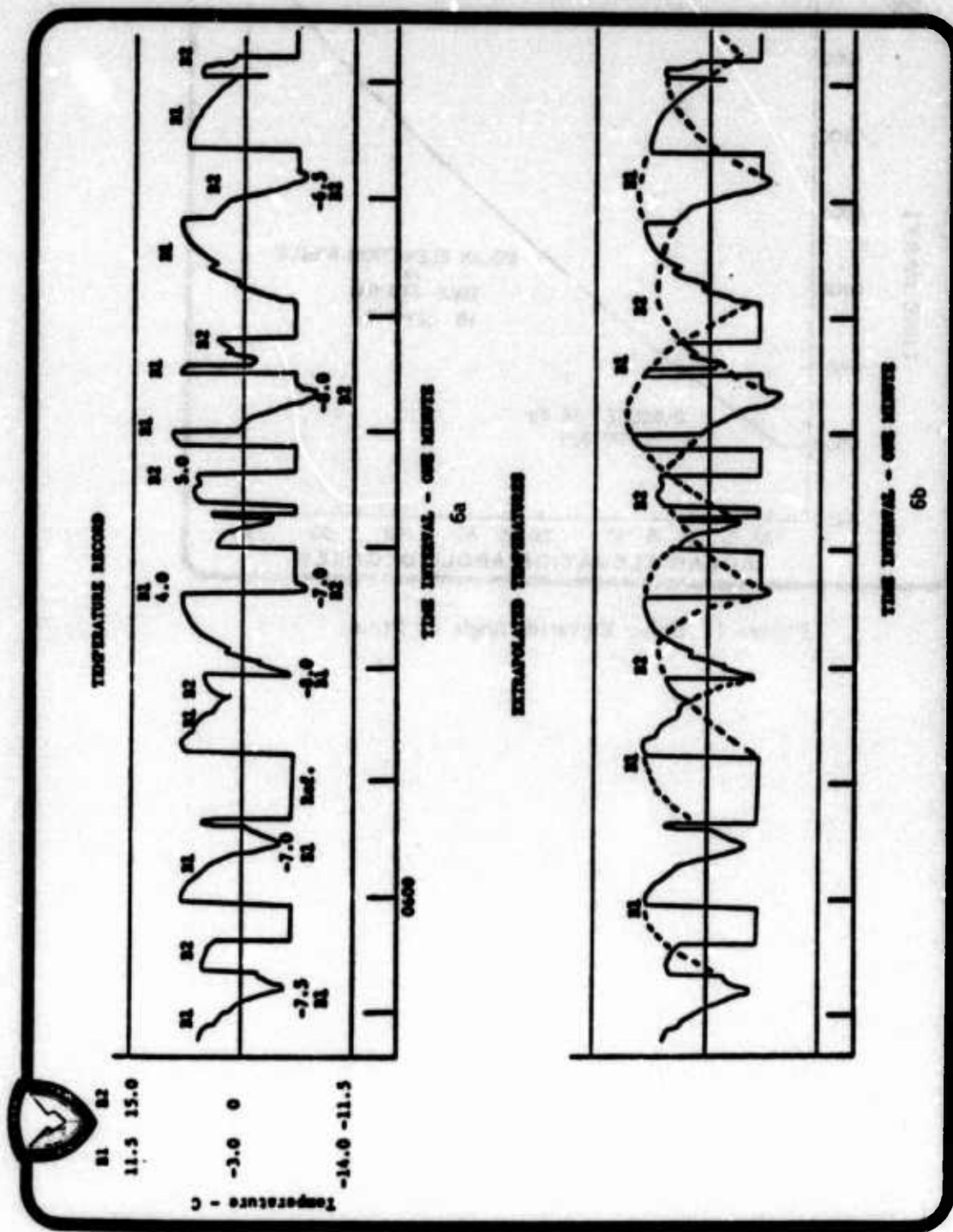


Figure 6. Expanded Temperature Record vs Time (0559 - 0607 MST)

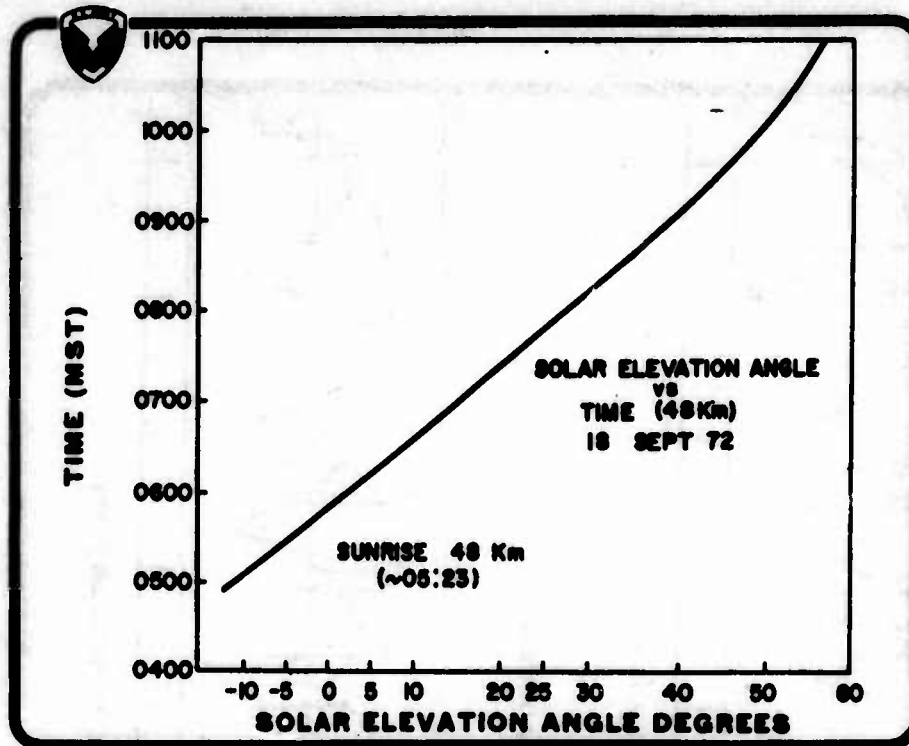


Figure 7. Solar Elevation Angle vs Time

References

- Ballard, H. N., 1961, "Response Time and Effects of Radiation on the VECO Bead Thermistor," Instrument Society of America, Preprint No. 157-LA-61, 27.
- Ballard, H. N., 1967, "A Guide to Stratospheric Temperature and Wind Measurements," COSPAR Technique Manual Series, COSPAR Secretariat, 55 Blvd. Malesherbe, Paris, France, 118 pgs.
- Ballard, H. N., 1968, "Reply," J. Appl. Met., 7, 306-310.
- Ballard, H. N., and R. Rubio, 1968, "Corrections to Observed Rocketsonde and Balloonsonde Temperatures," J. Appl. Met., 7(5), 919-928.
- Ballard, H. N., and B. Rofe, 1969, "Thermistor Measurement of Temperature in the 30-65 km Atmosphere Region," Progress in Astronautics and Aeronautics, Vol. 22, Academic Press, Inc., New York, 141-166.
- Ballard, H. N., N. J. Beyers, M. Izquierdo, and J. Whitacre, 1970, "A Constant Altitude Balloon Experiment at 48 Kilometers," J. Geophysical Research, Vol. 75, No. 18, 3501-3512.
- Ballard, H. N., N. J. Beyers, B. T. Miers, M. Izquierdo, and J. Whitacre, 1972, "Atmospheric Tidal Measurements at 50 km from a Constant-Altitude Balloon," J. Appl. Met., Vol. 11, No. 7, 1138-1149.
- Beyers, N. J., and B. T. Miers, 1970, "Measurements from a Zero-Pressure Balloon in the Stratopause (48 Km)," J. Geophysical Research, Vol. 75, No. 18, 3513-3522.
- Beyers, N. J., B. T. Miers, and R. J. Reed, 1966, "Diurnal Tidal Motions Near the Stratopause During 48 Hours at White Sands Missile Range," J. Atmos Sci., 23(3), 325-333.
- Drews, W. A., 1966, "An Improvement of Atmospheric Temperature Measurements Above 30 km by Means of the Bead Thermistor Mounting Arrangement," National Aeronautics and Space Administration Report, NASL-1611.
- Hind, H. D., 1966, "Temperature Corrections to a Bead Thermistor in the Upper Atmosphere," Weapons Research Establishment, Australian Defense Scientific Service.
- Hyson, P., 1968, "Thermistor Mountings," J. Appl. Met., 7(5), 908-918.
- Ney, E. P., R. W. Maas, and F. W. Huch, 1961, "The Measurement of Atmospheric Temperature," J. Appl. Met., 18, 60-80.
- Pearson, P. H. O., 1964, "Investigation into Response and Corrections to a Thermistor and a Platinum Wire Resistance Thermometer for Temperature Measurements in the Upper Atmosphere," Tech. Note P.A.D. 83, Dept. of Supply, Australian Defense Scientific Service, Weapons Research Establishments.
- Thompson, D. C., and D. P. Kelly, 1967, "The Accuracy of Thermistors in the Measurement of Upper Air Temperatures," J. Appl. Met., 6, 380-385.
- Thompson, D. C., 1968, "On the Errors of a Thin-film Mounted Rocketsonde Thermistor," J. Appl. Met., 7, 306.
- Wagner, N. K., 1961, "Theoretical Time Constant and Radiation Error of a Rocketsonde Thermistor," J. Appl. Met., 18, 606-614.

References

Wagner, N. K., 1964, "Theoretical Accuracy of a Meteorological Rocketsonde Thermistor," J. Appl. Met., 13, 461-469.

"A Survey for Naval Ordnance Laboratory of High Altitude Atmospheric Temperature Sensors and Associated Problems." Contract N-60921-6136, Wright Instruments, Inc., 1961.

Scientific Ballooning And Radiations Monitoring Organization (SBARMO): Origin, Purpose And Possible Future

Harald Trefall
Department of Physics
University of Bergen
Bergen, Norway

Abstract

SPARMO (Solar Particles and Radiations Monitoring Organization) was originally organized mainly for the purpose of coordinating balloon recordings of solar particle radiations, but in recent years the collaborative work of SPARMO groups has focused mainly on recordings of auroral-zone X-ray events associated with precipitation of high-energy electrons. The Organization has tried to further standardization of equipment and the development of safety rules for scientific balloon flights. Because of the increasing attention to practical and technical aspects of balloon flights it has been decided to change the name to SBARMO (Scientific ballooning and Radiations Monitoring Organization). As an international organization it has been affiliated with FAGS (Federation of Astronomical and Geophysical Services), but may in the future possibly be associated with COSPAR (Committee on Space Research) instead.

1. ORIGIN AND ORGANIZATIONAL STATUS

SPARMO was created in October 1961, when a group of European scientists met in Paris to investigate possibilities for cooperation in the scientific use of stratospheric balloons. The principal founders of the Organization were the late Prof. Alfred Ehmert of the Max-Planck-Institut für Aeronomie in Lindau/Harz, Germany, who became the first President of the new organization; and Mr J. P. Legrand of the Laboratoire de Physique Cosmique in Meudon, France, who has served as the Director of the Organization throughout its existence. Official international status was acquired in 1965 through membership in the Federation of Astronomical and Geophysical Services (FAGS) of the International Council of Scientific Unions (ICSU), with the International Astronomical Union (IAU) and the International Union for Geodesy and Geophysics (IUGG) as sponsors.

Quite early a scientific/technical journal entitled the "SPARMO Bulletin" was established, with Mr Legrand as Editor. Its first issue appeared in June 1964. The Bulletin is devoted to technical reports about the use of balloons for scientific purposes and summaries of data from such flights. The Bulletin is now being edited jointly by Mr Legrand and Dr G. Kremser, the latter of the Max-Planck-Institut für Aeronomie, Lindau/Harz, Federal Republic of Germany.

At the annual meeting in 1972 (in Graz in Austria), the future aims of the Organization were discussed, and it was decided that more emphasis ought to be placed upon the technical problems associated with stratospheric balloon flights. In order to reflect this fact, it was proposed to change the name of the Organization to SBARMO (Scientific Ballooning and Radiations Monitoring Organization).

2. MAIN ACTIVITIES

During SPARMO's first years the activity was largely devoted to recordings of solar and galactic cosmic rays and associated modulation effects. Standardized detectors were developed; specifications for solar activity forecasts were drawn up; and a fruitful collaboration was started with the International Ursigram and World Days Service (IUWDS). The importance of this kind of work declined, however, as satellites and interplanetary platforms became available for

more direct measurements of such radiations. On the other hand, some SPARMO groups had already from the beginning been interested in the study of electron precipitation events at high latitudes through the recording of associated bremsstrahlung X-rays. As it was realized that multiple simultaneous recordings over large areas were absolutely necessary for further progress in this field, an increasingly greater emphasis has been placed on the organization and coordination of such flights within SPARMO. This is a field where balloon observations provide information which can be obtained neither by ground observatories nor by rocket-borne or satellite instruments. However, there is now a tendency towards increasing use of balloons for solar and astrophysical studies, not only in countries without opportunities for satellite experiments, but also in satellite-launching countries as opportunities for space flights have become more scarce.

The institutes comprising SBARMO profit from their membership by the exchange of technological and scientific information at annual meetings and through the SBARMO Bulletin. In 1971 a symposium on the "Technology and Utilization of Stratospheric Balloons" was organized in connection with the 14th Plenary Meeting of the Committee on Space Research (COSPAR) in Seattle, U.S.A. Another Symposium, entitled "Research with the Aid of Balloons", is now under preparation by the Deutsche Gesellschaft für Luft- und Raumfahrt with SBARMO as co-sponsor, to be held in October this year.

3. PRESENT COLLABORATIVE EFFORTS

One main reason for SBARMO's existence is as already mentioned the furtherance of cooperation and coordination of the efforts of different groups where such coordination is necessary for scientific reasons. The field where such cooperation is presently most needed is that of measurements of various auroral-zone phenomena, which are themselves manifestations of magnetospheric disturbances.

One of the most important manifestations of magnetospheric disturbances is the precipitation of charged particles, especially electrons, into the earth's atmosphere. Effects observable from the ground are visual emissions (aurora) and enhanced absorption in the ionosphere of radio waves of extra-terrestrial origin. The morphology and time-variations of these phenomena can be linked to processes in the distant magnetosphere, and are therefore important objects

for study. However, when it comes to electrons of relatively high energy (≥ 30 keV), both the sensitivity of the recordings and their response to fast time-variations can be improved by sending scintillation counters to balloon altitudes (typically 30-40 km, corresponding to atmospheric depths of $12-3 \text{ gcm}^{-2}$), to record the associated bremsstrahlung X-rays. They are produced when such electrons are stopped in the atmosphere, at heights around 80-90 km.

Another important phenomenon is the presence of horizontal electric fields in the ionosphere, the gross features of which can be adequately sensed and measured at balloon altitudes, though they could not have been detected from the ground.

VLF-emissions should also be mentioned as an important field for balloon-borne measurements, even though such emissions can be reasonably well detected also from the ground. But problems with man-made noise are largely absent in balloon recordings, and then such measurements provide an opportunity for more direct comparison with balloon-recordings of X-rays and electric fields than is possible when the VLF-measurements are made from the ground. This is particularly important in connection with X-ray measurements, as it is thought that wave-particle interactions are largely responsible for the precipitation of electrons from the outer radiation belts.

Even though rockets or satellites are needed to measure the primary precipitating electrons or in-situ ionospheric electric fields, properly planned balloon recordings have several important advantages with respect to measurements from rockets or near-earth satellites, namely:

- a) In balloon recordings there is, even though balloons do drift with the stratospheric winds, no difficulty in distinguishing between temporal and spatial variations on the timescales in question, whereas this is a major problem in the interpretation of recordings from rockets or near-earth satellites.
- b) Balloons can whilst drifting slowly along the auroral zone, provide the full time history of precipitation events during a whole disturbed period.
- c) Morphological studies of the phenomena in question over large areas are in actual practice possible through simultaneous multiple balloon flights, whereas a corresponding number of rockets or near-earth satellites will hardly ever be simultaneously available in suitable locations, and if so only for very short periods.

Coordinated balloon measurements of X-ray events have been carried out in northern Scandinavia by SBARMO groups since 1960, on some occasions also with simultaneous flights from stations in Iceland or Greenland. The whole region from Scandinavia to Greenland will be of special importance during the forthcoming International Magnetospheric Study (1976-78), because the GEOS satellite will be on a geomagnetic field line connecting with that part of the auroral zone. Also, one of the few practical possibilities for conjugate studies of auroral-zone phenomena exists within that region, as Reykjavik in the northern auroral zone and Syowa station in the southern are geomagnetically conjugate.

Under arctic summer conditions, simultaneous coverage of the region between northern Scandinavia and Greenland can be obtained by launching balloons from a north-south line of stations in Scandinavia and let them drift westwards as they regularly do during that season. The feasibility of this has already been demonstrated during the summers of 1973 and 1974. With normal wind speeds, the balloons take 2-3 days from Scandinavia to eastern Greenland, and another day across Greenland. Telemetry coverage turns out to be possible from land-based stations only, and the problem of determining balloon positions has been largely solved by utilizing the network of CONSOL stations established for navigational purposes.

4. FUTURE STATUS OF SBARMO

The present affiliation of SBARMO with FAGS may not be ideal, as SBARMO cannot provide the kind of continuous or steady monitoring of phenomena like magnetic or solar observatories can. A more proper organizational niche may perhaps be found through an affiliation with COSPAR. Complete integration would not be possible under the present COSPAR statutes however, which limits the activity of COSPAR to measurements from rockets, satellites or space probes. Also it would hardly be desirable from the point of view of SBARMO. On the other hand, the above-mentioned limitation in COSPAR's activities represents a handicap for that organization from the scientific point of view, for the underlying phenomena are of course the same irrespective of whether they are observed from outer space, or from within the atmosphere. The same attitude could of course also be taken to

groundbased measurements. But most balloon measurements are actually more closely related to rocket and satellite measurements than to groundbased measurements, and an affiliation of SBARMO with COSPAR would thus supplement the activities of the latter in a rather natural way. The SBARMO annual meetings might then be coordinated with COSPAR meetings. This possibility is presently being explored.

But irrespective of what decisions may be taken regarding SBARMO's future, we believe it has a useful role to perform. Presently, about 15 groups from 3 continents are members of SBARMO and we hope to increase the membership in the years to come, as we believe this would be to the mutual benefit of all groups involved in this kind of work.

Session 4
Balloon-Borne Experiments

Alvin H. Howell, Chairman
Tufts University

Contents

1. Introduction
2. Historical Footnote
3. Accomplishments With Plastic Balloons
4. Scope of Recent Work

Background On Balloon-Borne Experiments

**Alvin H. Howell
Tufts University
Medford, Massachusetts**

Abstract

A background for the new experiments that are being described at this session is presented by reviewing some of the work that has been done in the past, and summarizing the flight program by AFCRL and NCAR for the past two years to indicate the kind of research that is now being done.

1. INTRODUCTION

Each of the preceding sessions of this Symposium has been devoted to vehicles-tethered, powered, and free balloons. An impressive capability has been demonstrated, and it will surely become more exciting by the time the next symposium is convened. Now it is the user's turn to say what is being done with the marvelous facility. Specific needs by users provide much of the drive, and more importantly, they often generate the funds to keep balloon development going in diverse directions. But as the capability to carry experiments aloft has grown, for whatever reasons, the number of users has multiplied, and each new experimenter has brought

a new job to be accomplished.

Those of you who have attended the preceding symposia and workshops are well aware that a large variety of experiments, and results, have been presented at these meetings. Yet this particular record is only a sample of a much larger number and variety of balloon-borne experiments that have been conducted during this 11-year period. In this session, seven additional papers are being added to the experimenters list.

In presenting a brief review of this topic, as has been requested, it seems appropriate to recall some of the experiments that have been done in the past and then to summarize in somewhat more detail those that have been conducted by AFCRL and by NCAR at their various launch sites, including those from remote locations, during the period since the last symposium. A look at this record will show what is now going on.

Extent of the present activity is most impressive--it amounts to approximately one flight per working day throughout the year. Some experiments are purely scientific, but many are engineering studies or systems tests that certainly must be included in the experimenter's program.

2. HISTORICAL FOOTNOTE

When this Symposium convened on Monday it happened to mark the 190th anniversary of the first balloon-borne scientific experiment. For it was on 30 September 1784 that the American physician John Jeffries and the French balloonist Jean Pierre Blanchard went aloft to make barometric, thermometric, and hygrometric observations. This followed by only 17 months the very first balloon flight ever made, the well known ascent by the Montgolfier brothers who reached the lofty height of 6000 feet, and traveled a carefully measured 7668 feet, in their hot-air aerostat. It is notable that from this very early beginning balloon vehicles were put to use as soon as they became available. What those early experimenters lacked in the way of equipment was surely made up by courage because the experimenters rode with their gear. To fully appreciate how remarkable this pioneering experiment was, it should be noted that it took place only three years after the War of Independence was concluded, only a year after the Treaty of Peace was signed recognizing the independence of the 13 rebelling colonial states, and three years before the first state ratified the new constitution.

Numerous other daring investigators followed, including the renowned chemist and physicist Joseph Louis Gay-Lussac who in 1804 ascended to 23,000 feet to study temperature, humidity, and magnetic phenomena. He also took air samples and found that, except for less water vapor, the chemical composition up to the altitude he

reached was the same as at ground level. In today's session, exactly 170 years later, a paper is offered on air sampling as of 1974. Non-scientific experimentation began early too, a notable example being balloon-borne reconnaissance during the Civil War. President Lincoln established the first air squadron, and put in charge a reckless college professor, meteorologist, and inventor, one Thaddeus Sabiesky Constantine Lowe. He was named Chief Aeronaut of the Union Army, and he commanded a fleet of eight balloons, each 38 feet in diameter with gas capacity of 32,000 cubic feet.

Use of the ancient fabric-type balloons for making measurements at upper altitudes ended in the 30's. Some here can remember the scientific flight in Belgium in 1931 by the Swiss physicist Auguste Piccard, and in America by his brother Jean Felix Piccard and wife in 1934. Also remembered is the meticulously planned Explorer II flight of Stevens and Anderson in 1935, a bonafide scientific balloon-borne experiment that reached 72,395 feet.

3. ACCOMPLISHMENTS WITH PLASTIC BALLOONS

After the war, polyethylene balloons came on the scene, and balloon-borne experiments began to multiply. Although the new vehicle wasn't very reliable, it was immediately used in unmanned flights to examine cosmic rays, make meteorological studies, and carry animals aloft in aeromedical experiments. Balloons and their design improved rapidly in the early 50's, and the uses multiplied. By the end of that decade, in addition to the study of high-energy nuclear particles from outer space, which has continued to the present, concentrations of ozone, carbon dioxide, carbon-14, and nitrous oxide were determined; isotope ratios of oxygen and nitrogen were measured; the presence of radioactive dust from nuclear blasts was detected; radar and photoreconnaissance systems were developed; solar spectroscopy was done; terrestrial magnetism was studied; turbulence, winds, and jet streams at higher altitudes were researched; an artificial moonlight experiment to determine the amount of natural sodium present at upper levels was accomplished; more was learned about radio propagation; many types of instruments and devices were tested, including high-mach parachute systems; satellite equipment was pretested; and rockets were fired from balloons to send experiments up 300,000 feet; to mention a few.

Riders reentered the picture by the middle of the 50's to make geophysical observations, acquire aeromedical research data, and take photographs and spectrograms of the sun and Venus with the aid of a manually operated, servo-stabilized telescope. A qualified astronomer first saw the heavens from the edge of space in the manned Stargazer flight. Most impressive was a live bail-out by Captain Joseph

Kittinger, Jr. from 102,800 feet to study high altitude escape procedures and test a pressurized space suit.

An excellent sample of on-going work since the beginning of the 60's is had by looking at the proceedings of earlier symposia where experiments are described. Many really sophisticated payloads were carried by ever more worthy balloons. A good number of these used precise pointing systems, either uniaxial, biaxial, or triaxial. Some were controlled from the ground, and others had on-board control. Areas of research expanded to include gamma-ray, X-ray, and infrared astronomy, and ultraviolet stellar spectroscopy. Atmospheric science studies continued and expanded using new and better techniques and equipment. Balloon-borne instruments utilized counters, telescopes, chambers, emulsions, radiometers, spectrophotometers, interferometer spectrographs, spectropolarimeters, cryogenically cooled elements, and many other devices. Control of experiments, and the means of storing and handling data improved, including the use of computer-compatible, on-board digital recording. Manned flights are also described, one of which used unique clusters of small balloons to support the pressurized gondola and associated telescope. The record contains many carefully prepared papers that deserve rereading by those having particular interest in the subjects discussed. Numerous of these present results as well as descriptions of the experiments and apparatus.

4. SCOPE OF RECENT WORK

Information about balloon-borne experiments during the past two years has been provided by Tom Danaher of AFCRL and by Robert Kubara and Ralph Harju of NCAR. Activities by these two groups represent a major portion of the total flight program.

A fundamental feature of the AFCRL operation is that roughly half of it is devoted to the development of new capability, including tethered balloons, and the testing of systems and equipment. Scientific experiments are concerned with relevant Air Force mission requirements, and are not solely aimed at advancing scientific knowledge. A good many of the scientific studies of the last two years relate to atmospheric sciences, but some are in the area of cosmic-ray, gamma-ray, X-ray, and infrared astronomy, and some are concerned with high-energy particles. Experiment types which have usually been flown several times include measurements of aerosol particle concentration and size distribution as a function of altitude; measurement of scattering and absorption characteristics versus altitude; turbulence measurements; auroral studies; particulate debris sampling from specific altitudes in the Northern Hemisphere; lower atmospheric composition and temperature experiments to determine solar radiation spectral intensities in the UV, cosmic

radiation flux, atmospheric constituent number densities in the mass number range 12-100, positive ion number densities, and related atmospheric temperature, pressure, and wind velocity; measurement of ozone, water vapor, nitrous oxide and nitric acid concentrations in the lower atmosphere; study of processes important in distribution of pollutants; polarization characteristics and measurements of angular light scattering properties; testing of air quality devices; laser experiments to determine effects of the atmosphere on optical propagation over a vertical path; radio transmission experiments from balloon to balloon to study ducting; infrared background measurements; infrared radiance from the planets and stars; gamma-ray spectral measurements.

Strictly engineering and evaluation experiments include UHF beacon tests; use of balloons in a UHF relay arrangement; evaluation of parachutes, including packed configurations; test of VIKING lander decelerator; test of all kinds of flight equipment; evaluation of the design of a solar flare particle detector prior to satellite use; evaluation of the capabilities and limitations of acoustic and infrared homing equipment; test of Pathfinder instrumentation; test of powered balloon components.

While many balloon flights are devoted to a single experiment, a number of those in the AFCRL record have involved a multiplicity of equipments to measure a variety of parameters simultaneously. A fine example is the stratospheric composition experiment which consisted of 24 individual experiments aimed at determining simultaneously the incident solar ultraviolet radiation; atmospheric composition; thermal, flow, and charged particle structure; cosmic radiation levels; and aerosol layers as they vary in time and space. Involved in this experiment were ultraviolet spectrometers; water vapor, ozone, and nitric oxide sensors; cryogenic atmospheric sampler for the determination of the nitrogen, oxygen, water vapor, and carbon dioxide concentrations; temperature and pressure sensors; cameras to photograph falling chaff and small spheres; three component anemometers for the determination of air flow relative to the balloon; radar reflectors for the determination of wind speeds from the radar track of the balloon; atmospheric turbulence sensors; positive ion and Gerdien condenser probes; cosmic ray sensors; and cameras to photograph aerosol layers.

Special mention should also be made of the lower atmosphere composition and temperature experiment (LACATE) which involved multiple experiments by a number of agencies done within a confined geographical area and conducted within a two-day interval. This large scale study of a cone in the atmosphere involved six multiple-experiment balloon flights, three by AFCRL, one by NCAR, and two by the University of Wyoming. These balloon-borne experiments were coordinated with other data-collecting means including aircraft and rocketsondes.

An especially notable feature of some of the AFCRL flights is the total isolation of the experiment from the balloon environment by reeling the experiment down to a position far below the balloon itself. This capability often has particular value.

A summary prepared by Mr. Harju shows particularly well the nature of the scientific balloon-borne experiments that were flown by NCAR since the beginning of 1972. Statistics were provided by him in the following categories: astronomy flights which include ultraviolet and infrared measurements of celestial bodies; polarimetry, photography, solar, gamma, and X-ray experiments; cosmic ray flights which include search for primary and secondary cosmic rays, high-energy particles and interactions and emulsions; atmospheric sciences and research and development flights.

There is breakdown about the experiments to show such things as use of precise or rough pointing, use of cryogenics in cooling detectors or optics, whether the experiment was programmed from the ground or by on-board means, whether the data were recorded or telemetered or both, whether the experiment was a nighttime or a daytime study, whether the data were collected on ascent and descent as well as at ceiling altitude, and whether the experiment was linked with the computer facility at Palestine. Also included in the summary is the average payload weight and the average flight duration.

Breakdown of the 71 flights made during 1972 is:

<u>Astronomy Flights</u>	36
Telemetry used	36
On-board data recording also	1
Precise pointing used	32
Rough pointing used	1
No pointing	3
Cryogenics used	11
<u>Far Infrared Experiments</u>	9
Near infrared experiments	4
Ultraviolet experiments	4
Programmed with no update by command	2
Programmed and updated by command	28
Linked with the computer facility	0
Night flights	20
Day flights	6
Both day and night flights	10
Data collected on ascent and float	1

<u>Cosmic Ray Flights</u>	14
Telemetry used	12
On-board data collection also	6
Emulsion flights	2
Cryogenics used	2
Linked with computer facility	0
Night flights	2
Day flights	3
Both night and day flights	9
<u>Atmospheric Sciences Flights</u>	11
Telemetry used	6
Data collected on ascent	2
Data collected on ascent, float and descent	3
Data collected at float and descent	3
Night flights	1
Day flights	10
<u>Research and Development Flights</u>	10
Telemetry used	7
Night flights	1
Day flights	8
Both night and day flights	1

The average payload weight was 1971.6 pounds during 1972. One flight had a payload of 6155 pounds, which was the heaviest payload launched by the dynamic method to this date. The average time at float altitude was 8.4 hours for all the flights excluding the Research and Development flights.

During 1973 a total of 94 flights were made with breakdowns as indicated in the following tabulation.

<u>Astronomy Flights</u>	50
Telemetry used	50
On-board data recording used also	1
Precise pointing used	43
Rough pointing used	2
No pointing	5
Cryogenics used	21
Programmed and updated by command	39
Far infrared experiments	20
Ultraviolet experiments	1
Near infrared experiments	1
Linked with the computer facility	14

Night flights	21
Day flights	16
Both day and night flights	13
Data collected on ascent and float	1
Multiple experiments	1
<u>Cosmic Ray Flights</u>	21
Telemetry used	12
On-board data recording also	4
Emulsion flights	9
Cryogenics used	1
Linked with computer facility	2
Night flights	5
Day flights	1
Both night and day flights	15
<u>Atmospheric Sciences Flights</u>	16
Telemetry used	9
On-board data collection only	7
Data collected on ascent	5
Data collected on ascent, float and descent	4
Data collected at float and descent	4
Data collected at float only	3

Research and Development had a total of seven flights, two of these were zero pressure balloons, flown during the day and one used telemetry. The other five were superpressure flights launched from Toowoomba, Australia. In addition to being Research and Development flights, two of them had gamma ray experiments, two had micro-meteorite collectors and the other had a cosmic ray experiment.

The average float time of all flights, excluding the two Research and Development flights and the five superpressure flights, was 8.3 hours and the average payload was 1638.1 pounds.

Contents

- 1. Introduction**
- 2. Science Objectives and Implementation**
- 3. Mission Implementation**
- 4. Technology Problems**
- 5. Conclusions**

Venus Balloon Systems

Patrick C. Carroll
Senior Staff Engineer

Charles L. Deets
Senior Engineer

Martin Marietta Corporation
Denver Division
Planetary Programs Department
P. O. Box 179
Denver, Colorado

Abstract

The planet Venus is shrouded with a very dynamic carbon dioxide atmosphere, dense cloud layers containing sulphuric acid and mercury compounds, and surface temperatures near 800°K. Recent Mariner 10 TV pictures of Venus cloud formations, as well as data obtained by flyby and descent probes, have increased the scientific interest in this planet. This paper describes the preliminary design of balloon systems that could complement Venus probe and orbiter missions being planned by NASA. Probe-deployed balloons into the Venus atmosphere offer the potential for determining circulation patterns as well as direct measurements of composition, structure, and cloud physics. Also, with the addition of droppable payloads, both vertical profile measurements through the atmosphere and surface structure measurements can be obtained.

Comparison of environments shows that at comparable ambient pressures the Venus atmosphere temperature is about 50°K higher than that of Earth. Also, above the heavy cloud tops, at about 200 mb pressure, the ultraviolet radiation damage to the balloon becomes important for long-life missions because of the equivalent two-sun intensity.

The challenges unique to the Venus balloon mission include entry into the Venus atmosphere, reliable balloon deployment and inflation, survival in the environment, and balloon tracking from either an orbiter or directly from Earth. A typical balloon system design that meets these requirements is described, and some mission options including dropsonde operations for vertical wind profiles and penetrometers for surface structure measurements are included.

1. INTRODUCTION

Although the subject of this symposium is the development and use of balloon systems for scientific exploration of Earth's atmosphere as well as commercial or other applications, the balloon system technology provides a unique opportunity to contribute to NASA's long-range programs to explore the solar system. NASA's plans include a balanced program of exploration of the planets, their satellites, comets, asteroids, and out-of-ecliptic missions.

However, of immediate interest are the atmospheres of Earth's two nearest and most similar planets, Mars and Venus. On Mars, the thin atmosphere appears to be nearly in radiative equilibrium and dynamic effects on temperature distribution are small. Although a simple physical situation, it represents one extreme of Earth's atmospheric behavior. On Venus, the opposite extreme is true because its atmosphere has very large densities and dense clouds minimize the effects of radiation so that the temperature field is expected to be dominated by dynamical wind systems. This concept tends to be confirmed by the UV photos of the upper cloud structures of Venus shown in Figure 1. In Earth's atmosphere, the radiative and dynamical influences are more nearly of equal importance, resulting in a complex problem. We therefore can expect fundamental gains by studying these simpler atmospheric systems provided by nature. Indeed, any knowledge of the state represented by the atmosphere of Venus may be overwhelmingly important as Earth's atmosphere becomes more turbid through progressive pollution (Space Science Board, 1970).

In the past, both US Mariner spacecraft and Russian Venera probes have made important measurements of the Venus atmosphere, and the current NASA Pioneer Venus probe mission will send entry descent probes to the surface of the planet. As important as these missions are, it still remains for a series of balloon probe missions to define the large-scale atmospheric circulation patterns at various altitudes around the planet and to measure the heat flux at various levels within the clouds.

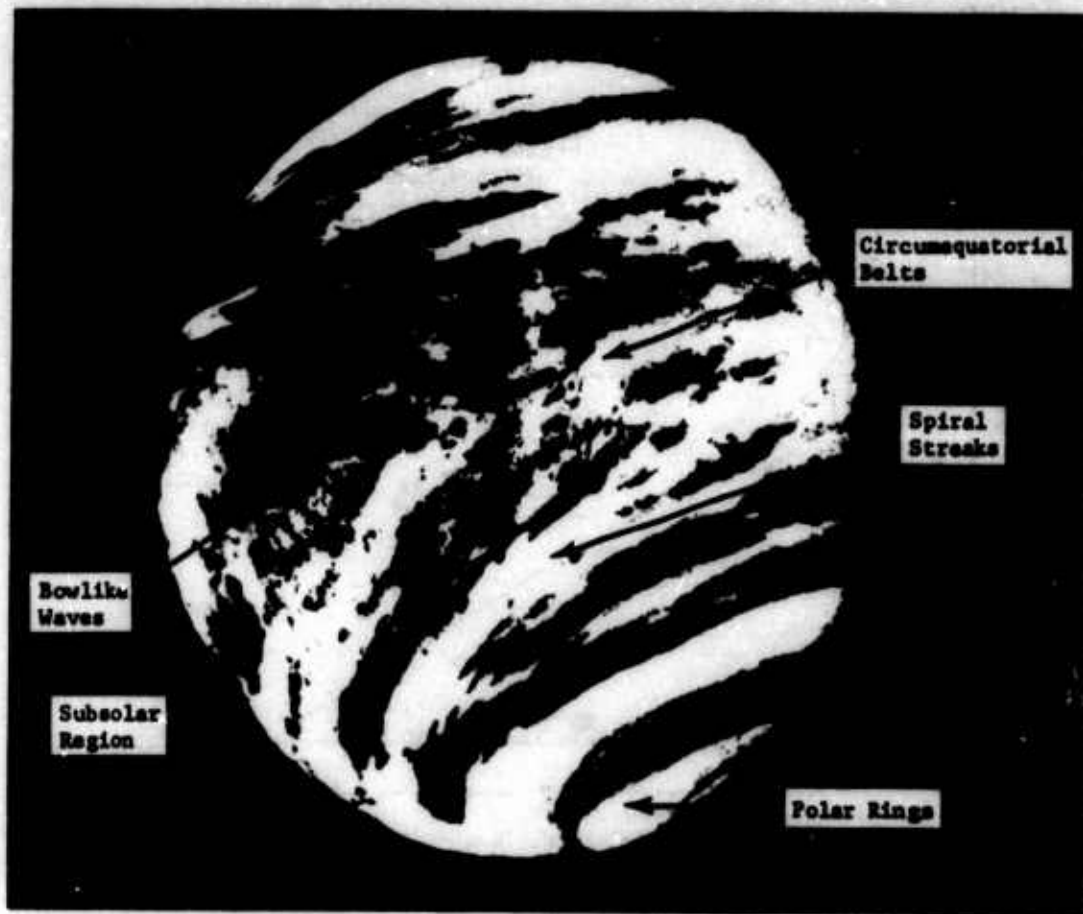


Figure 1. Venus Cloud Patterns, Ultraviolet View (NASA-JPL Mariner 10 Photo)

Comparison of the environments in Figure 2 shows that at typical float altitudes and comparable ambient pressures, the Venus atmosphere temperature is about 50°K higher than that of Earth. Also, above the heavy cloud tops, at about 200 mb pressure, the ultraviolet radiation damage to the balloon becomes important for long-life missions because of the equivalent two-sun intensity.

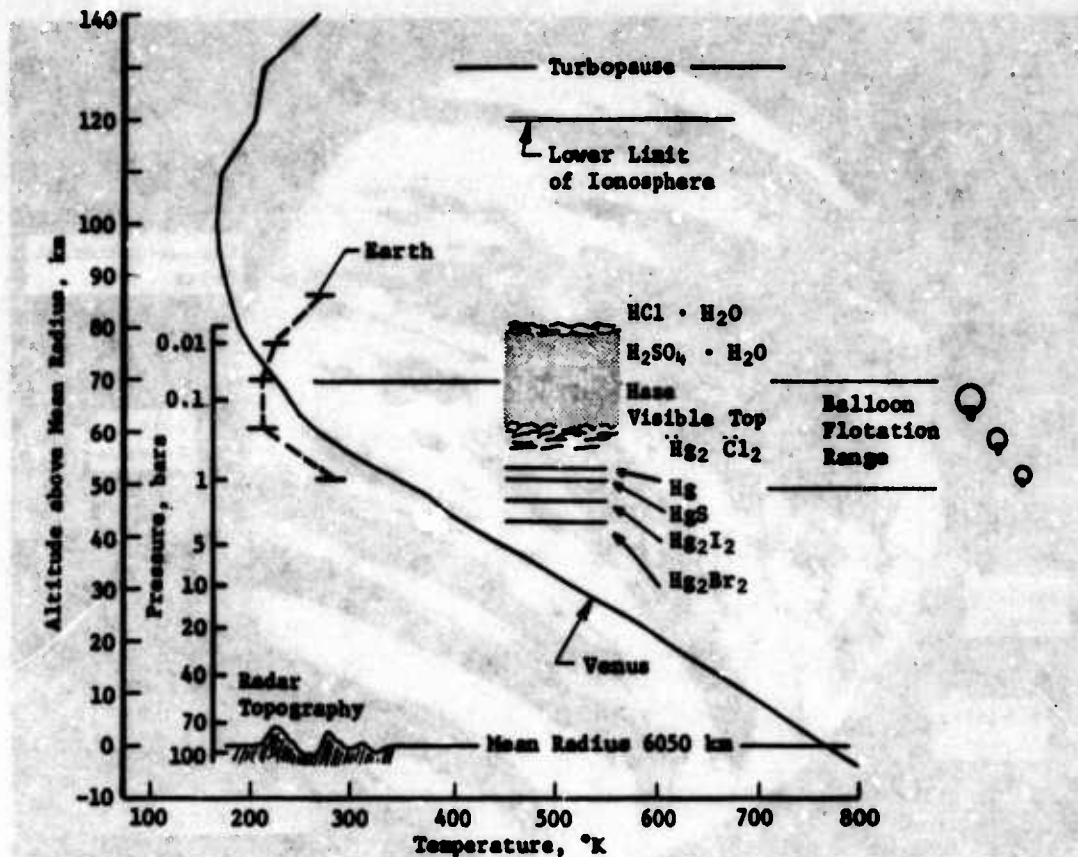


Figure 2. NASA SP8011 Venus Atmosphere (1972) with Earth Comparison

2 SCIENCE OBJECTIVES AND IMPLEMENTATION

In order to answer some of the fundamental questions about the Venus atmosphere, it is necessary to establish certain scientific objectives--which then provide the basis for the mission and balloon probe design criteria. These scientific objectives are listed in Table 1 and the science instruments that can provide measurements to support these objectives are also shown. The primary objective of a balloon mission is to determine the large-scale circulation patterns of the planet's atmosphere and only balloons can reasonably accomplish this. However, many balloon mission options are possible and if sufficient payload capacity is available, many or all of the objectives of Table 1 can be accomplished. Studies have been made to compare several small balloons targeted to various altitudes with a single, large balloon that carries all of the science instruments shown. The actual mission science objectives and specific instruments to be flown will be chosen to complement previous data obtained by the Pioneer Venus descent probes and by flyby or orbiting spacecraft.

Table 1. Science Objectives and Related Instruments

Science Objectives	Instruments											
	Balloon Position Tracking	Mass Spectrometer	Gas Chromatograph	Solar Flux Spectrometer	IR Flux Spectrometer	Nephelometer	Pressure	Temperature	3-Axis Accelerometer	Dropsonde	Radar Altimeter	Penetrometer
Atmosphere Circulation	D	N	N	R	R	N	R	R	N	D	R	N
Atmosphere Composition and Structure	R	D	D	R	R	N	R	R	D	D	N	N
Cloud Composition and Structure	R	D	D	D	R	D	R	R	N	N	N	N
Thermal Balance	R	R	R	D	D	N	R	D	N	N	N	N
Density, Pressure and Temperature	N	N	N	N	D	N	D	D	R	R	N	N
Small-Scale Turbulence*											R	N
Surface Profile*									N		D	N
Surface Structure*									N		R	D

D = Direct Measurement
R = Related
N = Not Related
* = Secondary Objective

Atmospheric circulation patterns would be measured by tracking the balloon as it drifts with the wind using range and range rate techniques. This tracking can be accomplished by the Earth-based Deep Space Network (DSN) when the balloon is on the Earth side of Venus. Tracking from an orbiting spacecraft would provide more accuracy and allow the balloon to be tracked on the backside of the planet. If atmospheric circulation is the major consideration for the Venus balloon mission, then several small balloons at various altitudes would be used. A typical mission that has been investigated uses 10 small balloons in conjunction with the Venus Orbiting Imaging Radar (VOIR) mapper. The balloons carry pressure and temperature sensors and a tracking transponder.

A more sophisticated atmospheric circulation mission would include two balloons in conjunction with the Venus Orbital Imaging Radar mission. These balloons would contain pressure and temperature sensors, a solar flux sensor, radar altimeter, and seven dropsondes as shown in Figure 3.

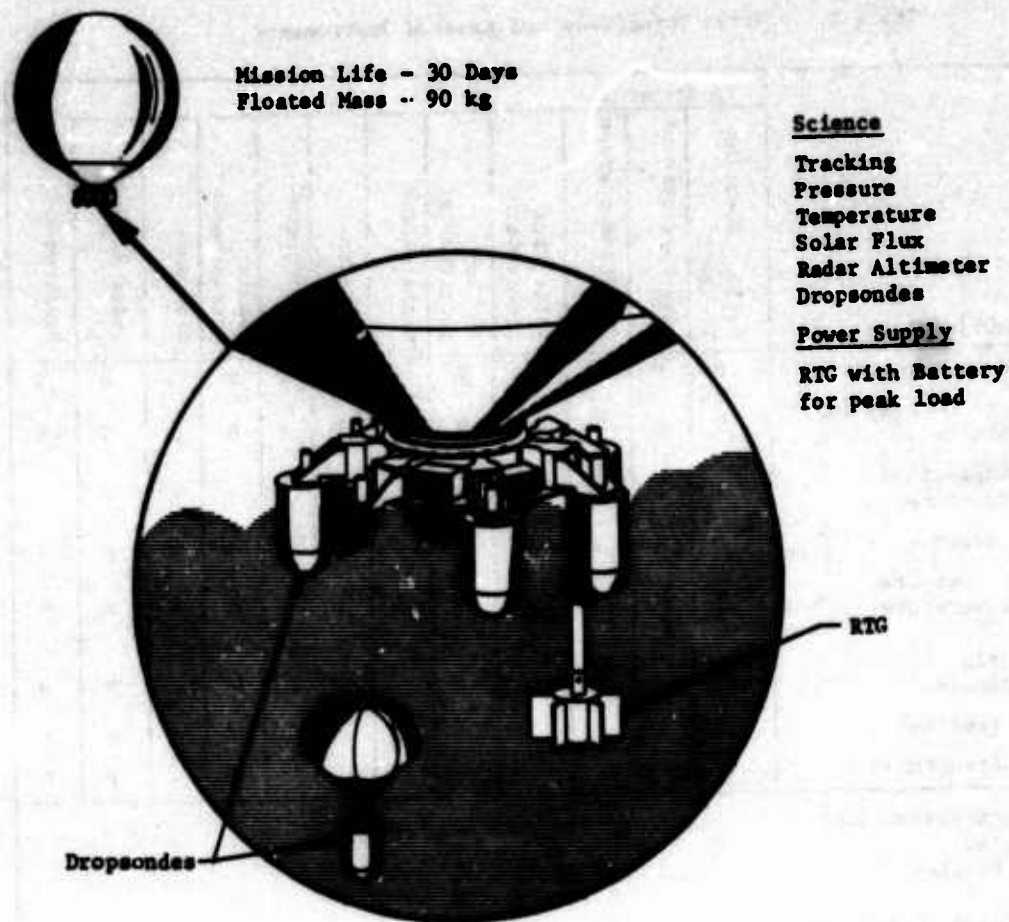


Figure 3. Venus Balloon System, Floated Configuration

The dropsondes would contain pressure and temperature sensors and a tracking transponder. The tracking transponder would provide a link to the Earth Deep Space Network. Using Doubly-Differenced Long Baseline Interferometry (DLBI) techniques, it is possible to obtain wind velocity profiles accurate to 1 meter per second and position errors on the order of 1 kilometer. To take advantage of this technique, the wind profile dropsondes would be released only on the Earth side of Venus. The pressure and temperature telemetry would be transmitted to the balloon for storage and/or relay to the orbiter.

The atmosphere and cloud composition can be accurately determined by appropriate instruments because the balloon provides a long mission time. The balloon may float into various cloud formations and changing latitudes. Because super-pressure balloons maintain a constant density altitude, it would be desirable to target balloons to float at several altitudes.

Both variable-altitude balloons and dropsondes have been studied to provide vertical profiles of winds and other measurements. The variable-altitude balloon has some very interesting possibilities; however, it is more complex and carries less useful payload than the conventional system. The dropsondes not only provide the vertical data but act as ballast release, thus giving the balloon added endurance.

Another interesting instrument is the penetrometer that when dropped onto the surface provides clues to the surface structure for a meter or two of depth. It is difficult to obtain more penetration because of the low terminal velocities of the device due to the extremely dense atmosphere. However, 1 meter of penetration is sufficient to correlate with radar maps to be obtained by the Venus orbiting mappers that may fly simultaneously with this mission. With prior target areas identified, the penetrometers can be released on command reasonably near these areas or, with some luck, directly into the target regions.

Another Venus balloon mission that has been evaluated is a large floating laboratory to study atmosphere composition. This balloon system would contain a mass spectrometer and a gas chromatograph for chemical analysis and isotope ratio experiments. Cloud particle and dust detection will be accomplished by a nephelometer or an attenuated total reflectance spectrometer. Light levels would be measured by a solar flux sensor and an IR spectrometer. The solar flux instrument would have four sensors to measure solar input from all directions. Turbulence would be sensed by a triaxial accelerometer. A radar altimeter would give a rough surface profile.

At the end of the mission, the balloon would be deflated on command and would take measurements as it descends. Studies indicate that the balloon could descend to about 30 kilometers altitude before the electronics temperature limits are exceeded.

3. MISSION IMPLEMENTATION

3.1 Launch Opportunities

Venus mission launch opportunities occur about every 18 months with the period of interest including September 1978, March 1980, November 1981, and May 1983. The Pioneer Venus descent probes are to be launched in September 1978 and will arrive at Venus about 4 to 5 months later. Although NASA's long-range plan shows

a Venus balloon mission early in 1985, these plans are subject to change in priority depending on the discoveries of earlier missions to Venus; therefore, the earliest balloon mission might occur in 1980 or 1981. Studies of a balloon mission in conjunction with a Venus orbiter radar mapper in 1983 have shown some very interesting mutual benefits. The orbiter could provide balloon tracking and the balloon could provide penetrometers to be targeted to areas of interest on the planet surface.

3.2 Balloon System Design

The balloon system will arrive at the planet Venus packaged inside an entry aeroshell and be deployed as shown in Figure 4.

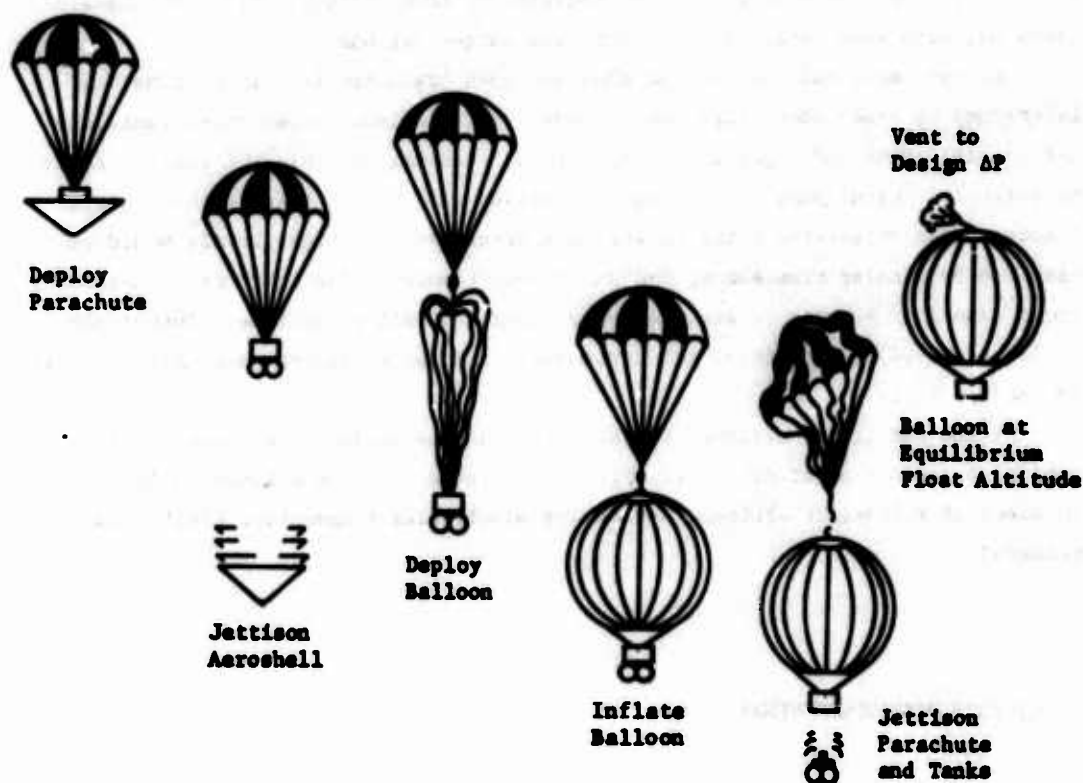


Figure 4. Deployment Sequence

After the entry vehicle has experienced the entry loads and heating and slowed to a subsonic velocity, a barometric switch will signal parachute deployment and aeroshell jettison. The balloon system would then be descending through the atmosphere at approximately 10 meters per second. At the design float altitude, another barometric switch signal deploys the balloon. The control unit sends sequenced signals to inflate the balloon and jettison the parachute and tanks. Additional signals from the control unit deploy the Radioactive Isotope Generator (RTG) and activate the superpressure control system. The balloon is initially inflated with about 10% excess gas. The balloon begins to recover and rise as the inflation gas heats and expands. As the balloon approaches its design altitude, the excess gas is vented and the superpressure is limited to its design value. The superpressure is adequate to allow the balloon system to cross from the light to the dark side of the planet.

Packaging the balloon system inside the aeroshell is a significant problem. The balloon must be packed inside a canister of minimum volume and stored for several months. The gondola must be minimum weight yet withstand the 400-g entry environment. If an RTG power supply is used, the excess heat must be transmitted outside the aeroshell during the 4- to 5-month interplanetary cruise period. For most balloon system designs, an oblate spheroid-shaped inflation gas tankage system is required to maintain the aeroshell center of gravity within proper limits to assure stability during entry and descent through the atmosphere. A typical balloon system inside the aeroshell is shown in Figure 5.

The balloon system entry vehicle is carried on board a spacecraft or bus during the launch and interplanetary cruise portion of the mission. Figure 6 shows two balloon system entry vehicles installed on the Venus Orbiter spacecraft in the launch configuration. The balloon system entry vehicles would be deployed and spun-up for stabilization prior to the orbit insertion burn of the spacecraft. The balloon system would then transmit data to the orbiter for storage and/or relay to Earth. A Pioneer spacecraft could also be used for the balloon entry probe bus and orbiter.

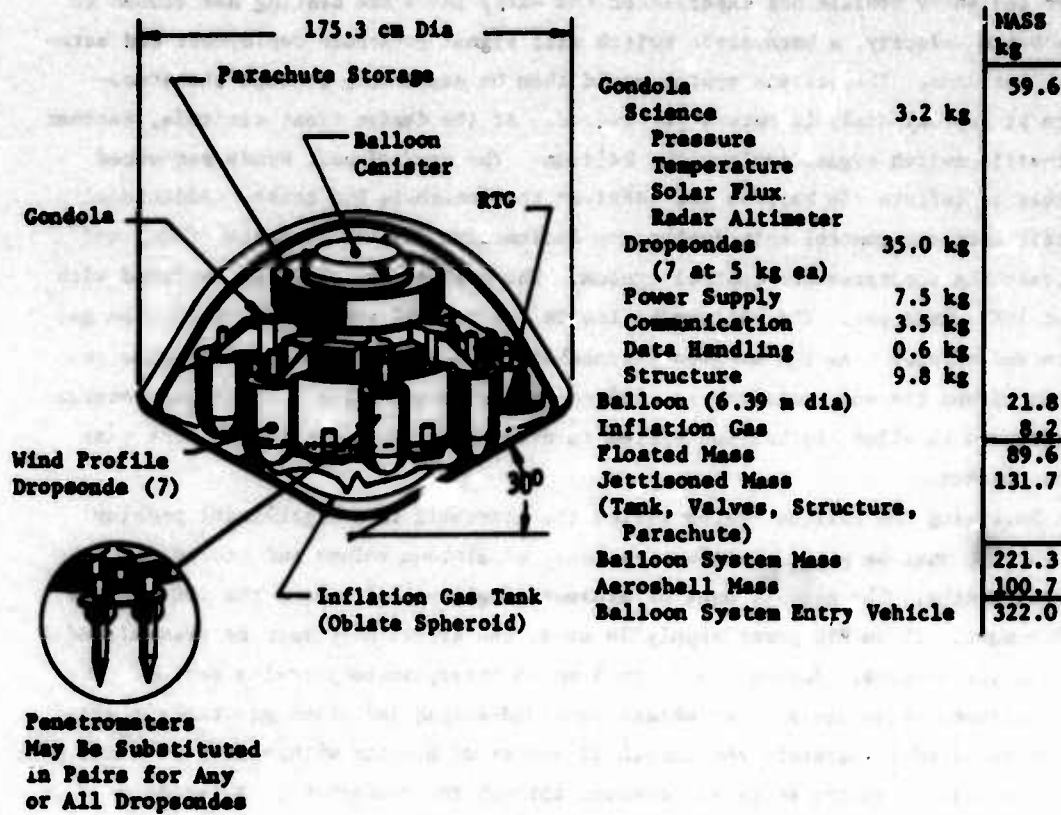


Figure 5. Venus Balloon System, Dropsonde Configuration

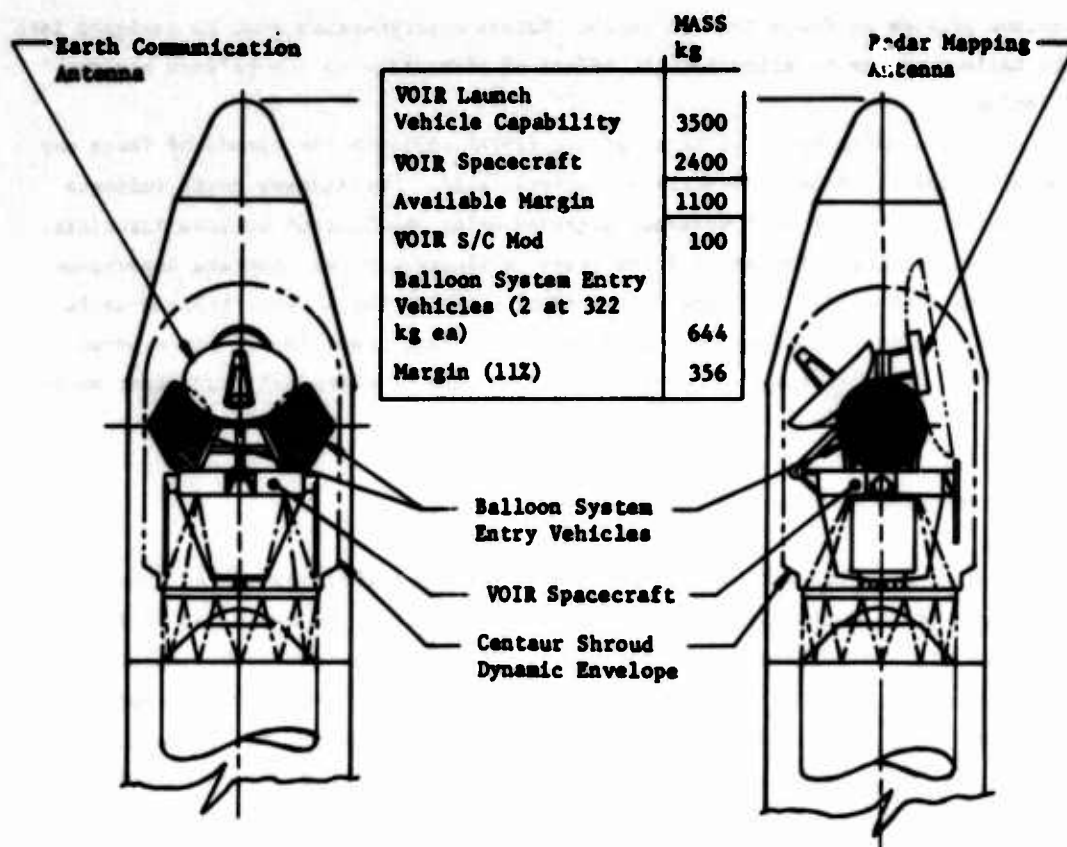


Figure 6. Venus Balloon System on VOIR Spacecraft

The Venus balloon system must withstand the launch, interplanetary cruise, entry, deployment, and operational environment. Tests indicate the balloon can be packed to a density of approximately 384 kg/m^3 (24 lb/ft^3). The balloon must be deployed and inflated at a descent velocity of approximately 10 meters per second. This has been accomplished in a wind tunnel with a 5-meter diameter Mylar* balloon. The flapping effects on the balloon can be minimized by rapid inflation of the balloon (approximately 1 minute). The balloon design superpressure is influenced by the attenuation of the solar flux through the Venus atmosphere. Current analysis indicates the balloon would receive approximately one Earth sun at 500 mb pressure altitude (56.6 km). At float altitudes of interest, the ambient temperature on Venus is about 50°C higher than the same pressure altitude on Earth. This means the inflation gas permeation through the balloon material is a much more

*Mylar is an E. I. DuPont de Nemours trade name for polyethylene terephthalate.

serious problem on Venus than on Earth. Excess superpressure must be designed into the balloon system to allow for the effect of permeation on the balloon mission lifetime.

Recent studies by J. L. Regas *et al.* (1974) indicate the clouds of Venus may contain droplets of 80% concentrated sulfuric acid. Preliminary tests indicate this concentration of acid severely degrades Mylar and Dacron* balloon materials. But there are other classes of films (such as fluorocarbons) that are impervious to concentrated acids. It appears the ideal material for a Venus balloon would be a trilaminate consisting of a permeation-resistant inner layer, and a woven scrim material for strength, covered by a thin film of chemically resistant material.

3.3 Balloon System Tracking

Balloon tracking can be accomplished by various techniques either directly from Earth or in conjunction with an orbiter. On Earth, the use of an orbiter satellite with range measurement for balloon tracking provides position location of approximately 3- to 5-kilometer accuracy. A Venus orbiter with the capability of providing both range and range rate measurements can locate the balloon within about 1 kilometer under ideal conditions; however, if the balloon is directly under the orbital path, the accuracy degrades. The most powerful tracking technique available uses Earth-based tracking stations of the Deep Space Network in conjunction with an orbiter. The technique is called Doubly-Differenced Long Baseline Interferometry, and this technique can provide position accuracy of less than 1 kilometer and rate accuracy (for wind profiles) of less than 1 meter per second. In this technique, the orbiter provides a known reference and the Earth-Venus transmission errors are differenced or cancelled out. For determination of the large scale atmospheric circulation, the position location capability is well within the required accuracy; for determination of vertical wind profiles using dropsondes, the DLBI technique is sufficient.

*Dacron is an E. I. DuPont de Nemours trade name for the fiber form of polythethylene terephthalate.

3.4 Dropsonde Operation

Dropsondes may be released from the balloon system to obtain vertical wind profiles. The wind profile dropsondes shown in Figure 7 weigh 5 kg each. They contain pressure and temperature sensors and a one-way link to the DSN for tracking. The sondes are designed to drop from 60 km altitude to 15 km in approximately 31 min for maximum tracking accuracy. A cross parachute is used to slow the descent of the sonde. Existing data indicates that most of the winds are above 15-kilometer altitude (Ainsworth and Herman, 1974). A slightly different configuration dropsonde could be used to investigate the atmosphere to the surface. A parachute would not be used on this configuration. It would descend from 60 to 15 km in approximately 21 min and from 60 km to the surface in 39 min. This configuration would allow investigation of the surface at the expense of tracking accuracy. The dropsonde to the surface would weigh approximately 0.6 kilogram more than the 15-kilometer dropsonde because of the extra insulation required.

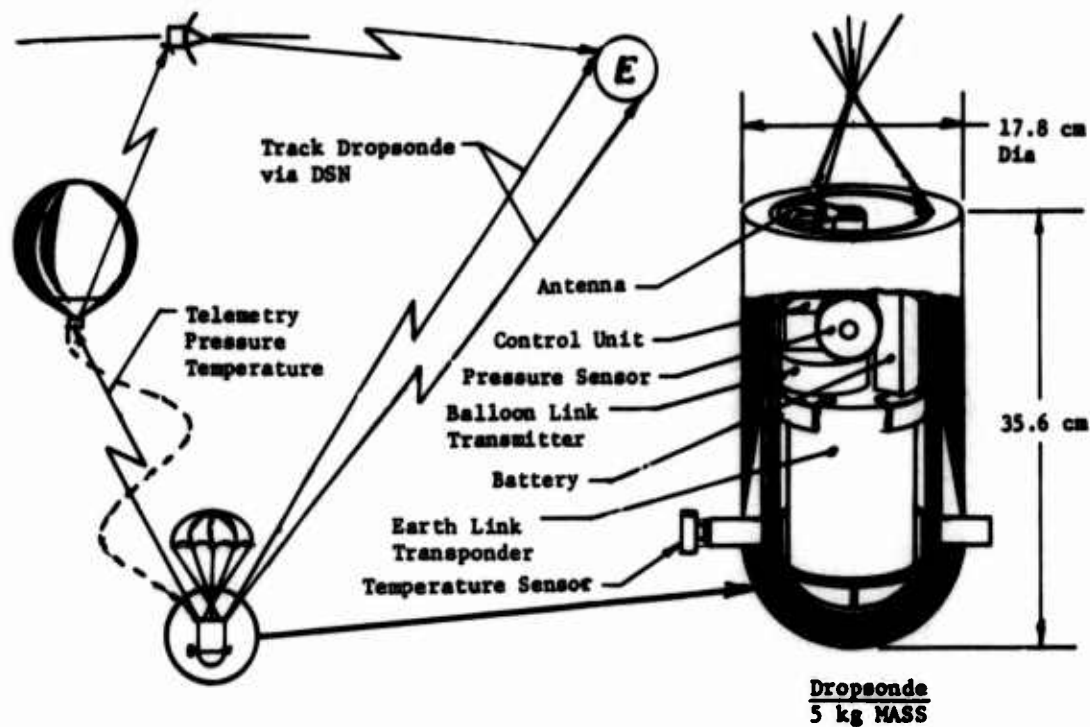


Figure 7. Wind Profile Dropsonde, Venus Balloon System

3.5 Penetrometer Operation

Surface penetrometers can replace dropsondes as required; two penetrometers could be installed for each dropsonde. When the balloon floats over previously mapped features on Venus, the penetrometers would be released to obtain an indication of the surface composition. The penetrometers would be released in salvos; probably three per salvo to reduce the uncertainty of the measurements. The accelerometer data is used to infer subsurface material properties and layering. This technique has found extensive use on Earth for investigating remote sites. On Venus, the high atmospheric density limits impact velocities to approximately 100 meters per second for even the most efficient aerodynamic shapes. S. J. Ducaai *et al.* (1970) estimate the surface of Venus to be between a sandstone type rock and hard dry silt or clay. Figure 8 shows a typical penetrometer design and expected depth of penetration into the Venus surface. This penetration is considered adequate for correlation with the Venus radar map.

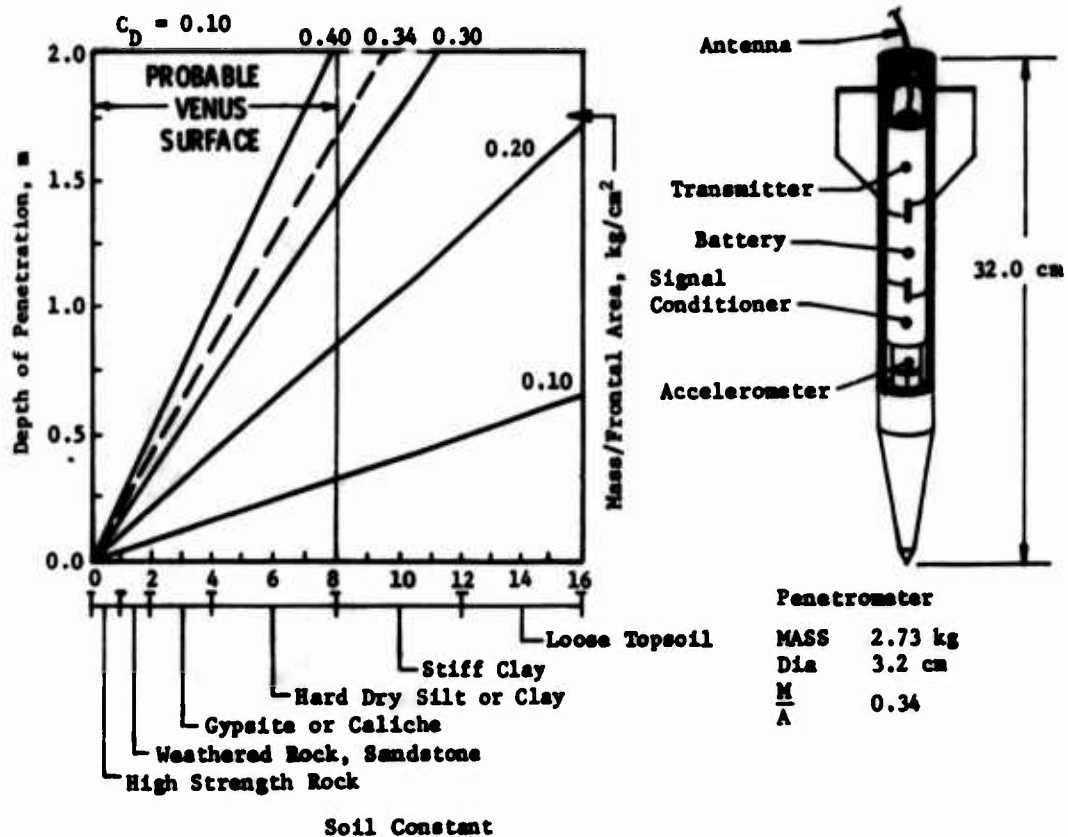


Figure 8. Surface Penetrometer, Venus Balloon System

4. TECHNOLOGY PROBLEMS

The Venus balloon mission presents two technology problems that are considerably more difficult to solve for the Venus application than for the Earth case. These are balloon deployment and balloon materials development to provide a reliable balloon system that can survive the chemical, thermal, and ultraviolet environment for a sufficient period of time.

A reliable packaging, deployment, and inflation technique is critical to the success of the Venus balloon mission. For a typical Venus balloon probe mission, the entry vehicle must decelerate to subsonic velocity, deploy a parachute to separate the balloon probe, and further decelerate it to a very low descent velocity suitable for balloon deployment. When the balloon is deployed, it is subjected to the airstream and is susceptible to flutter and large-scale flapping. Possibility of damage at this time can be reduced by rapid inflation to minimize exposure time and by the inherent ruggedness built into the balloon skin. Balloon size and descent velocity also affect the behavior of the balloon during this critical period.

By contrast, scientific balloons used on Earth are unpacked, deployed, and launched with the greatest of care and gentle handling. Balloon damage is usually sustained during handling, shipping, or launching; however, once the balloon reaches its operating altitude its chances of mission survival are very good. In some cases, such as with the superpressure balloons used in the National Center for Atmospheric Research (NCAR) GHOST program, the balloons are tested for leakage and other damage before launch. No such opportunity is available for the Venus probe balloon. Therefore, packing, deployment, and inflation concepts must be capable of providing a minimum of abuse to the balloon. Acceptable concepts will probably vary with balloon size and ruggedness because a large, fragile balloon designed for higher float altitudes will be more difficult to deploy and inflate than a small, rugged balloon.

Balloon materials development can probably be done using state-of-the-art materials. Nevertheless, new combinations are required that can resist UV damage, control permeation at elevated temperatures, resist sulfuric acid degradation to both strength and optical properties, and resist leakage due to packaging and deployment stresses. Various laminates have been under study for some time and the appropriate combination for this balloon mission appears to be attainable with additional research.

Martin Marietta, under contract to NASA, has conducted extensive screening tests of candidate balloon materials (P. C. Carroll, 1969). An attempt was made to simulate many of the anticipated environmental conditions that would be

encountered on a Venus mission, including initial handling abuse, packing sterilization (no longer a requirement), long-term storage, entry high-g loading (400 g), and ultraviolet exposure equivalent to a typical mission in the upper atmosphere of Venus.

Test results showed that single films do receive pinhole damage if subjected to certain types of abuse and that bilaminates of these films do effectively control pinholing as was expected. Testing provided a relative ruggedness comparison for the various materials that was not previously available. Scrims (loose net weaves) and fabrics demonstrated a much higher strength-to-weight ratio than the films alone, and provided a rugged rip-stop character to the outer surface of the material. There was evidence of damage to varying degrees on all materials due to the environmental exposures; however, certain materials proved superior for the balloon application.

Tests are under consideration that were not included previously. These involve a chemical environment test in which the candidate materials are exposed to the anticipated cloud compounds, temperature, UV, and atmospheric environment of Venus for durations equal to typical mission times. For the expected usable float altitudes between 1200 mb (50 km altitude, 350°K) and 50 mb (69.5 km altitude, 225°K), the current Venus atmosphere models indicate various mercury compounds and hydrochloric and sulphuric acids. The sulphuric acid is estimated to be an 80% concentration in droplet form. Study and testing is in order to determine whether extended exposure of balloon materials at the environmental temperature, pressure, and solar radiation conditions might result in significant degradation of strength or optical properties.

5. CONCLUSIONS

Probe-deployed balloons into the Venus atmosphere offer the potential for determining circulation patterns as well as direct measurements of composition, structure, and cloud physics. Also, with the addition of droppable payloads, both vertical profile measurements through the atmosphere and surface structure measurements can be obtained.

Past studies have shown that many Venus balloon mission options are practical and these options range in complexity from a simple balloon with a tracking transponder to large, scientifically complex, buoyant stations with droppable payloads. These balloon missions may be flown with or without a supporting orbiter for use in tracking and data relay. Earth-based tracking and direct link communications are practical and provide necessary coverage on the Earth-facing hemisphere of the planet. However, a supporting orbiter adds the capability of balloon tracking over a much larger area of the planet and provides an accurate reference vehicle when applying the powerful tracking techniques of DLBI.

A Venus orbiting spacecraft provides an excellent support vehicle for the balloon mission. Likewise, the balloon probe can provide valuable support to a radar mapping mission by dropping surface penetrometers on command. The penetrometers can provide correlating surface structure measurements a few meters into the surface. Penetrometer impact data can detect differences in such surface structures as alluvial planes, sandy soil, volcanic flows, and rocky areas. The nearly real-time balloon positions can be determined for use in penetrometer targeting.

References

- Ainsworth, J. E., and Herman, J. R. (1974) An analysis of Venera 8 measurements. Goddard Space Flight Center, Greenbelt, Maryland.
- Carroll, P. C., Arnett, J. (1969) Materials feasibility tests, Buoyant Venus Station. Report No. PR-22-69-17. Martin Marietta Corporation, Denver, Colorado.
- Ducsay, S. J. *et al.* (1970) Delta class balloon and lander missions for the exploration of Venus. Martin Marietta Corporation, Denver, Colorado.
- Regas, J. L., Giver, L. P., Boese, R. W., and Miller, J. H. (1974) Spectroscopic constraints on the clouds of Venus. American Astronomical Society, Division of Planetary Sciences, 5th Annual Meeting, Palo Alto, California.
- Space Science Board, National Academy of Sciences (1970) Venus, strategy for exploration. Washington, D.C.

Contents

1. Introduction
2. Background
3. Mission Statement
4. Sampling System Requirements
5. Control and Telemetry Equipment Requirements
6. Primary Instrumentation Package
7. Back-up Package
8. Ground Station
9. Acknowledgements

A Control And Telemetry System For A Balloon Borne Air Sampling Package

R. H. Cordella, Jr., Capt, USAF
Air Force Cambridge Research Laboratories
Bedford, Massachusetts

1. INTRODUCTION

The Aerospace Instrumentation Laboratory is charged with the support of an air sampling program sponsored by the Atomic Energy Commission (AEC). The sampling program utilizes several types of samplers to obtain specimens of gases and particles at various altitudes on a cyclical yearly schedule. Although the sampling system in use is functioning at a reasonable level of efficiency, the growing concern in environmental quality has spurred requests for an increased data gathering capability in conjunction with the ability for refined control over several samplers. This control and data telemetry system is the topic of this paper.

2. BACKGROUND

In the early 1950's the Office of Naval Research was conducting experiments to collect samples of the atmosphere under the name Project 201. Figure 1 is a

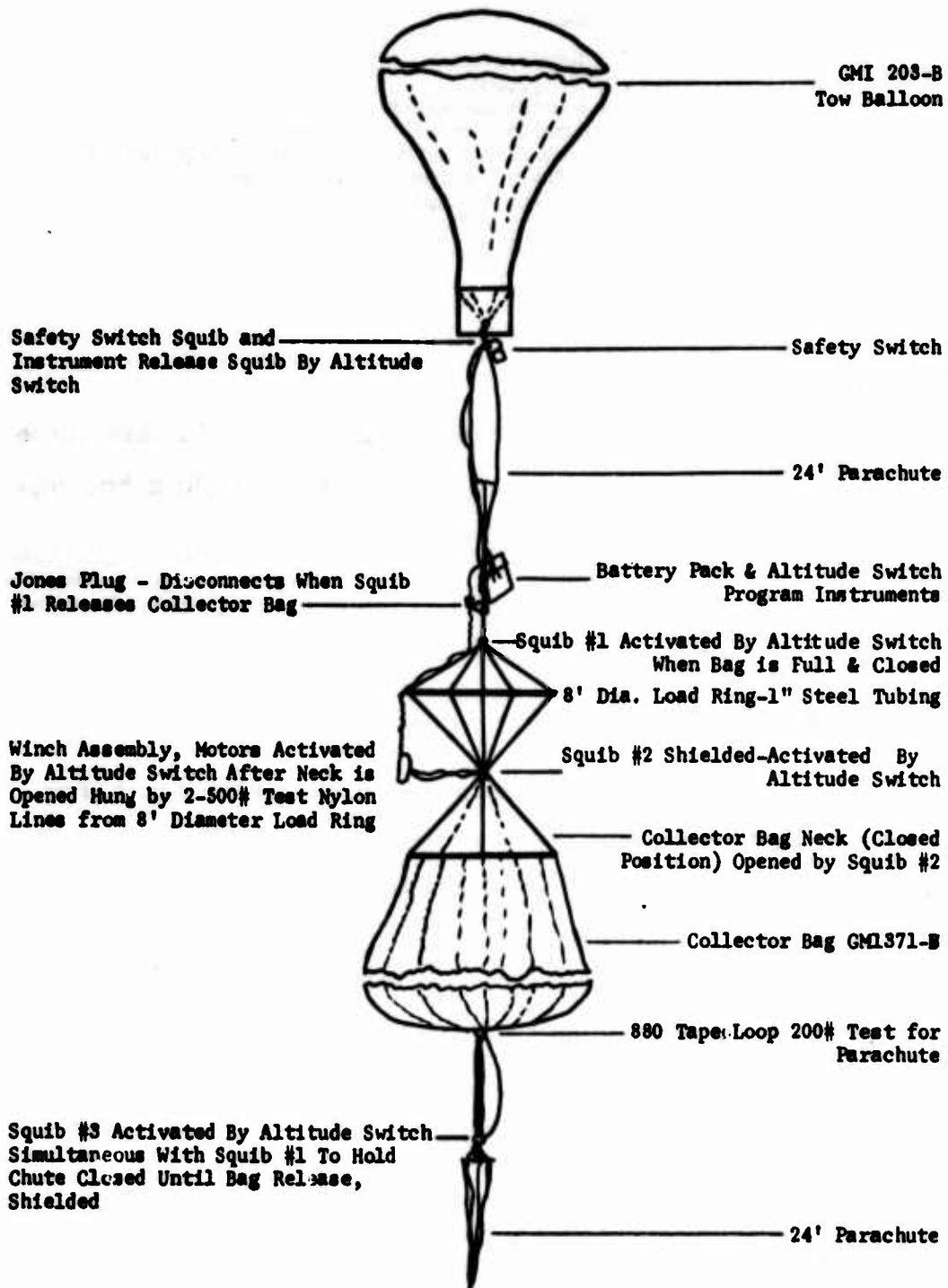


Figure 1. Project 201 Flight Configuration

sketch of the system used. The balloon weighed 19.5 pounds and the collection system was a large polyethylene bag which was opened at altitude, dropped and closed during descent. Total load on the balloon was 128.8 pounds and the maximum altitude was 16.1K feet.

By the 1960's the idea of bringing the atmosphere down to earth to look at it was superseded by the concept of gathering a sample of the particulate matter or certain gases in the air and returning them to earth. Work was carried out by an Air Force Weather Wing and was code named Cold Ash because at the time radioactive debris in the atmosphere was a prime concern. The control and telemetry equipment used on this program was more refined than on Project 201 but it does not approach the present state of the art. In 1971 responsibility for support of the air sampling mission was transferred to AFCRL and the project name was changed to Ash Can. This paper concerns the redesign of the instrumentation needed to support the samplers. This instrumentation will control the samplers and the balloon. A telemetry link will be provided to transmit data to the ground.

3. MISSION STATEMENT

Carry sampling device(s) and support equipment to a preselected altitude and maintain this position for a certain minimum time. Collect and preserve the specimen(s) through proper operation of the samplers. Gather data necessary for optimum utilization of the specimen and retain it in a usable format. Return the specimen and data to the ground with a minimum of damage to the equipment and subsequently deliver it to the experimenter.

4. SYSTEM REQUIREMENTS

The primary requirements for support of the sampling mission were levied by the AEC. In addition to the requirements in the mission statement the AEC stipulated that the data must be recorded on board as well as transmitted. Also, the system's operational deployment necessitates the inclusion of those devices

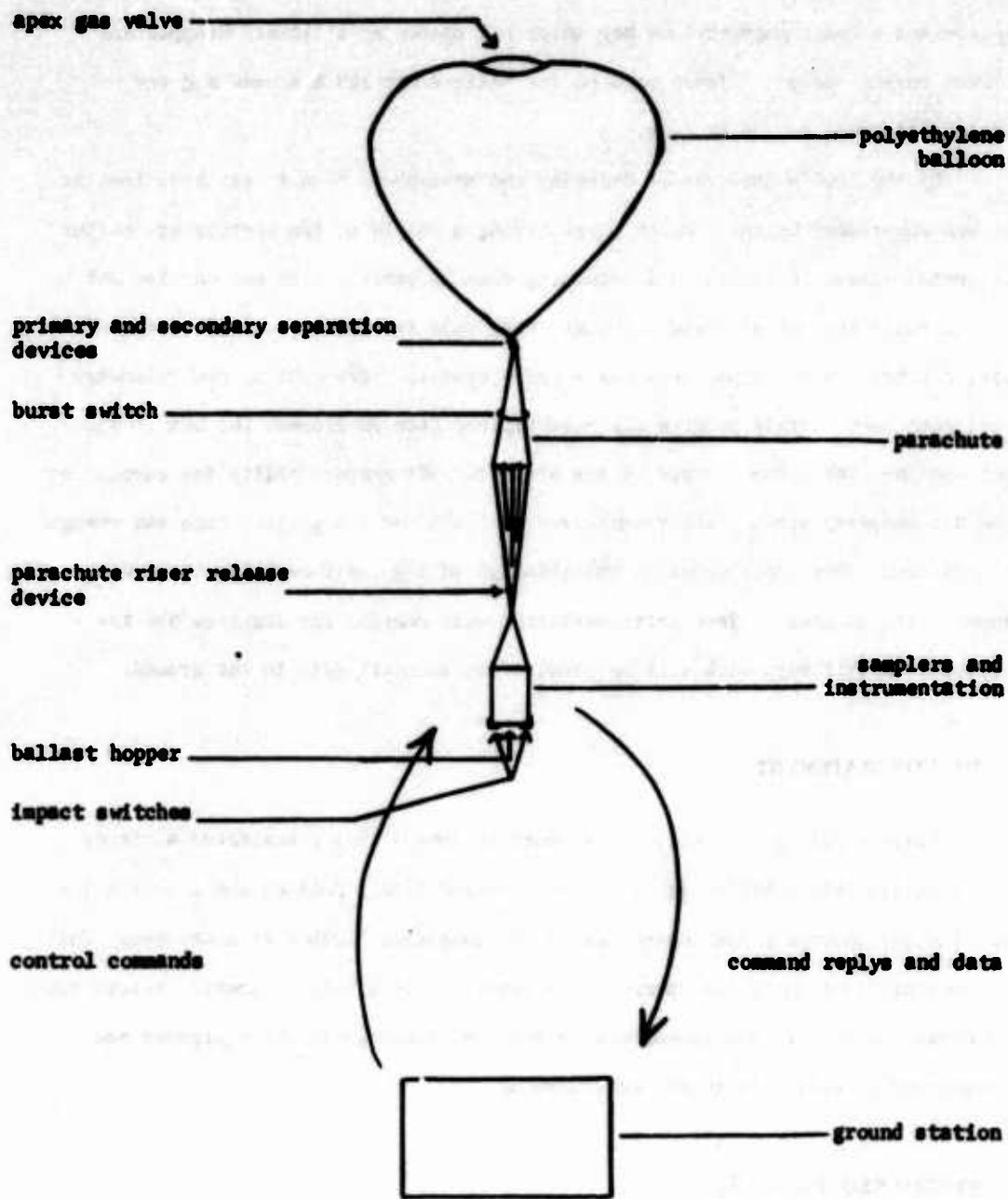


Figure 2. Typical Sampling System Flight Configuration

necessary to control the balloon and protect the equipment during all phases of the flight.

Figure 2 depicts the typical sampling flight configuration in a very simplified sense and intends only to point out the major system components which will be mentioned in the following sections.

The apex gas valve is used to vent helium from the balloon. The primary and secondary separation devices function to release the parachute and its payload from the balloon at the end of a flight or if rapid descent due to premature balloon failure is detected by the burst switch.

The impact switches operate the parachute riser release device to dump the air from the parachute as it touches the ground and thus prevents dragging of the payload.

5. CONTROL AND TELEMETRY EQUIPMENT REQUIREMENTS

The control and telemetry equipment can be categorized as balloon borne equipment or ground equipment as shown in Figure 2. The balloon borne equipment must control the balloon and the samplers, collect the data, store the data and transmit the data. The instrumentation to accomplish this is contained in the Primary Package and includes a controller, transmitter, command receiver, altitude sensors, a data encoder, a data recorder and, a homing beacon. It was decided at CRL that all balloon systems will have a back-up instrumentation package to preclude loss of balloon control beyond radio line of sight. In Figure 3 it is labeled Back-up Package. The control lines for the gas valve and ballast hopper from the primary controller pass through the back-up controller where redundant control is added. The control lines for the primary separation device pass through without interruption. Instead, a secondary separation device is added at the parachute apex and it is activated solely by the back-up instrumentation.

The standard samplers which must be controlled on most flights are known as direct flow sampler (DFS) and the Carbon 14 (C_{14}) sampler. The DFS is battery

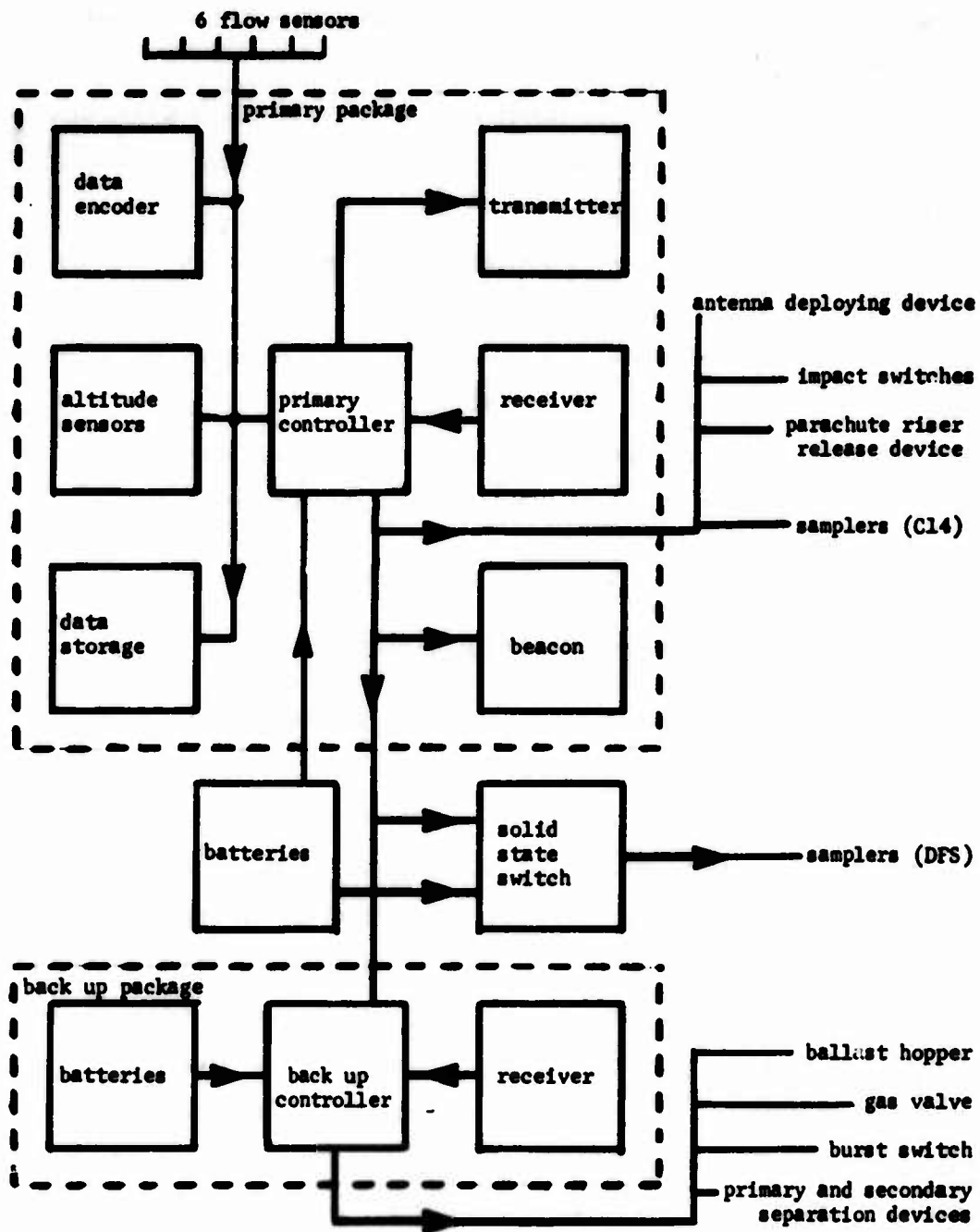


Figure 3. Balloon Borne Instrumentation Packages and the devices they control or monitor

powered and contains a motor which requires about 17 amps. The C₁₄ is operated by exhausting compressed nitrogen through the sampler.

The ground station contains transmitters to issue commands, a receiver to receive the data and, recorders. It also provides mission support liaison communications but this is not of direct interest to us in this paper.

6. PRIMARY INSTRUMENTATION PACKAGE

6.1 The Controller

The smooth implementation of the various functions necessary to carry out a successful mission rests on a high degree of system control and reliability. Various functions are controlled by pressure (altitude), time, command from the ground station or some combination of these or other forcing functions. The sensing of several variables and the proper regulation of their implementation rests with the controller.

The controller is the orchestrator of the whole mission. It has a crystal controlled clock which is started at the time power is applied to the package prior to balloon release and, if necessary could regulate the flight should ground control of the flight be lost. By aneroid pressure sensor or timer the controller would deploy a transmitting antenna, activate the samplers, activate the data encoding device, provide an auto-expand data mode, turn off the samplers, safeguard the sample, terminate the flight and, upon return to earth, separate the parachute from the package.

The command and time methods of implementing a function are designed with equal weight as far as the logic is concerned. However, the times are usually set for the maximum elapsed time from balloon release so if a command cannot activate a function at the earliest possible time, then the timer will activate it after enough time has elapsed to ensure achieving float altitude, etc.

Figure 4 parts a and b is a block diagram of the controller. Its logical and regulatory functions can be grouped into seventeen major categories all of

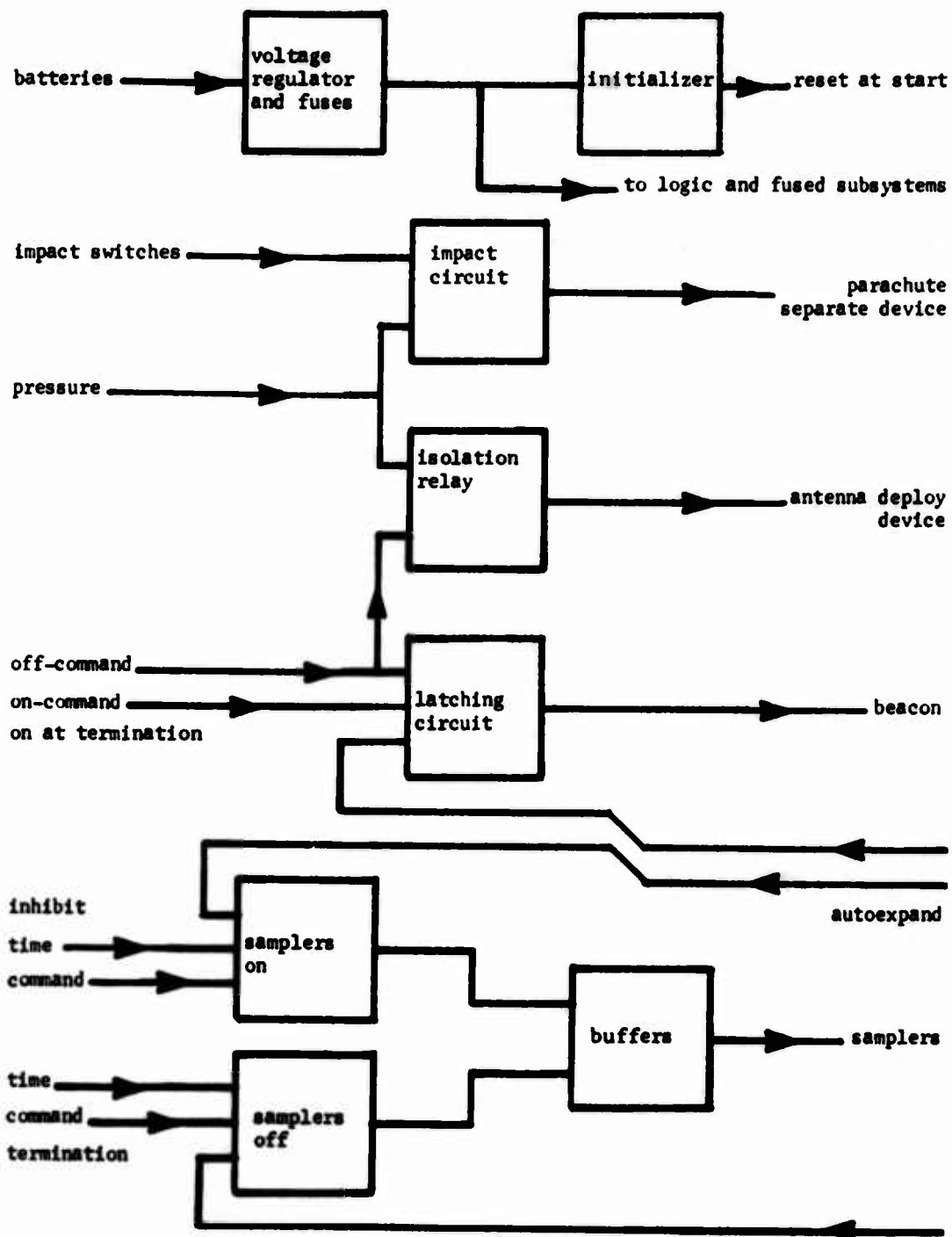


Figure 4a Controller (partial)

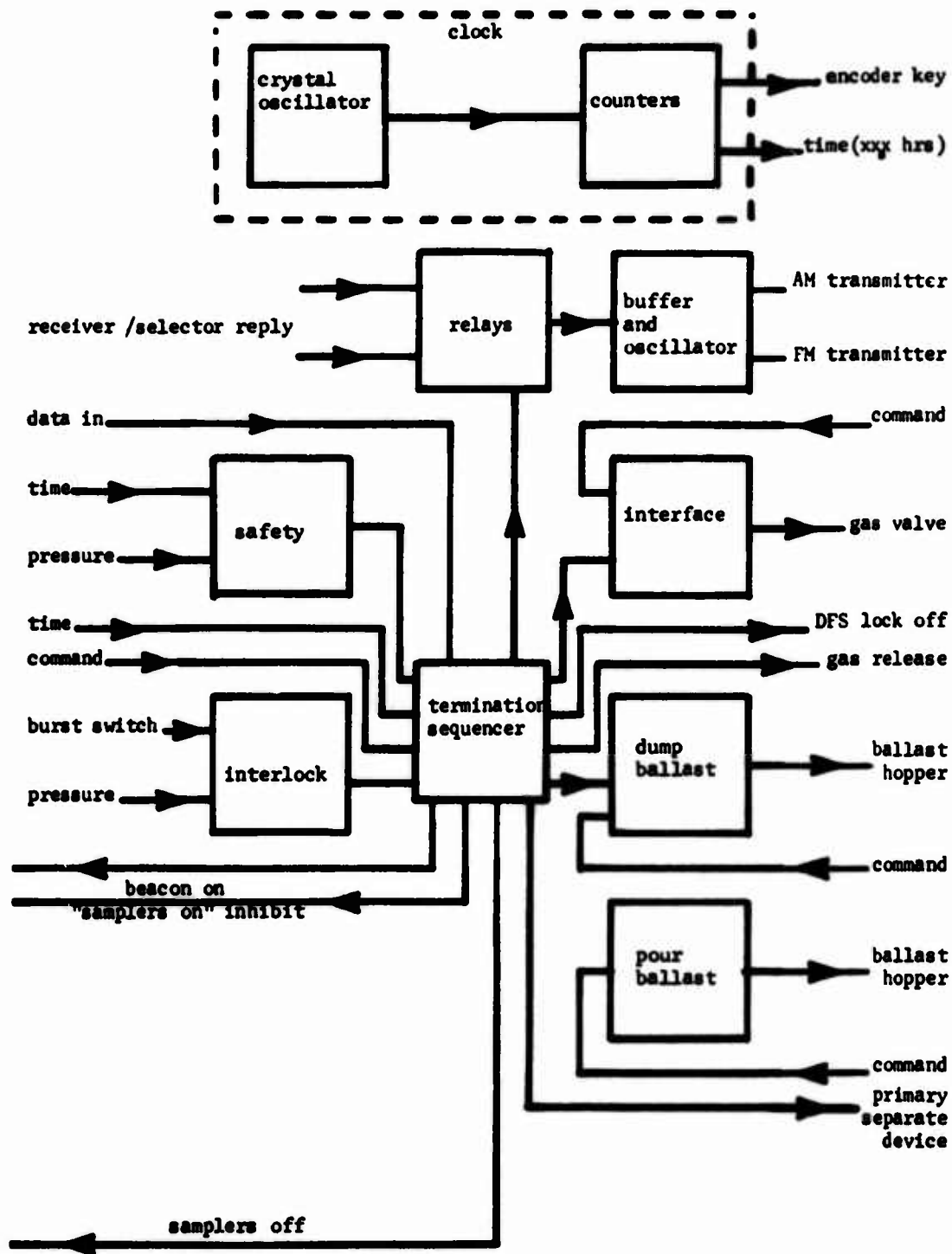


Figure 4b Controller (partial)

which are dependent upon external power to act in response to their input forcing functions. These forcing functions are grouped into two categories: primary, which are externally supplied to the controller and secondary, which are internally generated and therefore dependent on the primary inputs. The outputs of the functional blocks can likewise be grouped into two classes. First, there are those signals generated for the internal use of the controller and therefore never leave the controller but are essential to its proper operation. Second, there are the outputs which leave the controller and act upon the balloon or the sampling system. The primary inputs are the batteries, impact switches, several aneroids, eight commands, the burst switch, the receiver/selector reply signals and the data. This last input does not act on the control unit but rather passes through the control unit on its way to the transmitters and is acted upon by the controller when the receiver/selector is activated by the ground station. The secondary inputs are beacon on at termination, samplers on inhibit, samplers off at termination and, time in tenth-hour increments. These secondary inputs are, as mentioned before, the set of signals generated for internal use only. Each of the function blocks and their interactions will be discussed.

The Voltage Regulator and Fuse block contains an overvoltage regulator and reverse polarity protection plus capacitive filtering to eliminate noise. This voltage is used as V_{DD} for the logic.

The initializer is a non-capacitive reset pulse generator which functions right after the power has been connected and then locks itself out of operation until power has been disconnected for more than 15 seconds. The non-capacitive feature was incorporated because the voltage regulator sees fluctuations in the batteries voltage as various pieces of equipment function and some of the transients will appear on V_{DD} . If the initializer was capacitive it would be possible to retrigger it by noise on the V_{DD} line. The integrated circuit initializer enables the reset line on the entire circuit to follow any V_{DD} line fluctuations with no time delay other than the internal chip setup time. The reset circuit is realized by feeding nine outputs of a binary counter into a nand

gate and driving the counter through a gate with the output of the crystal oscillator in the clock. When the counter is full the output of the nand gate goes from high to low and the reset pulse has just ended. Simultaneously the input pulses to the counter are stopped by locking the input gate with the reset pulse line. The counter remains full and the output of the circuit low until power is disconnected long enough for the V_{DD} to fall below 1.5 volts.

The impact circuit is used at the touchdown of the package after the parachute has returned it to earth. Its function is to separate half the parachute risers from the package to preclude the parachute dragging the package. This circuit also turns off the FM transmitter to prevent possible thermal run-away prior to the arrival of the recovery crew. The aneroid pressure sensor serves as an arming device, the system must ascend through 10K feet to pre-arm and then descend through 10K feet to arm. Only then are the impact switches connected to the riser separating device. At the prearm stage any impact switches which are inadvertently shorted, are disconnected from the circuit. The same sensor which arms the impact circuit serves as a back-up for the command to deploy the transmitting antenna.

The command which is used for antenna deploy is also used to deactivate the homing beacon (242.0 MHz). The circuit for the beacon control is latching and, if the beacon is off will not effect the circuit. The beacon is automatically activated at termination but a requirement could exist to shut it off after a brief period of operation. Therefore, a command off capability is provided. If after it is automatically activated and turned off by command, it is necessary to reactivate it, a beacon "on" command is available. The beacon may be turned on and off as often as required by tracking aircraft or ground recovery teams.

The "samplers on" control block can be activated by either time or command. The time is set by a thumb wheel switch for 00.0 to 99.9 hours. After termination the inhibit line is used to prevent the samplers from being activated by either mode. The "autoexpand" ensures that the fifteen channels of data are activated

The "samplers off" function block also is activated by time and command in

a similar fashion as the sampler on function. However, the "off at termination" line also energizes the circuit. This signal does not override the functioning of the off command. If the samplers were not turned off by time, or a command, and if the "off at termination pulse" was not applied the samplers could still be deactivated by command.

The buffer stages are tailored to the samplers presently being used but are easily adaptable to any type of sampler. The first buffer stage drives a solid state switch for two high current direct flow samplers. The second buffer stage drives magnetically latching gas valves which control the C₁₄ samplers.

The System Clock uses a crystal oscillator and several binary dividers and decimal counters to derive tens hours, hours and, tenths hours. It also generates a trigger pulse for the data encoder 1.5 minutes after the application of power and every three minutes after that. The system clock possesses a speed up feature used to check out the system in 1/1024 the normal time.

The termination sequencer is a set of chips driven by its own internal clock which regulates the timing of events which should occur at the end of the flight. The circuitry can be activated in four ways. First, the safety time and altitude interlock will terminate the flight if a certain preset altitude is not reached within a set number of hours. Second, if the burst switch is closed when the package is above a preset altitude the flight will be terminated or if the burst switch is closed on the flight line or during launch, the flight will terminate when the balloon reaches the preset altitude. Third and fourth, the circuit can be activated by command or timer. It was noted above that the termination sequencer has its own internal clock. This is necessary to make the timer and command circuit activation modes truly independent and redundant. If the timer mode failed to operate because the system clock had stopped operating then there would be no guarantee that the termination sequence would work if it derived its clock pulses from the system clock. Instead, a 0.50Hz oscillator is built into the termination sequence. This oscillator is activated with the application of a start signal from any of the four modes and clocks the circuit through the

proper sequence of events. The bottom and right side of the termination sequencer block (Fig 4) are annotated with the control functions which originate within the block. Note that the bottom is used for functions relative to the samplers and the right side is used for functions relative to the balloon. Two functions relating to the samplers have been explained previously the third function, DFS latch off, controls a latching relay in the solid state switch which controls the direct flow samplers. When this relay is latched, it is impossible for the samplers to be activated. The fourth function, gas release, fires a squib which cuts the plastic tubing leading from a gas container to the C₁₄ samplers. This expells any remaining gas and renders the sampler inoperative. Two functions on the right hand side of the block are related to the balloon control. The upper control line opens the valve and, the second line blows out two panels in the ballast hopper to dump any unused ballast. Continuing clockwise, the third line on the bottom of the block fires a squib which releases the package and parachute from the balloon. The fourth line activates the homing beacon. The circuits represented at the top of the package regulate how the balloon and samplers reply to the ground station. The line labeled receiver/selector reply will be explained in the next section. The line labeled data originates in the encoder where the raw data is digitized, serialized and, converted to Morse code. This data line is a stream of Morse Code words which is routed through the controller to the transmitters. At termination this line is interrupted and the transmitters are fed a signal which originates in the controller. If the termination has been normal then a dashing signal is transmitted for 63 seconds. This dashing is taken directly from the multivibrator in the termination sequencer. It has about a 50% duty cycle and supplies approximately a one second dash and one second of silence. If the flight has been terminated via the burst switch line than a 63 second solid tone is heard. On the sixty fourth (2⁶) pulse the circuit is returned to its reset state. This releases the relays which have been energized and therefore conserves energy and removes the possibility of heat damage should the package stay in the desert for an extended period of time. During a normal termination

the sequence is as follows: At the reception of the input signal the samplers are turned off, the electrically driven samplers are latched off, power is applied to open the gas valve, 63 seconds of dashing commences. At termination plus 8 seconds the beacon is energized. At termination plus 32 seconds the squibs are fired to dump excess ballast, release unused gas for the gas driven samplers and separate the flight package and parachute from the balloon. At this time balloon destruct occurs by means of rip lines extending from the balloon to the apex point of the parachute. At termination plus 64 seconds the termination sequencer is deactivated, all relays that have been energized are deenergized and, the dashing signal stops. A termination caused by the pulling of the burst pin activates the same timing chain as described above but the separation, releasing of gas and dumping of ballast take place at the application of the signal. Also, the warning that termination has been activated is changed from a dashing to a steady tone which lasts for 63 seconds.

6.2 The Transmitters

The previous section refers to the transmitters several times. They are obviously used to relay information from the airborne system to the people on the ground. The control unit and the primary instrumentation system package have provision for driving either an HF keyed CW transmitter or a VHF FM transmitter or both. The keyed transmitter is driven with a relay contact that is normally open and then grounded to produce the data words. The FM transmitter is driven by a relay contact that is normally open and switched to a 720Hz tone to produce the data words. The primary and recommended transmission will be the FM system because, in transmitting a known and accurately controlled tone, the output of the receiver can be phase locked to the frequency of the tone to increase the system's ability to communicate in a high noise region. Normally only the FM transmitter will be flown. Since both transmitters are commercially obtained they will not be discussed in detail. The role of FM transmission will be fully discussed in section seven.

6.3 The Receiver/Selector

Like the transmitters, the existence of the receiver and selector has been more or less accepted and the commands have been discussed without saying what they really are. Any receiving system of acceptable frequency range able to produce closures to ground will serve as the command receiver. The system under discussion uses nine independent commands which are outputs of the receiver/selector. Each command output is a normally open relay contact which is connected to ground to enable a circuit somewhere in the system to be activated. Eight of the commands are used in the controller and have been discussed. The other command is used in the data encoder and will be discussed with it. Since the receiver/selector is obtained commercially it need not be discussed in detail. A feature of the HF command system now in use is the reply which is transmitted when one of the channels is selected. The controller has provisions to handle replies from any state of the art receiver/selector. In this fashion the operator of the ground station knows that the receiver/selector will act on the channel he intends to use.

The order of priority of transmitted signals is first, receiver/selector replies; second, balloon monitor warning tones; and third, data.

6.4 The Data Acquisition System

This subsystem encompasses the monitoring of the balloon functions as well as the monitoring of the flow sensors used on the samplers. The inputs are power, primary altitude data, gas valve reply voltage, ballast hopper reply ground, burst switch (ground closure), back-up altitude and six sets of flow and temperature data. The maximum system output is a stream of fifteen four letter Morse Code words every three minutes from the encoder and, a printed record of this same data stream.

The heart of the Data Acquisition System is the data encoder. The inputs to the encoder are analog signals from various sources which were already listed. The information from the primary altitude sensor and the flow sensor is in the

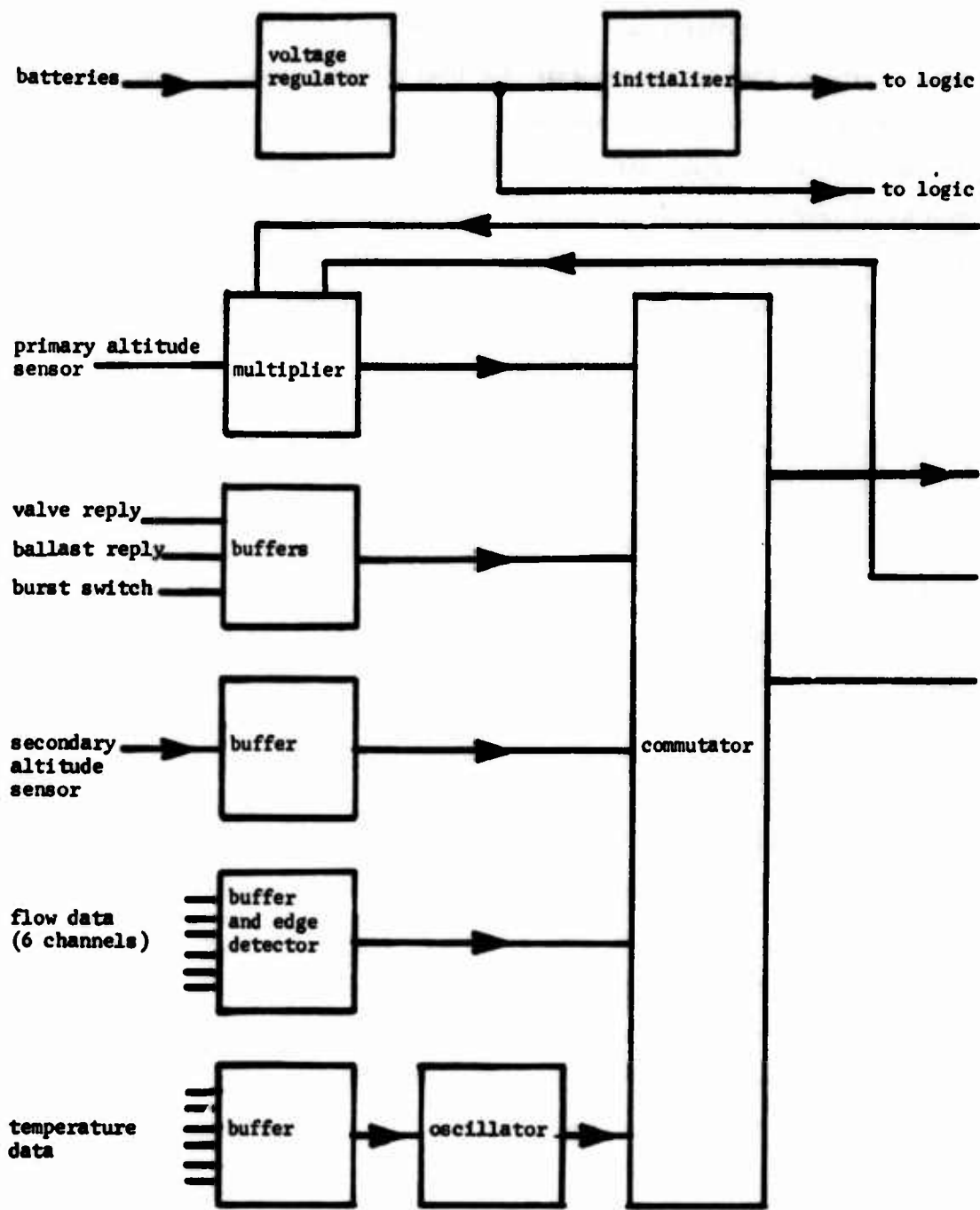


Figure 5a Encoder (partial)

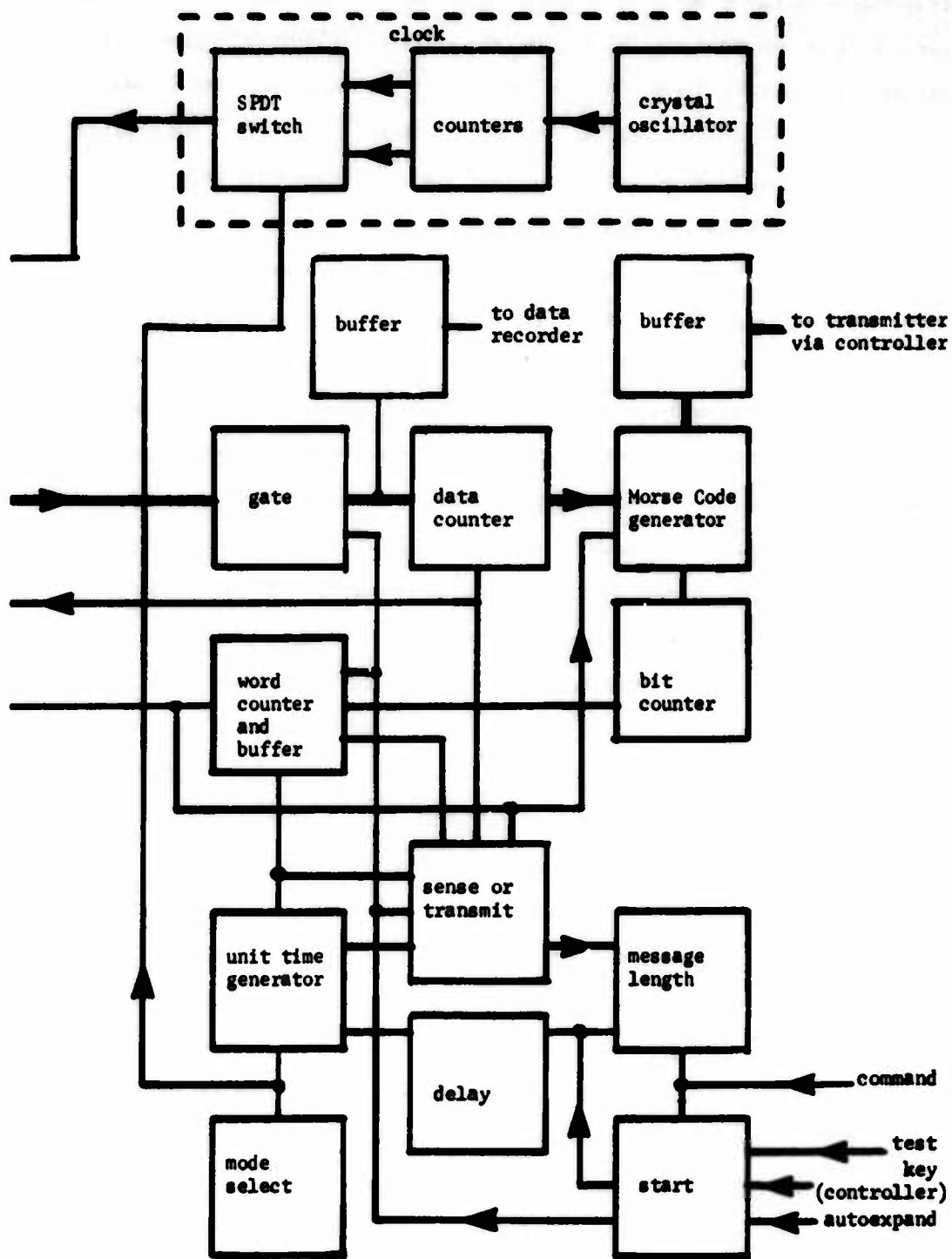


Figure 5b Encoder (partial)

frequency of a pulse train. The output of the back up altitude sensor is a voltage but it is converted to a binary signal, where the data is contained in the frequency, before it is applied to the encoder. The majority of the signals applied to the encoder contain the information in the frequency of the applied signal. To enable uniform data processing, the temperature data from the thermistors is changed into a variable frequency.

The format of the applied signals points to a mechanism which would be frequency sensitive and not detect various signal levels or duty cycles. The frequency sensitive element of the system had to be an edge detector or counter which would be gated on for a controlled period of time. This approach goes back to the basic definition of frequency from which the standard cycles per second is based; i.e., number of periods per unit time. The unit time and the size of the counter were chosen to accommodate the input signals. The central concept of the encoder is: all the raw data is in the form of frequency which is applied to a counter for x number of seconds. The number of events registered in the counter is a direct result of the frequency (the unknown) and the controlled unit time (known). This digitized form of the data must be transmitted and the incoming signals must be commutated into the counter but these are peripheral operations to the basic acquisition of the data.

A block diagram of the encoder is displayed in figures 5a and 5b. The double width line is the flow of data from the raw signal, through the counter, to the Morse Code generator and out of the encoder. All the other function boxes are support functions. The encoder is really a special purpose micro computer. The buffers, unit time generator and, speed and type of word output are tailored to the application under discussion. Its operation is too complicated to review in detail but fig 5 is very representative. Let's look at some of the function blocks and describe their part in the encoder's operation.

The buffer for the primary altitude sensor, which is located on channel one, consists of a level changer to assure that the voltage to the logic does not exceed but does meet V_{DD} , a frequency doubler and a single period gating circuit.

See figure 6. The signal in the sensor originates with a blocking oscillator (waveform 1) which is then applied to the input of a flip flop within the sensor to produce waveform 2 for transmission to the encoder. Wavefore #2 is reshaped by the level changer and returned to its original form by the frequency doubler (waveform 3). When channel one is energized (waveform 4) the period gating circuit selects the next whole period (waveform 5) and uses this to gate a string of pulses derived from the crystal oscillator (waveform 6) into the counter. The signal is processed in this manner because its period varies over eight octaves

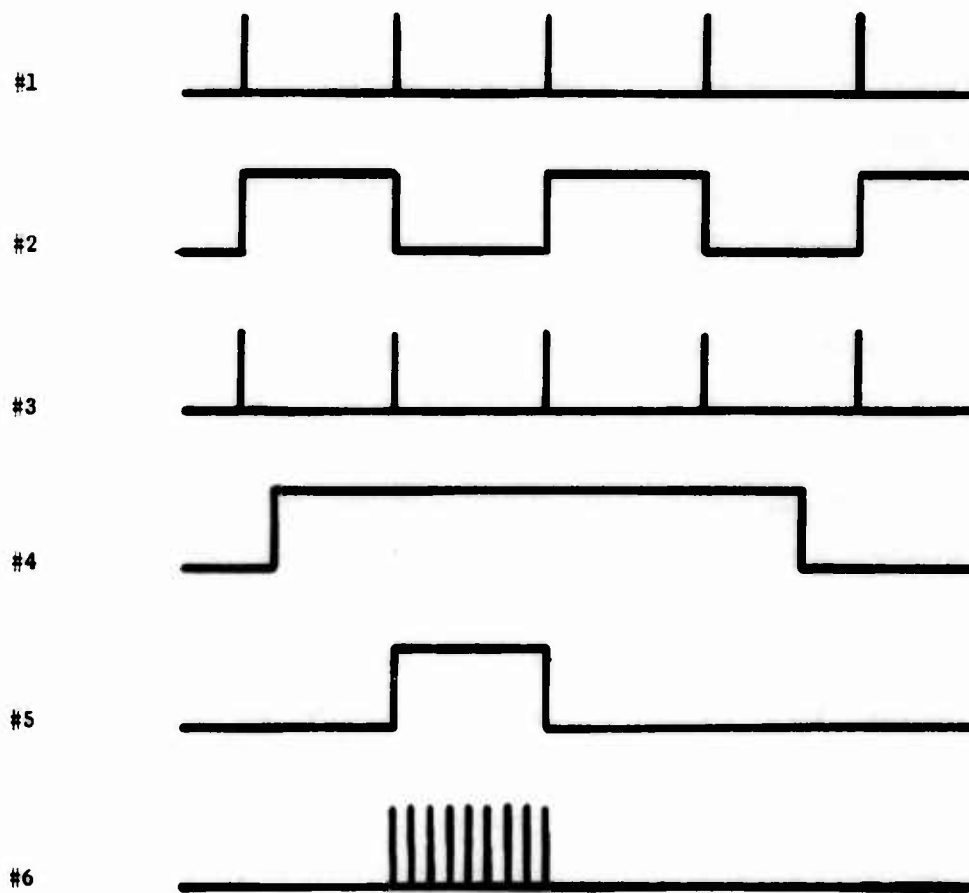


Figure 6. Waveforms generated in processing the primary altitude sensor signal.

and this multiplication technique enables the encoder to use one channel to cover 0 feet to 135K feet in altitude.

The buffer for the second channel interfaces the burst switch and the replies from the ballast hopper and the valve with the commutator. These reply signals are converted to frequencies. Each function therefore generates its own code and, if no signal is present a negative reply is produced.

The back-up altitude data is on the third channel and serves as a stand by sensor in case the primary altitude sensor should fail. The sensor used in this application is a diaphragm pressure sensor.

These three channels convey all the data necessary to monitor balloon control and, they can be cycled preceded by a keying pulse in about thirty seconds. It was decided that during the time when the balloon was rising to the float altitude and there is no data from the flow sensors it would be advantageous to only cycle the first three channels of the encoder. To accomplish this the "message length flip flop" is provided. It starts off in the state to provide the first three channels recycled and remains so until activated by command number one. It then changes states and enables the full fifteen channels to be cycled once every three minutes. The fifteen channels and the preceding warning pulse are generated in about two minutes depending on the ratio of dots to dashes. After the last channel there is no code from the encoder until the controller keys the encoder start circuit. See clock section of figure 3b. The length of the message can be switched between three and fifteen words (one four letter word per channel) as often as required. If, at the time the samplers are energized the encoder is in the three word state then it will automatically be placed in the other state by the auto-expand pulse generated in the controller.

The last twelve channels are devoted to the acquisition of six sets of data from the flow sensors. Each flow sensor has a chopper which generates a pulse train proportional to the speed of the air passing over the fan blades and a thermistor which senses the air temperature. The even numbered channels (4,6,8, 10,12,14) are devoted to the flow data and are buffered for overvoltage and point

bounce of the choppers. The odd numbered channels are devoted to the thermistors and are buffered primarily for RF interference. The thermistors are employed to generate a frequency suitable for the counter by switching them into a simple RC multivibrator where the R (resistance) is supplied by the thermistor as a function of temperature. The components of the oscillator are chosen so that the thermistor provides usable temperature data over a range of -80°C to $+40^{\circ}\text{C}$ with the most accurate range being around the -60°C to -30°C . The accuracy is always within 0.5°C .

The variety of signals applied to the encoder and the accuracy and resolution necessary to yield a viable system led to the choice of a twelve bit binary counter as the data counter. A twelve bit counter can have 4096 states; i.e., it can count from 0 to 4095. To produce Morse code from the counter outputs, the data is jammed into a shift register with spaces added between every three bits. This produces a format of

$$W = \text{XXX XXX XXX XXX}$$

where each X is a binary one or a zero or respectively, in Morse code, a dash or a dot. The count from each channel of the encoder is transformed into a four letter word. The letters come about because each of the three variables in an XXX group has two states 0 or 1 (dot or dash). Therefore, only eight possible combinations (000, 001, 010, 011, 100, 101, 110, 111) exist and if the zeros are dots and the ones are dashes they correspond to S,U,R,W,D,K,G,O in Morse code. The total message (M) is fifteen words

$$M = \text{W W W W W W W W W W W W W W W}$$

where each word is as described above, four letters or twelve binary bits.

To facilitate the decoding of the words a dictionary is generated by computer for each of the major signals: primary altitude data, back-up altitude data, flow data and, temperature data. A typical page of one of the dictionaries is shown in Figure 7.

TEMPERATURE IN DEGREES CENTIGRADE

	S	U	R	N	O	K	G	O
USS	-86.8	-86.6	-86.5	-86.4	-86.3	-86.2	-86.1	-86.0
USU	-85.9	-85.8	-85.7	-85.6	-85.5	-85.4	-85.3	-85.2
USR	-84.8	-84.9	-84.8	-84.7	-84.6	-84.5	-84.4	-84.3
USW	-84.2	-84.1	-84.0	-83.9	-83.8	-83.7	-83.6	-83.5
USO	-83.4	-83.3	-83.2	-83.1	-83.0	-82.9	-82.8	-82.7
USK	-82.6	-82.5	-82.4	-82.3	-82.2	-82.1	-81.9	-81.8
USG	-81.7	-81.6	-81.5	-81.4	-81.3	-81.2	-81.1	-81.0
USO	-80.9	-80.8	-80.7	-80.6	-80.5	-80.5	-80.4	-80.3
UUS	-80.2	-80.1	-80.0	-79.9	-79.8	-79.7	-79.6	-79.5
UUU	-79.4	-79.3	-79.2	-79.1	-79.0	-78.9	-78.8	-78.7
UUR	-78.6	-78.5	-78.4	-78.3	-78.2	-78.1	-78.0	-77.9
UUN	-77.8	-77.7	-77.6	-77.5	-77.5	-77.4	-77.3	-77.2
UUD	-77.1	-77.0	-76.9	-76.8	-76.7	-76.6	-76.5	-76.4
UUK	-76.3	-76.2	-76.1	-76.1	-76.0	-75.9	-75.8	-75.7
UUG	-75.6	-75.5	-75.4	-75.3	-75.2	-75.1	-75.0	-75.0
UUG	-74.9	-74.8	-74.7	-74.6	-74.5	-74.4	-74.3	-74.2
URS	-74.1	-74.1	-74.0	-73.9	-73.8	-73.7	-73.6	-73.5
URU	-73.4	-73.3	-73.3	-73.2	-73.1	-73.0	-72.9	-72.8
URR	-72.7	-72.6	-72.6	-72.5	-72.4	-72.3	-72.2	-72.1
URW	-72.0	-72.0	-71.9	-71.8	-71.7	-71.6	-71.5	-71.4
URO	-71.4	-71.3	-71.2	-71.1	-71.0	-70.9	-70.8	-70.8
URK	-70.7	-70.6	-70.5	-70.4	-70.3	-70.3	-70.2	-70.1
URG	-69.8	-69.9	-69.8	-69.8	-69.7	-69.6	-69.5	-69.4
URO	-69.3	-69.3	-69.2	-69.1	-69.0	-68.9	-68.9	-68.8
UNS	-68.7	-68.6	-68.5	-68.4	-68.4	-68.3	-68.2	-68.1
UNU	-68.0	-68.0	-67.9	-67.8	-67.7	-67.6	-67.6	-67.5
UNR	-67.4	-67.3	-67.3	-67.2	-67.1	-67.0	-66.9	-66.9
UNW	-66.8	-66.7	-66.6	-66.5	-66.5	-66.4	-66.3	-66.2
UNO	-66.2	-66.1	-66.0	-65.9	-65.9	-65.8	-65.7	-65.6
UNK	-65.6	-65.5	-65.4	-65.3	-65.2	-65.2	-65.1	-65.0
UNG	-64.9	-64.9	-64.8	-64.7	-64.6	-64.6	-64.5	-64.4
UNO	-64.3	-64.3	-64.2	-64.1	-64.1	-64.0	-63.9	-63.8

Figure 7. Typical Dictionary Page

6.5 Data Storage - Airborne

The requirement for on board data storage is accomplished with a commercially available battery operated printer which prints six columns of information on paper tape. One package of tape can more than accommodate an eight to ten hour mission including the preflight checkouts. At present all the data is printed as (binary coded octal) numbers but in the future printing wheels with letters will be used for the data printing wheels. This will enable the same dictionary to be used to decode either the printed record or the transmitted record. The printer is driven by an interface buffer which is in turn driven by the buffer in fig 5b which is tied into the system between the gate and the data counter. A time code is generated in the interface buffer by counting the encoder keying pulses from the controller and, it is printed with the data.

7. BACK-UP INSTRUMENTATION

Safety considerations and concern for the samplers necessitate the inclusion of back-up instrumentation in the total flight system. The back-up package contains batteries, a receiver and a small controller (Fig 3). The receiver has three command outputs which are used to control termination, the gas valve and ballast pouring. The back-up controller interfaces these functions with the same functions originating in the main controller and also has an internal clock for back-up timed termination. The back-up termination redundancy is further increased by having its own release device at the parachute apex. Likewise, the valve redundancy is assured by having the valve control lines switched to the back-up package batteries rather than assume that the primary system batteries are in working order.

8. THE GROUND STATION

The control of the balloon borne system and the retrieval of the telemetry signals are the primary purposes of the ground station. The transmitter and

receiver are purchased rather than produced in-house. The function of the transmitter is to generate a coded signal which will energize a certain closure to ground in the on-board receiver. This has been previously discussed.

The receiver in this station is a crystal controlled FM device operating in the 40 MHz region. This is important because the data acquisition technique is being automated. Initially the Morse Code was copied by hand and this was the only record. For the past several flights the data has been recorded on a chart recorder as a stream of dots and dashes which can be read as the code. This recording is not accomplished by sensing when there is a signal of sufficient amplitude at the receiver output but rather when a signal of a certain frequency is present at the receiver output. As mentioned before, the FM transmitter is keyed with a 720 Hz tone to form the dots and dashes. A phase locked loop (PLL) tuned to 720 Hz is driven by the receiver and when the proper signal is applied to it the output changes from a low to a high. This is applied to the chart recorder and the string of dots and dashes is recorded.

In the future the same PLL technique will be used but its output will be shifted into a circuit which will take the serially entering Morse Code, convert it to ones and zeros, and parallel print it as a four letter word using the aforementioned eight letters. This will produce a real time, readable copy of the entire flight.

9. ACKNOWLEDGMENTS

This system design has been influenced by many people. SMSgt John Ground devoted many hours discussing the operational aspects of air sampling. Mr. Hans Laping is deserving of special credit for his discussions on circuit design. Sgt Robert Dumont volunteered many suggestions to facilitate the operational use of the equipment. Lt Peter "Terry" Miller wrote the programs which generate the dictionaries used with the encoder. Mr Ralph Cowie read the draft manuscript and commented on areas that needed clarification. Naturally, all the people

whose discussions and comments led to the inclusion of an idea in the system implementation cannot be listed. But, what I consider to be a comprehensive and adaptable system has been the result of many inputs, especially the ever present comments of the technicians of (AFCRL) LCC.

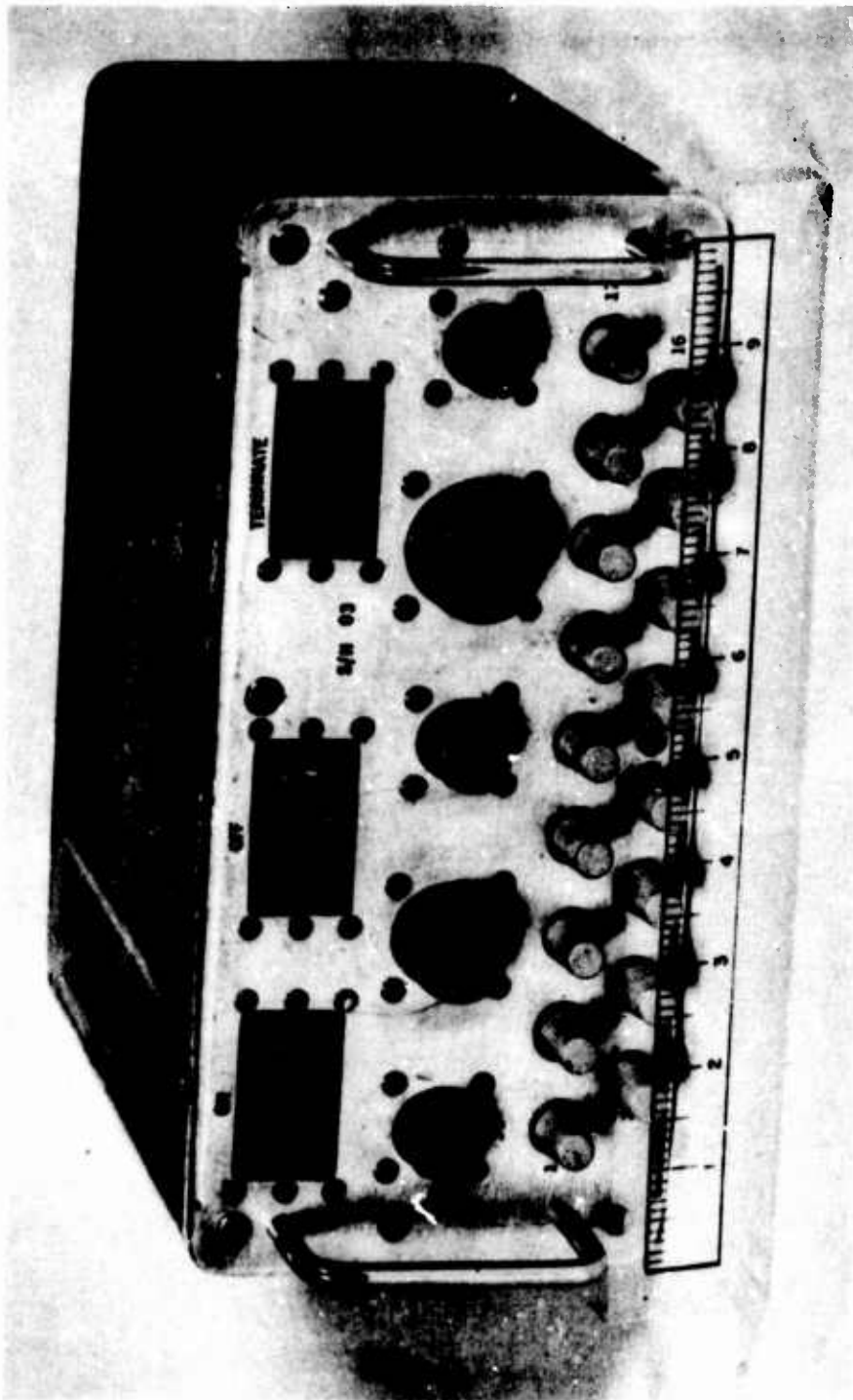


Figure 8. Primary Controller

Contents

1. INTRODUCTION
2. THE EXPERIMENT & INSTRUMENTATION
3. DATA INTERPRETATION
4. SUPPORTING MEASUREMENTS PROGRAM
5. RESULTS & DISCUSSIONS

**A Description Of The Lacate Balloon Experiment
And Some Preliminary Results**

James M. Russell, III*
NASA, Langley Research Center
Hampton, Virginia

John C. Gille
National Center for Atmospheric Research**
Boulder, Colorado

Richard E. Davis
NASA, Langley Research Center
Hampton, Virginia

Paul L. Bailey
National Center for Atmospheric Research**
Boulder, Colorado

Abstract

The Lower Atmospheric Composition and Temperature Experiment (LACATE) was launched from the White Sands Missile Range on May 5, 1974. The purposes of this mission were to flight test a model of a ten-channel horizon scanning radiometer destined for application on a future satellite and to obtain data on a number of

*This work was completed in part while the author was a visitor at the National Center for Atmospheric Research.

**The National Center for Atmospheric Research is sponsored by the National Science Foundation.

trace constituents in the stratosphere. The radiometer was carried to a maximum altitude of 42.6 km by a balloon having a volume of 45 million cubic feet. Infrared horizon radiance profiles were obtained for a period of approximately five and one-half hours including about forty-five minutes of pre-sunrise data. The experiment uses these radiance data to provide vertical profiles of temperature, ozone (O_3), water vapor (H_2O), nitrogen dioxide (NO_2), nitrous oxide (N_2O), nitric acid (HNO_3), methane (CH_4), and aerosols. A supporting measurements program was conducted at the time of the flight to obtain data for comparison with LACATE results. This program included aircraft, balloon, and rocket experiments conducted by several government agencies and two universities. Preliminary radiance profiles will be presented and the inversion of these data to yield constituent density profiles will be discussed. The planning, outcome, and operational considerations for the supporting measurements program will also be described.

1. INTRODUCTION

There has been an increasing concern in recent years that human activities or natural events might disrupt the fragile chemical balance of the stratosphere. The main concern has been that chemical species injected into the stratosphere, especially by high-flying aircraft, might reduce natural ozone levels by catalytic action, thus allowing passage of more biologically harmful ultraviolet radiation to the surface. The first studies suggested that water vapor might have strong effects (SCEP, 1970). It now appears that the nitrogen oxides (referred to as NO_x) are more important in this regard (Crutzen, 1970, 1974a; Johnston, 1971). More recently it has been realized that chlorine compounds are capable of initiating catalytic chains which are faster than those for NO_x . Sources of such chlorines are the combustion products from solid rocket fuel of the type to be used on the space shuttle (Stolarski and Cicerone, 1974) but perhaps more importantly from freons diffusing up from the troposphere (Crutzen, 1974b; Molina and Rowland, 1974).

Reacting to a growing unrest over the ozone question, the Congress, in 1971, directed the Department of Transportation to establish the Climatic Impact Assessment Program (CIAP). This action launched a national effort which has proven to be a stimulus for stratospheric research. One of the major goals of current efforts is to establish baseline values for the concentrations of gases that have important roles in the ozone photochemistry. Such a baseline is essential if we are to assess the consequence and extent of any future changes. A number of experiments have been conducted from balloons, rockets, and aircraft and these efforts have revealed new and significant information especially as regards the stratospheric distribution of nitric acid and the nitrogen oxides. However one deficiency in the present data bank is that the measurements are representative of specific geographic locations. Global scale baseline data are ultimately needed as well as measurements that support studies of stratospheric dynamics. Anticipating this need, the Lower

Atmospheric Composition and Temperature Experiment (LACATE) was conceived in 1971 as a satellite experiment to provide vertical profile measurements of O_3 , NO_2 , HNO_3 , N_2O , H_2O , CH_4 , aerosols, and temperature. The experiment was designed to provide measurements on a grid approaching 400 by 400 km around the globe. These data coupled with the thermal wind equation will allow calculations of mass flux divergence in direct support of dynamics studies. The experiment is based on the use of horizon radiance profiles measured in the principal emission bands of the gases listed. These profiles are mathematically inverted to infer temperature and gas concentrations.

This paper describes the first flight test of the LACATE instrument. The device, which is a 10 channel horizon scanning radiometer operating in the infrared, was launched from the White Sands Missile Range at 1 a.m. local time on May 5, 1974. The 45 million cubic feet balloon used in the test was launched by personnel of the Air Force Cambridge Research Laboratories Balloon Branch. The gondola was carried to a peak altitude of 42.6 km. Payload impact occurred at 11:15 a.m. at a point only about 36 km from the launch site. The ascent rate during the flight was only about one-third to one-half the planned rate and as a result, the instrumentation reached a much lower temperature than anticipated in going through the tropopause region. A cover over the radiometer entrance aperture to retard convective heat transfer during ascent was not removed until 5 a.m. at an altitude of about 36 km. The aperture cover was originally scheduled to be removed much earlier in the flight but it was decided to delay the time of removal to allow time for the instrument heaters to gain positive control of the instrument temperature. After the cover was removed, radiance profiles were obtained for a period of five and one-half hours including about forty-five minutes of the pre-sunrise period.

2 THE EXPERIMENT AND INSTRUMENTATION

The objectives of the LACATE balloon mission were to (1) test a model of the LACATE radiometer prior to its use on a satellite, (2) evaluate algorithms for inversion of the radiance data, (3) determine experimental accuracies of LACATE results through comparison with direct measurements, (4) assess the validity of cloud detection using radiometer data, (5) obtain basic data on the long path atmospheric transmittance, and (6) study diurnal changes in temperature and trace gas concentrations. These objectives led to the definition of the balloon experiment parameters. The second objective leads to a requirement on balloon altitude. Most of the measurements from a satellite are expected to be valid from 10 to at least 40 km. A balloon instrument looking toward the limb sees signals very similar to satellite measurements for atmospheric regions 10 km or more lower than the balloon

altitude leading to a desire for a flight to at least 50 km. Objective (6) requires a flight of several hours spanning sunrise. For most times of year, the large wind velocities at 50 km preclude long duration flights. In the spring and fall, during wind reversal conditions, the mean winds are near zero, allowing long duration flights to be made within the range of telemetry stations. A small balloon drift has additional benefits since payload recovery operations are simplified, and the instrument observes the same volume of the atmosphere during the flight. This also simplifies the planning for a network of supporting measurements, which are required by objectives (3) and (5). (A description of the design and planning for the supporting measurement program is included below.) The fourth objective dictates that the height and characteristics of clouds within the field of view be available. This can be met in part by placing a camera on the gondola looking at the atmospheric volume being scanned by the radiometer.

The gondola and instrumentation, exclusive of balloon ballast, weighed approximately 272.4 kg (600 pounds). The scientific instrumentation consisted of the 10 channel LACATE radiometer, a three axis rate gyro system, a two axis magnetometer system, two aluminum oxide water vapor sensors, a thermal conductivity type pressure gauge, two atmospheric temperature sensors fabricated by the University of Texas at El Paso, and a Hasselblad 70 mm camera. The camera exposure was 1/125 and Ektachrome type 5256 film was used.

A cut-away view of the LACATE radiometer is shown in Figure 1. Energy coming in the entrance aperture reflects off an elevation scan mirror which is being scanned approximately 7.3° down from local horizontal. An elevation angle sensor is included to give very precise readings of elevation scan mirror angular displacement. Radiance samples are taken every 0.013° of mirror movement. An inflight calibrator operating at a temperature of 317K is inserted at the top of each scan to allow updating of radiometer responsivity. The primary mirror focuses the energy onto a derotating "K" mirror and after passing through two sets of relay optics and the chopper plane, it is focused on a detector array mounted to a cold sting. The "K" mirror is included since otherwise the azimuth scan feature of the radiometer would cause the rectangular horizon image to rotate at the detector plane as the lower section of the radiometer is rotated in azimuth. The horizon image covers 7.5 milliradians by 0.25 to 1.0 milliradian for the various channels. Mercury-cadmium-telluride detectors are used and cooled to 80K by a liquid nitrogen dewar. Interference filters are mounted in front of each detector to admit only energy from the principal emission band of a given gas.

The radiometer design contains two channels in the $15 \mu\text{m}$ band of CO_2 for temperature inference. One is a broad band channel covering the entire CO_2 band and the other has a narrow filter covering only the central portion. The narrow band channel malfunctioned prior to flight and did not operate during

the mission. In addition to these channels, the radiometer has an ozone channel centered at 9.6 μm , a water vapor channel at 6.3 μm , a nitrogen dioxide channel at 6.2 μm , two nitric acid channels (for improved signal to noise ratio) both centered at 11.2 μm , a nitrous oxide channel at 17.1 μm , a methane channel at 7.8 μm , and an aerosol channel at 10.8 μm .

The remaining sensors used on the gondola are commercially available and will not be described. The rate gyro system was included to provide data needed in correcting the indicated angular spacing between any pair of radiance samples as given by the elevation angle sensor for additional movement of the radiometer line of sight due to pendulation motion of the balloon train. The magnetometers were included to measure the azimuth of the radiometer line of sight at any point in time. The camera was pointed toward the horizon to provide an indication of clouds in the radiometer field of view as well as information regarding the stratospheric aerosol layer. The principal reason for inclusion of the temperature and water vapor sensors was to obtain data needed in correcting radiance errors introduced by the presence of temperature and water vapor wakes which surround the balloon. This effect can be quite large. Reynolds and Wallis (1970) and Ballard, et al. (1972) show in the case of temperature, a difference of up to 20K or more between the disturbed air and ambient. No work has been reported on the water vapor wake. An extensive modeling effort was undertaken to model both types of disturbances surrounding the LACATE balloon and these studies will be described in a subsequent paper. The preliminary results indicate that a correction of as much as two or three times the noise equivalent radiance is required in the temperature channel and as high as 8 to 10 times the noise in the water vapor channel.

Unfortunately, the payload release mechanism on the launch crane failed during the launch run and the gondola was dragged on the ground a short distance. This occurrence destroyed the two atmospheric temperature sensors which were suspended below the main gondola section. Consequently, any temperature wake corrections will rely solely on the model. In addition, the camera jammed early in the flight after 34 frames and it appears that the photographs obtained will not be very useful. However, all other sensors including the radiometer functioned properly during the mission.

3. DATA INTERPRETATION

Figure 2 represents the horizon viewing geometry. The limb sensing approach has several advantages for the measurement of stratospheric gases. First, there is up to 60 times more gas in a horizon path than there is through the same atmosphere in the nadir direction. Thus, it is possible to sense smaller concentrations.

Also, the combination of the limb geometry and the exponential fall off of density with altitude gives rise to data heavily weighted towards the tangent point making it possible to achieve high vertical resolution. Finally, the background in the horizon experiment is the cold blackness of space. This greatly simplifies the inversion process over that required for a nadir experiment. In general, the radiance measured by the radiometer can be represented by

$$N(\Delta\bar{\nu}, H_0) = \int_{\Delta\bar{\nu}} \int_{\tau_b}^1 \phi(\bar{\nu}) B[\bar{\nu}, T(H)] d\tau[\bar{\nu}, q(H)] d\nu \quad (1)$$

where $N(\Delta\bar{\nu}, H_0)$ is the radiance measured over a bandwidth $\Delta\bar{\nu}$, $\phi(\bar{\nu})$ is the instrument response function, $B[\bar{\nu}, T(H)]$ is the Planck intensity at wave number $\bar{\nu}$ and temperature $T(H)$, $\tau[\bar{\nu}, q(H)]$ is transmittance, H is altitude, H_0 is tangent height or the point of closest approach of a ray path to the earth surface, and τ_b is the transmittance from the instrument to a point at the outside edge of the atmosphere for a given gas. A profile of N is measured as a function of H_0 for each spectral band by causing a mirror to scan the view direction vertically across the horizon or earth limb.

If the mixing ratio $q(H)$ is known, the temperature $T(H)$ can be inferred from these profiles and vice-versa. The 15 μm band of CO_2 is used to infer temperature since the CO_2 mixing ratio is known and taken to be constant with altitude. Originally, the "two color" approach described by Gille and House (1971) was to have been used to infer temperature versus pressure directly, independent of absolute altitude information. However, because of the loss of the narrow band CO_2 channel prior to flight, another approach described by Gille and House and used by McKee (1972) and McKee and Cox (1973) will be adopted. Basically, in this approach the inferred temperature profile is "anchored" to a rawinsonde temperature profile in the lower altitude range through adjustment of an initial assumed pressure for one radiance sample point. After the temperature profile has been determined, the measured radiance in the emission band of another gas, e.g. ozone, can be used to infer the gas concentration. Inversion studies for the inference of water vapor have been described by Gille and House (1971) and for the inference of ozone by Russell and Drayson (1972). Similar techniques will be used here for the inference of the various gases. All of these methods are iterative approaches where the parameter of interest, whether it be temperature or gas concentration, is changed at each altitude according to a special relaxation equation. The iteration continues until the root-mean-square residual radiance difference between measured and calculated radiance averaged over all measurement points is within given error limits, e.g. the noise level. In most cases it was not possible to select a spectral region where only one gas emits energy. Consequently, special methods have

been developed in some cases to reduce the LACATE data. The general inversion sequence that will be used is shown in Figure 3.

4. SUPPORTING MEASUREMENTS PROGRAM

The measurement of stratospheric trace gases is a difficult task for both remote and direct sensing techniques. Many of the constituents have concentrations in the parts per billion range requiring measurement techniques with high sensitivity. As a result, our present knowledge of the concentrations of stratospheric trace gases is rather limited. In view of these facts, it seemed highly desirable for this mission to try to obtain simultaneous measurements of the constituents measured by LACATE using other techniques. The cooperation of other researchers and organizations was solicited in this regard and excellent participation was obtained. This is mainly because all involved recognized the advantages of having a set of simultaneous measurements for intercomparison of results and evaluation of sensing techniques.

The first consideration in planning the location of various supporting measurements was definition of the atmospheric region measured by LACATE. Figure 4 shows the location of the radiometer line of sight tangent point as a function of altitude. When all azimuth positions are included, an ellipsoidal type atmospheric volume is defined. The cross section of this volume at the earth surface defines the measurement area for LACATE data and this is shown in Figure 5. Also shown in Figure 5 are the locations of the various supporting measurements conducted at the time of the flight. The open circles in the figure represent the regular rawinsonde sites of the National Weather Service. The solid circles denote two of three Meteorological Rocket Network (MRN) sites supporting the mission. The third MRN site was Wallops Island, Virginia. Triangles denote the approximate location of sites where scientific balloons were launched. Dashed lines with arrows are drawn for each of the supporting aircraft and the location of a ground lidar system is also noted. Wherever possible, the tracks of the research aircraft were chosen to be within a radius of the launch site corresponding to the area viewed by the LACATE radiometer when the line of site was above 5 km tangent height. Compromises were made where necessary, due to operational constraints, and to aid other researchers. For example, a four-way comparative experiment was planned for the San Angelo, Texas area. A dustsonde launch was planned, together with an overflight by a USAF WB-57F carrying the DOT/CIAP package. Lidar soundings were also planned to be concurrent with these two elements and in turn with LACATE. Tracks of research balloons were planned in the same way, and appropriate launch sites selected accordingly, within the constraints of radar tracking availability, and

suitability of the site for launch of large research balloons. The same applied for rocket-borne payloads, with safety and range operational status being strong additional constraints. A summary of the elements of the supporting measurements program is given in Figure 6 and a breakdown of the measurements according to platform, investigator, altitude and constituent is given in Table 1. Most of the planned measurements were successfully carried out on the day of the mission although some experiments were not conducted for various reasons. The data obtained are listed in Table 2.

5. RESULTS AND DISCUSSION

Figure 7 shows a typical horizon radiance profile measured during the flight in the ozone channel. Measurements in the other channels, with the exception of the N_2O , NO_2 , and aerosol channels, were of similar quality. These latter channels were more noisy but still of good enough quality to extract useful data. At point A in Figure 7, the radiometer is viewing horizontally and is just beginning a scan down toward the earth surface. Shortly thereafter (~ 0.1 sec) the inflight calibrator (IFC) is inserted as evidenced by the strong feature labeled warm calibration. The IFC stays in the field of view for about 1.6 sec and then is removed. During the entire time the IFC is being used, the elevation scan mirror is scanning downward which is why the radiance after the IFC is removed is higher than before it was inserted. This is also the reason for the radiance slope in the IFC region. This behavior arises because the radiometer was not out of the ozone atmosphere. The same effect also appears in the other channels. The channels least affected in this way are the HNO_3 and aerosol channels. If the planned float altitude of 50 km had been achieved, the effect would have been much smaller by as much as an order of magnitude in some cases. The radiance continues to increase as the mirror scans down to the region of the ozone maximum where it becomes virtually constant until energy is received from the lower troposphere. The strong temperature gradient in this region causes the radiance to increase again until the line of sight intersects the solid earth at which time the channel saturates. Some radiance features in this latter region of the profile appear to be due to clouds and these points are indicated in the figure. As time continues to point B, the mirror scans upward giving virtually the mirror image of the down scan radiances. Slight differences between consecutive scans are expected since the balloon train is pendulating and rotating in azimuth. Both types of motion would cause the radiometer to sample a slightly different atmospheric volume in the two scans. Work is now underway to invert these radiance data to obtain temperature and constituent information.

Table 1. Launch Sites, Altitude Ranges, and Constituent Measurements Planned for the Supporting Measurements Program

Total No. Missions	Platform	Agency	Investigator(s)	Launch Site/Ground Track	Altitudes (or Alt. Range)	Sampled Constituents
AIRCRAFT						
1	U-2	NASA-ARC	Loewenstein	ARC/See Fig. 3	60, 65, 70 Kft.	O ₃ , NO
2	WB-57F	USAF/DAT	CIAP-Mason	Kirtland AFB, NM/ (See Fig. 3)	55, 63, Kft	NO, O ₃ , H ₂ O HNO ₃ , H ₂ SO ₄ , CH ₄ , Aerosols Aitken nuclei
1	Suborbiter	NCAR	Ehhalt, ^a Munkin	Broomfield, CO/ (See Fig. 5)	to 40 Kft	H ₂ O, SO ₂ , H ₂ O, HNO ₃ , CH ₄ , CO ₂ , CO, O ₃ , H ₂ , NO
1	WC-135	USAF- AFMPC	AFMPC	McClellan AFB, CA/ (See Fig. 5)	to 40 Kft	H ₂ O, CH ₄ , Aerosols, Total Hydrocarbons, CO ₂ , CO
ROCKETRY						
12 (4 each site)	LOKI	NSA	Quires- DANA/USAF	Ft. Meigs, CA White Sands Missile Range Malloy I., VA**	0ft-55 km	Temp., Wind
3	ARCAS	USA-ASL	Randhava	USMR	10 - 60 km	O ₃
1	ARCAS	USA-ASL	Ballard	USMR	near 30 km	H ₂ O
1	ROCOE	NASA- GSFC	Krueger	USMR	50 - 30 km	O ₃
RESEARCH BALLOONS						
1	2x10 ⁶ cu ft	NCAR	Ehhalt	Midland, TX	35 km down to tropopause in 16 discrete steps	CH ₄ , H ₂ O, H ₂ O, CO ₂ , CO, NO, H ₂
1	10 ⁵ cu ft	A/C/ NCAR	Loewenstein	Midland, TX	50 km	H ₂ , NO ₂ , HNO ₃ , HCl, Na ⁺ , Ca ²⁺ , NH ₄ ⁺ , Cl ⁻
1	10.6m 10 ⁶ cu ft	U. of Denver/ US Army Ball. Res.Lab	Murphy	Holloman AFB, NM	Float at ~40 km. Scans South angles 45-95°	Atmospheric Emission Spectrum 5-15 μm to derive SO ₂ , H ₂ O, CH ₄ , H ₂ O, HNO ₃
	N/A	NASA- GSFC	Hilseforth	Holloman AFB, NM	40 km	O ₃
3	1x10 ⁵ cu ft	U. of Wyo.	Reese, Pepin, Hoffman	1 km from Winslow, AZ, Holloman AFB, NM and Goodfellow AFB, TX	to 40 km	O ₃ , temp. particulates
1	1x10 ⁵ cu ft	U. of Wyo.	Pepin	Holloman AFB, NM	Remote Infrared 5-30 km	Aerosols
OTHER						
1	N/A	NASA- LSC	McCormick	Goodfellow AFB (San Angelo, TX)	0ft-36 km	Relative aerosol distribution

^aTo sample some constituents as payload II

**Plus additional Rocketsones from CNS sites, as available.

Table 2. Data Obtained from the Supporting Measurements Program

Quantity	Mission	Alt. Range (km)	Accuracy	# Mission	Location	Flight Date	Time (GMT)
Temperature	1) NWS/MRN Balloon	0-24	-1K	-20	WSMR, MTR, Wallops, NWS Sites	5/5/74	08, 11, 12, 14, 17Z
	2) WC-135	8-12	-1K	1	See Fig. 5	5/5/74	09-15Z
	3) WB-57F	18, 21	-1K	2	See Fig. 5	5/5/74	10-16Z, 20-21Z
	4) MRN LOKIsonde	55-24	1-3K	11	WSMR, MTR, Wallops	5/5/74	09, 12, 15, 18Z
Ozone	1) UWY Dust/Ozone sonde	0-30	10Z	2	Winslow, Az HAFB, NH	5/5/74	10-14Z 11-15Z
	2) Sabreliner	8-12	10Z	1	CAPB, Tx	5/7/74	10-14Z
	3) WB-57F	18, 21	20Z	2	See Fig. 5	5/1/74	11-14Z
	4) U-2	19, 21, 23	20Z	1	See Fig. 5	5/5/74	10-16Z, 20-21Z
	5) ROCOZ	50-15	10Z	2	WSMR	5/5/74	17Z, 20Z
	6) ASL Ozone sonde	62-10	10Z	3	WSMR	5/5/74	10, 13, 16Z
Water Vapor	1) NWS/MRN Balloon	SFC-8	20Z	-20	WSMR, MTR, Wallops, NWS Sites	5/5/74	08, 11, 12, 14, 17Z
	2) Sabreliner	8-12	10Z	1	See Fig. 5	5/1/74	11-14Z
	3) WC-135	8-12	20Z	1	See Fig. 5	5/5/74	11-17Z
	4) WB-57F	18, 21	10Z	2	See Fig. 5	5/5/74	10-16Z, 20-21Z
	5) NCAR Balloon	35, 34, 33	10Z	1	Midland, Tx	5/8/74	14-16Z
Nitrogen Dioxide	1) Sabreliner	8-12	50Z	1	See Fig. 5	5/1/74	11-14Z
	1) Sabreliner	8-12	2Z	1	See Fig. 5	5/1/74	11-14Z
Nitrous Oxide	1) Sabreliner	35, 34, 33	2Z	1	Midland, Tx	5/8/74	14-16Z
	2) NCAR Balloon	35, 34, 33	2Z	1	Midland, Tx	5/8/74	14-16Z

Table 2. Continued

Quantity	Mission	Alt. Range (km)	Accuracy	# Mission	Location	Flight Date	Time (GMT)
Nitric Oxide	1) WB-57F	18,21	20%	2	See Fig. 5	5/5/74	10-16Z, 20-21Z
	2) U-2	19, 21, 23	30%	1	See Fig. 5	5/5/74	17-21Z
Nitric Acid	1) Sabreliner	8-12	50%	1	See Fig. 5	5/1/74	11-14Z
	2) AEC Balloon (Repeat Mission)	28	75%	1	HAFB, NM	5/13/74	08-14Z
Methane	1) Sabreliner	8-12	2%	1	See Fig. 5	5/1/74	11-14Z
	2) WC-135	8-12	Unknown	1	See Fig. 5	5/5/74	11-17Z
	3) NCAR Balloon	35, 34, 33	3%	1	Midland, Tx	5/8/74	14-16Z
Aerosols, Particulates	1) UYD Dust/ Ozoneonde	0-30	10%	2	Winslow, Az HAFB, NM	5/5/74 5/5/74	10-14Z 11-15Z
	2) LaRC Lidar	0-36	2%	300 shots	GAFB, Tx	5/7/74	10-14Z
	3) WC-135	8-12	Unknown	1	GAFB, Tx	5/5/74	07-13Z
	4) WB-57F	18, 21	Unknown	2	See Fig. 5	5/5/74	11-17Z
	5) AEC Balloon (Repeat Mission)	28	30%	1	See Fig. 5 HAFB, NM	5/5/74 5/13/74	10-16Z, 20-21Z 08-14Z
Total Hydrocarbon	1) WC-135	8-12	Unknown	1	See Fig. 5	5/5/74	11-17Z
Carbon Dioxide	1) Sabreliner	8-12	1%	1	See Fig. 5	5/1/74	11-14Z
	2) WC-135	8-12	Unknown	1	See Fig. 5	5/5/74	11-17Z
	3) NCAR Balloon	35, 34, 33	1%	1	Midland, Tx	5/8/74	14-16Z
Carbon Monoxide	1) Sabreliner	8-12	Unknown	1	See Fig. 5	5/1/74	11-14Z
	2) WC-135	8-12	Unknown	1	See Fig. 5	5/5/74	11-17Z
	3) NCAR Balloon	35, 34, 33	Unknown	1	Midland, Tx	5/8/74	14-16Z

However no inversion results were available at the time of submission of this manuscript. These results will be reported in a subsequent paper.

Based on the preliminary analysis made to date, it appears that virtually all objectives of the mission can be achieved to some degree. The very slow balloon ascent rate with attendant low instrument temperatures and the lower float altitude achieved will certainly compromise some of the objectives. The low altitude requires a greater reliance on assumptions and supporting measurements than is desirable. This may cause the accuracy of the results to suffer somewhat. Also, the effect of the very low instrument temperature around the sunrise period will have to be very carefully evaluated to assess the reliability of the measurements during this time. This could seriously affect attempts to measure diurnal change. Even without instrument effects, however, the low float altitude just prior to sunrise (36 km) will compromise the diurnal change objective especially for temperature and ozone. This is because diurnal effects are more pronounced at higher altitudes. Viewed generally, the mission was very successful. The instrument performed well during the flight apparently even while operating at an unusually low temperature. A good body of supporting measurements were obtained which should prove to be very useful in evaluating the results. Radiance data were obtained for an extended time period making it possible to average data from successive scans and reduce effective noise levels. Using the low noise data and supporting measurement results, transmittance studies can be performed. Even though the on-board camera jammed early in the flight, ATS satellite photographs taken during the mission will be useful in partially providing data that would otherwise be lost. In addition, the pressure sensor on the gondola functioned properly during the test and two redundant aluminum oxide water vapor sensor measurements tracked each other fairly well although this measurement has not yet been fully evaluated.

Future efforts will be devoted to a detailed analysis of radiance profiles and inverted results. The data will be examined for correlation between various parameters such as temperature and ozone profile fine structure features and these features will be compared to direct measurements to assess the realism of such correlations. Similar studies will be done using the nitric acid and aerosol channel results. The constituent profiles will be compared with photochemical model results and these data will also be examined to assess the magnitude of any spatial variability that may exist.

Even though most of the objectives of the experiment will be realized, a second LACATE balloon mission would be desirable. Data are needed from a 50 km or higher altitude platform for reasons discussed earlier. In addition correlations are required between on-board camera photographs and radiometer signals in order to properly evaluate cloud detection capabilities. The effect of the temperature wake on LACATE results should be studied further using on-board temperature sensors.

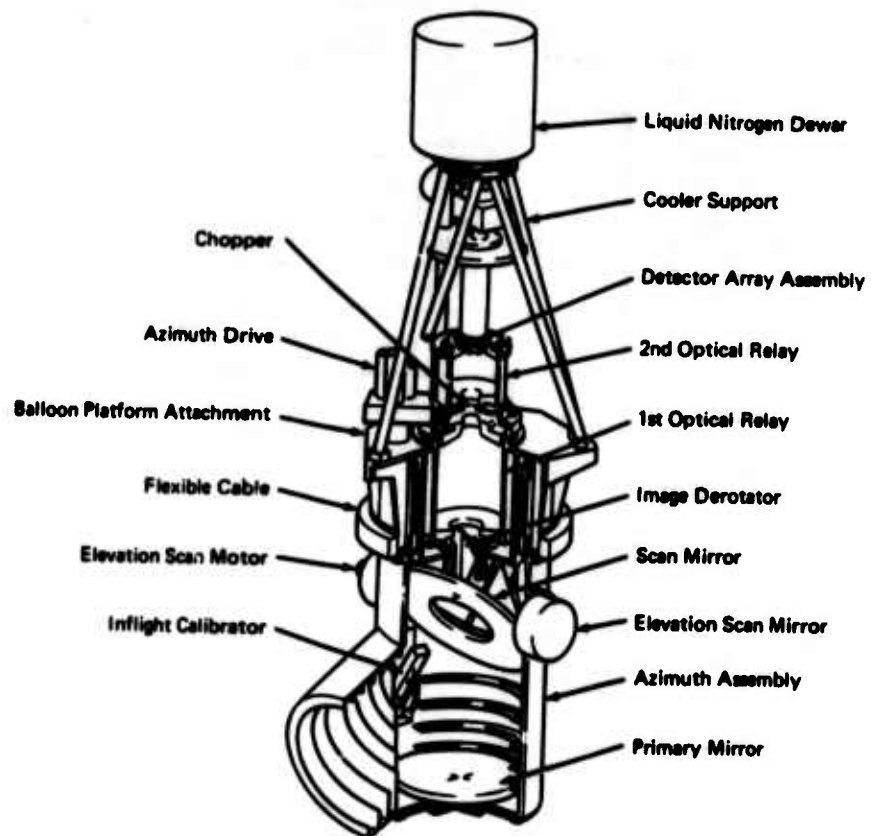


Figure 1. LACATE Radiometer

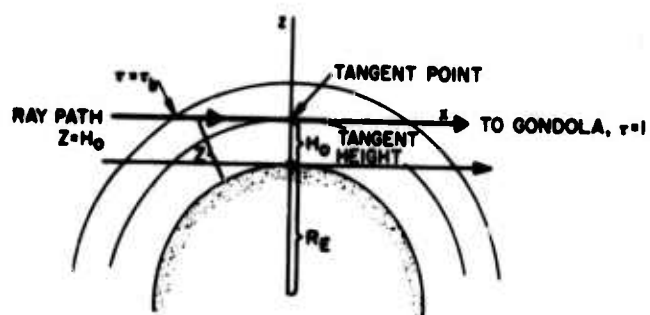


Figure 2. Limb Viewing Geometry

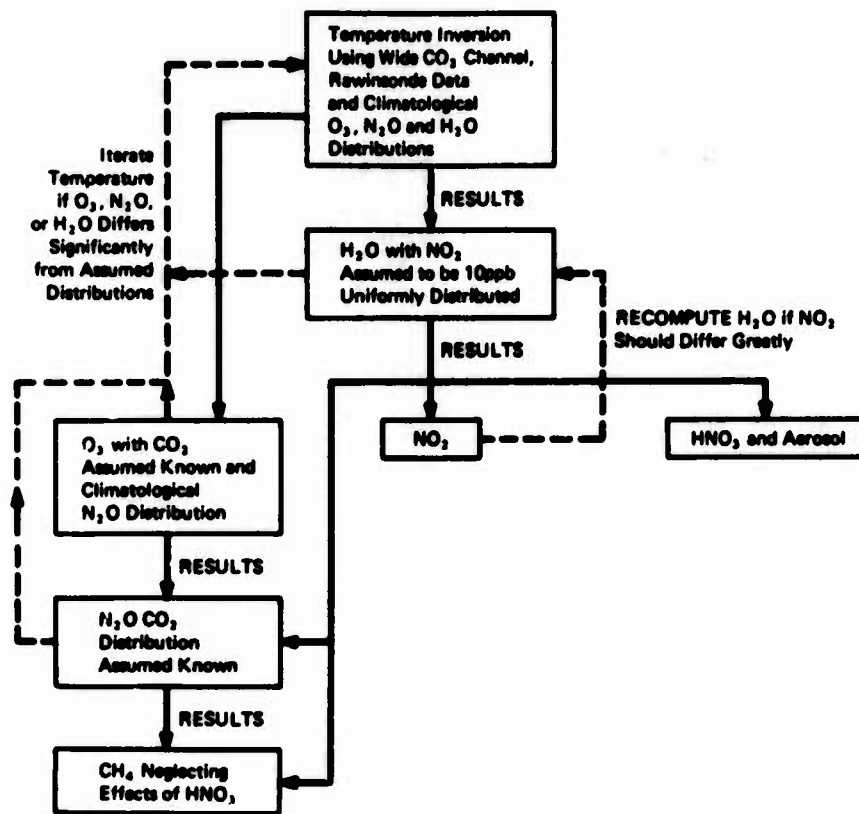


Figure 3. Inversion Flow Diagram

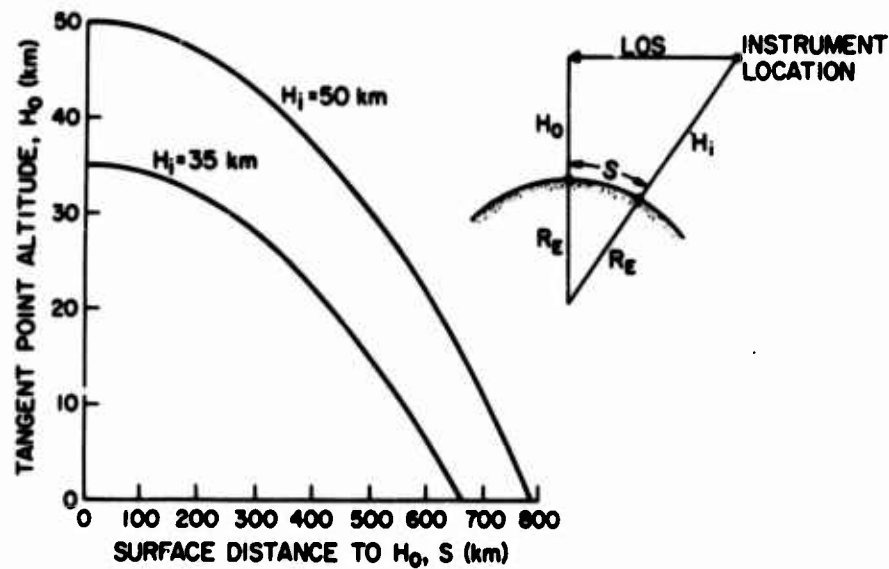


Figure 4. Variation in Location of the Tangent Point Subpoint as a Function of Tangent Height, H₀ and Two Balloon Float Altitudes, H₁

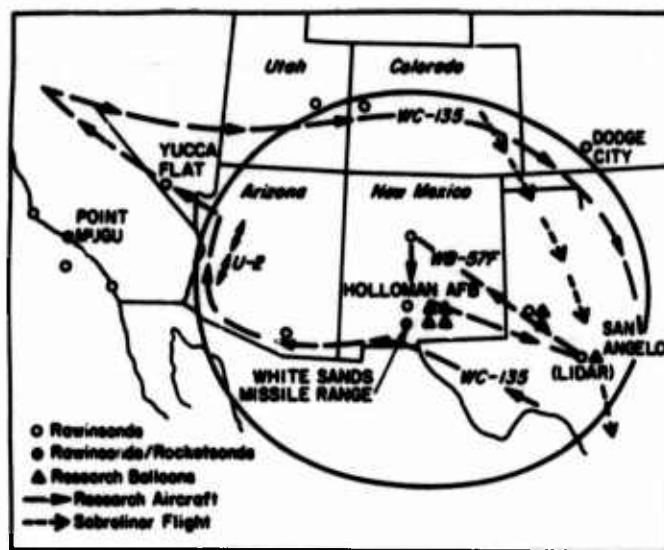


Figure 5. Location and Tracks of LACATE Balloon Program Supporting Measurements

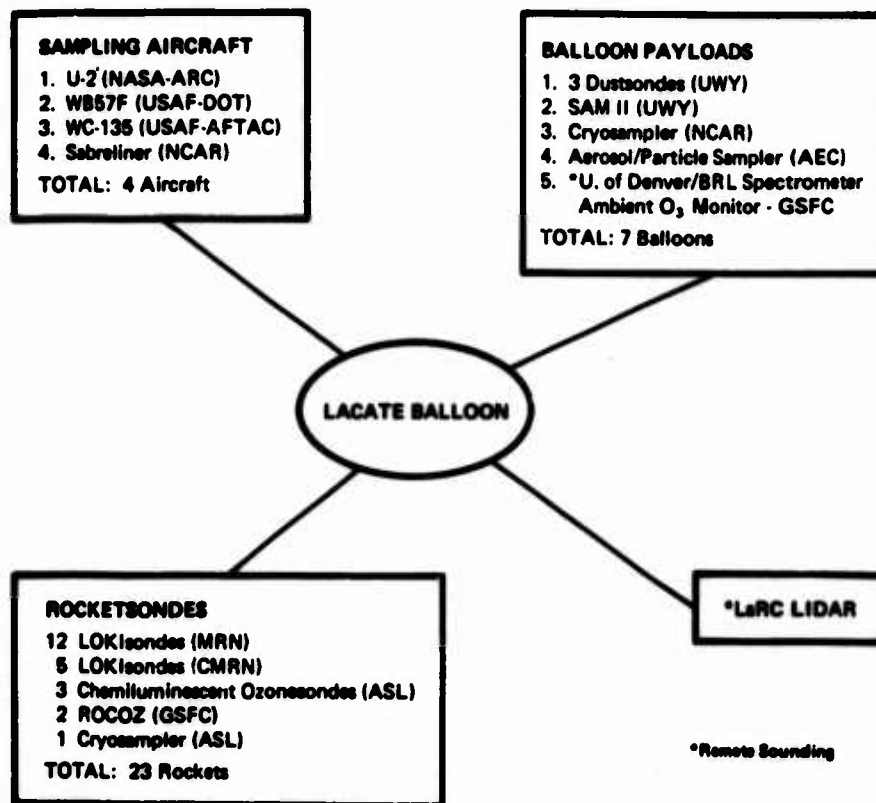


Figure 6. LACATE Balloon Mission Elements of Supporting Measurements Program

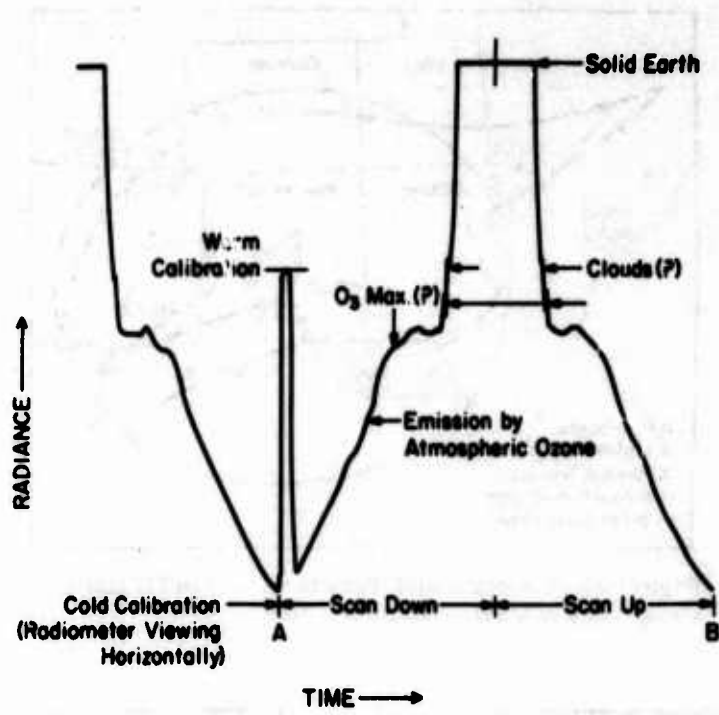


Figure 7. Limb Radiance Profiles, 9.6 μm Ozone Band Measured by Balloon LACATE From 41 KM Altitude Above Holloman, AFB May 5, 1974

Finally, the radiometer should be tested again with all channels operating at noise levels commensurate with those that will ultimately be realized in a satellite instrument.

References

- Ballard, H.N., Beyers, N. J., Miers, B. T., Izquierdo, M., and Whitacre (1972) Atmospheric tidal measurements at 50 km from a constant-altitude balloon, J. Appl. Met. 2(No. 7): 1138-1149.
- Crutzen, P. (1970) The influence of nitrogen oxides on the atmospheric ozone content, Quart. J. Roy. Met. Soc. 96: 320-327.
- Crutzen, P. (1974a) A review of upper atmospheric photochemistry, Can. J. Chem. 52: 1569-1581.
- Crutzen, P. (1974b) Estimates of possible future ozone reductions from continued use of fluoro-chloro-methanes (CF₂Cl₂, CFC1₃), Submitted to Geophys. Res. Ltrs.
- Gille, J. C., and House, F. B. (1971) On the inversion of limb radiance measurements I: Temperature and thickness, J. Atm. Sci. 28(No. 8): 1427-1442.
- Johnston, H. S. (1971) Reduction of stratospheric ozone by nitrogen oxide catalysts from supersonic transport exhaust, Science 173: 517.
- McKee, T. B. (1972) Inference of stratospheric temperature and water vapor from limb radiance profiles. Atm. Sci. Paper No. 178, Colorado State University, Fort Collins, Colo., 111 pp.
- McKee, T. B., and Cox, S. K. (1973) Stratospheric temperature profiles from limb radiance measurements, J. Appl. Met. 12: 867-873.
- Molina, M. J., and Rowland, F. S. (1974) Stratospheric sink for chlorofluoromethanes - chlorine atom catalyzed destruction of ozone, Nature 249: 810-812.
- Reynolds, R. D., and Wallis, A. L., Jr. (1970) An analysis of the boundary layer associated with floating balloon systems. Proc. 6th AFCRL Balloon Symposium: 471-476.
- Russell, J. M., III, and Drayson, S. R. (1972) The inference of atmospheric ozone using atmospheric horizon measurements in the 1042 cm⁻¹ band, J. Atm. Sci. 29: 376-390.
- Stolarski, R. S., and Cicerone, R. J. (1974) Stratospheric chlorine: A possible sink for ozone, Can. J. Chem. 52: 1582-1591.
- Study of Critical Environmental Problems (SCEP) (1970) Man's Impact on the Global Environment. The MIT Press, Cambridge, Mass.

Contents

1. Introduction
2. Design Criteria
3. Performance
4. Operating Experience

Design And Operating Characteristics Of A Balloon-Borne Vacuum System

R. O. Woods
Sandia Laboratories
Albuquerque, New Mexico

Abstract

Many instruments used for atmospheric research require vacuum pumps. Such pumps typically expend amounts of electrical energy which are large by ballooning standards or depend upon systems which operate only for limited times after being separated from their supplies of cryogenic liquids. In relatively low-altitude experiments it is possible to fly enough weight (batteries or cryogenic reservoir capacity) to support laboratory style vacuum pumps. This has been done successfully by earlier experimenters. At higher altitudes, particularly when flight times on the order of days are planned, use of conventional laboratory hardware ceases to be practical.

This paper will describe a vacuum pump which was specifically intended for use in balloon experiments at altitudes approaching 50 kilometers. In addition to light weight, the system was designed for a prolonged liquid nitrogen holding time and an unusually high intermittent pumping speed. It differed in several important respects from pumps of the conventional laboratory configuration.

The hardware has been briefly described in the literature¹. This presentation will stress performance data along with the sort of operational details which only intrude themselves when a system is taken to the field.

¹"A Cryopumping System for Balloon-Borne Mass Spectrometers,"
R. O. Woods and T. K. Devlin, Rev. Sci. Instrum. 45 1, pp 136-137.

1. INTRODUCTION

A program of atmospheric mass spectrometry performed from rockets has existed at Sandia Laboratories for a number of years. In 1971 the prospect arose of performing measurements at lower altitudes using balloons as carriers. Our experience in rocket instrumentation provided a good background for such measurements, but considerable work remained to be done in order to adapt the basic mass spectrometer to the new environment.

The mass analyzers themselves were modified by installing new ion sources which were capable of looking at ambient ions as well as neutrals. Pulse counting circuitry was developed to extend the sensitivity of the instruments below the range of the electrometers which had previously been exclusively used. In addition, the vacuum pump described here was developed specifically for the balloon environment. This equipment has been flown twice on the "Stratcom" series and is currently scheduled to fly again in the spring of 1975.

2. DESIGN CRITERIA

Stratcom I was to fly at a nominal altitude of 50 kilometers for a period on the order of 24 hours. Net payload weight was to be 250 pounds, of which the mass spectrometer system was to comprise a small fraction. The payload was to be recovered by parachute, and it was hoped that the mass spectrometer would survive to the extent that it could be flown on subsequent experiments with a minimum of refurbishing.

The pump and an enlarged view of the modified ion source are shown in Figure 1. The reader is referred to Reference 1 for additional details. In order to establish scale, note that the entire assembly shown in the drawing is 120 cm high.

A zeolite pump was chosen because of the prohibitively great weight of batteries required to power an active pumping system for the required length of time.* It was found, however, that no

*As a matter of interest, the energy densities of several typical flight-type batteries are given below. This information was furnished by Preston Herrington of Sandia Laboratories:

AgZn	40 watt hr lb ⁻¹	
AgCd	25-35 watt hr lb ⁻¹	
Nicad	15 watt hr lb ⁻¹	
Pb-Acid	10 watt hr lb ⁻¹	(max)

suitable laboratory style zeolite pump was available. In fact, little effort has even now been expended to optimize laboratory pumps of this type. Zeolite and liquid nitrogen are relatively cheap and the weight and volume of laboratory equipment are not normally of any great consequence. Price of the initial investment tends to be the most important consideration in the design of laboratory zeolite pumps, hence designs tend to be straightforward and fairly primitive. The flight environment, on the other hand, places great premiums on weight reduction and economy of cryogenic fluids. Initial cost, within reason, is not an overriding criterion.

The design was chosen to satisfy five basic criteria: (1) High intermittent pumping speed to handle the gas load while data were being taken, (2) the ability to recover pumping speed while holding the pressure at an acceptable level between data cycles, (3) prolonged liquid nitrogen holding time, (4) ease of refurbishing after parachute recovery, and (5) light weight. Each of these will be discussed in turn below.

2.1 Pumping Speed and Recovery

Pumping by zeolite is essentially a surface effect; thus a large surface-to-volume ratio for the zeolite package is desirable if high pumping speed is to be attained. A longer term effect, the diffusion of gas to greater depths in the package, has the effect of reducing the concentration at the surface and thus restoring the pumping speed of an assembly which has been subjected to a pulse of gas. Because of this capability, zeolite was recognized as being uniquely suited to our pumping problem.

The mode of application, gas pulse followed by a relatively longer recovery time, was established by the characteristics of the mass analyzers and payload power supplies. The mass spectrometers had the capability of operating in either an ions or neutral mode using either pulse counting or electrometer detectors. They could be operated in either a scanning or single peak mode. These functions as well as valve opening and closing were controlled from the ground. A typical data-gathering run would involve running through most of the permutations of the control functions and allowing several two-second scans in each. This typically took less than a minute. Such a sequence would be repeated at half-hour intervals

throughout the flight. During the times between data runs the payload would be shut down to conserve power.

22 Liquid Nitrogen Holding Time

The geometry of our design was radically different from that of a laboratory pump for reasons which were dictated primarily by liquid nitrogen economy. As mentioned earlier, the objective was to produce a system which could function for something over 24 hours, i.e., from one sunrise through sunrise the following day. This strongly suggested that the customary arrangement wherein the entire pump is surrounded by a liquid nitrogen reservoir would not be suitable. Such a geometry, while convenient and usually inexpensive to fabricate, has the disadvantage of holding the greatest possible external area at cryogenic temperatures. This creates an insulation problem.

In our design we have chosen to place the liquid nitrogen reservoir at the center of the vacuum chamber, thus modifying the conventional dewar geometry. The evacuated space itself serves to insulate the reservoir, with radiative heat transfer being reduced by polished aluminum shields in the radiation path. The primary route for heat absorption is conduction along the neck of the dewar, and this is mitigated by the cooling effect of gaseous nitrogen flowing out through the same tube. In order to take full advantage of this effect, the neck is elongated; this gives the dewar its traditional shape. The intrinsically good heat transfer situation was improved by adding a layer of aluminized mylar "space" insulation to the outside in order to reduce heating of the stainless steel shell by solar radiation.

23 Refurbishing After Flight

The requisite large surface area could have been obtained through the use of cryopanel in which zeolite material is bonded directly to the surface of metal plates. This arrangement has the advantage of providing excellent heat transfer, although the relatively small quantity of zeolite might not have had a recovery in pumping speed caused by diffusion of gas into deeper layers of a thicker package. A fair amount of art is involved in cryopanel design and fabrication, much of it proprietary and hence not available to us. Both of these factors argued against use of cryopanel in our application, but the most telling reason for choosing another method of packaging the

zeolite was the fact that mechanically bonded assemblies could not be as easily replaced as bulk zeolite during refurbishing of a recovered pump for future use. We settled upon an arrangement wherein the zeolite is carried in eight screened pouches which may be seen assembled to U-tubes filled with cryogen in Figure 1. Flat plates brazed to the tubes provided a heat conduction path much like that of the metal substrate of a cryopanel. This geometry had the great advantage of making it possible to replace a charge of zeolite with a minimum of handling. Insurance was thus provided against the possibility of a pump being contaminated by accidental venting during preflight preparation or as a result of landing impact after flight. It was also arranged that internal damage to the pump could be repaired by machining open a single joint in order to gain access to the interior. It seemed likely that this would be used after the first flight, since recovery was to be by parachute with a nominal impact speed of 30 feet per second.

24 Weight Reduction

The external shell of the pump was made as thin as practical, thus requiring external stiffening rings. Since the reservoir was subjected to internal pressure and hence immune to problems of elastic stability, it could be made relatively light without needing additional reinforcement. The heaviest single part of the system was a modified commercial flange with copper O-ring seal. This was used to provide a bolted joint at which the pump could be separated from the mass spectrometer. The analyzer, along with all electrical feed-throughs, was mounted on a flange which mated with the bottom of the pump. This arrangement made it possible to work with the mass spectrometer in the laboratory simply by connecting it to a ground-based vacuum system. By the same token, it was possible to work with the pump without degrading the analyzer by, for example, venting the electron multiplier.

25 Additional Details

The material used in the outer shell was 304L stainless steel, a very common choice for such purposes. This was also used for flanges, stiffening rings, and fittings. Assembly of these portions was by electron beam welding. The manifold and U-tubes assembly was made of OFHC copper, primarily because of its good properties in cryogenic

systems and to provide good heat transfer. The liquid nitrogen reservoir was made of Nickel 200 because of the high strength at cryogenic temperatures of welded seams as well as the parent metal. Transition was made between the nickel inner structure and the stainless steel outer shell by brazing a stainless steel boss to the inner assembly and electron beam welding it to the outer.

While not strictly pertinent to the pump portion of the system, a remark concerning the electrical feedthroughs might be of interest. During our rocket work we had experienced difficulty caused by corona discharge around exposed high-voltage terminals at reduced atmospheric pressure. In the case of feedthroughs entering vacuum systems, the solution was complicated by the fact that the best connectors for high-voltage cables did not fit any available vacuum feedthrough. The solution involved using a preferred vacuum feedthrough which emerged in a fitting which was sealed at one atmosphere and had an hermetically sealed cable connector on the outer end. This connector mated with the high-voltage cable. Such an arrangement was used on the high voltage and radio-frequency leads to the mass spectrometer with complete success. No electrical breakdown occurred despite the presence of potentials on the order of several kilovolts, and the system had excellent vacuum integrity.

3. PERFORMANCE

Liquid nitrogen holding time has been measured in the laboratory as in excess of 25 hours. This was at an ambient temperature of 27°C, approximately one atmosphere, and without external "Space" insulation. In flight, the holding time should be appreciably longer.

The mass of the entire system, ready to fly, was 23 kg. This includes a 5 kg charge of liquid nitrogen.

Pumping speed was investigated by installing on the pump a shell which carried an adjustable leak and vacuum gauges. Pressure was set to a given value for a time on the order of one mass spectrometer data cycle, the leak quickly valved off, and the pressure decay curve was recorded using an oscilloscope and camera to record the early transient. Additional data were recorded manually over an extended period. Data thus obtained are shown in Figure 2.

Figure 3 shows pumping speed as computed by differentiating the curve of Figure 2 and considering the total volume of the system.

The only similar data which we have seen in the literature is plotted on the same figure for comparison. It pertains to a laboratory style pump charged with several times the mass of zeolite contained in our pump. Unfortunately, these data do not extend far into the pressure range of interest, primarily because the authors were concerned with roughing pump applications and, for their purposes, the pumps hardly worked in our pressure range.

It can be seen that we have a pumping speed nearly two orders of magnitude higher than a commercial pump at the high pressure end. This, incidentally, is substantially higher than the very conservative values which we reported in Review of Scientific Instruments. It should not be naively thought that our pump is capable of maintaining such a high rate for extended periods. The cited reference reports a quasi steady-state pumping speed, i.e., one which the pump can maintain for periods of several minutes. It is closely related to the rate at which air can diffuse to the depths of the package. What we have reported is essentially a transient case (or surface effect) which can be interpreted as the behavior of the pump after "swallowing" a quantity of gas which approximates the amount to which it would be subjected during one cycle of a mass spectrometer experiment. This is the aspect of pump performance which is meaningful to us.

4. OPERATING EXPERIENCE

Check-out and calibration of the mass spectrometer was carried out independent of the flight pump by installing the large flange which carried the entire assembly on a conventional vacuum system. In some cases, it was placed in a bell jar, the bottom flange containing the inlet aperture being removed. In others, where the differential pumping feature of the flight pump was required, only the interior of the mass spectrometer housing would be evacuated to the 10^{-7} Torr or 10^{-8} Torr range which was typical of pressure over the zeolite. In these cases the instrument would communicate with the outside world via the pinhole inlet aperture. This was normally covered by another flange having a tube leading to a leak detector pumping station. The pressure in this portion of the system could be controlled, normally being held in the range of ambient pressures at flight altitude. It was thus possible to simulate the flight

environment for instrument check-out. The tube could also be clamped off in order to prevent leakage into the system through the inlet aperture.

Conditioning of the zeolite for flight was carried out by mating the cryopump with an oven. This was merely a stainless steel box containing four 500-watt commercial heat gun elements. It was equipped with an inlet tube through which cool air could be admitted, a pyrometer, and an exit tube which engaged the vent tube seen running halfway up the neck of the dewar in Figure 1. Power was supplied through a large Variac. An external pump circulated roughly two litres of air per second through the system. Power input was normally in the vicinity of 600 to 700 watts, although as much as 900 watts was used on occasion. Air temperature at the inlet to the cryopump ranged between 150°C and 350°C. A bake cycle would normally last on the order of 12 hours. During this time the system would be continually pumped by the leak detector station. At the end of the bake cycle, power to the oven was turned off allowing air to be circulated at ambient temperature for gradual cooling of the internal portions of the pump. When cooling began, pressure over the zeolite was typically in the vicinity of one Torr. This dropped into the 10^{-5} Torr range as the zeolite reached room temperature. The fact that the pressure reached this range proved to be a convenience since it made it possible to turn on the mass spectrometer for check-out without having to chill the zeolite.

Because of the well known improvement in pumping speed which takes place when zeolite is heat cycled several times, the above bake cycle should be repeated four or five times before flight. In our case this happened naturally in the course of pump check-out.

Actual final preparation for flight began with the installation of the mass spectrometer on the cryopump. Since this involved opening a partially conditioned zeolite system, the pump was vented to atmospheric pressure. This and subsequent venting was done using helium. This preserved the pumping capability of the zeolite, although it made difficult the use of a helium leak detector.

After the mass spectrometer was installed, pumping was performed by connecting the leak detector station to the cryopump via a copper tube pinchoff. This was used in order to save flying the weight of a high-vacuum valve. The pinchoff provided a fairly versatile pumping port since it was possible to make intermediate connections using a flexible tube which had been slid over the copper. This tube

could itself be temporarily clamped off. In many cases it was possible to reconnect to the system after the copper tube was pinched by reinstalling the flexible tube and then breaking the pressure welded pinch joint from outside without venting the system.

Transporting of the system to the field could be accomplished with the pump in any of several conditions. Ideally, it would be done with the pump conditioned and evacuated and the sampling valve installed over the inlet aperture. This would allow the system to be flown with no further preparation than charging with cryogen. This was not possible in practice because the sampling valve was always the least reliable part of the system. Any leakage at this point during shipment would ruin the conditioning of the zeolite. A more conservative approach was taken in which the pump was shipped with a flange installed over the inlet aperture in place of the valve, a flexible tube connected to the copper pinchoff and clamped shut, and the system filled with helium at one atmosphere. This made it possible to check out the mass spectrometer after reaching the field, vent the system once to install the valve and then finally condition the zeolite for flight.

The sampling valve shown as the bottom-most assembly in Figure 1 was not entirely successful and was replaced, after the first flight, with a more shock resistant design. The first valve was a rotary solenoid operated mechanism which moved a Teflon plug to open or close the sampling aperture. Its weakness lay in the fact that in order to apply a following load to the valve plunger it had been necessary to spring load the entire assembly against the mass spectrometer housing. This allowed enough random motion to permit the valve to be momentarily shaken open during a particularly rough launch. At this point we abruptly evolved a design philosophy for balloon payloads, i.e., design to the same shock and vibration standards used for rocket payloads. The solenoid-operated valve was replaced with a pneumatic system designed on this basis, and the system functioned satisfactorily on a subsequent flight.

At least two days before the scheduled flight date, final chill-down of the system was begun by charging the reservoir with liquid nitrogen. This was done by simply inserting a tube from a large storage dewar into the neck of the cryopump and pressure feeding the cryogen. Liquid level was monitored using a simple dipstick. If any possibility existed that water had condensed inside the reservoir, it was blown out for several hours beforehand with dry air.

The exact time at which filling began involved a trade-off. It was desirable that the pump be operating for check-out as early as possible since, if it became necessary to open the system to repair any problems found during testing, a turnaround time of at least two days would be required to recondition the pump for flight. On the other hand, the flight sampling valve was subject to creep problems which made it advisable to replace the Teflon plunger after about a week under pressure. This entailed venting the system.

Once the pump was chilled, a turnaround cycle involved blowing out the charge of liquid nitrogen and warming to room temperature, a 12-hour operation. The system would then be vented with helium, opened, repaired, and closed. This would be followed by a day and a half of baking, then another cool-down period of roughly half a day.

The performance of the pump as liquid nitrogen was added to a system initially at room temperature is shown in Figure 4. It will be noted that in this particular case the room temperature pressure over the zeolite was 2.5×10^{-5} Torr, a fairly respectable vacuum. The ability of zeolite to pump at room temperature has only recently been explored.²

When liquid nitrogen was added a dramatic drop in pressure began almost instantly. After a period on the order of 10 minutes, when the pressure was in the mid 10^{-7} Torr range, an equally abrupt rise in pressure would begin. This behavior is explained as being due to cryopumping on the metal walls of the reservoir. The process begins immediately, but becomes ineffective when the walls are saturated. At this point, the pressure again tends to the equilibrium pressure over the zeolite which has barely begun to cool. Subsequent reductions in pressure reflect the rate at which the zeolite package cools.

It can be seen in Figure 4 that the pressure in the pump was down to the 10^{-7} Torr range after about four hours. On this run the zeolite had been particularly well conditioned, and the final pressure was in the high 10^{-8} range. The exact value is not given because the vacuum gauge used to monitor pump pressure had not been calibrated below 10^{-7} Torr. The discontinuity in the curve is an artifact caused by temporary heating and outgassing when the mass spectrometer was turned on.

²Luches, A., and Zecca, A., J. Vac. Sci. Technol. 9 5, pp. 1237-1240 (1972)

A last operation performed only after the payload was committed to fly was the installation of a pressure relief valve set to one atmosphere (gauge). The purpose of this was to avoid unnecessary boil-off of liquid nitrogen by keeping the pressure in the reservoir at approximately one atmosphere at all times. If it becomes necessary to remove this valve after it has been in place for any length of time, one finds himself dealing with a reservoir filled with superheated liquid nitrogen. The preferred way to vent the reservoir is to partially unscrew the plug and allow the pressure to drop gradually. On one occasion the plug was removed prematurely by unscrewing it too far and allowing it to blow out, with results which were more spectacular than edifying.

The pump which we have described was successfully recovered after a parachute landing and reflown without any repairs having been necessitated. After the second flight, it was found to be badly deformed by landing shock but still had vacuum integrity. A backup unit of the same design is to be used on a third flight.

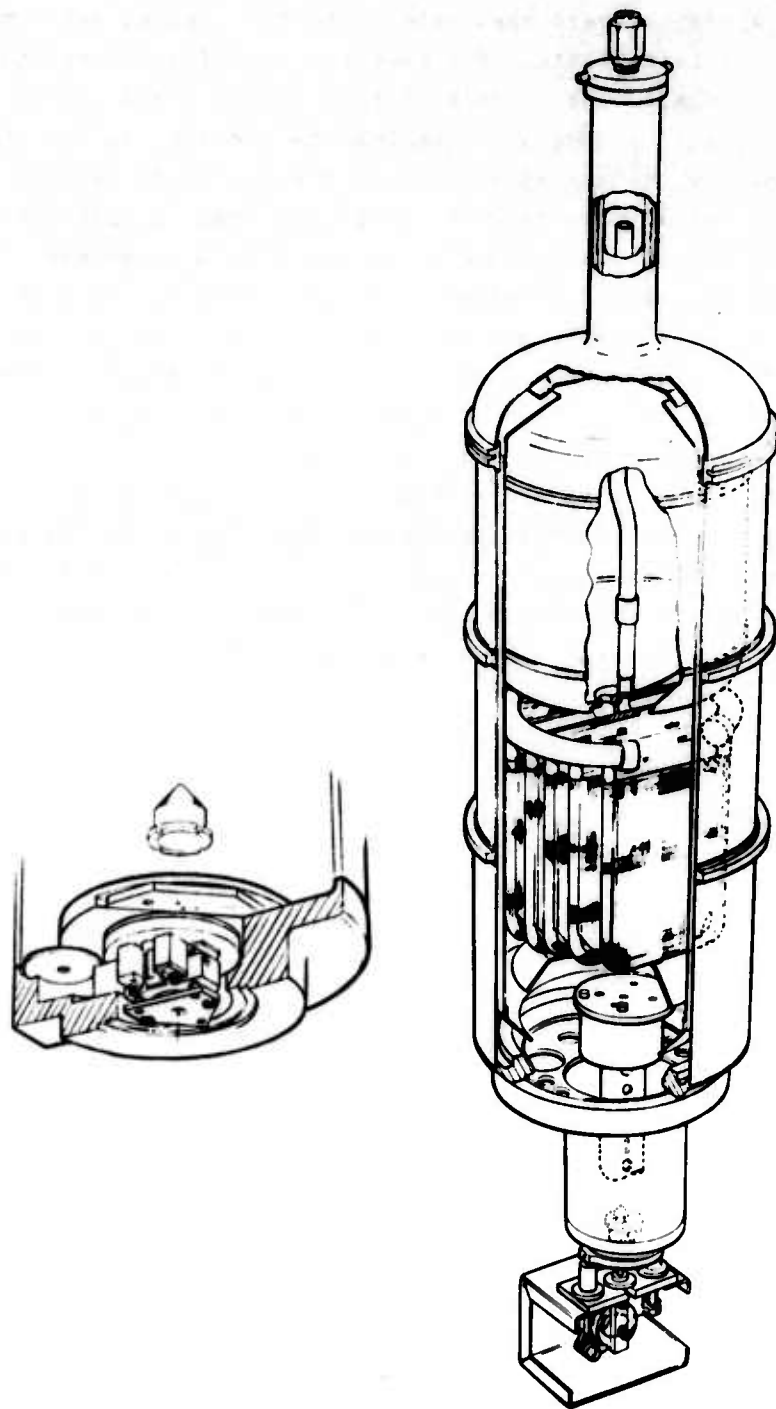


Figure 1. Flight Cryopump with Mass Spectrometer Installed
(The enlarged auxiliary view shows a special ion source intended for balloon experiments.)

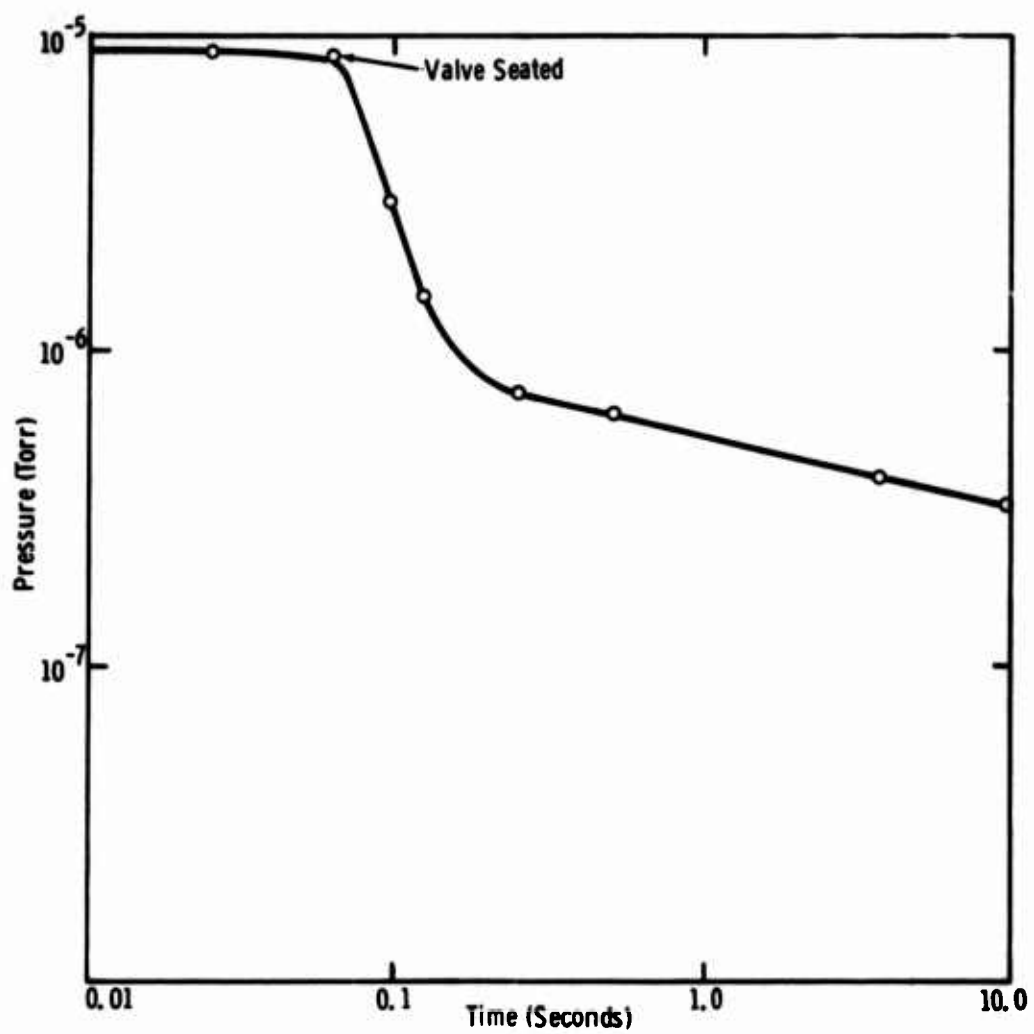


Figure 2. Pressure Transient Inside Pump as a Calibrated Leak Is Valved Off

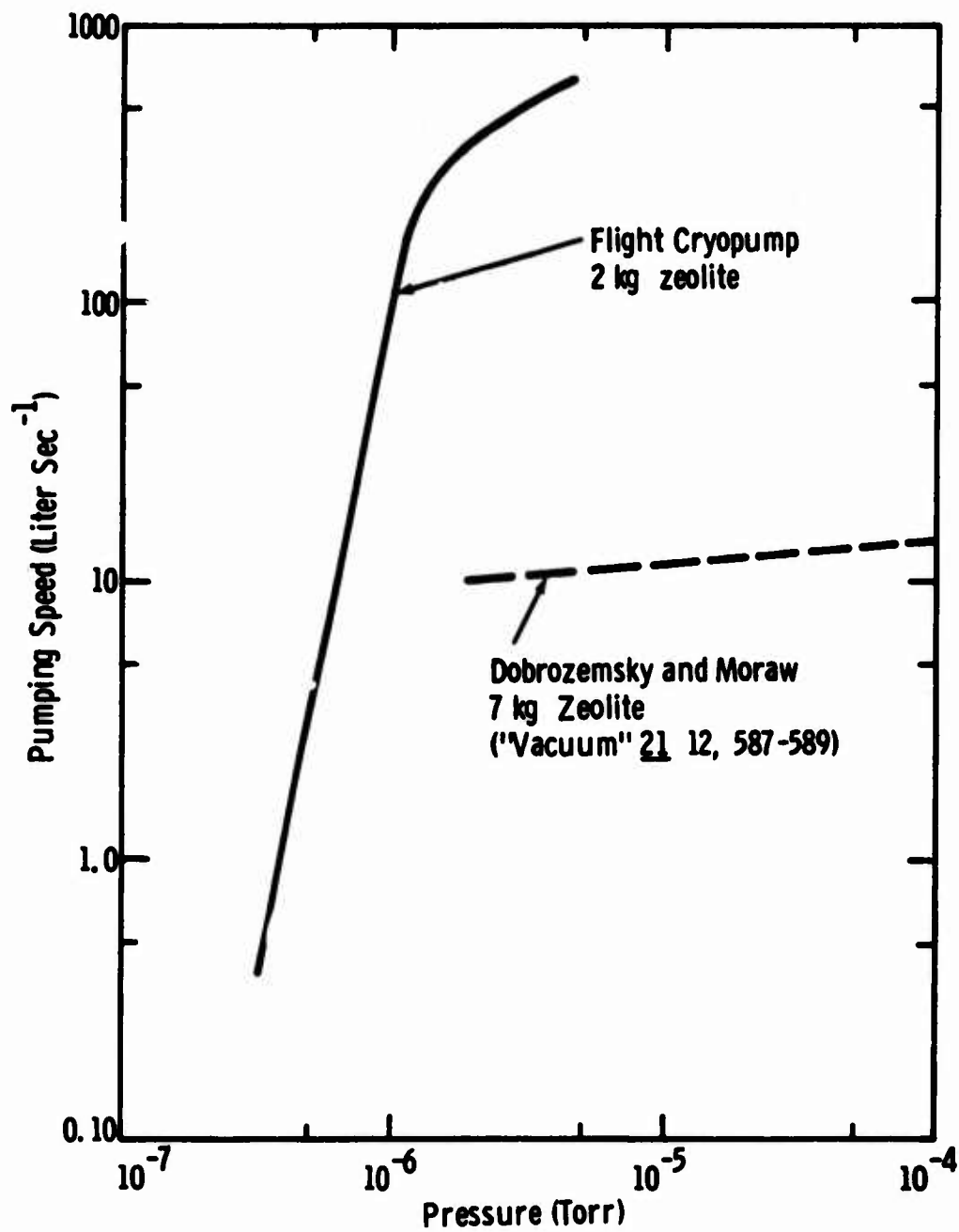


Figure 3. Pumping Speed Computed by Differentiating the Curve of Figure 2. (Similar data from the literature are plotted for comparison.)

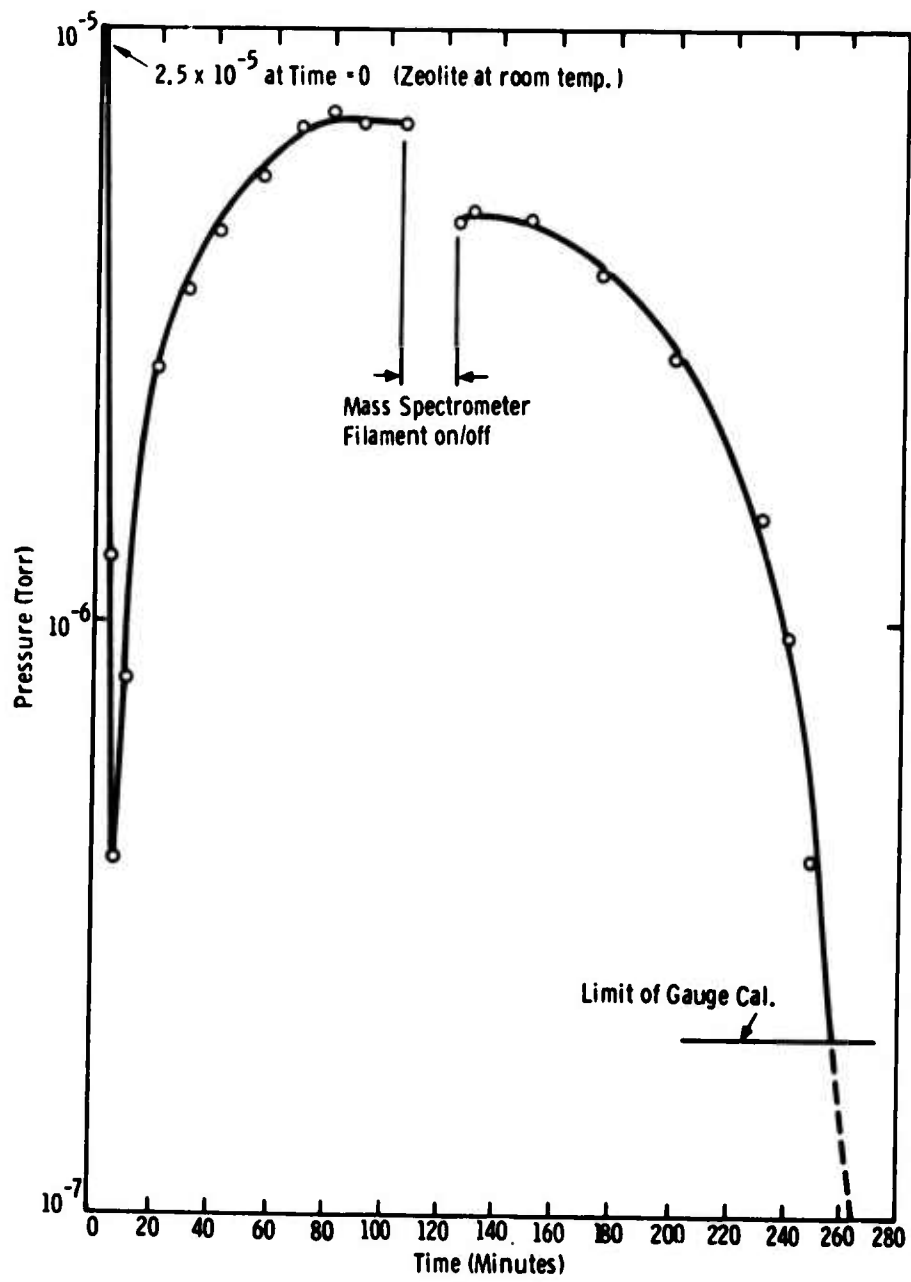


Figure 4. Pressure Inside a Pump Initially at Room Temperature as a Function of Time After Filling with Liquid Nitrogen

Contents

1. Introduction
2. Spin Rate
3. Frame Temperature
4. Levelness

Balloon Gondola Measurements

Preston B. Herrington
Sandia Laboratories
Albuquerque, New Mexico

Abstract

This paper describes measurements of gondola attitude made during a stratospheric balloon flight on September 18, 1972.

1. INTRODUCTION

Spin rate and frame temperature of the gondola and levelness of the main electronics housing were measured during a stratospheric balloon flight on September 18, 1972. The balloon, which had a fully inflated volume of 38.8 cubic feet, was launched by Air Force Cambridge Research Laboratories Balloon Branch from Holloman Air Force Base, New Mexico. The balloon reached a float altitude of 165 thousand feet. The scientific gondola which was approximately 6 feet in diameter and weighed 250 pounds was reeled down to 1200 feet below the balloon on a nylon rope.

The measurements described in this report were not made in order to obtain basic information about gondola attitude or temperature but instead were made to provide support data for the scientific instruments on the gondola. Data were obtained from the instruments continuously for one hour during sunrise and for short periods (approximately 2 minutes) on 18 other occasions.

2 SPIN RATE

A single-axis flux-gate magnetometer (Heliflux^(R) RAM-5C) was used to measure the spin rate of the gondola. The flux-gate used in the RAM-5C is comprised of a tubular-shaped permeable magnetic core surrounded by an excitation winding and a second winding designated as the signal-pickup winding.

An alternating current is passed through the excitation winding such that if there is no other field acting on the core the waveform of the flux produced by the core will contain only the fundamental and odd-order harmonics of the excitation frequency. With a component of the earth's magnetic field intersecting the core, the flux waveform contains even-order harmonics of the fundamental frequency in addition to the odd-order harmonics.

The construction of the sensor is such that the pickup winding is relatively insensitive to odd-harmonic flux but sensitive to even-harmonic flux. The signal conditioning circuits of the magnetometer are tuned to the second harmonic of the fundamental frequency.

A field magnitude within the range of ± 600 millioersted is converted to an analog output voltage, E , defined by

$$E = 2.40 + .004H \cos \theta$$

where H is the ambient field strength in millioersteds, and θ is the angle between the magnetic field vector and the magnetometer reference axis.

The gondola rotation as a function of time is shown in Figure 1. When Figure 1 is compared to the balloon flight profile shown in Figure 2, it can be seen that with one exception the spin rate during ascent is much higher than after float altitude was reached. The one exception occurred between 11:05 and 11:10 GMT. The maximum measured spin rate occurred during ascent at approximately 10:23 GMT and was approximately 1 rpm.

3. FRAME TEMPERATURE

The gondola frame temperature was measured with a bead thermistor which was mounted in thermal contact with a cylinder which was mounted to the gondola frame. The cylinder was 2 inches long and had an outside diameter of

0.75 inch. Both the cylinder and the gondola frame were painted with gloss white epoxy base paint (EPO-LUX No. 100 Type E-1 white).

The variation of gondola frame temperature with time is shown in Figure 3. The minimum measured temperature of -70°F was measured as the gondola ascended through the tropopause. Immediately before payload cut-down, the temperature was 110°F . If the balloon had been left at float altitude throughout the day, it is predicted that the gondola frame temperature would have stabilized at less than 120°F .

4. LEVELNESS

Two potentiometric pendulums were used to determine the levelness of the main electronics housing relative to the levelness during prelaunch tests. The main electronics housing was rigidly mounted to the gondola frame. The full scale measurement range along both axes was ± 5 degrees with a sensitivity of 0.5 volt/degree. The axis of one pendulum was orthogonal to the axis of the other pendulum.

The readings from one of the pendulums throughout the experiment were within ± 0.01 degree of the prelaunch reading. The other pendulum showed an offset of 0.3 degree between the prelaunch reading and the first data point. This offset remained throughout the experiment.

The pendulum data reflects only the levelness of the gondola. The pendulum effect of the gondola on the 1200-foot rope between the gondola and the balloon could not be detected with this device.

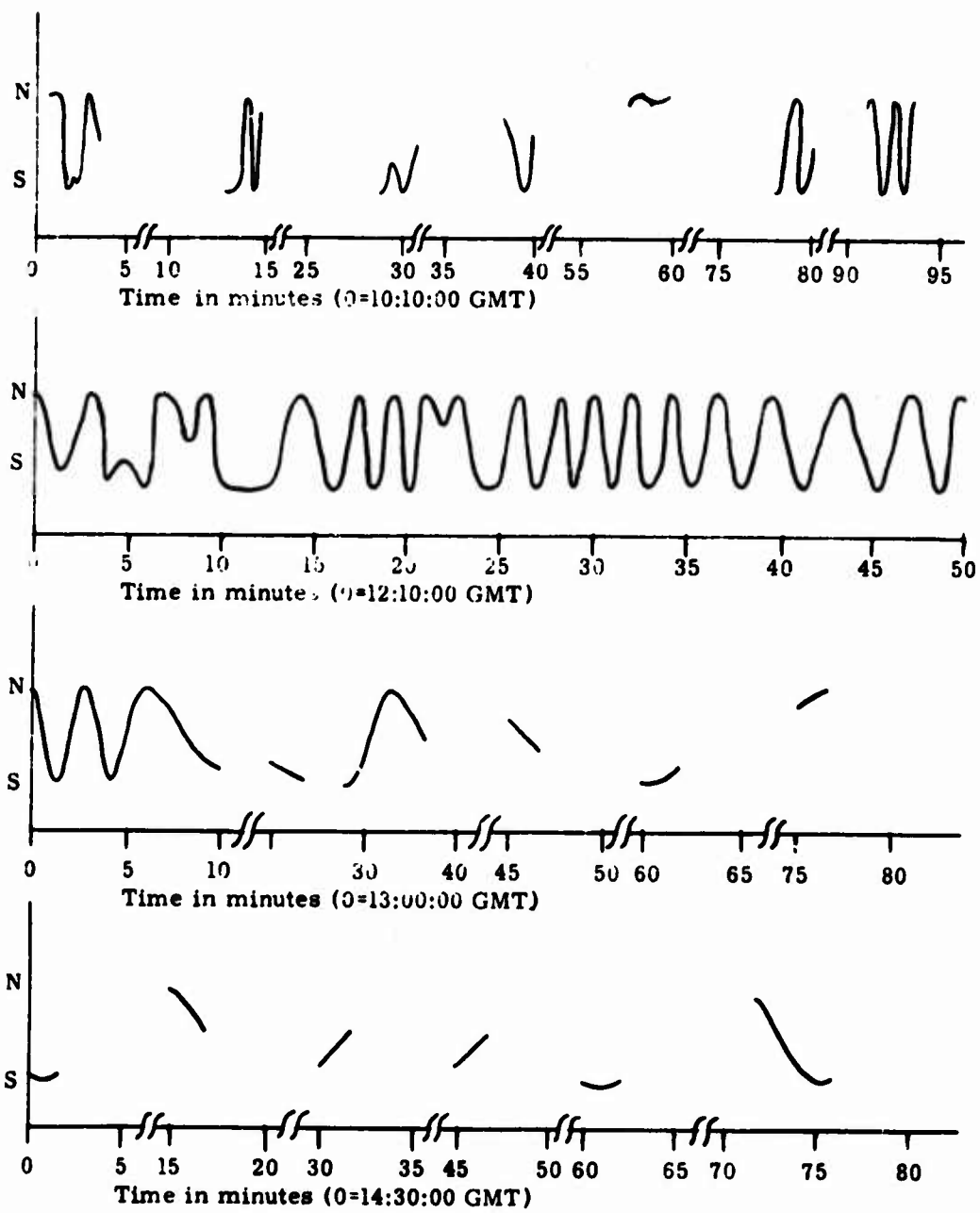


Figure 1. Gondola Rotation

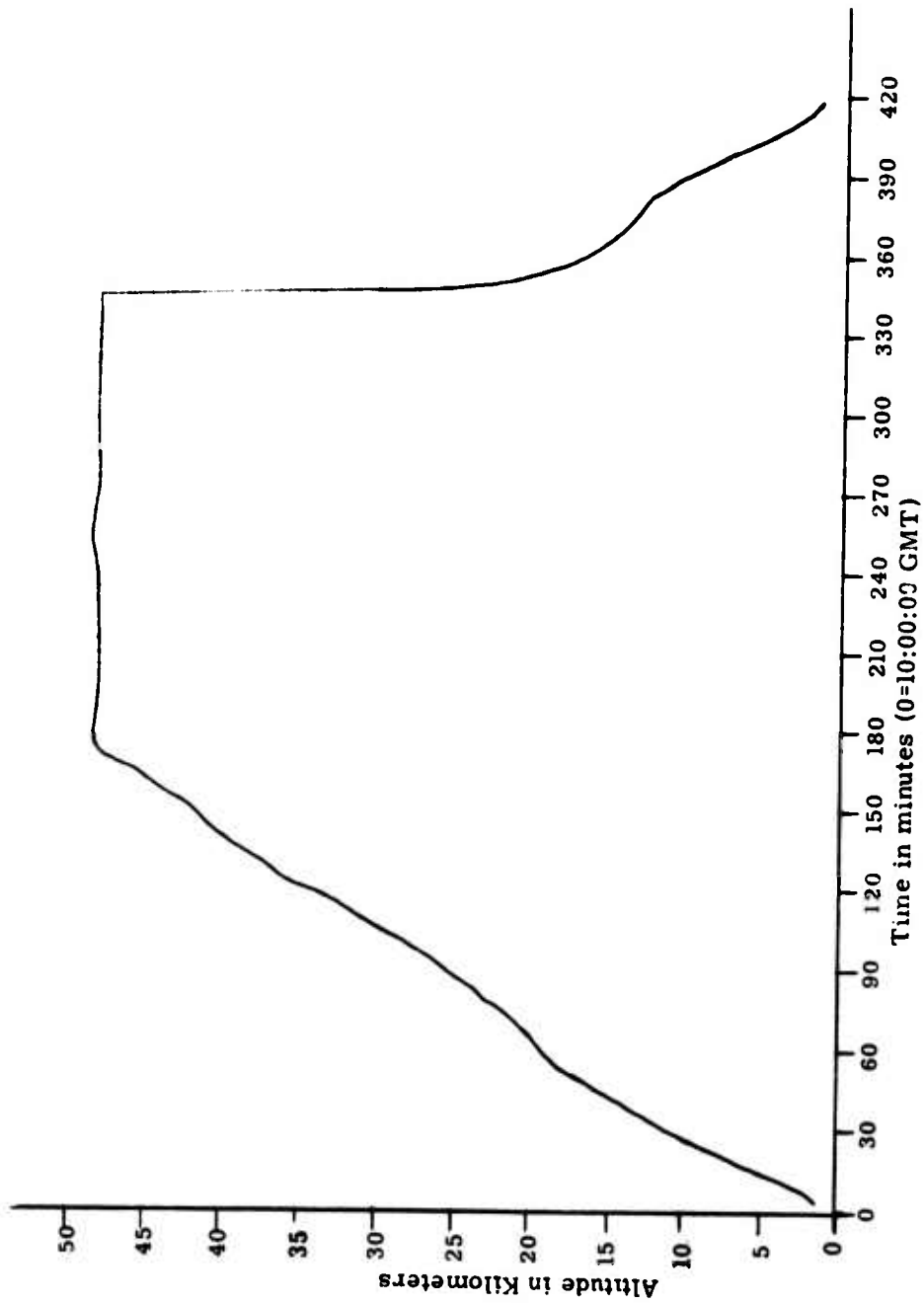


Figure 2. Balloon Flight Profile

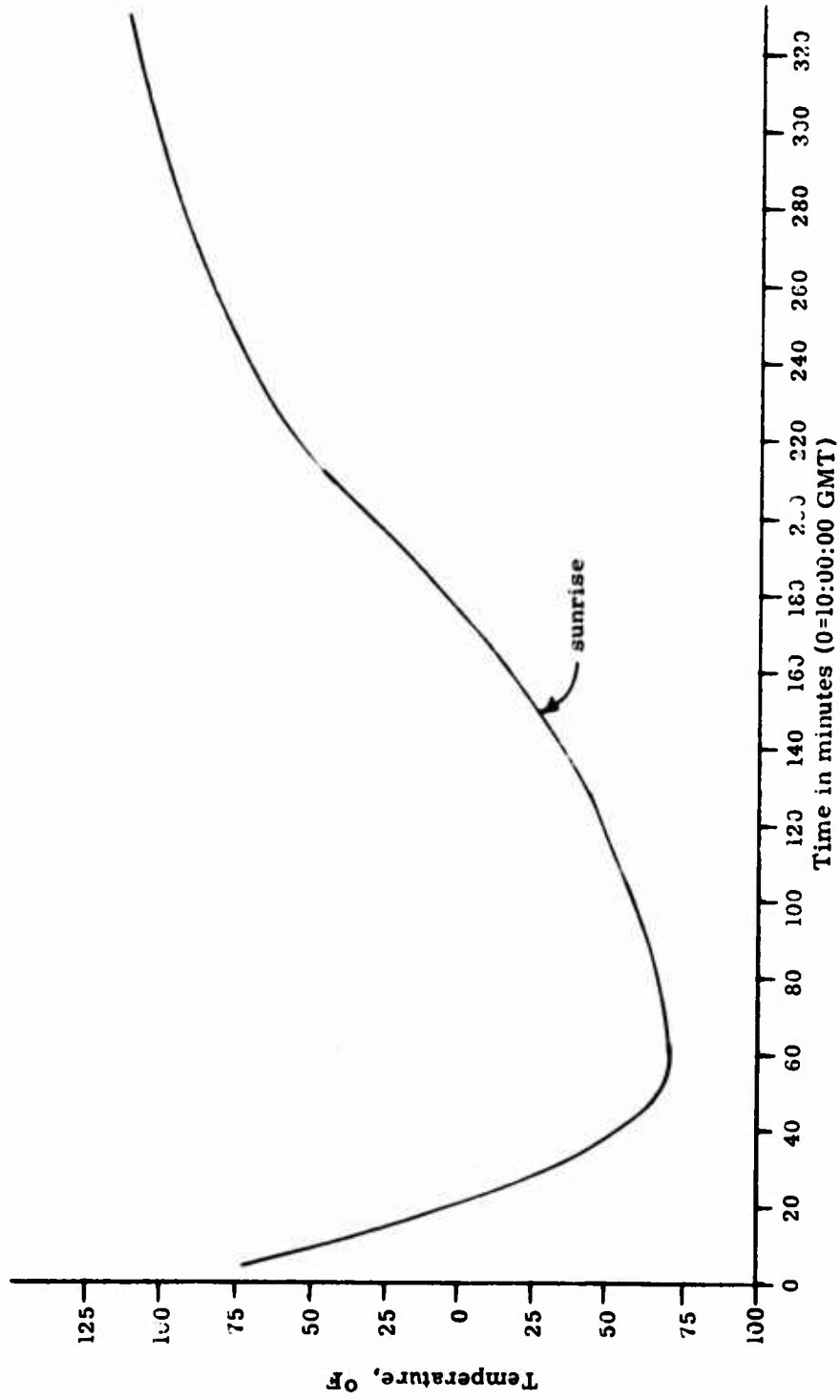


Figure 3. Gondola Frame Temperature

Ames Balloon-Borne Telescope For Infrared Astronomy

Charles D. Swift
Ames Research Center, NASA
Moffett Field, California

Abstract

Ames Research Center is developing a balloon-borne telescope for use in infrared astronomy investigations. It is a 28-inch cassegrain with an oscillating secondary mirror for phase lock detection of sources. Stabilization and star tracking are provided by a video inertial pointing system (VIP), which combines star field information from an onboard TV camera with rate-integrating gyros in a closed-loop system to track visible objects both on or off the optical axis of the telescope. Command and telemetry subsystems are included on the gondola. Ground facilities for this system include a mobile ground station that allows the investigator to control the telescope and focal plane instruments. All data can be monitored and recorded from the gondola, including star field information from the TV camera. Other ground facilities include laboratories for instrument development and calibration and an observatory for the balloon-borne telescope. It is possible to operate the telescope suspended in complete flight readiness in this observatory. The goal of this balloon-borne astronomy project is to develop a vehicle and ground facilities that allow maximum use of the vehicle for research and development.

Ames Research Center has developed a balloon-borne telescope as part of its program in infrared astronomy. The far-infrared astronomy under consideration is described briefly to help explain the requirements placed on the design of this system.

The wavelength range of interest is from 10 μ to 1 mm. Observations from the ground are impossible over most of this range because of absorption by the earth's atmospheric water vapor. Many celestial objects radiate great amounts of radiation in the far IR. The sun, of course, is the strongest source viewed from earth, followed by the moon and the planets, which actually radiate most of their power between 10 and 100 μ .

Beyond our solar system, the strongest sources are no longer associated with bright visible objects but with gas and dust. The brightest sources are the galactic center, the Orion Nebula, and other HII and molecular cloud regions. Outside our galaxy, the strong sources are unusual faint galaxies where apparently there is violent thermal or nonthermal activity.

The objectives in IR astronomy are to find and to identify these sources of infrared radiation and to determine the mechanisms responsible for the radiation. This information is valuable in understanding stellar and galactic evolution.

These objectives generate four major technical requirements. First, it is necessary to develop and use detector systems cooled to below 4°K in order to have sufficient sensitivity in the far IR. Second, it is necessary to observe from above the earth's water vapor - above about 45,000 ft with real advantages above 100,000 ft or all the way into space. Third, it is necessary to find and track nonvisible objects with a pointing accuracy of better than 2 arcmin. Finally, it is necessary to use techniques to discriminate (or eliminate) the background radiation from the atmosphere and the telescope itself, which is at the same wavelength as the source radiation and many orders of magnitude more intense. The design of the Ames balloon-borne telescope attempts to meet these requirements.

AIROscope (fig. 1) was originally developed as Polariscope at the University of Arizona by T. Gehrels and his associates for observations at ultraviolet wavelengths (Coyle & Gehrels, 1968). It is about 15 ft tall and weighs about 1500 lb. This system has been modified at Ames for IR astronomy (Koontz & Scott, 1974).

Table 1 includes the important details of the system - a 28-inch-diameter Dall-Kirkham telescope with a secondary mirror figured for an f/12 beam. The secondary mirror can be oscillated by command to allow the liquid-helium-cooled detector at the focal plane to alternately view areas to the right or left of the centerline of the telescope. This oscillation is square wave and not, for example, sinusoidal. It has an amplitude of typically 5-10 arcmin, and two frequencies of 11 and 21 Hz are selectable.

Table 1. Description of AIROscope

Optics:	71-cm-diameter, f/12 Dall-Kirkham with oscillating secondary mirror; 11 and 21 Hz selectable
Gondola:	5 by 2 by 2 m; total weight, 950 kg
Stabilization:	Magnetic compasses for coarse acquisition Gyrostabilized in elevation and cross elevation Video star tracking in an 8° field of view to 2 arcmin
Commands:	256 commands with an RF frequency of 405.4 MHz
Telemetry:	10 bit words at a rate of 20,480 bit/sec with an RF frequency of 1483.5 MHz
Detector:	Gallium-doped germanium bolometer cooled to 2°K with liquid helium
Wavelength:	Selectable cooled filters provide bandpasses (as many as 12) between 10 and 400 μ
Sensitivity:	100 flux units between 22 and 90 μ

Before observations, the telescope is carefully baffled and aligned so that the detector views equal amounts of the telescope and sky in each of the two displaced positions of the secondary mirror. During observations, the object of interest is tracked in either the right or left beam, the sky being observed in the other beam. The output of the detector is amplified by a phase lock amplifier synchronized to the oscillations of the secondary mirror. The amplifier output is the difference between the signal in the left beam and the signal in the right beam and is therefore proportional to the source intensity. This is the method used to cancel the background from the sky and telescope.

The instrument currently being used is a filter spectrometer and gallium-doped germanium bolometer both cooled to 2°K. These are housed in a liquid helium cryostat designed to maintain the low temperature for as much as 20 hours. As many as 12 bandpasses are selectable in flight. Bandpasses between 10 and 400 μ are presently used. System sensitivity was measured to be 100 flux units ($10^{-24} \text{ W-m}^{-2}\text{-Hz}^{-1}$).

Figure 2, a block diagram of the system, includes the command and telemetry subsystems which make possible control and data retrieval at the ground station. Another major portion of the system is the tracking and stabilization subsystem. It utilizes magnetic compasses for coarse pointing, gyros for stabilization in elevation and cross-elevation, and a TV camera for star field recognition and fine

pointing. Except for the television, this is a conventional gyrostabilized system (Murphy & Lorell, 1974).

The television is used for the offset tracking required because most of the objects of interest are not bright enough at visible wavelengths to track them directly. Tracking is done using the video signals from the stars adjacent to the infrared source. This is simple in concept but requires fairly sophisticated electronics to accomplish. (The reader is referred to a complete description by Deboo et al. (1974).)

Only half of a complete balloon-borne telescope system is launched; the other half, of course, is the ground station. Figure 3 is a drawing of the ground station associated with AIROscope. It is housed in a 40-ft semitrailer van, which is used to transport the telescope to the launch site and as a field shop facility as well.

The telescope is controlled during testing and flight from the ground station. A video display is used by the astronomer to recognize the star field being observed. There are controls for commanding the telescope tracking and other functions. The equipment is controlled at the focal plane from an investigator's console. Various readouts and controls are provided at the engineer's console to monitor and control engineering functions.

All commands and all data including the video are tape recorded. Timing information from WWV is recorded. All conversation in the ground station is recorded. Therefore, it is possible, after the investigation, to replay the entire investigation for analysis and diagnosis of the system.

Since the ground station is the center of activity after launch, a description of these activities will illustrate the capabilities of the system. Three people are directly involved in the operation: one at the engineering console monitors the performance of the system during ascent as well as during observations; one is at the pointing and stabilization console with its video monitor; and one at the investigator's console monitors the performance of the cryogenic equipment at the focal plane.

After reaching float altitude, the telescope is focused and aligned by moving the secondary remotely from the engineering console for best image and for best cancellation of the infrared background. While the compasses are monitored, the telescope is commanded to turn to the azimuth of the infrared source. It is then commanded to the correct elevation. The astronomer then observes the stars on the TV monitor in the field of view. After calculating the angles between the unseen infrared source and the visible stars, the observer sends commands to properly set electronic tracking gates so that the visible star can be tracked while the infrared source remains focused on the detector. These gates are moved periodically to correct for the earth's rotation and balloon drift. During this time, the

instrumentation at the focal plane is operated by sending commands from the investigators console. The entire operation is recorded. When sufficient data have been obtained, the telescope is reoriented onto the next source in the observing plan.

Although this system has been used for observation, it is still in a development phase. Part of this development is on-going in response to requirements of the investigations planned. In addition, improvements of a general nature are under way. The major one is to strengthen the gondola structure so that repeated launches can be made with essentially no repairs needed. Also, the stabilization system is to be completely rebuilt. The expected advantages are better pointing accuracy and the capabilities to use multiple instruments at the focal plane and to carry other experiments "piggyback" on the gondola. The video stabilization is being developed further to allow tracking on two stars simultaneously. This will provide automatic corrections required by earth rotation and balloon drift.

This system is being developed to meet the requirements of infrared astronomy as outlined earlier. It illustrates that, with modern engineering techniques, it is possible to provide astronomers with a reliable, rugged telescope suitable for balloon-borne research. This telescope and other balloon-borne telescopes will be valuable evolutionary steps toward the future use of telescopes in space.

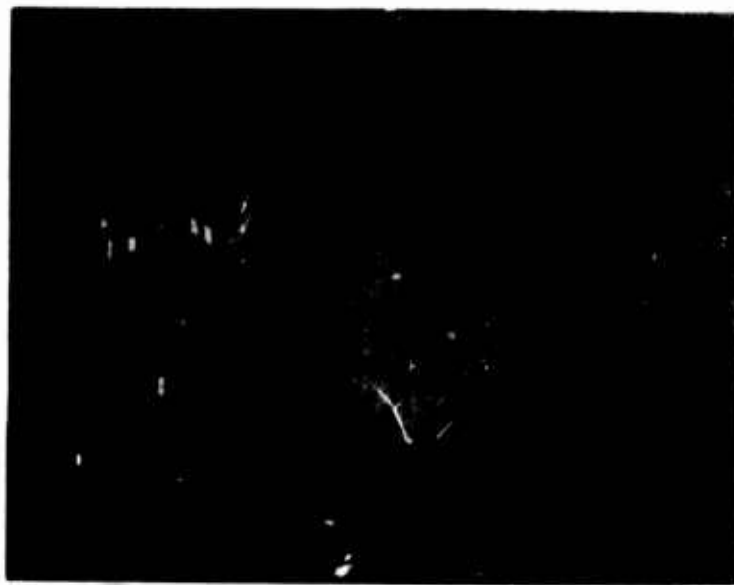


Figure 1.- AIRScope ready for launch.

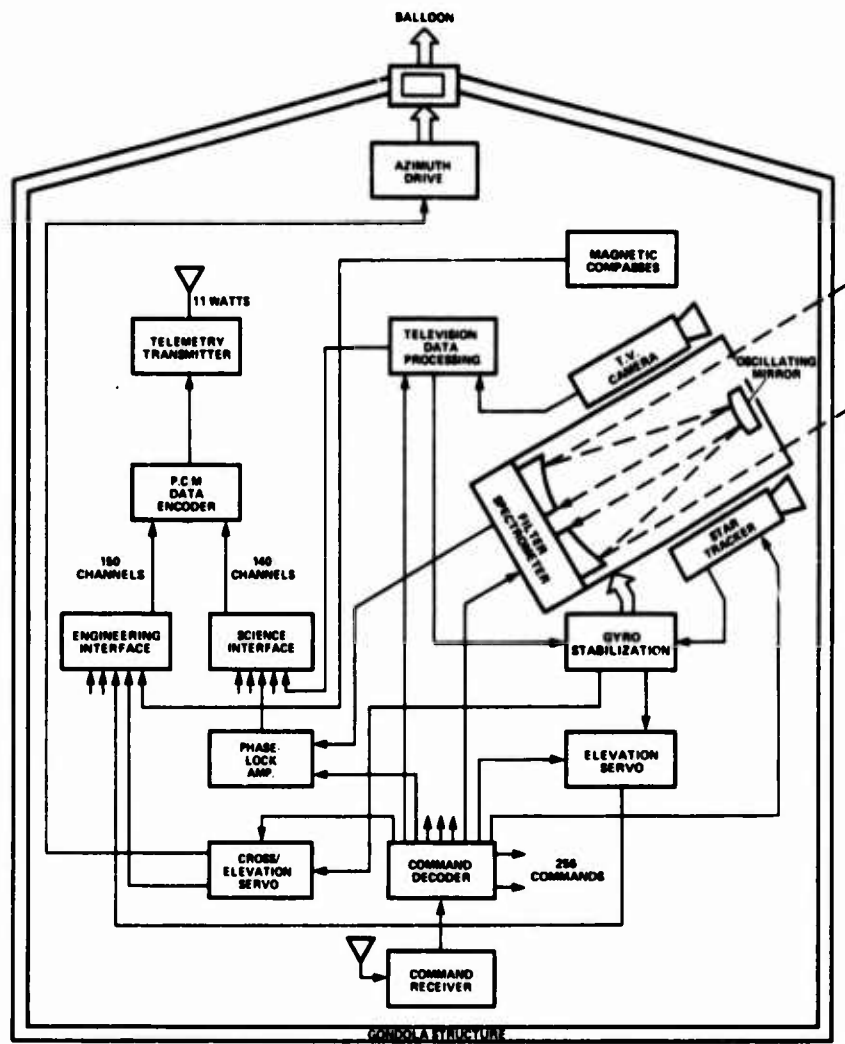


Figure 2.- Block diagram of AIRscope.

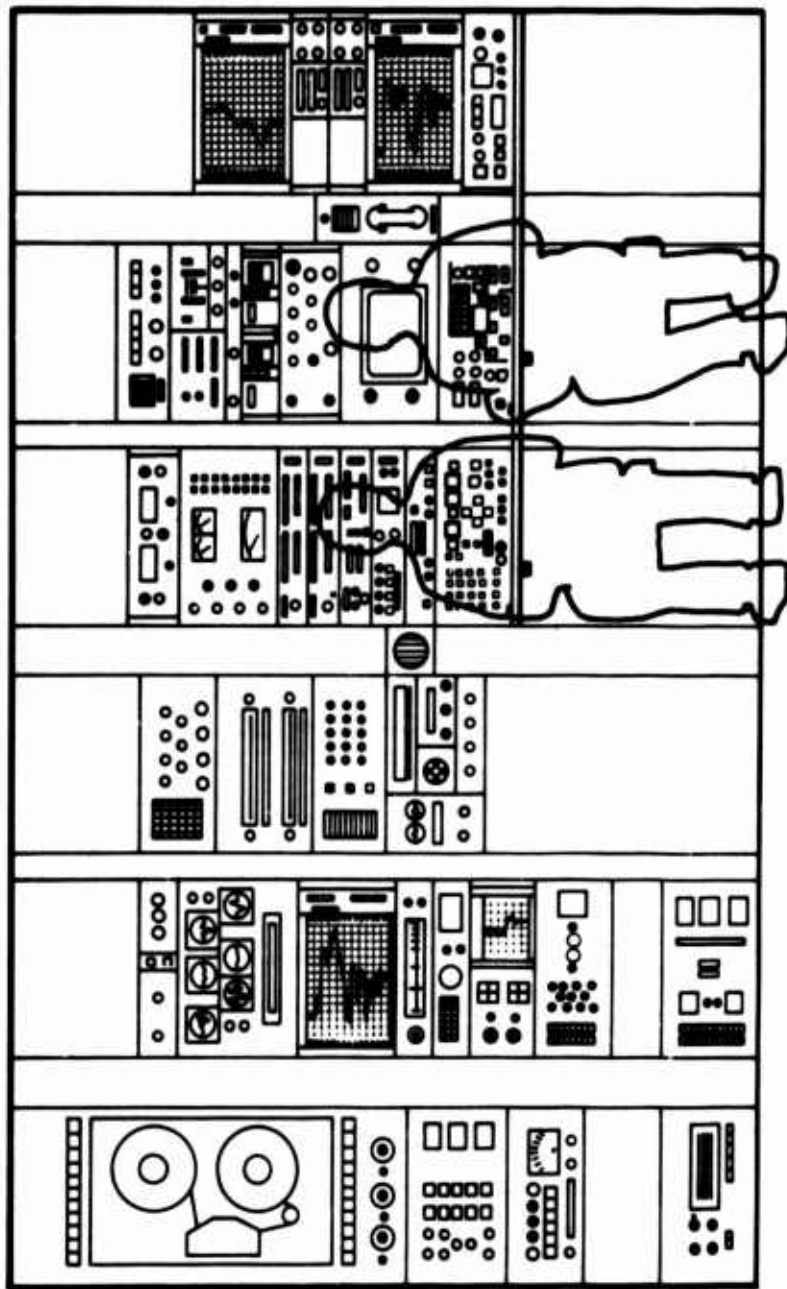


Figure 3.- AIMOScope ground control station.

References

- Coyne, G. V. and Gehrels, T. (1968) Polarimetry from high-altitude balloons, Communication of Lunar and Planetary Laboratory No. 108.
- Deboo, G., Parra, G., and Hedlund, R. (1974) AIROscope stellar acquisition, Proceedings of the Symposium on Telescope Systems for Balloon-Borne Research (to be published).
- Koontz, O. L. and Scott, S. G. (1974) AIROscope, Ames infrared balloon-borne telescope, Proceedings of the Symposium on Telescope Systems for Balloon-Borne Research (to be published).
- Murphy, J. P. and Lorell, K. R. (1974) The AIROscope pointing and stabilization system, Proceedings of the Symposium on Telescope Systems for Balloon-Borne Research (to be published).

Contents

1. INTRODUCTION
2. PLATFORM
3. STAR TRACKER
4. TV CAMERA
5. TARGET ACQUISITION
6. COARSE ATTITUDE CONTROL
7. FLIGHT PERFORMANCES

Flight Performances Of The Geneva Stellar Platform

Daniel A. Huguenin
Geneva Observatory
CH-1290 Sauverny, Switzerland

Abstract

This paper describes the new stellar balloon platform of the Geneva Observatory and gives the performances of the pointing system during the flight of April 1974. It explains how the compound pendulum motion was suppressed by an inertial viscous damper, how 12 targets were acquired and measured during a two-hour period, and how pointing at stars was accomplished during twilight.

I. INTRODUCTION

The interest of astronomical UV experiments from stratospheric balloons has been underlined by Kondo et al. (1974) and Navach et al. (1973). Rigaud (1973) demonstrated that it was possible to determine the reduced thicknesses of several atmospheric constituents, in particular ozone, and their variation at sunrise, by measuring the atmospheric extinction of UV stellar fluxes from balloon. Courtès and his team

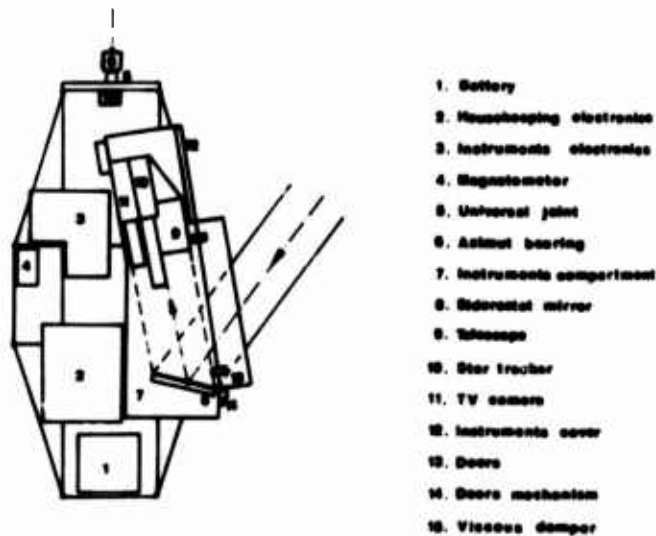


Figure 1. Schematic outline of the gondola

at the Laboratoire d'Astronomie Spatiale, in Marseille, designed several fine instruments for wide angle UV photography of the night sky.

Because of the present budget restrictions, it is often impossible to find a vehicle to launch these payloads. The balloon would sometimes be an excellent back-up for rockets, but stellar platforms capable of carrying a wide variety of scientific payloads are very scarce, if they at all exist. We tried to fill this gap by building a gondola with the following characteristics:

- Low weight (230 kg). An altitude of 40 km can be reached with a 350 000 m³ balloon.
- Star tracker completely independent from the scientific payload (siderostat), with a stability better than 1' of arc on a 6th magnitude star.
- Star field TV camera for fast target acquisition.
- Offset pointing capability of $\pm 1.5^\circ$ from the guide star.

2. PLATFORM

The schematic lay-out of the sub-systems inside the main structure of the gondola is shown in Figure 1. The structure is oriented in

azimut with an accuracy of $\pm 1^\circ$ by a 75 watts torque motor located in the suspension dynamic bearing. The azimut reference magnetometer, mounted on a rotating table, can be oriented in any direction by an on-board punched tape programmer. The scientific telescope, the star tracker and the TV camera see the sky by reflection in a 31 x 31 cm flat mirror. The elevation of the line of sight is adjusted, under the control of the on-board punched tape programmer, by rotating the flat mirror around its elevation axis.

In the tracking mode, the mirror is controlled by the star tracker electronics. Two DC servomotors drive the elevation and cross-elevation axes of the mirror so as to maintain the guide star on the line of sight. The flat mirror weights only 5 kg. It is the only mobile part of the system. The coarse attitude control electronics constantly updates the coordinates of the star so as to follow the apparent motion of the celestial objects which would otherwise drive the mirror beyond its mechanical tracking range.

70 telemetry channels are supplied by two PCM encoders. The 8 channel CNES telecommand is utilized to update the coordinates of the star, to switch the fine guidance into tracking mode, and to select the field of view of the TV camera. The other functions of the platform are controlled by the 48 commands of the on-board punched tape programmer.

3. STAR TRACKER

The optical schematics of the star tracker is given in Figure 2. The modulator is a classical D-Shaped rotating knife edge driven at 8000 RPM by a DC motor. The photomultiplier is an EMI 9558A with an exceptional sensitivity of 480 microamperes per lumen. The detection is made by single photoelectron counting and the error signals are generated by a digital C-POS electronics. Target brightness differences are compensated automatically by a pulse rate divider over a 6 magnitude range.

The field of view is defined by an iris. In the acquisition phase it has a diameter of 2° . When the tracking mode is initiated by telecommand, the field iris reduces the field of view in five seconds down to 22 minutes of arc, thus lowering the sky noise by a factor 30 and occulting bright background stars. With this small tracking field of view, we have been able to lock on a 2nd magnitude star until a few

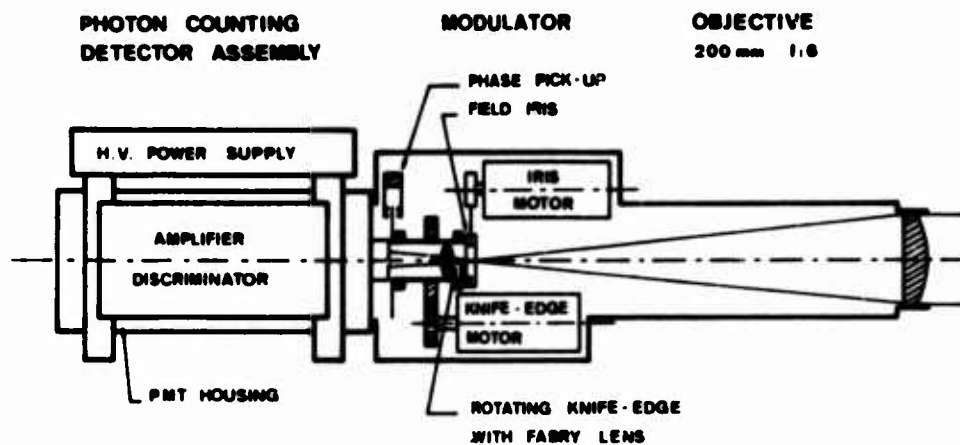


Figure 2. Schematic view of the star-tracker

minutes after sunrise. A blue filter was placed in front of the detector so as to cut down the red radiation of the twilight sky.

4. TV CAMERA

The camera is used for star identification and acquisition. The tube is an ITT FW-130 image dissector. The image definition is 1024 pixels (32 x 32) covering a field of view of 100 x 100 minutes of arc. The field can be magnified by two by telecommand during the acquisition. Like in the star tracker, the detection is made by single photoelectron counting. The camera transmits one picture per second to the ground. The video signal is stored at the receiving station in a random access memory and displayed on a regular laboratory oscilloscope at the rate of 50 frames per second to avoid flicker. The contrast range is 512 : 1 with logarithmic compression.

5. TARGET ACQUISITION

The on-board punched tape programmer is turned on at a given sideral time, approximately 1 1/2 hour before launch. The tape is driven at constant speed (10 characters per minute). At a given time, the programmer reads the coordinates of the guide star and drives the magnetometer and the flat mirror of the siderostat to the commanded azimuth and elevation. Any point of the celestial sphere can be reached

in less than 3 minutes. The coordinates are then adjusted by telecommand for the geographic position of the balloon at that time. Tables of geographic and magnetic declination corrections are calculated in advance for each star. The star now appears on the television screen. Most of the time, it is even in the 2° field of view of the star tracker and a tracking command is sent to the gondola. While the experimenter is looking at his star, the programmer reads the coordinates of the next star and stores them into the memory of the azimuth and elevation control system. It takes on the average 4 minutes to change the star, and 6 minutes to measure it with our six colour UV photometer, including the measure of the sky background in the vicinity of the star with the offset pointing command. These times are given for stars brighter than $m_v = 5$.

During the flight of April 1974, the gondola responded perfectly to the commands and we were able to keep this tempo of six stars per hour during two hours.

6. COARSE ATTITUDE CONTROL

The problem of the stability of the primary azimuth control system has for years been our stumbling block. From the flight data, it seemed that sometimes the azimuth motor, located in the suspension bearing, was sustaining the too well known compound pendulum oscillation of the gondola around its center of mass. We thought that the wind was also a possible cause of trouble. But a simple calculation indicated that a relative wind velocity of 1 m/s produces, at an altitude of 40 km, a drag of 2×10^{-3} newton (0.2 grams) on a 1 m^2 thin plate. Therefore, it was not the wind. Finally, we found that a misalignment of a fraction of a millimeter between the suspension shaft of the platform and the cable was enough to sustain compound pendulum oscillations.

A simplified gondola is shown in Figure 3, and the Figure 4 represents the parasitic loop which was responsible for the oscillations. At the level of the azimuth motor a rotation of the shaft produces a rotation of the platform around its center of mass if the shaft and the suspension cable are not perfectly lined up. This static unbalance produces a light coupling between the azimuth axis and cross-azimuth axes (pitch and roll for instance). The second element of the loop of the Figure 4 is the platform. It is after more than 300 periods

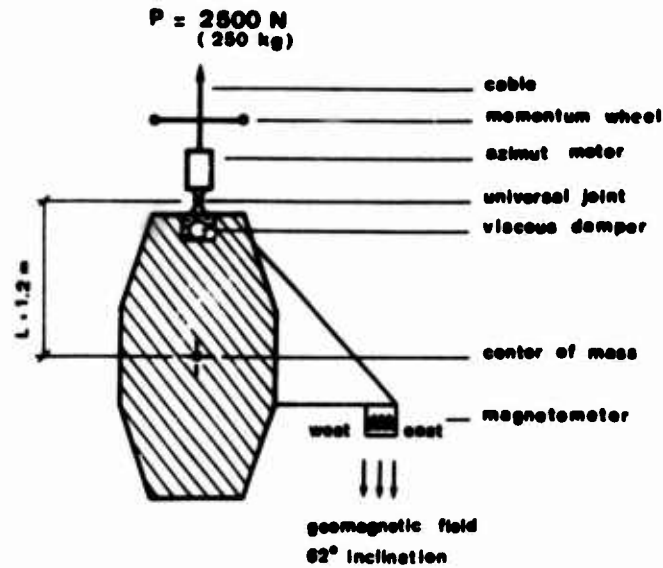


Figure 3. Schematic platform with azimuth control

that its compound pendulum motion is attenuated by a factor $1/e$. Thus the quality factor Q of the compound pendulum is approximately 1000. The loop is closed by the magnetometer. Because of the 62° inclination of the geomagnetic field, it responds to rotations around the north-south cross-azimuth axis as well as to changes of azimuth.

We broke the loop in two points. We designed a coaxial coupler which keeps the suspension shaft and the cable aligned within 0.2 mm. We mounted a momentum wheel on the suspension shaft. It acts as a low pass filter, preventing the shaft from rotating more than a few degrees when driven at full torque by the azimuth motor at the frequency of the compound pendulum oscillation (approximately 1 Hz).

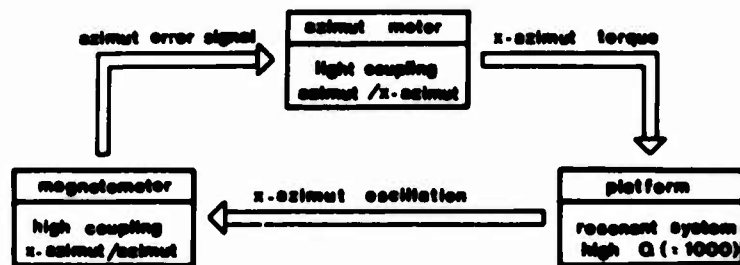


Figure 4. Axis coupling in the azimuth control system

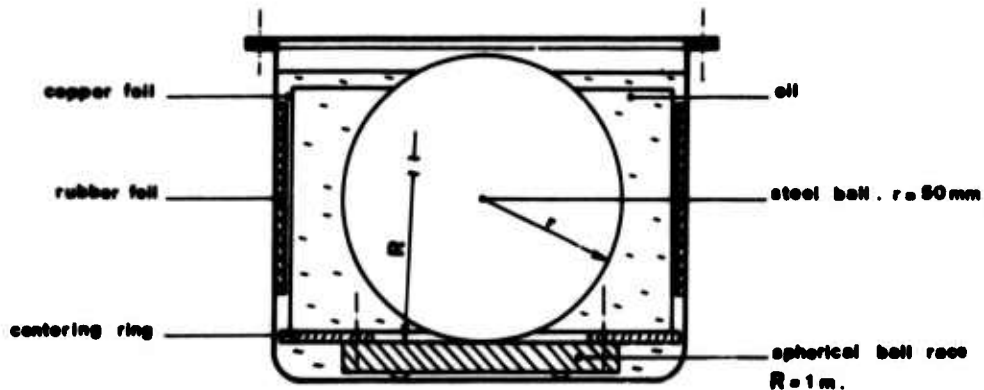


Figure 5. Inertial viscous damper

Finally, we designed an inertial viscous damper which reduced the quality factor of the compound pendulum by 20. This damper is shown in Figure 5 and its location in the gondola appears in Figure 1 and 3. The main element of the damper is a 4.2 kg steel ball sitting on a slightly concave spherical race with a radius of curvature of 1 m. The system is immersed in oil. In the absence of oil the period of oscillation of the ball on the spherical race is 2.2 seconds, more than twice the period of the compound pendulum oscillation of the gondola, which is 1 second. The viscosity and the level of the oil are chosen so as to achieve a critical damping of the ball. When released from the side of the container, the ball goes back to the center practically without overshoot. So the damper is a perfectly safe aperiodic system. It is mounted in the gondola as far away as possible from the center of mass. When compound pendulum oscillations occur, the platform drives the oil back and forth laterally. The ball, owing to its inertia, lags behind the motion of the oil; kinetic energy is absorbed by viscous friction. The oil used for night flights is a synthetic lockheed fluid for car brakes with a viscosity of 2 poises (90 SAE) at -45°C and a drop point of -57°C . Without damper, the amplitude of the oscillation decreased to $1/e$ in 300 periods, and with the damper, in only 15 periods. Such a system was calculated applying the classical differential equation of a damped resonant system to the platform and using the Poiseuil formula to calculate the drag created by the motion of the oil around the ball.

This damper has the advantage, over other systems, that dry friction is practically inexistant. In the absence of a mechanical

threshold, it is still efficient in damping oscillations of 1 minute of arc. The viscous friction torque, referred to the center of mass of the platform, produced by this damper is 12 newton.meter at an angular velocity of 1 radian per second. Measured and calculated values agree very well.

7. FLIGHT PERFORMANCES

The platform made a short test flight in France in October 1973. Star tracking was intermittent because of severe compound pendulum oscillations of the platform. This problem was solved as described in paragraph 6. The first scientific flight took place in April 1974 in France. Two experiments were programmed. A sample of rotating and non-rotating hot stars were measured in six colours between 2100 Å and 3100 Å, by a photon counting photometer for scientists of the Geneva Observatory. Twelve stars were measured during a two-hour period. The last hour of flight was devoted to an experiment of the Laboratory for Atmospheric Physics, University of Paris, consisting in measuring the ozone thickness and its variation at sunrise. The UV photometer pointed at a hot star throughout twilight, and recorded the variation of the atmospheric transmission in the absorption band of the ozone at 2550 Å.

The float altitude was 38 km and the average wind velocity 45 km/h (25 knots).

The stability of the primary attitude control system was good. In azimuth the short term peak error over periods of 10 seconds was ± 4 minutes. The Foucault pendulum motion of the line-gondola system and the wind introduced very low frequency errors never exceeding 25 minutes of arc, with periods longer than 20 seconds. The viscous damper kept the compound pendulum motion below ± 2 minutes of arc, with a period of 1.2 seconds.

Owing to the stability of the gondola, the pointing accuracy of the star tracker went beyond our most optimistic expectations: 15 seconds of arc rms on stars brighter than $m_v = 4$ and 30 seconds rms on the faintest star tracked during this flight ($m_v = 4.85$).

Acknowledgments

We would like to express our gratitude to our sponsors, the Swiss Foundation for Scientific Research, the University of Geneva, and particularly the French Space Agency (CNES) and the Laboratory for Atmospheric Physics of the University of Paris for taking the risk of being the first "passengers" of this platform and for their support to this programme.

References

- Huguenin, D. (1974) The stellar and solar tracking system of the Geneva Observatory gondola. Paper presented at the NASA-NCAR symposium on Telescope systems for balloon-borne research, Mountain View.
- Kondo, Y. and Wells, C. (1974) Ultraviolet stellar spectrophotometry from a balloon platform. Paper presented at the NASA-NCAR symposium on Telescope systems for balloon-borne research, Mountain View.
- Navach, C., Lehmann, M., Huguenin, D. (1973) Feasibility of UV Astronomy by Balloon-Borne Observations. Astron. and Astrophys. 22: 361-379.
- Rigaud, P. (1973) Mesure de la variation de l'ozone crépusculaire au moyen d'un photomètre stellaire embarqué à bord d'une nacelle stratosphérique. Thesis No. A.O.9045, University of Paris VI.

Session 5
Special Applications

James A. Winker, Chairman
Raven Industries

537

Preceding page blank

Contents

1. Introduction
2. Detonable Gas Balloons
3. Tethered Hot Air Balloons
4. Thermal Airships
5. Air Launched Balloons
6. Heavy Lift Balloons

Special Applications; An Overview

J. A. Winker
Raven Industries, Inc.
Sioux Falls, South Dakota

Abstract

Balloons have an almost unlimited range of potential applications. Some of the more unusual and unique of these are described, including explosive balloon envelopes, thermally buoyant balloons, air launched systems and industrial balloons.

1. INTRODUCTION

The earlier sessions of this symposium have had fairly definite or restricted subject matter. This session is something of a catch-all, with a variety of miscellaneous topics. In one sense, this makes an overview more difficult because there is no cohesive theme. However, it is really more interesting, because it allows the session chairman to pick and choose from a wide variety of interesting applications.

The scope of this session runs from "balloons" whose sole purpose is to contain an explosive gaseous mixture which is subsequently detonated, to different applications of thermally buoyant balloons, to a complex system for air launching moderate size balloon loads on a moment's notice, and finally to balloons which are used in the timber industry for harvesting logs from mountainsides.

2. DETONABLE GAS BALLOONS

The first topic in this session concerns balloons which are inflated with an explosive mixture of gasses and then are ignited to produce large scale blast effects. These are not balloons in the classic sense of a buoyant envelope carrying a payload, yet much of the structural design and handling techniques are borrowed directly from scientific ballooning.

It seems that if you look back far enough you can find in early ballooning history a precedent for almost any present day balloon application. The first known detonable gas balloon was built and flown in 1785. This was a hybrid envelope using hydrogen in a top compartment and hot air in a lower section. It wasn't intended, but inevitably the two got mixed up and the result was quite explosive and quite fatal to the two passengers. That episode was, of course, inadvertent whereas in current experiments the explosions are very intentional. Being intentional makes them no less hazardous and therefore precautions are most elaborate. The present day series of blast experiments started approximately ten years ago with test detonations of small spheres in the range of 1 to 4 meters diameter. Since then, balloon size and explosive yield have increased and the experiments refined. There have been many successes and a few failures. Past development has included solutions to some very critical materials and operational problems brought on by the fact that most of the feasible barrier materials tend to generate static electricity, and static electricity, combined with explosive gasses, tends to "expedite" the test schedule.

The paper to be presented describes a recent series of detonations using improved static-free materials and new handling techniques.

3. TETHERED HOT AIR BALLOONS

In the previous topic there was certainly a lot of hot air generated with the balloons described. It was a bit uncontrolled, however, and this second topic describes what can be done using a controlled source of hot air as a balloon buoyancy medium. The paper to be presented discusses the use of a tethered natural shape hot air balloon in warm fog research. The work was done at the Naval Weapons Center, China Lake, California. NWC procured its first hot air balloon test platform in 1964 and in the intervening decade they have owned several different hot air balloons for use in a considerable variety of experimental programs. In these programs the balloon has

served variously as a platform for observation, for dropping test articles, or as a test bed for carrying experimental equipment.

In one typical example, the development schedule for fuel air explosive (FAE) warheads was greatly speeded up. As a part of advanced FAE development, it was necessary to make drop tests with prototype warheads. Aircraft were not readily available for the drops, would be expensive in any case, and would necessitate a more widespread observing facility. No other technique appeared completely practical. The hot air balloon allowed rapid repetition of tests, at the rate of about one every half hour, and allowed dropping the warheads in a very narrow observation zone. The success of this program is all the more remarkable since the balloon had an open base and was not pressurized to resist the wind. It was simply an adaptation from free flight sport balloons.

There are a number of other NWC programs using tethered hot air balloons which are of interest, but rather than elaborate on these, I would like to digress and turn from technical to other uses. Having the platform, I can't resist the opportunity to mention the rising popularity of sport ballooning. Modern hot air ballooning started with a military requirement, almost died when that requirement was discontinued, but was rejuvenated when a few pioneers started flying the balloons for fun. The sport grew from a handful of balloons in the mid 60's to something like 300 balloons and 500 pilots at the present, with both populations rising exponentially. The real foundation for this growth came in 1967 and 1968 when the Federal Aviation Administration approved various designs and granted type certificates. Six years ago it was difficult to get a dozen balloons together for a rally or competition. Now there are sponsored events (balloonists receive expense money to attend) every few weeks in various parts of the country, and in 1974 the National Championships at Indianola, Iowa, attracted 135 balloonists all paying their own way plus a \$25 entry fee. Figure 1 shows a number of balloons participating in the First World Hot Air Balloon Championship at Albuquerque, New Mexico in 1973. The Great Adventure balloon shown in Figure 2 is currently the world's largest hot air balloon, with a volume of 400,000 cubic feet.

This tremendous increase in ballooning activity has brought us back full circle and technical fallout from the sporting activities is now benefitting commercial and scientific users. An improved tethered hot air balloon has been derived by fitting the basic sport balloon with an enclosing skirt at the base and adding an electrically driven blower to keep the envelope full and tight. Electricity and fuel may be supplied from the ground, allowing the balloon to remain tethered at altitudes up to about 150 feet for hours at a time, or may be carried on board, allowing higher altitudes, but shorter durations.



Figure 1. Albuquerque Balloon Fiesta



Figure 2. 400,000 cu. ft., 23 Man Balloon

The most common present use for superpressure hot air balloons is in advertising, grand openings and other types of promotion. Pressurized balloons have been used as movie props (Walt Disney's "High Flying Spy") and as a night spectacular display at Disney World. Workaday applications are also coming and an experiment that was tried some years ago was to lift a man into the top of a pine tree to pick pine cones for their seed (Figure 3). In scientific tree farming, as in agriculture, there are many improvements which can be made in "crop" yield and quality by selective breeding. The only way to achieve the desired results is to choose trees with the proper characteristics and harvest the cones before they fall to the ground. Unlikely as it may seem, the most effective present methods of gathering selected cones is to shoot them off the tree with a rifle, or simply cut down the whole tree and hand pick them. Hand picking from a balloon is still considered a good possibility and both helium and hot air balloons are being considered.

A tethered hot air balloon was recently used in a difficult repair job on the Omega antenna system on Hawaii. Plastic warning balls are installed on the antenna to alert aircraft of its presence. One



Figure 3. Tethered Hot Air Balloon Used in Pine Cone Picking Experiment

of these became dislodged and when power was applied to the antenna, corona discharge caused the ball to partially burn. A hot air balloon was raised 1600 feet on a tether to reach the antenna and was maneuvered to the area where the ball was burned off. The antenna was cleaned up and made ready for operation again. At last report a corona discharge ring was to be installed, again by bringing a hot air balloon up to the wires.

Experience has shown that tethered natural shape hot air balloons have many useful applications. It seems obvious that the applications would be expanded if aerodynamically shaped envelopes were used. Such designs have been proposed for many years but as yet have had no takers. This is the next logical step in development of tethered hot air balloons.

4. THERMAL AIRSHIPS

While the subject of tethered aerodynamically shaped hot air balloons has been almost completely ignored, the powered thermal airship certainly has not. Hot air ballooning as a sport had barely been revived when people began exploring the possibilities of adding engines and propellers to provide horizontal motion relative to the wind. In an early experiment a portable engine-driven fan was carried on board the gondola of a standard sport balloon. The two horsepower engine provided enough thrust to produce a perceptible, but otherwise negligible deviation in the balloon's flight path.

In 1965 and 1966 the first serious attempt at developing a thermal airship was undertaken in England. Malcolm Brighton (recently killed in a Transatlantic balloon flight attempt) and Anthony Smith constructed an 85,000 ft³ aerodynamically shaped envelope which they named the WASP (Warm Air Ship Project). This was a non-pressurized vehicle and was inflated but never flown. The WASP concept was revived by Don Cameron, also of England, and a flyable model was constructed and flown early last year. This feasibility model had a volume of 96,000 ft³ and achieved a speed of approximately 10 kn. It has undergone continued development, including considerable modification on the vertical stabilizers for yaw stability. It now has a speed capability of 15 kn, which may be a practical limit because of its unpressurized hull. The Cameron Airship will be available for commercial sale this year. The prototype gondola car is shown in Figure 4 and the airborne vehicle in Figure 5.

Two short papers will be presented describing thermal airships having a considerably greater degree of design refinement. One of the papers describes a pressurized thermal airship designed to make use of proven, off-the-shelf hardware and materials. It borrows directly

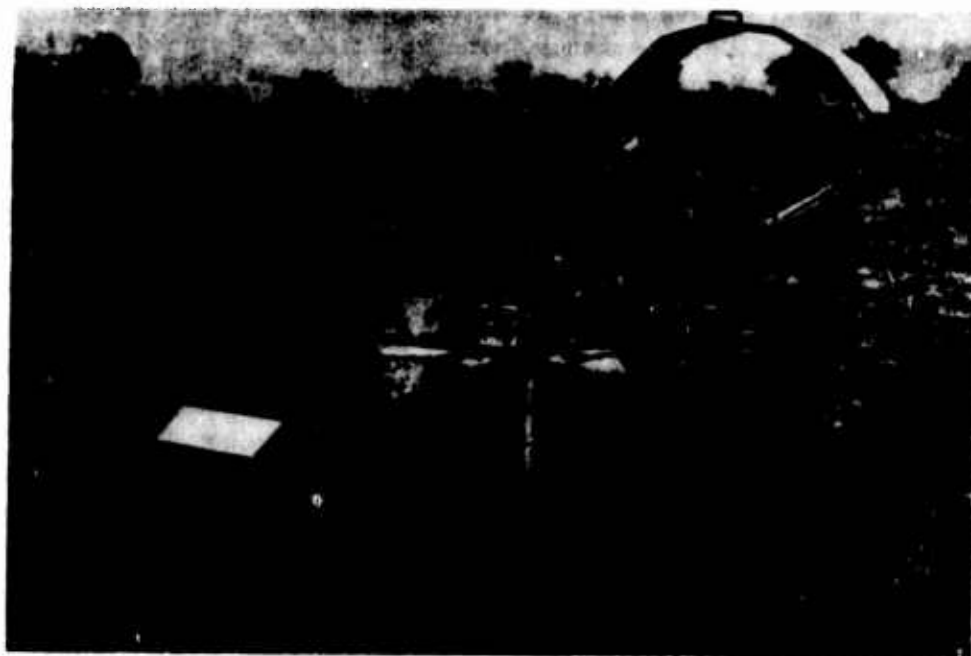


Figure 4. Gondola Car of the Prototype Cameron Airship



car for first public flight at Newbury on January 7th 1973.

Figure 5.

from equipment and operational techniques now common in free and tethered natural shape balloons. The result will be an operational vehicle which will be available at an early date and will allow accumulation of flight experience. The vehicle is designed for refinement and growth based on such experience. The second paper treats the design problems at a higher level of sophistication and arrives at a more elegant design solution.

5. AIR LAUNCHED BALLOONS

One of the most difficult things you can expect of a balloon is to throw it into the atmosphere, inflate it while it is falling to earth, tidy up the sky by recovering all of the inflation paraphernalia, and then expect the balloon to perform as though it had received tender loving care by a devoted launch crew. There have been many air launched systems developed in the last 20 years and most were considered somewhat daring in their time. The latest concept, to be described in today's paper, includes a rather large balloon, a substantial payload, lifting gas in liquidified form, and all of the supporting inflation equipment, to be packaged in the nose of a rocket and held on standby for virtually instantaneous launching. After being fired to desired altitude, the system deploys, inflates and floats away in a matter of minutes. Such a concept might have seemed incredible only a few years ago, and yet it shows excellent feasibility on paper. It is a measure of the maturity of balloon technology that such a system can even be considered.

My association with air launched balloons began in 1952 when a Navy meteorological squadron was looking for a way to put a marker in to the eye of a hurricane so radar could track it. The idea was to float a radar reflective balloon at such an altitude that natural air currents within the eye would keep it somewhere near the center. Since tracking airplanes already routinely penetrated hurricanes, it was natural to consider launching the radar balloons from these aircraft. Once the eye was seeded with radar balloons, tracking of the storm could be done from ships or airplanes outside of the severe wind area, reducing the need for aircraft penetrations. At that time the whole concept was extremely sketchy, including balloon performance, launchability, radar tracking capabilities, and even the meteorological question of whether the balloons would stay centered or would be sucked into the storm area. This required either a massive funding effort to study and solve all of the problems, or a minimum feasibility effort to determine how serious the problems were and to nibble away at their solution. The minimum approach was chosen and the magnificent sum of \$5000 was allocated to the program. This automat-

ically eliminated any approach where a package could be dropped on a parachute for mid-air inflation. The balloons had to be inflated within the aircraft and launched ready to fly. This in turn limited their size and their ability to carry a tracking payload. The end result was a pillow shaped balloon of 10 to 20 ft³ carrying a passive radar reflector. The balloons were launched through a plywood chute adapted to a door opening in the rear, underside of a Navy P4Y2 patrol plane (Figure 6).

The first attempts used a corrugated cardboard carton to "protect" the balloons during egress. This turned out to be more damaging than helpful and the most successful balloons were launched with no protection at all. Movie sequences (Figure 7) showed that much of the acceleration (relative to the airplane) took place within the launch chute, minimizing shock to the balloon by the time it was exposed. Many successful launchings were made, but nevertheless there was some tendency toward film degradation which shortened flight time. Long duration superpressure balloons had not been developed at that time, and at best the polyethylene pillow balloon would have had a marginal duration capability. Further, the small radar reflectors which showed up well on ground radar did not have a sufficient return for aircraft radar.

Later work on preinflated air launched balloons was done at Air Force Cambridge Research Labs and included the launching of neoprene meteorological balloons from C-119 aircraft and polyester superpressure pillow balloons from the bomb bay of a B-29. There is an obvious limit in the size attainable in preinflated mid-air launch systems and this practical limit has probably been reached in a recent AFCRL program which successfully demonstrated the launching of 8 foot diameter preinflated balloons out of the rear door of a C-130 cargo aircraft.

Air launching of preinflated balloons is quite inexpensive, but it is also quite limited in potential applications. By packaging the entire balloon system and its inflation equipment in a drop pod or nose cone, the possibilities open up tremendously. Small systems of this type were developed in the mid 1950's by AFCRL and Winzen Research. One of the AFCRL applications addressed the hurricane tracking problem again, but with considerably more background information available and with a better level of funding. The balloon system which was developed was complete with an active tracking transmitter and a ballaster which allowed a reasonable flight duration.

Figures 8 and 9 show the packaged and inflating stage of a mid-air launched radar jammer which was to be carried as an underwing store on fighter aircraft. The weight efficiency of this system is probably the highest achieved to date. For each kilogram of airborne mass in the buoyant balloon system, only 4 kg of inflation and structural hardware was required. With larger systems and cryogenic lift-



Figure 6. Launch Chute For Hurricane Tracking Balloon

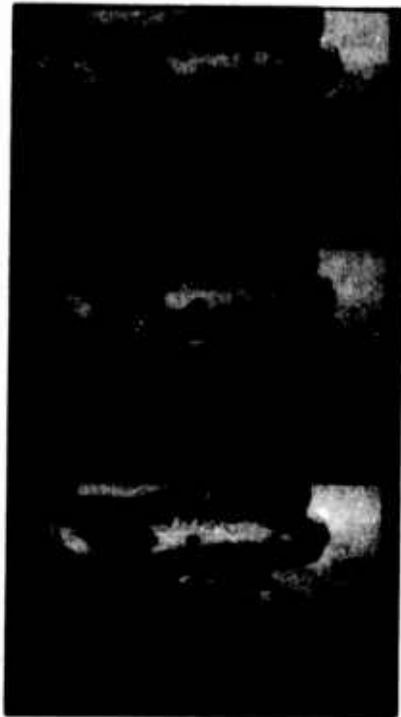


Figure 7. Launch Sequence of Hurricane Tracking Balloon

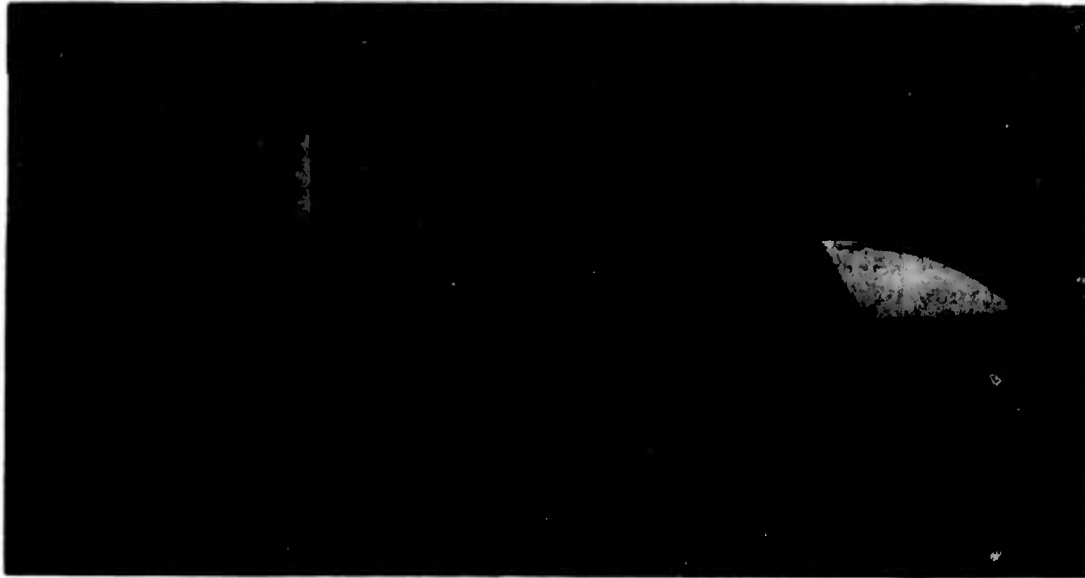


Figure 8. Air Launch Package for Radar Jammer

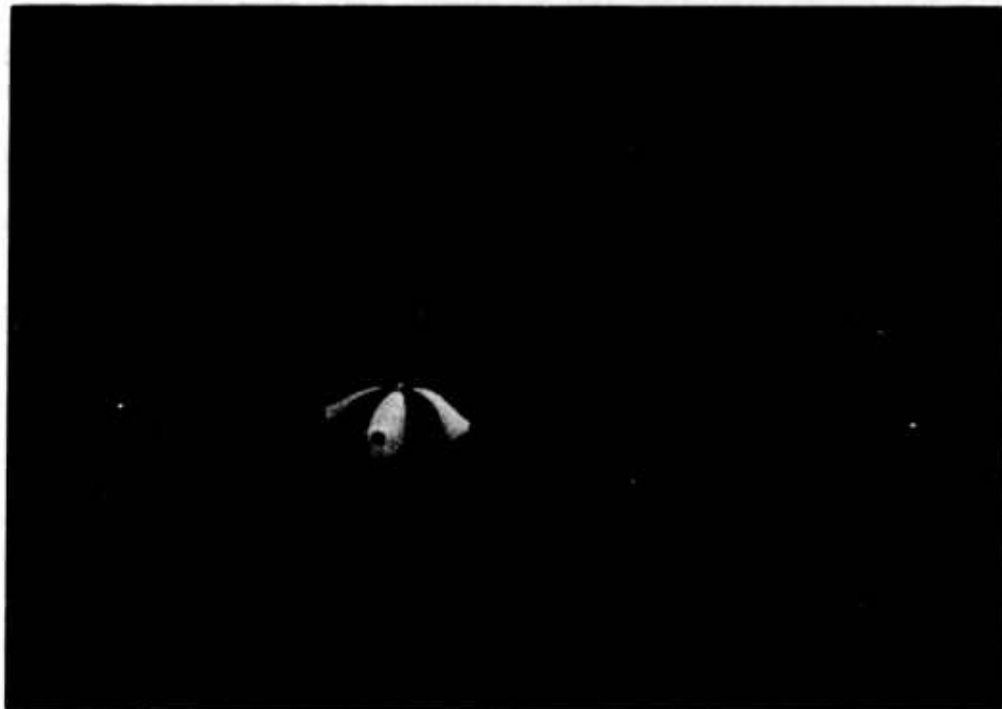


Figure 9. Radar Jammer Just Separating From Parachute

ing gasses as are now being proposed, this weight ratio should be bettered.

6. HEAVY LIFT BALLOONS

The list of applications for balloons--successful and unsuccessful, practical and impractical--is almost endless. Within that list there is almost nothing that can properly be termed an industrial balloon application. Among those few uses which qualify is the heavy lift logging balloon. One of the reasons there are so few industrial applications of balloons is that they can only be justified on an economic basis. Harvesting timber with balloons, while still undergoing development, has graduated from the strict experimental status of a few years ago and is competing with other logging systems on a sound economic basis. There are presently five balloon logging sites operating on a routine production basis and their cumulative inflation time is in excess of 100,000 hours. All of the operational systems and most of the preceding experimental setups have utilized a closed loop cableway with a double drum winch to move the balloon out and back from the winch site. The balloon provides direct lift to the load of logs which is then moved laterally by the winch (Figure 10). The present standard balloon size is 530,000 ft³ which provides a net lift of 24,000 lbs and a usable average logging load of about 18,000 lbs (Figure 11). A new model to be put into service next spring will have a volume of 700,000 ft³ and a capacity for an average usable load of 25,000 lbs.

New heavy lift balloon techniques have been proposed which would utilize a stationary balloon as a skyhook to support a cableway. A self-powered carriage would ride the cableway, picking up and delivering loads located under its path. This configuration, as applied to a ship-to-shore unloading operation, is shown in Figure 12. The paper to be presented describes how this type of balloon lift could be applied to a logging operation.*

*The paper on logging balloons was to have been published in the proceedings. Unfortunately, due to unforeseen circumstances it could not be completed in time for publication.

Contents

1. Introduction
2. Platforms for Fog Studies
3. A Balloon-Borne Droplet Charging System
4. Hygroscopics Sprayed From The Balloon
5. Future Fog Studies With Hot-Air Balloons
6. Summary

Manned Hot-Air Balloons As Warm Fog Research Vehicles

Roger Reinking
Earth and Planetary Sciences Division
Naval Weapons Center
China Lake, California

Abstract

The utility of tethered and free, manned hot-air balloons for warm fog research is examined. Advantages and limitations of the balloons in comparison to other air-borne platforms are considered. The manned hot-air balloons are very suitable platforms for studies that require that heavy payloads be carried with minimum disturbance to the fog.

Tethered, manned hot-air balloons have been successfully used by the Earth and Planetary Sciences Division of the Naval Weapons Center to test droplet charging and hygroscopic spray devices for dispersing fog. An instrumented hot-air balloon is being readied for a study of fog properties that regulate potentials for fog modification.

1. INTRODUCTION

Fog is cloud at ground or sea level. Fog inhibits visual observation and presents navigation hazards for airborne, sea-going and land-based vehicles. For example, a fog that reduces visibility to less than one-half mile and ceiling to less than 200 feet will close most airports. Warm fog, as compared to supercooled fog, is colloiddally relatively stable. Supercooled fog may be quite simply and rapidly

dissipated by triggering a phase change by introducing ice. However, a very simple, quick-acting, and practical method for triggering the dissipation of warm fog has yet to be developed. Some 95% of all fog occurrences are warmer than freezing, so research leading to effective warm fog dissipation techniques is vital.

Laboratory and field research of warm fog is being conducted by the Earth and Planetary Sciences Division (EPSD) of the Naval Weapons Center (NWC). This research has two basic aspects: (1) Identification and measurement of fog processes and properties that affect potentials for fog modification; (2) development and testing of experimental fog dissipation techniques, including monitoring of the effects on fog and the fog environment.

In the field, either aspect of this research requires platforms for observation and for operation of fog-dispersing and measuring devices. The information needed, or the nature of the dispersal technique, dictates what types of platform should be used. The manned, hot-air balloon is one alternative. Some advantages and limitations in using these balloons in warm fog work are recognized here. Past and planned applications by the EPSD are discussed.

2. PLATFORMS FOR FOG STUDIES

The platforms used in warm fog research may be mobile or stationary, ground-based or airborne. Ground level platforms are usually stationary; the fog is treated or observed as it drifts past a fixed point or array of points. Towers extend the capability of ground-based platforms to the vertical dimension, up to, say, 100 feet above ground level. The total depth of shallow fogs such as newly developing radiation fogs may thus be studied or treated. Towers reach into only the lower portions of most fogs, which commonly exceed depths of 500 feet.

Observations of fog made from stationary, ground level platforms and towers are very useful, although they do not represent the total fog system. Targeting fog dissipating materials and treating sufficient depths of fog from these platforms is difficult, even when expensive arrays are employed.

Airborne carriers can be used to complement ground-based measurements by extending the dimensions of the fog volumes observed. Also, targeting seeding material and treating appropriate fog volumes is most readily accomplished from aloft, when the fog dissipating device is compatible to mounting in or on an airborne carrier.

The various space and time requirements of airborne fog research operations are listed in Table 1. Fixed-wing aircraft, helicopters, kytoons, free constant-level balloons, and hot-air balloons all offer advantages and disadvantages. Operational space and time requirements that could be met with hot-air balloon flights are indicated in the Table.

In the tethered mode, manned hot-air balloons add to the vertical dimension of fixed-point tower measurements, and are suitable for certain small-area tests of fog dispersal devices. Since the tethered balloon system is portable, the point of launch may be readily changed between flights. Thus, for example, the testing position may be coordinated with the wind field that prevails at the time of launch. Vertical profile measurements may be acquired with a tethered hot-air balloon by raising and lowering the balloon itself, or by lowering and raising an instrument package from the balloon. Either a movable package or a package suspended at a fixed distance below the balloon avoids contaminating effects on the fog due to heat, water and particulates from the burner that powers the balloon. Ideally, the hot-air balloon is used to locate fog top, and operation is maintained just above fog top. Measurements at a desired position relative to fog top and profiles on ascent and descent through the fog depth and the fog/clear-air boundary can thus be obtained. This type of operation allows visual observation of fog top structure, which is important to characterizing fog life cycles .

Fixed level or profile measurements from a free, manned hot-air balloon can be obtained in much the same manner. The balloon pilot can control the level of any suspended instrument package relative to fog top, and thus eliminate the need for remote-control devices. The advantage of a free balloon is that it will drift with a given fog volume or "parcel". A given section of fog top and a specific flowing volume of foggy air can thus be continuously monitored and/or treated with dispersing materials, with minimum disturbance of the fog by the carrier. Such an operation has not been experimentally tried but might well provide valuable information on the evolution of fog. The balloon operating at fog top with an instrument package suspended into the fog may be expected to track a given fog volume in cases when (1) wind shear is near zero between balloon and package, (2) airflow is consistent, calm, or changing quite slowly so momentum does not cause the balloon to overshoot or lag drift of the fog volume, and (3) vertical mixing in the fog is minimal or accounted for by measurement or calculation.

Most time requirements for airborne fog operations (Table 1) can be met with a manned, hot-air balloon. The main exception occurs when a large foggy area is to be treated or observed in a short time. The only other real restriction is the limit on flight duration imposed by the fuel supply and the size of the payload. For example, the payload of NWC's balloon can be as heavy as 1,400 lbs, but flight time is limited to 1-3 hours with one fuel tank. However, a tethered balloon can be landed, refueled and launched again with an interruption in measurement of less than an hour, provided the refueling technique allows the balloon to remain inflated. Free hot-air balloons present a greater logistics problem, but free flights exceeding three or four hours would be an uncommon requirement in fog operations.

The hot-air balloons and fixed-wing aircraft serve quite different functions in fog research. On the other hand, hot-air balloons, kytoons, constant-density-level balloons, and helicopters can serve relatively similar purposes. Table 2 summarizes some advantages and disadvantages of manned hot-air balloons in comparison to these other vehicles. A principal advantage of the hot-air balloon is the

TABLE 1. Various Space and Time Requirements of Airborne Fog Operations

<u>SPACE</u>	<u>EXAMPLES OF PURPOSE</u>
Specific Level(s)	
Line paths boxing large or small area	Measure net flux of fog liquid water through volume
Cross-wind path	Line seeding, to enhance targeting
* Path of drift with wind and fog parcel	Monitor changing fog properties (e.g., droplet size) in given volume; continuously treat same fog volume.
* Fixed point(s) aloft	High point-source testing of fog dispersal devices.
Vertical Profiles	
* Over fixed point(s)	Extend vertical dimension of tower measurements.
In cross-wind plane	In-fog sampling of liquid water to measure effect of line seeding
* In plane parallel to wind, moving with air/fog volume	(Same as at specific level, vertical dimension added)
<u>TIME</u>	
Increments	
* Continuous	Monitor evolution of fog properties, especially during seeding.
* Fixed intervals	
seconds	(same as with continuous monitoring)
minutes	Repeat line-path seeding to increase dosage
hours	Monitor gross changes in fog (extent, depth, density)
Duration	
* Seconds	Accomplish line-path seeding
* Minutes	Induce and monitor changes in fog properties
* Hours	Monitor fog life cycles

* Feasible with manned hot-air balloon.

TABLE 2. Characteristics of Certain Airborne Carriers

	Vehicle Control	Payload	Operating Altitudes (above ground level)	On-station time
Manned hot-air balloon				
Tethered	Direct; altitude only, as modified by tether; wind gusts, speeds greater than 7-8 kts, reduce control; operation above and in fog OK	Up to 1,400 lbs (example)	Up to approx 2,000 ft	1-3 hr with each fueling; 2nd tank means more time, less payload. Fixed position.
Free	Direct, altitude only; risky within fog, but transponder aids navigation.	Same, but sacrifice some weight for maneuverability.	Unlimited	4-6 hr maximum; sufficient; follows airflow/fog volume.
Helium-filled kytoon	Tether; variable winds, etc., restrict constant altitude control; operate in or above fog.	Up to approx 120 lbs (standard models)	Limited by weight of tether	Order of 24 hr; limited only by diffusive helium losses; fixed position.
Constant-density-level balloon	None required, free, tracked by radar; operates in or above fog.	None or 1-2 lb package (serves to track airflow/fog parcel, may carry small telemetered sensors).	Unlimited	Many hours; normally very sufficient to follow air parcel across fog dimensions.
Helicopter	Direct (horizontal, vertical); good above fog, very poor in fog.	Maximum	Unlimited	Approx 2 hr, then relieve pilot; fixed position, or large or small area coverage.

TABLE 2. Characteristics of Certain Airborne Carriers—continued

	Night Flights	Disturbance to fog	Direct Visual Observations from operating level	Operating Expense
Manned hot-air balloon				
Tethered	OK if IFR equipped with rate of climb/descent indicator	Heat, H ₂ O, particles and gases from rising burner exhaust (Position sensors accordingly).	Yes	Moderate
Free	Not recommended	Same	Yes	Moderate
Helium-filled kytoon	Same as in daylight	Minimal	No	Minimal
Constant-density-level balloon	Same as in daylight	Minimal	No	Minimal
Helicopter	OK above fog	Downwash and exhaust constituents cause considerable fog modification over significant area, depth.	Yes	Substantial

heavy-payload capability. Direct visual observation from the operating level is also helpful. The crew of 5-7 men required for launching, controlling and piloting a hot-air balloon accounts for most of the moderate operating expense. A tethered hot-air balloon cannot be safely operated in winds exceeding about 8 knots. This restriction limits operations in advection fogs, in particular, but should not hinder studies of radiation fogs.

A helium-filled kytoon may be flown on station for a very long time, with a minimal crew. However, several kytoons operated individually or in tandem may be required to carry a complete payload. Hot-air balloons are generally more stable than kytoons.

Constant-level balloons are excellent for simply tracking airflow through fog, provided ground clutter does not interfere with the radar's function. This application would be useful for determining the lifetime of fog droplets, for example. This type of balloon could carry some miniaturized sensors, but it is not designed to carry a significant payload.

Helicopters are useful for fog dispersal tests in which the effects of the downwash are desired to act in combination with other dispersal agents such as hygroscopics. The disturbance to the fog greatly limits the utility of helicopters in fog characterization studies. The fog disturbance by hot-air balloons is relatively insignificant.

3. A BALLOON-BORNE DROPLET CHARGING SYSTEM

Warm fogs can be dispersed if the fog droplets can be induced to collide and coalesce, so as to gain sufficient mass to settle out. Electrically charged droplets are much more efficient collectors of other droplets than are uncharged droplets. Carroz, et al (1972) estimate significant increases in visibility in fogs that are sprayed with charged droplets of water or hygroscopic solutions. These potentials prompted development and testing of a droplet spraying and charging system by NWC with cooperation from the U.S. Army's Atmospheric Sciences Laboratory and the Federal Aviation Administration. During Project Foggy Cloud IV, charged water drops were sprayed from a hot-air balloon into small volumes of fog and open air, thus permitting laboratory type experiments to be conducted in the field. Details of the project and the results are reported by Loveland, et al (1972). Highlights are presented here to show how the balloon was used.

Field tests were conducted utilizing an induction charging system and pressurized water delivery system. This apparatus was lifted by a tethered manned hot-air balloon 60 feet in diameter with a payload capacity of about 1,400 pounds. Propane burners propel this balloon.

The charged drop-producing system in its field-ready form (Figure 1) used 48 Delavan 30-degree hollow-cone nozzles. Each nozzle is designed to give a median drop diameter of 100 μm and a spray rate of 8.8 gal/hr at 125 psi. Conical induction rings were utilized. The 30-degree angle of the rings coincided with the 30-degree nozzle spray pattern (Figure 2). The entrance openings were rounded to discourage arcing between nozzle and induction ring. All nozzles combined to produce a spray rate of approximately 6 gal/min. Negatively-charged spray was produced with the emf source attached as in Figure 2; positive spray was provided by reversing the source. The assembly plumbing which supported the nozzles, was an octagon (Figure 1) with sides about 12-feet long, supported by cables, and was 20 feet below the gondola. Twenty-four cables were used, as the plumbing itself was not rigid. A water tank pressurized by compressed nitrogen or helium fed the assembly. In early experiments, a ground-mounted emf source was used; however, a portable emf source (thirty 90-volt radio-type B batteries) was constructed for higher altitude testing. This source provided about 2,700 volts when fresh and declined to 2,200 volts after use.

Field tests were conducted at the Arcata-Eureka Airport and in Redwood Valley, both in the north coastal region of California. Clear air tests demonstrated that the balloon system could produce charged droplets, and that these droplets would hold their charges for times sufficient to produce interaction with fog droplets. The induction rings tended to collect the highly mobile, oppositely charged fine droplets ($< 20 \mu\text{m}$ diameter), thus eliminating possible fog enhancement by these particles. Effects of charging the spray could be seen visually. Under calm wind conditions, uncharged droplets settled downward from the spray boom as expected under the influence of gravity (Figure 2a). As droplets with one polarity were sprayed, they were attracted to the balloon system, which was grounded by the tether. Small and mobile charged droplets were drawn back and upward toward the balloon under the influence of the field produced between the balloon and the space charge of the spray.

An interesting question is that concerning the effect of the earth's natural field on charged droplets. Generally, the earth's natural field goes to positive with altitude, and may be of the order of 100 to 1,000 V/m in fog. Positive drops could be forced down faster than gravity alone would drive them; negative drops could be given an increased tendency to remain up. The experiments demonstrated, however, that the spray-generated local fields overshadow the earth's natural fields, except when drops drift enough horizontally to be out of the generated high local field. In field measurements using a field mill, fields of 4,000 V/m were consistently generated under the spray of charged drops. A field of this magnitude can substantially affect droplets with 16 μm diameters or less, as was visually observed. However, the predominance of spray droplets were considerably larger and relatively unaffected by either the induced or natural fields.

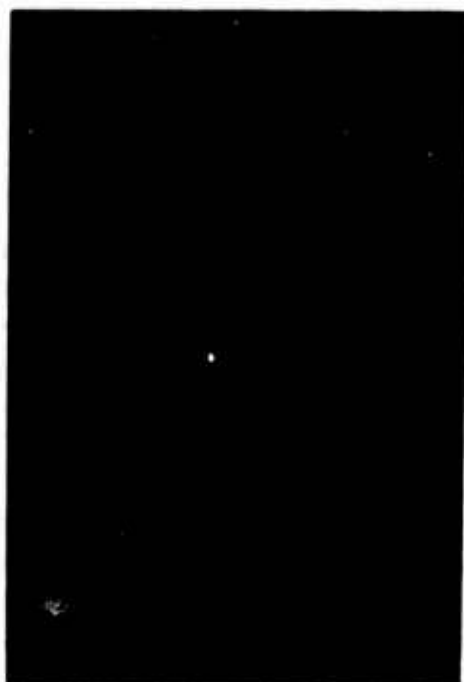


Figure 1. Spray Assembly Suspended From Balloon

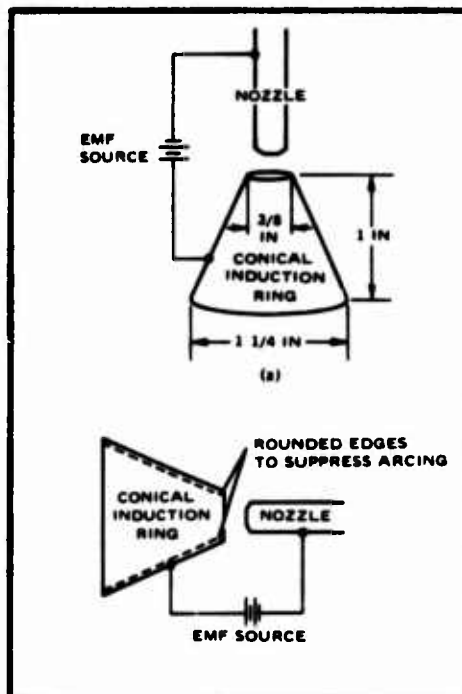
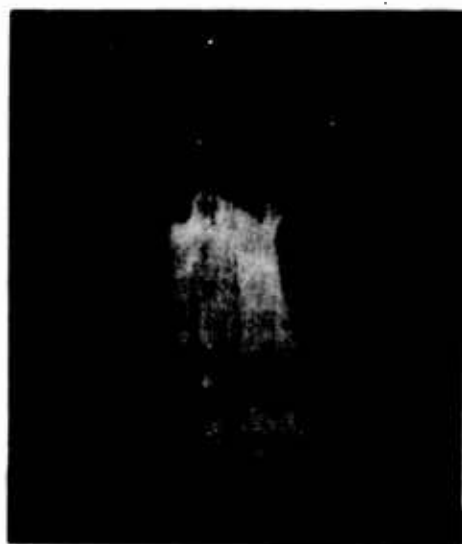
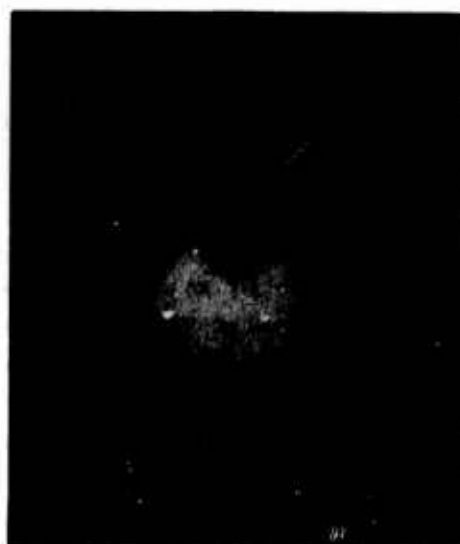


Figure 2. Conical Induction Ring. (a) Simplified view showing significant geometry; (b) mechanical details



(a) Uncharged spray



(b) Charged spray, showing drops rising and intercepting balloon

Figure 3

The small, charge-carrying droplets that return to the spray rig constitute a feedback current. Unless such droplets gain mass by collecting fog droplets during their transit, so as to avoid total return, they can reduce the effectiveness of this type of system. Therefore, procedures to reduce this feedback were tested. A feedback reduction is observed as an increase in current between the spray system and ground. An experiment was carried out to determine whether use of a blower would increase ground current by preventing the free charges, or charged droplets, from returning to the grounded spray assembly. First, a single nozzle system with the balloon-inflator blower was tested near ground level, as illustrated in Figures 4 and 5. Minus 2,250 volts were applied to the induction ring to produce a positive spray. With the blower off, measured ground current was 2 microamperes; with the blower on, measured ground current was 4.5 microamperes. The blower did reduce feedback.

To determine the effectiveness of the blower at higher altitudes, a specially constructed nine-nozzle system with the blower was constructed. The ground current was found to decrease with altitude between ground and 100 feet, but not as rapidly as without the blower; the feedback reduction was altitude-dependent. The pattern was apparently due to stronger droplet attraction by the earth at lower altitudes.

Fog was unfortunately not encountered during the scheduled test period, but the tests of the balloon-borne charging system did show that this fog dispersal method was worthy of further research. This research is in progress. The hot-air balloon was an excellent vehicle for the tests conducted.

4. HYGROSCOPICS SPRAYED FROM THE BALLOON

Hygroscopic particles rapidly grow by vapor diffusion in saturated, foggy air. The resulting solution droplets may be large enough to collide and coalesce with fog droplets. These effects can lead to fog dissipation as the large droplets settle out.

The FAA requested of NWC that liquid hygroscopic chemicals such as glycerine, diethylene- and tetraethylene-glycol, proposed and furnished by Dow Chemical Company, be tested using the hot-air balloon. The balloon system for these tests is depicted in Figure 6. The balloon carried 30 gallons of the test chemical in the gondola. The chemical was sprayed from the gondola using the Dow spinning disc particulator (see McDuff, *et al*, 1971). A cable carried power from the ground to the balloon and supported a vertical array of droplet samplers. These samplers were used to determine if the droplets of chemical changed in size by collecting either water vapor or the visibility-restricting droplets.

Clear-air tests were conducted with all three chemicals. The objectives of the clear-air tests were to measure the drop size-distribution from the particulators, and to observe the characteristics of the plume. In brief, drop size-distribution

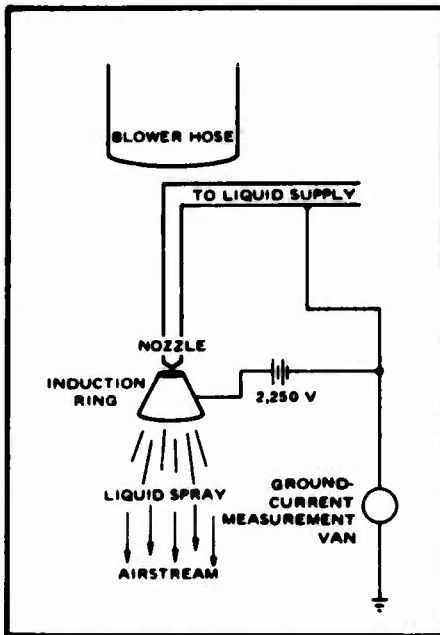


Figure 4. Single-Nozzle System With Blower



Figure 5. Single-Nozzle System With Blower; Ground Test Layout

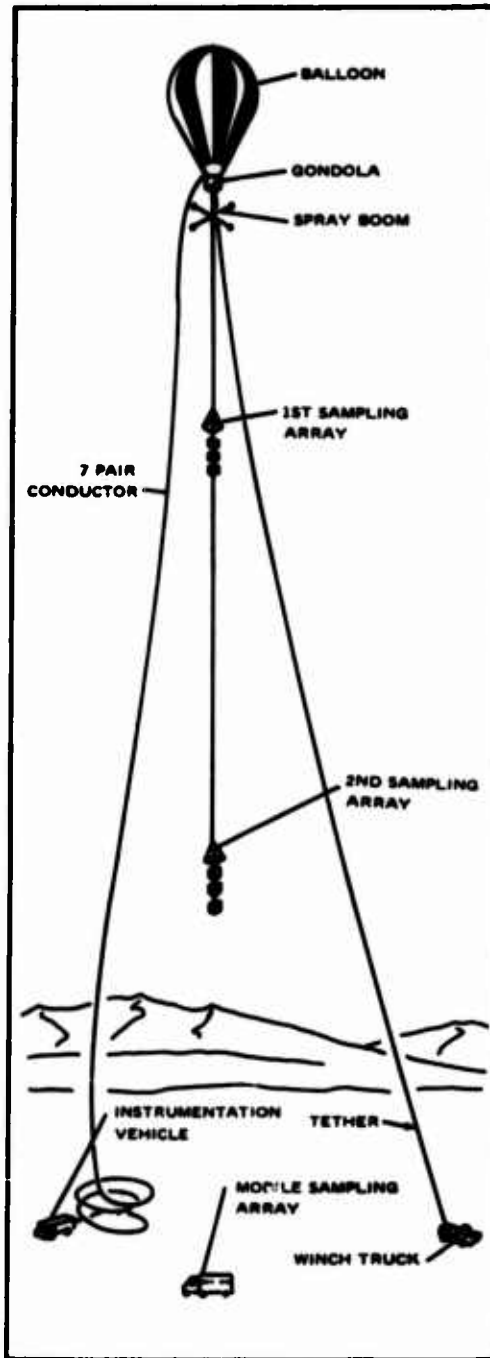


Figure 6. Hot-Air Balloon System for Hygroscopic Spray Tests

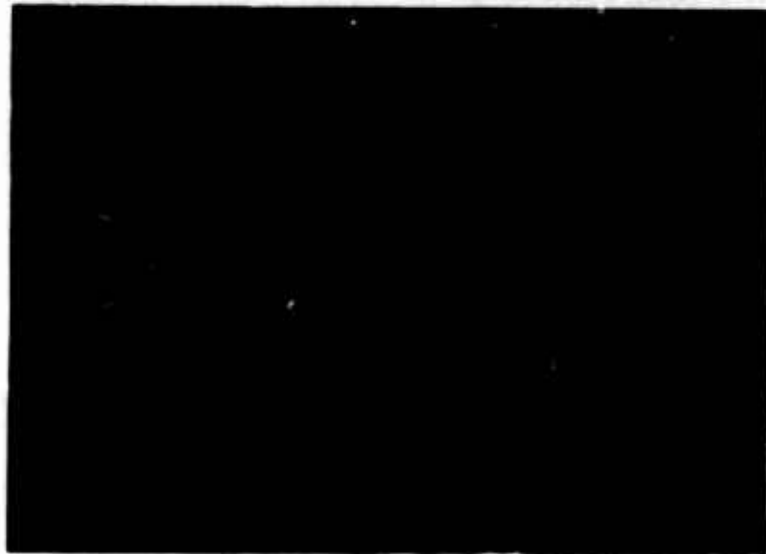


Figure 7a. Four Minutes After Spraying Began

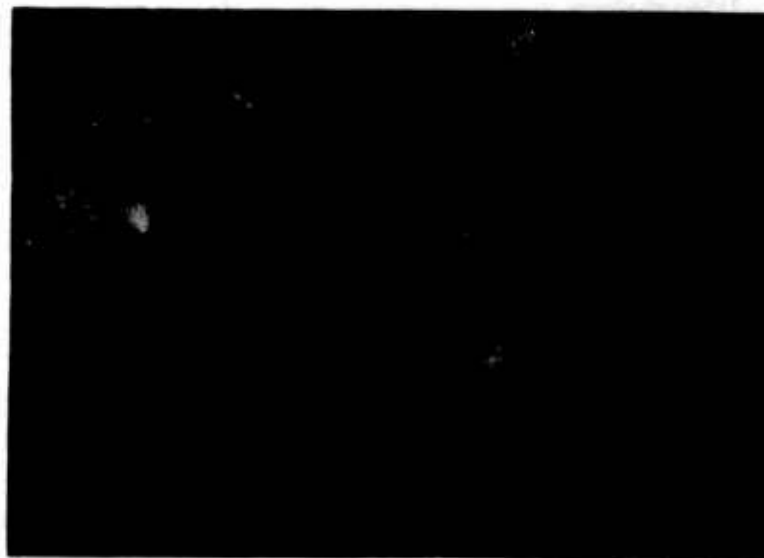


Figure 7b. Seven Minutes After Spraying Began

Figure 7. Photographs of the Fog-Abatement Test From the Navy U-3 Aircraft Flying at 10,000 ft. The balloon is in the center of each picture

samples obtained from the disc particulator showed that over 78% of all drops had diameters less than 30 μm , regardless of the collection distance below the balloon (Hindman and Clark, 1972). Evaporation of the chemical drops should not have caused a significant effect in the humid coastal environment. These droplets were somewhat smaller than desired for optimum effects on fog. The maximum flow rate from the disc particulator was 2.7 gal/min.

McDuff, et al (1971) report that the plume was approximately 10 feet in diameter immediately below the particulator which was at 100 feet AGL. In calm wind conditions the plume was observed to diffuse to approximately 20-25 feet in diameter. As the wind velocity increased to 2 to 3 knots the width of the plume increased to approximately 220 feet at the ground.

Because of the clear weather, only one cloud dispersal test was conducted. A stratus deck with base near 250 feet AGL, and top near 500 feet AGL, filled Redwood Valley. The balloon was loaded with glycerine preheated to 30°C to decrease viscosity and enhance the flow rate. Only 14.5 min after launch, the balloon was stabilized at 450 feet AGL and began spraying. Heat from the balloon was the most probable cause of the large depression around the balloon observed some 3 min after stabilization (Figure 7a). The balloon releases roughly $3 \cdot 10^6$ btu/hr in tethered flight, according to J. Craig, the pilot (personal communication). Each cubic meter of cloud that drifted by the balloon was calculated to receive about 453 calories, enough to cause local evaporation.

A small rift was cut through the fog depth well before the end of the 9.3 min spray period (Figure 7b). Droplets of glycerine water solution were observed at the ground under the hole. The amounts of glycerine sprayed amounted to 21 gal/acre, which was calculated to be more than sufficient to cause the hole by the processes of vapor diffusion plus droplet collision-coalescence (Hindman and Clark, 1972). Other studies by NWC indicate that certain liquid hygroscopics, and an ammonium nitrate-urea-water solution in particular, are reasonably effective in dissipating fog. More efficient means are still being sought.

5. FUTURE FOG STUDIES WITH HOT-AIR BALLOONS

The EPSD is currently funded to conduct a basic fog characterization study with the manned hot-air balloon. Emphasis will be placed on studying the boundary layer between dense fog and clear air above the fog. Acquisition of profiles of certain parameters through the fog will also be attempted. The study will be conducted primarily in the warm, winter radiation fogs that form in the San Joaquin Valley of California. The formative and ripening stages of these fogs are of particular interest, since processes at these stages may hold potentials for modification to prevent or dissipate fog.

The balloon will be operated in the tethered mode, such as shown in Figure 6. Sampling instrumentation will be carried in the gondola and on a platform suspended approximately 10 feet below the gondola. Samples will be gathered as the balloon ascends and descends through fog, and at fog top. As many fog properties as feasible will be monitored. The instrument package design calls for measurement of temperature and dewpoint, volumetric airflow, fog water content and chemistry, cloud condensation nucleus concentration and chemistry, solar and net radiation, and visual and/or infrared characteristics of fog top. If feasible, diffusion in and out of cloud top will be studied by observing colored smoke plumes. Measurements of size and electric charge of natural fog droplets are desired, but many improvements in current instrumentation are required.

The fog water will be sampled in bulk with a simple cylindrical, centrifugal collector. The particle information will be gathered with a Lundgren impactor and a MEE cloud condensation nucleus counter. Particle samples will be drawn through a 3-inch tube that extends to at least 10 feet below the platform, so as to avoid exhaust of the balloon burner. Weather Measure instruments will be used to measure the radiation fluxes, provided radiative effects of the balloon are sufficiently consistent to be subtracted from the readings. The suspended platform will be mounted on a gimbal to maintain a level orientation, especially for the radiation sensors. Simple thermometry, airflow devices and cameras will be used to sample the remaining parameters. Power will be supplied by a 750-foot cord from the ground.

The balloon measurements will be complemented with measurements from the EPSD's 60-foot instrumented tower.

6. SUMMARY

The manned hot-air balloon is very suitable for specialized studies of warm fog properties and warm fog dissipation techniques. In the tethered mode, the hot-air balloon may be used to complement tower measurements so as to provide relatively complete vertical characterizations of fog layers. The effect of fog dispersing agents may be observed over a small control area when tested from a tethered balloon. Free hot-air balloons drift with the fog, and offer the potential for continuous monitoring or treating of given fog volumes. The hot-air balloons can carry heavy payloads while causing only minor disturbances in the fog.

Tethered, manned hot-air balloons have been successfully utilized by the NWC's EPSD to test droplet charging and hygroscopic spray techniques for dispersing fog. An instrumented, tethered hot-air balloon will be used in a project now underway to study properties of fog top during formative and ripening stages.

Contents

1. Introduction
2. Hull Design
3. Heat Generators and Hull Pressurization
4. Gondola and Power Plant
5. Controls and Instrumentation
6. Operations

A Manned, Nonrigid Thermal Airship

R. A. Pohl
Vice President, Raven Industries, Inc.
Sioux Falls, South Dakota

Abstract

Airships have classically utilized helium or hydrogen as a buoyancy medium. In general, these gases were used due to availability and the operational mode of the airship. An airship can use hot air as a buoyancy medium. Such a vehicle has obvious limitations; however, as a low altitude, multihour flight duration airship it has many advantages over the helium/hydrogen "classics". Some of the primary advantages are initial and operational costs and ease of storage between flights. The primary and obvious disadvantages are flight duration and payload capacity.

Since hot air is a time function degradable buoyancy medium, a continuous energy source is required to maintain any significant flight duration. Hot air sport balloons, which have become quite common today, use onboard burners with a hydrocarbon fuel to accomplish flight duration of hours. These same type of burners and fuel, coupled with a pressurization fan are basically the buoyancy and hull pressurization source for the thermal airship.

This paper describes the design and expected performance of a hot air airship presently under construction. Flight tests are scheduled to begin during the fall of 1974. The flight characteristics of the airship are based on commercial markets with low, slow and light payload requirements. The nonrigid hull has a 2.5:1 fineness ratio

with inflated fins. A gondola which is close-coupled to the hull, will contain the air-cooled engine which drives a single propeller. A heat generator and hull pressurization system, along with propane fuel tanks, are in the gondola. Provisions for controls and pilot plus copilot and/or passenger are made in the forward gondola section.

1. INTRODUCTION

Hot air sport balloons with a natural shaped configuration have been demonstrated to be a reliable and economical method of free ballooning at low altitudes. These balloons are used primarily as sport vehicles and in some cases, for advertising and promotion. With an onboard burner(s) and a hydrocarbon fuel source for maintenance and control of the buoyancy state, these balloons float with the wind and have practically no directional control other than the wind vector variations as a function of altitude. This flight regime is acceptable for the type of flying done by sport balloonists.

Hot air is an economical buoyancy medium for relatively short duration, low altitude flights with manned balloons. The obvious advantage of thermal buoyancy in a balloon is that it can be "generated" as needed or desired by the combustion of liquid fuels in relatively simple onboard burners. This basic fact has made hot air ballooning a popular sport that is quite commonplace throughout the United States.

The obvious next generation of hot air ballooning is a thermal airship with a low drag hull and an onboard power plant so the balloonist can control his direction. Such an airship is presently under construction and is scheduled for flight testing in the October-November period of this year. The general design and operating characteristics of this vehicle are described herein. This project and the vehicle are called STAR.

2. HULL DESIGN

The hull of the STAR airship is based on a class C shape with a fineness ratio of 2.5:1 and a volume of 140,000 ft³. These parameters result in a hull length of 120 feet and a diameter of 48 feet. As noted in Figure 1, four inflatable fins are located on the aft hull section for stability and directional control. The fins are inflated through gas transfer ports located in the fin root/hull interface. Interweb sections maintain the fin thickness and determine taper an-

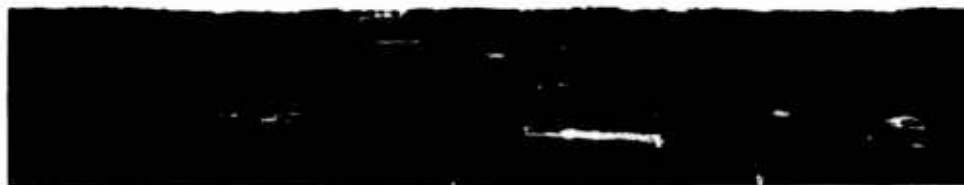


Figure 1. STAR Thermal Airship

gles. A movable rudder section is located on the upper vertical fin while both horizontal fins have elevator control surfaces.

The hull is constructed of a urethane coated polyester ripstop fabric (3 oz/yd²) with a MD/TD strengths of 100 and 70 lb/in. Longitudinal gores constructed of panel sections are utilized to maximize the fabric properties. The hull is a single compartment cell with catenary suspensions located near the top of the hull as shown in Figure 2. These load suspensions are used to transfer the gondola loads into the hull at maximum lift locations and distribute the center of buoyancy/gravity intersection planes. Temperature distribution in the hull is anticipated to yield a somewhat uniform center of buoyancy area; however, one of the twin burners used to supply heat to the ship is gimballed to permit burner plane variations along the longitudinal axis.

3. HEAT GENERATORS AND HULL PRESSURIZATION

Twin burners with a combined output of 4.5 million BTU/hr. are used to heat the air in the hull. The burners are located on the top of the gondola and within the hull with a pressurization fan which will maintain the hull at 0.5 in. of H₂O. Liquid propane is used as a fuel and is contained in stainless steel tanks located in the gondola. Both the burners and pressurization fan are standard hot air sport balloon components. The pressure fan is powered by a small gasoline engine. A redundant feature of this fan power source is an engageable takeoff from the main power plant.

4. GONDOLA AND POWER PLANT

A fabric covered, aluminum frame gondola is located under the hull at a location which will yield a 6° negative angle of pitch with zero power application. This ten foot long gondola is configured for a side-by-side pilot/copilot in the forward section with the main power plant, fuel tanks, and blower/burner in the aft section as shown in Figure 3. A pusher propeller located on the gondola aft section is driven by a 65 horsepower Revmaster Volkswagen aircraft engine with single ignition starter and a 12 volt generator. Aviation 100 octane gasoline is the fuel source. The prop is coupled via a direct drive to the engine. An annular ring duct around the prop is used to maximize prop efficiency and thrust direction.

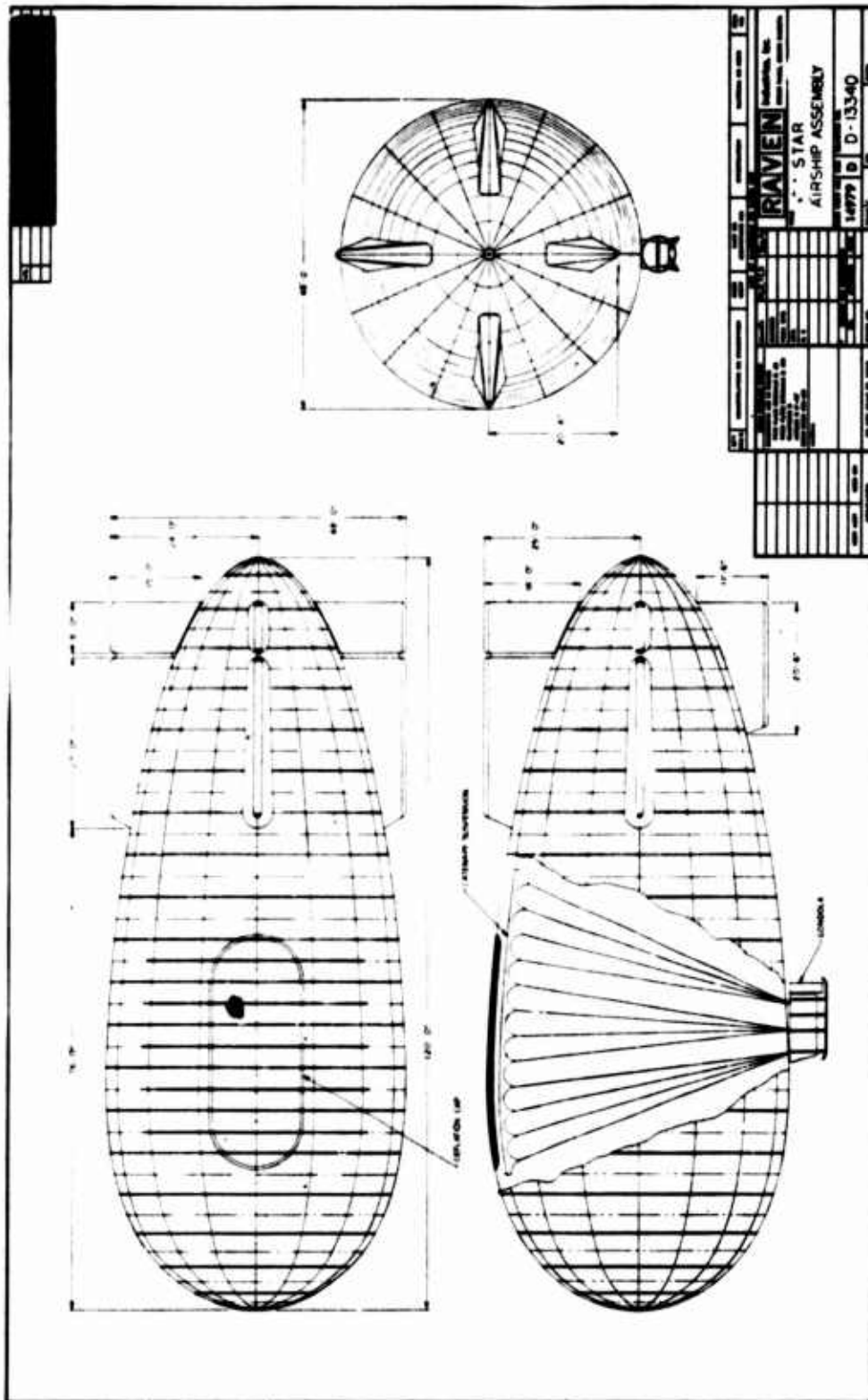


Figure 2. STAR Airship Assembly



Figure 3. STAR Gondola Under Construction

5. CONTROLS AND INSTRUMENTATION

Controls include rudder, elevators, propane flow to burners, main power plant throttle, burner override, propane pressure to burners, blower speed, aft burner gimbal. These basic controls are used for flight direction and internal hull temperature variations for gross lift modification. As is commonplace in manned hot air sport balloons, the large inertia mass of the ship will yield a somewhat slow response to the heat and/or rudder-elevator control inputs.

The panel in the forward section of the gondola will have the standard engine condition monitoring instrumentation. Also included on the panel are an airspeed indicator, altimeter, rate-of-climb, balloon internal temperature, hull pressure, fuel quantity and pressure gages.

6. OPERATIONS

The STAR airship with its 65 horsepower engine is intended to a service ceiling of 4,000 feet at a gross load of 2030 pounds which includes 78 gallons of propane and a 100 pound payload. The anticipated flight duration is three hours. Under these conditions and at the maximum available thrust of approximately 350 pounds STAR is predicted to have a top airspeed of 25-30 mph.

As has been noted, airship response to control surface deflection will not be rapid. For example, analysis indicates that at low airspeeds (up to 10 fps), large elevator deflections will have little impact on the pitch of the airship. This analysis predicts elevator deflections in excess of 40° (upwards) to achieve trim at airspeeds in this range. On the other hand, at maximum speed, response in pitch to elevator deflection is predicted to be quite sensitive, to the extent that pilot experience will be a major factor in achieving level flight. Nevertheless, since altitude control of STAR is for all practical purposes a function of thermal rather than aerodynamic considerations, these response characteristics will not affect system usability and the flying attitude accepted by the pilot will be largely a function of the flight conditions and his comfort.

Figure 4 indicates the elevator deflections required to achieve an angle of attack of 0° . The system weights for which this information has been derived are as follows:

2187 lb. - Full load, Pilot and copilot, 100% fuel.

2007 lb. - Full load, Pilot only, 100% fuel.
1827 lb. - Full load, Pilot and copilot, 20% fuel.
1647 lb. - Full load, Pilot only, 20% fuel.

In this figure, the lack of low speed response is evident. Also, it is here seen that the low speed "reversal" of control surface deflection at low speeds common in airships is predicted for STAR. However, since the medium static pitch angle is only approximately 6° at the maximum gross weight (approximately -1.5° at the minimum listed system weight), it will probably be found that no elevator deflections will be necessary at these speeds to give acceptable performance, and that the region of the flight envelope in which reversal occurs will be a factor only under higher gross weight conditions.

The size of all control surfaces was selected on the basis of those surfaces which have provided controllability in previous manned and unmanned airships. This predicted controllability in yaw has been verified by comparison to wind tunnel data available in general circulation for a specific airship model (not STAR). However, response to rudder deflection is expected to be quite slow, to the extent that it may be necessary under certain conditions to accelerate to the upper range of airspeed in order to achieve the required response characteristics.

Control surface deflection will be achieved through a cable and hand crank system which will provide some mechanical advantage in deflecting the surfaces. Application of this force will be near the trailing edge of the control surfaces, approximately 7 ft. from the hinge line. Since the predicted hinge moment for a 30° deflection of the rudder at near the maximum airspeed is approximately 500 lb.ft., the control surface forces are seen to be quite low, approximately 70 lb. applied normal to the rudder axis. Tests conducted on a full scale upper vertical fin and rudder assembly have confirmed these low predicted values for control surface forces.

Normal flight operations are to be VFR in light to moderate wind conditions. Both takeoff and landings are the same as normal airship operations. VTOL operations will also be possible in light wind conditions. Since the hull is nonrigid and the buoyancy medium is generated onboard, the vehicle will be inflated at the takeoff site and deflated upon landing. The deflated hull, along with the gondola, can be transported with a medium-sized truck.

Handling lines are located around the hull to aid the ground crew in their operations. A deflation panel located on the hull top-side will be pulled out by the pilot upon landing. The type of "pull out panel" is the same basic configuration as that used in hot air

sport balloons. Once the hull is deflated, the panel is manually replaced.

The STAR vehicle is intended for the low and slow flight regime with directional control. It is designed for ease of maintenance, low operational costs and relatively simple logistics.

Pressure Hot Airship Design And Performance

John F. Hebel
Buoyant Flight Systems
Nashua, New Hampshire

Abstract

Pressure hot airships have unique design problems. The basic problem is control of heat loss through the surface of the envelope. Heat loss data collected from experiments with several different configurations of low heat-loss envelopes point up the limitations of economically available fabrics for balloon construction. The stresses due to internal pressure and forward motion of the ideal airship, based on a specific envelope configuration, have been derived via digital computer design of the contour of the envelope. The weight of the fabric required to carry these stresses has been calculated for the envelope under consideration, along with the lift of the envelope. From an estimate of the weights of other necessary airship components, the useful load has also been calculated. Variations in range and duration, at a variety of airspeeds and altitudes, have also been worked out. In addition, the unique operating characteristics of this class of aircraft have been identified. Extremely good efficiency of utilization of the heat content of the fuel is promised. The conclusion is that for certain missions, pressure hot airships are practical and viable in the energy-started future.

Contents

- 1. Introduction and Background**
- 2. Potential Mission Applications**

X74-845/034A

Rocket-Launch Balloon-Borne Systems (RLBS)

**Robert C. Geiss
Missile Systems Division
Rockwell International
Anaheim, California**

Abstract

DOD-sponsored studies have described the technical feasibility and the potential mission payoff of payloads supported by balloon platforms that are rocket-launched to deployment altitude. Company-sponsored investigations of representative payload configurations have uncovered a gamut of scientific and potential military mission applications that could be accommodated by a platform supporting capability of about 230 kilograms net payload weight on station. The feasibility of such a rapid launch technique is described and assessed. The mission capabilities of representative payloads are described and cost and weight estimates are made. Qualitative assessments are made of the overall characteristics and utility of a launch, deployment and on-station operational employment sequence that would take less than five minutes.

1. INTRODUCTION AND BACKGROUND

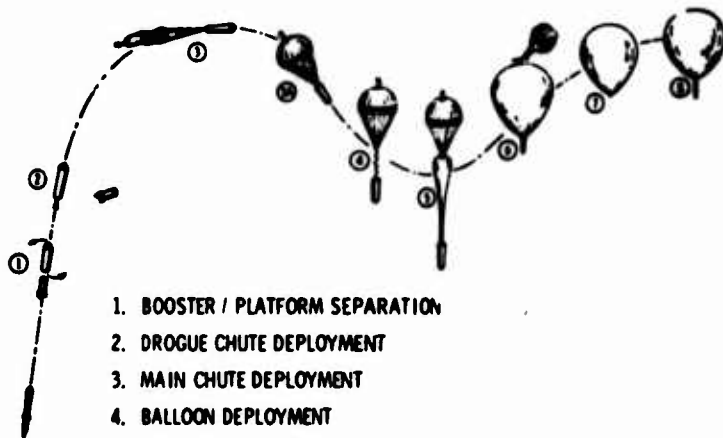
Over the past four years, various industry studies under Government sponsorship have identified the potential utility of balloon-borne sensor and equipment platforms in support of mission objectives (reference 1, 2). Particular mention was

made of the advantages concerning cost and mission utility if such balloon-borne platforms could be rapidly rocket-launched and deployed on warning. Industry and Government studies have addressed the feasibility of such deployment techniques (reference 3, 4). While differing in detail, the study conclusions generally agree that such launch techniques are feasible, within the state of the art, require certain engineering developments, and should be demonstrated.

This paper will highlight results of the Rockwell study (reference 3) regarding the characteristics of a rocket-launch technique and balloon platform deployment for optical payloads supporting BMD mission needs. A representative rocket-launch mission profile is shown in Figure 1. Nominal mission altitude was chosen as 80 kilo feet (24.4 km). Mission guidelines concerned: long storage periods in launch-ready condition, 2 to 4 minute launch to on-station time, and on-station up to 15 hours or more. Feasibility study conclusions included: deployment and inflation is feasible and reasonable, practical upper altitude limit is about 90 K ft. (27.4 km); deployment parachutes are state-of-the-art; active gas replenishment was preferred for altitude maintenance, although ballast methods are adequate for other missions examined; liquid H_2 /gaseous O_2 was preferred inflatant with liquid He/H_2O_2 as a second choice; gas generation system is state-of-the-art. A representative conceptual balloon and payload configuration is depicted in Figure 2. The study results also highlighted that a relatively wide range of payload weights and functions could be accommodated on rocket launchers already in the DOD inventory and available at nominal cost. Gross launched payloads to 2,000 pounds (909 Kg) can be handled by surplus Honest Johns, for instance. Time and space do not permit discussion of the throw weight, range, altitude profiles of the various candidate boosters. It is sufficient to state that they exist and are capable of providing the weight, payload volume and altitude capability for the platform functions subsequently analyzed.

The characteristics of the launch and deployment environments were found to be compatible with all payloads investigated. The understanding of the launch environmental parameters are well in hand and documented for all launch vehicles studied. It was discovered that the parameters of deployment and subsequent sequences can be tailored to be no more severe than the launch environment. For instance, in certain launch vehicles, maximum "g" loading approach 6 gravities. The deployment sequence, by judicious choice of drogue and deceleration chutes, can be held within that "g" profile. The mission hardware examined for rocket-launched balloon platform applications are compatible for such environments. As Carten states . . . "there are subtle differences, such as involving flight Mach number and altitude density experienced . . ." (reference 4) by aircraft launched balloon system versus a rocket-launched system. These differences lead to a lower gross weight launched to net payload ratio for the rocket launched system.

CONCEPTUAL SYSTEM DEPLOYMENT



1. BOOSTER / PLATFORM SEPARATION
2. DROGUE CHUTE DEPLOYMENT
3. MAIN CHUTE DEPLOYMENT
4. BALLOON DEPLOYMENT
5. INITIATE INFLATION (BALLOON CONTAINER SEPARATION)
6. MAIN CHUTE SEPARATION
7. INFLATION COMPLETE (INFLATION SYSTEM RETENTIONS)
8. PAYLOAD DEPLOYMENT

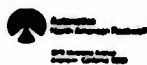


FIGURE 1 - ROCKET-LAUNCHED BALLOON PLATFORM - MISSION DEPLOYMENT

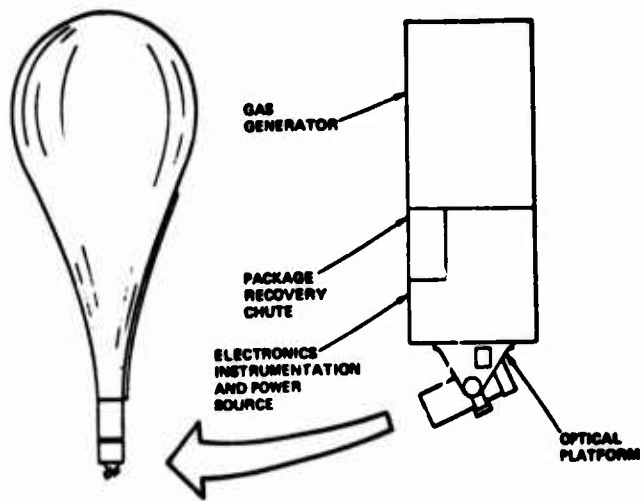


FIGURE 2 - CONCEPTUAL BALLOON/PAYLOAD CONFIGURATION

2. POTENTIAL MISSION APPLICATIONS

The primary thrust of Rockwell's initial investigations of rocket-launched balloon-borne platforms was to support ballistic missile defense surveillance requirements. As described earlier, the results of feasibility investigations were positive for such a mission application. Subsequent analyses uncovered a gamut of potentially useful missions or capabilities that could be supported by a rapid-launch and deployment technique for a high altitude platform. These can be grouped as follows: surveillance or astronomical observations payloads, communications, and command and control. Each application was treated in a generic way. That is, a representative configuration established, capabilities assessed, and weight and cost estimates made. Finally, the payload requirements were folded into balloon, drogue, and parachute system parameters to establish nominal subsystem characteristics. It must be emphasized that the payload components were chosen from contemporary, off-the-shelf items. No attempt was made to optimize the components toward a given goal. Rather, we accepted existing performance and described that performance as the capability.

Surveillance payloads were sized to accomplish the following missions: battlefield TV surveillance at one foot resolution out to 40 miles as depicted in Figure 3. Such surveillance capability is useful for other than conflict scenarios

SURVEILLANCE

BATTLEFIELD TO COMMAND AND CONTROL CENTER

- PERIMETER COMMUNICATION TO HORIZON - 300 NMI
- EXCELLENT VISUAL IMAGERY - SLANT RANGES ≤ 40 NMI
- HIGH RESOLUTION COVERAGE WITHIN 5400 SQ MI AREA
(One Foot Resolution, 230 K Ft Slant Range, 6-in. Dia Optics)
- ≥ 15 HR STATION TIME
- ROCKET OR AIRCRAFT LAUNCH

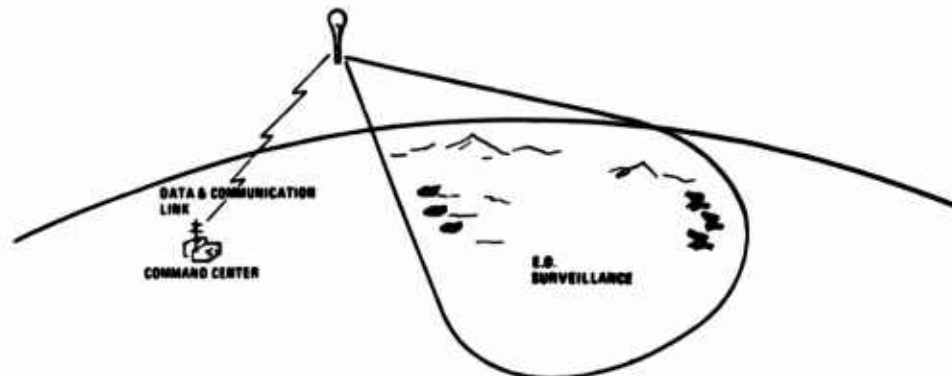


FIGURE 3 - BATTLEFIELD TV SURVEILLANCE CAPABILITIES

as well. The payload weight bill is shown in Figure 4. Space surveillance or astronomical observations utilize a cryogenically-cooled LWIR telescope to typify such mission requirements. Figure 5 portrays the mission scenario and Figure 6 presents a typical weight bill.

	<u>WEIGHT (LB)</u>
● TELEVISION SURVEILLANCE SYSTEM	150
● SURVEILLANCE DATA LINK (UP-DOWN EQUIP)	35
● BALLOON ACQUISITION SYSTEM (BEACON)	30
● LOS BEARING SYSTEM	35
● MISC HARDWARE ITEMS	15
● POWER SOURCE (5000 WATT-HOUR)	<u>143</u>
NET PAYLOAD	408
	===

FIGURE 4 - BATTLEFIELD SURVEILLANCE PAYLOAD WEIGHT ESTIMATES

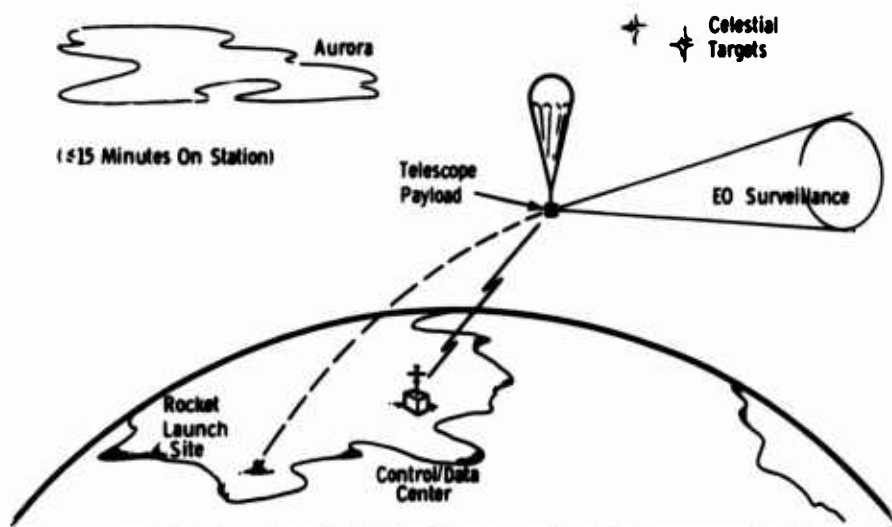


FIGURE 5 - SCENARIO FOR SPACE SURVEILLANCE OR ASTRONOMICAL MISSIONS

	<u>WEIGHT (LB)</u>
● LWIR SENSOR SYSTEM	190
● GROUND/BALLOON DATA LINK (UP-DOWN)	50
● BALLOON ACQUISITION SYSTEM	30
● LOS BEARING SYSTEM	35
● MISC HARDWARE ITEMS	15
● POWER SOURCE (5000 WATT-HOUR)	<u>143</u>
NET PAYLOAD	463
	===

FIGURE 6 - WEIGHT ESTIMATES FOR SPACE SURVEILLANCE
OR ASTRONOMICAL MISSIONS

Communication requirements were addressed to support a postulated NORAD communication outage. The scenario is depicted in Figure 7 and the net payload weight bill is outlined in Figure 8. Similar weight bills can be established for derivatives of communication and command/control missions. Secure emergency fleet communication requirements are depicted in Figure 9 and the weight bill in Figure 10.

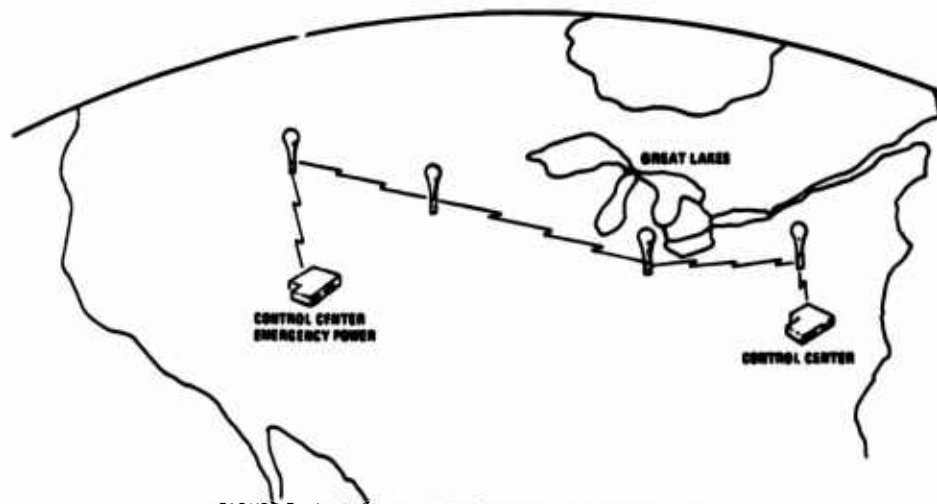
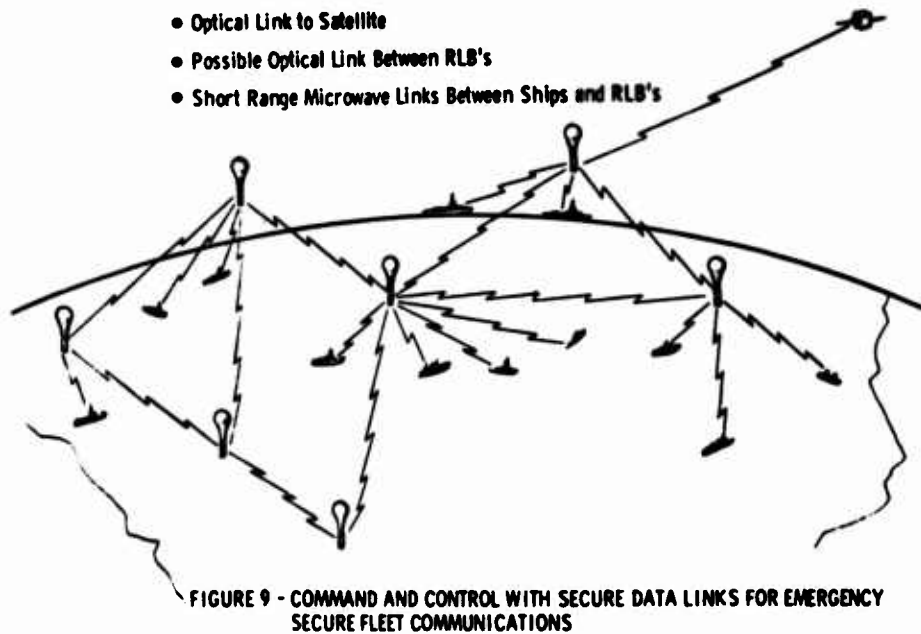


FIGURE 7 - EMERGENCY NETWORK (NORAD SUPPORT) SCENARIO

	<u>WEIGHT (LB)</u>
● GROUND/BALLOON DATA LINK	40
● GROUND/BALLOON ACQUISITION (BEACON)	30
● BALLOON/BALLOON DATA LINK	30
● BALLOON/BALLOON ACQUISITION SYSTEM (BEACON)	40
● LOS BEARING SYSTEM	35
● COMMUNICATION STORAGE AND PROGRAMMER	15
● MISC HARDWARE ITEMS	15
● POWER SOURCE (5000 WATT-HOUR)	<u>143</u>
NET PAYLOAD	348
	===

FIGURE 8 - EMERGENCY COMMUNICATIONS LINK WEIGHT ESTIMATE



	<u>WEIGHT (LB)</u>
● MULTICHANNEL SHIP/BALLOON COMMUNICATION SYSTEM	40
● SHIP/BALLOON ACQUISITION SYSTEM (BEACON)	30
● MULTICHANNEL BALLOON/BALLOON COMM SYSTEM	30
● BALLOON/BALLOON ACQUISITION SYSTEM (BEACON)	40
● MULTICHANNEL BALLOON/SATELLITE ACQUISITION AND COMM SYSTEM (OPTICAL)	170
● PRECISION LOS BEARING SYSTEM	50
● COMMUNICATION STORAGE AND PROGRAMER	15
● MISC HARDWARE ITEMS	15
● POWER SOURCE (5000 WATT-HOUR)	<u>143</u>
NET PAYLOAD	533
	===

FIGURE 10 - EMERGENCY SECURE FLEET COMMUNICATIONS WEIGHT ESTIMATE

Gross payload launched versus net payload on-station calculations had been made previously during parametric studies (reference 3). For the assumptions made (e.g., cryogenic H₂/liquid O₂ inflatants, 40 in. diameter system, given "q" and "g" profile) the payload weight characteristics table was developed as shown in Figure 11. These data were plotted in Figure 12. The range of data is valid for 200 to

	WEIGHT (LB)			
	90	100	130	260
DROGUE AND MAIN CHUTES	90	100	130	260
BALLOON	130	145	220	400
INFLATION SYSTEM	170	200	285	510
RECOVER CHUTE	20	25	30	50
NET PAYLOAD	250	300	400	650
GROSS PAYLOAD	660	770	1065	1870

FIGURE 11 - GROSS PAYLOAD LAUNCHED VERSUS NET PAYLOAD ON STATION WEIGHTS (NOMINAL 80K ALTITUDE)

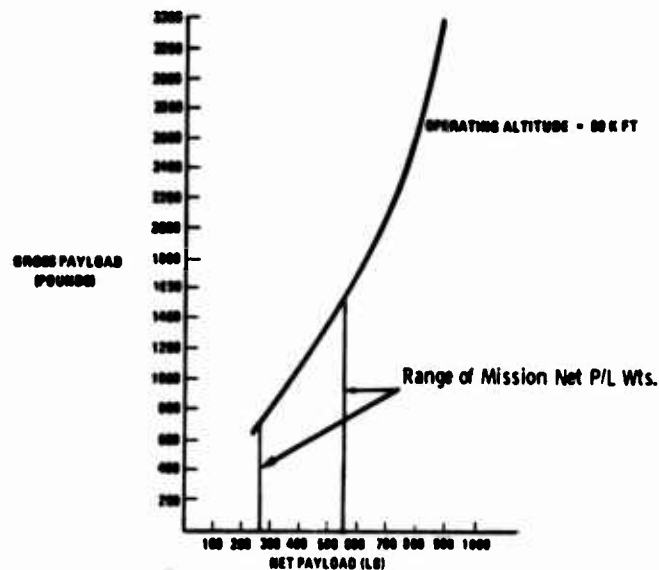


FIGURE 12 - GROSS PAYLOAD WEIGHT AS FUNCTION OF NET PAYLOAD WEIGHT

1000 pounds net payload weight. The range of net payload weights needed for the mission requirements are indicated by the two vertical lines which encompass the missions examined. A message which can be derived is that the maximum net payload weights generate gross payload requirements which are well within the capabilities of current or surplus launch vehicles and normally do not exceed 550 pounds (250 Kg) net payload weight.

Cost estimates for the mission requirements described before are tricky at best and misleading at worst. Assuming that the necessary development and demonstration activities are successfully completed, cost estimates for the booster hardware alone range from about \$15K for a modified surplus Honest John upward through \$150K for a Castor I configuration (Scout second stage plus two Recruit strap-on motors). The parachute/balloon subsystem to support a 600 pound (273 Kg) net payload would come to about \$15K. The net recoverable payload would range upwards of \$10K through \$200K depending on the payload components and their complexity. These estimates do not include support costs, but are indicative of hardware costs only.

References

1. Midcourse Surveillance System Study Program (Phase II). Volumes I, II, III, Philco-Ford, Aeronutronics Division, 1970.
2. Surface Optical Defense, Final Report on Contract DAHC60-70-C-0076 (SECRET), G.E., Space Sciences Laboratory, P.O. Box 8555, Philadelphia, Pa 19101. Volume I, Summary and Conclusions, 1 July 1971.
3. Optical Rocket-Launched Balloon (ORB) Feasibility Study Program (U). Final Report, Contract DAHC60-71-C-0073, Autonetics Division, Rockwell International, November 1972.
4. An Investigation of Techniques for Launching Large Balloon Systems from Aircraft or Rockets in Flight. A.S. Carten, Jr., AFCRL TR-73-0633, 9 October 1973.

Contents

1. Introduction
- 1.1 Background
- 1.2 General Considerations
2. Design
- 2.1 General Features
- 2.2 Materials
- 2.3 Seals
3. Conclusions

Sphere Design For A Static Detonable Gas Experiment - GEST

M. G. Marcucci, Capt., USAF
Air Force Cambridge Research Laboratories
Bedford, Massachusetts

Abstract

During the period Nov 73 - Jan 74, several detonations of CH_4/O_2 filled spheres were accomplished by the AF Weapons Lab in the Gas Explosion Simulation Technique (GEST) Program. These spheres were designed by AFCRL and manufactured by the Sheldahl Co. in Northfield, MN. Of importance in the design were the static discharge properties and sundry handling needs. These will be discussed relative to the material selected and the specific features of the spheres.

Preliminary results from the 4 detonations were strongly encouraging to the sponsor, the Defense Nuclear Agency, and further funding is expected for a Jan 75 detonation and an additional future series of larger spheres.

1. INTRODUCTION

Over the past ten years, an on-again, off-again series of projects and studies have been performed in the study of nuclear explosions using detonable gas balloons. These programs have been conducted under the auspices of the Defense

Nuclear Agency (DNA) and have varied in magnitude from a yield of a few tens of pounds to a yield of 20 tons of high explosives. The latest in this series was called the Gas Explosion Simulation Technique (GEST) Program and was conducted by the Air Force Weapons Lab (AFWL).

In preparation for this program, AFWL sought out the AFCRL and the General American Research Division (GARD) as engineering consultants. The Aerospace Instrumentation Lab was to design and procure the proper spheres, then to formulate the necessary handling procedures. GARD was to design the inflation system and to consult on its installation and operation.

This paper will describe briefly the background of detonable gases, and explain the design considerations of interest in the GEST spheres.

1.1 Background

The GEST tests were conducted on part of the Air Force Special Weapons Center testing range in New Mexico from November 73 to January 74. Three single shots were successfully performed in November and December, and a partially successful double shot took place in January.

This series culminated over a year's work by the participants. AFWL divisions were in charge of both the detailed theoretical work and the conduct of the testing. Their Theoretical Branch had planning responsibilities for gas mixtures, seedant powders, yield effects, and instrumentation, and coordinating responsibilities for test schedules and outside agencies. This branch is also evaluating the test data for DNA. The Civil Engineering Branch, Experimental Division, was responsible for site preparation and construction, and for conducting the test series.

1.2 General Considerations

1.2.1 ADVANTAGES OF DETONABLE GASES

An observer's questions might include why detonable gases instead of high explosives (HE)? This has been argued before, but to make the discussion appli-

cable to GEST, let's take a cursory view at it's purpose. In general, GEST was designed to study of the entrainment of oxygen into the fireball of a low altitude nuclear explosion. Photographic and pressure measurements would document the movements of both the explosive "fluid" and its surrounding medium. The torus formed by the explosion was of particular interest. Photographs were to be in the visible and the infrared and were to be compared with AFWL's theoretical behavior model.

To do this, detonable gases offer several hard advantages over HE - the most noticeable being cleanliness. Because the burst height for our experiment was about 150 feet (see Figures 1, 3, and 4) a tower would have been necessary for the HE. In past experiments, observations have been hindered to an extent by debris thrown about by HE blasts. The destroyed tower along with unburned portions of the TNT pack would degrade the visual portion of the test and distort pressure patterns. Detonable gas eliminates this debris.

In simulating air bursts, according to an article in Technology Week (1966), there are further advantages. The article mentions that the shock wave from the detonation is much more distinct than TNT in the higher overpressure regions. Granted that GEST is not specifically concerned with blast and shock effects as was the SLEDGE program; however, their byproduct - the torus - should also be cleaner to distinguish.

In addition, another advantage lies in the reproducibility of the blast. Incomplete burning or non-burning of various segments of a TNT package can result in minutely different blast patterns. Given that a sphere with good quality control measures has a uniform thickness, with complete gas mixing, the sphere should have no such problems. We may assume excellent correlation from one shot to the next if wind conditions are similar and we accurately measure the amount of gas.

A fourth advantage of using the detonable gas sphere for this program was to build proficiency with buoyant systems. For future work involving high yield nuclear simulations at high altitudes (10-20 tons at 20K-100K feet), a buoyant

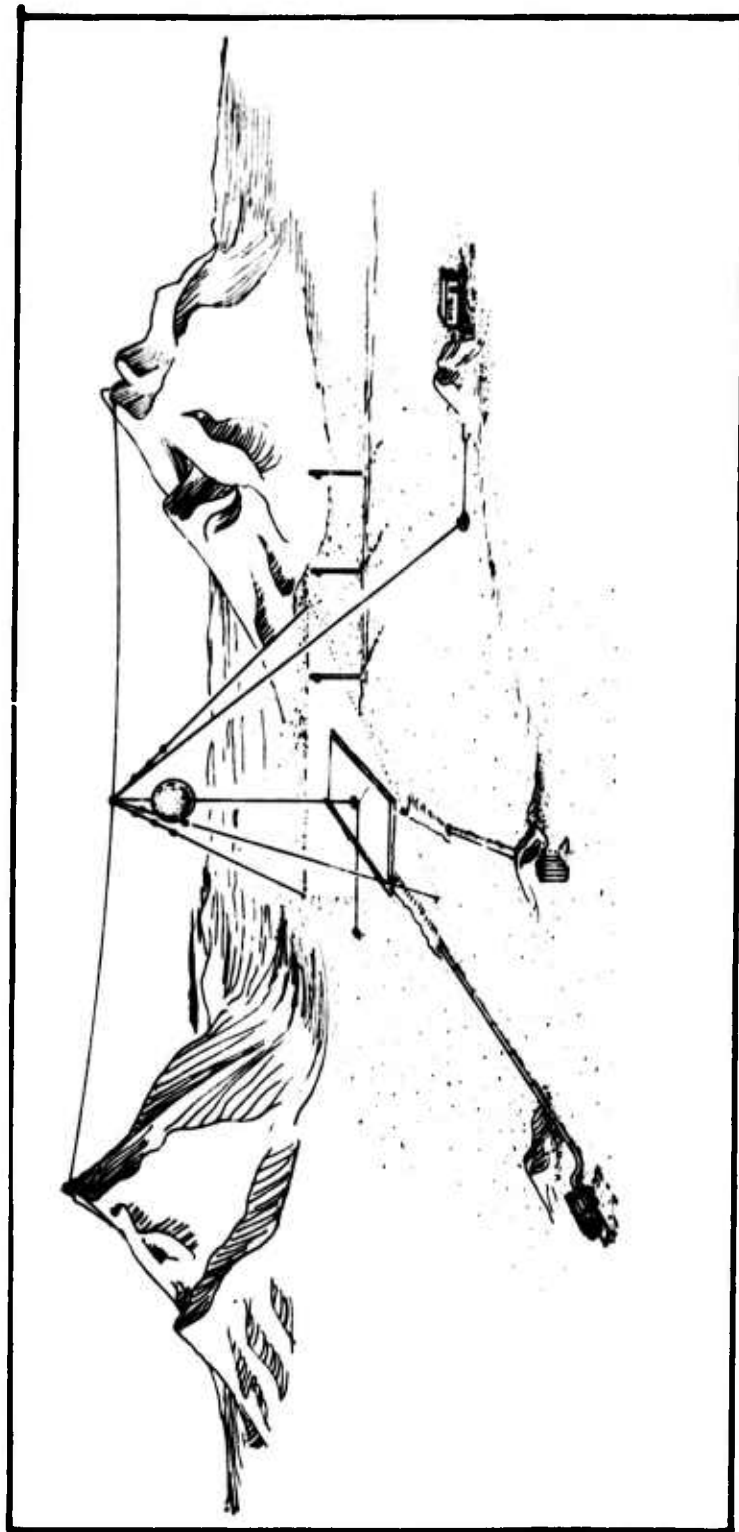


Figure 1. GEST Site Layout

Table 1. Detonable Gas Programs

Date	Program	Size	Material	Remarks
May 65	SLEDGE Phase I	3', 5' spheres 10', 13½' spheres	rubber Dacron scrim over Mylar	GTS*
Oct 65	SLEDGE Phase II	32', 40' spheres	Dacron scrim between metallized Mylar	GTS X-850
Jun 66	Distant Plain	17' hemisphere	Dacron scrim between Mylar	GTS
Jul 66		110' sphere	Mylar between Dacron scrim	GTS
		125' hemisphere	Dacron scrim over Mylar	GTS
1969-1971	SLEDGE	4.0x10 ⁶ ft ³ natural shape	Dacron scrim between Mylar w/silver grids	G115200**
1972	SLEDGE	10' spheres	Dacron scrim over Mylar	G001200
Nov 73	GEST	32' spheres	Metallized Mylar bilaminate	G131900

*G. T. Sheldahl Co.
** GTS designation



Figure 2. The Inflated Sphere Over GZ

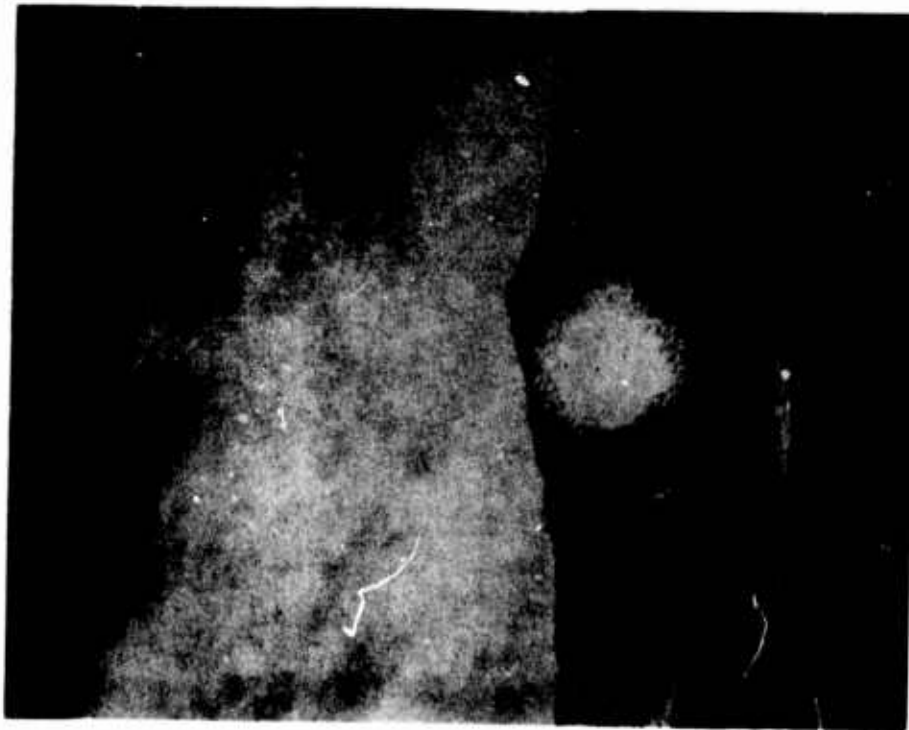


Figure 3. A Daylight Picture of a Detonation

detonable array is perhaps the most economical system.

At today's prices as described in Nolan (1973), lifting 10 tons of HE to 20,000 ft would incur a balloon cost of approximately \$30,000, while the same load to 100,000 ft would cost approximately \$300,000.* Keep in mind that these costs do not include support, instrumentation, or the payload itself. According to sources at AFWL, the present cost of 10 tons of TNT would be somewhat over \$20,000. These costs have risen considerably in the past few years, and we could expect this trend to continue. Only four years ago, the former balloon above would have cost approximately \$20,000 and the latter \$130,000. The costs of detonable gas balloons vary also. They are expensive because of the unique design (see examples in Table 1), and at low yields, in fact, are perhaps more expensive than HE. They become cost-effective quickly, though, as one moves up the yield-altitude curve. Their actual cost varies with the specific material used, but there are a few general related factors which may be considered.

The large cost for the HE balloons is due to their geometric size increase as altitude requirements go up. However, detonable mixtures of CH_4/O_2 or H_2/O_2 are buoyant in themselves and, instead of being dead payload weight, can act as all or part of the lifting medium. A considerable reduction of the system gross weight is the result and a smaller balloon is required for the same burst height. The reduced weight also lessens the gross lift needed at launch making the system easier to handle.

1.2.2 PREVIOUS PROGRAMS

In past detonable gas experiments, balloon materials have differed from this program. Table 1 summarizes these designs. The differences were caused mainly by the particular inflation scheme or the material strength needed based on planned handling. Some of the key decisions which led to eliminating scrim from the GEST design were, likewise, based on expected handling and usage. Extra strength would

*A 10 ton payload is the present practical limit for the Mylar/scrim design without a materials development program.

have been needed if equipment in addition to the inflation tube were to be placed on the gore material or if handling patches were needed. Planners decided against both of these points, instead, incorporating all miscellaneous parts on the bottom end fitting (BEF) and replacing the need for patches with a restraining stand for the BEF. (See Figure 5).

1.2.3 TEST PLAN

A GEST scenario for a single shot would last approximately 5 hours if the planned schedule were followed. A brief summary of events is as follows:

T-4 3/4 hours	personnel arrive on site
T-4 hours	lay out sphere
T-3 1/4 hours	insert support cable and close up sphere
T-2 hours	place sphere in suspended position
T-1 1/4 hours	begin inflation
T-15 minutes	raise sphere to burst height
T-0	detonate

The basic work could be done by 4 men. In a little more detail, it included laying the sphere out from the box, installing the time of arrival (TOA) gauges, internal support cable, and both end fittings, attaching to the upper restraining cable, using a truck to raise the sphere over ground zero (GZ), fitting the BEF on to its holding stand, attaching to the lower restraining line, inflating from a remote location, and, finally, raising the sphere to its burst height (using the truck again).

In our design, we had to consider this basic list and modify either the spheres or the procedures to complement one another. Our main theme consisted of minimum handling throughout. In keeping with this, the above work was all to be accomplished at the site.



Figure 4a. 1 ms. After Initiation



Figure 4b. 6.4 ms. GZ Camera Set At 5000
Frames Per Second



Figure 4c. 12.4 ms. Notice the Position
Marks On the Camera

2 DESIGN

2.1 General Features

To serve as a starting point for our design, we were given certain fixed conditions with respect to the data from the experiment which was to be collected in several ways. First, blast pressure sensors were to be installed in strategic locations around the GZ. Several of these may be identified in Figure 1. Then, TOA gauges were to be fitted to the skin of the sphere to measure the symmetry of the blast, and, lastly, both visible and IR photographs and motion pictures were to document the physical processes. A metallic dust seedant was to aid the visible photography.

In addition, the unique factor present at the chosen test site was a 1" steel cable spanning the valley at a height of 200 ft. This would lend itself well towards restraining the sphere at both the bottom and top.

Basic requirements for the sphere were laid out so that an explosion of 1000 lbs of TNT could be simulated with minimum risk to personnel and max reuse of equipment. The appropriate sphere for this yield would have a 32 ft diameter and a volume of 17,157 ft³. The risk factor would be considered in the detail design and in the handling procedures.

The main components of our end product included two end fitting structures, an internal support cable, the sphere material proper, the TOA gauges, an inflation tube, a pressure relief valve, an inflation poppet valve, and a gas diffuser.

2.1.1 TOP END FITTINGS

The TEF, in addition to gathering and sealing the top ends of the sphere gores, served as the top attach point to the overhead cable. It consisted of an eye-bolt in the middle of an 18 inch I.D. removable aluminum plate held to an outer structural ring (which held the sphere material) with 12 bolts. It was removable to allow inserting the internal support cable.

2.1.2 INTERNAL SUPPORT CABLE

This cable internal to the sphere was designed as a load supporting member. It was subject to a tensile load of 1500 lbs. exerted between the upper and lower restraining lines.

We were fortunate to have had a predecessor program of the same magnitude. It was carried out in October 1965 by GARD as part of the SLEDGE program (refer to Table I). The GEST site, while not as flat of terrain, had, as mentioned in 2.1, the overhead cable. The sphere, then, could be held in place by a taut line through its middle rather than by handling lines attached to its skin. This line also allowed us to raise the sphere after inflation.

One consideration on the composition of the support line entered our planning. A synthetic line would contaminate spectrographic pictures less than a steel one. However, with the latter, we hoped the system would remain intact during the explosion rather than clatter to the ground. This internal support cable, unique to our design, was to be used in raising or lowering the sphere, for hanging the detonators and metallic dust container(s), and for stability during inflation.

2.1.3 BOTTOM END FITTING

The BEF served as the attach point for the lower restraining line, but, more importantly, had openings in it for the inflation poppet valve and the pressure relief valve. In order to accommodate these, its inner diameter was 42".

Its eyebolt in the middle could be attached to the lower restraining line. Offset from this were two openings, one 12" in diameter and the other 5" in diameter. (Refer to Figure 5 for a schematic). The two valves were bolted into these openings. The TEF and BEF were directly opposed.

As previously mentioned in paragraph 1.2.2, a major decision in our design was that of no handling patches. This impacted the material itself, the inflation sequence, and all ground handling. Instead, we incorporated a rigid stand at GZ to hold the BEF in place five feet above the ground. A fixed standpipe below this was to be used for inflation. Three pins on the stand fit into matching

receptacles on the BEF which was held in place by the lower restraining line. The purpose of this arrangement was to give us a fixed geometry during inflation. We desired as close to a hands-off inflation as possible, and the stand let us dispense with the handling lines which would have been necessary to prevent rotation.

2.1.4 SPHERE MATERIAL

A 32 ft diameter sphere has about 3220 ft² for the end fittings leaves a little more than 3200 ft² of surface to be constructed out of an appropriate conductive material. This material is fully described in section 2.2.

2.1.5 TIME OF ARRIVAL GAUGES

As part of the instrumentation requirements set forth for the spheres, 4 TOA gauges were to be installed at specific locations on the surface material. These were to measure the symmetry of the detonation wave and were to be located mutually 120° from one another at the corners of an imaginary tetrahedron. They measured 1/2" in diameter by 1/16" thick.

The pockets for these devices, consisted of two circular patches of the same material as the sphere proper. They were 6" and 5" in diameter and were heat sealed to the surface leaving an unbonded 135° section for inserting the gauge. The associated wiring was installed by GTS at the factory. Final connections were made in the field.

2.1.6 INFLATION TUBE

A flexible, conductive, appropriately sized tube connected the fixed stand-pipe to the inflation poppet valve (refer to Figure 8). It was banded rigidly at the top, but open at the bottom so that it could slip off the delivery pipe as the sphere was elevated. A remotely controlled clamp provided a seal during inflation.

2.1.7 PRESSURE RELIEF VALVE

As a safety measure against overinflating or superheating, a 5" relief

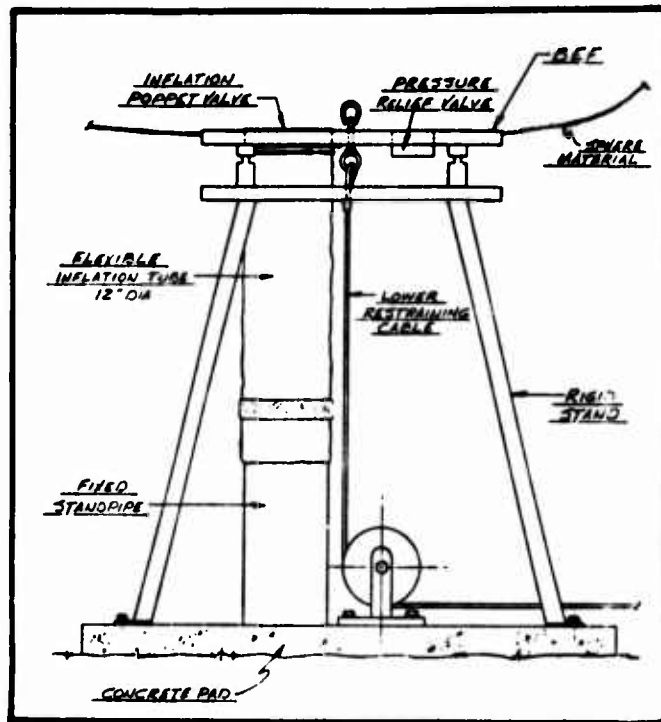


Figure 5. The Rigid Standoff at Ground Zero Holding the Bottom End Fitting in Place

valve was installed on the BEF to combat any pressure above 3" H₂O. This amount of superpressure was not considered detrimental. It was equipped with a manual override so that during the acceptance pressure test, it could be held shut while internal pressures of up to 7.4" H₂O were present.

2.1.8 INFLATION POPPET VALVE

To prevent backflow during inflation and to provide an automatic seal after inflation, the design required that a poppet valve be an integral part of the inflation port. Since excess velocity across the sphere material was liable to cause a charge buildup, it was required to be large enough to keep inflatant velocities below 12 ft/sec. GARD recommended that limit after studying the static charges caused by fluid flow across non or semi-conductive materials. Part of the function of the gas diffuser was also to help prevent such an occurrence.

2.1.9 DIFFUSER

We attempted to use the normal inflation sequence to help mix the oxygen and methane. Putting the gas entrance at the bottom of the sphere, therefore, would not hinder the mixing as long as the heavier gas were forced in first. Afterwards the lighter gas, in this case methane, would help mix itself as it rose.

To assist this mixing process even further, we required an internal diffuser to be incorporated with the inflation port. GTS satisfied this item with a conductive, half torus around the poppet valve. It diffused the flow and protected the adjoining area in two ways. It prevented a concentrated flow of gas from impinging on the sphere inner surface, reducing the static charge buildup possibilities. And, secondly, by doing so, it also reduced the chances of destructive flutter in that area.

The diffuser was grounded directly to the BEF.

2.2 Materials

An interesting summary of static electricity problems and considerations in the SLEDGE program is given by Major Brown (1968). The evaluations of coating

materials and the balloon materials themselves, such as in these studies, were part of the background study for in the selection of a suitable material for the GEST spheres.

2.2.1 PREVIOUS PROGRAMS

Table 1 is meant to contrast the different materials which have been used previously. Usually, a combination of Dacron scrim and Mylar sheets were used for safety purposes. In these programs, the necessity for handling patches on several of the large balloons made the likelihood of small tears high. To combat the total loss of a sphere through propagation of any of these tears, a pattern of crisscrossing scrim was designed to act as a "ripstop" measure.

2.2.2 THE GEST BILAMINATE

As the GEST designers, however, we were allowed a different viewpoint. The internal support cable, as described earlier, allowed us to dispense with the costly scrim laminates because of the smaller possibilities of tears. It was more cost effective to design the handling procedures to conform to the material than to relax the handling requirements in exchange for the safer, more expensive material. Figure 6 shows the metallized laminate proposed by GTS. In choosing a basic material for the sphere surface, GTS considered, besides the bilaminate, a single thickness sheet and a foil laminate (Figure 7). We were interested in a material with at least a calculated minimum strength and without unmanageable handling requirements. For GEST, GTS decided on the bilaminate for several reasons:

- a. Resiliency - The bilaminate is more elastic and more pliable than either of the others. This is a plus for handling.
- b. Fault Count - The whole does not equal the sum of its parts. It would be highly coincidental if a fault in one of the sheets matched up with a fault in the other. The double sheet, then will have less faults than either of the singles. This reduces the possibility of leaks.
- c. Stiffness - Thicknesses of greater than 2.5 mils in mylar are very stiff and very difficult to seal. A single sheet of 3 mil Mylar with a

vacuum deposit of aluminum would have fallen in this category. This violates our handling criteria.

d. Tri-corners - The scheme for field inflation and the specification requirement for a pressure test before acceptance meant that each sphere would undergo considerable handling before a detonation. Tears caused by tri-corner folds are a likely possibility in a foil laminate and in a thick single sheet of mylar, whereas the bilaminate weathers this treatment quite well.

As a point in fact, during the test series, each sphere ended up heavily creased from usage. Numbers 2 and 3 (of 8) were retested several times before passing acceptance because of leaky fittings but did not develop a single flaw from creasing or tri-cornering. None of the spheres developed any flaws from any handling.

2.2.3 PROPERTIES

Every material to be used near detonable gases should have certain electrical and handling properties which make it safety compatible. By way of review, we should look at several of these. They are: a) static charge and sparking possibilities b) abrasion characteristics, and c) spontaneous combustion preventative measures.

a. Static charge and sparking

The aim of the specification was to assure adequate, complete conductivity among all components of the balloon, making the possibilities of a charge buildup negligible. By providing a common ground at the BEF (See para 2.1.3) and by grounding the BEF through the lower restraining line, which was constructed of steel cable, we hoped to bleed off even the slightest accumulated charge.

Paragraph 2.5 in the performance specifications covers the electrical continuity requirements, and paragraph 3.2 states the electrical resistivity limits for the sphere. The measures taken by Sheldahl Company to conform to these included the 1200Å aluminum coating, the K017000 silver ink, and conductive tabs

at the midpoint of each gore to furnish the inner/outer surface conductivity.

The manufacturer used silver ink to provide conductive paths around the end fittings, from one gore to the next at the seals (ref. Figure 8), and around the pockets for the time-of-arrival gauges. This was painted on during the manufacturing process as the various seals were made. The ink replaced the electrical path which may have been broken wherever adhesive was used.

Fortunately, we had no instances of sparking. We believe, however, that the conductivity provisions functioned efficiently, and, though not cost effective for large balloons because of a heat transfer problem, could be equally effective in smaller future work. There are no quantitative measurements available on actual charging because of our difficulties in obtaining a reliable and accurate instrument.

b. Abrasion characteristics

We classify most balloon material as delicate because of its susceptibility to tears. With a total thickness of somewhat over 3 mils, the GEST material was not so prone to tears as it was to wear. As part of their acceptance testing before qualifying the G131900 for use, GTS found that the electrical resistance of the surface after the aluminum coating had been subjected to rubbing increased significantly. They also crumpled it, crimped it, folded it, scrubbed it, sealed it, and peeled it to investigate further resistance and abrasion characteristics. Wear through handling was to be the area of most concern. Though not as tough as a foil laminate, the G131900 was acceptable with careful handling.

c. Spontaneous Combustion

Wherever an environment of pure oxygen is present, the danger of spontaneous combustion exists. Designers had to be concerned with the interiors of the inflation lines, the standpipe at GZ, the inflation tube, and the sphere, and try to assure that there were no oily surfaces present. To do this, we required gloves to be worn whenever personnel handled the sphere, and periodic cleaning of the equipment to be performed with a proper solution. The inflation lines were kept pressurized with nitrogen and the standpipe covered to prevent introducing

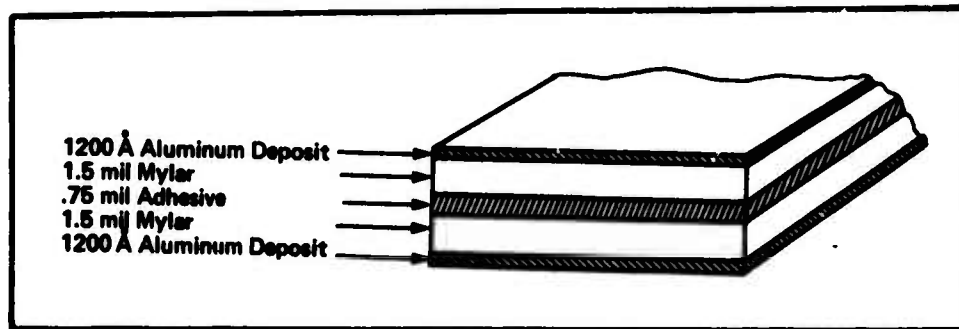


Figure 6. Detail of the GEST Metallized Laminate - G131900

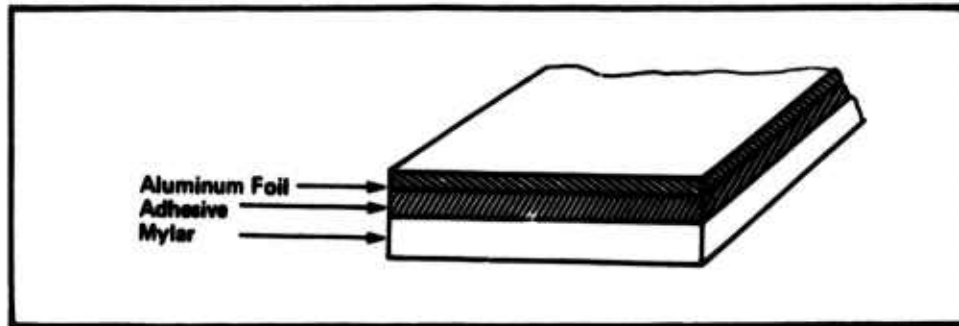


Figure 7. A Foil Laminate - one of the alternate materials

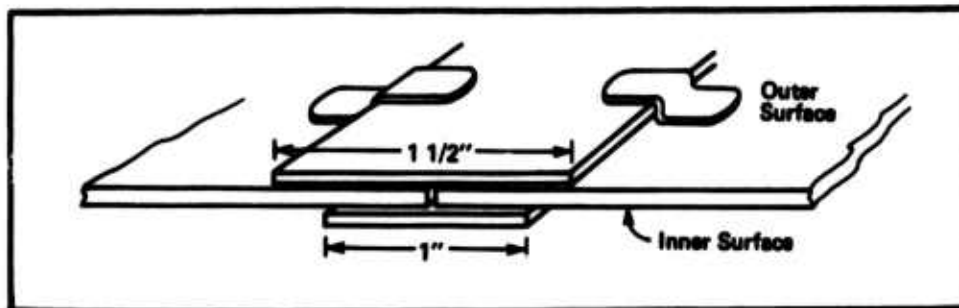


Figure 8. Cutaway View of a Gore Seal Showing the "Jumpers" of Silver Ink

impurities into the sphere. We stressed the importance of preventing combustion to the handlers and inspected procedures continually.

2.3 Seals

According to Slater (1958) and others, one of the disadvantages of Mylar in balloons is that it cannot be heat sealed to itself. Fortunately previous research in superpressure spheres had uncovered sealing techniques appropriate for our program. With adhesive tape on the inside and the outside of the seal (See Figure 8), the strength requirements as noted in paragraph 2.2 of the GTS proposal are satisfied.

3. CONCLUSIONS

3.1 Design Results

Of the basic design, there has not been undue criticism. Its structural integrity, conductivity, ease of inflation, wear against abrasion, etc. were all within the specifications. The two main problems concerned attached equipment.

The more serious of the two involved the inflation poppet valve. The specifications for this item (see para 2.1.8) included size, flow velocities, and opening and closing pressures. These figures were not only correct but had been examined and approved beforehand by AFCRL as part of the work statement on the spheres. When the valves were delivered out of spec for opening and closing pressures, time restraints on the field tests did not allow GTS to launch into a contract dispute, so they modified each with a pneumatic opening device. The first few acceptance inflations were performed with difficulty until these devices could be retrofitted.

A similar problem ensued with the pressure relief valves. Again, they did not open or close at the proper pressures, and the Sheldahl engineering staff had to modify their mainsprings.

Both difficulties were time-consuming to repair and caused testing delays

and changed procedures. Fortunately, the "fixes" were satisfactory and the tests were not impaired.

3.2 Usage Results

We drew two conclusions from the field tests on procedures impacted by the design. They concerned preparing the sphere as it came out of its shipping box and raising it to the vertical before inflation.

Originally, we wanted to perform all work in the field to minimize the time the sphere would be subject to accidents out of its box. By November, though, weather conditions were more severe than we had imagined. The crew was severely taxed on simple tasks because of the cold and we were thus forced into readying the sphere at the nearest suitable indoors location which was 15 miles away.

We conclude from our experience that the cleanliness, lighting conditions, and warmth of the work building more than compensated for any extra wear on the sphere during the ride to the test site. We used a 50 ft flatbed truck to transport the sphere which had all internal work completed and both end fittings installed. This procedure reduced arrival time on a detonation day from T-5 hours to T-2 hours. I would recommend this as the normal procedure for a future similar program regardless of the weather because of the overall improvement in working conditions.

Secondly, when ready to raise the sphere, the original plan called for attaching the BEF to the standoff before raising the TEF to the vertical. TSgt Dew from AFWL suggested that the order be reversed, and the idea was adopted. Using handling lines attached to the top end fitting, we, in fact, raised the sphere directly from the flatbed. This was considered a very worthwhile improvement.

AFWL concluded this satisfactory test series in January 74, and, using the same design, plan to follow up with future supplementary tests.

Acknowledgments

I would like to thank several people who have generously contributed time and knowledge to this paper. First, the GEST program and, second, this write-up would not have been possible without their efforts.

Mr Frank Doherty of AFCRL has been involved in detonable gas programs since their beginning. His background knowledge provided immensely helpful guidance. Mr Jim Dwyer, also of AFCRL, was instrumental in material design from the SLEDGE efforts to today. Our discussions and evaluations resulted in a very satisfactory material and a commendably safe test series.

Mr Gene Brieland from GTS spent many unrewarded overtime hours with this program overall and the sphere manufacturing in particular. His cooperation was appreciated.

Lt Col Pat O'Toole and Capt Jim Teague lived with GEST for many months. The proper design would not have been of much help unless it was properly handled during the testing. Along with advising me on HE programs, they are responsible for the past and the future conduct of the GEST tests.

References

- Anonymous (1966) "Exploding Gas Bags May Aid ABM Effort", Technology Week 14 Nov 66.
- Balcerzak, M. J. (1966) Detonable Gas Explosion: A Unique Application, Proc. Fourth AFCRL Scientific Balloon Symposium, AFCRL-67-0075, January 1967.
- Balcerzak, M. J., Johnson, M. R., Kury, F. R. (1966) Nuclear Blast Simulation Part I Detonable Gas Explosion. GARD report for DASA-1792-I, Contract No. DA-49-146-XZ-422.
- Balcerzak, M. J., Johnson, M. R., Lucole, S. W. (1967) Nuclear Blast Simulation Detonable Gas Explosion, Operation Distant Plain. GARD final report for DASA - 1945. Contract No. DA-49-146-XZ-400. April 1967.
- Brieland, G., Niccum, R., et al. "Proposal for Detonable Gas Balloons" Vol I. GT Sheldahl Proposal No. 51982. 21 March 73.
- Brown, R. M., Major, USAF (1968) Conductive Balloon Material Study, Proc. Fifth AFCRL Scientific Balloon Symposium, AFCRL-68-0661.
- Fields, S. F., Dr. (1972) High Altitude Blast Generation System: Detonable Gas Mixing Experiments, Proc. Seventh AFCRL Scientific Balloon Symposium, AFCRL-TR-73-0071, January 1973.
- Grass, L. A. (1972), Superpressure Balloon for Constant Level Flight, Instrumentation for Geophysics and Astrophysics #21, AFCRL-62-824. August 1962.
- Korn, A. O. (1970) Polyethylene and Scrim Balloons - Size and Cost. AFCRL Report, July 1970.
- Nolan, G. F. (1973) Balloon Program Facilities and Capabilities. AFCRL Report, January 1973.
- Schaefer, R. A. (1961) Final Report, Mylar Balloon Fabrication Study. ARDC Report, Contract AF19(604) 7254, Feb 61.

References

Slater, R. J. (1958) Superpressure "Mylar" Polyester Balloons, Final technical summary of contract AF19(604) 2286, AFCRC-TR-58265, Mar 1958.

Personal communications. Lt Col P. O'Toole and Lt W. Smith, AFWL(DEX), High explosive blast research, past and present.

Appendix A

Publications of Proceedings of Past AFCRL Balloon Symposia and Workshops

Due to interest expressed in the proceedings of past AFCRL balloon symposia and workshops, and because the report series for these reports has been changed, a listing of the Proceedings of all past AFCRL balloon symposia and workshops follows.

<u>TITLE</u>	<u>AFCRL REPORT NO. AND DATE</u>
Proceedings of the AFCRL Balloon Symposium	AFCRL-63-919, Dec. 1963 (AD614065)
Proceedings, 1964 AFCRL Scientific Balloon Symposium	AFCRL-65-486, Jul. 1965 (AD619695)
Proceedings, AFCRL Scientific Balloon Workshop, 1965	AFCRL-66-309, May 1966 (AD634765)
Proceedings, Fourth AFCRL Scientific Balloon Symposium	AFCRL-67-0075, Jan. 1967 (AD656692)
Proceedings, AFCRL Tethered Balloon Workshop, 1967	AFCRL-68-0097, Mar. 1968 (AD676037)
Proceedings, Fifth AFCRL Scientific Balloon Symposium	AFCRL-68-0661, Dec. 1968 (AD685726)
Proceedings, Sixth AFCRL Scientific Balloon Symposium	AFCRL-70-0543, Oct. 1970 (AD717149)
Proceedings, Seventh AFCRL Scientific Balloon Symposium	AFCRL-73-0071, Jan. 1973 (AD767582)